CERN Yellow Reports: Monographs CERN-2025-010

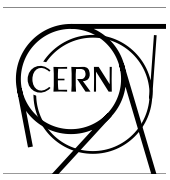
70 years of particle physics

Daniel Treille

CERN, Geneva, Switzerland

Felicitas Pauss

ETH Zurich, Switzerland



CERN Yellow Reports: Monographs
Published by CERN, CH-1211 Geneva 23, Switzerland

ISBN 978-92-9083-716-9 (paperback)
ISBN 978-92-9083-717-6 (PDF)
ISSN 2519-8068 (Print)
ISSN 2519-8076 (Online)
DOI https://doi.org/10.23731/CYRM-2025-0010

Copyright © CERN, 2025
Creative Commons Attribution 4.0

This volume should be cited as:
70 years of particle physics, Daniel Treille and Felicitas Pauss, CERN Yellow Reports: Monographs, CERN-2025-010 (CERN, Geneva, 2025), doi:10.23731/CYRM-2025-0010

Corresponding author Daniel.Treille@cern.ch.
Accepted, in December 2025, by the CERN Reports Editorial Board
(contact Carlos.Lourenco@cern.ch).
Published by the CERN Scientific Information Service (contact Jens.Vigen@cern.ch).
Indexed in the CERN Document Server and in INSPIRE.
Published Open Access to permit its wide dissemination, as knowledge transfer is an integral part of the mission of CERN.

Preamble

This document presents a selection of topics in Particle Physics, from the early periods of its existence until today.

It is aimed at specialists in the field, hoping to inform the young ones about the past and recalls important moments to the seniors who want to refresh their memory.

Many highlights of our field are described, but less bright periods, doubts, and temporarily wrong paths are not kept hidden, and problems are presented as they appeared at the time.

An attempt was made to find the right balance between technology and physics, and to acknowledge in a fair way the important contributions of actors with very different profiles.

The document includes various comments and points of view, but always only drawn from published material.

The document proposes many references, which are mostly publications, entries in the INSPIRE data base or free access books, e.g., the book "Technology Meets Research" [i]. However, it also contains interesting figures that have been taken from public lectures given by experts at conferences, workshops and in physics schools, with the relevant sources cited. As far as possible, the reference gives direct access to the relevant material.

Furthermore, this document describes the most up-to-date results and presents the major questions left open. From these, one can deduce possible guidelines for the future, but considerations of strategy and discussions on what should come next in terms of machines and programmes are not part of this document.

The fundamentals of the different subjects are usually only referenced to, but some topics are explained by including short introductory texts.

Besides the Particle Physics Standard Model another "Standard Model" exists, including what we know about our universe, its content and possibly its history. This document also deals with the relations between both domains.

The work started as a review of 60 years of Particle Physics at the Société Française de Physique, and initially emphasised the French contributions to these fields. This aspect has been largely removed, and the document attempts to cover contributions from key players around the world, although activities involving CERN programmes still occupy a large part. This is motivated by CERN's 70th birthday, celebrated in 2024.

[i] Technology Meets Research. 60 Years of CERN Technology: Selected Highlights. Editors C. Fabjan, T. Taylor, D. Treille and H. Wenninger. https://inspirehep.net/files/02de568d4897c555515de27f0b96af4d

Acknowledgements

We are very grateful to Robert Barate for his careful reading of the manuscript and for providing numerous comments and suggestions. We thank Yves Zolnierowski for several comments on cosmology. Our warm thanks go to Jean Iliopoulos, Günther Dissertori and Ralph Eichler for their comprehensive feedback on multiple sections. We are indebted to Carlos Lourenço for his numerous constructive comments on the document. We are particularly thankful to Fabiola Gianotti and Christian Fabjan for their supportive and encouraging feedback.

Contents

Preamble iii

Acknowledgements iv

1. Short news from prehistory 1

2. Outline of the adventure 3

3. Establishment of the CERN Organisation 6
- 3.1 Mission of CERN
- 3.2 Other large Laboratories world-wide
- 3.3 Education: some famous schools of physics

4. The "great reduction" 11
- 4.1 Towards the quark model
- 4.2 Intermède: a bit deeper in complexity

5. What is the proton? 17
- 5.1 Probes and structure functions
- 5.2 The path to Quantum Chromodynamics
- 5.3 From QCD foundations to its manifestations in high-energy collisions
- 5.4 Back to the proton
- 5.5 Modern fixed-target electron scattering

6. Evolution of detectors 30
- 6.1 The sequence of detector types
- 6.2 Various aspects of HEP instrumentation
- 6.3 Intermède

7. Towards the Standard Model 41
- 7.1 The successes
- 7.2 What is missing in the SM?
- 7.3 Some possible directions beyond the SM
  - 7.3.1 Grand Unification
  - 7.3.2 Extra Dimensions
  - 7.3.3 Asymptotic safety
  - 7.3.4 Effective theory
- 7.4 An aside on anomalies
  - 7.4.1 From the classical theory to the quantum theory
  - 7.4.2 What about anomalies in the SM?
  - 7.4.3 What about global anomalies?
  - 7.4.4 A first encounter of non-perturbative aspects of the SM
  - 7.4.5 A bit more on topology
- 7.5 Intermède 1: a brief introduction to the SM
  - 7.5.1 Local invariance
  - 7.5.2 The Brout–Englert–Higgs mechanism in brief
  - 7.5.3 Electroweak symmetry breaking: the BEH boson and some pre-discovery thoughts

7.6 Intermède 2: the Higgs mechanism, analogies
7.6.1 The crowd analogy
7.6.2 Higgs-elementary particle interaction
7.6.3 Superconductivity
7.6.4 An identity crisis
7.6.5 The “added mass effect”
7.6.6 A math amusement
7.6.7 Mass without mass

8. The GIM mechanism 62
8.1 Origin of the mechanism
8.2 Flavour Changing Neutral Current Processes

9. Neutral Currents 68
9.1 The Gargamelle discovery
9.2 The consequences

10. Accelerators in brief 76
10.1 The Proton Synchrotron
10.2 The Super Proton Synchrotron
10.3 The Intersecting Storage Rings
10.4 Stochastic cooling
10.5 The proton-antiproton collider
10.6 The Large Hadron Collider
10.7 Key moments and figures at CERN
10.8 HERA at DESY
10.9 The Tevatron at Fermilab
10.10 The present status and achievements of R&D
10.11 Some applications of the accelerators
10.12 Crystal channelling
10.13 A major turning point
10.14 Programmes in USSR and Russia
10.14.1 Accelerators
10.14.2 The Era of Electron-Positron Colliders
10.14.3 Absolute Neutrino Mass Measurements
10.14.4 Non-Accelerator physics
10.15 Programmes in China
10.16 Programmes in Japan
10.16.1 KEK
10.16.2 KEKB
10.16.3 J-PARC
10.16.4 Neutrinos
10.17 The High Intensity Proton Accelerator Facility at the Paul-Scherrer-Institute

11. ISR physics and technology 98
11.1 Instrumental highlights
11.2 Machine highlights
11.3 Main physics results

12. W and Z discovery 101
12.1 The UA experiments at the CERN proton-antiproton collider
12.2 What followed in the antiproton world

13. CP Violation 107
13.1 The kaon story
13.2 The third generation

14. CP – a continuation 111
14.1 Towards the Unitarity Triangle and CKM
14.2 Any new physics?
14.3 The present status
14.4 Perspective
14.5 Note on non-separability
14.6 The strong CP problem

15. The e^+e^- colliders 119
15.1 Historical comments
15.2 The Stanford Linear Collider and beyond
15.3 The Large Electron Positron Collider at CERN

16. Florilège of LEP 129
16.1 LEP1
16.2 LEP2
16.3 Two brave attempts
16.4 More on the top story
16.5 A four-jet story
16.6 A comment on LEP cost

17. LEP2 and its fate 138

18. Final message from LEP/SLC 142
18.1 Combined results
18.2 The 97/98 GeV hint at LEP
18.3 The LEP/SLC global variables
18.4 The LEP paradox
18.5 Digression on SUSY
18.6 A different track?
18.7 After LEP

19. About neutrinos 153
19.1 Accelerator neutrino physics
19.2 The number of neutrinos
19.3 The advent of neutrino astrophysics
19.4 Present status of oscillations
19.5 Present activities
19.6 Heavy Neutral Leptons
19.7 The vMSM
19.8 The hunt for HNLs
19.9 HNL as DM
19.10 The gallium anomaly
19.11 Neutrino detectors at accelerators
19.12 Astrophysical domain of ν physics
19.13 Details on oscillations
19.14 Summary
19.15 Some synoptic plots

20. Heavy ions 180
20.1 The scenery
20.2 Summary of results at ultra-relativistic energies
20.2.1 The measurements of the EW probes and the parton distribution functions
20.2.2 Soft particle production
20.2.3 Studies of hard probes
20.2.4 Differential measurements of onia and evidence of deconfinement
20.2.5 Study of rare probes
20.3 Conclusion
20.4 Brief historical overview
20.5 Searches with HI at colliders
20.6 On the ridges

21. The LHC challenges 193

22. LHC: from doubts to confidence 197

23. Instrumental highlights of LHC 201
23.1 Images of some instrumental breakthroughs
23.2 Details about the main highlights
23.3 Particle flow
23.4 Aspects of LHC computing
23.5 Evolution of data analysis

24. LHC Physics 210
24.1 Higgs Boson physics at LHC
24.1.1 Discovery and properties
24.1.2 Higgs interactions
24.1.3 Higgs self-interaction
24.1.4 A deep mystery
24.1.5 More on baryogenesis
24.1.6 More on the sphaleron and the search for it
24.2 Exploration of an eventual extended Higgs sector
24.3 Other searches at LHC
24.3.1 The scenarios
24.3.2 Back to Supersymmetry
24.3.3 Effective field theory
24.4 Other LHC measurements and top physics
24.4.1 Overview
24.4.2 Double parton scattering
24.4.3 Top production and mass
24.4.4 Toponium
24.4.5 The M_W measurement by CMS
24.4.6 About running masses

25. More on precision: Atomic parity violation 252

26. More on precision: the g–2 factor of the muon 254
26.1 Basics of g–2
26.2 Measurements and predictions
26.3 Some history of a_μ
26.4 g–2 of the tau and electron

26.5 Another access to the hadronic vacuum polarisation: a^{HVP}
26.6 To conclude

27. Flashback, for the pleasure: the π meson 264
27.1 History and studies of π^0
27.2 Recap about baryon number non-conservation

28. New spectroscopy from LHC and elsewhere 267
28.1 From expected to unexpected spectroscopy
28.2 Exotic states
28.3 Diquark, all-charm tetraquarks, glueball?

29. Overview and timeline of discoveries 275

30. Change of perspective: news from the sky 277
30.1 The expanding Universe
30.2 The quark-hadron transition
30.3 Big Bang Nucleosynthesis
30.4 The Cosmic Microwave Background
30.5 Re-ionization
30.6 Supernovae and the acceleration
30.7 Baryon Acoustic Oscillation
30.8 One more big problem?
30.9 Towards the origin?
30.10 More on inflation
30.11 More on cosmology
30.12 Digression 1: The Universe in logM-logR coordinates
30.13 Digression 2: An interesting but controversial topic

31. Dark matter 304
31.1 Dark matter overview
31.1.1 Brief historical account
31.1.2 Dark matter particles or MOND
31.1.3 Dark Matter: Hypotheses and classification
31.1.4 The three types of Dark Matter searches
31.1.5 Short overview of Dark Matter search techniques
31.2 Weakly Interacting Massive Particles and Feebly Interacting Particles
31.2.1 Characteristics of Weakly Interacting Massive Particles (WIMPs)
31.2.2 WIMPs exclusion
31.2.3 Complementarity with collider results
31.2.4 Seasonal variation and directional detection
31.2.5 Feebly interacting particles: few keV - GeV light dark matter
31.2.6 Direct DM detection strategies
31.3 Axions and Axion-Like Particles
31.3.1 Presentation of the axion
31.3.2 Scenarios
31.3.3 Searches for axions
31.3.4 Axion exclusions
31.3.5 Collider searches
31.3.6 Overview of searches
31.3.7 Detection concepts, detector target materials and technologies
31.3.8 More information on axions

31.4 The dark stars
31.4.1 The contribution of microlensing
31.4.2 A brief account of Weak Gravitational Lensing
31.4.3 Primordial black holes: presentation
31.4.4 Primordial black hole searches

32. Some very hot topics …… 347
32.1 Neutrinos: a key question remains
32.1.1 Neutrinoless double beta decay
32.1.2 Backgrounds
32.1.3 Interpretation and identification
32.1.4 Current and future experiments
32.2 Electric Dipole Moments
32.2.1 EDM limits
32.2.2 More on two of the last eEDM experiments
32.2.3 Some more on neutron EDM
32.2.4 A nice by-product
32.3 Still more on FCNCs
32.4 GUTs, Proton decay searches and the Neutron lifetime problem
32.4.1 Proton decay searches, history and prospects
32.4.2 More towards baryogenesis
32.4.3 The Neutron problem

33. A singular point: The Paul-Scherrer-Institute …… 373

34. Brief status of the physics of gravitational waves …… 375

35. Astroparticle physics …… 381
35.1 Overview
35.2 Imaging Atmospheric Cherenkov Telescopes
35.3 Neutrino telescopes and other instruments like e.g. air shower detectors using water tanks
35.4 The Alpha Magnetic Spectrometer
35.5 The Large Area Telescope

36. Some conclusions …… 392

1. Short news from prehistory

Let's recall some aspects of the physics landscape when Particle Physics (PP) started to bloom [1].

Quantum Electro Dynamics (QED) [2], the first quantum field theory, born in 1948-49, earned Shin'ichiro Tomonaga, Julian Schwinger and Richard Feynman the 1965 Nobel Prize. In 1947, the **Lamb shift**, a quantum effect describing the energy difference between two levels of the hydrogen atom, was discovered by Willis Lamb and Robert Retherford.

In the 1950s, Chen-Ning Yang and Robert Mills proposed a type of non-abelian gauge theory (i.e. whose vector bosons self-interact), called **Yang–Mills gauge theory** [3], the first example of which concerns the nuclear force in the nucleus. In a different direction, its developments were promised to a bright future.

Bell's inequalities [4], stated in 1964 by John Stewart Bell, are relations that measurements on entangled states must respect in the hypothesis of a local deterministic theory with hidden variables. In 1982 the experiments of Alain Aspect (Nobel Prize 2022) showed definitively that they are violated in the EPR [5] cases. This validates Quantum Mechanics (QM) and forces us to admit the non-separability of entangled states. Today, it is a precious tool in flavour physics.

In 1948 Ralph Alpher and Robert Herman predicted the **Cosmic Microwave Background (CMB)** [6], closely related to the work of George Gamov. The same year the Alpher–Bethe–Gamow paper on Big Bang nucleosynthesis was published. The CMB was discovered in 1964 by Arno Allan Penzias and Robert Woodrow Wilson (Nobel Prize 1978).

In early electronics, the **bipolar transistor** was produced for the first time in December 1947 and won the 1956 Nobel Prize for its authors (William Shockley, John Bardeen and Walter Brattain).

In 1937, Louis Leprince-Ringuet had created the first laboratory of the École Polytechnique, devoted to cosmic rays at Argentière-la-Bessée (France). In 1946, the Laboratoire Cosmiques was inaugurated.

The detectors used were emulsions, dating from before 1900, the Wilson chamber (1912), Geiger–Müller counters (1928) and scintillators, which appeared from 1947 to 1950. The bubble chamber (BC) was invented in 1952 by Donald Glaser, who received the Nobel Prize in 1960.

---

[1] For instance, the PP branch of the French Society of Physics appeared in 1969.

[2] For a very elementary introduction of QED see Technology Meets Research. 60 Years of CERN Technology: Selected Highlights. Editors C. Fabjan, T. Taylor, D. Treille and H. Wenninger.
https://inspirehep.net/files/02de568d4897c555515de27f0b96af4d , p. 25
For a less elementary introduction by S. T. Epstein in 1965:
https://ntrs.nasa.gov/api/citations/19650023652/downloads/19650023652.pdf
For a basic historical QED paper by R. P. Feynman (1949): https://journals.aps.org/pr/pdf/10.1103/PhysRev.76.769
An excellent introductory book on PP, we shall often refer to, is Particle Physics and Cosmology, by Collins, Martin and Squires,1989: https://onlinelibrary.wiley.com/doi/book/10.1002/3527602828
A more recent introductory book to PP is from M. Thomson, Modern Particle Physics, Cambridge University Press 2013:
https://doi.org/10.1017/CBO9781139525367
A quite advanced document on gauge theory is: D. Tong https://www.damtp.cam.ac.uk/user/tong/qft/six.pdf

[3] L. Maiani, An Elementary Introduction to Yang–Mills Theories and to their Applications to the Weak and Electromagnetic Interactions. https://cds.cern.ch/record/872007/files/23.pdf

[4] J. S. Bell, On the problem of hidden variables in quantum mechanics. *Rev. Mod. Phys.38, 447 (1966)*

[5] J. S. Bell, On the Einstein Podolsky Rosen Paradox. https://cds.cern.ch/record/111654/files/vol1p195-200_001.pdf

[6] https://www.esa.int/Science_Exploration/Space_Science/Herschel/Cosmic_Microwave_Background_CMB_radiation

In non-accelerator physics, a shock for the PP community, **parity (P) violation** in the weak interaction was discovered in 1956 in the nuclear β decay experiment of Mrs Chien-Shiung Wu [7], inspired by Tsung Dao Lee and Chen Ning Yang (Nobel Prize 1957).

On the PP side, in 1947, long after **Hideki Yukawa** postulated them in 1935 [8], Cecil F. Powell, César Lattes and Giuseppe Occhialini of Bristol University discovered the first mesons, **the π^+ and π^- pions**, using very high-altitude balloons and emulsions. In 1946, Louis Leprince-Ringuet and Michel Lhéritier published *"the probable existence of a particle with a mass 990 times that of the electron"*, the **K meson**. Strange particles thus appeared from 1946 to 1953.

"No klystron, no HEP" was a motto when PP started. Let us mention their inventors, Russell and Sigurd Varian, and a figurehead of the first Stanford linacs, Wolfgang "Pief" Panofsky [9]. The first US synchrotron projects at Brookhaven and Berkeley in 1947 closely followed the invention of the synchrocyclotron. Around 1952, the invention of **strong focusing or alternating gradient** magnetic lattices brought a revolution for synchrotrons [10].

Towards the end of 1954, at Stanford's MARK III (1 GeV) linac, the e^- scattering on hydrogen showed that the proton is a finite-sized object with a radius of $(0.74 \pm 0.24)\times10^{-13}$ cm. This opened up a large sector of PP and Robert Hofstadter received the 1961 Nobel Prize.

For the **colliders**, so familiar now, it was a long time before anyone dared to consider them. The first were e^-e^- tangent rings [11], but Bruno Touschek, visionary, focused on e^+e^-, requiring only one ring [12].

[7] R. Webb, Chien-Shiung Wu: Chinese-American particle physicist who was denied a Nobel prize. https://www.newscientist.com/people/chien-shiung-wu/

[8] L. M. Brown, How Yukawa Arrived at the Meson Theory. https://lib-extopc.kek.jp/preprints/PDF/1985/8512/8512140.pdf

[9] Early linacs. In symmetry | volume 02 | issue 06, https://www.symmetrymagazine.org/article/august-2005/early-linacs

[10] P. J. Bryant, A Brief History and Review of Accelerators. https://cds.cern.ch/record/261062/files/p1_2.pdf
Erika Peters, Happy 100th Birthday to Ernest Courant. Brookhaven Lab celebrates the father of modern particle accelerators. https://www.bnl.gov/newsroom/news.php?a=217140

[11] S. Tazzari, Short History of Particle Accelerators. Zakopane 2006, https://cas.web.cern.ch/sites/default/files/lectures/zakopane-2006/tazzari-history.pdf

[12] CERN Courier, Vol 54 (2014): AdA – the small machine that made a big impact. https://cds.cern.ch/record/2064501

2. Outline of the adventure

Figure 2-1 schematically illustrates the outline of the adventure.

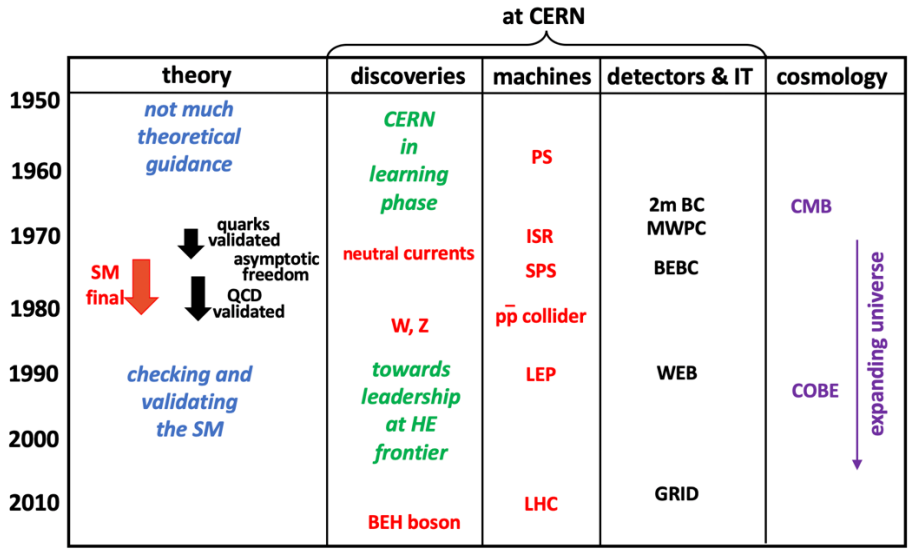


Fig. 2-1: Schematic outline of the adventure seen from CERN. For the broad view see Fig. 2-4. Figure by D. Treille.

Particle physics can be divided into two very contrasting periods: an initial phase where only a few guidelines emanated from theory and during which, Europe and CERN being in a learning phase, with discoveries mostly coming **from the United States**. This was followed by a phase of great clarity in the relationship between theory and experiment, with the progressive development and validation of the Standard Model (SM), while Europe and CERN had reached maturity and could point to a series of successes.

The turnaround can be illustrated by the ***mirabilis year* 1964**, which witnessed major discoveries as summarized in Fig. 2-2.

Conceptually, after these breakthroughs, a complete change occurred in the late 60s, early 70s. The experimental work focused on tests and, until now, validation of the SM. And CERN moved on to its current leadership at the high-energy frontier, achieving a remarkable sequence of accelerators.

As for cosmology, it was only with the discovery of the CMB [13] in 1964 that the idea of an expanding U Universe with an initial hot big bang prevailed, opening up a new point of view on our field: the **microscopic recreation of physics** which prevailed at the beginning of the Universe, beyond the curtain of invisibility that the original plasma imposes on its electromagnetic observation. A schematic view of the history of the Universe is illustrated in Fig. 2-3.

Figure 2-4 shows a worldwide and more detailed version of Fig. 2-1.

[13] See Section 30.4
For an interesting anecdote: Denis Puy, Le fond de rayonnement cosmologique ou la première lueur de l'Univers. https://www.ac-sciences-lettres-montpellier.fr/academie_edition/fichiers_conf/PUY-2015.pdf p. 217

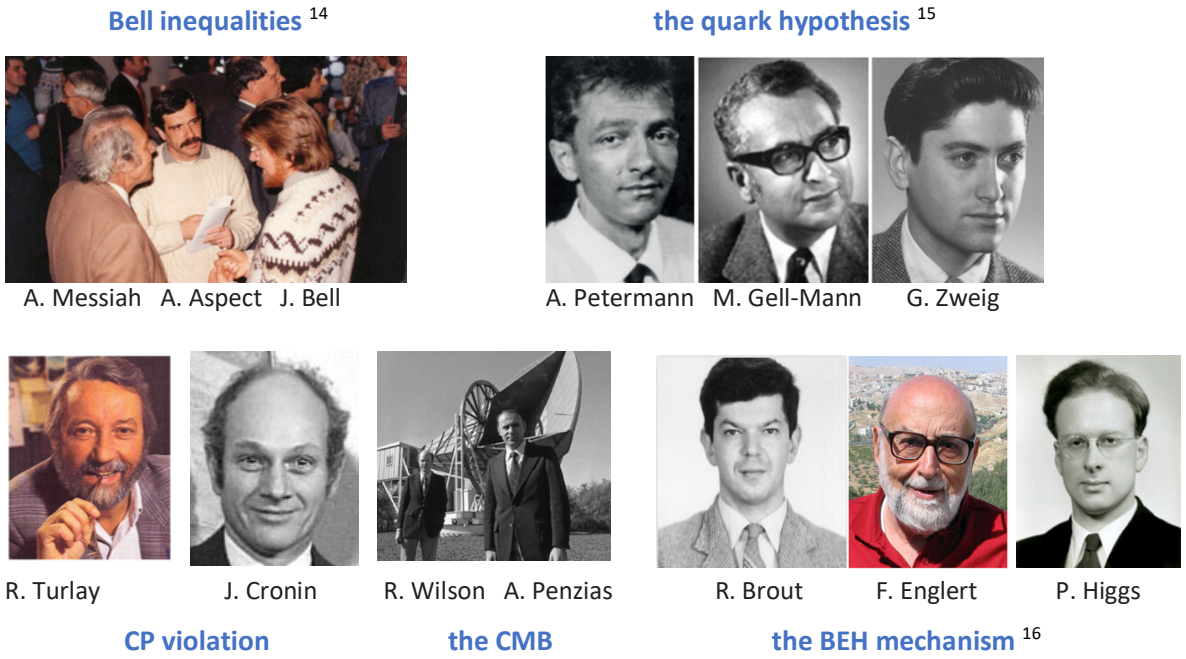


Fig. 2-2: Major discoveries during 1964.

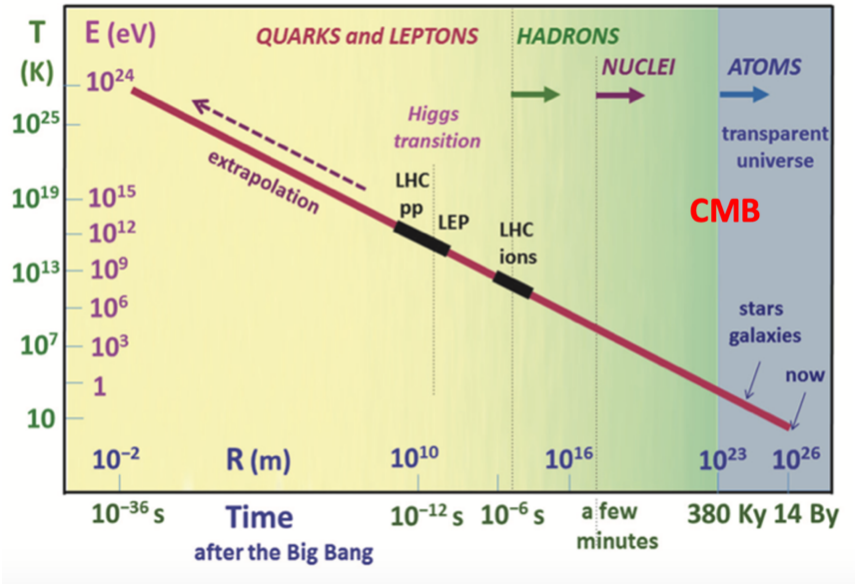


Fig. 2-3: History of the Universe: temperature T or mean energy per photon (E = kT) as a function of age (time after the Big Bang), in logarithmic coordinates. Also shown is what would have been the radius R of the Universe observable now. Figure by F. Pauss.

---

[14] J. S. Bell, On the problem of hidden variables in quantum mechanics, *Rev. Mod. Phys.38, 447 (1966)*
Photo taken at the 1985 Paris conference honouring the memory of Alfred Kastler.

[15] V. A. Petrov, The idea of quarks: towards restoring of historical justice. https://arxiv.org/abs/2001.04843 , he will tell you if Petermann must also be quoted.
See also A. de Rujula, Archeology and evolution of QCD. https://arxiv.org/abs/1610.07466
C. Llewellyn Smith, From concrete quarks to QCD: a personal perspective. *EPJ H 48, 13 (2023),* https://link.springer.com/article/10.1140/epjh/s13129-023-00061-4

[16] For an elementary introduction: https://inspirehep.net/files/02de568d4897c555515de27f0b96af4d p. 271
For a tentative historical account: R. E. Allen, The London-Anderson-Englert-Brout-Higgs-Guralnik-Hagen-Kibble-Weinberg mechanism and Higgs boson reveal the unity and future excitement of physics. https://arxiv.org/abs/1306.4061

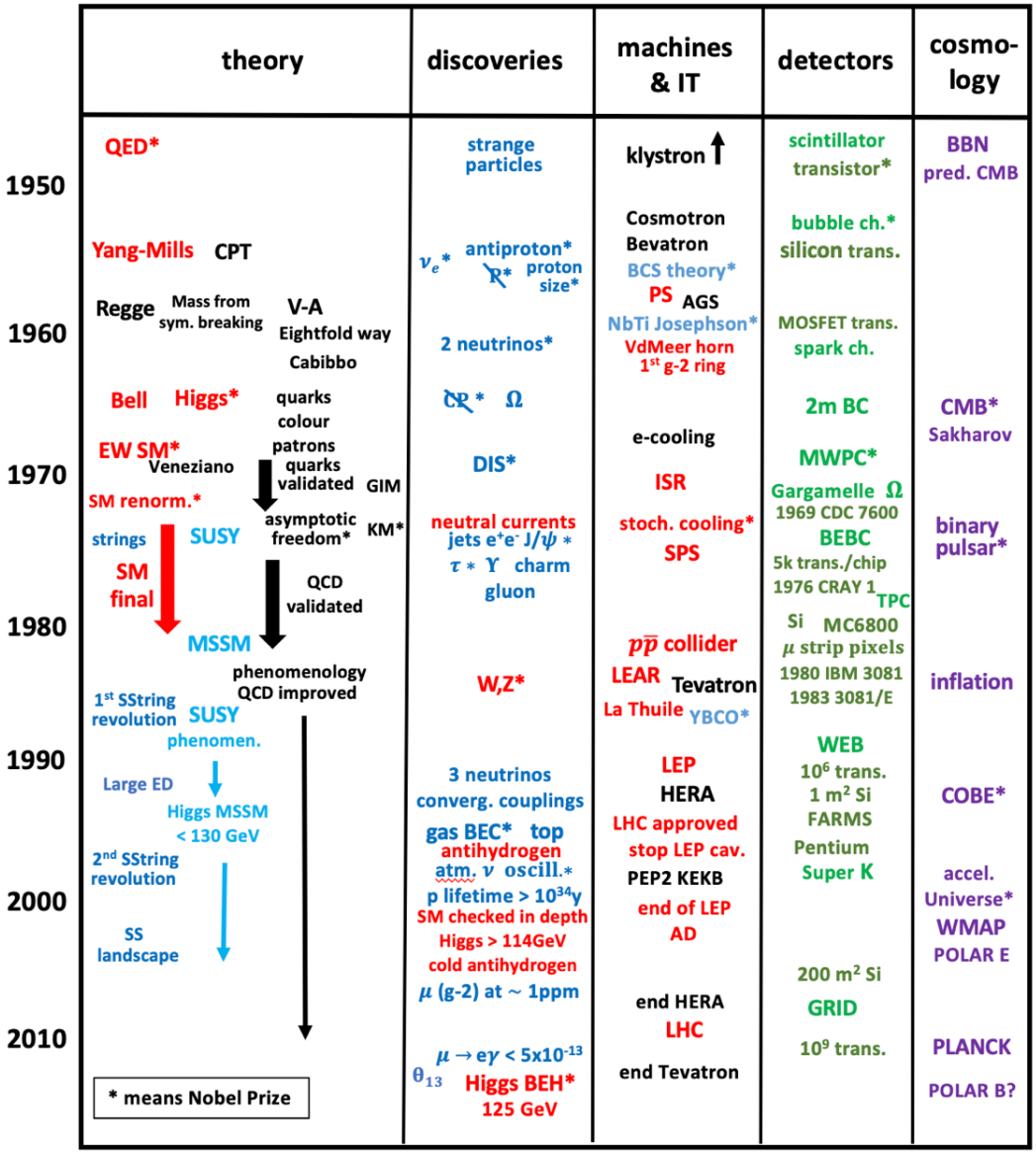


Fig. 2-4: A more detailed presentation of the schematic outline of the adventure of Fig. 2.1. Figure by D. Treille.

3. Establishment of the CERN Organisation

CERN is one of Europe's finest scientific achievements [17], an "institutional feat" and, to date, a political success, proving that States – 12 founding member states, 25 today [18] and 10 associate members, not counting the non-member states who participate in CERNs programs – can agree on ambitious projects.

Its official existence dates back to 29 September 1954, with the entry into force of the convention ratified by the founding states, the culmination of a long process begun after the Second World War, in a context marked by the hegemony of the research in the US and in Europe through a strong desire for reconciliation.

It is around "subatomic" physics (and not nuclear energy, a reserved domain) that the hope of scientific cooperation is born, with passionate defenders such as Eduardo Amaldi, Lew Kowarski, Pierre Auger and Francis Perrin, the reinforcement of prestigious scientific figures, such as Louis de Broglie and Isidor Rabi, and the help of UNESCO. The objective was a laboratory with a 6 GeV machine and the canton of Geneva was chosen as the site.

3.1 Mission of CERN

The first machine to be built, the 600 MeV Synchrocyclotron, SC [19], was a milestone for CERN (Fig. 3- 1).



Fig. 3-1: The 600 MeV SC in December 1957, ready for physics.

The absence of the $\pi \rightarrow e\nu$ decay at the expected rate in previous US experiments posed a real theoretical problem. The novelty and power of the SC experiment solved it and led to the discovery of the $\pi \rightarrow e\nu$ decay, **rare and precious**, in agreement with theory.

[17] D. Guthleben, Le Cern, quelle histoire! https://lejournal.cnrs.fr/billets/le-cern-quelle-histoire
C. Sutton and H. Wenninger, in Technology Meets Research.
https://inspirehep.net/files/3f8e83db02057bf400ac8380b82ae0a7

[18] https://en.wikipedia.org/wiki/CERN , All member states are European, except Israel.

[19] B. Allardyce and G. Fidecaro, The 600 MeV Synchrocyclotron: Laying the Foundation.
https://inspirehep.net/files/53479a7bd7931662e81f61632e1e8c8f

In 1958, at the SC, the first CERN "g–2" experiment (1958–1964) started, aiming to measure the anomalous magnetic moment of the muon [20].

Furthermore, the SC originally fed the ISOLDE facility which started delivering radioactive ion beams (RIBs) in 1967. This facility, upgraded several times and moved in 1992 to be connected to the proton synchrotron booster (PSB), is currently the longest-running facility in operation at CERN at the forefront of science with RIBs [21].

Seven decades later, CERN has become a quasi-global laboratory (about 40% of its users are from non-member countries). It still has great prestige and the CERN Model is often given as an example. The prestige of CERN is, of course, linked to the remarkable series of large machines that have been built thanks to collaboration, to the successes of their physics output, and, last but not least to the fact that these series of powerful accelerators were built on the original site. It is likely that if these accelerators had been built elsewhere in the world, people would talk less about the CERN Model now.

Apart from a few avatars, CERN has fulfilled its mission and its European members have played the game, while keeping, e.g. in Germany, a strong program in parallel.

CERN was the model for other joint ventures like ESO. It always contributed to a good understanding of the scientists concerned, keeping in touch with those who were in difficulty in the USSR during the Cold War, bringing together communities that politics could make adversaries, launching the idea of the SESAME project, etc., Ref. [22]. CERN has thus served as a model for international organizations looking to foster collaboration, manage complex resources, drive innovation, and promote transparency and openness across various scientific and technological domains.

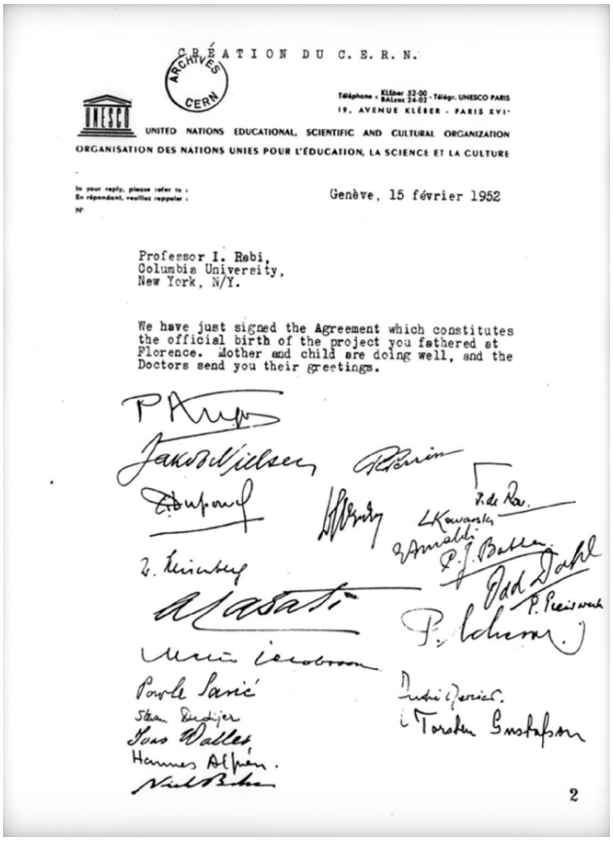
CERN has generally met its objectives, not exceeding the planned budgets by more than twenty percent. It stuck to the practice of a **fair return**, industrial and otherwise, to member countries.

But one can also underline less positive aspects:

- concerning this last point, the impossibility for European industry, due to a lack of competitiveness, to carry out parts of its programs, such as large-scale arrays of silicon detectors;
- as in other domains, an exaggerated recourse to subcontracting, the skills of employees in the early days of CERN in terms of welding, metrology, largely lost afterwards;
- it is also obvious that the two host countries benefit from certain advantages that others may envy. It is also clear that the contribution of the laboratories of around the world involved in CERN programs has been a key of its success and the outside world may have sometimes felt, rightly or not, not recognized enough for its contributions.

A very thorough account of the activities in the CERN theory division up to the mid-nineties can be found in Ref. [23]. For images of the past see Ref. [24]. Figure 3-2 shows the key agreement establishing the CERN Organization.

[20] B. L. Roberts, The history of the muon (g−2) experiments. https://scipost.org/SciPostPhysProc.1.032/pdf . See also Chapter 26.
[21] ISOLDE: https://home.cern/news/series/meet-isolde/meet-isolde-where-did-it-all-begin
and https://en.wikipedia.org/wiki/ISOLDE
[22] However, the 1992 UN embargo against Serbia and Montenegro and the war of Russia against Ukraine had an impact on CERN policy.
[23] J. Iliopoulos, Physics in the CERN theory division. https://cds.cern.ch/record/261679/files/CERN-CH-39.pdf
[24] https://library.cern/archives/history_CERN/historical_images?page=0



CRÉATION DU C. E. R. N.

ARCHIVES CERN

UNITED NATIONS EDUCATIONAL, SCIENTIFIC AND CULTURAL ORGANIZATION
ORGANISATION DES NATIONS UNIES POUR L'ÉDUCATION, LA SCIENCE ET LA CULTURE

19, AVENUE KLÉBER - PARIS XVI

Genève, 15 février 1952

Professor I. Rabi,
Columbia University,
New York, N/Y.

We have just signed the Agreement which constitutes the official birth of the project you fathered at Florence. Mother and child are doing well, and the Doctors send you their greetings.

2

Fig. 3-2: Agreement which constitutes the official birth of CERN on 15 Feb 1952.

3.2 Other large Laboratories world-wide

Here is a list of labs which played and/or play an important role in PP. The US labs, with the first new machines, led the field, until Europe and CERN reached maturity.

- United States
  - SLAC National Accelerator Laboratory, https://en.wikipedia.org/wiki/SLAC_National_Accelerator_Laboratory
  - Brookhaven National Laboratory, https://en.wikipedia.org/wiki/Brookhaven_National_Laboratory
  - Lawrence Berkeley National Laboratory, Berkeley, California, https://en.wikipedia.org/wiki/Lawrence_Berkeley_National_Laboratory
  - Fermi National Accelerator Laboratory, Batavia, Illinois, https://en.wikipedia.org/wiki/Fermilab
- Canada
  - TRIUMF, Vancouver, Canada's Particle Accelerator Center, https://triumf.ca
- Japan
  - The High Energy Accelerator Research Organization, KEK, https://en.wikipedia.org/wiki/KEK
- China
  - IHEP, Beijing, https://english.ihep.cas.cn/ https://en.wikipedia.org/wiki/Institute_of_High_Energy_Physics

- Russia
  - Joint Institute for Nuclear Research (JINR), https://en.wikipedia.org/wiki/Joint_Institute_for_Nuclear_Research
  - Institute for High Energy Physics, IHEP, Protvino, https://en.wikipedia.org/wiki/Institute_for_High_Energy_Physics
  - Budker Institute of Nuclear Physics, Akademgorodoc, https://en.wikipedia.org/wiki/Budker_Institute_of_Nuclear_Physics
- Europe (other than CERN)
  - DESY, Deutsches Elektronen-Synchrotron, Hamburg, Germany, https://desy.de/index_eng.html
  - GSI Helmholtzzentrum für Schwerionenforschung, Darmstadt, Germany, https://www.gsi.de/en/start/news
  - PSI, Paul-Scherrer-Institute, Villigen, Switzerland, https://www.psi.ch/en
  - Laboratori Nazionali di Frascati, Italy, https://w3.lnf.infn.it
  - IJCLab, Orsay, France, https://www.ijclab.in2p3.fr/en/home/
  - RAL, Rutherford Appleton Laboratory, UK, https://www.ukri.org/who-we-are/stfc/facilities/rutherford-appleton-laboratory/

The first two US machines, the Cosmotron (1952–1966) at the Brookhaven National Laboratory (BNL) and the Bevatron at Berkeley, were completed in 1951 and 1954, respectively. Previously, the 184-inch cyclotron at Berkeley produced the first human-made mesons in 1948. The Cosmotron, a proton synchrotron, produced a series of strange particles, such as the K-meson, and demonstrated the principle of associated production. The Bevatron (Billions of eV proton synchrotron) produced the antiproton in 1955 (Emilio Segrè and Owen Chamberlain, Nobel Prize 1959). The Bevatron and subsequent proton synchrotrons were the principal instruments of particle physics and, after the discovery of strong focusing at Brookhaven in 1953, produced increasingly higher energies, as the Brookhaven Alternating Gradient Synchrotron (AGS) in 1960 and the CERN PS in 1959 (see Section 10.1).

Two of the earliest Alvarez linacs with strong focusing magnets were built at CERN and BNL. In 1947, while Luis Alvarez was developing his proton linac concept, William Webster Hansen constructed the first travelling-wave 6 MeV electron accelerator at Stanford University. Later, electron acceleration at Stanford Linear Accelerator Center (SLAC) extended to 2 miles length and an ultimate energy of 50 GeV (construction started in 1962, completed in 1966). Some of the earliest superconducting linacs included the Superconducting Linear Accelerator (for electrons) at Stanford and the Argonne Tandem Linear Accelerator System (for protons and heavy ions) at Argonne National Lab.

SLAC successes will be recalled in Chapter 4. The circular e^+e^- colliders built at some of these laboratories and elsewhere will appear in Chapter 15. DESY and Fermilab will be considered in Sections 10.8 and 10.9, respectively.

3.3 Education: some famous schools of physics

Newcomers to PP had to be trained and the creation of physics schools was mandatory.

The **Aspen Center of Physics (Colorado)** first opened as the Physics Division of the Aspen Center for Humanistic Studies (now the Aspen Institute) in 1962. It became the Aspen Center for Physics, an independent non-profit institution for physics research, in 1968.

The original **CERN Schools of High-Energy Physics** [25] were established in the early 1960s. Starting in 1970, every second school was organized jointly with the Joint Institute for Nuclear Research (JINR), CERN's sister organization in the Soviet Union [26].

The **Rencontres de Moriond** were born in 1966 at the initiative of Jean Tran Thanh Van. Very successful, the Rencontres grew rapidly, adding biology meetings in 1970 and astrophysics in 1981. Becoming an annual event, they triggered other rencontres, like for example Aoste Valley, Blois and Vietnam. Jim Cronin, at "20 years of Moriond", said that the Rencontres had "*a deep effect on the way we communicate in Particle Physics*". Summaries of fifty years of Moriond can be found in Ref. [27].

The **Les Houches School of Physics** was created in 1951 thanks to the French physicist Cécile DeWitt-Morette, with the aim to improve the level of modern physics in post-war Europe and accelerate international exchanges. Thousands of physicists, including many Nobel Prize winners, passed through this place for meetings, scientific exchanges and training in Physics of a very high level. In 1977, a physics centre was created, specialised for shorter conferences, all year round. In 1988, a pre-doctoral school was opened for young researchers starting their PhD theses. "Les Houches School of Physics" is now a joint unit of service which brings together several French institutes. According to Jean Zinn-Justin, the Les Houches School is the **"*mother of all modern schools of physics*"**.

Yves Rocard and Maurice Lévy, inspired by this school, founded in 1961 a summer school in **Cargèse, Corsica**, which they called the *"Les Houches on the beach".*

Subsequently, other scientific summer schools opened up all over Europe, and around the world, following the same model. Some of them supported by the Advanced Study Institutes program of NATO.

[25] N. Ellis, Training young physicists: a 20-year success story.
https://cerncourier.com/a/training-young-physicists-a-20-year-success-story/
[26] https://en.wikipedia.org/wiki/Joint_Institute_for_Nuclear_Research
[27] J. Lefrançois, Personal memories on how particle physics apparatus and experiments evolved in the 50 years since the first Moriond. https://inspirehep.net/files/72f9855444a790bf6180d629dfa5cd58
D. Treille, 50 years of Moriond: a personal view. https://inspirehep.net/files/d3b2dcd8fee51f79b72d841724b910b9 ,
https://webcast.in2p3.fr/video/50-years-of-moriond

4. The “great reduction”

4.1 Towards the quark model

After decades of calm in our field, the new machines led to the discoveries of an avalanche of new particles (Fig. 4-1), up to a hundred hadronic states in 1970. Order had to be put in place.

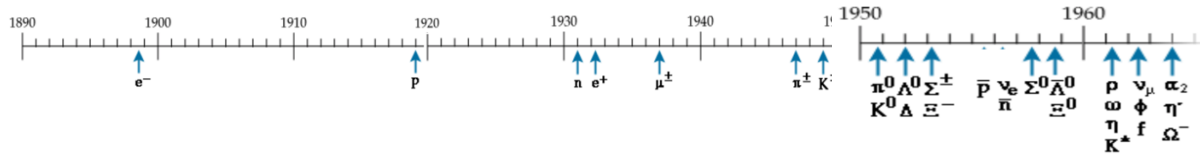


Fig. 4-1: The 1950s avalanche [28].

It was proposed either to distribute them along the Regge trajectories, mass squared as a function of spin (Fig. 4-2), or according to the multiplets of the flavour SU(3) (nothing to do with the current colour SU(3)), strangeness versus the third component of isospin, such as the 3/2+ baryon decuplet shown in Fig. 4-3.

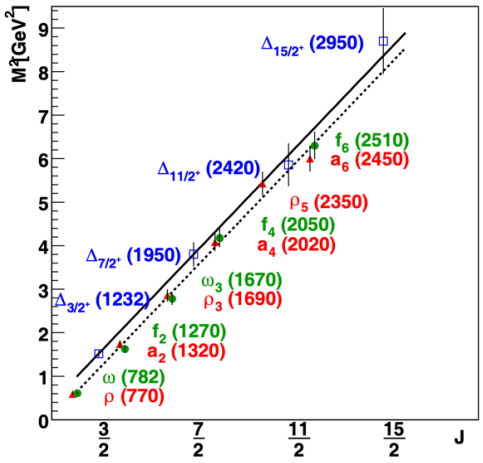


Fig. 4-2: The leading Regge trajectories [29].

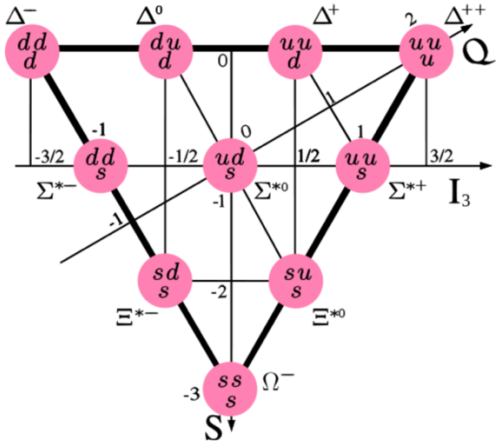


Fig. 4-3: The baryon decuplet [30].

Regge's theory was built on the angular momentum analyticity of scattering amplitudes and located the particles on the eponymous trajectories. Next the Dolen–Horn–Schmid duality was introduced, saying that the s and t channels [31] are two ways of expressing the same physics encoded in the Veneziano formula. This approach culminated with the Bootstrap of Geoffrey Chew, postulating a total democracy between the particles: none is fundamental, the axioms of the S matrix are the only basic principles.

---

[28] Quantum Theory timeline, https://ccwww.kek.jp/pdg/particleadventure/other/history/quantumt.html

[29] E. Klempta and B. C. Metsch, Multiplet classification of light-quark baryons. *Eur. Phys. J. A (2012) 48: 127*, https://link.springer.com/article/10.1140/epja/i2012-12127-1

S. Alef *et al.*, K⁺Λ photoproduction at forward angles and low momentum transfer. *Eur. Phys. J. A 57, 80 (2021)*, https://arxiv.org/abs/2006.12350 , Regge theory, https://en.m.wikipedia.org/wiki/Regge_theory

[30] Baryon: https://en.wikipedia.org/wiki/Baryon

[31] In the s channel, two particles create another one; in the t channel they exchange another one.

In 1960 the "eightfold way" [32] of Murray Gell-Mann and Yuval Ne'eman appeared, situating the hadronic states at the nodes of the diagrams corresponding to the representations of the SU(3) group of flavour, for example the decuplet of Fig. 4-3. In 1962, the *sss*-state (Ω^-) still missing at the tip of the decuplet was predicted to have a mass around 1685 MeV and the Ω^- hyperon was discovered in 1964 at Brookhaven.

Finally, in 1964 Murray Gell-Mann and George Zweig [33] found it easier to focus on the smallest representation of SU(3) and proposed a triplet of quarks (or "aces") with fractional charge: u, d and s (Fig. 4-4). You have to read these authors to guess how they felt about their physical reality. With the introduction of the colour quantum number in 1964 came the now usual representation for hadrons. The famous reduction à la Mendeleev could then occur, very welcome given the growing crowd of hadrons.

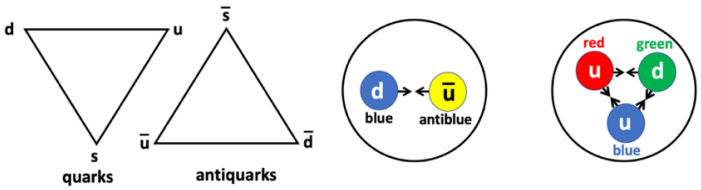


Fig. 4-4: The quark model.

At the Ecole des Houches in 1965, led by Maurice Jacob, between the message of Marcel Froissart, Roland Omnès and Geoffrey Chew speaking of S matrix and bootstrap, thus of *"democracy"* between particles, and of Richard Dalitz dealing with *"Quark models for elementary particles",* conceptually a priori the opposite, a beginner could feel a bit schizophrenic. For a more scholarly chronicle of this "confrontation", see Ref. [34].

However, after the evidence of the finite size of the proton (Fig. 4-5), the Deep Inelastic Scattering (DIS) of e^- (Jerome Friedmann, Henry Kendall and Richard Taylor, Nobel Prize in 1990) revealed the substructure of the proton, the existence of "partons" of spin ½, charged and pointlike [35] (Fig. 4-6). With the parton model [36] (Richard Feynman) and its scale invariance [37] (James Bjorken), the idea of quarks as fundamental objects began to take hold.

With the victory of the quarks [38], the minds not being ripe to accept confinement, came the interlude of free quarks searches. Murray Gell-Mann complains: *"A friend of mine ... rings me up, sometimes at midnight, to report his progress in a search for quarks in sea water, … grinding up oysters and looking for quarks in them."*

---

[32] M. Gell-Mann, The Eightfold Way: a Theory of String Interaction Symmetry. https://www.osti.gov/servlets/purl/4008239/
https://en.wikipedia.org/wiki/Eightfold_way_(physics)

[33] G. Zweig, Memories of Murray and the Quark Model. https://arxiv.org/abs/1007.0494

[34] D. Gross, The Discovery of Asymptotic Freedom and the Emergence of QCD. Nobel lecture 2004,
https://www.nobelprize.org/uploads/2018/06/gross-lecture.pdf
H. Pietschmann, On the Early History of Current Algebra. https://arxiv.org/abs/1101.2748.pdf

[35] M. Riordan, The Discovery of Quarks. Slac-Pub-5724,
https://www.slac.stanford.edu/pubs/slacpubs/5500/slac-pub-5724.pdf

[36] J. Friedman, Deep Inelastic Scattering: Comparisons with the Quark Model. Nobel Lecture 1990,
https://www.nobelprize.org/uploads/2018/06/friedman-lecture.pdf , https://cds.cern.ch/record/422985

[37] In the naive model of partons, structure functions depend only on the fraction x of proton impulsion taken by the quark and not on the "scale" Q^2.

[38] One must however read what the fathers of quarks actually thought: *"So we must face the likelihood, Gell-Mann concluded, that quarks are not real. They might appear in mathematical equations-but not in particle detectors."*
M. Riordan, The Hunting of the Quark. https://orcascurrents.com/the-hunting-of-the-quark/
C. Llewellyn Smith, From concrete quarks to QCD: a personal perspective. *EPJ H 48, 13 (2023),*
https://link.springer.com/article/10.1140/epjh/s13129-023-00061-4

In 1973, the ISR (Chapter 11) observed the scattering of hadrons at large angles, showing that the partons, pointlike for electromagnetism, are **also pointlike for the strong interaction**.

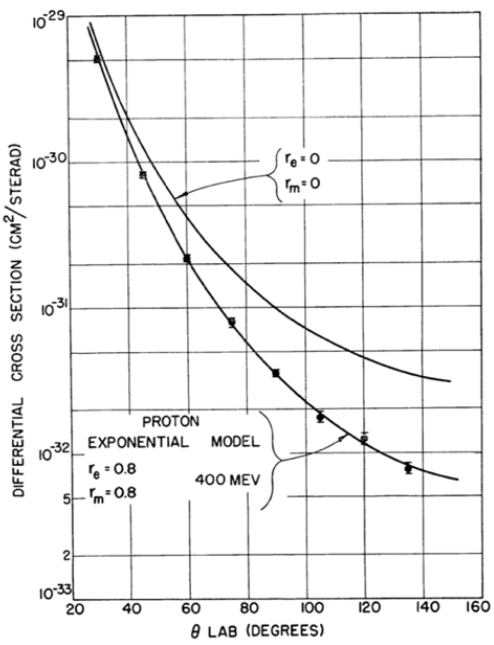


Fig. 4 -5: The proton finite size [39].

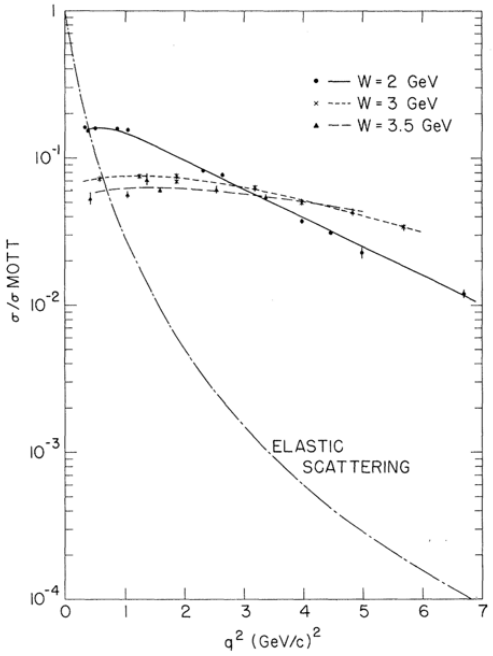


Fig. 4-6: Pointlike scatterers inside the proton [40].

The **Constituent Interchange Model** (CIM) [41] was then proposed, introducing partons into the game without having to solve the problem of confinement and parametrizing the hard scattering of hadrons according to **the number of fundamental constituents** involved in the process (Fig. 4-7). The CIM reproduced well the elastic scattering of hadrons at wide-angle and helped the idea of quarks to penetrate in minds.

Presently a new avalanche is in progress. In addition to the qqq triplet of baryons and the quark-antiquark pair of mesons, and as anticipated by MGM who envisaged more complex combinations, many **tetraquark and pentaquark** candidates have appeared at B Factories and at the LHC (Fig. 4-8). It started with the $X(3872) \rightarrow J/\Psi\pi\pi$. Heavy quarks play an important role here. Is it tight coupling of multiquarks or loose molecules? We will come back to this in more detail in Chapter 28.

[39] E. Chambers and R. Hofstadter, The Structure of the Proton. https://cds.cern.ch/record/1241692/files/p295.pdf https://www.nobelprize.org/prizes/physics/1961/hofstadter/lecture/

[40] M. Breidenbach, *et al.,* Observed Behavior of Highly Inelastic Electron-Proton Scattering. *Phys. Rev. Lett.23, 935 (1969),* https://journals.aps.org/prl/pdf/10.1103/PhysRevLett.23.935

J. Friedman, Nobel Lecture, 1990, https://www.nobelprize.org/uploads/2018/06/friedman-lecture.pdf

[41] S. Brodsky and R. Blankenbecler, Large Transverse Momentum Processes and the Constituent Interchange Model. https://inspirehep.net/files/5784835c43b45ffb0ae39c2f68c5c7cb

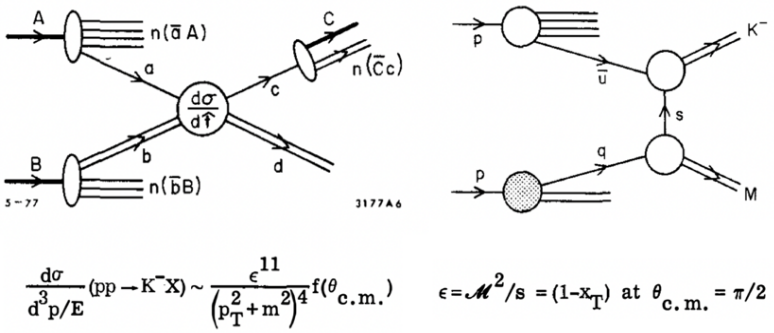


Fig. 4-7: Sketch of the CIM model [42].

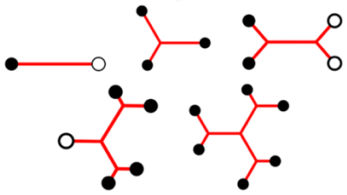


Fig. 4-8: Multiquark systems [43].

4.2 Intermède : a bit deeper in complexity

A very simplified historical account of the field may not pay justice to the elaboration of ideas paving the road between the Yang–Mills idea and the Standard Model. Figure 4-9 recalls the sequence of achievements [44].

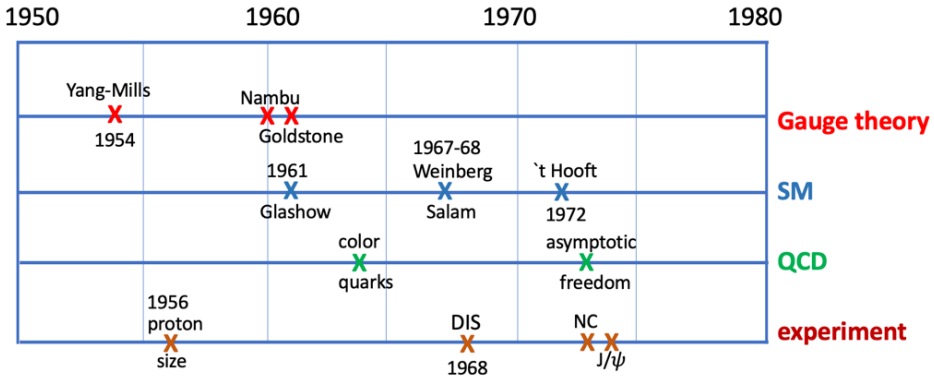


Fig. 4-9: Time table of major advances in gauge theory, the SM (EW and QCD) and experiments.

An excellent reference is the book *Particle Physics and Cosmology* [45]. Very complete but more difficult is, for instance, Ref. [46]. It is important to realize that most key ideas have been developed also or even appeared first in neighbouring fields of physics, as condensed matter physics and superconductivity.

Let us simply recall a couple of ideas which became essential to our physics.

---

[42] ibid

[43] N. Brambilla *et al.*, Substructure of Multiquark Hadrons (White Paper), Snowmass 2021, https://arxiv.org/abs/2203.16583 with references to "Pioneering papers on multiquark hadrons" by R. L. Jaffe, p. 3

[44] C. N. Yang and R. Mills, Conservation of Isotopic Spin and Isotopic Gauge Invariance. *Physical Review 96(1): 191–195 (1954),* https://journals.aps.org/pr/abstract/10.1103/PhysRev.96.191

Y. Nambu, Quasiparticles and Gauge Invariance in the Theory of Superconductivity. *Physical Review 117(3): 648–663 (1960),* https://journals.aps.org/pr/abstract/10.1103/PhysRev.117.648

J. Goldstone, Field Theories with "Superconductor" Solutions. *Nuovo Cimento. 19 (1): 154–164 (1961),* https://link.springer.com/article/10.1007/BF02812722 , https://cds.cern.ch/record/343400/files/CM-P00057225.pdf

[45] P. D. Collins, A. D. Martin and E. J. Squires, Particle Physics and Cosmology. Copyright © 1989 by John Wiley & Sons, Inc. ISBN: 0-471-60088-1 https://onlinelibrary.wiley.com/doi/book/10.1002/3527602828

[46] D. Tong, Lectures on Gauge Theory. http://www.damtp.cam.ac.uk/user/tong/gaugetheory.html

Concerning strong interaction and QCD, before quoting the restauration of **chiral symmetry** (Chapter 20), it would be appropriate to recall **what is this symmetry and why it is broken.**

Following wiki [47]: **Massless fermions** have spin either aligned (right-handed (RH) chirality) or counter-aligned (left-handed (LH) chirality) with their momenta. Chirality is then a conserved quantum number of the given fermion, of whom left and right-handed spinors can be **independently phase transformed**. They can form multiplets under some symmetry group G_L x G_R. Thus, one naturally expects hadron physics to manifest **chiral symmetry (CS)**.

A Dirac mass term explicitly breaks the chiral symmetry. In the absence of mass and quantum loops, **QED** would have a $U(1)_L$ x $U(1)_R$ CS, but the electron Dirac mass breaks it to a single U(1) symmetry that allows a common phase rotation of left and right together. The local version of this symmetry is the **gauge symmetry of QED**. At the quantum loop level, the CS is broken, even for a massless electron, by the **chiral anomaly**, but the U(1) gauge symmetry is preserved (Chapter 7).

In **QCD**, the lightest quarks are nearly massless, and an **approximate chiral symmetry** is present. In this case the LH and RH quarks are interchangeable in bound states of mesons and baryons, so an exact CS of the quarks would imply that every state should appear in a pair of equal mass particles, called **"parity partners".** In the notation, $(\text{spin})^{\text{parity}}$, for instance a pseudoscalar 0^- meson would therefore have the same mass as its parity partner, a scalar 0^+ meson.

But it is **not at all what the observed hadron spectrum shows**. The 0^- pion is much lighter than any other particles. The same happens for the 1^- vector mesons, such as the ρ meson, the scalar mesons 0^+ and pseudovector mesons 1^+ are heavier short-lived resonances, far (in mass) from their parity partners. Therefore, something must **break this symmetry**.

This breaking of chiral symmetry in the strong interaction results from a special case of what is called **Spontaneous Symmetry Breaking (SSB)**. In SSB, although the equations of motion of the theory are invariant under some symmetry group, the ground state of the theory, and hence the observed physics, is not. The symmetry is then said to be realized in the **"Nambu–Goldstone"** mode.

In QCD, if we assume the 3 light quarks as massless and ignore electromagnetic and weak interactions, the theory has an exact global $SU(3)_L \times SU(3)_R$ **chiral flavour symmetry**. Under SSB, the CS is spontaneously broken to the "diagonal SU(3) flavour subgroup", generating low mass **Nambu–Goldstone bosons**, which are identified with the **pseudoscalar mesons** and form an octet representation of the diagonal SU(3) flavour group.

The breaking of CS is **dynamical**, i.e. arises through scalar particles that are **composite states** made of the fundamental quarks. Thus, the QCD Lagrangian must produce ($q\bar{q}$) **scalar condensates** which acquire nonzero vacuum expectation values. A static **vacuum condensate** can form, composed of bilinear operators involving the quantum fields of the quarks in the QCD vacuum, known as a fermion condensate. This takes the form driven by quantum loop effects of quarks and gluons, $< \bar{q}_R^a \, q_L^b > = v \, \delta^{ab}$ with $v \approx -(230 \text{ MeV})^3$. The π decay constant $f_\pi \approx 93$ MeV may be viewed as measuring the strength of the CS breaking.

The quark condensate is induced by **non-perturbative strong interactions** and spontaneously breaks the $SU(3)_L$ x $SU(3)_R$ down to the diagonal vector subgroup $SU(3)_V$ (containing as a SU(2) flavour subgroup the original symmetry of nuclear physics called **isospin**, which acts upon the up and down quarks). The unbroken SU(3) flavour group constitutes the original "Eightfold Way", presented above, as a successful classification scheme of the elementary particles, including strangeness.

[47] Chiral symmetry breaking. https://en.wikipedia.org/wiki/Chiral_symmetry_breaking

For the light quarks, the chiral symmetry breaking condensate can be viewed as inducing the so-called **constituent quark masses (CQM).** Hence, the up quark, with *explicit* mass $m_u \approx 2.3$ MeV, and down quark, with *explicit* mass $m_d \approx 4.8$ MeV, now acquire CQMs of about $m_{u,d} \approx 300$ MeV. QCD then leads to the **baryon bound states** whose masses are approximately given by the sums of their CQMs.

One aspect of SSB, in general, is the existence of these Nambu–Goldstone bosons. In QCD these appear as approximately massless particles. Corresponding to the eight broken generators of the original $SU(3)_L \times SU(3)_R$, they include eight mesons (pions, kaons, eta). These states have small masses due to the explicit masses of the underlying quarks and are called **"pseudo-Nambu–Goldstone bosons"** or **"pNGB's".** pNGB's are a general phenomenon and arise in any Quantum Field Theory (QFT) with **both spontaneous and explicit symmetry breaking, simultaneously.**

The fact that the pions are bound states of fundamental fermions and yet can also be viewed as **Goldstone bosons** was first suggested by Yoichiro Nambu in the early 1960s, ten years before the formulation of QCD and several years before Murray Gell-Mann and George Zweig introduced the idea of quarks.

Chiral symmetry breaking is also apparent in the **mass generation of nucleons** since no degenerate parity partners of the nucleon appear. Chiral symmetry breaking and the **quantum conformal anomaly** account for approximately 99% of the mass of a proton or neutron, as we just saw, and these effects account for most of the mass of visible matter. The light quark *explicit* masses only contribute about 1% of the proton mass.

It was also understood how a symmetry at the classical level may be **broken through quantum corrections**, which is referred to as **"anomalies"** (Chapter 7). For instance, the CP $U(1)_A$ symmetry is **anomalous**, broken in QCD by gluon effects known as **instantons** that we present in Section 7.4 and will also encounter in other chapters.

Such anomalies can spoil the renormalizability of the theory, so that it may be essential for them to cancel out, which places important restrictions on the theory. On the other hand, the presence of other types of anomalies is essential to obtain agreement with experiment. Examples include the decay of the neutral pion (Chapter 27) and the non-conservation of the U(1) axial current. The latter is linked to the existence of gauge fields with **nontrivial topologies** that may play an important role in the quantized theory because of **quantum tunnelling** (Chapter 24 and Section 32.4) and that might be relevant for **baryogenesis**.

5. What is the proton ?

5.1 Probes and structure functions

Knowing what protons are is of primary importance because the visible Universe is made of protons and because they are the projectiles of the LHC. Most laboratories, notably CERN (SPS) and Fermilab, then DESY, have invested heavily in exploring the proton structure, using all possible probes.

Muon scattering, an **electromagnetic** (EM) **probe** (Fig. 5-1), has been studied at CERN by EMC and NA4, exploiting the excellent μ beam at the CERN SPS (Chapter 10), still in use, and at Fermilab by the E203 and E665 experiments.

At CERN, neutrino scattering, the **weak probe** (Fig. 5-2), has been achieved with the remarkable ν-beams from the PS and SPS [48]. Using the van der Meer horn to focus the parent hadrons, they fed the large bubble chambers (BCs), BEBC and GARGAMELLE, as well as the large electronic detectors, CDHS (1976–1984), CHARM, then NOMAD and CHORUS. Pictures of the Van der Meer horn, of BEBC and of CDHS are shown in Fig. 5-3. Similar programs have taken place in the USA.

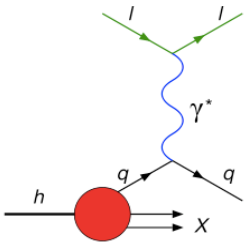


Fig. 5-1: The electromagnetic probe.

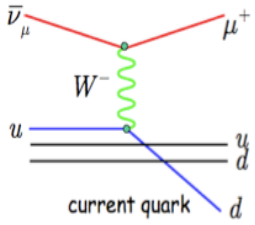


Fig. 5-2: The weak probe.

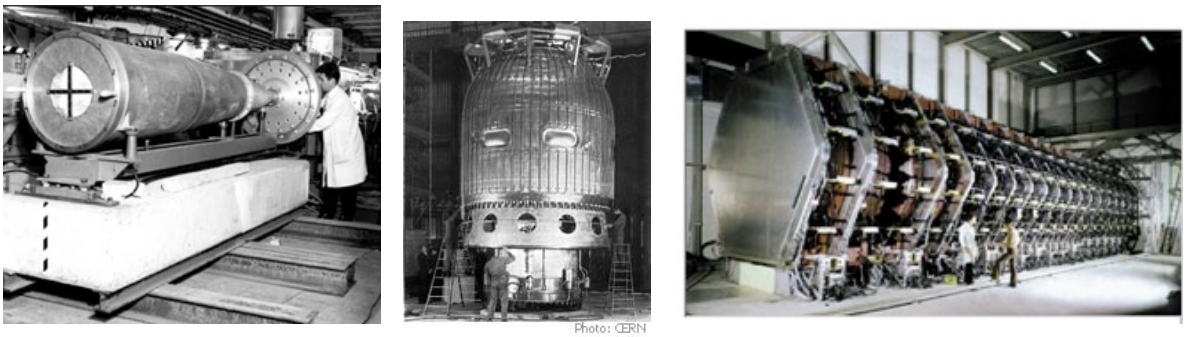


Fig. 5-3: Van der Meer Horn (left), BEBC (middle) and CDHS (right).

Hadron scattering, selecting in the final state a pair of leptons (Fig. 5-4) or a "prompt" photon (Fig. 5- 5), resulting from the hard collision of partons, was an active fixed-target CERN program, also measuring the structure functions (SF) of identified incident particles, as done in WA11, NA3, WA70, etc.

[48] These are ν_μ beams, with a tiny fraction of ν_e. Enriched ν_e beams were considered but not used, e.g. D. Treille, R. Turlay and K. Winter, A possible ν_e beam. CERN/ECFA/72-4 (1972), vo.1, p. 167. https://cds.cern.ch/record/102521
See also B. Jongejans *et al.,* Proposal for the Study of the ν_e and anti-ν_e interactions in BEBC with an enriched ν_e K^0_L beam. CERN/SPSC/80-77, https://cds.cern.ch/record/601295/files/cm-p00045379.pdf

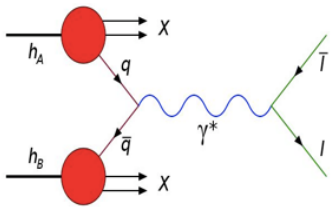


Fig. 5-4: Hard hadron scattering.

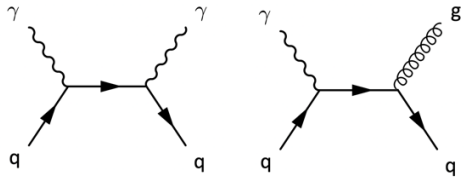


Fig. 5-5: Hard photoproduction: Compton QED (left), Compton QCD (right).

From the very beginning of these programs, we can highlight the evidence of the **violation of scale invariance,** namely the fact that the structure found depends on the resolving power of the measurement, as QCD predicts. It was first observed by large BCs (Fig. 5-6) [49], then confirmed by electronic detectors, with better statistics, but after a long fight against systematic uncertainties. Wolfgang Panofsky, referee of one of them, correctly predicted that it would take 10 years to master them.

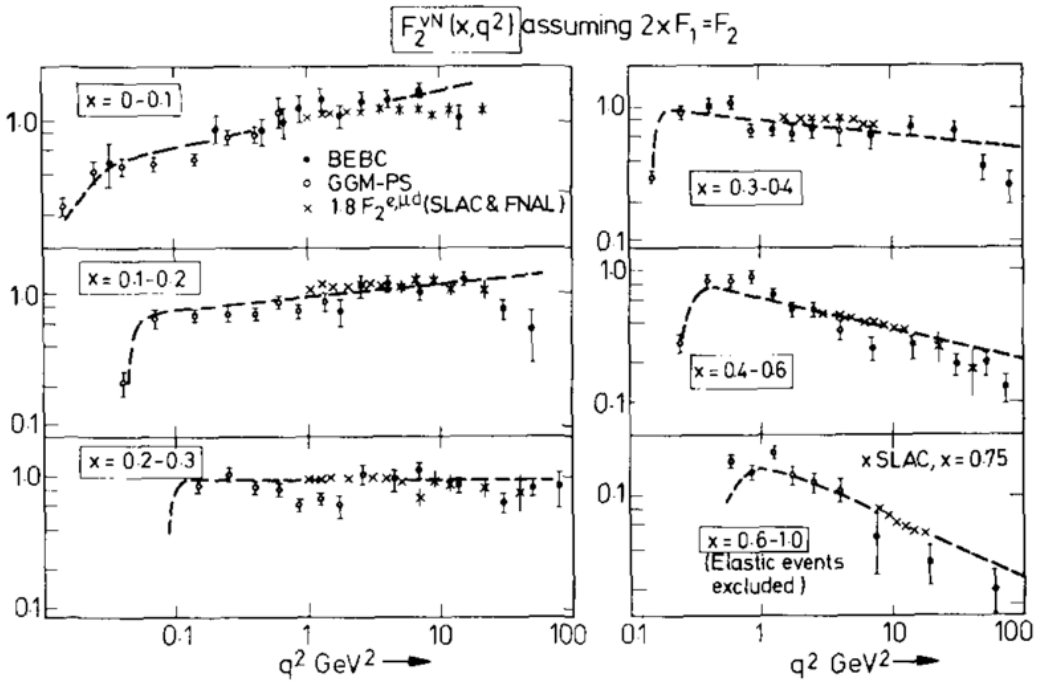


Fig. 5-6: Historical plots: first evidence of scaling violation.

Hard hadron scattering led, in 1979, to the discovery of the "**K-factor**", the discrepancy between the experimental result and the theoretical prediction, at the time at the lowest order. This called for a more elaborate estimation of the process.

[49] J. Blietschau *et al.,* Observation of scaling deviations in the energy distribution of secondary hadrons in inelastic neutrino-proton interactions. *Phys.Lett. B87 (1979) 281*
https://www.sciencedirect.com/science/article/abs/pii/0370269379909833?via%3Dihub
P. C. Bosetti *et al.,* (BEBC), Analysis of nucleon structure functions in CERN bubble chamber neutrino experiments. *Nucl. Phys. B 142, 1 (1978),* https://www.sciencedirect.com/science/article/abs/pii/0550321378903991

μ-scattering revealed the **EMC effect** [50] in 1983, showing that the structure of the nucleon depends on the nucleus in which it is immersed, and the **spin crisis** in 1987, indicating that valence quarks carry only a fraction of the spin of the nucleon.

Then HERA (e-p) took over this monumental task, leading to the structure functions currently used [51]. See Figs. 5-7 to 5-9.

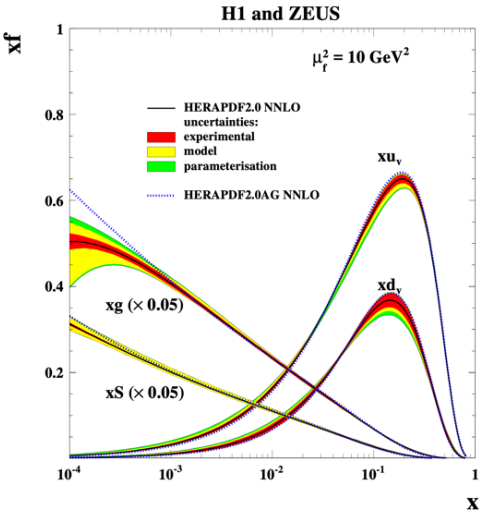


Fig. 5-7: The parton distribution functions from HERA.

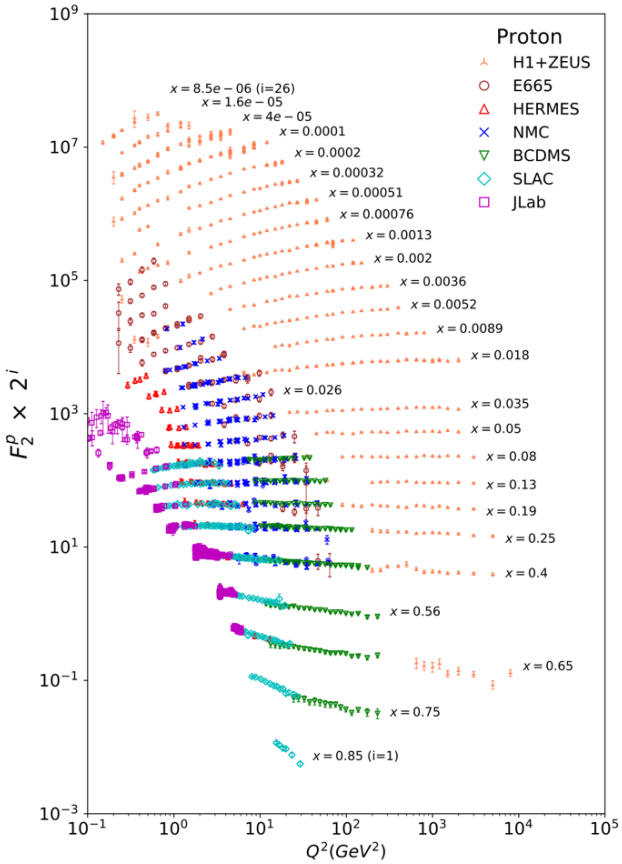


Fig. 5-8: Patterns of scaling violation [52].

Studies indicate that further improvements of our knowledge of SFs can be achieved at the LHC [53] (Fig. 5-10). Progress is needed: differences between PDF sets are still present both in central values and in uncertainties of Higgs cross sections [54].

[50] D. Higinbotham *et al.,* 30th Anniversary of the EMC Effect: Thirty years on CERN's EMC effect still puzzles experimentalists and theorists. https://arxiv.org/abs/1305.7143

[51] V. Chekelian, Proton structure and parton distribution functions from HERA. *EPJ Web of Conferences 126, 02005* (2016) https://inspirehep.net/files/77b7c2c650aac7f21f44eff6cf6e2b29

[52] Particle Data Group, E. C. Aschenauer *et al.,* Structure Functions. https://pdg.lbl.gov/2020/reviews/rpp2020-rev-structure-functions.pdf

[53] R. A. Khalek *et al.,* Towards Ultimate Parton Distributions at the High-Luminosity LHC, https://arxiv.org/abs/1810.03639.pdf
F. Giuli, High-x quark density and their impact on Z'-boson dilepton searches. EPS-HEP 2023, https://pos.sissa.it/449/444/pdf
ATLAS Collaboration, Determination of the parton distribution functions of the proton using diverse ATLAS data from pp collisions at $\sqrt{s}$ = 7, 8 and 13 TeV. https://arxiv.org/abs/2112.11266

[54] J. Rojo, PDFs for Higgs boson production at the LHC. Higgs Hunting, Paris, 2025. https://indico.ijclab.in2p3.fr/event/11484/contributions/37590/attachments/25998/38406/rojo-HiggsHunting-PDFs.pdf

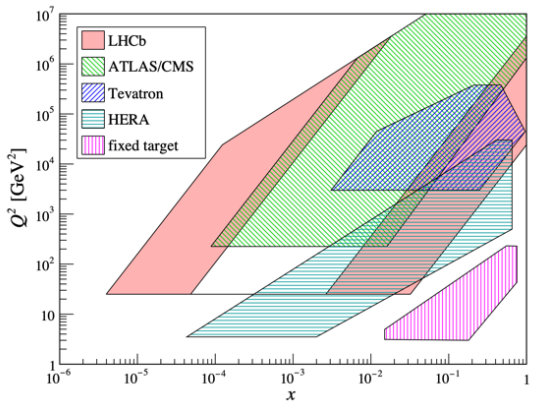


Fig. 5-9: Q^2 – x diagram: regions covered by different experiments [55].

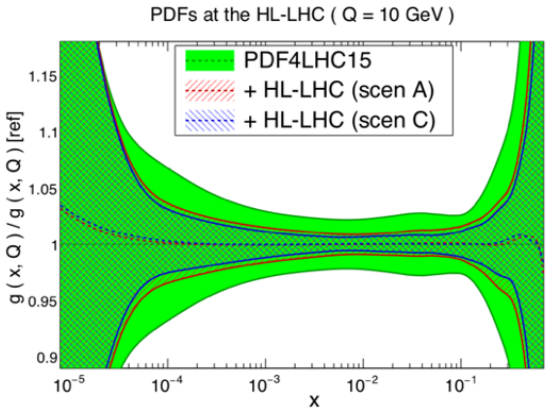


Fig. 5-10: Potential improvements on g(x) expected at the HL-LHC.

5.2 The path to Quantum Chromodynamics

Figure 5-11 summarizes the basic properties of **Quantum ChromoDynamics (QCD)**: **confinement** (trend of the curve at left) and **asymptotic freedom** (right side). Let us briefly recall the path towards its validation [56] .

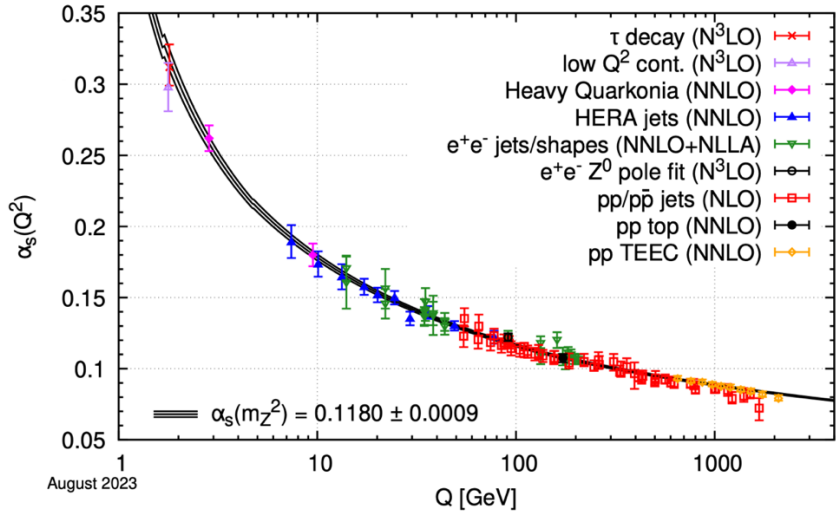


Fig. 5-11: The key facts of QCD: Summary of determinations of α_s as a function of the energy scale Q compared to the predicted running of the coupling α_s [57].

[55] T. Boettcher *et al.,* A direct probe of the intrinsic charm content of the proton. *Phys. Rev. D 93, 074008 (2016),* https://arxiv.org/abs/1512.06666

[56] F. Wilczek, QCD Made Simple. *Physics Today, 53-N8 22-28, (2000),* https://frankwilczek.com/Wilczek_Easy_Pieces/298_QCD_Made_Simple.pdf
H. Fritzsch, The History of QCD. CERN Courier vol 52-issue8-p021, https://cds.cern.ch/record/1734855/files/vol52-issue8-p021-e.pdf
For a brief and very elementary introduction: In Technology Meets Research: https://inspirehep.net/files/02de568d4897c555515de27f0b96af4d p. 98

[57] J. Huston *et al.,* Quantum Chromodynamics. https://arxiv.org/abs/2312.14015.pdf

The invention of the **colour quantum number**, attributed among others to Oscar Greenberg in 1964, was initially motivated by some spin/statistical mysteries. The quark model then accounted for the lifetime of the π^0 (Chapter 27) and for the ratio R ($e^+e^- \rightarrow$ hadrons / $e^+e^- \rightarrow \mu^+\mu^-$) [58], as illustrated in Fig. 5-12.

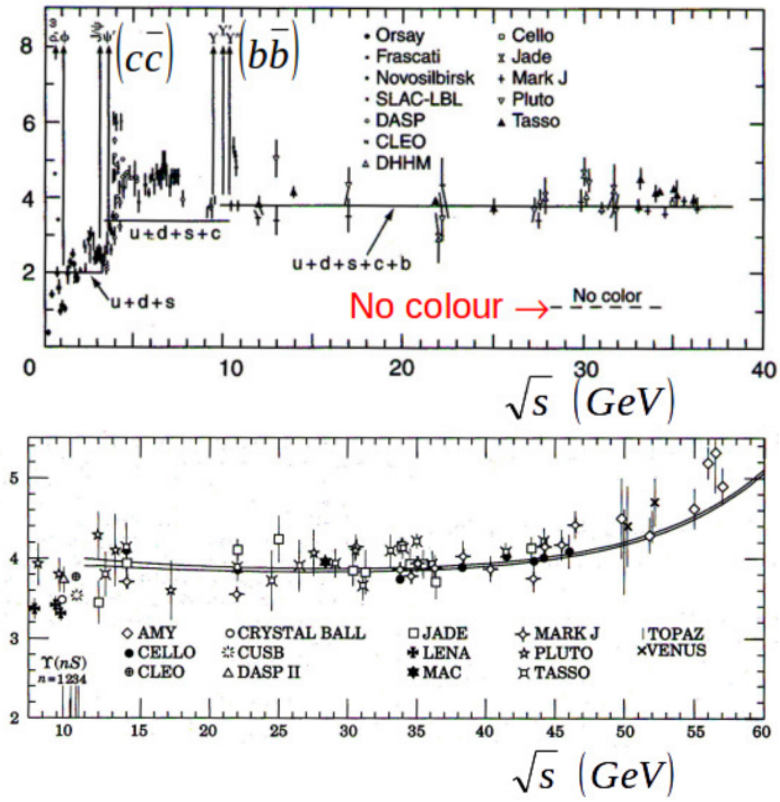


Fig. 5-12: Two views of the R ratio R = $\frac{\sigma(e^+e^- \rightarrow \text{hadrons})}{\sigma(e^+e^- \rightarrow \mu^+\mu^-)}$ shown in the y-axis (from T. Potter [59]).

In 1965 Han–Nambu used colour to propose three sets of quark triplets with integer electric charge. Deciding between the two versions of quarks led to much discussion around 1974. The comparison of the SFs obtained from the EM and weak probes and the direct measurement of the QED Compton effect, elastic scattering of real photons on quarks (NA14 [60], Fig. 5-5), decided in favour of fractional electric charges.

In 1971–1972, Harald Fritzsch and Murray Gell-Mann [61] defined the main lines of the new strong interaction theory and coined the words "gluons" and "QCD". In 1972–1977 came the DGLAP evolution equations [62]. In 1973, David Gross, David Politzer and Frank Wilczek demonstrated **asymptotic freedom** (AF), that is to say the decisive fact that the strong coupling constant actually tends to zero at a very small distance (large Q-value) between quarks (Fig. 5-11).

[58] T. Potter, QCD: Particle and Nuclear Physics.
https://www.hep.phy.cam.ac.uk/~chpotter/particleandnuclearphysics/Lecture_07_QCD.pdf
[59] ibid
[60] G. Wormser, Point-Like Interactions of Photons in High p_T Photoproduction.
https://lib-extopc.kek.jp/preprints/PDF/1990/9007/9007450.pdf
[61] H. Fritzsch, The History of QCD. CERN Courier vol 52-issue8-p021,
https://cds.cern.ch/record/1734855/files/vol52-issue8-p021-e.pdf
[62] D. Diakonov, QCD scattering: from DGLAP to BFKL. https://cerncourier.com/a/qcd-scattering-from-dglap-to-bfkl/,
Dokshitzer–Gribov–Lipatov–Altarelli–Parisi (DGLAP), Balitsky–Fadin–Kuraev–Lipakov (BFKL)

The gluon was required [63]. Experimental evidence of its existence came from PETRA at DESY in 1979. Later, LEP measured the evolution with energy of the strong coupling and, together with DIS, etc., contributed many measurements of the unique QCD parameter at the $m_{quark} = 0$ boundary, $\boldsymbol{\alpha_S(M_Z)}$.

For the current state of $\alpha_S(M_Z)$, obtained from 7 categories of observables, $\alpha_S(M_Z) = 0.1179 \pm 0.0009$, see Ref. [64]. It nevertheless remains the least well known of the coupling constants (Fig. 5-13), as shown by this series:

$$\delta\alpha \sim 10^{-10} \ll \delta G_F \sim 10^{-7} \ll \delta G \sim 10^{-5} \ll \delta\alpha_s \sim 10^{-2}$$

Anticipating on more recent times, Fig. 5-14 shows the progress made on the theoretical side and the good convergence of the α_S determination using different orders of resummation series.

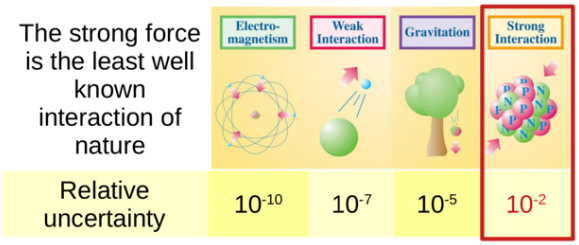


Fig. 5-13: Relative uncertainty of the coupling constants [65].

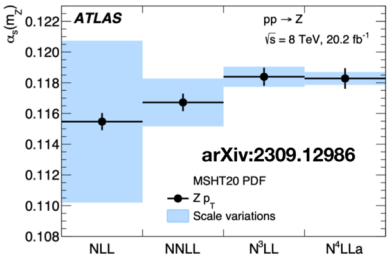


Fig. 5-14: Improvements on $\alpha_S(M_Z)$ [66].

5.3 From QCD foundations to its manifestations in high-energy collisions

A monumental task remained to be accomplished: the tremendous work it took to get from the foundations of QCD to the **details of its manifestations** in high-energy collisions. These two undertakings, absolutely vital for the physics of the LHC, have been completed.

On the last point, Fig. 5-15 explains that the simplest process, the emission of a gluon shown in (a) evolves, once the self-interaction of the gluons is included (b). Their conversion in pairs of quarks and the transition from partons to particles [67] is depicted in (c), illustrating the great complexity. Finally, a hadronic event as recorded by the OPAL experiment is shown in (d).

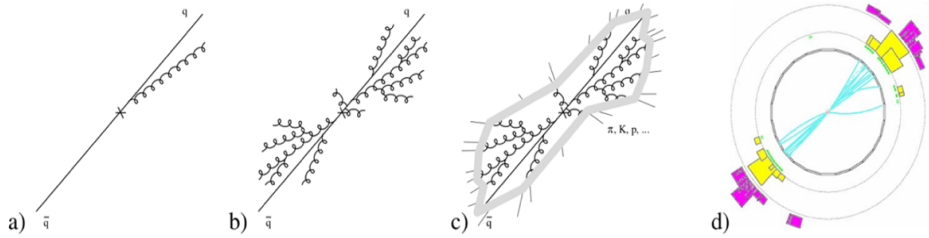


Fig. 5-15: Emission pattern from a $q\bar{q}$ event: from gluon radiation to a full hadronic Z event in OPAL [68].

[63] J. Ellis, M. K. Gaillard and G. G. Ross, Search for Gluons in e^+e^- Annihilation. *Nucl. Phys. B111 (1976) 253*

[64] D. d'Enterria *et al.,* The strong coupling constant: State of the art and the decade ahead. https://arxiv.org/abs/2203.08271 , also presented in Moriond QCD 2023: https://moriond.in2p3.fr/QCD/2023/ThursdayAfternoon/Enterria.pdf

[65] S. Camarda, Measurement of Z-boson cross sections and strong-coupling constant with ATLAS. Moriond EW, 2023, https://indico.in2p3.fr/event/29681/contributions/122547/attachments/76644/111342/07-SCamarda-v2.pdf

[66] ATLAS Collaboration, A precise determination of the strong-coupling constant from the recoil of Z bosons with the ATLAS experiment at $\sqrt{s}$ = 8 TeV. https://arxiv.org/abs/2309.12986

[67] B. R. Webber, Fragmentation and Hadronization.https://cds.cern.ch/record/419784/files/9912292.pdf
These were fitted to data from PETRA and LEP and used in Monte Carlo simulations of the physics processes.

[68] G. P. Salam, Elements of QCD for hadron colliders. https://arxiv.org/abs/1011.5131

This work concerns:

- jetology: how to best define and measure a jet;
- simulation program for particle collisions [69] (Figs. 5-16 and 5-17, plots from T. Sjöstrand);
- fixed-order calculations, from lowest to highest order: LO, NLO, NNLO, NNLL, N3LL, etc.;
- matrix element generator for the simulation of parton-level events [70];
- simulation of the passage of particles through matter using Monte Carlo methods [71];
- Lattice QCD [72].

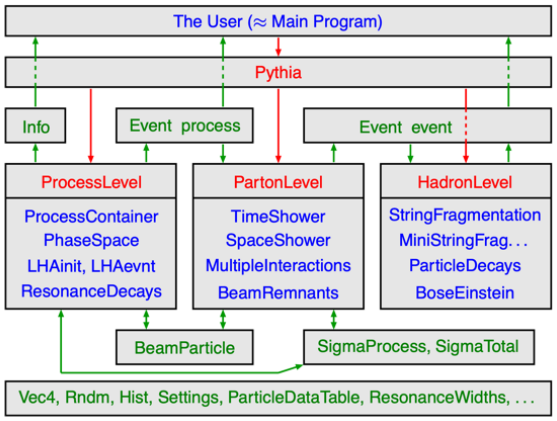


Fig. 5-16: Structure of the Pythia code.

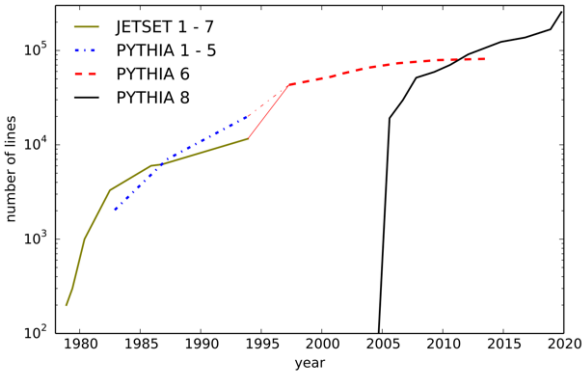


Fig. 5-17: Evolution of the Pythia code size.

Figures 5-18 to 5-21 give more references and details about the higher order computations.

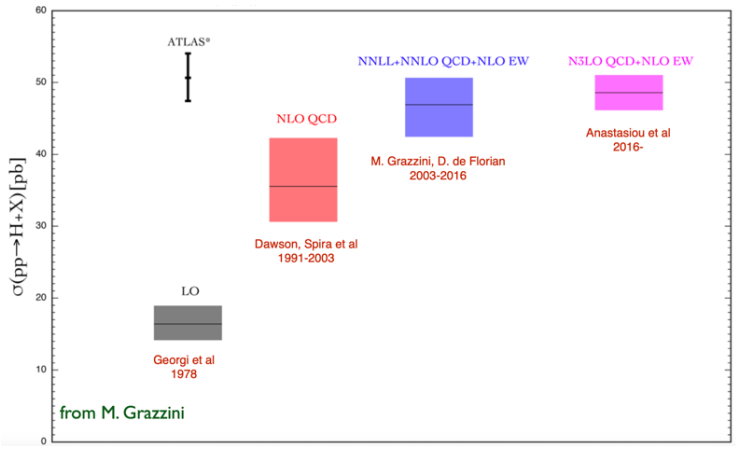


Fig. 5-18: The Higgs boson production cross-section at various orders [73].

[69] T. Sjöstrand, The PYTHIA Event Generator: Past, Present and Future. https://arxiv.org/abs/1907.09874
See also G. Marchesini and B. R. Webber, HERWIG: A new Monte Carlo event generator for simulating Hadron Emission Reactions with Interfering Gluons., https://lib-extopc.kek.jp/preprints/PDF/1988/8804/8804021.pdf
[70] See for instance: J. Alwall *et al.,* MadGraph/MadEvent v4: The new web generation. https://arxiv.org/abs/0706.2334
[71] Geant4 (for GEometry ANd Tracking) is a platform for *"the simulation of the passage of particles through matter"* using Monte Carlo methods. https://en.wikipedia.org/wiki/Geant4
[72] O. Pène, An Introduction to Lattice QCD. https://arxiv.org/abs/hep-ph/9504271.pdf ,
S. Hashimoto *et al.,* Lattice Quantum Chromodynamics. https://pdg.lbl.gov/2019/reviews/rpp2018-rev-lattice-qcd.pdf ,
A. Gérardin, Introduction to Lattice QCD.
https://indico.in2p3.fr/event/17541/contributions/62625/attachments/49566/63068/GIF18_gerardin2.pdf
[73] D. de Florian, Standard Model and Higgs Theory. European Physical Society HEP 2023,
https://indico.desy.de/event/34916/contributions/142209/attachments/84141/111406/EPSdeFlorian.pdf

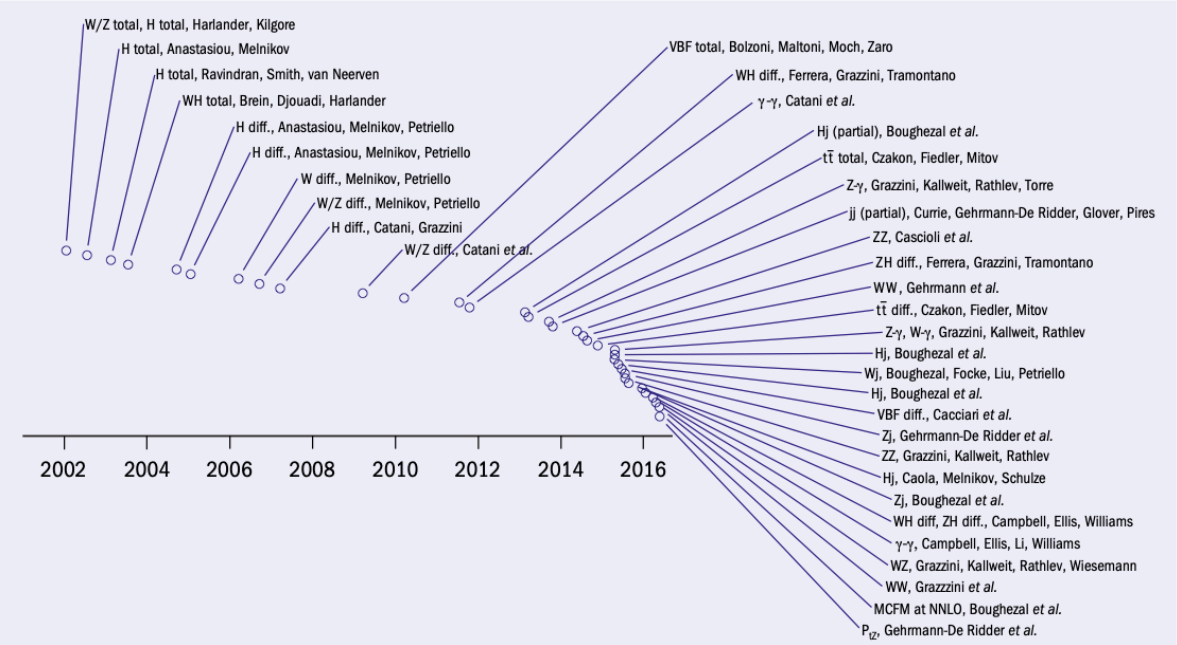


Fig. 5-19: Overview of the higher order revolution. From G. Zanderighi. The completion date and main authors of various NNLO calculations, with vertical separations for display purposes [74].

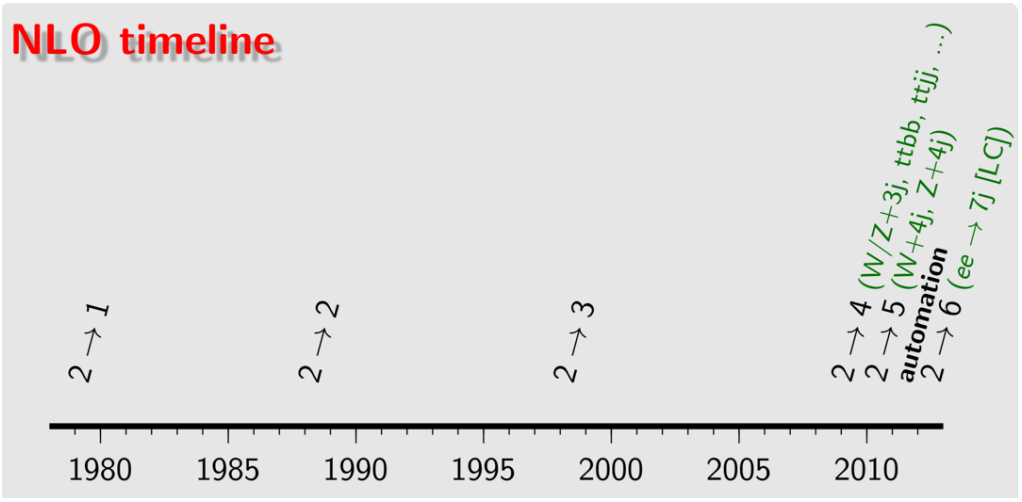


Fig. 5-20: Steps of the N3LO revolution for Drell–Yan like processes [75].

And finally, Figs. 5-22 and 5-23 complete the information about the highest orders.

[74] G. Zanderighi, The two-loop explosion. CERN Courier April 2017, https://cds.cern.ch/record/2256135/files/CERN%20Courier%20Volume%2057%20Issue%203%20April%202017.pdf

[75] G. Salam, QCD in hadron collisions. https://gsalam.web.cern.ch/gsalam/talks/repo/2012-LaThuile-collider-QCD.pdf

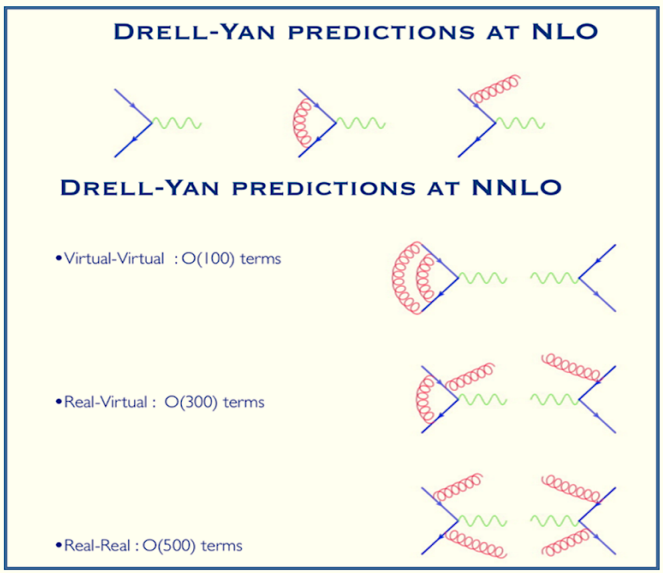


Fig. 5-21: Drell–Yan predictions at NLO and NNLO, giving an idea of the diagrams involved in this case [76].

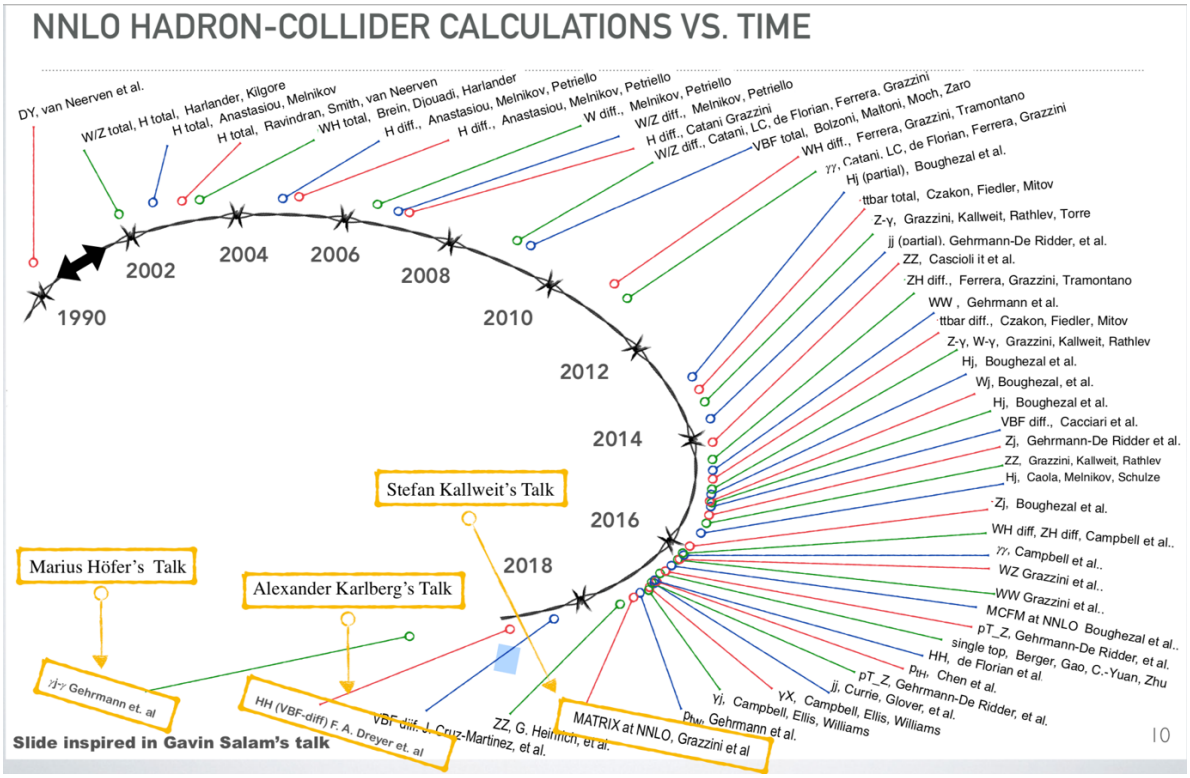


Fig. 5-22: The NNLO Standard: Beauty of figure and quantity of information [77].

[76] F. Maltoni, Basics of QCD for the LHC. https://indico.cern.ch/event/208901/contributions/1501068/attachments/323332/450949/Maltoni_L4.pdf

[77] L. Cieri, Higgs Production Using the Q_T-Subtraction Formalism at N^{3}LO. Rencontres de Moriond QCD & HEI 2019, https://moriond.in2p3.fr/QCD/2019/ThursdayAfternoon/Cieri.pdf

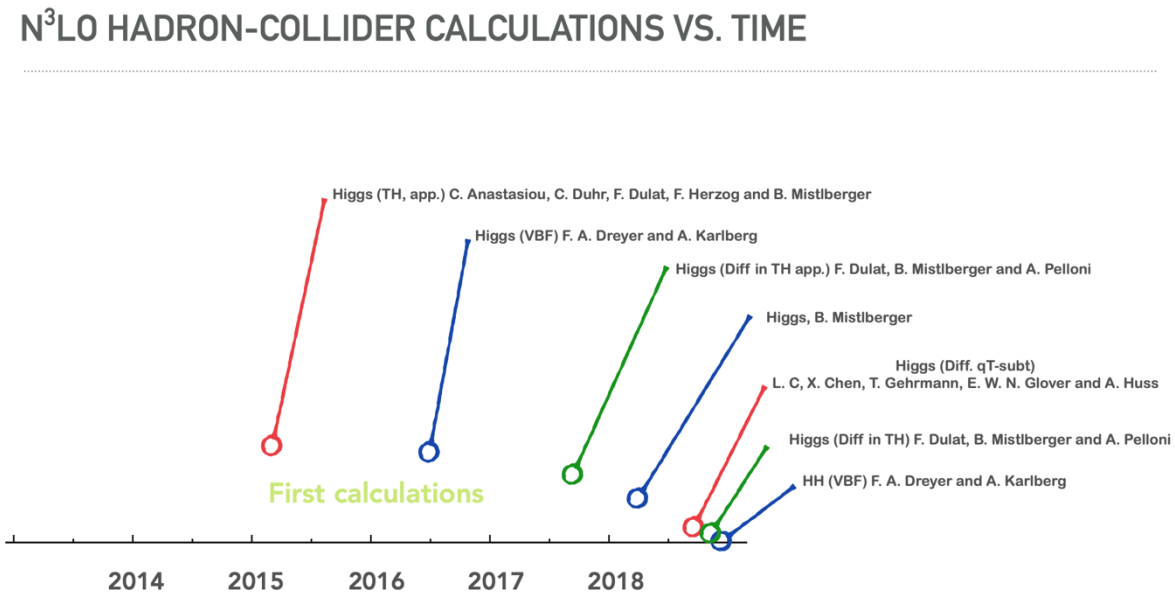


Fig. 5-23: Steps of the N3LO revolution for Drell–Yan like processes [78].

5.4 Back to the proton

The modern image of the nucleon, still a "cartoon", illustrates its complexity. An important fact is that its mass [79] is not due to that of its constituents but, at ~ 99%, to their kinetic energy, their ***dance***.

In other words, from this point of view, proton and antiproton are almost identical. It will be interesting to see what gravity will say when antihydrogen is submitted to it [80]. It is likely that a possible effect will be beyond the sensitivity (% to ‰) of the first generation of such experiments or of muonium.

The physics of heavy ion collisions (Chapter 20) has experienced great developments, which in 2000 allowed CERN to announce the observation of **a new state of matter** [81], **the quark-gluon plasma.**

What is the proton **charge radius**? Figure 5-24 [82] shows seven standard deviations of disagreement between on the one hand the Lamb shift of muonic hydrogen and on the other hand electron scattering on the proton and the Lamb shift of "normal" hydrogen. Doubts exist as to the estimate of

[78] ibid , S. Camarda, L. Cieri and G. Ferrera, Drell–Yan lepton-pair production: q_T resummation at approximate N⁴LL+N⁴LO accuracy. https://arxiv.org/abs/2303.12781
S. Camarda, L. Cieri and G. Ferrera, Drell–Yan lepton-pair production: q_T resummation at N³LL accuracy and fiducial cross sections at N³LO. https://arxiv.org/abs/2103.04974

[79] F. Wilczek, Origins of Mass, https://arxiv.org/abs/1206.7114 ,
https://physics.mit.edu/wp-content/uploads/2021/01/physicsatmit_03_wilczek_originofmass.pdf
MAGE Collaboration, Studying Antimatter Gravity with Muonium. https://arxiv.org/abs/1802.01438

[80] The BASE collaboration measured the electric charge-to-mass ratios of the proton and the antiproton with record precision. The results found these are identical to within an experimental uncertainty of 16 parts per trillion.
https://home.cern/news/news/physics/base-breaks-new-ground-matter-antimatter-comparisons

[81] New State of Matter created at CERN: https://home.cern/news/press-release/cern/new-state-matter-created-cern

[82] T. Walcher, The Lamb shift in muonic hydrogen and the electric rms radius of the proton.
https://arxiv.org/abs/2304.07035
R. B. Lumpay *et al.,* The Proton Radius Puzzle and Discrepancies in Proton Structure Measurements.
https://arxiv.org/abs/2501.11195
T. A. Rostomyan, Status of the MUSE experiment.
https://indico.psi.ch/event/16492/contributions/58976/contribution.pdf

the Lamb shift of muonic hydrogen [83]. But measurements belonging to the same technique (same colour in Fig. 5-24) also disagree.

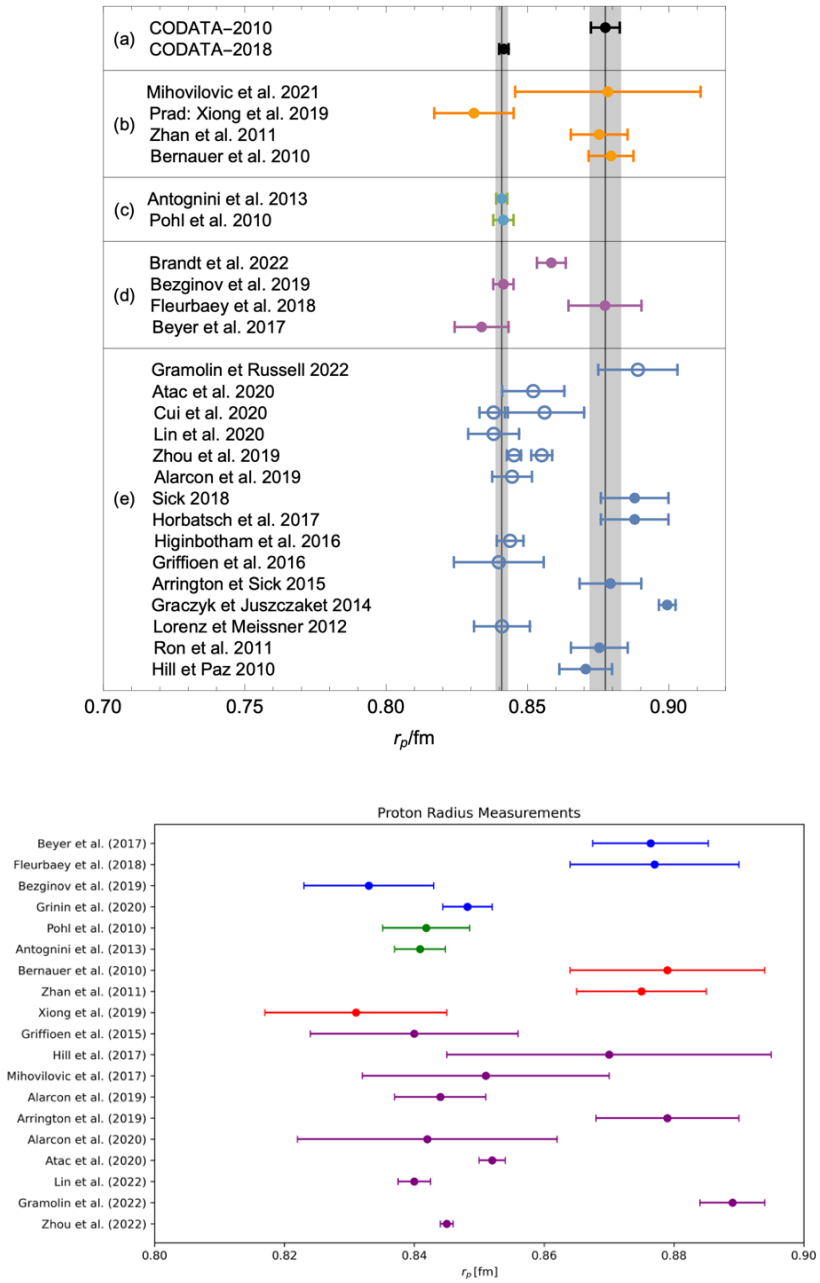


Fig. 5-24: Top: Data on proton charge radius. Bottom: Proton radius measurements categorized by technique. The blue points represent results from Hydrogen Spectroscopy, the green points are from μ-Hydrogen Spectroscopy, the red points are from e-p Scattering, and the purple points are from re-analyses of data.

[83] T. Walcher, The Lamb shift in muonic hydrogen and the electric rms radius of the proton. https://arxiv.org/abs/2304.07035
See also A. Gasparian *et al.,* PRad-II: A New Upgraded High Precision Measurement of the Proton Charge Radius. https://arxiv.org/abs/2009.10510

By "sniffing gluons", using J/ψ photoproduction at threshold, one can infer a **mass radius** of the proton [84] (0.75 fm) and a **scalar proton radius** [85] (1 fm) related to the gluon content, which suggests a proton structure made of three distinct regions, with a gluonic inner core providing most of the mass.

A related question is that of the **spin of the proton** [86]. Only about 30% of the spin comes from quark spins. The spins of the gluons contribute about 30-50%, and the rest is thought to come from orbital angular moments of quarks and gluons. RHIC polarized pp collisions played an important role. Further measurements and theoretical analyses are needed to solve the puzzle of spins. Figure 5-25 proposes one more cartoon, which is probably not the last.

Let us pay tribute to the role in spin physics of the spin program of RHIC [87] (Chapter 20) and of the fixed-target experiment COMPASS [88], using the polarized CERN μ beam and **polarized targets** [89], a highlight of PP.

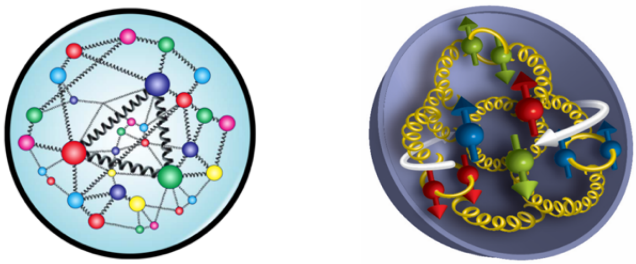


Fig. 5-25: Left: cartoon of the proton suggesting its complexity. Right: another cartoon: q/$\bar{q}$ (balls with arrows) and gluons (yellow "springs").

5.5 Modern fixed-target electron scattering

The Continuous Electron Beam Accelerator Facility (CEBAF) [90] at the Jefferson Lab (USA) consists of a polarized electron source, an injector and a pair of superconducting RF linacs 1400 m long and connected to each other by two arc sections that contain steering magnets. The electron beam makes up to five successive orbits. Effectively, CEBAF, first large-scale application of multipass beam recirculation, is a linear accelerator that has been folded up to a tenth of its normal length.

In early 1987, the construction of the accelerator began. The first beam was delivered to the experimental area on 1 July 1994 at an energy of 4 GeV. Along the years, the facility was upgraded to

[84] E. Kharzeev, The mass radius of the proton. https://arxiv.org/abs/2102.00110.pdf
J. Timmer, Proton's mass radius is apparently shorter than its charge radius. https://arstechnica.com/science/2023/04/protons-mass-radius-is-apparently-shorter-than-its-charge-radius/ , Proton structure consists of three distinct regions. https://cerncourier.com/a/locating-the-proton-mass/
[85] B. Duran *et al.,* Determining the gluonic gravitational form factors of the proton. *Nature 615 813 (2023).*
[86] Smashing Polarized Protons to Uncover Spin and Other Secrets, https://www.bnl.gov/newsroom/news.php?a=111699
[87] Spin Physics, https://www.bnl.gov/rhic/spin.php , A. Bazilevsky for the RHIC Spin collaboration 2016, The RHIC Spin Program Overview. J. Phys.: Conf. Ser. 678 012059, https://iopscience.iop.org/article/10.1088/1742-6596/678/1/012059/pdf
[88] L. Silva, Gluon polarisation results from the COMPASS experiment. https://inspirehep.net/files/44851668183717c8b6df683dc88808ab
[89] T. Niinikoski, Polarized Targets: Pointing to New Directions. https://inspirehep.net/files/10d44588132b3ba669a11fc258d9577e
[90] P. A. Adderley *et al.,* The Continuous Electron Beam Accelerator Facility at 12 GeV. https://arxiv.org/abs/2408.16880

the present 12 GeV energy. Since 2018, the CEBAF accelerator delivered electron beams to all four experimental halls simultaneously.

One of the key features of Jefferson Lab is the continuous nature of the electron beam, with a bunch length of less than 1 picosecond. Another one is its use of Superconducting Radio Frequency (SRF) technology, with liquid helium cooling niobium to ~ 2 K. This was one of the first large-scale implementations of SRF technology.

Jefferson Lab conducts a broad program of research, see Ref. [91], using the electromagnetic interaction to probe the structure of the nucleon, the production and decay of light mesons, and aspects of the interactions of nucleons in the atomic nucleus. The main tools are electron scattering and the creation and use of high energy real photons. In addition, both electron and photon beams can be made highly polarized, allowing exploration of spin degrees of freedom in searches. The four experimental halls have different but overlapping research goals, but with instrumentation unique to each.

Experimental results about the electromagnetic form factors, nuclear femtography and the generalized parton distributions of the nucleon pointed towards the importance of positron beams in determining these fundamental quantities of the nucleon structure, and such a program Ce+BAF is under development [92].

[91] J. Arrington *et al.,* Physics with CEBAF at 12 GeV and Future Opportunities. https://arxiv.org/abs/2112.00060
[92] E. Voutier, The Jefferson Lab Positron Physics Program. https://arxiv.org/abs/2401.16223

6. Evolution of detectors

6.1 The sequence of detector types

The following figures give an idea of the evolution over time of the different classes of detectors. What is plotted in Fig. 6-1 is simply the number of entries in the INSPIRE data base whose title refers to a given technique. The fall of the curves does not necessarily mean that the technique is no longer used but means that it no longer deserves a publication on its own.

Our field first saw the reign of the BCs [93], from the years of learning at CERN to the success of its large liquid hydrogen (LH) and heavy liquid (HL) chambers. The methods of analysing their images evolved in parallel. The roles of France and the École Polytechnique in this saga have been major ones [94]. See Chapters 5 and 9.

A remark: in Fig. 6-1 a surprising red tail appears for the BC technique. Besides retrospective papers, it includes a pursued activity concerning dark matter searches with **special BCs** [95].

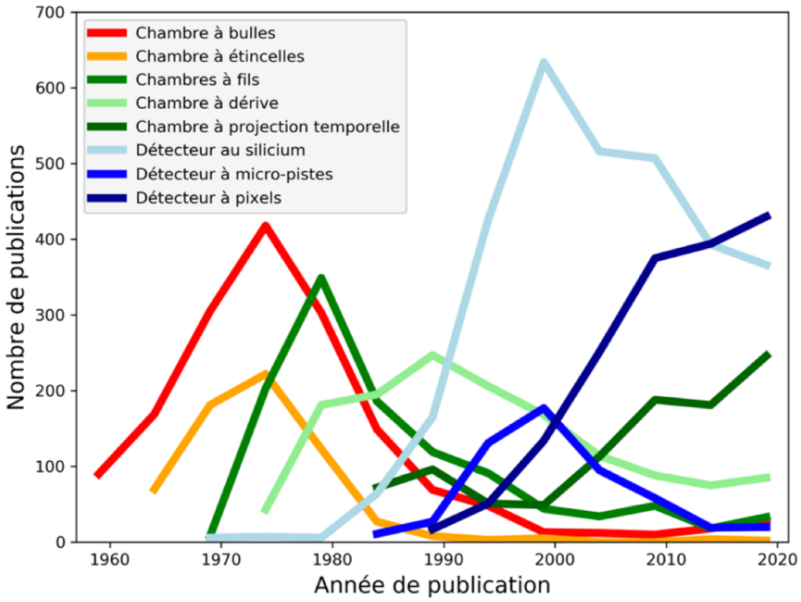


Fig. 6-1: The series of detector types. From Ph. Rosnet and D. Treille.

Triggered detectors then appeared, with the development of **spark chambers** (SC, 1949–1959), their different reading methods, from film to filmless, and variants such as streamer chambers [96]. The first massive use of SCs took place at BNL in 1962, in the experiment that proved the existence of ν_μ .

[93] H. Wenninger, In the tracks of the bubble chamber. https://cerncourier.com/a/in-the-tracks-of-the-bubble-chamber/
[94] M. Bloch *et al.,* Propane and heavy liquids bubble chambers at the École Polytechnique, Paris. https://inspirehep.net/files/3c00e9d4e1f31a472e599109fcc72bdd
[95] C. Amole *et al.,* PICASSO, COUP and PICO – search for cold dark matter with bubble chambers. EPJ Web of Conferences 95,04020 (2015), https://inspirehep.net/files/c9be4e854fc6b659abc399a545150308 , C. Amole *et al.,* Dark Matter Search Results from the Complete Exposure of the PICO-60 C_3F_8 Bubble Chamber. https://arxiv.org/abs/1902.04031.pdf
[96] F. Bulos, *et al.,* Development of streamer spark chambers. https://inspirehep.net/files/6ff42d9efbbbdb4a4b3b260213405aa4

Around 1964 came the first online computers. The optical OMEGA spectrometer was commissioned in 1972. Hybrid systems, from BEBC and its muon identifier, for neutral currents (Chapter 9), to the European Hybrid Spectrometer (EHS), for charm physics, have played an important role.

1968 saw a radical change in the course of our physics with the "revolution" of Georges Charpak, inventor of the **Multiwire Proportional Chamber** (MWPC), which then led to the drift chamber, to multi-stage chambers, a series culminating with the time projection chamber (TPC) [97]. The first large-scale use of MWPCs was in 1971 with the CERN-Heidelberg experiment at the PS, dealing with CP violation, and the Split Field Magnet at the ISR. In Ref. [98], Ioanis Giomataris pays tribute to Georges Charpak and describes recent developments, as Micromegas detectors, already in use in major experiments. See also Ref. [99].

For tracking and particle identification, **transition radiation** [100] played a specific role: a close relative of the Cherenkov effect, emitted in the transit between media, it produces X-rays only for $\gamma > 1000$ (γ is the Lorentz factor), and is therefore particularly useful to identify electrons. To absorb X-rays efficiently, Xenon was selected.

Cherenkov detectors, from threshold and focusing devices (DISC) to the ring imaging technique (RICH), have played a key role in particle identification. The **RICH**, invented by Thomas Ypsilantis and Jacques Séguinot (Fig. 6-2), after having been used in the era of LEP (DELPHI) at SLD and ALICE at LHC, is continuing a fine career, illustrated by the example of LHCb.

Regarding **calorimetry** [101], important breakthroughs have been the understanding and exploitation of the compensation mechanism and the evolution towards pointing geometries, from Spaghetti to the ATLAS Accordion [102]. Liquid argon and scintillating crystals [103], increasingly radiation hard, are essential techniques as used at the LHC (much more in Chapter 23).

An important development was the gradual rise of **silicon (Si) detectors** (Fig. 6-3). While the focus was on flavour labelling in the LEP era, they are now also used as primary trackers. We have gone from a few cm^2 at the SPS to m^2 at LEP and 200 m^2, or even more, at the LHC [104].

---

[97] F. Sauli, The Gas Detector (R)evolution. In Technology Meets Research,
https://inspirehep.net/files/4c15209795cee451737b0be5630774b1

[98] G. Charpak – a true man of science. https://cds.cern.ch/record/1734475 ,
H. Jarlett, Fifty years since Charpak revolutionised particle detectors.
https://home.cern/fr/news/news/detectors/fifty-years-charpak-revolutionised-particle-detectors

[99] H. J. Hilke and W. Riegler, Gaseous Detectors. In Technology Meets Research,
https://inspirehep.net/files/8f6cf687d1af68dcff4d884060535c7a

[100] C. Fabjan, Transition Radiation: Imaging Relativistic Particles. In Technology Meets Research,
https://inspirehep.net/files/02de568d4897c555515de27f0b96af4d, p. 121

[101] C. Fabjan *et al.,* Hadron cascades in iron and uranium. *Phys. Lett. 60B (1975) 105*; C. W. Fabjan *et al.,* Iron liquid-argon and uranium liquid-argon calorimeters for hadron energy measurement. *Nucl. Instr. and Meth. 141 (1977) 61.*
C. Fabjan and W. J. Willis, Physics Limitations on Calorimetry.
https://inspirehep.net/files/00f794c198c039406f3f03eacab91532
R. Wigmans, 70 years of calorimetry. *J. Phys.: Conf. Ser.* 928 012001 (2017)
https://inspirehep.net/files/71f572a3e7df7fdb9af9dcdf294cdf8a
H. Burmeister *et al.,* Electromagnetic calorimetry using scintillating plastic fibers. *Nucl.Instrum.Meth.A 225 (1984) 530,*
https://cds.cern.ch/record/1034268/files/CM-P00062340.pdf
F. Gianotti *et al.,* Liquid argon calorimetry with LHC performance specifications, *Nucl.Instrum.Meth.A 315 (1992) 285*
C. Fabjan, Precision Calorimetry: Honing an Essential Tool.
https://inspirehep.net/files/21e59791dffe28bfbec1d89abe0652c6 p. 125

[102] D. Fournier, Le Défi des Détecteurs.
https://indico.in2p3.fr/event/8302/contributions/44880/attachments/36471/45104/Fournier_24Avril.pdf

[103] P. Lecoq, BGO for the L3 Experiment: Betting on Precision.
https://inspirehep.net/files/d8317e2490824c0916b765874b74d84b , p. 253

[104] E. Heijne, The Silicon Age: Micrometre Precision Millions of Times a Second.
https://inspirehep.net/files/4cd45e76228bc106df801e1ab69247cc , p. 170

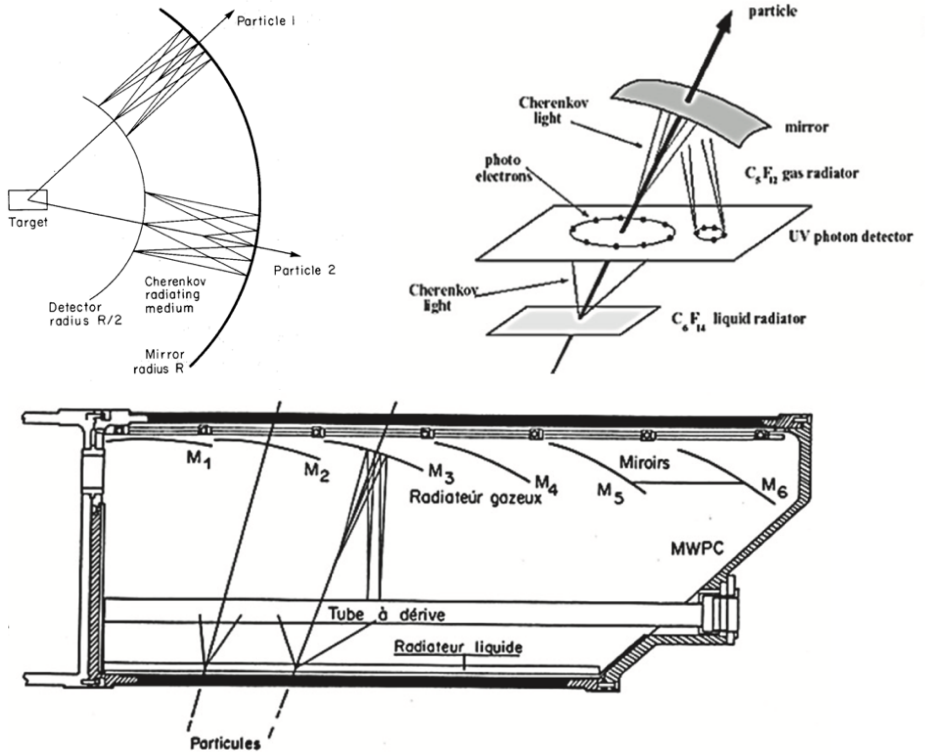


Fig. 6-2: The RICH [105] saga: Upper Left: the original idea of a spherical device. Upper right: the two-radiator arrangement. Bottom: sketch of the DELPHI Barrel Rich. Drift length of 155 cm.

The development of **pixel and CCD** detectors [106] is also spectacular.

It is clear that these advances have been made possible by various formidable **breakthroughs in microelectronics**, in particular the advent of **submicron processes,** which are inherently resistant to radiation, a very welcome feature for the LHC experiments. One of the authors of this document is seven years older than the transistor, and there are now billions of them per chip, as illustrated in Fig. 6-4.

[105] T. Ypsilantis and J. Seguinot, Développement de compteurs Cerenkov à image annulaire pour l'identification des particules. https://lss.fnal.gov/archive/other/lpc-94-48.pdf
J. Seguinot and T. Ypsilantis, Photo-Ionization and Cherenkov Ring Imaging. https://lib-extopc.kek.jp/preprints/PDF/1977/7703/7703161.pdf ,
P. Baillon, DELPHI RICH: The Luminous Footprint of Particles. https://inspirehep.net/files/02de568d4897c555515de27f0b96af4d , p249
T. J. C. Ekelöf *et al.,* The Cerenkov ring-imaging detector: recent progress and future development. *Phys. Scr. 23, 4 pt.2 (1981) p. 718*
C. D'Ambrosio *et al.,* The Future of RICH Detectors through the Light of the LHCb RICH. https://arxiv.org/abs/1703.09927
[106] C. Damerell, Tracking the rise of pixel detectors – CERN Courier https://cerncourier.com/a/tracking-the-rise-of-pixel-detectors/
P. Delpierre, A history of hybrid pixel detectors, from high energy physics to medical imaging. *Journal of Instrumentation, Volume 9, May 2014,* https://iopscience.iop.org/article/10.1088/1748-0221/9/05/C05059
E. H. M. Heijne, History and future of radiation imaging with single quantum processing pixel detectors. https://cds.cern.ch/record/2747957/files/1-s2.0-S1350448720302146-main.pdf

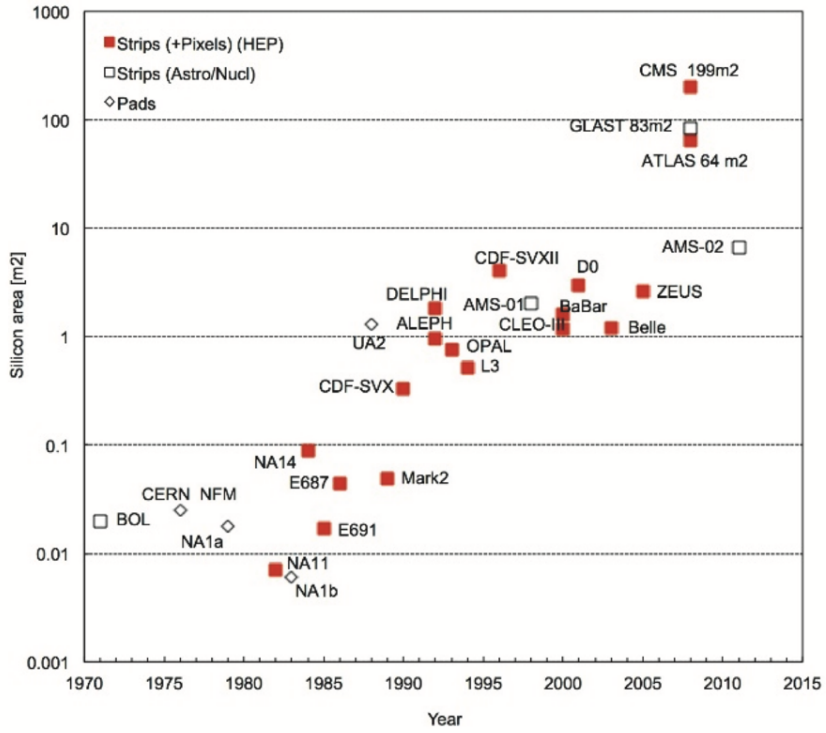


Fig. 6-3: The development of Si detectors [107] (courtesy Y. Unno, KEK). Missing in the figure is the H1 silicon vertex detector [108].

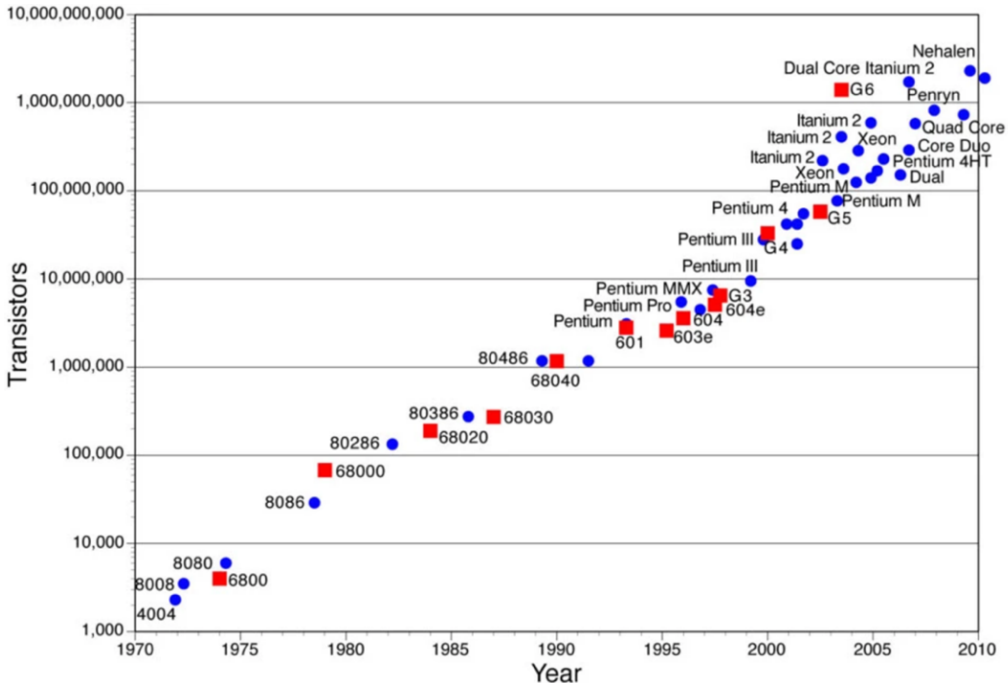


Fig. 6.4: The growth of microelectronics [109].

[107] E. Heijne, The Silicon Age: Micrometre Precision Millions of Times a Second. In Technology Meets Research, https://inspirehep.net/files/818b65cb5004b2f8c5f23faf63571c33 p. 170

[108] D. Pitzl *et al.,* The H1 silicon vertex detector. https://arxiv.org/pdf/hep-ex/0002044

[109] Moore's Law: https://cielotech.wordpress.com/2016/06/10/moores-law/

It is imperative to underline the crucial role of the continuous and vigorous **R&D programs**, in particular the robust DRD program [110] undertaken to learn how to exploit the full luminosity of the LHC, for example concerning the radiation hardness of the Si detectors. It is also clear that, if we want to go further, such R&D efforts must continue. Regardless of the physics goal and the machine being considered, some requirements are similar. Optimal **tracking** requires real 3D information obtained from pixels, micro or macro, rather than microstrips in stereo, perhaps vector information (position and direction), thinner, faster detectors, even still radiation harder and cheaper. **Calorimetry** is looking for a completely satisfactory design with regard to its granularity and the integration of the electromagnetic and hadronic parts (the CALICE program [111]).

We can also note the significant repercussions of HEP accelerators and detectors, for example in **medical physic**s [112]. For **analysis/programming** see Ref. [113] (ROOT). For **electronics** see Ref. [114]. The story of the evolution of **HEP computing,** from the early days to now, is described in Ref. [115].

The organisation in the domain of nuclear and particle physics varies with the country. Taking the French example, it involves a collaboration between CNRS/IN2P3, CEA/IRFU and universities [116]. For historical information on the start and growth of the French PP laboratories, see Ref. [117].

6.2 Various aspects of HEP instrumentation

Much more information on detectors will be given in the following chapters.

The following tables (Table 6-1 to 6-9) and figures (Figs. 6-5 to 6-8), borrowed from the Particle Data Group (PDG) [118] and elsewhere, summarize the history and status of various aspects of HEP instrumentation.

Let us start with a key item of particle physics birth and growth, the **photomultiplier** (Table 6-1).

---

[110] DRD Programme at CERN: https://scientific-info.cern/archives/history_CERN/Exp-Programme-04#DRD

[111] CALICE (Calorimeter for Linear Collider Experiment): https://en.wikipedia.org/wiki/CALICE

[112] C. Benvenuti *et al.*, Knowledge and Technology: Sharing with Society.
https://inspirehep.net/files/8dab861cf947a6ec6fdf61cff4e079f2 , p. 365
U. Amaldi and A. Degiovanni, Proton and Carbon Linacs for Hadron Therapy.
https://inspirehep.net/files/d1efdfdd8435f962a35e704d4da7cdb4

[113] R. Brun, Data Analysis and Programming Environment: Distilling Information.
https://inspirehep.net/files/daabafb2586d8d41916a586321539079 p.353
J. Apostolakis *et al.,* The path toward HEP High Performance Computing. *Journal of Physics: Conference Series* 513 (2014) *052006*, https://inspirehep.net/files/f27be78c90cf7dde675ba082c41b2ead
R. Brun, The Evolution of Software in High Energy Physics. *Journal of Physics: Conference Series 396 (2012) 052016,*
https://inspirehep.net/files/7fae909d97691512000734107d703112

[114] C. de la Taille, 15 ans d'OMEGA + 35 ans de microélectronique = 50 ans d'IN2P3.
https://llr.in2p3.fr/IMG/pdf/50ans-christophe-delataille_c.pdf

[115] F. Hemmer and P. G. Innocenti, Data Handling and Communication.
https://inspirehep.net/files/87110a239677f4cf66a65ff562b7586d p. 327
A short history of the Web. https://home.cern/science/computing/birth-web/short-history-web
C. Jones, Computing at CERN: the mainframe era. https://cerncourier.com/a/computing-at-cern-the-mainframe-era/
D. Ball, Computing at CERN. https://cds.cern.ch/record/1729450/files/vol12-issue3-p062-e.pdf

[116] This scheme has been frequently praised and one can quote its founders: A. Berthelot, R. Aymar, J. Teillac, J. Yoccoz and P. Falk-Vairant.

[117] U. Bassler and D. Guthleben, L'essor de la physique des particules en France.
https://cerncourier.com/a/lessor-de-la-physique-des-particules-en-france/
J. Laberrigue-Frolow and C. de la Vaissière, Les débuts de la physique des particules élémentaires à l'Institut de physique nucléaire d'Orsay. https://doi.org/10.4000/histoire-cnrs.9275

[118] Particle Data Group: Particle Detectors at Accelerators.
https://pdg.lbl.gov/2021/reviews/rpp2021-rev-particle-detectors-accel.pdf

Type	λ (nm)	$\epsilon_Q\,\epsilon_C$	Gain	Risetime (ns)	Single photon time resol. (ps)	Area (mm^2)	1-p.e noise * (Hz/mm^2)	HV (V)
PMT †	115–1700	0.15–0.25	10^5–10^7	0.7–10	∼200	10–10^5	10^{-2}–10^2	500–3000
MCP-PMT†	115–650	0.01–0.10	10^3–10^7	0.15–0.3	∼20	1–10^4	1–10	500–3500
HPD†	115–850	0.1–0.3	10^3–10^4	$O(1)$	∼1000	10–10^5	10–100	$\sim 2 \times 10^4$
HAPD†	115–850	0.1–0.3	10^4–10^5	$O(1)$	∼30	10–10^5	∼1	$\sim 1 \times 10^4$
GPD†	115–500	0.15–0.3	10^3–10^6	$O(0.1)$	∼100	$O(10)$	∼1	300–2000
APD	300–1700	∼0.7	10–10^8	$O(1)$	- ‡	1–10^3	$O(10^7)$ §	400–1400
SiPM	125–1000	0.15–0.4	10^5–10^6	∼ 1	∼50	1–36	10^4–10^5	30–60

Table 6-1: Characteristics of some photodetectors used in particle physics. From PDG, revised August 2011 by P. Križan (Ljubljana University). For the definition of symbols please consult the PDG article.

Among other remarkable features, one can underline the role of very large PMTs in neutrino physics (Kamiokande, Figs. 6-5 and 6-6) [119] and of devices working in magnetic fields, as Avalanche Photo Detectors (APD, read out of CMS crystals). A review of the use of SiPMs can be found in Ref. [120].



Fig. 6-5: Picture of a very large PMT used in the Kamiokande ν physics experiment (Japan).



Fig. 6-6: A multi-PMT photodetector system used in the Hyper-Kamiokande experiment.

Let us move to **electromagnetic calorimetry**, crucial instruments as proven again by the Higgs boson discovery at the LHC in 2012. Table 6-2 recalls the properties of some inorganic crystals. Table 6-3 [121] lists all major crystal calorimeters so far. Figure 6-7 illustrates the radiation lengths of various crystals. Table 6-4 provides the resolution of typical electromagnetic calorimeters.

Concerning the BGO crystals of L3 see Ref. [122] and Ref. [123] concerning the $PbWO_4$ crystals of CMS. More on the latter will come in Chapter 23.

[119] Developing the 20-inch semispherical photomultiplier tubes.
https://ethw.org/w/images/c/c0/Developing_the_20-inch_semispherical_photomultiplier_tubes.pdf
[120] F. Simon, Silicon photomultipliers in particle and nuclear physics.
https://www.sciencedirect.com/science/article/pii/S0168900218316176
[121] R.-Y. Zhu, Inorganic Scintillators for Future Crystal Calorimeters.
https://indico.phy.ornl.gov/event/38/contributions/189/attachments/231/772/ryz_210316_EIC_Crystal_CAL.pdf
[122] P. Lecoq, BGO for the L3 Experiment: Betting on Precision.
https://inspirehep.net/files/d8317e2490824c0916b765874b74d84b p. 253
[123] B. Joshi *et al.*, Predicting the Future of the CMS Detector: Crystal Radiation Damage and Machine Learning at the LHC.
https://scispace.com/pdf/predicting-the-future-of-the-cms-detector-crystal-radiation-2z1srbbu.pdf

Parameter:	ρ	MP	X_0*	R_M*	dE/dx*	λ_I*	τ_{decay}	$\lambda_{\max}$	$n^\dagger$	Relative yield‡	Hygro-scopic?	$d(\text{LY})/dT$
Units:	g/cm^3	°C	cm	cm	MeV/cm	cm	ns	nm				%/°C§
NaI(Tl)	3.67	651	2.59	4.13	4.8	42.9	245	410	1.85	100	yes	−0.2
BGO	7.13	1050	1.12	2.23	9.0	22.8	300	480	2.15	21	no	−0.9
BaF_2	4.89	1280	2.03	3.10	6.5	30.7	650^s	300^s	1.50	36^s	no	−1.9^s
							<0.6^f	220^f		4.1^f		0.1^f
CsI(Tl)	4.51	621	1.86	3.57	5.6	39.3	1220	550	1.79	165	slight	0.4
CsI(Na)	4.51	621	1.86	3.57	5.6	39.3	690	420	1.84	88	yes	0.4
CsI(pure)	4.51	621	1.86	3.57	5.6	39.3	30^s	310	1.95	3.6^s	slight	−1.4
							6^f			1.1^f		
$PbWO_4$	8.30	1123	0.89	2.00	10.1	20.7	30^s	425^s	2.20	0.3^s	no	−2.5
							10^f	420^f		0.077^f		
LSO(Ce)	7.40	2050	1.14	2.07	9.6	20.9	40	402	1.82	85	no	−0.2
PbF_2	7.77	824	0.93	2.21	9.4	21.0	-	-	-	Cherenkov	no	-
CeF_3	6.16	1460	1.70	2.41	8.42	23.2	30	340	1.62	7.3	no	0
$LaBr_3(Ce)$	5.29	783	1.88	2.85	6.90	30.4	20	356	1.9	180	yes	0.2
$CeBr_3$	5.23	722	1.96	2.97	6.65	31.5	17	371	1.9	165	yes	−0.1

Table 6-2: Properties of some inorganic crystals. From PDG, revised August 2021 by C. L. Woody (BNL) and R.- Y. Zhu (HEP California Inst. of Technology).

Date	75-85	80-00	80-00	80-00	90-10	94-10	94-10	95-Now	10-Now
Experiment	C. Ball	L3	CLEO II	C. Barrel	KTeV	BaBar	BELLE	CMS	BES III
Accelerator	SPEAR	LEP	CESR	LEAR	Tevatron	PEP	KEKB	LHC	BEPC
Laboratory	SLAC	CERN	Cornell	CERN	FNAL	SLAC	KEK	CERN	IHEP
Crystal Type	NaI:Tl	BGO	CsI:Tl	CsI:Tl	CsI	CsI:Tl	CsI:Tl	PWO	CsI:Tl
B-Field（T）	-	0.5	1.5	1.5	-	1.5	1.0	4.0	1.0
r_{inner} (m)	0.254	0.55	1.0	0.27	-	1.0	1.25	1.29	0.94
Crystal number	672	11,400	7,800	1,400	3,300	6,580	8,800	75,848	6,240
Crystal Depth（X_0）	16	22	16	16	27	16 to 17.5	16.2	25	15
Crystal Volume（m^3）	1	1.5	7	1	2	5.9	9.5	11	5.3
Light Output（p.e./MeV）	350	1,400	5,000	2,000	40	5,000	5,000	2	5,000
Photo-detector	PMT	Si PD	Si PD	WS+Si PD	PMT	Si PD	Si PD	Si APD	Si PD
Gain of Photo-detector	Large	1	1	1	4,000	1	1	50	1
σ_N/Channel（MeV）	0.05	0.8	0.5	0.2	Small	0.15	0.2	40	0.2
Dynamic Range	10^4	10^5	10^4	10^4	10^4	10^4	10^4	10^5	10^4

Table 6-3: All major crystal calorimeters so far.

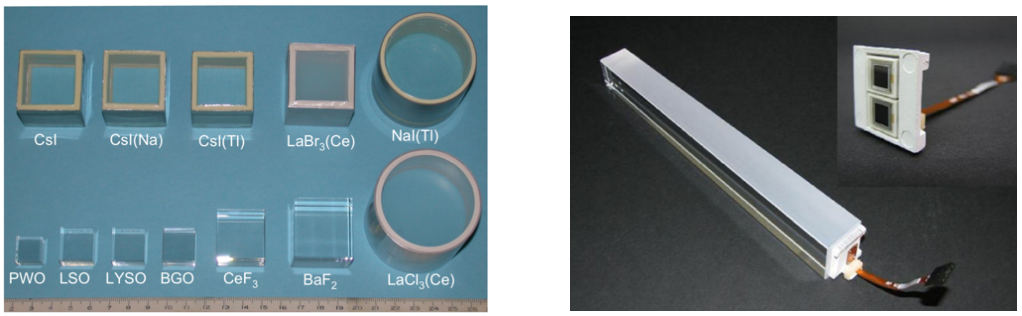


Fig. 6-7: Left: Picture showing twelve crystal scintillators with dimension of 1.5 X_0 [124]. Right: Picture of a $PbWO_4$ crystal (about 28 X_0 with photodetector attached), used in CMS.

[124] R.-Y. Zhu, Precision Crystal Calorimeters in High Energy Physics: Past, Present and Future. *AIP Conf. Proc.* 867, 61 (2006)

The goals for improvements in electromagnetic calorimetry involve:

- High Granularity Sampling calorimetry, reconstructing and identifying individual particles in showers, allowing to measure the energy of each particle with the most appropriate detector subsystem;
- Dual Readout Calorimetry of both scintillation and Cerenkov photons to disentangle EM and hadronic components event-by-event, which allows to appropriately correct each response.

Technology (Experiment)	Depth	Energy resolution	Date
NaI(Tl) (Crystal Ball)	$20X_0$	$2.7\%/\mathrm{E}^{1/4}$	1983
$Bi_4Ge_3O_{12}$ (BGO) (L3)	$22X_0$	$2\%/\sqrt{E} \oplus 0.7\%$	1993
CsI (KTeV)	$27X_0$	$2\%/\sqrt{E} \oplus 0.45\%$	1996
CsI(Tl) (BaBar)	16–$18X_0$	$2.3\%/E^{1/4} \oplus 1.4\%$	1999
CsI(Tl) (BELLE)	$16X_0$	1.7% for $E_\gamma > 3.5$ GeV	1998
CsI(Tl) (BES III)	$15X_0$	2.5% for $E_\gamma = 1$ GeV	2010
$PbWO_4$ (PWO) (CMS)	$25X_0$	$3\%/\sqrt{E} \oplus 0.5\% \oplus 0.2/E$	1997
$PbWO_4$ (PWO) (ALICE)	$19X_0$	$3.6\%/\sqrt{E} \oplus 1.2\%$	2008
Lead glass (OPAL)	$20.5X_0$	$5\%/\sqrt{E}$	1990
Liquid Kr (NA48)	$27X_0$	$3.2\%/\sqrt{E} \oplus 0.42\% \oplus 0.09/E$	1998
Scintillator/depleted U (ZEUS)	20–$30X_0$	$18\%/\sqrt{E}$	1988
Scintillator/Pb (CDF)	$18X_0$	$13.5\%/\sqrt{E}$	1988
Scintillator fiber/Pb spaghetti (KLOE)	$15X_0$	$5.7\%/\sqrt{E} \oplus 0.6\%$	1995
Liquid Ar/Pb (NA31)	$27X_0$	$7.5\%/\sqrt{E} \oplus 0.5\% \oplus 0.1/E$	1988
Liquid Ar/Pb (SLD)	$21X_0$	$8\%/\sqrt{E}$	1993
Liquid Ar/Pb (H1)	20–$30X_0$	$12\%/\sqrt{E} \oplus 1\%$	1998
Liquid Ar/depl. U (DØ)	$20.5X_0$	$16\%/\sqrt{E} \oplus 0.3\% \oplus 0.3/E$	1993
Liquid Ar/Pb accordion (ATLAS)	$25X_0$	$10\%/\sqrt{E} \oplus 0.4\% \oplus 0.3/E$	1996

Table 6-4: Resolution of typical electromagnetic calorimeters. From PDG, revised October 2021 by C. L. Woody (BNL) and R.-Y. Zhu (HEP California Inst. of Technology).

For **charged particle detectors**, the comparison of dead times of BC and wire chambers, shown in Table 6-5, illustrates the impact of Charpak's invention. Spark chambers nevertheless played an important role. For modern developments of BC see Ref. [125]. The table shows also which detectors lead the race towards time resolution, in the tens of ps domain.

The **main magnets of large experiments** are major pieces of equipment of which, besides field quality, long term reliability is an absolute must. Table 6-6 provides a list of superconducting magnets used in particle physics detectors.

For the magnets of giant detectors see Ref. [126] and Chapter 23. Figure 6-8 gives some details on the superconductors: for CMS the high-purity Al used to stabilize the superconductor was not strong enough to withstand the stress on the conductor when the magnet was operated at 4 T. The alternative was to solder or weld Al alloy flanges to the pre-extruded insert, a process subject of a development made in collaboration between CERN and ETH Zurich. In collaboration with industry, it was found that by using electron-beam welding the process was both feasible and practical and resulted in a superconductor degradation of less than 5%. For the ATLAS central solenoid (CS), a doped

[125] B. Broerman, The Scintillating Bubble Chamber Experiment. *SciPost Phys. Proc. 12, 023 (2023),* https://inspirehep.net/files/bea7671bf4f6f30f5d32bb24e208d411 ,
C. Amole *et al.,* Dark Matter Search Results from the Complete Exposure of the PICO-60 C_3F_8 Bubble Chamber. https://arxiv.org/abs/1902.04031.pdf

[126] A. Hervé, P. Jenni and T. Taylor in Technology Meets Research. https://inspirehep.net/files/d59e7aaf7b366b4da3ed4a0798e7a8e9 , p. 318.

pure aluminium, sufficiently strong but with low resistivity, was developed as in-kind contribution of Japan.

Detector Type	Intrinsinc Spatial Resolution (rms)	Time Resolution	Dead Time
Resistive plate chamber	50 μm	50–1000 ps*	10 ns†
Liquid argon TPC	0.5–1 mm‡	0.01-1 μs§	—¶
Scintillation tracker	∼100 μm	100 ps/n‖	10 ns
Bubble chamber	10–150 μm	1 ms	50 ms**
Wire chambers (proportional and drift chambers)	50–100 μm	5–10 ns††	20–200 ns‡‡
Micro-pattern gas detector	30–40 μm	5–10 ns††	20–200 ns‡‡
Silicon strips/pixels	$\lesssim$ 10 μm§§	few ns¶¶ ‡‡	$\lesssim$ 50 ns‡‡

Table 6-5: Resolution and dead time of charged particle detectors. From PDG.

Experiment	Laboratory	B [T]	Radius [m]	Length [m]	Energy [MJ]	X/X_0	E/M [kJ/kg]
TOPAZ*	KEK	1.2	1.45	5.4	20	0.70	4.3
CDF*	Tsukuba/Fermi	1.5	1.5	5.07	30	0.84	5.4
VENUS*	KEK	0.75	1.75	5.64	12	0.52	2.8
AMY*	KEK	3	1.29	3	40	†	
CLEO-II*	Cornell	1.5	1.55	3.8	25	2.5	3.7
ALEPH*	Saclay/CERN	1.5	2.75	7.0	130	2.0	5.5
DELPHI*	RAL/CERN	1.2	2.8	7.4	109	1.7	4.2
ZEUS*	INFN/DESY	1.8	1.5	2.85	11	0.9	5.5
H1*	RAL/DESY	1.2	2.8	5.75	120	1.8	4.8
BaBar*	INFN/SLAC	1.5	1.5	3.46	27	†	3.6
D0*	Fermi	2.0	0.6	2.73	5.6	0.9	3.7
BELLE*	KEK	1.5	1.8	4	42	†	5.3
BES-III	IHEP	1.0	1.475	3.5	9.5	†	2.6
ATLAS-CS	ATLAS/CERN	2.0	1.25	5.3	38	0.66	7.0
ATLAS-BT	ATLAS/CERN	1	4.7–9.75	26	1080	(Toroid)†	
ATLAS-ET	ATLAS/CERN	1	0.825–5.35	5	2 × 250	(Toroid)†	
CMS	CMS/CERN	4	6	12.5	2600	†	12
SiD**	ILC	5	2.9	5.6	1560	†	12
ILD**	ILC	4	3.8	7.5	2300	†	13
SiD**	CLIC	5	2.8	6.2	2300	†	14
ILD**	CLIC	4	3.8	7.9	2300	†	13
FCC**		6	6	23	54000	†	12

* No longer in service
** Conceptual design in future
† EM calorimeter is inside solenoid, so small X/X_0 is not a goal

Table 6-6: Superconducting magnets for PP detectors. From PDG.

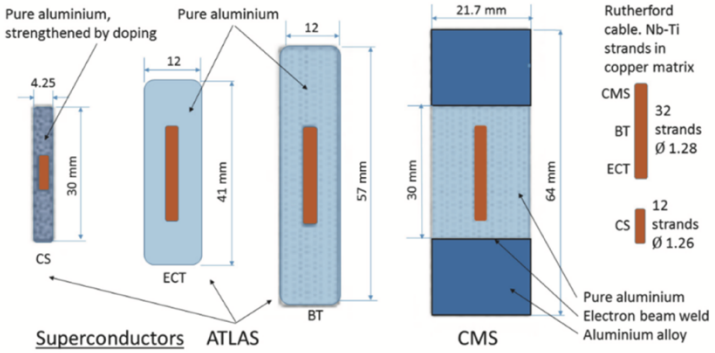


Fig. 6-8: Structure of the superconductors of the ATLAS and CMS solenoids at LHC [127].

[127] A. Hervé, P. Jenni and T. Taylor in Technology Meets Research. https://inspirehep.net/files/d59e7aaf7b366b4da3ed4a0798e7a8e9 , p. 318.

Let us proceed with data, coming mostly from test beams, of **hadronic and combined calorimetry**, with Tables 6-7 and 6-8, from PDG.

Calorimeter	Passive	Active	Resolution	Ref.
Bernardi *et al.*	Pb	Scintillator layers	$44.2\%/\sqrt{E}$ §	[442]
CALICE AHCAL	Fe	Scintillator tiles	$44.3\%/\sqrt{E} \oplus 1.8\%$ †	[434]
CALICE W-AHCAL	W	Scintillator tiles	$57.9\%/\sqrt{E} \oplus 4.6\% \oplus 0.065/E$ §	[443]
CDHS	Fe	Scintillator layers	$58\%/\sqrt{E}$ ♯	[431]
DREAM/RD52	Pb	Scint.+ Quartz fibers	$70\%/\sqrt{E}$ *	[440]
HELIOS	U	Scintillator layers	$34\%/\sqrt{E}$ §	[444]
SPACAL	Pb	Scintillating fibers	$33.3\%/\sqrt{E} \oplus 2.2\%$ §	[445]

§ Bernardi *et al.*, CALICE W-AHCAL, HELIOS, SPACAL: (near-)compensating calorimeters.
† CALICE AHCAL: Local software compensation exploiting the high granularity of the calorimeter.
♯ CDHS: Offline weighting using longitudinal information.
* DREAM/RD52: Due to the relatively small transverse size of the detector lateral leakage was significant, deteriorating the energy resolution with respect to the full potential of the dual readout method.

Table 6-7: Hadron calorimeters and their resolution for single charged hadron (test beam). From PDG, revised August 2021 by F. Sefkow (DESY, Hamburg) and F. Simon (Werner-Heisenberg-Institute).

Experiment	technology (ECAL, HCAL)	Combined hadronic resolution	Reference
H1	Pb/LAr, Steel / LAr	$46\%/\sqrt{E} \oplus 2.6\% \oplus 0.73/E$	[447]
ZEUS	depleted U / plastic scintillator	$35\%/\sqrt{E}$	[448]
CDF	Pb/plastic scint., Steel/plastic scint.	$68\%/\sqrt{E} \oplus 4.1\%$	[449]
D0	depleted U / LAr	$44.6\%/\sqrt{E} \oplus 3.9\%$	[450]
ATLAS	Pb/LAr, Steel/plastic scintillator	$52\%/\sqrt{E} \oplus 3.0\% \oplus 1.6/E$	[451]
CMS	$PbWO_4$, brass/plastic scintillator	$84.7\%/\sqrt{E} \oplus 7.4\%$	[452]

Table 6-8: Energy resolution in combined e.m. and hadronic calorimeters for single hadron (from test beam).

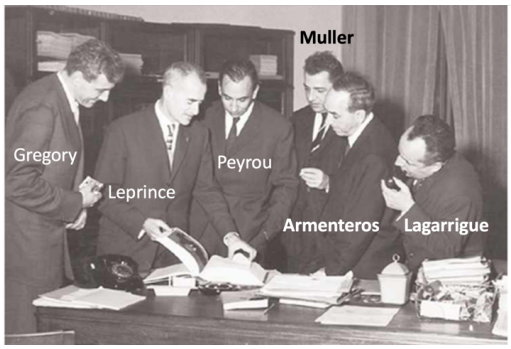
And let us close with the sector that presently shows the major growth, the **semiconductor detectors**, by recalling their properties. Figure 6-3 gives an idea of their developments.

Property	Si	Ge	GaAs	CdTe (CZT)	Diamond
atomic number (Z)	14	32	31/33	48/(30)/52	6
density ρ (g/cm^3)	2.328	5.327	5.32	5.85	3.51
semiconductor type	indirect	indirect	direct	direct	indirect
bandgap E_G (eV)	1.12	0.66	1.424	1.44(1.44–2.2)	5.5
intr. carrier density (cm^{-3})	1.01×10^{10}	2.4×10^{13}	2.1×10^{6}	10^7	≈ 0
radiation length X_0 (cm)	9.36	2.30	2.29	1.52	12.15
average energy w_i for (e/h) creation (eV)	3.65	2.96	4.35	4.43	13.1
mobility (cm^2/Vs)					
electrons μ_n	1450	3900	8500	1050	≈1800*
holes μ_h	500	1800	400	90	≈2300*
lifetime					
electrons τ_e	>100 µs	∼ms	1–10 ns	0.1–2 µs	≈100 ns
holes τ_h	>100 µs	∼ms	20 ns	0.1–1 µs	≈ 50 ns

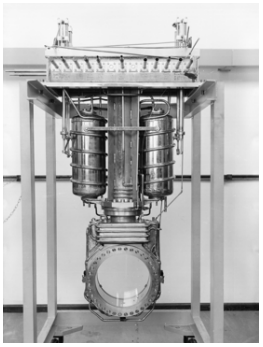
Table 6-9: Properties of some detector-relevant semiconductors; temperature-dependent quantities given at 300 K. From PDG, revised August 2021 by N. Wermes (Bonn University).

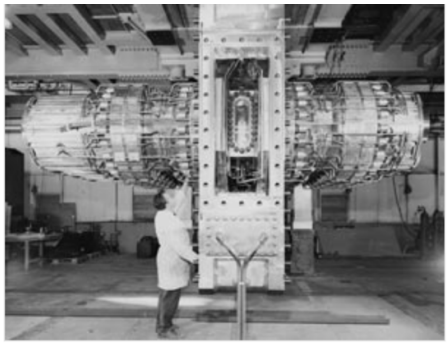
6.3 Intermède

Some decades ago, a CERN motto was: *"CERN is its member states, plus l'X"*. L'X in French jargon is the École Polytechnique, and this sentence underlines the pioneering role of its Bubble Chamber physicists led by Louis Leprince-Ringuet.

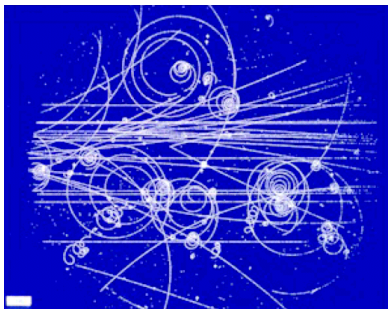


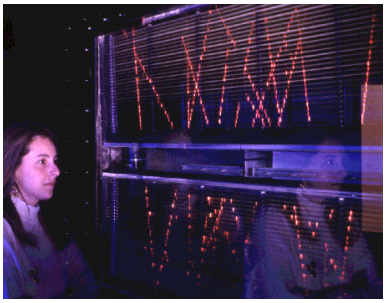
Louis Leprince-Ringuet and his état-major.

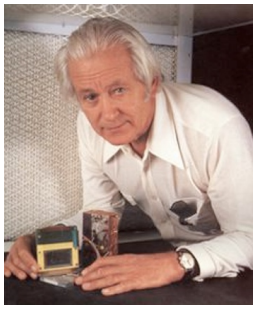

The 30cm Bubble Chamber.

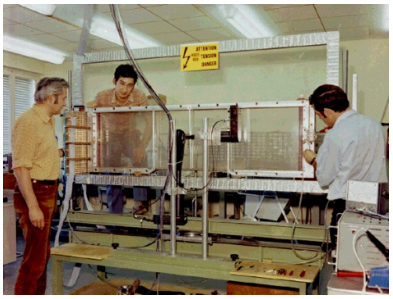

The 2m Bubble Chamber.

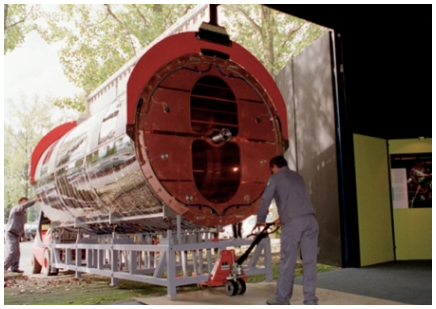

A plea of Charles Peyrou for still bigger.


Bubble chamber.


Spark chamber.


G. Charpak and his small chamber.


G. Charpak (left) with F. Sauli (middle) and C. Santiard (right).


The UA1 trajectograph.

7. Towards the Standard Model

We start with a brief recap (Sections 7.1 to 7.3). This story has been told and explained in detail, for instance by Jean Iliopoulos [128, 129]. Then we will tell more about the topic of **anomalies** (Section 7.4). Finally, will come two intermèdes, **the SM in words** (Section 7.5) and a choice of possible **analogies to the Higgs (BEH) mechanism** (Section 7.6).

7.1 The successes

We recall that after QED, built on the basis of local gauge invariance, Chan Ning Yang and Robert Mills, in 1954, extended local gauge invariance to the non-abelian case, i.e. when vector bosons are **self-interacting**.

In 1961 Sheldon Glashow gave the **correct algebra** of the Standard Electroweak Model (SEM), SU(2) x U(1), but for **massless objects**. In 1967–1968 Abdus Salam and Steven Weinberg brought a happy ending to the story, using the **BEH mechanism** (Brout–Englert–Higgs mechanism, Nobel Prize in 2013), proposed in 1964. Sheldon Glashow, Abdus Salam and Steven Weinberg obtained the Nobel Prize in 1979. Finally, in 1971, Gerard t' Hooft showed that the SEM was **a "true" quantum theory, renormalizable.** He obtained the 1999 Nobel Prize together with Martinus Veltman.

Alongside the GIM mechanism (1970, Chapter 8), the paper of Claude Bouchiat, Jean Iliopoulos and Philippe Meyer gave an anomaly free version of the Weinberg model [130].

Once the SEM was established, after the discovery of Neutral Currents in 1973 (Chapter 9), a clear mission was defined: to experimentally proof the existence of the W, Z and the Higgs (BEH) boson. In this respect, as we shall see, CERN has done very well (see Chapter 12 and Chapter 24). Figure 7-1 recalls the predictions and observations of all SM particles.

However, there was **some delay in the minds** before the SM was fully accepted (Chapter 29). In fact, even QED was still under inspection.

For example, in 1972, Howard Georgi and Sheldon Glashow proposed an alternative model, without Z, but with a heavy lepton [131].

---

[128] J. Iliopoulos, The Making of the Standard Theory, https://inspirehep.net/files/d3cf88043545b69efc7d759615eb1eec , The Nobel path to a unified electroweak theory.
https://cerncourier.com/a/the-nobel-path-to-a-unified-electroweak-theory/
T. W. B. Kibble, History of electroweak symmetry breaking. https://arxiv.org/abs/1502.06276.pdf
S. Weinberg, The Making of the Standard Model. https://cds.cern.ch/record/799984/files/0401010.pdf
S. Glashow, The Standard Model. https://inference-review.com/article/the-standard-model

[129] J. Iliopoulos, Fifty years that changed our physics. https://inspirehep.net/files/51ad7449c5d9b351b16c72fac1e1e989
J. Iliopoulos, Introduction to the STANDARD MODEL of the Electro-Weak Interactions. https://arxiv.org/abs/1305.6779.pdf
J. Iliopoulos, From Many Models to ONE THEORY. https://arxiv.org/abs/2501.10233

[130] C. Bouchiat, J. Iliopoulos and Ph. Meyer, An Anomaly-Free Version of Weinberg's Model. *Physics Letters B 38, no. 7 (1972): 519–23*
S. L. Adler, Anomalies to All Orders. https://arxiv.org/abs/hep-th/0405040.pdf

[131] H. Georgi and S. L. Glashow, Unified Weak and Electromagnetic Interactions without Neutral Currents. *Phys.Rev.Lett. 28 (1972) 1494*

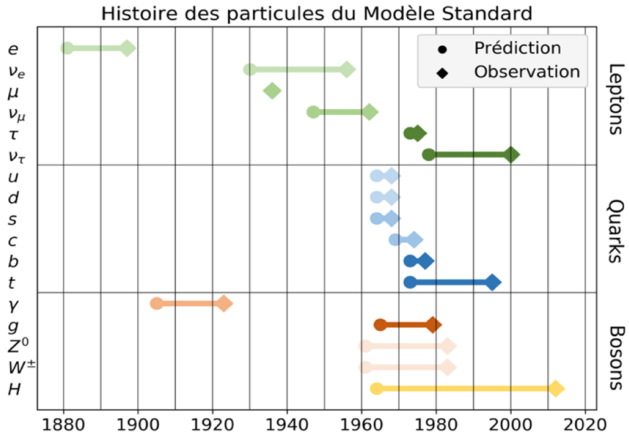


Fig. 7-1: From prediction to observation (courtesy Philippe Rosnet).

From quotes in Moriond some doubts were still expressed. In 1976, John Ellis [132] spoke of quantum asthenodynamics *"which many people now believe exists although no one knows what it is"*. James Bjorken, Jun John Sakurai in 1980, and others, proposed the idea of Technicolor [133].

Others were convinced very early on, as Jean Iliopoulos in Moriond 1973 [134] (BEH was then called Higgs-Kibble). In 1973, Jonathan Rosner was *"waiting for W, Z, charm, heavy lepton"*.

Christopher Llewelyn Smith in his conclusion of Moriond 1981 found the SEM *"sound"* but asked for W and Z and proof of confinement. In the Weinberg model (1976), it was possible, end of the seventies, to predict $m_W = (78 \pm 3)$ GeV, $m_Z = (89 \pm 3)$ GeV, plus 3 GeV of radiative corrections [135]. It just remained to discover these bosons.

Concerning the SM, i.e. the SEM completed by $SU(3)_C$, in addition to the major discoveries, the increasingly close confrontation between many precision measurements and SM predictions played a decisive role. It was a long friendly match between theorists, pushing their estimates to higher orders, and experimentalists refining their detection and analysis techniques. We described that for QCD and will return to it later with LEP, LHC, etc.

7.2 What is missing in the SM?

The PP story went on with a series of experimental confirmations of the SM. However, **the SM incompleteness is also manifest** [136].

The SM has three different gauge interactions, each with its own coupling strength. The quantization of electric charge is not explained, and the observed equality, with opposite signs, of the e^- and p charges, which must be good to at least 1 part in 10^{20} to account for the observed electrical neutrality of bulk matter, remains a mystery.

---

[132] J. Ellis, Charmonium and gauge theories. https://inspirehep.net/files/bc5f58dadf9407400326da3672686049
[133] J. Ellis, Technicolour - Oasis or Mirage? https://lib-extopc.kek.jp/preprints/PDF/1981/8110/8110130.pdf
[134] J. Iliopoulos, Yang-Mills models of weak and electromagnetic interactions.
https://inspirehep.net/files/b3b16670b8c0e11c7eb9a446c7abe6c5
[135] Z. Hioki, How Does the Discovery of Z Boson Improve the Prediction for $W^\pm$ Boson Mass?
https://lib-extopc.kek.jp/preprints/PDF/1983/8302/8302066.pdf
E. A. Paschos, The Weak Mixing Angle and its Relation to the Masses M_Z and M_W.
https://lib-extopc.kek.jp/preprints/PDF/1982/8206/8206244.pdf ,
[136] J. Ellis, Beyond the Standard Model for Hillwalkers. https://arxiv.org/abs/hep-ph/9812235

The SM contains at least **19 arbitrary parameters**: three independent gauge couplings and a possible CP-violating strong-interaction parameter, six quarks and three charged-lepton masses, three generalized Cabibbo weak mixing angles and the CP-violating Kobayashi–Maskawa phase (Chapter 14), and two parameters (M_H, M_W) for the Higgs sector.

The ν world (Chapter 19) requires more parameters to account for the oscillations: if neutrinos are Dirac particles, there are three ν masses, three real mixing angles, and a CP-violating phase, in principle observable in ν oscillation experiments. If neutrinos turn out to be Majorana, as a ν-less $\beta\beta$-decay observation would confirm it (Section 32-1), two more phases intervene.

The big questions can be formulated as:

- If the origin of elementary particle masses is due to a Higgs boson, **why are most masses so small** and why such a **large spectrum of fermion masses**?
- Can all particle interactions be **unified in a simple symmetry group**? Would it predict relations between SM parameters such as gauge couplings or fermion masses?
- Why **so many different types** (flavours) of fermions and why, in weak interactions, this **peculiar way of mixing**?

Another shortcoming of the SM is, if the **dark sector** is relevant to the particle world, the absence of any explanation for and of candidate(s).

More generally, the SM **ignores gravity.** How would a theory comprising PP and gravity, valid for all energies, look like? This leads us to the domain of **quantum gravity** (QG) whose effects manifest at the Planck scale of 10^{19} GeV.

7.3 Some possible directions beyond the SM

An improvement over the SM would certainly be the advent of **Supersymmetry (SUSY)** at a not too high energy scale, a topic we will consider in Chapters 16 to 18 and 24. SUSY would solve the crucial problem of **hierarchy**, but not other ones, and would still be considered as an **effective theory** [137].

Presently, apart from the Higgs boson mass, found in the range expected by the MSSM [138], and the improvement of the convergence of couplings at high energy that SUSY brings, no proof of its existence at the needed scale exists yet. So, let us first consider other roads beyond the SM.

7.3.1 Grand Unification

Grand Unified Theories (GUTs), unified descriptions of e.m., weak and strong interactions at high energy scales, offer a very interesting completion of the SM, in a group-theoretical framework, resolving some of the quoted problems [139]. For instance, in a GUT, charge quantization would no longer be surprising. **Note that GUTs are not an alternative to SUSY.**

GUTs appeared in 1974 when Howard Georgi and Sheldon Glashow proposed to unify the SM gauge group into a simple group, SU(5). **One can also consider as a GUT the 1974 Pati–Salam model** [140].

GUTs require that the unified group be a simple group, e.g. SU(5), SO(10) or E_6, but one may also consider product groups as SU(4) $\times$ SU(2) $\times$ SU(2). Candidate groups for a realistic GUT model must

[137] Not everyone shares the assumption that there exists a "true theory", which is not effective.
[138] MSSM is the minimal supersymmetric standard model as it considers only the minimum number of new particle states and new interactions.
[139] Chapter 7 of the book by P. D .B. Collins, A. D. Martin, E. J. Squires, Particle Physics and Cosmology.
[140] https://en.wikipedia.org/wiki/Pati%E2%80%93Salam_model

contain the SM group as a subgroup and have **complex representations** reproducing the chiral structure of the SM.

This larger gauge group is spontaneously broken at a scale M_{GUT}, above 10^{16} GeV, according to the proton lifetime constraints. New particles, predicted to have masses around that scale, still well below the Planck scale, are beyond reach. However, the breaking of such large groups to the SM one may occur through different phases, offering states at intermediate lower scales.

In addition to the SM gauge bosons, GUTs must have gauge bosons X, linking quarks and leptons lying within the same group multiplet. These X bosons will mediate new interactions violating baryon number (B) and lepton number (L) conservation. These new interactions have not been "felt" so far, meaning that the X bosons must be very massive.

GUTs inspire low energy beyond the Standard Model (BSM) theories, as left-right symmetric or supersymmetric models, and fill the gap between the experimental domain and ultraviolet (UV) physics. The **renormalization equations** provide the link between the two scales. The convergence of couplings of the three forces at about 10^{16} GeV, quasi perfect in the case of the MSSM (Chapter 16), is a famous example and an encouragement to pursue the GUT track.

Even if "simplified" models with more specific phenomenology took the lead, it is essential to recall the importance of GUTs in particle physics [141].

A possibility to grasp GUT is to search for TeV scale observables arising from abelian groups embedded in GUT constructions, e.g. a signal of a Z' gauge boson of coupling strength to SM fermions as predicted by the construction. Progress of experiments permits to test the predictions of GUTs at different energy scales.

For instance, Ref. [142] focuses on heavy dilepton resonances and obtains limits on the Z' mass for several GUT-models using current and future proton-proton colliders. If the Z' is seen as a mediator between DM and SM, a connection with the DM problem is established.

If GUTs play a role in **inflation** they could leave tracks in the CMB observations. They could manifest themselves in tests of the proton stability, which already excluded the simple SU(5) version (see Section 32-4). Some GUTs relate the Baryon (B) asymmetry to contributions to the neutron **electric dipole moment, d_n** (Section 32.2). In the absence of unforeseen cancellations, one can obtain an approximate cosmological lower limit on this key parameter.

The predictions of specific GUT models could be tested at pp colliders, via searches for exotic states or additional contributions to flavour anomalies.

However, such GUTs **are also incomplete**. They ignore gravity, do not explain the number of generations of fermions, the fermion masses and mixing angles. The larger the GUT group, the more arbitrary is the Higgs sector. The hierarchy of mass scales and how can it be naturally sustained is a new fundamental problem associated with GUT. Despite these problems, GUTs have rightly started many theoretical investigations.

7.3.2 Extra Dimensions

Let us briefly evoke another domain of speculations beyond the SM.

String theory introduced a new fundamental energy scale associated with the string tension, or equivalently with the inverse string size. Its value can be high, near the four-dimensional Planck mass,

[141] D. Croon *et al.,* GUT Physics in the era of the LHC. https://arxiv.org/abs/1903.04977

[142] G. Arcadi *et al,* GUT Models at Current and Future Hadron Colliders and Implications to Dark Matter Searches. https://arxiv.org/abs/1704.02328

compatible with traditional (supersymmetric) grand unification. However, it has also been suggested that it may be lower, down to the TeV scale.

Reference [143] proposed TeV^{-1}-size Extra Dimensions (EDs) related to supersymmetry (SUSY) breaking, and Ref. [144] showed that an ED $\sim (10^{12}\ GeV)^{-1}$ in M-theory can lower the string scale to the grand unified (GU) scale $M_{GUT} \sim 10^{16}$ GeV, unifying gravity with other forces at that scale. The discovery of D-branes in string theory (Ref. [145]) provides a natural framework for various fields that exist in different number of EDs.

The idea of EDs became popular in phenomenology after Ref. [146] (1998) considered large ED as a solution to the hierarchy problem, in an appropriate String and D-branes framework in which the SM can be embedded. Subsequently, searches for ED were carried out in many physics programmes.

The Randall–Sundrum (RS) model [147], with a single, "warped" extra dimension, realized in five-dimensional anti-deSitter space-time (AdS_5), proposes two 3-dimensional branes with equal and opposite tensions, positioned at fixed points in the AdS_5 space, the SM brane and the Planck brane. Gravity is generated on the Planck brane, while at least some of the SM particles are confined to the SM brane, separated from the Planck brane in the ED. Due to the warping of the ED, operators with the characteristic size of M_P on the Planck brane give rise to exponentially suppressed energy scales on the SM brane: $M_D = \bar{M}_P\, e^{-\pi kR}$, where $\bar{M}_P \equiv M_P/\sqrt{8\pi}$ is the reduced Planck scale, k the warp factor and R the radius of the compact dimension. Thus, one can connect the electroweak symmetry breaking (EWSB) scale to the Planck scale by requiring the product $kR \sim 10$. R could have a "natural" value of $\sim 1/M_P$, thus solving the hierarchy problem.

For a review of ED, see Ref. [148]. Anticipating, for a review in relation with searches at LHC, see Ref. [149].

In our space-time the phenomenology of all models involves a tower of **Kaluza–Klein (KK) excitations** of particles propagating in extra dimensions. For compactified ED, their momentum projection on the compact dimensions has only **quantized values**. For a 3D observer, this quantized momentum in the direction orthogonal to the 3D brane appears as a "tower" of massive states, with masses $m^2_n = m^2_0 + (n/R)^2$, R being the compactification radius and m_0 the mass of the zeroth KK mode, representing the ground state, or the particle confined to a 3D brane.

The **5D minimal UED model (MUED),** of compactification radius R, is an effective theory, valid below a cut-off scale Λ. Because of the presence of missing energy (escaping to ED or as gravitational radiation), its phenomenology resembles in many aspects to the MSSM one [150] (see Section 24.3.2 for an update on SUSY searches). Each SM particle has a partner particle at the first KK mode level, but of the same spin. The MUED model possesses a "KK parity" and the lightest partner of the $U(1)_Y$ gauge

---

[143] I. Antoniadis, A possible new dimension at a few TeV. *Phys. Lett. B 246, 377 (1990)*

[144] I. Antoniadis and M. Quiros, Large radii and string unification. https://arxiv.org/abs/hep-th/9609209
P. Horava and E. Witten, Eleven-Dimensional Supergravity on a Manifold with Boundary. *Nucl.Phys.B. B 475, 94 (1996)*, https://arxiv.org/abs/hep-th/9603142

[145] J. Polchinski, Dirichlet-Branes and Ramond-Ramond Charges. *Phys. Rev. Lett. 75, 4724 (1995)*, https://arxiv.org/abs/hep-th/9510017

[146] N. Arkani-Hamed, S. Dimopoulos and G. R. Dvali, The Hierarchy Problem and New Dimensions at a Millimeter. *Phys. Lett. B 429, 263 (1998),* https://arxiv.org/abs/hep-ph/9803315

[147] L. Randall and R. Sundrum, An Alternative to Compactification. *Phys. Rev. Lett. 83, 4690 (1999).* https://arxiv.org/abs/hep-th/9906064

[148] H. C. Cheng 2009 TASI Lecture – Introduction to Extra Dimensions. https://arxiv.org/abs/1003.1162

[149] G. Landsberg, Searches for Extra Spatial Dimensions with the CMS Detector at the LHC. https://arxiv.org/abs/1506.00024

[150] N. Deutschmann *et al.,* Current LHC Constraints on Minimal Universal Extra Dimensions. https://arxiv.org/abs/1702.00410
See also. J. Beuria *et al.,* LHC Collider Phenomenology of Minimal Universal Extra Dimensions. https://arxiv.org/abs/1702.00413

boson is a dark matter candidate, reproducing the observed DM relic density if 1.25 TeV $\leq R^{-1} \leq$ 1.5 TeV, while larger R^{-1} would overclose the Universe. Via loop corrections, the KK resonances contribute to EW precision observables and flavour physics, which impose bounds on $R^{-1} \geq$ 600–750 GeV [151].

Figure 7-2 shows limits obtained by ATLAS and CMS in the MUED model. No sign of any ED has been obtained up to now.

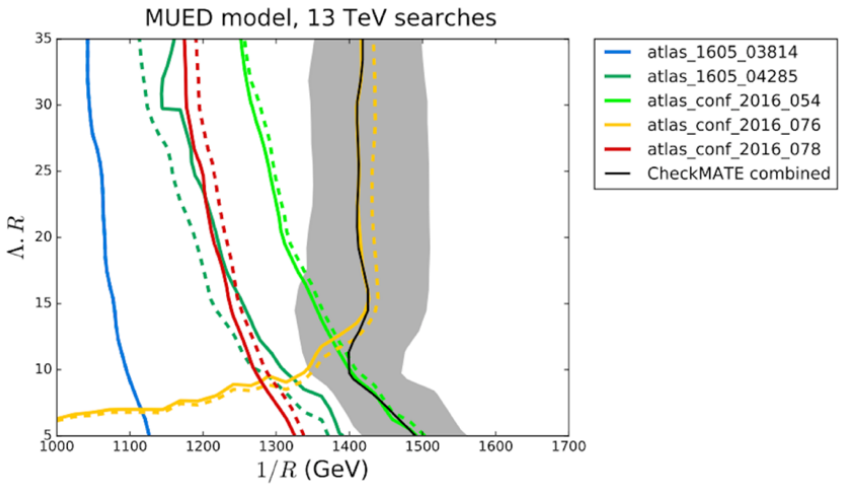


Fig. 7-2: 95% confidence level limit in the ΛR – R^{-1} plane from searches performed at the LHC centre of mass energy √s = 13 TeV. R: compactification radius, Λ: cut-off scale of the effective theory [152].

7.3.3 Asymptotic safety

Unless the existence of extra-dimensions brings it to much lower energy, a fact of which we have presently no hint, one scale is guaranteed to exist, the Planck scale (1.22×10^{19} GeV) [153], where the gravitational force is expected to meet the other forces, the domain of **Quantum Gravity (QG**) and **Superstrings**.

String theory is a promising candidate for a consistent description of both physics but connecting this theory to the SM has shown to be very hard. See, however, Ref. [154].

The **"asymptotic safety"** [155] approach towards Quantum Gravity [156] may offer a better option for implementing the top-down idea since it uses the language of Relativistic Quantum Field Theory (RQFT).

Trying to upgrade General Relativity to a quantum theory, **quantum fluctuations** make things go wrong rapidly, unless, following the idea of **renormalisation**, they are properly organised and integrated out, which creates the Wilsonian renormalisation-group "flow" of the theory. Satisfactory high-energy

[151] ibid. https://arxiv.org/abs/1702.00410 and references therein.
[152] N. Deutschmann *et al.,* Current LHC Constraints on Minimal Universal Extra Dimensions. https://arxiv.org/abs/1702.00410
[153] Fundamental physical constants: https://physics.nist.gov/cgi-bin/cuu/Value?plkmc2gev
[154] F. Marchesano *et al.,* The Standard Model from String Theory: What Have We Learned? https://arxiv.org/abs/2401.01939
[155] R. Percacci, Asymptotic safety. https://arxiv.org/abs/0709.3851
M. Shaposhnikov and C. Wetterich, Asymptotic safety of gravity and the Higgs boson mass. https://arxiv.org/abs/0912.0208
S. Weinberg, Asymptotically Safe Inflation https://arxiv.org/abs/0911.3165
[156] A. Ashtekar and E. Bianchi, A Short Review of Loop Quantum Gravity. https://arxiv.org/abs/2104.04394

completions are provided by **renormalisation-group fixed points (RGFP)** [157], special points where the theory becomes **scale-invariant**, hence free of divergences. The existence of RGFP with non-vanishing interactions is referred to as asymptotic safety.

Actually, the existence of a RGFP suitable to make gravity asymptotically safe is supported by a number of first principle computations [158]. The link to particle physics follows from the fact that "*the asymptotic-safety construction remains operative once gravity is supplemented by the matter fields of the SM*". Asymptotic-safety predicts relations between the couplings of the SM effective field theory, which can be confronted with observations, testing whether the observables measured in PP or astrophysics obey these constraints.

Such bold considerations are beyond the level of this document, which just points to various references. **How should the SM be considered** in practice?

7.3.4 Effective theory

Without any new discovery up to now (besides the BEH Boson), we should treat the SM as an **effective theory** and start to systematically explore its "UV completion" (see the SMEFT in Chapter 24). PP went through such a phase with the **Fermi theory** (Chapter 8) and its 4-fermion vertex, until the IVBs (Intermediate Vector Bosons W and Z) provided an element of its "UV completion".

Meanwhile, the **search for new effects** should be pursued by all means. It is not excluded that some new discovery, such as a trio of **right-handed neutrinos** (the νMSM, Chapter19), the observation of **proton decay** and thus the evidence of grand unification (GU, Section 32.4), the discovery of the **axion** (Section 31.3) or other Higgs bosons and/or SUSY partners, etc., will provide us with important answers.

7.4 An aside on anomalies

7.4.1 From the classical theory to the quantum theory

Anomalies, intervening in SM and BSM sectors and playing a key role, are worth being considered [159]. This is however a difficult topic and **our main concern will be to point at references**. A few recaps first.

Repeating what was said in Chapter 4, a **chiral** phenomenon is one that is not identical to its mirror image. The **chirality** of a particle is determined by whether the particle transforms in a right- or left-handed (**RH or LH**) representation of the Poincaré group. Chirality for a Dirac fermion ψ is defined through the operator γ^5. A theory asymmetric with respect to chiralities is called a **chiral theory**, while a non-chiral (i.e., parity-symmetric) theory is sometimes called a **vector theory** (meaning opposed to axial-vector). **QCD is a vector theory**, since both chiralities of all quarks appear in the theory, and couple to gluons in the same way. **The EW theory is a chiral theory.**

Quantum anomalies occur when quantum corrections do not respect a symmetry of the classical Lagrangian. A **chiral anomaly** is the anomalous non-conservation of a chiral current.

---

[157] Renormalization group: https://en.wikipedia.org/wiki/Renormalization_group A fixed point appears when the relevant β functions are equal to 0.

[158] F. Saueressig and M. Becker, A safe approach to quantum gravity.
https://cerncourier.com/a/a-safe-approach-to-quantum-gravity/ and references therein.
See also A. Bonanno and F. Saueressig, Asymptotically safe cosmology – a status report. https://arxiv.org/abs/1702.04137

[159] D. Tong: Lectures on Gauge Theory. https://www.damtp.cam.ac.uk/user/tong/gaugetheory.html , Part 3
R. Jackiw, The Chiral Anomaly. https://www.europhysicsnews.org/articles/epn/pdf/1991/04/epn19912204p76.pdf
See Chapter 5 of P. D. B. Collins, A. D. Martin, E. J. Squires, Particle Physics and Cosmology.

From Roman Jackiw [160]: *"Anomaly phenomena arise when fermions are coupled to gauge fields. An aspect that was believed to carry over intact from the classical theory to the quantum theory are symmetry properties and conservation laws… However, today we know that this is not always so, and the violation of classical symmetries and conservation laws by the quantization procedure is called the* ***anomaly phenomenon****, for which a better name would be* ***quantum mechanical symmetry breaking****. Anomalous or quantum mechanical symmetry breaking affects symmetries associated with masslessness: both scale and conformal invariance of massless fields, as well as chiral invariance of massless fermions, are broken by quantum effects".*

The **Adler–Bell–Jackiw (ABJ) anomaly** [161] of QED is a symmetry of **classical electrodynamics** that is **violated by quantum corrections** (Table 7-1). Considering the classical (non-quantized) theory of EM coupled to **massless** fermions (electrically charged Dirac spinors), one expects to have **two conserved currents**: the ordinary electrical current (the **vector current**), described by the Dirac field $J_V^\mu = \bar{\psi}\gamma^\mu\psi$ and an **axial current** $J_A^\mu = \bar{\psi}\gamma^\mu\gamma_5\psi$ When moving from the classical theory to the quantum theory, one may compute the **quantum corrections** to these currents, which at first order are the **one-loop Feynman diagrams**. However, the axial current cannot be regularized in such a way as to preserve the axial symmetry [162]. The axial symmetry of classical electrodynamics is **broken by quantum corrections**. See Table 7-1.

For a massless fermion coupled to an external classical e.m. field

$L = i\bar{\psi}\gamma^\mu\partial_\mu\psi + eJ_V^\mu A_\mu$ with $J_V^\mu = \bar{\psi}\gamma^\mu\psi$

Invariance under vector and axial phase rotations of the spinor field

$U(1)_V : \psi \to e^{i\alpha}\psi$ $U(1)_A : \psi \to e^{i\alpha\gamma_5}\psi$

Implies the conservation of the vector and axial currents

$\partial_\mu J_V^\mu = 0$ $\partial_\mu J_A^\mu = 0$ where $J_A^\mu = \bar{\psi}\gamma^\mu\gamma_5\psi$.

However the correct result is

$$\partial_\mu J_A^\mu = -\frac{e^2}{8\pi^2}F_{\mu\nu}\tilde{F}^{\mu\nu}$$

where $F_{\mu\nu}$ is the e.m. field strength and $\tilde{F}^{\mu\nu} = \frac{1}{2}\epsilon^{\mu\nu\rho\sigma}F_{\rho\sigma}$.

This is the ABJ anomaly.

In QCD the equivalent result is

$$\partial_\mu J_A^\mu = -\frac{g_s^2}{32\pi^2}N_f\epsilon^{\kappa\lambda\mu\nu}G^a_{\kappa\lambda}G^a_{\mu\nu} = -N_f\frac{g_s^2}{8\pi^2}\mathrm{Tr}(G_{\mu\nu}\tilde{G}^{\mu\nu})$$

where $G_{\mu\nu} \equiv \frac{\lambda^a}{2}G^a_{\mu\nu}$ with a sum on the colour index a =1,8

with $G^a_{\mu\nu} = \partial_\mu G^a_\nu - \partial_\nu G^a_\mu - g_s\sum_{b,c} f_{abk}\, G^b_\mu G^c_\nu$. and $\tilde{G}^a_{\alpha\beta} = \frac{1}{2}\epsilon_{\alpha\beta\rho\mu}G^{\varrho\mu a}$

λ^a are the colour SU(3) matrices with $\mathrm{Tr}(\lambda^a\lambda^b) = 2\,\delta^{ab}$

We note that $\sum_a G^a_{\mu\nu}G^{a\mu\nu} = 2\,\mathrm{Tr}(G_{\mu\nu}G^{\mu\nu})$.

Table 7-1: The ABJ axial anomaly with massless fermions. For QCD the trace is over color indices, the index f in N_f is for flavour. For the weak $SU(2)_L$, the anomaly is similar to the QCD version, with the proper components, coupling, field strengths, as listed in Table 7-2. The anomaly is a pure quantum effect: if we abandon natural units ($\hbar = 1$), the formulae must be multiplied by $\hbar$.

[160] R. Jackiw, Anomalies and Topology. https://lib-extopc.kek.jp/preprints/PDF/2000/0033/0033239.pdf

[161] M. A. Vazquez-Mozo, Anomalies. http://tp.lc.ehu.es/TAE/lectures/lecture4.pdf

[162] This is a shortcut: one could preserve the conservation of the axial current at the cost of violating the vector current conservation.

The anomaly was discovered in the early 1970s in an attempt to explain the observed decay rate of the neutral pion to a pair of photons. See Chapter 27.

In four dimensions and for massless fermions, the axial charge changes if we turn on both a magnetic field **B** and an electric field **E** lying in the same direction [163].

$$\dot{\rho}_A = \frac{eB}{2\pi}\frac{eE}{\pi} = \frac{e^2}{2\pi^2}\vec{E}\cdot\vec{B}\,.$$

This formula is equivalent to the ABJ anomaly of Table 7-1.

Is an anomaly bad? For a **global symmetry**, not necessarily (Section 7.4.3). For a **local symmetry**, yes, it corresponds to the loss of unitarity and of renormalizability. In Section 7.4.2 we will check that the EW SM is indeed free of anomalies.

Then **topology comes in!**

Another aspect, which does not happen in the 4-dimensional Abelian Maxwell theory, is the following. Quoting again Roman Jackiw [164]: *"Physical states are invariant against infinitesimal gauge transformations. Finite gauge transformations, which can be obtained by iterating infinitesimal ones, will also leave the states invariant. However, in a non-Abelian gauge theory, there are gauge transformations which cannot be implemented by such an iteration.*
All non-Abelian gauge transformations, for compact, simple Lie groups, can be categorized by equivalence classes labelled by the integers, called ***winding numbers****".*

A hint of the aspect of this topological problem will be given in Section 7.4.5.

As a consequence, a non-Abelian pure gauge theory in four dimensions possesses, after quantization, a hidden P and T violating parameter, **the vacuum angle θ**, which can be moved to the Lagrangian as a **topological term**, affecting physical quantities, such as energy eigenvalues. One could think of choosing θ = 0. However, as we will see in Section 14.6, fermions and the associated anomaly phenomenon **induce their own non-zero angle**, even if the Yang–Mills theory does not possess one. Such a term is P and T or CP violating. But strong interactions show no evidence of CP violation. **How can two independent effects cancel is the strong CP problem.**

In the Yang–Mills theory, a zero-energy solution will be found if the field strength is **self-dual**. Such solutions, called **instantons or pseudoparticles**, do exist. Progressively, it became clear that the structure of the anomaly could be described, in math language, with bundles with a non-trivial homotopy group [165] or, in physics language, in terms of instantons that we will meet again in Chapter 24.

A brief interrupt: since we are meeting some formulae and equations, let us recap in Table 7-2 the ingredients they contain. For more explanations see Chapter 2 of the excellent Ref. [166].

7.4.2 What about anomalies in the SM?

From the ABJ anomaly we can deduce the type of anomalies that occur in a **chiral gauge theory**, where the gauge field couples to the LH component of the fermions differently from the RH ones.

---

[163] In non-relativistic terms $\epsilon^{\alpha\nu\beta\mu}F_{\alpha\nu}F_{\beta\mu} = 8\vec{E}\cdot\vec{B}$, pseudoscalar CP-odd.

[164] R. Jackiw, Anomalies and Topology. https://lib-extopc.kek.jp/preprints/PDF/2000/0033/0033239.pdf

[165] Gauge theory (mathematics): https://en.wikipedia.org/wiki/Gauge_theory_(mathematics) . Reading can be limited to the Table giving the comparison of concepts in mathematical and physical gauge theory.
To relate the traditional to the modern formulation of gauge theory, in particular Maxwell and Yang–Mills equations, a great book is J. Baez and J. P. Muniain, Gauge fields, Knots and Gravity. https://doi.org/10.1142/2324

[166] P. D. Collins, A. D. Martin and E. J. Squires, Particle Physics and Cosmology.
https://onlinelibrary.wiley.com/doi/book/10.1002/3527602828

Appearing in the formulae and equations

— for QED (U(1)) the vector potential A_μ and the field strength tensor $F_{\mu\nu} \equiv \partial_\mu A_\nu - \partial_\nu A_\mu$

— for the weak interaction ($SU(2)_L$) the three independent gauge vector potentials W_μ^k and the field strength tensors $W_{\mu\nu}^i = \partial_\mu W_\nu^i - \partial_\nu W_\mu^i - g\sum_{j,k} \epsilon_{ijk} W_\mu^j W_\nu^k$. Latin index from 1 to 3.

— for QCD ($SU(3)_C$) eight gluon vector potentials $G_\mu^i(x)$ with the gluon field strength tensors $G_{\mu\nu}^i = \partial_\mu G_\nu^i - \partial_\nu G_\mu^i - g_s\sum_{j,k} f_{ijk} G_\mu^j G_\nu^k$. f_{ijk} are structure functions. Latin index from 1 to 8.

In the Lagrangian, the term corresponding to gluon interactions is $-\frac{1}{4}\sum_i G_{\mu\nu}^i G^{i\mu\nu}$

The dual of a field strength tensor is $\tilde{F}^{i\mu\nu} = \frac{1}{2}\epsilon^{\mu\nu\alpha\beta}F_{\alpha\beta}^i$.

If $\tilde{F}_{\mu\nu}^i = \pm F_{\mu\nu}^i$ the field strength tensor is called self-dual.

The Lie algebra valued matrix form is $A_\mu \equiv \sum_i A_\mu^i T^i$ with $[T^i, T^j] = \frac{1}{2} f_{ijk} T^k$.

Table 7-2: Some useful formulae.

Chiral gauge anomalies also arise in a non-abelian gauge theory. If the **fermion matter content** consists of LH Weyl fermions [167] in the representation r of the gauge group G, the non-conservation of the gauge current is given by $\partial_\mu j_a^\mu = -\frac{i}{32\pi^2} d_{abc}(r)\epsilon^{\mu\nu\rho\sigma} f_{\mu\nu}^b f_{\rho\sigma}^c$, where the tensor of the representation r is defined by the group factor $d^{abc}(r) := \frac{1}{2}\mathrm{Tr}_r(T^a\{T^b, T^c\})$, where Tr_r is the trace over the representation; a, b, c run from 1 to N^2-1; f is the relevant field strength; the T^i matrices are the generators of the Lie algebra associated with G in the representation r. $\{T^b, T^c\}$ is the anticommutator of its terms.

If this anomaly is present, we have a **breakdown of gauge invariance** which cannot be compromised. Therefore, the net gauge anomaly **must vanish for a theory to be mathematically consistent**.

In the relevant triangle diagrams producing this anomaly (Fig. 7-3), consider a theory in which the fermions are coupled to N gauge fields through the currents

$$J_\mu^a = \bar{\psi}_R \gamma_\mu T_R^a \psi_R + \bar{\psi}_L \gamma_\mu T_L^a \psi_L \text{ , with } a = 1, \ldots, N \text{ ,}$$

in which we allow different matrix representations $T_{R,L}^a$ for RH and LH fermions.

For the theory to be renormalizable, there must be no anomalies arising from the coupling of any three currents (a,b,c) by diagrams like Fig. 7.3. The **condition for cancellation** [168] is that

$$\sum_{\mathrm{Rep}} \mathrm{Tr}\{(T_L^a T_L^b + T_L^b T_L^a)T_L^c - (T_R^a T_R^b + T_R^b T_R^a)T_R^c\} = \mathbf{0} \text{ ,}$$

where the sum is over all fermion representations while the trace sums over all the fermions in each representation. The anticommutators arise from the sum of the uncrossed and crossed diagrams.

Remarkably, given the basics of the Weinberg–Salam EW SM, **this condition is satisfied.** The SM fermion matter content in the loop, whatever be the trio of gauge groups involved at the summits, **cancels all possible gauge anomalies**. There is **no gauge anomaly in the SM**.

For instance, when the three groups are SU(3) this is automatic: QCD is vector-like. However, when all three groups are $U(1)_Y$, the condition to be satisfied **needs imperatively the colour** quantum number

[167] Weyl equation: https://en.wikipedia.org/wiki/Weyl_equation .
See also P. B. Pal, Dirac, Majorana and Weyl fermions. https://arxiv.org/abs/1006.1718

[168] P. D. Collins, A. D. Martin and E. J. Squires, Particle Physics and Cosmology
https://onlinelibrary.wiley.com/doi/book/10.1002/3527602828

of quarks [169] !

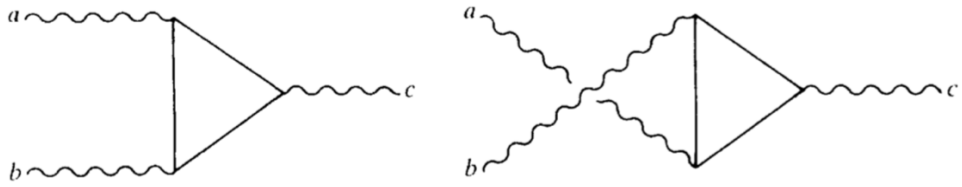


Fig. 7-3: Potentially anomalous couplings of currents a, b and c by a fermion triangle loop [170].

7.4.3 What about global anomalies?

SM **global anomalies** lead to most important effects, as baryonic charge (**B**) and leptonic charge **(L)** non-conservation (Section 32.4) [171].

The classic **EW Lagrangian** conserves **B** since quarks always enter in bilinear combinations, a quark disappearing only in collision with an antiquark as $\partial^\mu J^B_\mu = \sum_j \partial^\mu(\bar{q}_j \gamma_\mu q_j) = 0$ [172].

However, quantum corrections known as the **sphaleron** (see Section 7.4.4 and Chapter 24) destroy this conservation law: instead of zero in the right-hand side of this equation, for $SU(2)_L$ for instance, there is a **non-vanishing quantum term**

$$\partial^\mu J^B_\mu = \frac{N_F\, g^2}{32\pi^2} W^{a\mu\nu}\widetilde{W}^a_{\mu\nu}\,, \quad W^a_{\mu\nu} = \partial_\mu W^a_\nu - \partial_\nu W^a_\mu + g\, f^a_{bc} W^b_\mu W^c_\nu\,, \quad \widetilde{W}^a_{\mu\nu} = \frac{1}{2}\epsilon_{\mu\nu\alpha\beta} W^{\alpha\beta a}$$

with a sum over a implied, a = 1, 2, 3. The U(1) part is omitted. N_F is the number of families.

We will see in Section 7.4.5 that the anomalous current non-conservation is proportional to the total derivative of a vector operator. This is non-vanishing due to **instanton configuration** (see Chapter 24**)** of the gauge field. The **non-conservation of baryonic number** happens in a **tunnelling process from one vacuum to the other.** The definition of a particle is different in the two vacuum states between which the tunnelling occurs; so, a state of no particles in one vacuum corresponds to a state with some particles in the other vacuum.

But the same relation holds for the lepton number current: $\partial^\mu J^B_\mu = \partial^\mu J^L_\mu$.

So, the **global symmetry B − L**, where quarks have **B − L** = 1/3 and leptons have **B − L** = -1, is non-anomalous. This is called the **B – L symmetry** since it counts the number of baryons minus the number of leptons. **It is the only global symmetry of the SM** [173].

We will discuss the **role of anomalies** on several occasions: their role in the **strong CP problem** (Section 14.6), and in the possible solutions to the problem of **baryogenesis** (Sections 24.1.5 and 32.4.2), either **electroweak** or through **leptogenesis**.

---

[169] With the usual notation (SU(3), SU(2), Hypercharge) the SM fermions are ℓ_L = (**1, 2**, −1), e_R = (**1, 1**, −2), q_L = (**3, 2**, 1/3), u_R = ($\bar{\mathbf{3}}$**, 1**, 4/3), d_R = ($\bar{\mathbf{3}}$**, 1**, − 2/3). The $U(1)^3$ anomaly requires that the sum of hypercharges cube $\sum_{\text{left}} Y^3 - \sum_{\text{right}} Y^3 = 0$. Indeed $\text{tr}Y^3 = (-1)^3 \times 2_f - (-2)^3 + (1/3)^3 \times 3_c \times 2_f - (4/3)^3 \times 3_c - (-2/3)^3 \times 3_c = 0$. Important is that the sum of all electric charges inside any family is equal to zero.

[170] Ibid., P. D. Collins et al.

[171] The convention is: for a quark B=1/3, L=0, hence B=1 for a proton, for a lepton as e^- B=0, L=+1, and the opposite for antiparticles.I

[172] The sum over j is a shorthand notation. It implies summing on quark flavour and colour indices.

[173] If it happens to be violated, as B and L are through anomalies, then the only true symmetries of the SM will be gauge symmetries. See E. Witten, Symmetry and emergence. https://arxiv.org/abs/1710.01791

7.4.4 A first encounter of non-perturbative aspects of the SM

The wiki references help introducing the various terms appearing in this sector and just met in previous paragraphs: **soliton, instanton, sphaleron**.

A "**topological soliton**" [174] is a static, stable, finite-energy solution of the classical field equations for real time t ($t^2 \geq 0$).

An **instanton** [175] is a localized, finite-action solution of the classical field equations for imaginary time τ ($\tau^2 \leq 0$). Instantons are **tunnelling solutions between the vacua**. The BPST instanton [176] describes a transition between two different vacua of SU(2) Yang–Mills theory.

The Lagrangian of the EW sector of the SM has a possible nonperturbative solution, which includes a vacuum transition known as a "sphaleron" [177], term met in Section 7.4.3

The sphaleron is the saddle-point at the top of the barrier**.** As stated above, a sphaleron (σφαλερός "slippery") is a static, unstable, finite-energy solution of the classical field equations for real time t. Being unstable it should be distinguished from a soliton.

A sphaleron is a critical piece of **EW baryogenesis theory**, which explains the matter-antimatter asymmetry of the Universe by such processes. Indeed, its crucial feature, which allows such claims, is **the violation of baryon (B) and lepton (L) numbers, while B – L is preserved.**

As we saw in Section 7.4.3**, sphalerons are related to anomalies.** If one defines the **axial charge** as the integral of the usual anomalous term, then the integrated anomaly equation tells us that the change in the charge is an **integer number** [178] ΔQ_A

$$\Delta Q_A = Q_A|_{t=+\infty} - Q_A|_{t=-\infty} = \int d^4x \, \frac{e^2}{16\pi^2} \epsilon^{\mu\nu\rho\sigma} F_{\mu\nu} F_{\rho\sigma}$$

The left-hand side is an integer because of **quantum mechanics**. The right-hand side is an integer because of **topology**. The anomaly equation relates these two ideas.

For instance, mappings from the 3-sphere S_3 to the gauge group $SU(2)_L$, which has the **topology of a sphere**, are classified by an **integer winding number** or topological charge, counting the number of times SU(2) can be wrapped around S_3.

The value of the Higgs mass allowed to determine the EW couplings, giving an estimate of the energy required for the sphaleron transitions: $\mathbf{E_{sph} \approx 9\ TeV.}$ In Section 24.1.6 we will present **a search for such a sphaleron at the LHC.**

7.4.5 A bit more on topology

Let us come back [179] to the topological problem quoted in sentences in Section 7.4.1. It is clear from Table 7-1 that the **axial current is not conserved**. However, one can rewrite the anomaly in $SU(3)_C$ as a total divergence: $N_f \frac{g_S^2}{8\pi^2} \mathrm{Tr}\left(G_{\mu\nu}\tilde{G}^{\mu\nu}\right) = \partial_\mu K^\mu$, with $K^\mu = N_f \frac{g_S^2}{4\pi^2} \epsilon^{\mu\nu\varrho\sigma} \mathrm{Tr}(A_\nu \partial_\rho A_\sigma + \frac{2}{3} i g_s A_\nu A_\rho A_\sigma)$

[174] Soliton: https://en.wikipedia.org/wiki/Soliton
[175] Instanton: https://en.wikipedia.org/wiki/Instanton
[176] A. A. Belavin, A. M. Polyakov, A. S. Schwartz and Y. S. Tyuplin, *Phys. Lett. B 59 (1975) 85.*
BPST instanton: https://en.wikipedia.org/wiki/BPST_instanton
[177] Sphaleron: https://en.wikipedia.org/wiki/Sphaleron
F. R. Klinkhamer, Sphalerons and anomalies (an introduction).
https://www.itp.kit.edu/_media/research/korea-snu-sphalerons-14oct2015-v3.pdf
[178] It is linked to the Chern–Simons number that we shall meet in Section 24.1.5 and to the winding number of a gauge transformation introduced in words in Section 7.4.1.
[179] See Chapter 5 of P. D. B. Collins, A. D. Martin, E. J. Squires, Particle Physics and Cosmology.
A. Riotto, Theories of Baryogenesis. https://arxiv.org/abs/hep-ph/9807454

with the gluon fields expressed as $A_\mu = \frac{\lambda^a}{2} G^a_\mu$, and define a new conserved current $\hat{J}^\mu_5 \equiv J^\mu_5 + K^\mu$ with $\partial_\mu \hat{J}^\mu_5 = 0$, K^μ being not gauge-invariant.

Trying to deduce conservation of the **axial "charge"**, $\int \hat{J}^0_5 \, d^3x$, one meets a problem when trying to **discard its surface integral**. Usually, one can do this because the fields are assumed to be zero as $|x| \to \infty$ [180]. It is certainly essential that the **energy density should go to zero** as $|x| \to \infty$, but one can show that it only requires that, under a gauge transformation U, A^μ can be transformed to $A^\mu = 0$, i.e. that $A_\mu \to -\frac{i}{g} U^{-1} \partial_\mu U, \text{when } |x| \to \infty$, and becomes a **"pure gauge" configuration**. For such potentials, K^μ is in general not zero.

The problem is the following: although one can always **gauge away such potential locally**, there are situations in which, although the field behaves as a pure gauge over some closed boundary, it is **topologically nontrivial** and cannot be gauged away throughout all space by a (differentiable) gauge transformation.

If one works in a Euclidean space, whose surface is a large three-sphere, S_3, centred on the origin, U is then **a mapping of S_3 into the QCD gauge group SU(3).** One could try to transform U away by another gauge transformation U' (equal to U at infinity), but in fact this is not always possible because U is too **twisted up**. **Here topology enters the game!**

If this U at infinity cannot be continuously deformed into such a U', then one says that U and U' belong to **different "homotopy classes".** Two mappings (of one topological space into another) that can be continuously deformed into each other are said to belong to the same homotopy class. Different homotopy classes are characterized by different values of the **topological "winding" number** of S_3 onto the group space.

It may help to think of the map from the **unit circle S_1 onto U(1)**, which can involve n extra turns. Here the U are SU(3) matrices, so n is a property of the map from the surface S_3 onto SU(3). The **integer n** gives the number of times we go round the gauge group as we cover the three-sphere S_3. Thus, n is defined by the global characteristics of the field and for this reason it is called the **"topological charge".**

$$2\mathbf{n}N_f = -\int K^\mu dS_\mu = -\int \partial_\mu K^\mu d^4x = -\frac{N_f g_S^2}{8\pi^2} \int \mathrm{Tr}(G_{\mu\nu}\tilde{G}^{\mu\nu})\, \partial^4 x$$

The similarity of the integrand with the integrand of the **change in axial charge ΔQ_A** in Section 7.4.4 shows that the integer topological charge n describes the main physics.

In a field theory, the state of a system at a given time is specified by the field strengths over all of space, i.e., on a given 3-surface. Hence, **each vacuum state is associated with a topological quantum number** that gives the mapping of the S_3 surface into the gauge group.

Thus, the theory has an **infinity of degenerate vacuum** states $|n>$, labelled by their topological quantum number and **quantum tunnelling** can occur between them. The fields that interpolate between the pure-gauge fields at ±t are called **instantons.**

If, instead of using this complicated θ-vacuum, we insist on using a single vacuum state, we must add an extra term to the QCD Lagrangian $L_\vartheta = -n\theta = \theta \frac{g_S^2}{16\pi^2} \mathrm{Tr}(G_{\mu\nu}\tilde{G}^{\mu\nu})$. Here comes the $\boldsymbol{\theta}$ **term** considered in words in Section 7.4.1 and appears **the strong CP problem**. We will discuss it in Section 14.6 and describe a possible solution in Section 31.3.

[180] In $|x| \to \infty$, ∞ can mean a distance of M_W^{-1}. See later the sphaleron size (Section 24.1.6).

7.5 Intermède 1: a brief introduction to the SM

7.5.1 Local invariance

Here comes a 2-pages diversion, a retrospective, the SM described briefly in words [181], that experts can skip.

An idea to keep is that, besides existing in space-time, constituents live in other spaces, called "internal". Quarks do so in the colour space. All fermions do so in the weak isospin space. Left-handed fermions (their spin opposite to their momentum) live as couples, or doublets, right-handed ones live as bachelors, or singlets, another odd feature of the SM.
In these spaces one can perform "rotations" (true rotations or unitary transformations), or substitutions of particle species, which leave the physics invariant, for instance changing a red quark to a green quark, or a lepton to its neutrino inside a weak isospin left-handed doublet. These substitutions actually occur by emission or absorption of the corresponding bosons.

The SM is the math description of what was just said in sentences. It rests on two great principles

1. *its formulation is invariant when one interchanges particles, a priori different, as explained above;*
2. *this can only be done in a coherent way if one introduces the required bosons, which will operate the rotations mentioned.*

*This gives to the theory a **local invariance**, namely the freedom to perform, in each point of space-time, arbitrary "rotations". It is the locality of the invariance which gives all its power to the theory. Mathematicians will recognize Yang–Mills theories.*

*Unfortunately, this beautiful construction applies only to **massless particles**, which is not our world, and this delayed the advent of the SM for a while.*

But there is a happy end to the story …

7.5.2 The Brout–Englert–Higgs mechanism in brief

*Indeed, something in nature may **refuses this freedom** of performing arbitrarily such "rotations".*

*Inside a superconductor, the **field of Cooper pairs**, bosons acting coherently over macroscopic distances, forbids the freedom of rotating the phase of the wave function of an electron arbitrarily in each point. By interacting with this field, the photon gets a mass m. It is **the Meissner effect**. The magnetic field penetrates the superconductor only over a distance 1/m [182].*
*The BEH mechanism mimics such a situation, with however big differences. A field acting in the weak isospin space gives an orientation and suppresses the freedom to rotate arbitrarily in this space. The weak bosons then get a mass, e.g. $m_w = ½\ g\ v$, where v is the **"vacuum expectation"** of the Higgs field (246 GeV) and g is one of the two gauge couplings.*

*The BEH field is a complex doublet (4 components) in weak isospace. Spontaneous symmetry breaking is crucial. The resulting Nambu–Goldstone bosons are "eaten" by the gauge bosons W and Z and become their longitudinal modes (3 components). One component is left, a Lorentz scalar**, the BEH boson.** The **"how"** of the BEH mechanism in the SM is the following. The energy added by the Higgs field is $E = \mu^2\phi^2 + \lambda\phi^4$. With λ (quartic coupling) > 0 and μ^2 chosen negative, quite arbitrarily, one gets*

---

[181] D. Treille, Pourquoi les particules ont-elles une masse ? https://videos.cern.ch/record/1067493
For an elementary introduction: Technology Meets Research.
https://inspirehep.net/files/02de568d4897c555515de27f0b96af4d , p. 207

[182] L. Dixon, From Superconductors to Supercolliders.
https://indico.cern.ch/event/591196/contributions/2493992/attachments/1431464/2199061/higgs-supraleiter-dixon.pdf

the "mexican hat" potential, ensuring that the minimal energy is obtained for $\phi \neq 0$. The boson mass is ≈ v √λ, therefore unknown, as is λ (until the discovery!). It is only required to be neither too heavy, to avoid for instance a Landau singularity (i.e. the coupling becoming infinite), nor too light, as we will see later.

*However, **Supersymmetry (SUSY**) tells more about the **"why"** of the BEH mechanism. One can choose a normal potential, with $\mu^2 > 0$, at very high energy, and the evolution makes it "mexican" at the EW scale, provided that the **top quark**, dominating the evolution, is **heavy enough**, which is indeed the case.*

*The SUSY Higgs sector is more complicated. But the "smoking gun" is that in its minimal version one neutral boson at least must be **lighter than about 130 GeV**, a fact known since about 1991* (Chapter 17).

The exact nature of the electroweak phase transition (which order?) is an important question, since some authors associate a first order transition to the possibility of electroweak baryogenesis (Chapter 24).

7.5.3 Electroweak symmetry breaking: the BEH boson and some pre-discovery thoughts

*This brings us to our third and longer stop: the time of electroweak symmetry breaking and the Brout–Englert–Higgs (BEH) boson, the "goddamn" particle that became "God's particle" (*see also Section 10.13)!

It is the simplest version of the origin of mass, although one can imagine other mechanisms, as Technicolor, now disfavoured by experiment.

The boson gives to elementary particles a mass more or less heavy by interacting more or less with them (Section 7.9). We will come back in Chapter 19 to the case of neutrinos, massless in the SM, not in reality.

*Let us note also that this has almost nothing to do with our mass, nor the mass of the Universe, as seen in Chapter 5. We weight the mass of our nucleons, which, by far, do not weight the mass of their constituents, gluons, massless, and u and d quarks, nearly so (few MeV), but their **"dance".***

*While, before the discovery, the mass of the SM BEH was undetermined, within the limits described (see Chapter 16), one knew everything else about it. In brief, the boson couples to the **heaviest states available**. This is the case for its decay modes, as well as for its production. However, the dominant production mode, through gluon-gluon fusion, as well as its decay mode into a pair of photons, seems to contradict that statement. It is nevertheless true, since the boson communicates with these massless particles through **a loop of virtual heavy particles** involving the top quark and the vector bosons (and eventually other non-SM particles if we go beyond the SM). It is thus remarkable that, as we shall see in Chapter 24, the boson will have been discovered **purely through quantum effects.***

*Knowing the production cross-section and branching ratios of the SM boson, as well as the SM backgrounds, one could then, as a function of its mass and the integrated luminosity at LHC, anticipate what would be the significance of its observation. The **p-factor**, more precisely its local value, is defined as the probability that a similar or more extreme effect would be seen when the signal does not exist. **In 2012 ATLAS and CMS discovered a 125 GeV object**. See Chapter 24.*

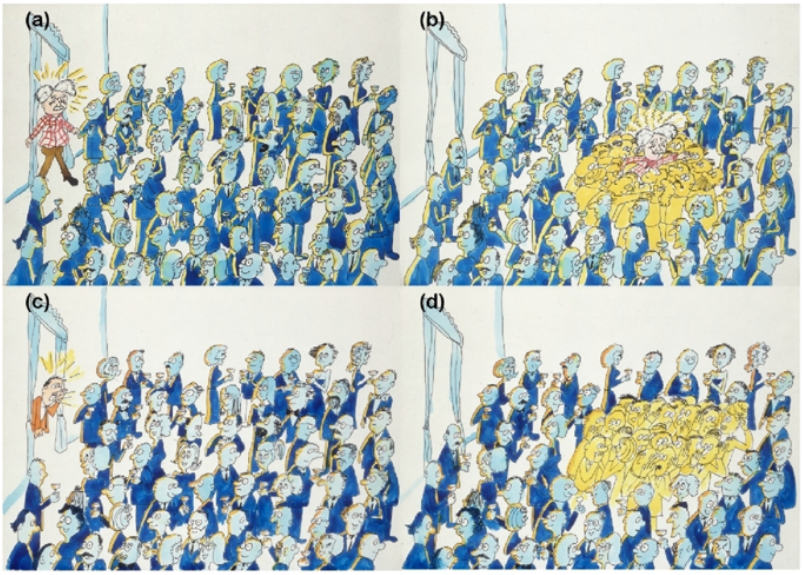
*The mass of 125 GeV found for what could be the SM BEH boson is particularly interesting. For too light a mass of the boson, the Higgs potential would not be bounded from below or would develop at a higher scale a minimum lower than the electroweak one, leading to the **instability, or metastability, of the vacuum**. With the known top mass and α_S the instability mass limit is estimated to be 127 GeV, with a few GeV uncertainty due to the uncertainties on these two quantities (see Chapter 24).*

Some authors, on the basis of arguments concerning the behaviour of the Higgs quartic coupling at high scale, have actually predicted that the SM boson mass would be found close to this limit, which was indeed the case. These authors also consider that the SM is valid up to arbitrary high scale, with no need for new physics (see Chapter 24 for precisions). This domain of mass is however also ***the region imposed by the MSSM*** *(Minimal SUSY SM) whose quest goes on.*

7.6 Intermède 2: the Higgs mechanism, analogies

Trying to give to the public (and to ourselves) an idea of what are the Higgs field and Higgs boson has led to a few metaphoric attempts, as "the celebrity in a crowd" (Fig. 7-4) or "walking in melasse". These are brave attempts … Let us also explore other possible analogies in more focused contexts.

7.6.1 The crowd analogy



	Crowd (simple)	Crowd (complex)	Medium (F–B)	Medium (B–F)
Particle	Celebrity	Celebrity	Various	Various
Higgs boson	Member of crowd	Cluster of crowd	Element of field	Excit. of field
Higgs field	Crowd	Crowd	Fluid	Fluid
Higgs mech.	Crowd/drag	Crowd	Drag	Drag

Politics	Model of conductivity	Higgs model
Crowd	Lattice of ions	Higgs field
Margaret Thatcher	Electron	W, Z bosons
Knot of people surrounding Thatcher	Effective mass of electron	Mass of W, Z bosons
Rumor-carrying cluster	Phonon	Higgs boson

Fig. 7-4: The crowd analogy (top) [183], and list of analogy features (middle and bottom).

[183] S. Alsop and S. Beale, Molasses or crowds: making sense of the Higgs boson with two popular analogies. *2013 Phys. Educ. 48 670,* https://iopscience.iop.org/article/10.1088/0031-9120/48/5/670/pdf
Higgs Without Molasses. https://woosterphysicists.scotblogs.wooster.edu/2020/03/29/higgs-without-molasses/

7.6.2 Higgs-elementary particle interaction

Figure 7-5 [184] visualizes the (Higgs-elementary particle) interaction. This cartoon introduces a heavy Majorana ν of brief existence 1/M, which gives the neutrino its average mass m^2/M (Chapter 19).
Explanation of Fig. 7-5: *"(a) According to the Higgs mechanism in the Standard Model, particles in the vacuum acquire mass as they collide with the Higgs boson. Photons (γ) are massless because they do not interact with the Higgs boson. All particles, including electrons (e), muons (μ) and top quarks (t), change handedness when they collide with the Higgs boson; left-handed particles become right-handed and vice versa. Experiments have shown that neutrinos (ν) are always left-handed. Since right-handed neutrinos do not exist in the Standard Model, the theory predicts that neutrinos can never acquire mass. (b) In one extension to the Standard Model, left- and right-handed neutrinos exist. These Dirac neutrinos acquire mass via the Higgs mechanism, but right-handed neutrinos interact much more weakly than any other particles. (c) According to another extension of the Standard Model, extremely heavy right-handed neutrinos are created for a brief moment before they collide with the Higgs boson to produce light left-handed Majorana neutrinos*."

The collision Higgs-particle is best seen in the "heavy wall" system, where the incoming and outgoing momenta of the particle are opposite. Since colliding with a scalar cannot change the spin, the particle handedness can only change, and the particle, able to have both handedness and to be overtaken by a faster observer, is thus massive.

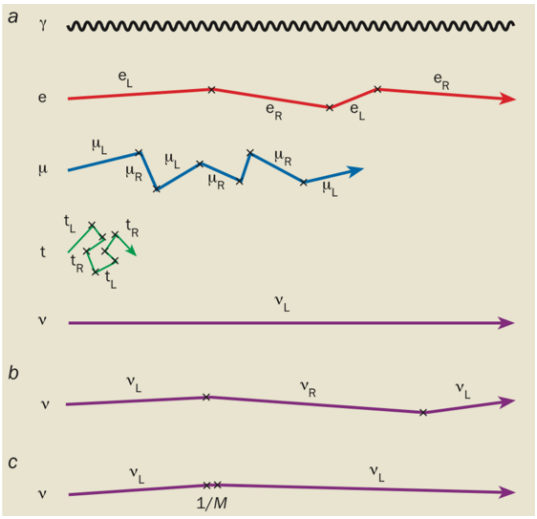


Fig. 7-5: Higgs-elementary particle interaction. See explanation in the text.

7.6.3 Superconductivity

Figure 7-6 illustrates the analogy of the Higgs mechanism and superconductivity (SC).

Explanation: "There are two important length scales in a superconductor. The first measures how efficiently the condensate expels a magnetic field. In fact, the expulsion is not quite complete. There is a thin layer of depth λ, called the London ***penetration depth****, over which the magnetic field drops exponentially to zero. The value for λ depends on the material, but a tenth of a micron is typical. In this same region, the magnetic field perturbs and reduces the condensate. The second length scale, called the* ***coherence length*** *ξ, governs how fast the condensate snaps back to its bulk value once the*

[184] H. Murayama, Implications of Neutrino Mass. http://sandman.berkeley.edu/neutrino/PhysicsWorld.pdf
H. Murayama, The origin of neutrino mass. http://hitoshi.berkeley.edu/neutrino/PhysicsWorld.pdf

magnetic field has gone to zero. Depending on the material, the coherence length can be either longer or shorter than the magnetic field penetration length; these two classes of superconductors (known as type I and type II) turn out to have quite different magnetic properties. In any case, it is this response of the condensate to a local disturbance that is the superconductor analogue of the Higgs particle.

The length scales λ and ξ, reinterpreted in EW context become the $\lambda_{Compton}$ or inverse masses of the W boson (λ) and of the Higgs boson (ξ)."

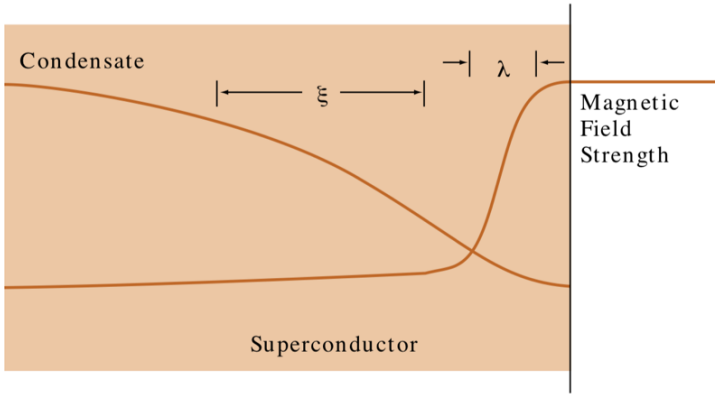


Fig. 7.6: The Higgs mechanism and superconductivity [185].

These **analogies with condensed matter physics** come from models of superconductivity that inspired the introduction of **spontaneous symmetry breaking** (SSB) into PP in the early 1960s. Reference [186] made an analysis of the analogies between the EW Higgs model and the Ginsburg–Landau (GL) and Bardeen–Cooper–Schrieffer (BCS) models of superconductivity, respectively (Table 7-3). This analysis concludes that both sets of analogies are purely formal and accompanied by **substantial physical differences**: analogies to models of SC cannot supply the basis for the physical interpretation of EW SSB. Nevertheless, contrasting the physical interpretations of SSB in SC and the Higgs model helps to clarify some basic issues. The distinction between the phenomenological GL model and the dynamical BCS model is not transposable to EW models. *"The development of the Higgs model illustrates how purely formal analogies can play a fruitful heuristic role in physics".*

7.6.4 An identity crisis

Figure 7-7 [187] evokes a particle "with an identity crisis".
"Consider the direction of the spin of the electron. In (a), whether it is left or right handed depends on the direction of the spin relative to the direction of motion. So, the two blue lines describe left handed massless electrons since the direction of spin is opposite to the direction of motion. In (b) we see a massive electron. Some of the time it behaves as a right-handed electron and sometimes as a left-handed electron. ***It switches from one to the other thanks to the Higgs field.*** *Going sometimes backward it progresses slower than light."*

[185] L. Dixon, From Superconductors to Supercolliders.
https://indico.cern.ch/event/591196/contributions/2493992/attachments/1431464/2199061/higgs-supraleiter-dixon.pdf
D. Fraser and A. Koberinski, The Higgs mechanism and superconductivity: A case study of formal analogies.
https://www.sciencedirect.com/science/article/abs/pii/S1355219816300739
[186] ibid
[187] J. Maldacena, The symmetry and simplicity of the laws of physics and the Higgs boson. https://arxiv.org/abs/1410.6753

Superconductor models	Higgs model
$U(1)$ broken (global) gauge symmetry group	$SU(2) \times U(1)$ broken (local) gauge symmetry group
(limited-range) photon with effective mass (two transverse components)	massive W, Z bosons
plasmon with massive longitudinal component	massive Higgs boson
no analogue	massless photon

Table 2: Analogies between the GL model and the Higgs model

GL model	Higgs model
free energy density of superconducting state $\mathcal{F}_s$	Lagrangian $\mathcal{L}$
$a\|\psi(\mathbf{x})\|^2 + \frac{b}{2}\|\psi(\mathbf{x})\|^4$	$V_H = \mu^2\|\phi(x)\|^2 + \lambda\|\phi(x)\|^4$
collective wave function for superconducting electrons $\psi(\mathbf{x})$ as the order parameter	scalar particle field $\phi(x)$ as the order parameter
T	*no analogue*

Table 3: Analogies between the BCS model and the Higgs model

BCS model	Higgs model
energy gap Δ as the order parameter	vacuum energy $\langle 0\|\,\phi\,\|0\rangle$ as the order parameter
composite Cooper pairs	*no analogue*
T	*no analogue*
Anderson-Bogoliubov collective mode	Higgs boson
no analogue	Higgs field

Table 7-3: Analogies between superconductor models and the Higgs mode [188].

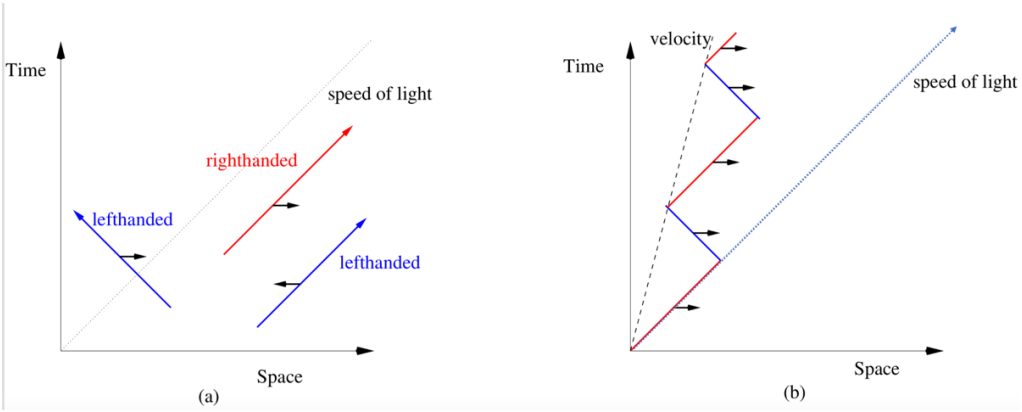


Fig. 7-7: A particle "with an identity crisis". See text for explanations.

7.6.5 The "added mass effect"

In the Higgs mechanism, the weak force mediators get masses by interacting with the Higgs condensate, leading to a **vector boson mass matrix**. On the other hand, a rigid body accelerated through a low or zero viscosity, incompressible and irrotational fluid feels an opposing force linearly related to its acceleration, via **an added-mass tensor** [189]. The reference uncovers a physical analogy between the two effects and offers a dictionary relating them. The correspondence turns the **gauge Lie algebra into the space of directions** in which the body can move, encodes the pattern of gauge symmetry breaking in the shape of an associated body and relates symmetries of the body to those of the scalar vacuum manifold (Table 7-4). The correspondence raises interesting questions, notably on

[188] D. Fraser and A. Koberinski, The Higgs mechanism and superconductivity: A case study of formal analogies. https://core.ac.uk/reader/78374190

[189] G. S. Krishnaswami and S. S. Phatak, Higgs Mechanism and the Added-Mass Effect. https://arxiv.org/abs/1407.2689

the fluid analogy of the broken symmetry and Higgs particle, and the field-theoretic analogue of the **added mass of a composite body** [190].

Higgs Mechanism	**Added-Mass Effect**
Gauge bosons (e.g. photons, $W^{\pm}, Z^0$ bosons)	Rigid body
Higgs scalar field	Fluid
Number of gauge bosons	Dimension of space in which fluid flows
Strength of Higgs condensate (vev)	Constant density of fluid
Direction in linear space spanned by gauge bosons	Direction of acceleration of rigid body
Gauge boson mass matrix M_{ab}	Added mass tensor μ_{ij} of rigid body
System of gauge bosons with equal masses	Spherical rigid body
System of $W^{\pm}$ and Z^0 gauge bosons with $m_{W^{\pm}} < m_Z$	Ellipsoid of revolution with semi-axes $r_1 = r_2 > r_3$
Massless photon	Zero added mass for acceleration along thin, flat direction of body
Pair of equally massive gauge bosons and a photon	Hollow right circular cylindrical shell
Spontaneous breaking of gauge symmetry on interaction with Higgs field	Breaking of fore-aft pressure symmetry when sphere is accelerated
Goldstone mode	'Benign' flow around body moving uniformly through inviscid fluid
Higgs boson – longest wavelength mode of Higgs scalar field	A long-wavelength fluid mode around an accelerated body
Quantum fluctuations around constant strength of Higgs condensate	Compressional waves in otherwise constant density flow
Semi-classical loop expansion in powers of $\hbar$	Expansion in powers of Mach number describing effects of compressibility

Table 7-4: The Higgs and added-mass correspondence.

7.6.6 A math amusement

In Table 7-5 [191] one sees that, because of the simple interaction between the S and Z fields with strength y, a non-zero equilibrium value S_0 for the S field gives the Z quantum a mass proportional both to y and to S_0. **The S field's non-zero value has given mass to the particle of the Z field** [192]**!**

Another argument [193], asking, for symmetry reason, that energy should always be expressed as **a product, either of a potential and a charge or of two fields**, as in electromagnetism, leads to introduce naturally the Higgs field.

7.6.7 Mass without mass

Let us finally recall a basic fact, already noted in Chapter 5 [194], concerning the proton mass, hence our and the Universe visible mass, which at about 99 % has no relation with the Higgs mechanism.

Figure 7-8 tells that the proton mass comes not from the mass of its constituents, but from their kinetic energy. A consequence already quoted is that, from the point of view of the origin of mass, p and $\bar{p}$ are nearly identical, and, submitted to gravity, they should essentially behave the same. Such

[190] G. S. Krishnaswami and S. S. Phatak, ibid and https://www.ias.ac.in/article/fulltext/reso/025/02/0191-0213
[191] G. Organtini, Unveiling the Higgs mechanism to students. https://arxiv.org/abs/1207.2146
[192] M. Strassler, The Basic Idea.
https://profmattstrassler.com/articles-and-posts/particle-physics-basics/how-the-higgs-field-works-with-math/1-the-basic-idea/
[193] G. Organtini, Unveiling the Higgs mechanism to students. https://arxiv.org/abs/1207.2146
[194] F. Wilczek, Origins of Mass. https://arxiv.org/abs/1206.7114

experiments must a priori be high accuracy ones to have a chance to detect a difference between matter and antimatter. Figure 7.8 illustrates the differences between mass and kinetic energy of an atom, a nucleus and a proton.

Consider a field Z (x,t) with equation of motion

- $d^2Z/dt^2 - c^2\, d^2Z/dx^2 = -(2\pi c^2/h)^2\ m^2 (Z-Z_0)$
- $m = h\, \nu_{min} / c^2$

ν_{min} is the minimum frequency allowed for waves in this field

Consider two fields, S massive, Z massless, with equilibrium values at 0

- $d^2S/dt^2 - c^2\, d^2S/dx^2 = -(2\pi c^2/h)^2\, m_S^2\, S$
- $d^2Z/dt^2 - c^2\, d^2Z/dx^2 = 0$

Add additional terms (different) where y is a number (0 to 1) called ***Yukawa parameter***

- $d^2S/dt^2 - c^2\, d^2S/dx^2 = -(2\pi c^2/h)^2\, (m_S^2\, S + y^2\, S\, Z^2)$
- $d^2Z/dt^2 - c^2\, d^2Z/dx^2 = -(2\pi c^2/h)^2\ y^2\, S^2\, Z$

Assume deviations from equilibrium very small
Keep $Z_0 = 0$, but not S_0, Z(x,t) stay very small, not S(x,t)

- $d^2S/dt^2 - c^2\, d^2S/dx^2 = -(2\pi c^2/h)^2\, (m_S^2\, [S - S_0] + y^2\, S\ Z^2)$
- $d^2Z/dt^2 - c^2\, d^2Z/dx^2 = -(2\pi c^2/h)^2\, y^2\, S^2\, Z$

Let s(x,t) be the variation of S, with s(x,t) very small

- $S(x,t) = S_0 + s(x,t)$
- $d^2s/dt^2 - c^2\, d^2s/dx^2 = -(2\pi c^2/h)^2\, (m_S^2\, s + y^2\, [S_0+s]\ Z^2)$
- $d^2Z/dt^2 - c^2\, d^2Z/dx^2 = -(2\pi c^2/h)^2\, y^2\, [S_0+s]^2\, Z$
  $= -(2\pi c^2/h)^2\, y^2\, (S_0^2 + 2\, sS_0+s^2)\, Z$

Drop products of two or more small fields

- $d^2s/dt^2 - c^2\, d^2s/dx^2 = -(2\pi c^2/h)^2\, m_S^2\, s + \ldots$
- $d^2Z/dt^2 - c^2\, d^2Z/dx^2 = -(2\pi c^2/h)^2\, y^2\, S_0^2\, Z + \ldots$

Consequently ***the quanta of Z field now have a mass***

- $m_Z = y\, S_0$

Table 7-5: How the quanta of a massless field get mass.

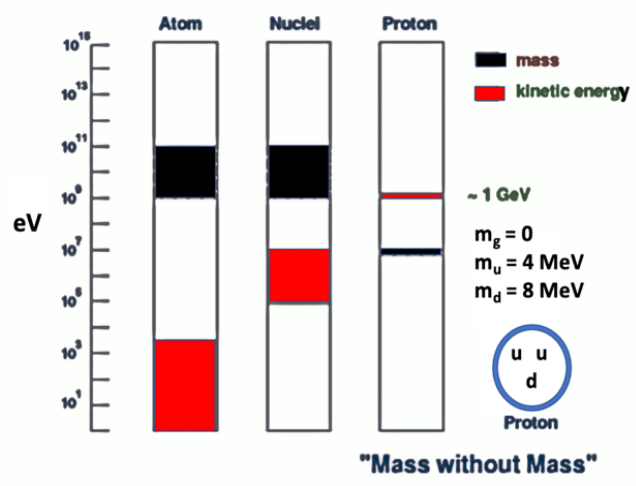


Fig. 7-8: Mass and kinetic energy from atom to proton.

The intermèdes are over and we resume the course of the presentation.

8. The GIM mechanism

8.1 Origin of the mechanism

At the beginning of the 1960s, the weak interaction was described by the Fermi theory reduced to the form V minus A **(V−A)** and a product of currents, in which only current vector V and axial vector A intervened [195]. The electron-muon universality of the weak interaction, similar to that of electric charge, seemed established. However, it was observed that the semi-leptonic decay of strange particles was suppressed compared to the nuclear beta decay, as if their Fermi constant, e.g. that of the baryon Λ, was smaller by a factor of 4 to 5. One then expected an identical suppression concerning for example the decay of the K_S, which was not the case [196].

Nicola Cabibbo had then proposed a modified expression for the weak leptonic and hadronic currents. In the modern version where flavour singlet quarks and gluons are the fundamental particles, the beta decays of leptons and hadrons boil down to d $\rightarrow$ u, s $\rightarrow$ u transitions and the weak Cabibbo current has the form $J_\lambda = \bar{u}\,\gamma_\lambda\,(1-\gamma_5)\,d'$, where $d' = d\cos\theta_C + \sin\theta_C$.

The Cabibbo angle, θ_C, is the mixing angle expressing the weakly interacting bottom quark, d', in terms of the eigenstates of mass d and s. We can also say that in SU(3) space this angle determines the orientation of the weak SU(2) group with respect to the strong SU(2) group. About a possible slight "Cabibbo anomaly" presently considered, see Chapter 14 and Ref. [197].

Cabibbo's theory thus extended to weak decays the idea of universality introduced by Fermi. It was a crucial development, indicating the correct way to include lepton-hadron universality, and a success in phenomenology. The Cabibbo angle, the new constant of nature, is $\theta_c = 0.22650 \pm 0.00048$ radian.

Cabibbo's contribution was generalized when the third family appeared (see Chapter 14). Let us first describe how the second family was completed.

The weak Fermi interaction was described by the product of weak currents, themselves made of universal parts, lepton and hadronic contributions. But its ultraviolet divergence suggested that it was only the effective expression of a less divergent and possibly renormalizable theory, which would be described later.

The simplest possibility, the hypothesis of an intermediate vector boson, IVB, was to admit that the current-current interaction was transmitted by such a massive and charged vector boson, the W. But then the calculation of amplitudes with exchange of two bosons like that of the $K^0 \rightarrow \overline{K^0}$ transition (Fig. 8-1) is divergent and must be regulated by an ultraviolet cut-off Λ.

In 1969 many weak interaction amplitudes could be calculated with precision in this 3-quark model (u, d and s) and their coupling by the Fermi constant and including the Cabibbo angle. However, there was a major exception and a mystery: the suppression of neutral currents with a change in strangeness.

The problem arose about processes like $K_L \rightarrow \mu^+\mu^-$ and the $K^0 \rightarrow \overline{K^0}$ mixture, whose one-loop amplitude was of order $G \sin\theta_C \cos\theta_C\,(G\,\Lambda^2)$ where G is the Fermi constant, Λ a UV cut-off and $G\Lambda^2$,

---

[195] R. P. Feynman, Proc. of "Neutrino-1974", U. of Pennsylvania, p. 300: *"We have a conventional theory of weak interactions invented by Marshak and Sudarshan, published by Feynman and Gell-Mann and completed by Cabibbo - I call it the conventional theory of weak interactions - the one which is described as the V-A theory."*
See also E. C. G. Sudarshan and R. E. Marshak, Origin of the Universal V-A theory.
https://pubs.aip.org/aip/acp/article/300/1/110/765193/Origin-of-the-Universal-V-A-theory

[196] Kaon: https://en.wikipedia.org/wiki/Kaon

[197] E. Passemar, Cabibbo Anomaly and Universality Tests.
https://indico.in2p3.fr/event/29681/contributions/122506/attachments/76502/111031/03-EPassemar-v1.pdf

dimensionless, the first term of a higher-order expansion. However, the limits at that time required a very low cut-off of the order of 2–3 GeV [198], whereas one could expect $\Lambda = G^{-1/2} \sim 300$ GeV.

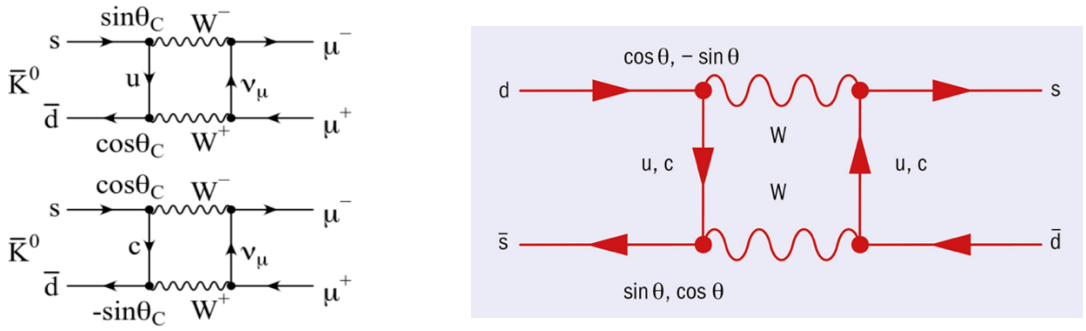


Fig. 8-1: Left: the GIM mechanism. Right: one-loop quark diagrams for the $K^0 \rightarrow \overline{K^0}$ mixing.

Taking this surprising result seriously, Sheldon Glashow, Jean Iliopoulos and Luciano Maiani (GIM) [199] then proposed the introduction of a fourth quark, charm, thus completing the first two families, [(ν_e, e), (u, d)] and [(ν_μ, μ), (c, s)] whose u and c quarks are coupled by the weak interaction with two superpositions of the d and s quarks : u ↔ d', with d' = d $\cos\theta_C$ + s $\sin\theta_C$, and c ↔ s', where s' = −d $\sin\theta_C$ + s $\cos\theta_C$ is the orthogonal combination.

The amplitudes of s → d with u and c on the same fermion line would exactly cancel for $m_c = m_u$. For $m_c >> m_u$, there would remain a residual neutral current effect of order G $\sin\theta_C$ $\cos\theta_C$ (Gmc^2), which links m_c to the previously mentioned cut-off Λ. A detailed study of the processes leads to $m_c \sim 1.5$ GeV.

8.2 Flavour Changing Neutral Current Processes

The GIM mechanism thus explained the suppression of the neutral current process (Chapter 9) which is e.g. the decay $K^0_L \rightarrow \mu^+ \mu^-$, relatively to the charged current process $K^+ \rightarrow \mu^+\nu$.

Flavour Changing Neutral Current Processes (FCNC), such as particle-antiparticle mixing, certain rare and radiative meson decays and CP-violating decays, played an important role in the construction of the SM. The GIM mechanism assures their natural suppression and there are no FCNC processes at the tree level. They result from the one-loop diagrams (Fig. 8-2), penguin [200] and box diagrams, and are most sensitive to contributions from physics beyond the SM. FCNC processes are thus very efficient for the determination of some parameters of the quark mixing matrix (Chapter 14).

Being acquainted with the FCNC, let's anticipate what followed as developments of this theme [201].

An example of FCNC involves the transition from a beauty quark to a strange quark. This process may occur via the same quantum loop transition as the GIM mechanism, but this time dominated by the top quark contribution.

---

[198] This low value was found in 1968 by B. L. Ioffe and E. P. Shabalin. The reference, meaning and impact of their result is described in L. Maiani, The GIM Mechanism: origin, predictions and recent uses. https://arxiv.org/abs/1303.6154

[199] H.-J. He and L. Maiani, 50 years of the GIM mechanism. https://cerncourier.com/a/50-years-of-the-gim-mechanism/, L. Maiani, The GIM Mechanism: origin, predictions and recent uses. https://arxiv.org/abs/1303.6154 https://cerncourier.com/a/50-years-of-the-gim-mechanism/

[200] Penguin diagram: https://en.wikipedia.org/wiki/Penguin_diagram

[201] F. Archilli *et al.,* Flavour-changing neutral currents making and breaking the standard model. *Nature 546, 221–226 (2017).* https://www.nature.com/articles/nature21721
M. Ardu and G. Pezzullo, Introduction to Charged Lepton Flavor Violation. https://doi.org/10.48550/arXiv.2204.08220

At the LHC, especially LHCb, but also ATLAS and CMS, have made precise measurements of FCNC decays of b hadrons. Previously BaBar and Belle at B-factories in the US and Japan, had also done it with fewer b produced but in the cleaner environment of e^+e^- collisions (Chapter 14).

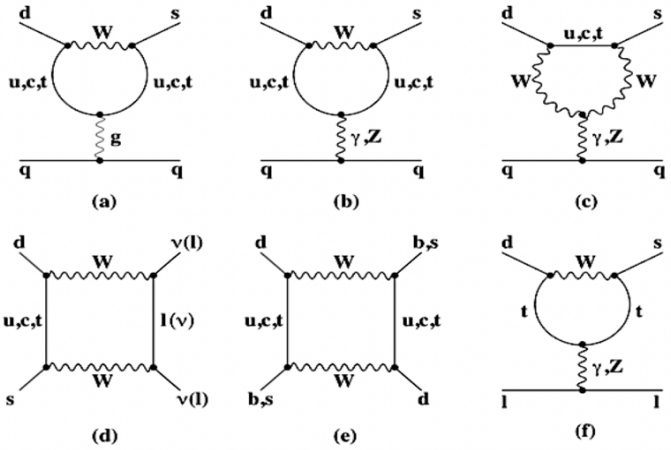


Fig. 8-2: Penguin and box diagrams.

A particularly rare FCNC process is the $B^0_s \rightarrow \mu^+\mu^-$ decay of the hadron made of a b-antiquark and s-quark into a pair of muons (Fig. 8-3). LHC data led to the evidence and study of this process, as well as of $B^0 \rightarrow \mu^+\mu^-$, 30 times rarer decay due to d quarks couple less than s quarks to the top, and still not accessible. Figure 8-4 shows the combined data of CMS and LHCb for Run1 and Fig. 8-5 represents the CMS update with full Run 2 data.

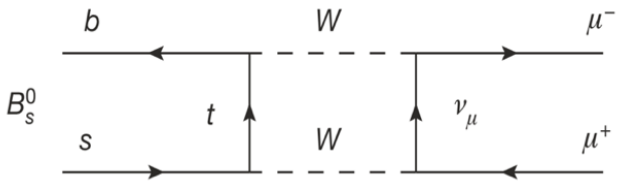


Fig. 8-3: $B^0_s \rightarrow \mu^+\mu^-$.

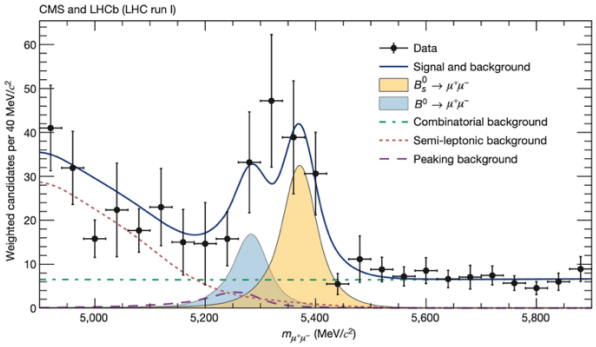


Fig. 8-4: Status of neutral $B^0 \rightarrow \mu^+\mu^-$ decays [202].

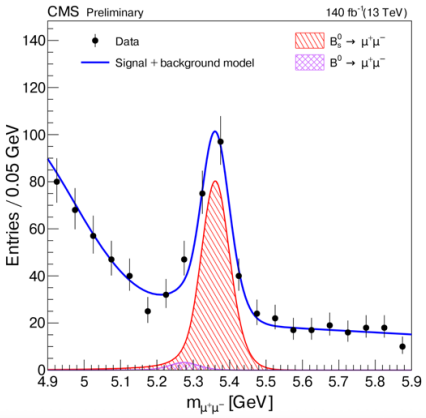


Fig. 8-5: Status of $B^0 \rightarrow \mu^+\mu^-$ in CMS with full Run 2 data [203].

[202] CMS Collaboration and LHCb Collaboration, Observation of the rare $B_s^0 \rightarrow \mu^+\mu^-$ decay from the combined analysis of CMS and LHCb data. *Nature 522, 68–72 (2015)*. https://www.nature.com/articles/nature14474

[203] CMS Collaboration, https://cms.cern/news/new-study-rare-b-meson-decays-two-muons

SM predictions for these modes are accurate, due to the purely lepton character of the final state, which reduces the role of the strong force.

One predicts the following branching ratios BR ($B^0_s \rightarrow \mu\,\mu$) = (3.66 ± 0.23) × 10^{-9} and BR ($B^0 \rightarrow \mu\,\mu$) = (1.06 ± 0.09) × 10^{-10}. The measured values are in agreement with the SM prediction [204] (Fig. 8-6).

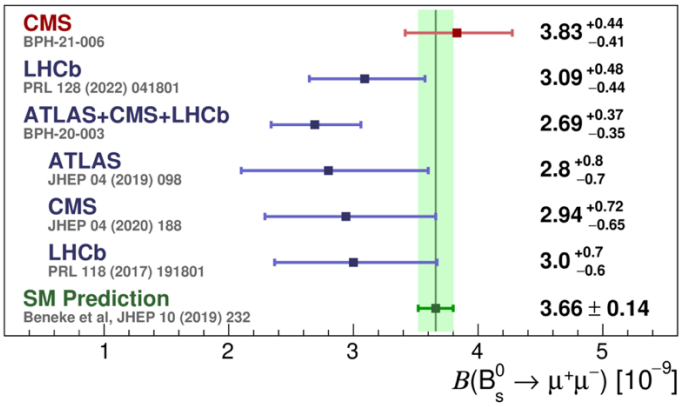


Fig. 8-6: BR ($B^0_S \rightarrow \mu\mu$) (10^{-9}).

Figure 8-7 gives the B^0_S effective lifetime measurements. The lifetime differences of the mass eigenstates are expected to scale as $1/m_Q^2$, where m_Q is the mass of the heavy quark.

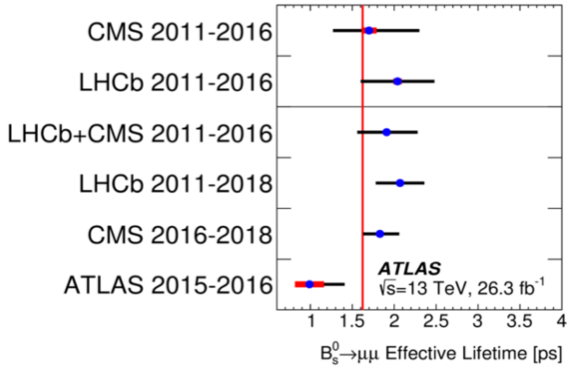


Fig. 8-7: $B^0_S \rightarrow \mu^+\mu^-$ effective lifetime (ps) [205].

[204] F. M. Simone, Status and prospects of rare decays at ATLAS and CMS, PoS WIFAI2023 (2024) 028. https://cds.cern.ch/record/2887139/files/CR2024_021.pdf
CMS Collaboration, https://cms.cern/news/new-study-rare-b-meson-decays-two-muons
CMS Collaboration, https://cms-results.web.cern.ch/cms-results/public-results/publications/BPH-21-006/index.html
D. Kovalskyi, CMS measurements of rare B meson decays to two muons. https://inspirehep.net/files/441a670372ec1083d0d2818bd73fc5c0
See also LHCb collaboration, Measurement of the $B^0_s \rightarrow \mu^+\mu^-$ decay properties and search for the $B^0 \rightarrow \mu^+\mu^-$ and $B^0_s \rightarrow \mu^+\mu^-\gamma$ decays. https://arxiv.org/abs/2108.09283

[205] B. Clerbaux, Experimental Summary Talk. Moriond EW 2024. https://indico.in2p3.fr/event/32664/contributions/137027/attachments/83769/124768/BClerbaux-v2.pdf or O. Kovanda, B-Physics in ATLAS and CMS. Moriond EW 2024. https://cds.cern.ch/record/2897507/files/ATL-PHYS-PROC-2024-033.pdf
For ATLAS: Measurement of the $B^0_s \rightarrow \mu\mu$ Effective Lifetime with the ATLAS Detector. https://arxiv.org/abs/2308.01171 .
In the SM hypothesis $\tau_{\mu\mu}$ coincides with the lifetime of the heavy B^0_s eigenstate. The experimental average of the B^0_s - $\bar{B}^0_s$ lifetimes and their difference yields the prediction $\tau^{SM}_{\mu\mu}$ = (1.624 ± 0.009) ps, with new physics effects perturbing it at most by the difference between the heavy and light eigenstate lifetimes (0.193 ps).

Another type of FCNC decay occurs when the b hadron does not annihilate, but its b quark decays into a new s quark and two leptons (Fig. 8-8), a semileptonic process 1000 times more frequent than the direct decay to μμ. For such processes, thousands of events are needed to allow more detailed analyses.

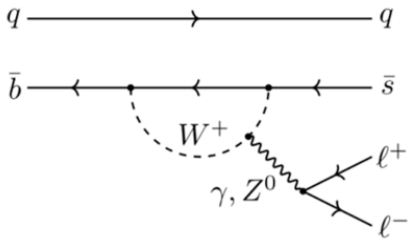


Fig. 8-8: Semileptonic B decay.

One of them consists in measuring the ratio of the branching ratios of the decays involving the electrons and the muons, R = BR ($B^+ \rightarrow K^+\mu^+\mu^-$) /BR ($B^+ \rightarrow K^+ e^+e^-$), after phase space correction, which, according to the principle of **lepton universality** of the SM, can deviate from unity only in the event of new physics. We will come back to this process in Chapter 14 concerning the determination of some parameters of the quark mixing matrix. We will show that presently these measurements have not revealed any deviations from the SM.

This is also the case for all the FCNC processes explored concerning strangeness, as BR ($K^+ \rightarrow \pi^+\mu^+\mu^-$) = $(9.15 \pm 0.08) \times 10^{-8}$. As for the top, limits at the level of 10^{-5} are presently set on the branching ratios of processes like $t \rightarrow \gamma u$, Zu, Zc, Hu, Hc (Fig. 8-9). We will complete this topic in Section 32.3.

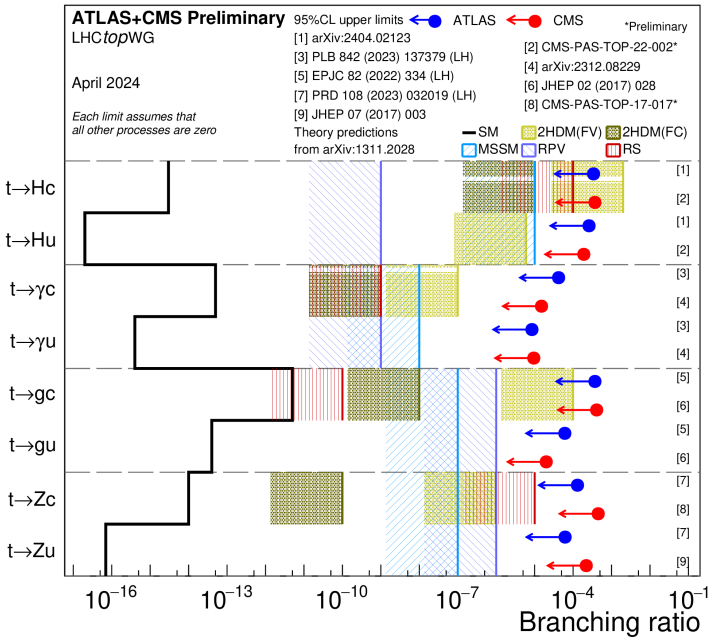


Fig. 8-9: Limits on top FCNCs [206].

[206] ATLAS Collaboration, Top Quarks + X Summary Plots April 2024.
https://atlas.web.cern.ch/Atlas/GROUPS/PHYSICS/PUBNOTES/ATL-PHYS-PUB-2024-005/

However, a puzzling channel is $B^+ \to K^+ \nu \bar{\nu}$ (Fig. 8-10) for which BELLE [207] determines a BR of $2.3 \pm 0.5\,(stat)^{+0.5}_{-0.4}\,(syst) \times 10^{-5}$, providing the first evidence for this decay at 3.5 standard deviations. The combined result is 2.7 standard deviations above the Standard Model expectation. Figure 8-10 shows the lowest-order quark-level diagrams for the $B^+ \to K^+ \nu \bar{\nu}$ decay in the SM, either of the penguin (a), or box type (b). The long-distance double-charged-current diagram (c) also contributes at tree level in the SM.

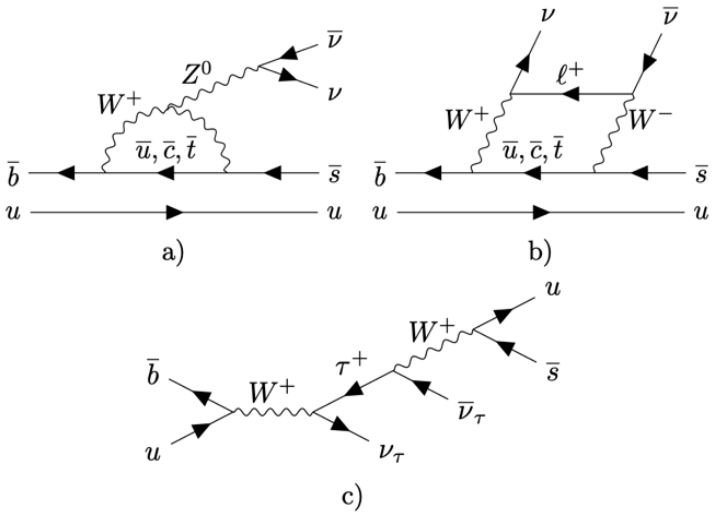


Fig. 8-10: Lowest-order diagrams for $B^+ \to K^+ \nu\bar{\nu}$. See text for explanation.

[207] The Belle II Collaboration, Evidence for $B^+ \to K^+ \nu\bar{\nu}$ decays. https://arxiv.org/abs/2311.14647

9. Neutral Currents

9.1 The Gargamelle discovery

This was the first major achievement of CERN's maturity. The observation of the elastic scattering of neutrinos on electrons and quarks in the Freon of the BC Gargamelle provided indirect proof of the existence of the weak boson Z.

Decided at the end of 1965, Gargamelle was built by CEA France and operated at CERN. Victor Weisskopf and Bernard Gregory were strong supporters of the project. It was a real odyssey, with a lot of scepticism to fight both on the theoretical side and on the experimental side. The adventure is well documented by several chronicles [208]. The present part is inspired from Bernard Degrange [209].

The search for Neutral Currents (NC), of low priority when proposed in 1970, became a major topic after the renormalizability of the electroweak model was demonstrated in 1971.

The muon-neutrino beam from the PS (neutrinos or antineutrinos depending on the polarity of the focusing horn, peak at 2 GeV, 10 GeV maximum) (Fig. 9-1) is directed towards Gargamelle (Figs. 9-2 and 9-3), whose size and Freon are adequate for good lepton identification.

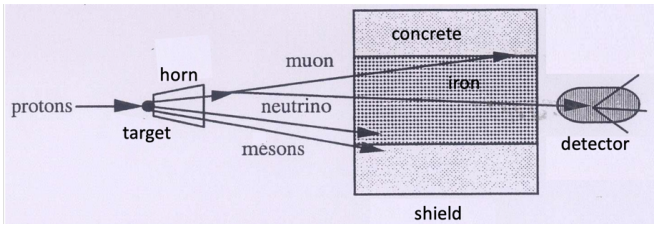


Fig. 9-1: The set-up.

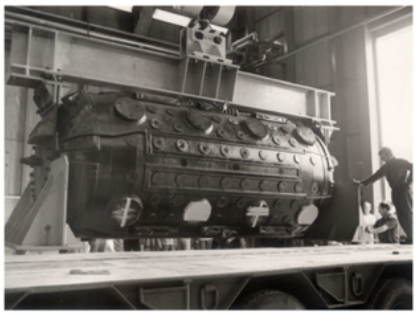


Fig. 9-2: The Gargamelle BC (length = 4.8 m, diameter = 1.9 m, about 20 t of Freon).

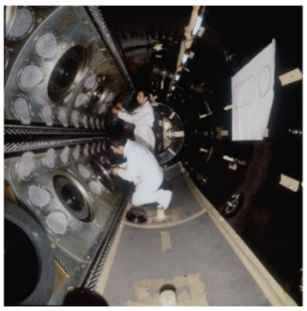


Fig. 9-3: Inside Gargamelle.

[208] D. Perkins, Neutral currents. https://cerncourier.com/a/neutral-currents/
D. Haidt, The discovery of the weak neutral currents.
https://cerncourier.com/a/the-discovery-of-the-weak-neutral-currents/
A. Pullia and J. P. Vialle, Weak neutral currents discovery: a giant step for particle physics. *Europhysics News* Vol. 41, No. 1, 2010, pp. 23-26. https://www.europhysicsnews.org/articles/epn/abs/2010/01/epn20101p23/epn20101p23.html
D. Perkins, Neutral currents. https://cds.cern.ch/record/1733411/files/vol43-Commemorative-Issue-p015-e.pdf
[209] B. Degrange, Gargamelle et la découverte des courants neutres.
https://llr.in2p3.fr/services/llr_seminaires/upload/ggm_cn_09.pdf
About André Rousset' book: Gargamelle et les courants neutres. Histoire d'une découverte cruciale.
https://cds.cern.ch/record/1739649/files/vol35-issue6-p040-f.pdf

Figure 9-4 displays an event without a lepton as observed with the Gargamelle experiment.

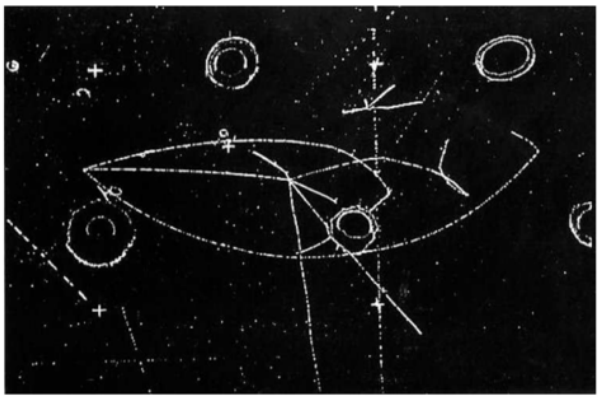


Fig. 9-4: An event without lepton (muon or electron) as recorded with Gargamelle. The neutrino coming from the left produces three secondary particles, all clearly identified as hadrons [210].

One observes events with lepton in the final state, of the charged current type (Fig. 9-5).

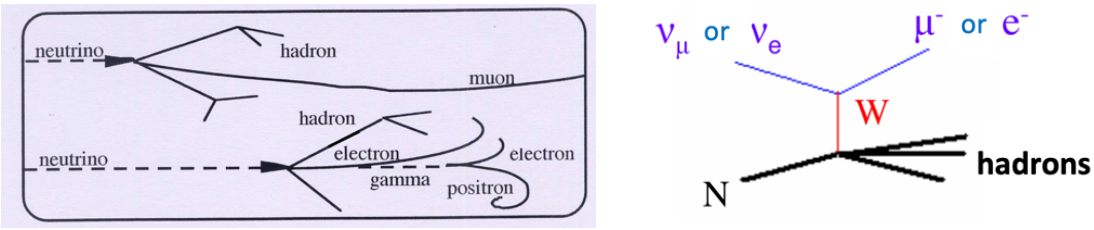


Fig. 9-5: Events with leptons and their interpretation.

But also purely hadronic events without a lepton (Fig. 9-6) were recorded.

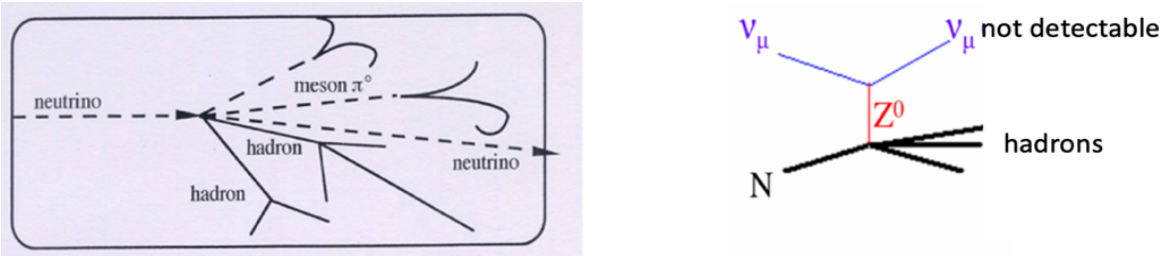
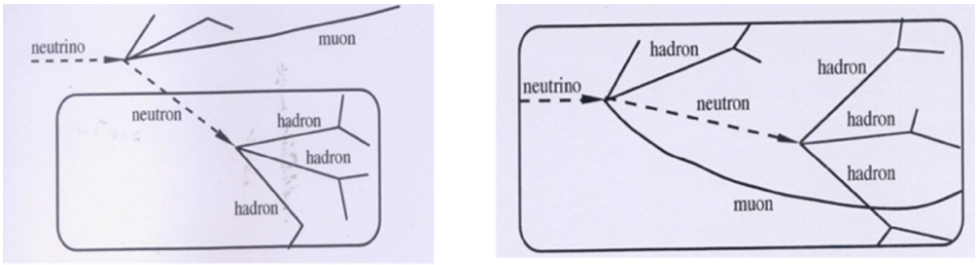


Fig. 9-6: Events without a charged lepton and their interpretation.

A probable background is that of neutrons created in an interaction outside the chamber and penetrating it, a possibility confirmed by "associated" type events, which show neutron production and "star" i.e. interaction (Fig. 9-7).

[210] D. Cundy and C. Sutton, Gargamelle: the tale of a giant discovery.
https://cds.cern.ch/record/1734418/files/vol49-issue7-p025-e.pdf



neutron interacting out of the detector event background B

neutron seen interacting inside Gargamelle event called "associated"

Fig. 9-7: Neutrons from neutrino interactions interacting.

Experimentally, the main problem was indeed the **neutron background**. The distinction between neutrinos and neutrons can only be made by studying the distribution of the penetration distances of the events in the chamber, expected to be flat for the former, sharp towards the entrance for the latter (Fig. 9-8). Elaborate Monte Carlo simulations [211] made it possible to overcome this problem, to be convinced of the existence of a population of the first type and to measure the rate of Neutral Currents.

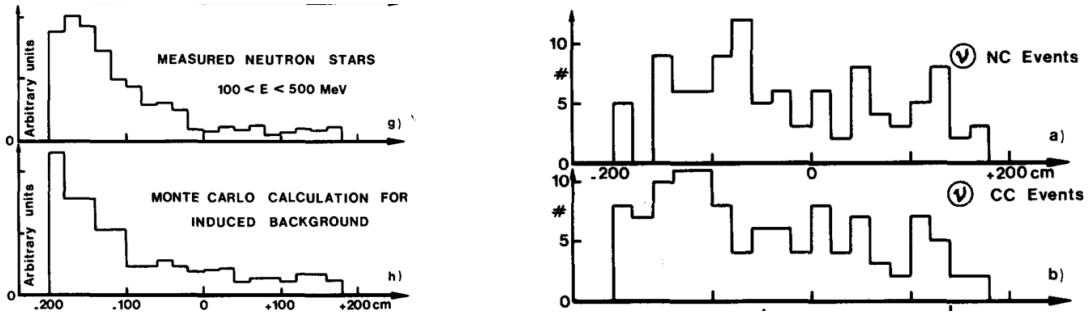


Fig. 9-8: Distributions along the chamber from neutrons (left) and from neutrinos (right) [212].

A more disturbing and less controllable background noise was the HPWF experiment [213] in the US, designed for the study of Charged Currents, at higher energy (Fig. 9-9). For the study of NCs it had to undergo transformations, the result being that NCs appeared and then disappeared [214], which earned them the name of "Alternating Currents", and this put enormous pressure on Gargamelle and CERN.

In particular, a "disappearance" after the NC announcement in Bonn in August 1973 led Gargamelle to perform a "proton experiment" to further verify the validity of the neutron background estimate. An important asset of Gargamelle was the observation of some events of the type of Fig. 9-10: an event that appeared very early, (Aix 1972), 3 other events later, where only one unchecked electron appears (one must then pay attention to the possible background $\nu_e n \rightarrow e^- (p)$) and therefore interpretable by the exchange diagram of a Z between neutrino and electron (Fig. 9-11). The predicted σ/E ratios are of the order of 10^{-42} cm^2/GeV, hence the low number of candidates.

[211] D. Haidt, The Discovery of Weak Neutral Currents. https://www.desy.de/~haidt/nc30_text.pdf
[212] F. J. Hasert *et al.,* Observation of neutrino-like interactions without muon or electron in the Gargamelle neutrino experiment. *Phys. Lett. 46B (1973) 138*
[213] D. Perkins, Neutral Currents. https://cds.cern.ch/record/1733411/files/vol43-Commemorative-Issue-p015-e.pdf
[214] For a somewhat different and very vivid account from the US side see L. Sulak, "The discoveries of weak neutral currents in the US". https://indico.ijclab.in2p3.fr/event/9830/contributions/31358/attachments/22508/32172/Sulak.pdf

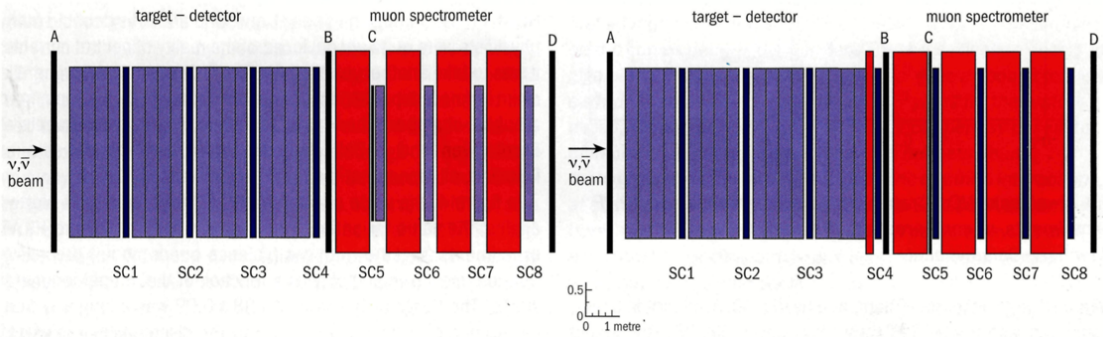


Fig. 9-9: HPWF experiment before (left) and after (right) modifications [215].

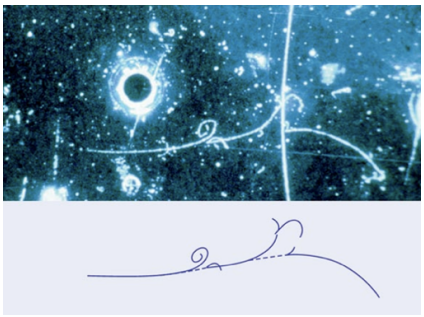


Fig. 9-10: A key event.

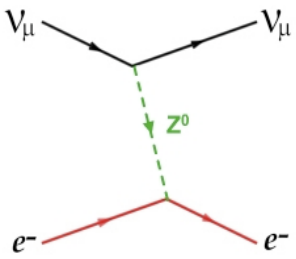


Fig. 9-11: Its interpretation.

The Gargamelle collaboration finally announced in 1973 the discovery of NCs (Fig. 9-12).

OBSERVATION OF NEUTRINO-LIKE INTERACTIONS WITHOUT MUON OR ELECTRON IN THE GARGAMELLE NEUTRINO EXPERIMENT

F.J. HASERT, S. KABE, W. KRENZ, J. Von KROGH, D. LANSKE, J. MORFIN, K. SCHULTZE and H. WEERTS
III. Physikalisches Institut der Technischen Hochschule, Aachen, Germany

G.H. BERTRAND-COREMANS, J. SACTON, W. Van DONINCK and P. VILAIN*[1]
Interuniversity Institute for High Energies, U.L.B., V.U.B. Brussels, Belgium

U. CAMERINI*[2], D.C. CUNDY, R. BALDI, I. DANILCHENKO*[3], W.F. FRY*[2], D. HAIDT, S. NATALI*[4], P. MUSSET, B. OSCULATI, R. PALMER*[4], J.B.M. PATTISON, D.H. PERKINS*[6], A. PULLIA, A. ROUSSET, W. VENUS*[7] and H. WACHSMUTH
CERN, Geneva, Switzerland

V. BRISSON, B. DEGRANGE, M. HAGUENAUER, L. KLUBERG, U. NGUYEN-KHAC and P. PETIAU
Laboratoire de Physique Nucléaire des Hautes Energies, Ecole Polytechnique, Paris, France

E. BELOTTI, S. BONETTI, D. CAVALLI, C. CONTA*[8], E. FIORINI and M. ROLLIER
Istituto di Fisica dell'Università, Milano and I.N.F.N. Milano, Italy

B. AUBERT, D. BLUM, L.M. CHOUNET, P. HEUSSE, A. LAGARRIGUE, A.M. LUTZ, A. ORKIN-LECOURTOIS and J.P. VIALLE
Laboratoire de l'Accélérateur Linéaire, Orsay, France

F.W. BULLOCK, M.J. ESTEN, T.W. JONES, J. McKENZIE, A.G. MICHETTE*[9], G. MYATT* and W.G. SCOTT*[6,9]
University College, London, England

Received 25 July 1973

Fig. 9-12: Publication of the discovery of NCs in 1973 [216].

[215] D. Perkins, Neutral Currents. https://cds.cern.ch/record/1733411/files/vol43-Commemorative-Issue-p015-e.pdf
[216] F. J. Hasert *et al.,* Observation of neutrino-like interactions without muon or electron in the Gargamelle neutrino experiment. *Phys. Lett. 46B (1973)*

Figure 9-13 displays some protagonists of this great adventure. Unfortunately, the premature death of project leader André Lagarrigue and other actors probably deprived this discovery of a Nobel Prize.



A. Lagarrigue. A. Rousset P. Musset V. Brisson A. Pullia J.P. Vialle

Fig. 9-13: Some of the protagonists of the discovery of the NC.

The measurement of the CC/NC ratio by Gargamelle, followed by other experiments, gave access to the weak angle (Table 9-1) and therefore to the W and Z masses.

Experiment	Value for the weak angle
Gargamelle	0.3-0.4
CDHS	0.24 ± 0.02
SLAC e-D 1978, 1979	0.20 (3), 0.224 ± 0.020
CHARM 1984	$0.236 \pm 0.005 \pm 0.003$
CDHS 1986	$0.225 \pm 0.005 \pm 0.003$
BEBc 1986	0.240 ± 0.030
NuTeV 2002	$0.2277 \pm 0.0013 \pm 0.0009$

Table 9-1: The weak angle evolution [217].

9.2 The consequences

After the discovery of the NC the road was traced: to discover the Wand Z bosons. In 1976, their masses were thus estimated: M_W between 60 and 80 GeV, M_Z between 75 and 95 GeV. See also Ref. [218] (published in March 1982).

And two proposals were made:

- Build the LEP collider: the LEP landscape anticipated by B. Richter in his founding paper on LEP was quite close to reality (Fig. 9-14).
- Turn the SPS into a proton-antiproton collider.

The second option, described in detail in Chapter 10 and Chapter 12, took priority.

As former UA2 spokesperson Pierre Darriulat wrote [219] in 2004: *"The pressure to discover the W and Z was so strong that the long design, development and construction time of the LEP project left most of*

[217] E. A. Paschos, The Weak Mixing Angle and its Relation to the Masses M_Z and M_W. https://lib-extopc.kek.jp/preprints/PDF/1982/8206/8206244.pdf , *"Determinations of the weak mixing angle including one loop radiative corrections are reviewed. The results restrict the masses of the heavy bosons in the ranges 78.9 < M_w < 84.6 GeV and 90.3 < M_z < 94.9 GeV".*

[218] ibid

[219] P. Darriulat, The W and Z particles: a personal recollection. https://cerncourier.com/a/the-w-and-z-particles-a-personal-recollection/

us, even the most patient, dissatisfied. A quick (but hopefully not dirty) look at the new bosons would have been highly welcome. But when proton–proton colliders such as the Superconducting Intersecting Storage Rings were proposed in this spirit, they were 'killed in the egg' by the management at CERN, with the argument that they would delay – or, even worse, endanger – the LEP project. The same argument did not apply to the proton–antiproton collider, as it did not require the construction of a new collider ring and could be proposed as an experiment …"

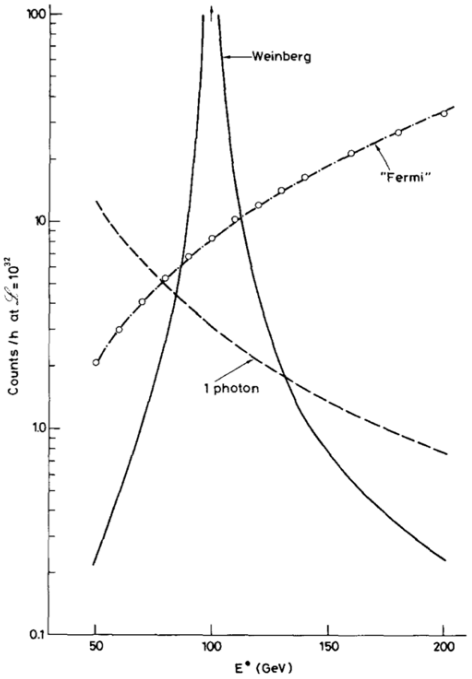


Fig. 9-14: A historical figure [220].

Regarding the weak angle [221], it is fun to tell a strange story that happened in 1981 and led to the *proton decay fever*. A value of $\sin^2\theta_W$ about 10% lower than the previous one, appeared on the market, see Ref. [222]. Such a value suited non-SUSY SU(5) better than its SUSY version (Fig. 9-15) [223]. And the first scenario predicted a fairly short lifespan of the proton, of the order of 10^{30} years. Experimenters were then strongly encouraged to rush to the nearest cavern and search for proton decay. Several did so. The fever stopped when the weak angle returned to a "normal" value. And Super Kamiokande did not find the proton decay but observed the first supernova neutrinos and later showed that the neutrino was not massless. *Ad augusta per angusta*.

Another hiccup in the determination of the weak angle was the NuTeV anomaly [224], which, with finer processing of QCD, in particular concerning the sea of strange quarks, almost disappeared.

---

[220] B. Richter, Very high energy electron-positron colliding beams for the study of the weak interactions, *Nucl. Instr. & Meth.* 136, 47 (1976), and SLAC-PUB-1738.

[221] W. J. Marciano, The Evolution of EW Theory. The Weak Mixing Angle. An Ode to $\sin^2\theta_W$. A Personal Perspective. https://indico.cern.ch/event/701949/contributions/3008077/attachments/1695224/2728432/03_SLAC2_ppt.pdf3.pdf

[222] D. Perkins, Neutral currents. https://cds.cern.ch/record/1733411/files/vol43-Commemorative-Issue-p015-e.pdf

[223] ibid, plot from S. Dimopoulos
J. Ellis, *et al.,* A Phenomenological Comparison of Conventional and Supersymmetric GUTs. (GUTs 3: SUSY GUTs 2), *Nucl.Phys.B 202 (1982) 43-62.*

[224] W. Bentz *et al.,* Reassessment of the NuTeV determination of the weak mixing angle. https://arxiv.org/abs/0908.3198

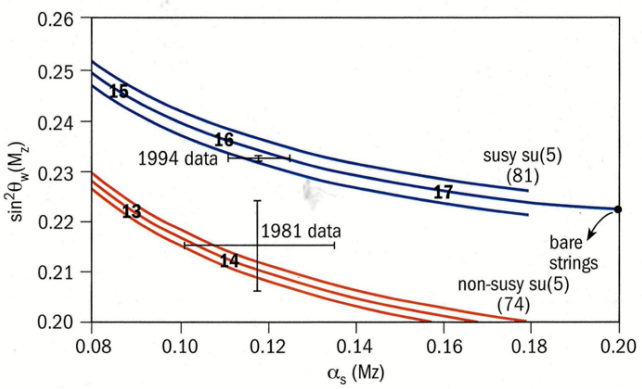


Fig. 9-15: A strange story.

Figure 9-16 [225] gives the evolution with the energy scale of the measured weak angle and Fig. 9-17 suggests its explanation [226]. Note in Fig. 9-16 the measurement of the weak charge of the proton by diffusion of polarized electrons on the proton (Q_{weak}) [227].

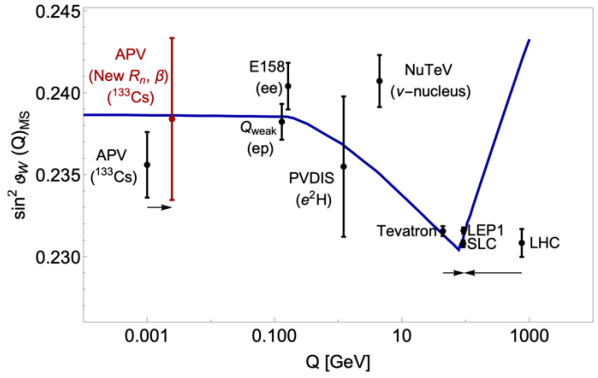


Fig. 9-16: Mind: numbers given in the $\overline{MS}$ renormalization scheme, different from Table 9-1.

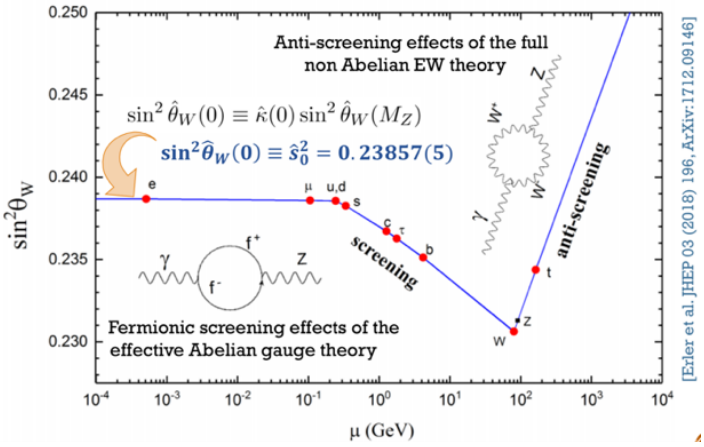


Fig. 9-17: Some explanations of Fig. 9-16.

[225] M. Cadeddu *et al.,* Neutrino, Electroweak and Nuclear Physics from COHERENT Elastic Neutrino-Nucleus Scattering with a New Quenching Factor. https://arxiv.org/abs/1908.06045

[226] J. Erler and R. Ferro-Hernández, Weak Mixing Angle in the Thomson Limit. https://arxiv.org/abs/1712.09146

[227] Q_{weak} collaboration, Precision Measurement of the Weak Charge of the Proton. *Nature 557, 207-211 (2018)*, https://arxiv.org/abs/1905.08283

Figure 9-18 [228] presents the results of low energy NC displayed in a plane spanned by two effective charge couplings $s^2(m_Z^2)$ and $g^2_Z(m_Z^2)$, which are related to sin θ_W and the overall neutral current strength. In the ellipse marked $\nu_\mu q$, a total of 41 ν_μ – experiments are combined. The figure shows the results from the e-d experiment at SLAC, the ν_μ– e data and results from atomic parity violating experiments. All low energy data agree well, as is evident from the thick ellipse representing the result of the combined fit. LEP and SLC will obviously bring much improvement (Chapters 16 and 18).

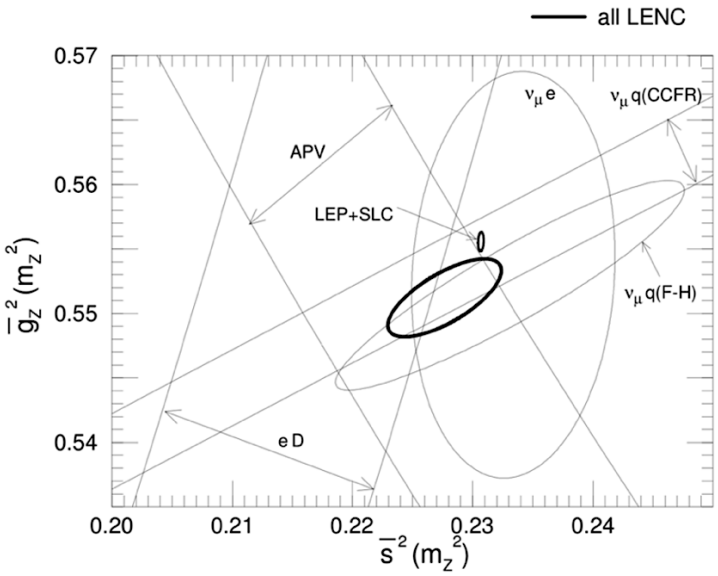


Fig. 9-18: The results of low energy NC. See text for explanations.

[228] D. Haidt, The Discovery of Weak Neutral Currents. https://www.desy.de/~haidt/nc30_text.pdf

10. The accelerators in brief

The CERN Large Electron-Positron (LEP) Collider and the Stanford Linear Collider (SLC), including also physics results, will be discussed in Chapters 15 till 18.

10.1 The Proton Synchrotron

The **Proton Synchrotron (PS)**, first of a long sequence of machines at CERN [229], besides the Synchrocyclotron (SC) and still in use today as an injector, was constructed between 1956 and 1959. The ring is a sequence of 100 combined-function magnets interleaved with 100 straight sections including auxiliary magnets, elements for injection and extraction, and accelerating radio-frequency cavities. The first beam was accelerated to 26 GeV in November 1959. In 1960 the PS accelerated routinely 10^{12} protons per pulse (ppp).

High energy physics started with internal targets, then in 1960 with beam lines receiving protons by fast or slow extraction.

The first injector to PS was a linac (Linac 1) providing 50 MeV protons. With the arrival of new "customers", a study on how to reach 10^{13} ppp was launched and led to the PS Booster (PSB), a compact slow-cycling 800 MeV synchrotron with four superimposed rings, inserted between Linac1 and the PS. Built between 1968 and 1972 it was integrated in the PS injection scheme in 1973, just for the Gargamelle neutrino experiment (Chapter 9). The PSB energy was later raised to 1 and 1.4 GeV. The 50 MeV Linac2 was introduced in 1978. Various developments and inventions allowed the PSB to reach 10^{13} ppp in 1974, 3×10^{13} by 1985, 4.2×10^{13} by 2003 (Fig. 10-1). Figure 10-2 displays the PS complex.

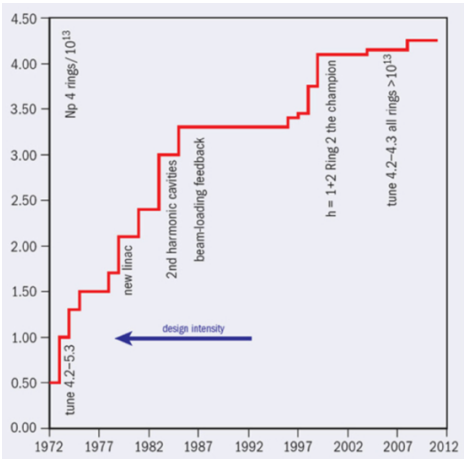


Fig. 10-1: The PSB peak intensity per pulse over the years.

For LHC a new linac (Linac 4) is used and the PSB has been pushed to 2 GeV.

[229] Technology Meets Research : 60 Years of CERN Technology: Selected Highlights
https://inspirehep.net/files/02de568d4897c555515de27f0b96af4d
D. Cundy and S. Gilardoni, in Technology Meets Research:
https://inspirehep.net/files/5398b0c8f10fc4834f2c81ed8ca32932 , p. 39
For a friendly competition between Brookhaven AGS and CERN PS see E. Courant, Brookhaven and CERN: the AGS and the PS. https://cerncourier.com/a/brookhaven-and-cern-the-ags-and-the-ps/

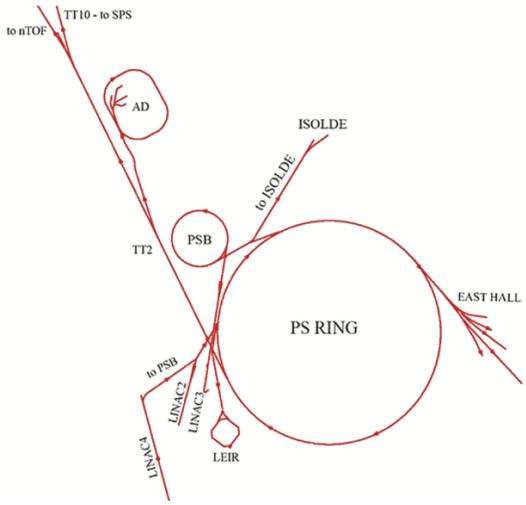


Fig. 10-2: The PS complex at CERN.

10.2 The Super Proton Synchrotron

In the early 1960s both sides of the Atlantic planned large proton synchrotrons of 200 GeV to 300 GeV, scaled up of **combined-function** (focusing and bending) magnet lattice used for the AGS and CPS [230].

In May 1970 CERN proposed to build a 300 GeV accelerator adjacent to CERN I (Meyrin) site in an underground tunnel of 7 km in circumference. Such a machine would reach 400 GeV with normal magnets installed in all the gaps. Installing the first half of the magnets (the missing dipole scheme) would even permit higher energies if the second half is filled with superconducting magnets.

The machine was approved in February 1971. Superconducting technology developing slower than expected, it was decided in 1973 to build a 300 GeV machine with normal-conducting magnets.

Five years later the **Super Proton Synchrotron (SPS)** machine was operational [231]. In the June 1976 Council meeting, John Adams announced the acceleration to 300 GeV and formally asked permission for the machine to reach 400 GeV operation, which was realised and announced a few hours later.

Figure 10-3 shows the competition in energy which followed between the SPS and Fermilab machines, its Main Ring, then its Tevatron after 1983, which discovered the top in 1995 [232]. LEP at CERN started in 1989.

The SPS physics programme was discussed in great detail in workshops and meetings [233], involving large audiences of the HEP community and studying a variety of possible beams from the SPS (hadronic, leptonic, charged and neutral) and their characteristics (intensity, momentum resolution) (Figs. 10-4 to 10-6).

[230] K. Brown, M. Giovannozzi and Th. Roser (BNL), The PS and AGS: The first strong focusing proton synchrotrons. https://www.worldscientific.com/doi/abs/10.1142/9789814436403_0008
[231] N. Doble *et al.,* in Technology Meets Research: https://inspirehep.net/files/818b65cb5004b2f8c5f23faf63571c33 , p. 135
[232] Fermilab, Accelerator History: https://history.fnal.gov/historical/accelerator/accelerator_history.html
American Physical Society: April 1995: Discovery of the top quark at Fermilab.
https://www.aps.org/archives/publications/apsnews/200204/history.cfm
[233] ECFA 300 GeV Working Group, https://inspirehep.net/files/039c309d041438681c4f74403c2bf6b9

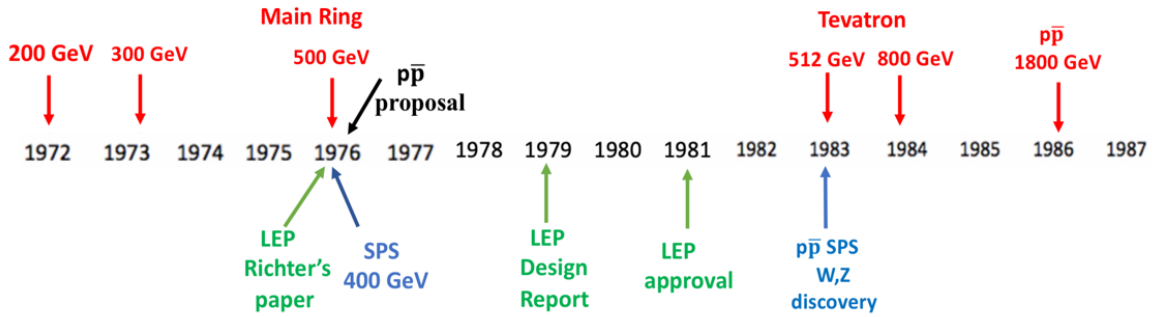


Fig. 10-3: Time schedule of Fermilab machines (above) and of SPS and preliminaries of LEP at CERN (below).

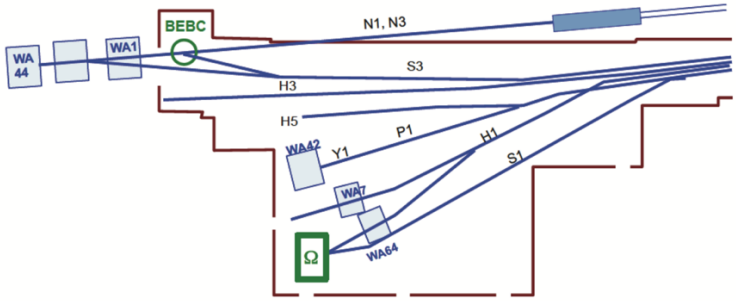


Fig. 10-4: The SPS beams to West Hall experiments.

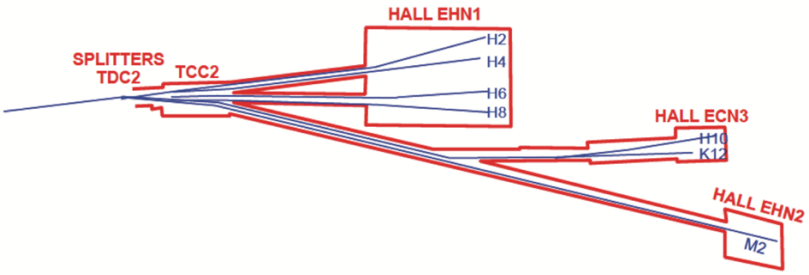


Fig. 10-5: The North Area beam lines.

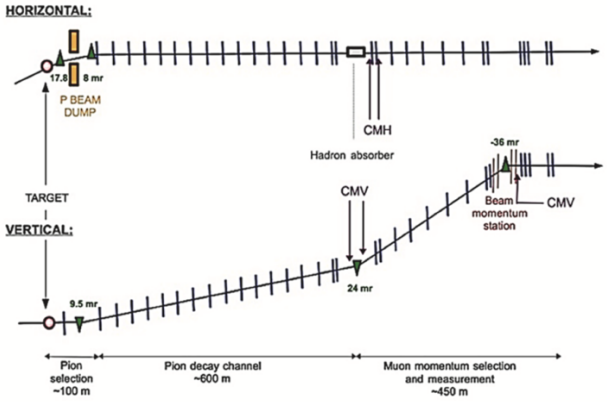


Fig. 10-6: The North Area muon beam exploiting the vertical plane.

This was a period of great activity and positive minds. It can be illustrated by an anecdote, which, by present standards, may sound as a miracle. One of the authors was called by the Director of the CERN Physics Department, Paul Falk-Vairant, who announced that spare money was available and asked him for ideas to spend it. The suggestion made was in favour of a new underground experimental zone, able to be fed by the most intense beams. This choice was probably backed by other actors and the realisation of the ECN3 zone was decided. It housed first the NA10 and NA14 experiments. Later it was used by NA48, followed by NA62. Recently it was decided that in the future the SHiP Beam Dump [234] would occupy ECN3.

The many facets of the research landscape of SPS included the exploration of the nucleon structure (Chapter 5), the study of heavy flavours (Chapter 14), heavy ions physics (Chapter 20) and CP violation (Chapter 14).

Later, the SPS provided a neutrino beam [235], pointing 730 km away to the OPERA detector, installed in the Italian Gran Sasso Underground Laboratory near Rome (see Chapter 19).

The SPS also provided a test bed for proton driven plasma wake field acceleration, the AWAKE project [236].

10.3 The Intersecting Storage Rings

The **Intersecting Storage Rings (ISR)** [237], operated from 1971 till 1984, was the first p-p collider in history. Even if, at least at the beginning, the physics left something to be desired (Chapter 11), the machine was a great success and in various aspects (high vacuum, small β quadrupoles) an essential step towards later machines (Fig. 10-7). The superconducting insertion at the ISR, with innovative cryogenics was the first superconducting magnet system routinely operated at an accelerator. It increased the luminosity of the collider by a factor of 2.3 in its final years of operation.

The ISR offered proton-proton collisions at a maximum energy of 62 GeV centre-of-mass and currents of 50 A per beam. Later, antiprotons were injected to test proton-antiproton collisions [238].

10.4 Stochastic cooling

The concept was invented by Simon van der Meer in 1968 [239]. The principle is simple (Fig. 10-8): information on the beam collected at one point is, via a shortcut, transmitted to another point where the required corrections are made. But in theory and in practice it is extremely complex and subtle.

Intense controversy arose over the impossibility of stochastically cooling a beam of charged particles, without violating Liouville's theorem. Simon van der Meer demonstrated that this theorem, based on

[234] The SHiP Collaboration: SHiP experiment at the SPS Beam Dump Facility. https://arxiv.org/abs/2504.06692
[235] E. Gschwendtner *et al.,* CNGS, CERN Neutrinos to Gran Sasso, Five Years of Running a 500-Kilowatt Neutrino Beam Facility at CERN. https://inspirehep.net/files/40731448b28871c2f4b834f0212dfbdc
[236] E. Gschwendtner *et al.,* The AWAKE Run 2 Programme and beyond. https://arxiv.org/abs/2206.06040
[237] C. Fabjan and K. Hübner, in Technology Meets Research.
https://inspirehep.net/files/21e59791dffe28bfbec1d89abe0652c6 , p. 87
[238] CERN70: The world's first hadron collider: https://home.cern/fr/news/series/cern70/cern70-worlds-first-hadron-collider
[239] F. Caspers *et al.,* Simon van der Meer: a quiet giant of engineering and physics.
https://inspirehep.net/files/e14ff390a96301f5f51d667ae3f48f69

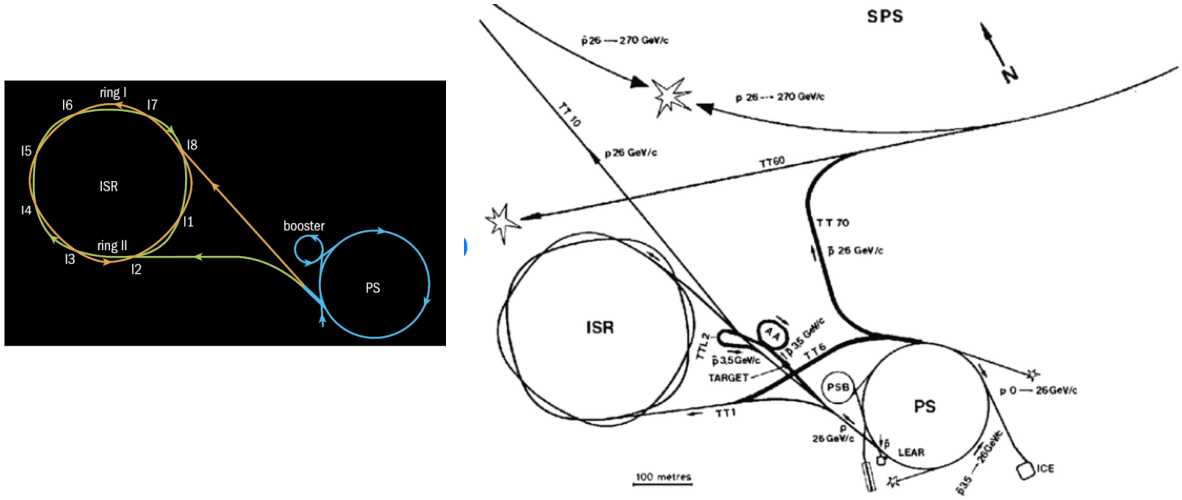


Fig. 10-7: The CERN accelerator complex: ISR and Ps (left), including the injector lines for the SPS (right).

statistics, is valid either for an infinity of particles, or for a finite number of particles if we have no information on the particles in phase space.

Finally, the idea of testing the stochastic damping of betatronic oscillations, in the ISR, was proposed in 1972. The measurements carried out justified the validity of the ideas put forward on betatronic damping (Fig. 10.9). A small dedicated ring, ICE (Initial Cooling Experiment) was installed (it was the ring of a g–2 experiment) to demonstrate that it was possible to reduce angular divergence and energy dispersion of a charged particle beam.

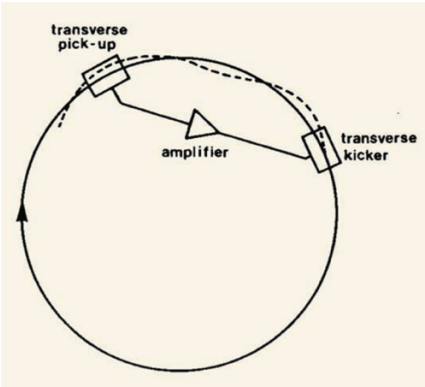


Fig. 10-8: Principle of stochastic cooling.

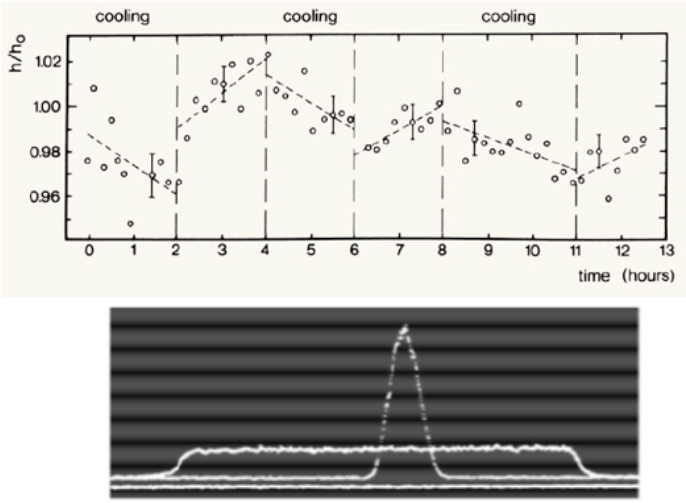


Fig. 10-9: Top: cooling at ISR; bottom: in momentum at ICE.

Following the successes, the AA (Antiproton Accumulator) was built, with first beam on 3 July 1980.

From 1981, antiprotons accumulated and “cooled” in the AA were injected and accelerated in the SPS, to carry out proton-antiproton collisions, a program to which we turn next. Stochastic cooling increased the luminosity of the collider and after the $W^{\pm}$ and Z^0 discovery (Chapter 12), Simon van der

Meer was awarded the Nobel Prize in 1984 together with Carlo Rubbia, spokesperson of the UA1 experiment [240].

About stochastic cooling, let us mention the exceptional trajectory of a major actor [241]. In Yosemite, Frank Sacherer was a legend for pioneering a new level of free climbing. He died in Grandes Jorasses in 1978 (aged 38).

10.5 The proton-antiproton collider

As early as 1966, Carlo Rubbia had realized the potential of the SPS to be used as a proton–antiproton collider [242] with Budker's electron cooling [243]. In 1968, as we saw, Simon van der Meer invented a method to increase the collision rate ("luminosity") of the ISR: Stochastic Cooling (SC), later proven experimentally at the ISR. This was the ingredient needed to propose in 1976 to use the CERN SPS as a single ring proton–antiproton collider [244].

In 1976 CERN decided to construct rapidly a small ring (Initial Cooling Experiment (ICE)) to study beam cooling and set up a design group for a proton–antiproton facility using the SPS as a storage ring and collider.

Meanwhile, tests in the ISR, theoretical developments and confirmation in ICE of cooling in all planes, gave the confidence that a final accumulated beam core of over 10^9 particles could be achieved. This led to build the Antiproton Accumulator (AA), key element of the scheme, a fixed magnetic field, single storage ring, accumulating antiprotons at 3.5 GeV, generated from 26 GeV (PS) protons impinging on a metal target.

The stochastic accumulation (stacking) process, essential feature in the AA scheme, could not be tested in ICE. This process involved simultaneous cooling in both transverse planes and increasing longitudinal density by four orders of magnitude while moving the particles into the dense core. The AA performed as expected.

The AA project was launched in 1978, with beam commissioning in July 1980. The first SPS proton–antiproton collisions at 270 GeV occurred in July 1981 and the first real period of physics runs in 1982.

After the W/Z discovery in 1983 (Nobel Prize in 1984), and the ever-increasing need of higher luminosities, the Antiproton Collector (AC) ring was built and commissioned in 1987, to bring a ten-fold increase in the accumulated antiprotons. The SPS ran as a collider as well as for short fixed-target runs during these years. After the last collider run in 1991 the SPS returned to its mode as a fixed-target physics accelerator.

---

[240] For an elementary introduction in Technology Meets Research: Stochastic cooling: Domesticating beams. https://inspirehep.net/files/02de568d4897c555515de27f0b96af4d p. 192
S. van der Meer, Stochastic cooling and the accumulation of antiprotons. *Rev.Mod.Phys, 57, 689-697 (1985)*
D. Möhl, Stochastic cooling of Particle Beams. Springer-Verlag, Berlin, 2013.

[241] M. Innocenti, Publications (up to his death) by Frank J. Sacherer on Work done at CERN. https://cds.cern.ch/record/2828611/files/PS-BR-Note-78-15.pdf

[242] H. Koziol and D. Möhl, The CERN Antiproton Collider Programme: Accelerators and Accumulation Rings. https://cds.cern.ch/record/806277/files/ab-2004-097.pdf
CERN Accelerator School Couse on Antiprotons for Colliding Beam Facilities, 1983. https://cds.cern.ch/record/157137/files/CERN-84-15.pdf

[243] About G. Budker's role: K. Johnsen, Gersh Budker. *Nature* 270, 459 (1977). https://www.nature.com/articles/270459a0

[244] C. Rubbia, P. McIntyre and D. Cline, Producing Massive Neutral Intermediate Vector Bosons with Existing Accelerators. https://cds.cern.ch/record/2137187/files/p175.pdf
V. Chohan and P. Darriulat, in Technology Meets Research: The CERN Antiproton Programme: Imagination and Audacity Rewarded. https://inspirehep.net/files/b6490184742632ba3b1c9481f1efb15a , p. 179

Improved systems were also used for the antiproton source at FNAL, leading to the top discovery at Fermilab in 1995 (Section 10.9).

The overall scheme (Fig. 10-7 right) implied major modifications to the PS and the SPS and new beam transfer lines for the antiprotons. The PS injectors and the 26 GeV PS were pushed to their limits to deliver an intense proton beam on the production target: up to 1.4×10^{13} protons per pulse, yielding up to 7×10^{7} injected antiprotons. The transverse emittances had to be small and the proton burst length had to correspond to the AA circumference, exactly one quarter of the PS.

Initially, the AA was used as a collector as well as an accumulator; in 1987 the construction of a large acceptance Antiproton Collector (AC) ring encircling the AA was launched, for collecting the antiprotons from the target. More accumulated particles, less momentum spread and stochastic cooling in the AC reduced the 6-dim phase space density by up to 4×10^{9} before the beam was extracted to the AA and accumulated over hours or days (Fig. 10-10) [245]. In the AA, over a day, a stack of up to several 10^{11} antiprotons was accumulated. An antiproton bunch was picked from the stack and moved to the ejection orbit. From there it was sent through a "loop" (TTL2 in Fig. 10-7 right) to the PS. In the PS, this bunch was accelerated to 26 GeV and sent to the SPS.

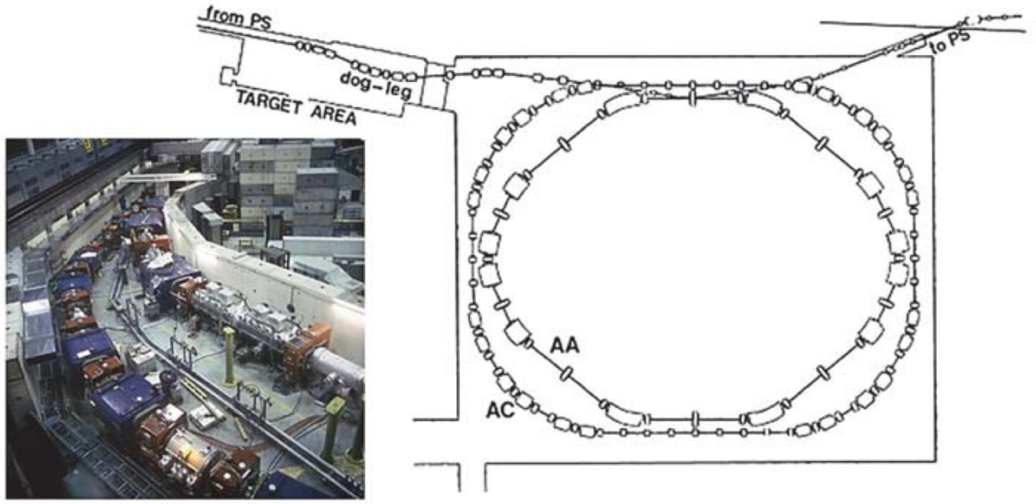


Fig. 10-10: View of the Antiproton Accumulation Ring (AA) and the Antiproton Collector (AC) (Chapter 12).

Before a transfer, checks were done on small "pilot bunch" of ~ 10^{9} antiprotons all the way from the AA to the SPS, assuring that a "big shot", a day of accumulated antiprotons, would safely find its way. The antiproton beam was accelerated in the SPS to 270 GeV simultaneously with the counter-rotating proton beam injected just before. After some adjustments the beams were brought to collision. The acceleration time of about 3.4 s was short, and the beams were kept colliding with up to 16 hours of useful beam lifetime.

[245] V. Chohan and P. Darriulat, in Technology Meets Research: The CERN Antiproton Programme: Imagination and Audacity Rewarded. https://inspirehep.net/files/b6490184742632ba3b1c9481f1efb15a , p. 179

10.6 The Large Hadron Collider

The Large Hadron Collider **(LHC)** [246] succeeded the LEP collider (Chapters 15 till 18) in the same 27 km circumference tunnel. Between 2000 and 2008, the dismantling of the LEP machine was followed by the installation of the LHC machine.

For the genesis of the LHC program see Ref. [247]. Born in the early eighties, LHC came in exploitation in 2009.

In 1978 John Adams, then CERN Director General, was already asking: "*What will happen at CERN in the nineties?* " In 1985 a working group was created, chaired by Carlo Rubbia and in 1987, study days were organised in La Thuile (Val d'Aoste, Italy) and the goal of reaching a luminosity of 10^{34} $cm^{-2}s^{-1}$ was adopted [248].

In 1990–1991 CERN created the committee for R&D on detectors (DRDC) to optimize the efforts undertaken for LHC. A goal was to increase the collaboration with external laboratories and industry concerning the high field magnets and detectors at high luminosity.

End 1991 the LHC evaluation committee convinced CERN Council that LHC was the right machine for CERNs future. In March 1992 CERN and ECFA organised the Évian-les-Bains general meeting on physics and detectors, "Towards the LHC Experimental Programme" [249]. Proto-collaborations were already formed and by the end of the same year Letter of Intents (LoIs) were presented at CERN. In 1994 Technical Proposals were handed in and negotiations started on how to reduce the number of proposals to have only two general purpose detectors, a dedicated experiment for beauty physics and one for heavy ion collisions in the LHC tunnel. By February 1996 the two large general-purpose detectors ATLAS and CMS were officially approved, followed by the approval of LHCb (in 1998) and ALICE (in 1997).

After some variants, it was finally decided to build LHC for completion in 2005, in a single stage, thanks to the participation of non-member states.

For the machine see Ref. [250]. The challenge was to produce 1232 innovative 2-in-1 Nb-Ti dipoles (Fig. 10-11) cooled to 1.9K with superfluid helium, and nearly 10 000 magnet elements in total. The conception, prototyping and realisation of these dipoles was an example of close collaboration and exchange between CERN and industry. For cryogenics see Ref. [251] and for the relation with industry see Ref. [252]. More will come in Chapters 21 to 24**.**

---

[246] G. Brianti and P. Jenni, in Technology Meets Research:
https://inspirehep.net/files/d59e7aaf7b366b4da3ed4a0798e7a8e9 , p. 263

[247] G. Brianti, The Large Hadron Collider project: historical account. *Phys.Rept. 403-404 (2004) 349-364*
C. Llewellyn-Smith, Genesis of the Large Hadron Collider. https://doi.org/10.1098/rsta.2014.0037
H. Ostrowiecki, Genèse d'un projet: du LEP au LHC, https://journals.openedition.org/histoire-cnrs/489?lang=en
Large Hadron Collider in the LEP tunnel, Proceedings of the ECFA-CERN workshop, ECFA 84/85, CERN 84-10.
http://cdsweb.cern.ch/record/154938/files/CERN-84-10-V-1.pdf
Early days: Lausanne LHC workshop (archive): https://cerncourier.com/a/early-days-lausanne-lhc-workshop-archive/

[248] Report of the High-Luminosity Study Group to the CERN Long-Range Planning Committee: The Feasibility of Experiments at High Luminosity at the Large Hadron Collider. https://lib-extopc.kek.jp/preprints/PDF/1988/8805/8805137.pdf

[249] General Meeting on LHC Physics and Detectors: Towards the LHC experimental programme, ECFA CERN Workshop 1992, https://cds.cern.ch/record/236265

[250] L. Evans, The Large Hadron Collider. https://inspirehep.net/files/bba804c9ffd7db0a5c8b4eaeda897128
Facts and figures about the LHC: https://home.cern/resources/faqs/facts-and-figures-about-lhc

[251] Ph. Lebrun, Twenty-Three Kilometres of Superfluid Helium Cryostats for the Superconducting Magnets of the Large Hadron Collider (LHC). https://inspirehep.net/files/807b2f3c8e0c07c2cc2a6fb82f2b7cb3

[252] Ph. Lebrun in Technology Meets Research, Building Large Accelerators with Industry: Lessons from the LHC.
https://inspirehep.net/files/d6d6c5fada7e8a77ea8690df3e8b3775

In 2004, a failure occurred in the cryogenic distribution line (QRL) made by the French company Air Liquide. The problem was solved, but a complete reorganization of the installation schedule was needed.

On 10 September 2008, the first beam of the LHC was injected, an event followed by worldwide media. Less than an hour later, a first beam made the complete turn of the ring. CERN was in the public spotlight for a while. However, a week later, during a rise in energy, one of the 10 000 superconducting connections between the magnets broke, causing massive damage [253]. It took more than a year to repair the damage and cure the weaknesses. On 29 November 2009 the beams circulated again in the LHC.



Fig. 10-11: An LHC dipole magnet.

These avatars aside, the LHC turned out to be the remarkable machine as expected. It has reached and even exceeded the high luminosity aimed at in 1987 of 10^{34} $cm^{-2}s^{-1}$. Another step, the HL-LHC (High Luminosity LHC) is presently in preparation.

A major piece of technology concerned the current leads to the magnet where an innovative solution involving high temperature superconductors (HTS) was massively used [254] (Chapter 23).

A curiosity: the LHC ring is “agitated by surface waves” in the tens of mHz range. Thus, on 5 September 2012 the earthquake of magnitude 7.6 in Costa Rica was recorded by the LHC (seismic event at 14:42 UTC, first waves arrived at 15:06 UTC) [255].

Since 2022 (Run 3), the LHC continues operating at a centre-of-mass energy of 13.6 TeV and has achieved a record-breaking integrated luminosity in 2025 [256], resulting in about 125 fb^{-1} for ATLAS and CMS, thus bringing the total luminosity delivered since the start of LHC operations to over 500 fb^{-1}. The LHC is scheduled to operate till middle of 2026 before a major upgrade programme for the HL-LHC (Chapter 22) will start. This large data set enables more detailed studies of the properties of the Higgs boson and searches for physics beyond the Standard Model (Chapter 24).

---

[253] CERN releases analysis of LHC incident:
https://home.cern/news/press-release/cern/cern-releases-analysis-lhc-incident
M. Bajko *et al.,* Report of the Task Force on the Incident of 19 September 2008 at the LHC. CERN-LHC-PROJECT-REPORT-1168, https://cds.cern.ch/record/1168025/files/LHC-PROJECT-REPORT-1168.pdf

[254] A. Ballarino in Technology Meets Research: High Temperature Superconducting Current Leads for the Large Hadron Collider. https://inspirehep.net/files/11a52d77c896d2e5425eb4f62c25883b , p. 287

[255] N. Biancacci *et al.,* Lessons Learned from the Civil Engineering Test Drilling and Earthquakes on LHC Vibration Tolerances. https://indico.cern.ch/event/448109/contributions/1942067/attachments/1216213/1800370/HL-LHC.VibrationsEarthquakes.paper.pdf ,

[256] R. Steerenberg, Accelerator Report: 2025 is another record-breaking year for protons in the LHC.
https://home.cern/news/news/accelerators/accelerator-report-2025-another-record-breaking-year-protons-lhc

10.7 Key moments and figures at CERN

Among the major figures of the past, John Adams played a leading role in the growth of CERN as a world leading laboratory, with the realisation of the PS and SPS. Bernard Gregory, first French Director General (DG) of CERN (1966–1970), oversaw the world's first hadron collider, the Intersecting Storage Rings (ISR). Herwig Schopper (1981–1988) started and led beautifully LEP preparation and realisation.

Carlo Rubbia (1989–1993), initiator of the proton-antiproton collider program, acted strongly in favour of LHC, followed by Christopher Llewellyn-Smith (1994–1998) who got the approval of LHC, and by Luciano Maiani (1999–2003).

In December 2001 Robert Aymar became chair of the LHC External Review Board, mandated to evaluate this project [257]. He presented the results to the Board Committee in June 2002. In 2004 he became the second French DG of CERN (2004–2008). The use of superfluid liquid helium, at 1.9 K, for the LHC magnets, benefited from his experience acquired on the Tore Supra in Cadarache. The collaboration between CERN and the CEA-DSM has been a key for the use of liquid helium. During the failure of the LHC cryogenic line in 2004, Robert Aymar was able to get the LHC back on its feet. It was during his mandate that the first beam of protons circulated in the LHC on 10 September 2008, with unfortunately the problem quoted above occurring soon after. It was also during his time that the construction of Linac 4 started, key proton injector for the HL-LHC project.

As the authors already noted, this document does not explicitly address the ongoing European Strategy process, which should ideally be driven by young and engaged scientists. Nonetheless, the authors have closely followed discussions and actively contributed [258] to certain aspects of proposed future projects and would like to extend warm thanks to the key figures in the strategy process, particularly the CERN Director General, Fabiola Gianotti, for her strong and compelling advocacy for what appears to be the favoured path forward: the FCC project, see e.g. Ref. [259].

Table 10-1 summarizes the present and former Direct Generals of CERN.

Year	Director General
2026 –	Mark Thomson
2016 – 2025	Fabiola Gianotti
2009 – 2015	Rolf-Dieter Heuer
2004 – 2008	Robert Aymar
1999 – 2003	Luciano Maiani
1994 – 1998	Christopher Llewellyn Smith
1989 – 1994	Carlo Rubbia
1981 – 1988	Herwig Schopper
1976 – 1980	DG for Research: Léon Van Hove Executive DG: John Adams
1971 – 1975	DG of CERN Laboratory I (Meyrin): Willibald Jentschke DG of CERN Laboratory II (Prévessin): John Adams
1966 – 1970	Bernard Gregory
1961 – 1966	Victor Weisskopf
1960 – 1961	John Adams
1955 – 1960	Cornelius Bakker
1954 – 1955	Felix Bloch
1952 – 1954	Secretary General: Edoardo Amaldi

Table 10-1: The present and former Director Generals of CERN.

[257] R. Aymar, The Origin of LEP and LHC. Pontifical Academy of Sciences, Scripta Varia 119, Vatican City 2014, https://inspirehep.net/files/e9345836adc2b0cf97ef3215260a5530

[258] U. Amaldi *et al.,* Charting the European Course to the High-Energy Frontier. https://arxiv.org/abs/1912.13466

[259] M. Benedict, F. Zimmermann *et al.,* Future Circular Collider Feasibility Study Report: Volume 1, Physics, Experiments, Detectors. https://arxiv.org/abs/2505.00272

10.8 HERA at DESY

The **Hadron-Elektron-Ring-Anlage (HERA)** at DESY in Hamburg is up to now the only **lepton-hadron collider**. It operated from 1992 to 2007 and used PETRA as a pre-accelerator for both e and p. With a circumference of 6.3 km, HERA collided e^- or e^+ at 27 GeV with protons at 820 GeV, then 920 GeV. The warm dipole magnets in the e-ring had a field of 0.165 T. The 416 superconducting 9-m long dipole magnets in the proton ring were operated at 4.65 T during the 820 GeV running. All magnets, with cold iron yoke, were industrially produced. Upgraded, HERA reached a peak luminosity of 5×10^{31} $cm^{-2}s^{-1}$ (total delivered luminosity was 800 pb^{-1}). Its main physics results were described in Chapter 5. For more details see Ref. [260] and for tribute to a key figure of DESY, Bjørn Wiik, see Ref. [261]. Figure 10-12 shows the layout of the HERA accelerator and the luminosity accumulated during the HERA-1 and HERA-2 periods.

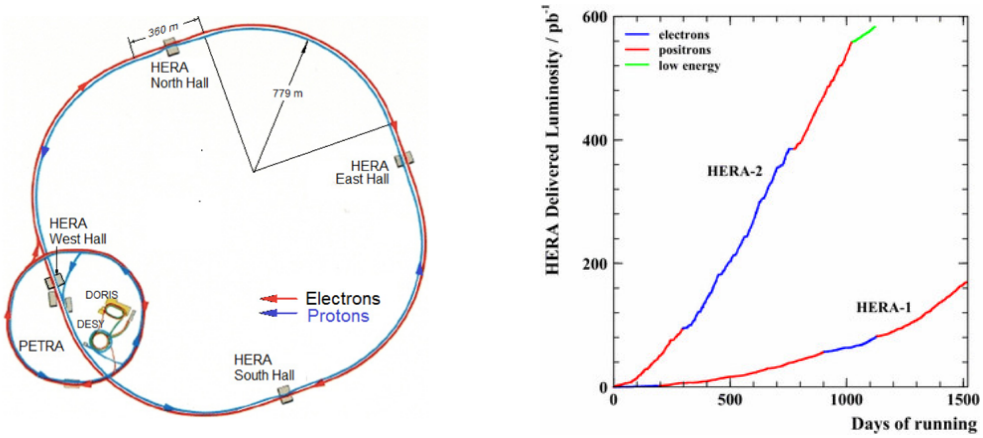


Fig. 10-12: HERA and its achievements in luminosity.

10.9 The Tevatron at Fermilab

The first synchrotron built with SC magnets, the Tevatron [262] p-$\bar{p}$ collider began operation in December 1985 and was shut off on 30 September 2011, overtaken by the LHC. The magnets, with still warm iron cores and a mechanical structure reinforced by collars, were cooled by forced circulation of supercritical helium.

The Tevatron offered centre-of-mass collision energies of up to 1.96 TeV. Its initial design luminosity was 10^{30} $cm^{-2}s^{-1}$, but, with two decades of upgrades, it was able to deliver 430 times higher luminosities to each experiment, CDF and D0. Owing its principle to the van der Meer stochastic cooling but expanding it over CERN design and adding electron cooling, it was an extremely complex research instrument known for many technological breakthroughs and discoveries, including the most famous

[260] M. Klein and R. Yoshida, Collider Physics at HERA. https://arxiv.org/abs/0805.3334.pdf
D. Trines, Constructing HERA, rising to the challenge. https://cds.cern.ch/record/1734158
[261] Bjørn Wiik: Eclipse of a visionary. https://cerncourier.com/a/eclipse-of-a-visionary/
[262] S. D. Holmes, Remembering the Tevatron, the Machine(s). https://arxiv.org/abs/1109.2937
V. Shiltsev, The Story of the Tevatron Accelerators: Accelerator Science and Technology Breakthroughs, Achievements and Lessons. FERMILAB-PUB-12-088-APC, https://inspirehep.net/files/14957246b24a3ed2387be7ee5943c9f2
L. M. Lederman, The Tevatron. *Scientific American, vol. 264:3, 1991,* https://doi.org/10.1038/scientificamerican0391-48

top discovery (Section 10.9). Figures 10-13 and 10-14 show the accelerator chain, the antiproton source and the achievements in luminosity.

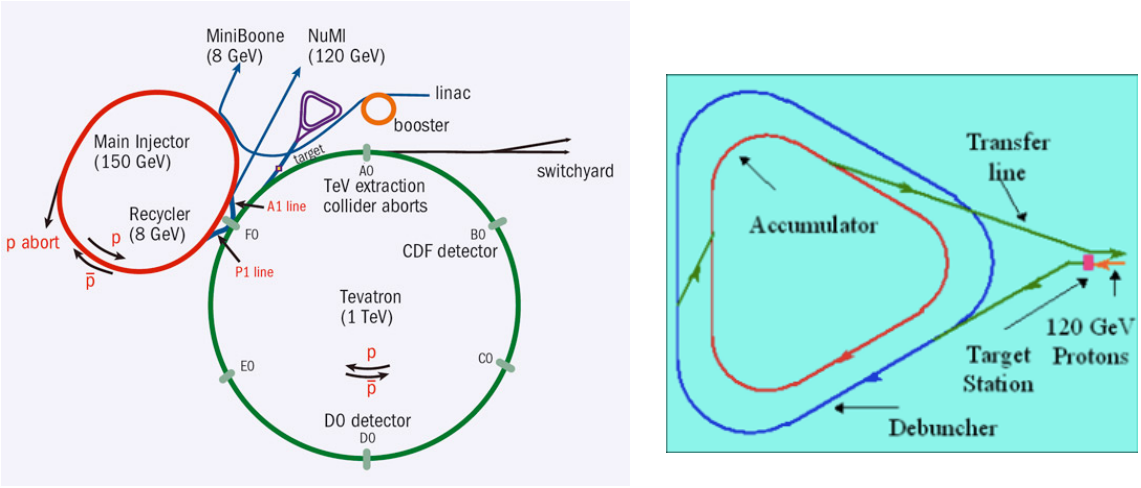


Fig. 10-13: Fermilab accelerator chain (left) and the Tevatron antiproton source (right).

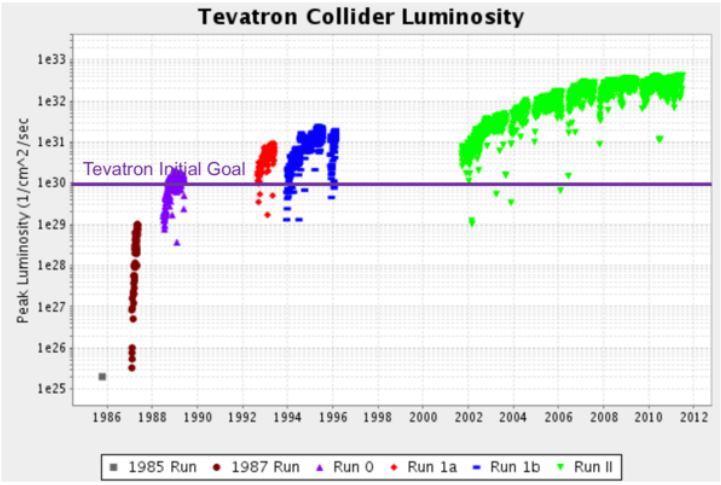


Figure 10: The luminosity history of the Tevatron Collider

Fig. 10-14: The Tevatron achievements in luminosity.

10.10 The present status and achievements of R&D

In the last decades much work and innovation has been put in the R&D efforts towards the worldwide future of HEP. Conceptional Design Reports (CDRs), Technical Design Reports (TDRs), Feasibility Studies and Project Readiness Reports of proposed future machines are available. But in this chronicle, as we said, we will only refer to the prospective documents concerning detailed studies and opinions about the future of our field at the HE frontier [263].

[263] K. Jacobs, Future Colliders.
https://indico.cern.ch/event/1283224/contributions/5405749/attachments/2729137/4743752/CPAN_Future_Colliders_2023.10.pdf
V. Shiltsev and F. Zimmermann, Accelerator Physics of Colliders.
https://pdg.lbl.gov/2023/reviews/rpp2023-rev-accel-phys-colliders.pdf

High-field SC magnets are the key technology for future hadron colliders, μ colliders, ν beams, etc.

Let us first pay tribute to the pioneers of the domain, as e.g. Peter Smith at RAL, who introduced the Rutherford SC cable (end sixties, early seventies), used since by all the big accelerators, and those who explored the properties of SCs as Nb_3Sn and High Temperature Superconductors (HTS). These are indeed the present candidates to reach the objective of 16–20 T field strength, and their technologies must be mastered and transferred to industrial production (Fig. 10-15) [264].

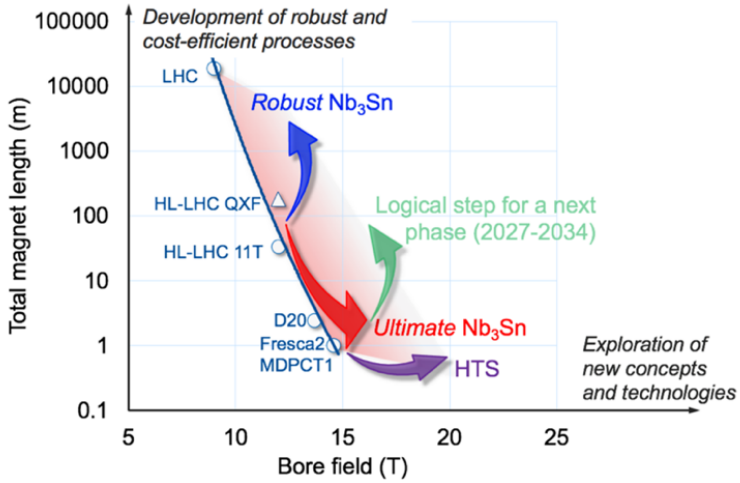


Fig. 10-15: Graphical representation of the objectives of the High Field Magnets R&D programme from 2021–2027. Both fronts of maximum field (red for Nb3Sn, purple for HTS) and large-scale production (blue) will be advanced. Also represented, in green, is a possible evolution for the longer term, 2027–2034.

HTS may have a major role in addressing the challenges of the next circular collider at the high energy frontier. HTS materials, rare-earth barium copper oxide (ReBCO) in particular, have very high critical fields and can carry high currents at field and temperature levels well above those of LTS materials. Operating at T significantly higher than liquid He, they offer **superior energy efficiency** and can reduce the **dependency on He**, whose price and availability may be at risks.

ReBCO is a material of choice for applications in several other fields of scientific and societal applications [265], offering the perspective of a sustainable market and of further cost decrease.

As for **accelerating RF cavities,** key of e^+e^- colliders, the application of SC materials has gained a huge interest over the last five decades. The accelerating gradients have been increased considerably due to a better understanding of the initial limiting factors, in particular multipacting, issues in surface preparation, etc. Advances in material technology played also a very important role.

Among the huge R&D efforts carried out on these topics, let us select in Ref. [266] a summary paper of each of the key objectives: the race towards larger accelerating fields of SC RF cavities and the race

[264] P. Védrine *et al.,* High-field magnets. CERN Yellow Reports: Monographs, CERN-2022-001. https://cds.cern.ch/record/2806281/files/document.pdf
European Strategy for Particle Physics - Accelerator R&D Roadmap: arXiv:2201.07895
L. Bottura and B. Bordini, HTS Potential and Needs for Future Accelerator Magnets. https://arxiv.org/abs/2503.23048
[265] REBCO high-temperature superconductors are ideal for tokamak magnets, study suggests. https://physicsworld.com/a/rebco-high-temperature-superconductors-are-ideal-for-tokamak-magnets-study-suggests/
[266] On high field magnets: L. Bottura, High Field Accelerator Magnets for Next Generation Colliders – Motivation, Goals, Challenges and R&D Drivers. https://www.worldscientific.com/doi/10.1142/9789811278952_0031

towards higher magnetic fields, in particular concerning high temperature superconductors (HTS). It is interesting to follow the corresponding evolution in neighbour domains as fusion [267].

10.11 Some applications of the accelerators

See Ref. [268] in particular for medical physics. Concerning synchrotron light sources and X-ray free-electron-lasers see Ref. [269] for a status. A common goal of light sources is low emittance, now based upon the concept of a **Hybrid Multi-Bend Achromat**, as illustrated in Ref. [270]. For an original source of X-rays, see ThomX [271].

Another domain of application of accelerators are the **Accelerator Driven Systems (ADS).** For the origin and a list of projects, see Ref. [272] and Ref. [273], respectively. The CiADS (China initiative Accelerator Driven System) project is under construction in Huizhou, Guangdong, with an estimated operational start date of 2028.

10.12 Crystal channelling

Crystal channelling [274], in which charged particles are guided along the interatomic corridors of a crystal, bring interesting advances in particle beam dynamics.

Hadron colliders suffer from halo of particles around the beam, threatening the stability and protection of the operation and requiring a multi-stage setup of collimators. Bent crystals as collimators can deflect the halo at larger angles and improve the power loss of hadron colliders [275] such as the LHC.

Bent crystals led to a reduction of losses during the slow extraction from the SPS by shadowing the electrostatic septum.

On SC RF cavities: S. Belomestnykh *et al.,* Key directions for research and development of superconducting radio frequency cavities. https://arxiv.org/abs/2204.01178
For a good recap see also: F. Caspers and S. Calatroni, Superconducting RF cavities.
https://cds.cern.ch/record/2928989/files/document.pdf

[267] Tokamak completes set of HTS magnets (2023):
https://www.world-nuclear-news.org/Articles/Tokamak-completes-set-of-HTS-magnets

[268] M. Dohlus *et al.,* Application of Accelerators and Storage Rings.
https://inspirehep.net/files/a01dbe11a03ad21e318278422fc1a1fb
K. Hübner, Medical Accelerators: A Tool for Tumour Therapy. In Technology Meets Research:
https://inspirehep.net/files/8dab861cf947a6ec6fdf61cff4e079f2%20%20%20%20%20%20K.Hubner, p. 374

[269] E. Prat, Synchrotron light sources and X-ray free-electron-lasers. https://arxiv.org/abs/2107.09131

[270] P. Raimondi *et al.,* Commissioning of the hybrid multibend achromat lattice at the European Synchrotron Radiation Facility. https://journals.aps.org/prab/abstract/10.1103/PhysRevAccelBeams.24.110701

[271] M. Jacquet *et al.,* First production of X-rays at the ThomX high-intensity Compton source. *Eur. Phys. J. Plus (2024) 139: 459,* https://epjplus.epj.org/articles/epjplus/abs/2024/05/13360_2024_Article_5186/13360_2024_Article_5186.html

[272] C. D. Bowman *et al.,* Nuclear energy generation and waste transmutation using an accelerator-driven intense thermal neutron source. *Nucl. Instrum. Methods A320, 336 (1992)*
F. Carminati, R. Klapisch, J. P. Revol, C. Roche, J. A. Rubio and C. Rubbia, An Energy Amplifier for Cleaner and in Inexhaustible Nuclear Energy Production Driven by a Particle Beam Accelerator. CERN/AT/93-47,
https://cds.cern.ch/record/256520/files/at-93-047.pdf

[273] Accelerator-driven Systems (ADS) and Fast Reactors (FR) in Advanced Nuclear Fuel Cycles. A Comparative Study:
https://www.oecd-nea.org/ndd/reports/2002/3109/nea3109ch9.pdf
B. Yee-Rendon, Overview of ADS Projects in the World. https://accelconf.web.cern.ch/linac2022/papers/tu2aa01.pdf

[274] Proposed by E. N. Tsyganov in 1976, demonstrated in DUBNA in 1979.

[275] W. Scandale and A. Taratin, Channeling and volume reflection of high-energy charged particles in short bent crystals. Crystal assisted collimation of the accelerator beam halo. *Phys. Rep., vol. 815, pp. 1–107, 2019.*
https://www.sciencedirect.com/science/article/abs/pii/S0370157319301498?via%3Dihub

Channelling of a 450 GeV proton beam was used to produce simultaneous particle beams.

A pair of simultaneous and nearly-collinear beams of long- and short-lived neutral kaons [276] were a key part of the NA48 experiment at CERN (Chapter 13).

The Underground Area 9 (UA9) [277] experiment is using beams from the CERN SPS to investigate how one could improve collimation in modern hadron colliders by using bent crystals.

Channelling in bent crystals has been observed at the CERN LHC [278].

In the future, it is planned to measure electric and magnetic dipole moments of short-lived particles with a double-crystal experiment in the LHC [279].

10.13 A major turning point

The Superconducting Super Collider (SSC) [280] arose from cancelling a previous project at Brookhaven called ISABELLE [281], during the Reagan administration. By 1983, ISABELLE, a 200 × 200 GeV p-p collider, had met problems, notably with its superconducting magnets. Furthermore, its primary goal was to discover the W and Z bosons, which were discovered in 1983 at CERN. US HEP Leaders decided to redirect the funds towards an even bigger accelerator, initially called the "desertron".

This very ambitious SSC project was recommended by the HEPAP [282] Subpanel on New Facilities in 1983. The planned ring circumference was 87 km with a CM energy of 40 TeV and a design luminosity of 10^{33} $cm^{-2}s^{-1}$. It would have been the world's largest and highest energy collider [283]. Construction started in 1991 in Texas near the town of Waxahachie.

During the planning and initial construction phase, there were heated debates about the high cost of the project. Initially estimated at around 4.4 B$ in 1987, the cost increased to 11.8 B$ by 1993, with some estimates suggesting it could even reach 21 B$ by completion. This escalation finally resulted in a US Congress vote in 1993 to cancel the SSC project [284], after about 2 B$ had been spent on the project. This cancellation was a significant setback for US particle physics and as a consequence many American scientists joined the LHC experimental programme. The SSC's cancellation led to valuable insights into the importance of long-term planning and sustained political support for large scientific projects and resulted in a greater emphasis on international cooperation in large-scale physics projects. Furthermore, it shifted the global balance of leadership in high-energy physics to Europe.

Leon Lederman, Fermilab director at that time, was a very strong supporter of the SSC project. He wrote a popular science book, published in 1993, to promote awareness of the significance of the scientific work which the SSC would have supported and to counteract the loss of congressional

[276] N. Doble *et al.,* A novel application of bent crystal channelling to the production of simultaneous particle beams. https://cds.cern.ch/record/280045/files/sl-95-016.pdf
[277] W. Scandale *et al.,* The UA9 setup for the double-crystal experiment in CERN-SPS. *NIM in Physics Research, A 975 (2020) 16175,* https://www.sciencedirect.com/science/article/pii/S0168900220305714?via%3Dihub
[278] R. Rossi *et al.,* Observation of channeling in bent crystals at the CERN LHC.https://hal.science/hal-03448426/
[279] G. Cavoto, Bent crystals for beam manipulations. https://indico.cern.ch/event/587927/contributions/2405610/attachments/1391363/2119652/LHC-b_fixedtarget.pdf
[280] Superconducting Super Collider: https://en.wikipedia.org/wiki/Superconducting_Super_Collider
[281] ISABELLE: https://en.wikipedia.org/wiki/ISABELLE
[282] HEPAP: https://en.wikipedia.org/wiki/High_Energy_Physics_Advisory_Panel
[283] For comparison, the LHC project at CERN has a ring circumference of 27 km, a design E_{CM} = 14 TeV and a design luminosity of L= 10^{34} $cm^{-2}s^{-1}$.
[284] US 'reneges' on SSC decision: https://cerncourier.com/a/us-reneges-on-ssc-decision/

support. The book with the title *"The God Particle: If the Universe Is the Answer, What Is the Question?"* made the nickname "God particle" he introduced for the Higgs boson very popular [285].

The debates about the SSC and the trauma experienced following its cancellation led to numerous statements [286] from scientists in HEP, other fields such as condensed matter physics, and various representatives from politics and society.

Here are the key takeaways from this story:

- the risk of conceiving a new project of this magnitude **out of nothing (the "desert")**;
- the lack of a clearly defined **international collaboration** from the beginning;
- the lack of a procedure **guaranteeing financing** over a sufficiently long period (as CERN's Bannier procedure [287]);
- the danger of announcing **minimized costs** to get approval. Cost escalation is worse than cost itself.

However, it is essential to recall the breakthroughs that R&D and early works on these programs brought and which were essential for subsequent machines. An example is the idea of "two-in-one" dipoles put forward by John Paul Blewett in 1971, considered for US projects and which was realized 30 years later for the LHC [288].

10.14 Programmes in USSR and Russia

10.14.1 Accelerators

At the Joint Institute for Nuclear Research (JINR) in Dubna, established in 1956, the Synchrophasotron (which featured 10 GeV protons and polarized deuterons) was inaugurated in 1957, with what was then the largest magnet in the world. This was followed by the NUCLOTRON, an accelerator complex for relativistic nuclei and polarized deuterons, which utilized advanced superconducting magnet technology [289].

U-70 is a proton synchrotron with 76 GeV final energy built in 1967 at the IHEP in Protvino. At the time of its construction, the accelerator held the world record for beam energy and is still the highest-energy accelerator in Russia. In 1970–1971 the hydrogen BC Mirabelle was installed on U-70.

In the mid-1980s, the Accelerating and Storage Complex (**UNK) project** of a proton accelerator and storage complex was launched, with a p-p collider of 3 × 3 TeV. It was planned that U-70 would become

---

[285] The story wants that Lederman foresaw as title the "Goddamn Particle" – owing to frustration over how difficult it was to detect. But his publishers changed the name to the "The God Particle", which often draws ire from religious communities.

[286] W. Thomas, The Superconducting Super Collider: Oral Histories (AIP's oral history collection).
https://www.aip.org/history/the-superconducting-super-collider
E. Payson Willard, The Demise of the Superconducting Super Collider: Strong Politics or Weak Management?
https://www.wcu.edu/pmi/1994/94PMI001.PDF
APS: This Month in Physics History. October 1993: Congress Cancels Funding for the SSC.
https://www.aps.org/archives/publications/apsnews/201310/physicshistory.cfm

[287] W. Kummer, A rich inheritance. https://cerncourier.com/a/a-rich-inheritance/
M. Hine, The beginning of long-term planning in CERN.
https://cerncourier.com/a/the-beginning-of-long-term-planning-in-cern/

[288] R. B. Palmer, Superconducting Accelerator Magnets: A Review of their Design and Training.
https://www.slac.stanford.edu/pubs/slacpubs/5750/slac-pub-5899.pdf
L. Botura and S. A. Gourlay, Superconducting Magnets for Particle Accelerators.
https://lss.fnal.gov/archive/2016/pub/fermilab-pub-16-709-td.pdf
L. Botura, Superconducting Magnets.
https://indico.cern.ch/event/643268/contributions/2610549/attachments/1608286/2554490/part_II.pdf

[289] Dubna synchrophasotron turned 65. https://www.jinr.ru/posts/dubna-synchrophasotron-turned-65/

an injector for the collider ring. In 1994, the construction was frozen, and in 1999 it was decided to close the UNK project, following the closure of the SSC (Texas, USA) project in 1993 (and probably following the USSR dissolution) [290].

Presently, the entire Accelerator Complex U-70 comprises four machines, two linear and two circular accelerators, and operates in proton or light-ion mode.

10.14.2 The Era of the Electron-Positron Colliders

At the Institute of Nuclear Physics in Novosibirsk, now called Budker Institute of Nuclear Physics (BINP), electron-electron scattering experiments were performed in 1965–1967 with the **VEP-1** collider, demonstrating that colliding beam experiments were possible in PP [291].

The first BINP **electron-positron experiment** was performed at the **VEPP-2** collider in 1967 on ρ-meson production [292]. ACO (Orsay), following AdA (Section 15.1), and CEA (Cambridge) were also at work. The VEPP-2 collider was in operation from 1967 to 1970.

The next Novosibirsk e^+e^- collider **VEPP-2M** operated for experiments from 1975 to 2000. Then came its upgrade, **VEPP-2000.** Currently, two modern detectors, **CMD-3** and **SND,** perform new set of important experiments (Section 26.2).

Now in preparation is a new **VEPP-2M upgrade.** Since 1980 the **higher energy e^+e^- collider VEPP-4 operates at Novosibirsk.**

Other topics were studied in BINP. Near 1971 a group around Vladimir Balakin and Alexander Skrinsky started to develop ideas for high energy linear colliders [293]. Other studies concerned the method of resonant depolarization for precise beam energy measurement in colliders, the development of the theory describing beam polarization in storage rings, spin rotators called Siberian Snakes, etc.

The synchrotron radiation cooling was crucial for the e^+e^- colliders. The first cooling method, applicable to protons**, electron cooling**, was proposed at BINP by Gersh Budker in 1965.

10.14.3 Absolute Neutrino Mass Measurements

At the Institute for Nuclear Research of the Russian Academy of Sciences in Moscow, the Troitsk experiment was built in 1970, a spectrometer studying the endpoint region of the tritium decay spectrum. An incorrect measurement in 1980 ($14\ eV < M_\nu < 45\ eV$) gave a boost to cosmology! But afterwards, from 1994 to 2019, Troitsk [294] and Mainz held the world's best upper neutrino mass limits, gradually improving from 4.5 eV to 2 eV. It is now the domain of KATRIN (Chapter 19).

---

[290] K. P. Myznikov and E. F. Troyanov, Status of U-70 Operation and UNK Project.
https://inspirehep.net/files/83cea6d8cbc192e0b8868940c9465cc1
N. Tyurin, Forty years of high-energy physics in Protvino.
https://cds.cern.ch/record/1733548/files/vol43-issue9-p031-e.pdf

[291] A. N. Skrinsky, Accelerator Field Development at Novosibirsk (History, Status, Prospects).
https://proceedings.jacow.org/p95/ARTICLES/MAD/MAD04.PDF

[292] On the precise chronology of e^+e^- collisions see V. Shiltsev, The first colliders: AdA, VEP-1 and Princeton-Stanford.
https://arxiv.org/abs/1307.3116

[293] V. E. Balakin and A. N. Skrinsky, Proceedings of the second ICFA workshop on Possibilities and Limitations of Accelerators and Detectors, 1979. https://lss.fnal.gov/conf/C791004/
V. E. Balakin, G. I. Budker and A. N. Skrinsky, Feasibility of Creating a Superhigh Energy Colliding Electron-Positron Beam Facility. https://inspirehep.net/files/15a7992c7c8f40267cfd1695c972e0a8

[294] V. N. Aseev *et al.,* Upper limit on electron antineutrino mass from the Troitsk experiment**.**
Phys.Rev.D84,112003, https://journals.aps.org/prd/abstract/10.1103/PhysRevD.84.112003

10.14.4 Non-Accelerator physics

It is clear that the contributions to cosmology of USSR and Russia giants as Andrei Sakharov, Alexei Starobinsky and several others, illustrated elsewhere in this document, have been crucial ones. Given history and language one may ask whether some pieces of work may have been overlooked. See for instance Ref. [295].

Let us focus on some experimental aspects.

At the Baksan Neutrino Observatory (INR of RAS) the solar neutrinos experiment **SAGE** was performed and the dedicated Baksan Experiment on Sterile Transitions (BEST) utilizing a neutrino source of unprecedented intensity (see Section 19.10 for an account of the **gallium anomaly** and references).

The Lake Baikal set-up offered the birth of high-energy neutrino astronomy, with in 1984 a one-string prototype, and in 1993 NT-36, the first underwater detector with the capability to perform full spatial muon track reconstruction. For the present status see Ref. [296] (Chapter 31).

10.15 Programmes in China

For a general introduction to the status of Particle Physics in China see Ref. [297].

Over the past many years, China has been involved in particle physics research, with the construction of several cutting-edge facilities like e.g. BEPC and the Daya Bay Neutrino experiment. China was and still is also a **partner of most PP world programs**, having participated or is presently actively involved in programmes at CERN, DESY, GSI/FAIR, Fermilab, KEK, BNL, AMS on the ISS, Kamioka observatory, etc.

The Independent **Institute for High Energy Physics (IHEP)** in Beijing was created in February 1973. The **Beijing Electron Positron Collider (BEPC)** was constructed from 1984 to 1988 with a beam energy of 1–2.8 GeV. It delivered both physics runs with luminosity of 10^{31} $cm^{-2}s^{-1}$ at 1.89 GeV for 5 month per year, and synchrotron radiation runs.

The **detectors BES I and II** focused on light hadron spectroscopy and J/ψ. BESII registered close to 60×10^6 J/ψ decays. The main results of BES were a precision measurement of the **τ mass** and **R-ratio measurement** from 2 to 5 GeV CM. BES performed systematic studies of ψ(2S) and J/ψ decays and observed new non-$q\bar{q}$ resonances (see Chapter 28).

Next IHEP performed upgrades of **BEPC to BEPCII** and, for the detector, from **BES II to BES III**. The **BEPCII double ring** design reached a luminosity of 10^{33} $cm^{-2}s^{-1}$ at 3.78 GeV CM. The first beam was stored on 18 November 2006.

After major upgrades, the forefront **BES III detector** started its physics run in Summer 2008. Physics included precision measurement of the CKM matrix elements, precision tests of the SM, baryon spectroscopy, charmonium spectroscopy, glueball searches, and searches for non-$q\bar{q}$ states. With now 10^{10} J/ψ recorded, measurements of very rare decays are guaranteed!

[295] A. F. Zakharov, Nearly forgotten results in development of physical cosmology. https://www.arxiv.org/abs/2511.06018
[296] G. Safronov, The status and astrophysics results of the Baikal-GVD neutrino telescope. https://inspirehep.net/files/08f1c04f302cfbae30f39f1af3d87f56
[297] Information from H. Chen, Prospect of Particle Physics in China. https://indico.cern.ch/event/21977/contributions/1522286/attachments/356769/496750/CPPM801a.pdf

A Circular Electron Positron Collider (CEPC) [298] is China's proposal for a future Higgs factory with a circumference of 100 kilometers and a maximum center-of-mass energy of 240 GeV. The upgrade plan foresees an energy increase to operate at the top-pair threshold. In a second phase, a possible upgrade to a pp collider is planned, with collision energies of about 100 TeV.

Chinese **Non-Accelerator Physics** is also very active. Concerning **astroparticle physics** let us quote the **Yangbajing cosmic-ray observatory** in Tibet, and the participation to the **AMS experiment** on the ISS. China has also its own satellite, the Dark Matter Particle Explorer, or **DAMPE**, also known as **Wukong**.

The China **Jinping underground laboratory** (CJPL) [299] is currently the deepest underground laboratory in the world and will become one of the largest. Its main focus are dark matter searches (CDEX, PandaX), nuclear astrophysics and low background screening techniques.

In ν physics (see details and references in Chapter 19) the **Daya Bay ν reactor experiment**, from its ground-breaking ceremony on 13 October 2007, exploited the $\bar{\nu}_e$ flux from four reactor cores (11.6 GW), with two more cores in 2011 for a total of 17.4 GW, and with identical near and far detectors.

The **JUNO** (Jiangmen Underground Neutrino Observatory), a medium baseline reactor neutrino experiment, is under construction in Southern China.

Big **scientific platforms** also exist in China:

- The **Synchrotron Radiation Light Sources**: Beijing synchrotron radiation facility (2.5 GeV), Hefei national synchrotron radiation light source (800 MeV), Shanghai Light source (3.5 GeV, under construction).
- The **Chinese Spallation Neutron Source**

And dozens of **PP and NP theory groups** are active in institutes and universities.

10.16 Programmes in Japan

The key role of great Japanese physicists in the birth of Particle Physics [300] is quite obvious (see Chapter 1 and Section 4.2).

10.16.1 KEK

KEK **(High Energy Accelerator Research Organization)** was founded in 1971. A 12 GeV Proton synchrotron (KEK PS) was constructed in 1976, a 2.5 GeV Photon factory in 1978.

The **Tri Ring Intersecting STorage Accelerators in Nippon (TRISTAN**) machine initially planned as a beam collider aiming at various types of beam collisions, $e^+ e^-$, ep, and pp, and with three rings: the 50 GeV proton/electron booster and both 180 GeV proton storage rings with superconducting magnets.

The e^+e^- collider TRISTAN was proposed in 1973 by Tetsuji Nishikawa, with a 3.016 km circumference, 32 GeV beam energy and 4.5×10^{31} cm^{-2}s^{-1} luminosity with experiments AMY, TOPAZ and VENUS. The physics goals included top search, QCD, 2γ physics.

[298] J. Gao, Y. Li and C. Yu, China's designs for a future circular collider.
https://cerncourier.com/a/chinas-designs-for-a-future-circular-collider/
CEPC Technical Design Report: Accelerator, https://arxiv.org/pdf/2312.14363
[299] H. Ma *et al.*, Status and prospect of China Jinping Underground Laboratory. https://inspirehep.net/literature/2037563
[300] Y. Nambu, Particle Physics since Lawrence and Yukawa. https://cds.cern.ch/record/1108080/files/p1.pdf

The design was to exceed the PEP (29 GeV) and PETRA (46 GeV) accelerators as much as possible, up to 60 GeV CM energy and to get ahead of LEP as early as possible.

The TRISTAN accelerator system consisted of a 2.5 GeV e^+ and e^- injector linac with a 0.25 GeV positron generation linac, an 8 GeV accumulation ring (AR), and a main collider ring (MR).

The ground-breaking ceremony took place in November 1981. TRISTAN [301], world highest energy e^+e^- collider before LEP, operated from 1986 to 1995. With a SC cavity system, SC quadrupole magnets for mini-beta insertion, the machine performed well with luminosity rising from 1986 to 1992 up to $4 \times 10^{31}\,cm^{-2}s^{-1}$.
Unfortunately, the top quark was out of reach and the Z manifested itself only by an increase in the R value and γ–Z interference studied through measurements of large charge asymmetries [302]. Thus, TRISTAN was stopped in 1995.

In 1986 it had been decided to start accelerator R&Ds immediately aiming at domestic construction of a future **TeV linear collider** (see Chapter 15).

10.16.2 KEKB

However, time was ripe for another domain of physics. In 1973 Makoto Kobayashi and Toshihide Maskawa had proposed the "KM-mechanism" of CP-violation. The third generation had been discovered. In 1980 CLEO at CESR (Cornell, US) discovered $\Upsilon(4S)$ with $m_\Upsilon = 10.55$ GeV. In 1987, the B-meson lifetime of $\tau = 1.29 \pm 0.2$ ps was measured by MAC at PEP, and in 1987 large $B\overline{B}$ oscillation of 0.21 ± 0.05 were observed by ARGUS at DORIS-II.

In 1986, Piermaria Oddone proposed an asymmetric e^+e^- collider. In 1994 KEKB and PEP-II were designed as such machines, to be constructed, and operated in parallel, with the same clear physics goal. The race started. TRISTAN was removed in 1995. First beams were stored in the KEKB rings in 1998–1999 and the BELLE experiment was operational from 1999 till 2010. KEKB operated with e^- at 8 GeV and e^+ at 3.5 GeV, reaching a luminosity of $2.1 \times 10^{34}\,cm^{-2}s^{-1}$.

Exploiting collisions with finite crossing angle, both machines exceeded their luminosity goals by a factor 2. A friendly race led them to **the discovery of CP violation in the B^0 system in 2001** [303]. Abundant flavour physics followed.

Then came SuperKEKB and SuperBELLE (Chapter 14).

10.16.3 J-PARC

The old 40 GeV KEK PS plan was realized about three decades after as the Japan Proton Accelerator Research Complex (**J-PARC**). J-PARC is composed of three proton accelerators (400 MeV linac, 3 GeV Rapid Cycle Synchrotron, and 50 GeV Main Ring) and three research facilities (Materials and Life Science Experimental Facility, Neutrino Experimental Facility, and Hadron Experimental Facility). The Main Ring feeds the T2K (Tokai to Kamioka) neutrino experiment (see below).

---

[301] Y. Kimura, From TRISTAN to B–Factory. https://www.nishina.riken.jp/researcher/seminar_past/nishina120/kimura.pdf
[302] T. Nozaki, Tests of the Standard Model of Electroweak Interactions at the e^+e^- collider TRISTAN https://inspirehep.net/files/ff81abfb842f9b456a7065dde274063f
[303] K. Abe *et al.,* Observation of Large CP Violation in the Neutral B Meson system. https://arxiv.org/abs/hep-ex/0107061
B. Aubert *et al*, Observation of CP violation in the B^0 meson system. https://arxiv.org/abs/hep-ex/0107013

10.16.4 Neutrinos

In 1979, Masatoshi Koshiba proposed the initial concept of **Kamiokande**. The Kamiokande tank construction started in late 1982 and the Kamiokande experiment on July 6, 1983.

During these studies, missing ν_μ (or a smaller μ-like/e-like ratio) were observed. IMB (US) had measured the same effect. In short, Kamiokande observed **supernova neutrinos** (1987), found **missing atmospheric muon-neutrinos** (1988) and confirmed the **missing solar neutrino problem (1989)**.

Super-Kamiokande (SK) started taking data on 1 April 1996. In 1998, SK concluded that the observed zenith angle dependence (and other supporting data) gave **evidence for neutrino oscillations** [304]. Much more information about neutrino physics will be given in Chapters 19 and Section 32.1.

Due to an accident in 2001, more than a half of the PMTs were broken. But SK was partially recovered with the survived PMTs in 2002 and fully recovered in 2006.

Super-Kamiokande continues contributing to ν physics, detecting atmospheric and solar ν, acting as far detector of K2K and T2K, looking for relic supernova neutrinos. It also pursues proton decay searches (Section 32.4).

The next step will be Hyper-Kamiokande (see Section 32.4 and references there).

10.17 The High Intensity Proton Accelerator Facility at the Paul-Scherrer-Institute

The very rich physics program at PSI will be treated in detail in Chapter 33. But let us here illustrate its jewel at the Intensity Frontier, the High Intensity Proton Accelerator Facility (HIPA) [305].

It provides a 1.4 MW proton beam for the production of mesons and neutrons used for materials science and particle physics. With a beam current of up to 2.4 mA, HIPA holds the world record for a cyclotron-based accelerator facility. With 10 trillion protons accelerated per second, a high intensity of secondary particles is produced for high-precision experiments.

HIPA drives the only continuous-beam spallation neutron source in the world (SINQ) and the world's most powerful continuous-beam μSR facility (SμS). It also serves the PP program (see Chapter 33) with pions, muons and ultracold neutrons.

Protons are accelerated in a three-stage process. The first stage consists of a microwave driven proton source providing a 60 kV DC proton beam with a net current of approximately 10 mA for the Cockcroft–Walton (CW) pre-Accelerator. The CW raises the beam energy from 60 keV to 870 keV. Between the CW and the Injector 2 cyclotron the continuous (DC) beam provided by the CW is converted into a bunched beam with a bunch frequency of about 50 MHz to match with cyclotron acceleration. The Injector 2 cyclotron collimates the beam and accelerates the remaining protons to 72 MeV as required for the injection into the Ring cyclotron. Besides a small fraction devoted to produce radio-isotopes, the main fraction of the beam is injected into the Ring cyclotron, which accelerates the proton bunches up to 590 MeV as required for the efficient production of secondary particles.

After extraction from the Ring cyclotron the beam is guided towards two targets where pions and muons are generated for user experiments. The remaining beam is transported to the SINQ target

[304] T. Kajita, Atmospheric neutrino results from Super-Kamiokande and Kamiokande – Evidence for ν_μ oscillations. https://arxiv.org/abs/hep-ex/9810001

[305] The High Intensity Proton Accelerator Facility. https://www.psi.ch/en/cas/hipa

for the production of neutrons. Every few minutes the full beam is kicked for several seconds to the beamline of the ultra-cold neutron source (UCN).

In the past years, an availability of 95% was achieved.

11. ISR physics and technology

According to Maurice Jacob [306], ISR physics had *"a brilliant start"* (1971–74), *"a somewhat difficult period"* (1975–77) and *"a very active and interesting program"* (1978–83).

Physics highlights [307] include:

- The total pp cross-section increasing with the energy [308].
  Instrumental for this measurement, the "Roman pot" technique was invented at the ISR to study particles scattered at very small angles. These particles travel close to the circulating beams, in fact inside the vacuum chamber.
- The demonstration in 1973 of the production of hadrons at large p_T, showing that the partons were also pointlike with respect to the strong interaction.
- The discovery in 1979 of the production of direct photons, and their in-depth study, an important QCD test.

Unfortunately, J/ψ, charm, beauty, tau and gluon were found elsewhere, while they were potentially accessible at the ISR. This was initially due to inappropriate detectors, focused on the forward region, by lack of theoretical guidance.

An example is the Split Field magnet, equipped of a system of 40 MWPCs of light-weight design with around 50 000 sense wires and the electronics to read the signals, completed in record time, and in 1972 ready to take data.

The proper detectors arrived later, as the Open Axial Field Magnet, with its clever structure allowing barrier-free access [309].

However, the hadronic rate at large p_T turned out to be a high background noise and forced to set high thresholds which prevented discoveries.

11.1 Instrumental highlights

Nevertheless, one can quote major innovative instrumental highlights [310].

An example is the demonstration by the R806 experiment of the interest of transition radiation detectors (TRDs).

Precision calorimetry became a focal point of detector R&D at the ISR. Indeed, with a sufficiently precise measurement of the energy balance in the transverse plane (the energy components should add up to zero), a neutrino will manifest itself as an unbalance in this transverse energy distribution.

The goal was to understand the underlying detector physics determining the intrinsic performance and to develop instrumentation reaching this performance and surrounding the collision point quasi

[306] L. Van Hove and M. Jacob, Highlights of 25 years of physics at CERN. *Phys.Rep. 62 (1980) 1-86.*
CERN: The second 25 years. Editors: J.R. Ellis, J. Gillier, M. Jacob, D.E. Plane and D. Treille, *Phys.Rep.403-404 (2004)1-504*
[307] M. Jacob and K. Johnsen, A Review of Accelerator and Particle Physics at the CERN Intersection Storage Rings. CERN-84-13, https://cds.cern.ch/record/156665/files/CERN-84-13.pdf
[308] U. Amaldi, An ISR Discovery: The Rise of the Proton–Proton Cross-Section.
https://cds.cern.ch/record/2103292/files/9789814644150_0011.pdf
[309] C. Fabjan, Evolution and revolution: detectors at the ISR.
https://cerncourier.com/a/evolution-and-revolution-detectors-at-the-isr/
[310] C. Fabjan and K. Hübner, The Intersecting Storage Rings (ISR): The First Hadron Collider. In Technology Meets Research: https://inspirehep.net/files/21e59791dffe28bfbec1d89abe0652c6 , p. 87

"hermetically". A crucial requirement is to equalize the calorimeter response to the electromagnetic and hadronic parts of the cascade.

Scintillators were mostly used, but their instrumental disadvantages led to the suggestion to replace them with liquid argon.

Among the proposals to achieve this equalization ("compensation"), an unconventional one was the idea to use depleted uranium 238 as absorber plates. A 300-ton uranium scintillator calorimeter with full azimuthal coverage was constructed for the Axial Field Spectrometer.

11.2 Machine highlights

The ISR machine was a superb machine, a test bed for ground-breaking accelerator and detector technologies.

For the ISR intersections, where the p–p collisions take place, a pressure lower than 10^{-10} Pa was required to minimize the proton–gas interactions. One of the ISR experimental areas was equipped with two large cryopumps, where a pressure lower than 10^{-10} Pa was achieved. This was a test bench for cryopumping on a large scale in LHC where it is now used successfully in the cold sectors over about 18 km.

Moreover, it is not trivial to measure such a level of vacuum. Gauges of improved design were produced by industry and used in the ISR, where they measured pressures typically in the low 10^{-10} Pa range. Improvements extended the access of the gauge to the low 10^{-12} Pa range, which was and still is the lowest pressure ever measured inside a vacuum system [311].

To squeeze beams to increase the luminosity, superconducting quadrupoles were used, but of greater size, strength and quality than had been previously attained.

Another achievement was the cryogenics for the Superconducting High Luminosity Insertion Magnets (one per beam), which started regular operation in 1981. This was the first ever superconducting magnet system in an operating accelerator.

Stochastic cooling was briefly discussed in the previous chapter.

At the end of the ISR in 1983, Maurice Jacob declared: *"I come to bury Caesar and not to praise him"* (Marc Antoine, in Jules César), while Victor Weisskopf tried to convince that *"no matter where the discoveries are done"*. The Pope and the Dalai Lama gave CERN moral comfort, but the real one came from the success of the proton-antiproton collider.

11.3 Main physics results

Figures 11-1 to 11-3 describe the main physics results of the ISR [312]:

---

[311] C. Benvenuti, Vacuum Pumping by Freezing Molecules and How to Measure Almost Nothing. In Technology Meets Research: https://inspirehep.net/files/21e59791dffe28bfbec1d89abe0652c6 p. 99 and p. 101
C. Fabjan and K. Hübner, The Intersecting Storage Rings (ISR): The First Hadron Collider. In Technology Meets Research: https://inspirehep.net/files/21e59791dffe28bfbec1d89abe0652c6 , p. 87

[312] G. Giacomelli and M. Jacob, Physics at the CERN ISR. *Phys.Rept. 55 (1979) 1-132*
C. Fabjan and N. McCubbin, Physics at the CERN Intersecting Storage Rings (ISR) 1978–1983. *Phys. Rep. 403–404 (2004) 165–175*
U. Amaldi *et al.,* 40th Anniversary of the First Proton-Proton Collisions in the CERN Intersecting Storage Rings (ISR). https://arxiv.org/html/1206.4876/

— cross-section increasing with energy (Fig. 11-1),
— particles emitted at large p_T (Fig. 11-2) and
— direct photons appear at large p_T (Fig. 11-3).

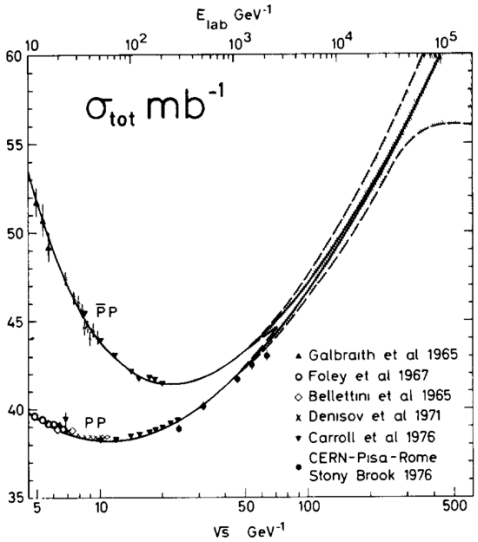


Fig. 11-1: Cross-section increasing with energy.

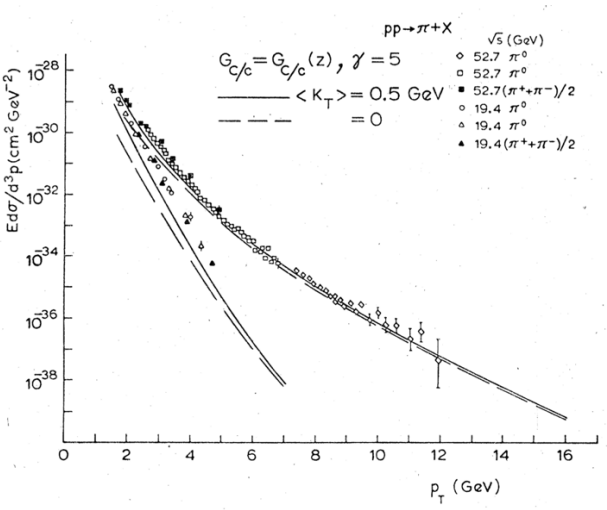


Fig. 11-2: Particles emitted at large p_T.

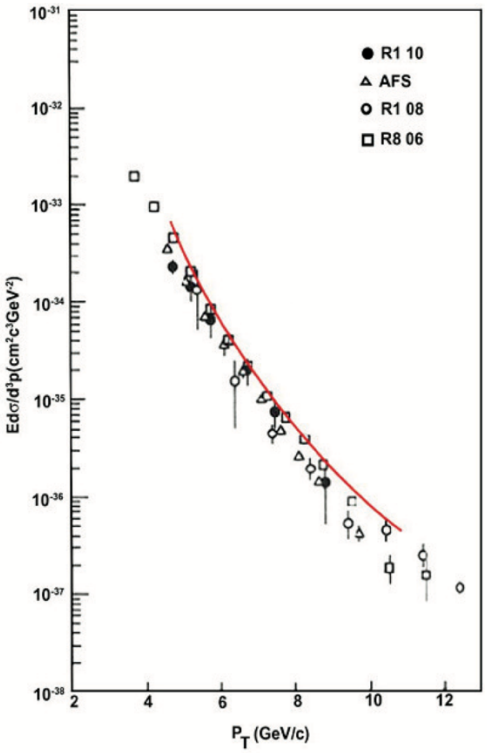


Fig. 11-3: Direct photons appear at large p_T.

12. The W and Z discovery

12.1 The UA experiments at the CERN proton-antiproton collider

Following the discovery of Neutral Currents, the goal of the collider program was clear: discover W and Z Bosons [313]. The two elements which made this program possible are, on the one hand, the vision of Carlo Rubbia from 1966 of the possibility of using the SPS as a proton-antiproton collider, on the other hand, the invention in 1968 by Simon van der Meer of the stochastic cooling.

A brilliant machine served excellent detectors combining hermeticity, redundancy of procedures and innovative techniques. It is fair to say that producing W and Z was more difficult than detecting them in their leptonic decay modes.

Key milestones towards the discovery were:

- 1976 paper by Carlo Rubbia, Peter McIntyre, David Cline [314];
- 1977 proposal made at CERN and Fermilab, feasibility studies;
- 1978 success of stochastic antiproton cooling at ICE, ring recycled from the first g–2 programme;
- 1978 approval of the UA1 and UA2 experiments;
- 1983 discovery of W and Z;
- 1984 Nobel Prize for Carlo Rubbia and Simon van der Meer.

Most striking was the speed with which the decisions were taken, with only seven years between the first article by Carlo Rubbia *et al.* (1976), and the success in 1983, via the proposal submitted to CERN and Fermilab in 1977, the feasibility studies and the successful stochastic cooling tests, the approval of the experiments, their construction and their commissioning. This is largely due to the determination of Carlo Rubbia in an initially somewhat unfavourable climate.

As former UA2 spokesperson Pierre Darriulat wrote in 2004 [315]: *"But when proton–proton colliders such as the Superconducting Intersecting Storage Rings were proposed in this spirit, they were 'killed in the egg' by the management at CERN, with the argument that they would delay – or, even worse, endanger – the LEP project. The same argument did not apply to the proton–antiproton collider, as it did not require the construction of a new collider ring and could be proposed as an experiment …*
Another argument also made it possible for the proton–antiproton project to break the LEP taboo: if CERN did not buy Carlo's idea, it was most likely that he would sell it to Fermilab.
Whether the weak bosons would have been discovered at LEP, at the Stanford Linear Collider (SLC), or at some other collider is another matter, but it would have taken another six years at least."

The ingredients that led from the idea to the conviction are in 1976 the implementation of ICE, its longitudinal cooling, showing that it was possible to cool in all planes, then the construction of the AA launched in 1978, the process of stochastic accumulation and the first comprehensive set of stochastic cooling systems.

---

[313] V. Chohan and P. Darriulat, The CERN Antiproton Programme: Imagination and Audacity Rewarded. In Technology Meets Research, https://inspirehep.net/files/b6490184742632ba3b1c9481f1efb15a , p. 179
F. Pauss, $S\bar{p}pS$ Collider Physics: a very exciting time in CERN's history.
https://indico.cern.ch/event/1068633/contributions/4495624/attachments/2327818/3965899/Pauss_ppbar_Physics.pdf

[314] C. Rubbia *et al.,* Producing Massive Neutral Intermediate Vector Bosons with Existing Accelerators.
https://lss.fnal.gov/conf/C7803272/p175.pdf

[315] P. Darriulat, The W and Z particles: a personal recollection, CERN COURIER Mar 31, 2004;
https://cerncourier.com/a/the-w-and-z-particles-a-personal-recollection/

The UA1 experiment was approved in June 1978, UA2 in December the same year. The first proton-antiproton collisions in the SPS took place in June 1981. The first physics run came in 1982, and the W and Z followed soon after. Detected via their lepton decays, their detection was less of a challenge than their production.

On the detector side, a lot of effort was made to ensure good hermeticity.

UA1 was a versatile detector, with a classic dipole magnet (which has since had a lively second life) (Fig. 12-1 left). Its central tracking detector [316], a veritable electronic bubble chamber, was pioneering work and a remarkable success. Bernard Sadoulet was a major player.

UA2, three times cheaper than UA1, without a central magnet, detected electrons but no muons. It had a high-quality, high-resolution lead-scintillator central calorimeter. Its central vertex detector, with several new technologies, scintillating fibres and a checkerboard of silicon pads, demonstrated the emerging power of this latest technology (Fig. 12-1 right).

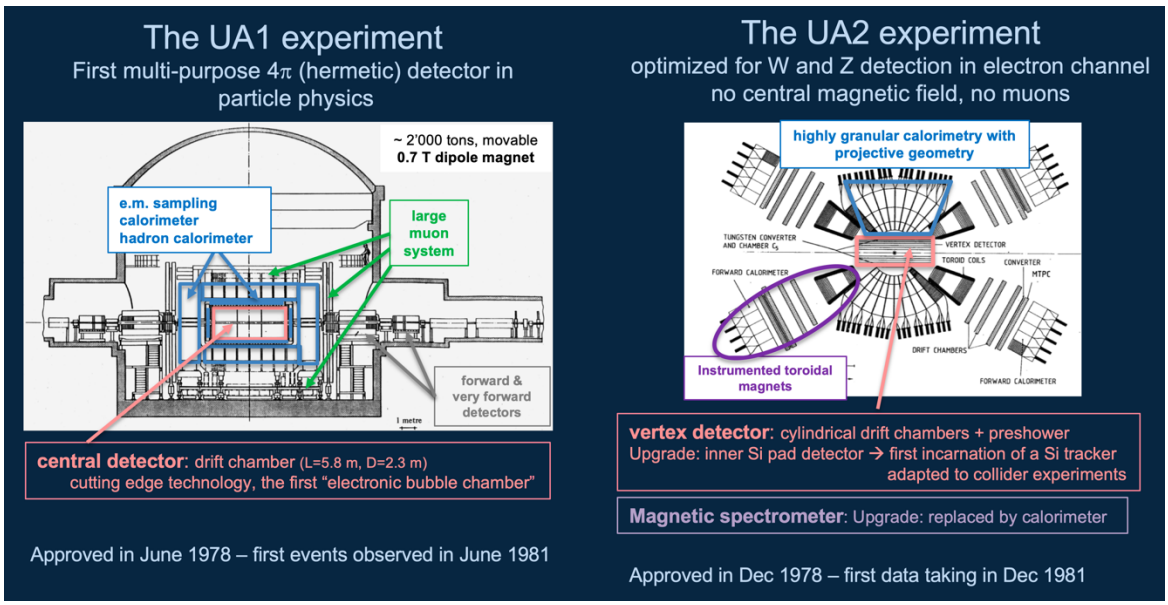


Fig. 12-1: Layout of the UA1 (left) and UA2 (right) experiment.

Figures 12-2 and 12-3 show pictures of UA1 and UA2 and Figs. 12-4 to 12-9 illustrate various aspects of UA1 and UA2.

We also like to mention UA5 and its large streamer chambers. This experiment also served as test benches for the LHC experiments.

In addition to bosons, the UA-experiments have brought other important physics results: the angular distribution of parton-parton scattering, information on proton structure functions, in particular on the role of small-x gluons, multijet final states, the p_T distribution of W's, the mixing of beauty, etc.

"L'espoir changea de camp, le combat changea d'âme" (Daniel Denegri et Victor Hugo) [317]. Hugo was actually referring to Waterloo, but for convinced Europeans, it doesn't matter.

[316] B. Sadoulet, The UA1 Tracker: An Electronic Bubble Chamber. In Technology Meets Research, https://inspirehep.net/files/b6490184742632ba3b1c9481f1efb15a , p. 201

[317] D. Denegri, When CERN saw the end of the alphabet. CERN Courier 43, 4 (2003) pp. 26-30, https://cerncourier.com/a/when-cern-saw-the-end-of-the-alphabet/

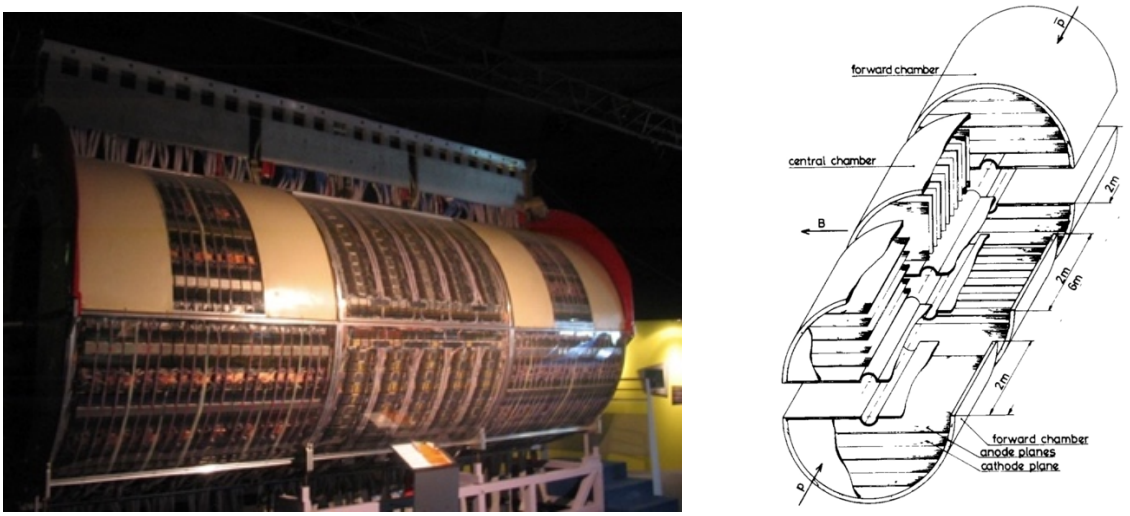


Fig. 12-2: UA1 trajectograph (left) and its structure (right).

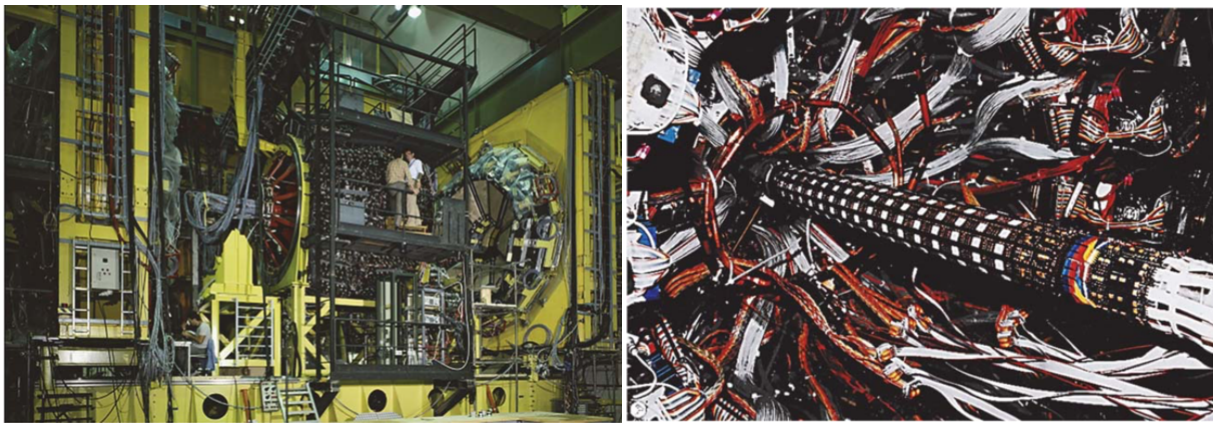


Fig. 12-3: UA2 detector (left) and its silicon pad detector (right).

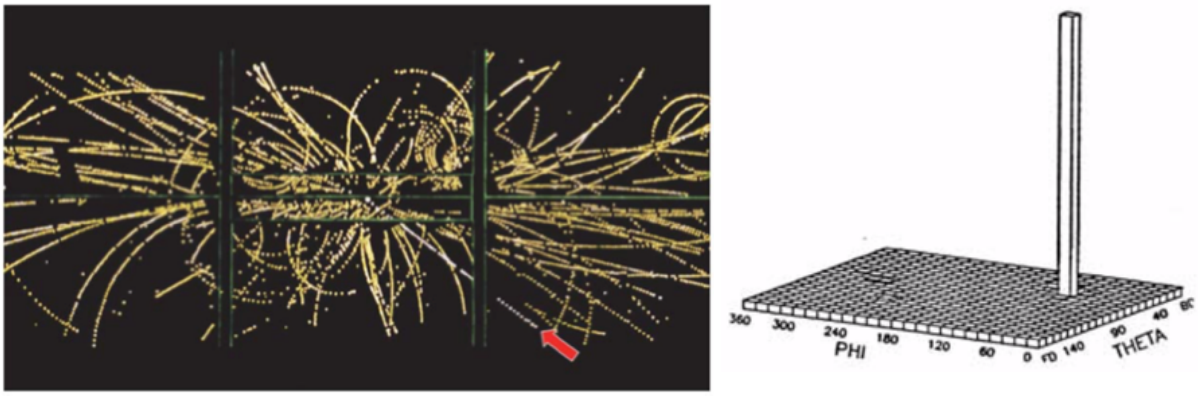


Fig. 12-4: First W candidate in UA1: interactive event display (Megatek) of the trajectograph (left) and the so-called lego-plot of the same event (right).

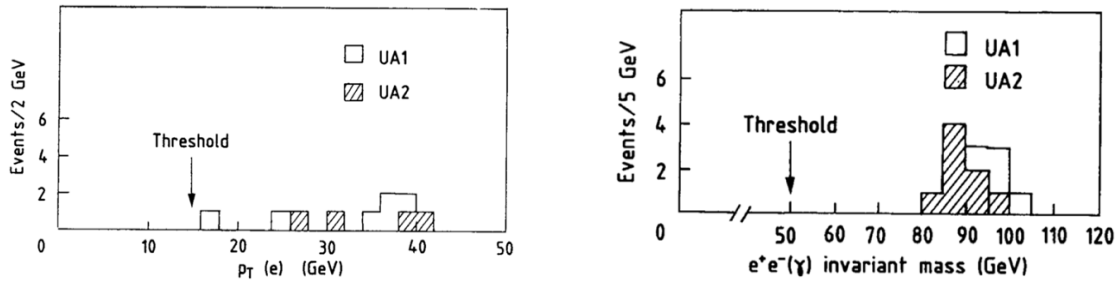


Fig. 12-5: The UA1 and UA2 discovery plots of the Z boson: the p_T spectrum of the electron (left) and the invariant mass distribution of the e^+e^- pair (right).

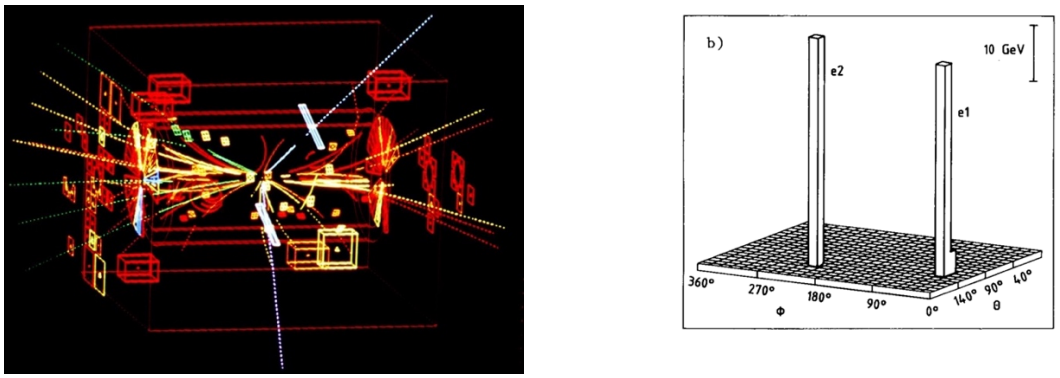


Fig. 12-6: UA1 event display of the first Z candidate recorded on 30 April 1983 at 18:53 (left) and lego-plot of a Z candidate in UA2 (right).

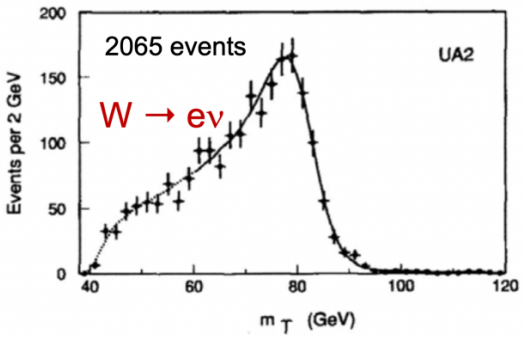


Fig. 12-7: The W transverse mass spectrum in UA2 [318].

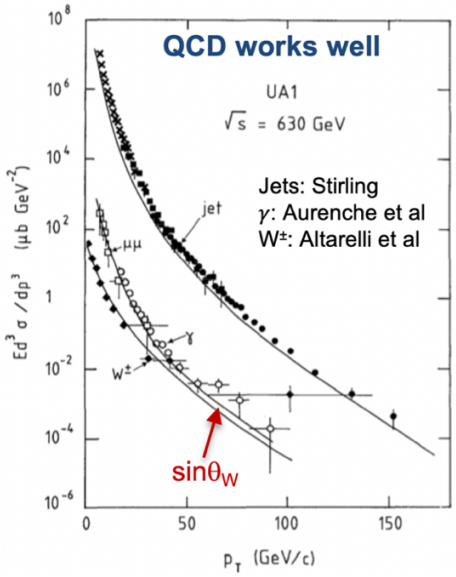


Fig. 12-8: The good understanding of QCD (jets) and the EW theory: prompt γ and W production getting closer as p_T increases [319].

[318] L. di Lella, Remembering the W discovery. CERN Courier 10 January 2023, https://cerncourier.com/a/remembering-the-w-discovery/

[319] F. Pauss, $Sp\bar{p}S$ Collider Physics: a very exciting time in CERN's history. https://indico.cern.ch/event/1068633/contributions/4495624/attachments/2327818/3965899/Pauss_ppbar_Physics.pdf



P. Darriulat



C. Rubbia and S. van der Meer



The Dalai-Lama at Megatek with C. Rubbia

Fig. 12-9: Personalities and moments of the W and Z discovery.

After the IVB discovery and taking benefit of the increase in luminosity described in Section 10.5 the UA experiments performed a lot more of elaborate physics analyses.

For instance, a summary of UA2 final achievements can be found in Ref. [320]. The large data sample collected from 1988 to 1990 at $\sqrt{s}$ = 630 GeV offered detailed tests of many aspects of the SM. Precise measurements of electroweak parameters were performed, predictions of perturbative QCD were tested, and a new mass range of possible new particles was explored.

Let us give two examples.
The final results of the W and Z masses measurements from UA2 are

$$m_w = 80.84 \pm 0.22 \text{ (stat)} \pm 0.17 \text{ (syst)} \pm 0.81 \text{ (scale) GeV},$$
$$m_z = 91.74 \pm 0.28 \text{ (stat)} \pm 0.12 \text{ (syst)} \pm 0.92 \text{ (scale) GeV}.$$

The largest errors result from the ±1% uncertainty on the absolute energy scale and mostly cancel in the ratio m_w/m_z. The ratio $m_w/m_z = 0.8813 \pm 0.0036$ (stat) ± 0.0019 (syst), multiplied by the LEP value of m_z, $m_z = 91.175 \pm 0.021$ GeV, gives a more precise value of the W mass:

$$m_w = 80.35 \pm 0.33 \text{ (stat)} \pm 0.17 \text{ (syst) GeV}.$$

This value agrees with the CDF W mass measurement in 1990, $m_w = 79.91 \pm 0.39$ GeV [321]. If both results are combined one gets

$$m_w = 80.14 \pm 0.27 \text{ GeV},$$

where the statistical and systematic errors have been added in quadrature.

The measurement of the ratio of the IVB masses is equivalent to the measurement of the weak mixing angle $\sin^2\theta_W$. Using the on-shell renormalization scheme, where $\sin^2\theta_W$ is defined to all orders as $\sin^2\theta_W = 1 - (m_W/m_Z)^2$, the collider measurements can be translated into:

$$\sin^2\theta_W = 0.2234 \pm 0.0072 \text{ (UA2)},$$
$$\sin^2\theta_W = 0.2274 \pm 0.0052 \text{ (UA2+CDF)}.$$

EW radiative corrections modify the Born level predictions for the boson mass values. Using the dependence of the *W* mass on the mass of the top quark and the mass of the Higgs in the SM, from the UA2 result it can be concluded that

$m_{top} = 160^{+50}_{-60}$ GeV or $m_{top} < 250$ GeV (95% CL) for $m_H = 100$ GeV and for $m_H < 1$ TeV, respectively.

---

[320] K. Jakobs, The Physics Results of the UA2 Experiment at the CERN proton-antiproton Collider.
https://lib-extopc.kek.jp/preprints/PDF/1994/9405/9405299.pdf
F. Pauss, Physics in proton-antiproton collisions.
https://lib-extopc.kek.jp/preprints/PDF/1989/8909/8909387.pdf

[321] F. Abe *et al.,* (CDF Collaboration), Measurement of the W-boson mass. *Phys. Rev. Lett. 65, 2243,*
https://journals.aps.org/prl/abstract/10.1103/PhysRevLett.65.2243

12.2 What followed in the antiproton world

All these innovations and breakthroughs were taken up and then adapted to FNAL, which led in particular to the discovery of the top in 1995 (Chapter 16). On the other hand, it gave birth to a long and rich program at low energy, with LEAR until 1966, then, still in progress, with the AD deceleration ring (the transformed AC).

The LEAR ring [322] was equipped with two 4-π detectors, the Crystal Barrel, whose CsI calorimeter provided good spectroscopy, and CP-Lear, whose interesting results are cited in Chapter 13. Some highlights of the LEAR program are the ultra-slow extraction of its antiproton beam, and, as antiprotons should be very slow, their slowing down by radiofrequency quadrupole.

The objective was precise measurements of the properties of antiparticles, antiproton then antihydrogen, which was observed in flight at LEAR in 1996, then trapped in a Penning trap in 2002 by ATRAP and ATHENA.

The AD continues the antimatter program. The antiprotons produced by the collisions of protons from the PS at 24 GeV, are filtered in mass and charge, then decelerated in the AD from a few GeV to 5.3 MeV. ELENA (Fig. 12-10) will complete the job. Trapping requires an energy reduction at keV. To be studied, hydrogen antiatoms must be either beam-formed (ASACUSA) or trapped (ALPHA).

A major goal will be the study of the gravitational behaviour of antihydrogen atoms. In AEgIS, GBAR, ALPHA, it is necessary to aim for a cooling of these atoms towards 2 mK [323].

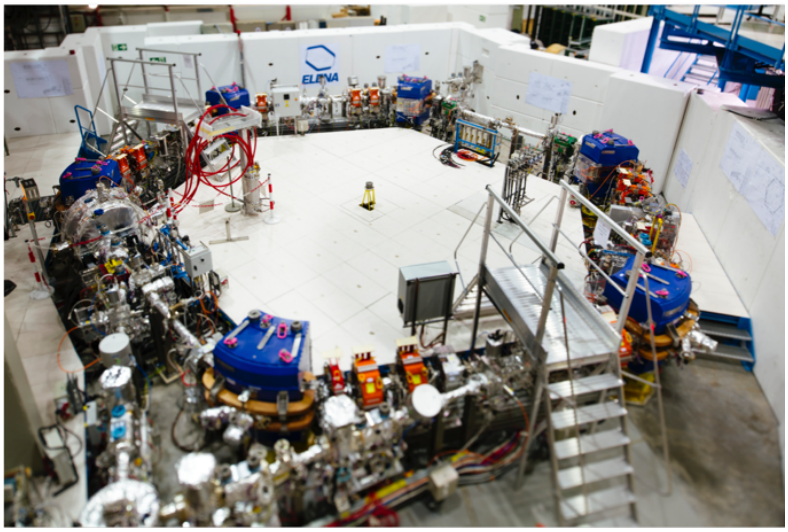


Fig. 12-10: The ELENA ring.

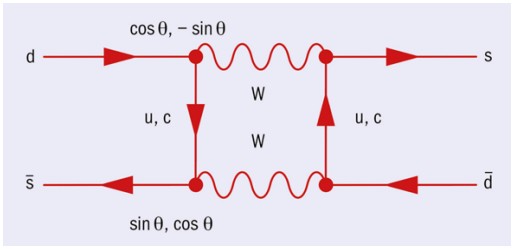
[322] P. Lefèvre, LEAR in the Nineties. https://cds.cern.ch/record/201428/files/CM-P00059198.pdf
D. Möhl, LEAR, History and Early Achievements. https://core.ac.uk/download/pdf/25260046.pdf
[323] M. Doser, Precision experiments with antihydrogen: an outlook.
https://inspirehep.net/files/2dc601df149ee083d625841c08c7dca9
A. Schaeffer, Exceptionally slow antiprotons.
https://home.web.cern.ch/news/news/accelerators/exceptionally-slow-antiprotons

13. CP Violation [324]

13.1 The kaon story

Figure 13-1 recalls properties of the K^0 system: the particle-antiparticle mixing and the definition of states.

In 1970 the **GIM mechanism** (Chapter 8 and Fig. 13-1) explained the near absence of flavour changing NC by postulating **charm**, which was discovered, first hidden (the J/ψ in 1974), then open (in 1976). Previously, the K^0 system had shown the existence of **mixing**, particle-antiparticle transformation, and offered a short-lived particle, K_1, and a long-lived one, K_2, with K_1 and K_2 + and – **eigenstates of CP**.



$$|K_1\rangle = \frac{1}{\sqrt{2}}\left(|K^o\rangle + |\bar{K}^o\rangle\right) \qquad CP\,|K_1\rangle = +1\,|K_1\rangle$$

$$|K_2\rangle = \frac{1}{\sqrt{2}}\left(|K^o\rangle - |\bar{K}^o\rangle\right) \qquad CP\,|K_2\rangle = -1\,|K_2\rangle$$

$$|K_S\rangle = \frac{1}{\sqrt{1+|\varepsilon|^2}}\left(|K_1\rangle + \varepsilon|K_2\rangle\right) \qquad K_2 \nrightarrow 2\pi$$

$$|K_L\rangle = \frac{1}{\sqrt{1+|\varepsilon|^2}}\left(|K_2\rangle + \varepsilon|K_1\rangle\right) \qquad K_L \neq K_2$$

ε degree of CP violation

Fig. 13-1: Properties of the K^0-system.

The surprise was great when in 1964 a Brookhaven experiment in a K_2 beam observed a clear signal of a decay into $\pi^+\pi^-$ (CP = +1) (Fig. 13-2) [325]. θ is the angle of the resultant of the two pion tracks with respect to the beam axis. René Turlay was very involved in this discovery [326].

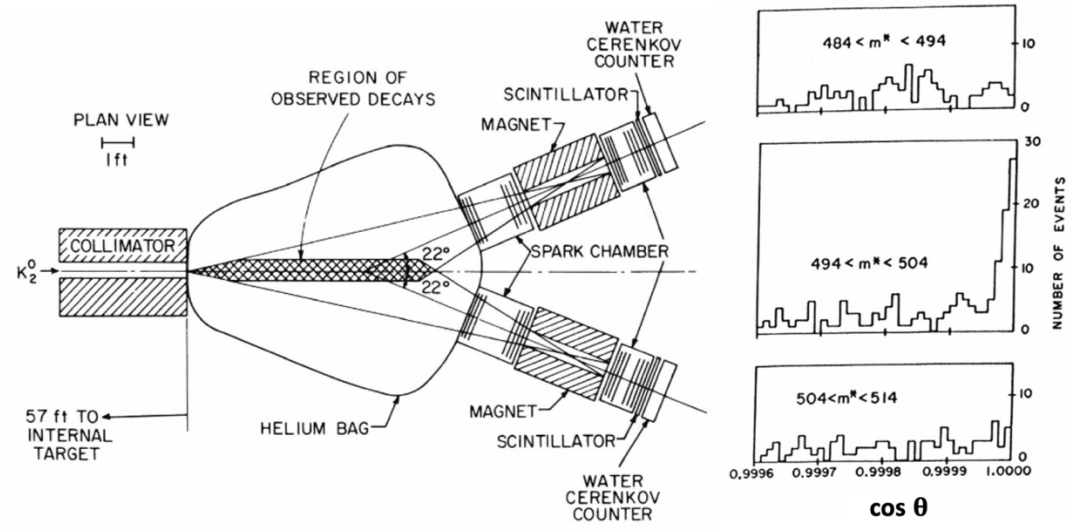


Fig. 13-2: Indirect CP violation: Nobel Prize in 1980 to James Cronin and Val Fitch. The set-up (left) and the signal (right).

[324] For an overview: Y. Nir, Flavour Physics and CP Violation. https://arxiv.org/abs/1605.00433
[325] J. Cronin, The Experimental Discovery of CP Violation.
https://inspirehep.net/files/90037f1ddee05a8e74c284ce5681b66e
[326] Hommage to R. Turlay, ScintillationS_N57.pdf (March 2003)

It was then explained that this violation of CP resulted from the fact that the long-lived particle, K_L, was not quite K_2 but had, via mixing, acquired a small component of CP = 1 (Fig. 13-1, right). It was then called **indirect CP violation.**

Demonstration of a direct (say Kobayashi–Maskawa-like) violation required the measurement of a double ratio shown in Fig. 13-3, involving K_L and K_S as well as both neutral and charged decay modes. It was a great transatlantic duel at that time, with a great deal of intelligence put into the experiments and the design of the kaon beams [327].

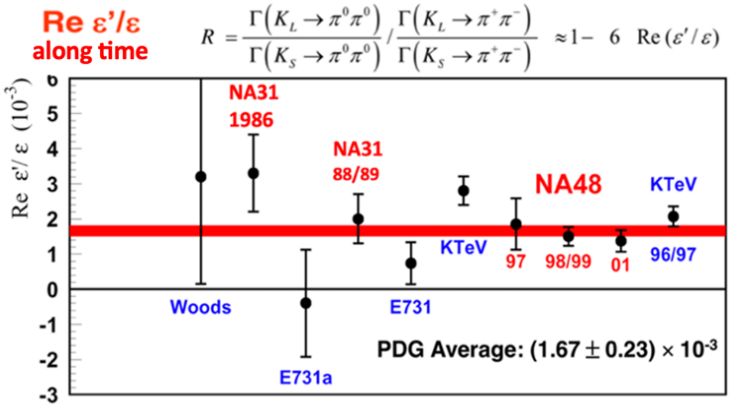


Fig. 13-3: Direct CP violation (courtesy A. Ceccucci, derived from Ref. [328]).

After some periods of doubt, agreement was reached on the evidence of a **direct CP violation** (an ordinate different from zero in the data of Fig. 13-3). This saga is well told in Ref. [329].

At CERN, NA48 later became NA62 [330], performing precision measurements as $K^+ \to \pi^+\mu^+\mu^-$ and $K^+ \to \pi^+\gamma\gamma$ ($BR(K_{\pi\mu\mu}) = (9.15 \pm 0.08) \times 10^{-8}$, $BR(K_{\pi\gamma\gamma}) = (9.73 \pm 0.19) \times 10^{-7}$) and exotic searches in the beam-dump mode. Figure 13-4 shows the NA48 beam line.

NA62 obtained a 5σ rejection of the background-only hypothesis for $K^+ \to \pi^+\nu\bar{\nu}$ decay [331] with a $BR = 13.0^{+3.3}_{-3.0} \times 10^{-11}$.

Still concerning the K^0, let us mention the work of **CP Lear** on the **LEAR antiproton ring** and the reactions $p\bar{p} \to K^{\pm}\pi^{\mp}K^0(\bar{K}^0)$ with direct measurement of **non-invariance by time reversal** [332] (Fig. 13- 5), namely $P(K^0 \to \bar{K}^0) - P(\bar{K}^0 \to K^0) \neq 0$ at $5\,\sigma$ and **CPT conservation** demonstrated 50 times more precisely than before.

---

[327] N. Doble and L. Gatignon, Two Very Special K^0 Beams: Discovery of Direct CP Violation.
https://inspirehep.net/files/818b65cb5004b2f8c5f23faf63571c33 p. 158
I. Mannelli, Liquid Krypton Calorimetry: Elucidating Nature's Subtle Asymmetries. ibid, p. 161

[328] K. Kleinknecht and H. Wahl, First observation of direct CP violation in weak decays of neutral K mesons. europhysicsnews, volume 37, number 2, p. 26, https://www.europhysicsnews.org/articles/epn/pdf/2006/02/epn06203.pdf

[329] L. Iconomidou-Fayard and D. Fournier, The Discovery of Direct CP Violation.
https://cds.cern.ch/record/2103283/files/9789814644150_0009.pdf

[330] NA62 experiment: https://na62.web.cern.ch/home/home.html

[331] G. Ruggiero, On the ultra-rare $K^+ \to \pi^+\nu\bar{\nu}$-decay at NA62. Moriond EW 2025.
https://indico.in2p3.fr/event/35965/contributions/152400/attachments/91530/139511/5_GRuggiero-v1.pdf
The SM prediction is $(K^+ \to \pi^+\nu\bar{\nu}) = 8.38(17)(25)(40) \times 10^{-11}$. The last and dominant uncertainty is parametric, in particular from $|V_{cb}|$.

[332] A. Filipcic, CP, T and CPT at CPLEAR. https://inspirehep.net/files/e2bd65b804a11c301d38e181d4a08c11
For a thorough discussion of time reversal: J. Bernabeu and F. Martinez-Vidal, Time-Reversal Violation. *Ann. Rev. Nucl. Part. Sci. 2015. 65:403–27*

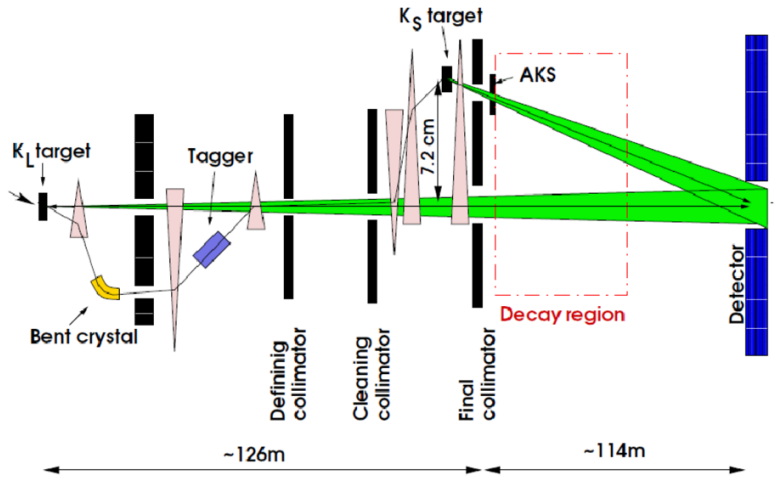


Fig. 13-4: The NA48 beam line [333].

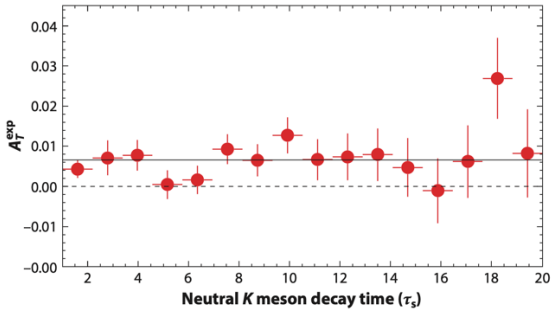


Fig. 13-5: T-Violation asymmetry versus decay time.

13.2 The third generation

But **Makoto Kobayashi and Toshihide Maskawa** had already proposed the **3rd generation hypothesis**, with a good reason for doing so: the possibility of a 3x3 mixing matrix, the **Cabibbo–Kobayashi–Maskawa (CKM) matrix** having **a phase** and therefore naturally explaining CP violation. This matrix (Fig. 13-6 left, approximate) leads **from the quark mass eigenstates to their weak interaction eigenstates.**

$$U_{CKM} = \begin{pmatrix} 1-\frac{1}{2}\lambda^2 & \lambda & A\lambda^3(\rho - i\eta) \\ -\lambda & 1-\frac{1}{2}\lambda^2 & A\lambda^2 \\ A\lambda^3[1-(\rho+i\eta)] & -A\lambda^2 & 1 \end{pmatrix}$$



Fig. 13-6: The **K–M matrix** and the authors, Kobayashi (left) and Maskawa (right) **(KM).**

[333] L. Iconomidou-Fayard and D. Fournier, The Discovery of Direct CP Violation.
https://cds.cern.ch/record/2103283/files/9789814644150_0009.pdf
N. Doble and L. Gatignon, Two Very Special K⁰ Beams: Discovery of Direct CP Violation. In Technology Meets Research,
https://inspirehep.net/files/818b65cb5004b2f8c5f23faf63571c33 p. 158

Their hypothesis was rapidly confirmed, by discovering the tau lepton (Martin Perl, 1975, Nobel Prize in 1995) and the beauty quark (Leon Lederman, 1977, Fig. 13-7) [334].

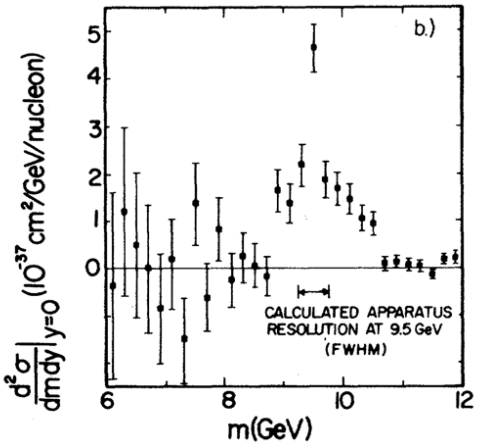


Fig. 13-7: Beauty discovery: Measured dimuon production cross sections as a function of the invariant mass of the muon pair [335].

Some comments about the CKM matrix (see Chapter 14): the true matrix is given in Fig. 14-7. It is unitary. The unitarity of the first line gives a limit on a possible fourth family. The orthogonality of lines and columns allows a visualisation by 6 triangles of same area (Figs. 14-2 to 14-11), more or less flat. The standard parameterization involves a product of 3 rotation matrices and 1 CP-violating phase: 4 real parameters, as shown in Fig. 13-8.

$$V_{\mathrm{CKM}} = \begin{pmatrix} 1 & 0 & 0 \\ 0 & c_{23} & s_{23} \\ 0 & -s_{23} & c_{23} \end{pmatrix} \begin{pmatrix} c_{13} & 0 & s_{13}e^{-i\delta} \\ 0 & 1 & 0 \\ -s_{13}e^{i\delta} & 0 & c_{13} \end{pmatrix} \begin{pmatrix} c_{12} & s_{12} & 0 \\ -s_{12} & c_{12} & 0 \\ 0 & 0 & 1 \end{pmatrix}$$
$$= \begin{pmatrix} c_{12}c_{13} & s_{12}c_{13} & s_{13}e^{-i\delta} \\ -s_{12}c_{23} - c_{12}s_{23}s_{13}e^{i\delta} & c_{12}c_{23} - s_{12}s_{23}s_{13}e^{i\delta} & s_{23}c_{13} \\ s_{12}s_{23} - c_{12}c_{23}s_{13}e^{i\delta} & -c_{12}s_{23} - s_{12}c_{23}s_{13}e^{i\delta} & c_{23}c_{13} \end{pmatrix}$$

Fig. 13-8: The VCKM matrix, where $s_{ij} = \sin\theta_{ij}$, $c_{ij} = \cos\theta_{ij}$, and δ is the phase responsible for all CP-violating phenomena in flavour-changing processes in the SM. The angles θ_{ij} can be chosen to lie in the first quadrant, so s_{ij} , $c_{ij} \geq 0$ [336].

It is known experimentally that $s_{13} \ll s_{23} \ll s_{12} \ll 1$ (see Fig. 14-7). Hence the Wolfenstein parameterization ($s_{12} = \lambda$, $s_{23} = A\lambda^2$, ...). Figure 13-6 gives a development at order $0(\lambda^3)$.

The least flat triangle, nearly rectangular, best measured, is given in Fig. 14-8. LEP, BaBar and Belle have measured its sides and angles, respectively, as we will see in the next chapter.

---

[334] These multiple discoveries were stimulating but generated some frustration at CERN. It made up for it by ensuring abundant spectroscopy of heavy flavours, especially charm, with 20 experiments at SPS and 60 in the Ω spectrometer, in particular of photoproduction, a process offering proportionally more charm than hadroproduction. Then came LEP.
[335] S. W. Herb *et al.,* Observation of a Dimuon Resonance at 9.5 GeV in 400-GeV Proton-Nucleus Collisions. *Phys.Rev.Lett.* 39 (1977) 252-255, https://journals.aps.org/prl/pdf/10.1103/PhysRevLett.39.252
[336] A. Ceccucci *et al.,* CKM Quark-Mixing Matrix. https://pdg.lbl.gov/2022/reviews/rpp2022-rev-ckm-matrix.pdf

14. CP – a continuation

14.1 Towards the Unitarity Triangle and CKM

In terms of CP and mixing, interest then turned from K^0 to **neutral beauty mesons**. In 1987, the ARGUS detector at DORIS (DESY) demonstrated the $\mathbf{B^0\overline{B}^0}$ **mixing** and found that $0.007 \leq V_{td} \leq 0.034$ (Fig. 14-1 and Section 14.3).

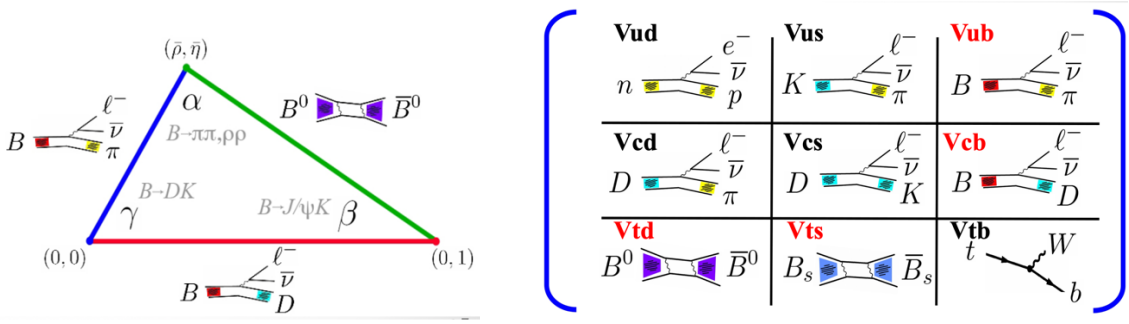


Fig. 14-1: Processes needed to build the unitarity triangle and the CKM matrix.

Then came the reign of the **asymmetric e^+e^- B Factories** [337], where the difference in beam energy gave a longitudinal boost to the products of the reaction and where the **non-separability** of the quantum state [338] became a working tool (Fig. 14-2, see also end of this chapter): PEPII at Stanford with the **BaBar** detector and KEKB in Japan with the **BELLE** detector.

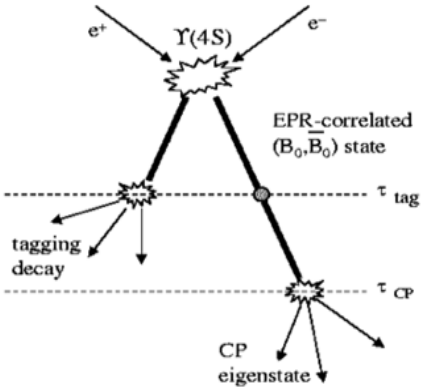


Fig. 14-2: An EPR (Einstein–Podolsky–Rosen)-correlated $(B^0\overline{B}^0)$ state.

Table 14-1 gives the huge volume of data accumulated by BaBar on the Upsilon resonances.

	Dates	fb^{-1}	Number of Upsilons
Υ (4S)	1999 – 2007	426	468 million
Υ (3S)	2008	28	122 million
Υ (2S)	2008	14	99 million

Table 14-1: Accumulated data on the Υ-resonances by BaBar.

[337] F. Martinez-Vidal, Asymmetric *B* factories: https://inspirehep.net/files/3abfa917111a92652abf128192538ab1
[338] Caltech Science Exchange: What Is Entanglement and Why Is It Important? https://scienceexchange.caltech.edu/topics/quantum-science-explained/entanglement

These experiments undertook the vast program of constructing the **Unitarity Triangle** (UT) and the **CKM matrix.** Figure 14-1 [339] shows which tools were used to determine the various elements and the coefficients of the matrix, essentially **semi-leptonic decays of B and frequencies of oscillation of B^0s.**

In addition to the measurements of the angles β, α, γ, the BaBar experiment, for example, demonstrated the **violation of T** symmetry [340] (but concerning anteriority see also CP Lear and corresponding reference), discovered new states such as **Υ(4260) and η_b** , carried out BSM researches and hadron production measurements $e^+e^- \rightarrow$ hadrons, input to the estimation of g−2 (Chapter 26).

Then came the large contributions of the LHCb, ATLAS and CMS experiments at the LHC, characterized by the abundance and variety of subjects offered by high-energy pp collisions: the sector of strangeness, the sector of charm (of which LHCb has shown direct CP violation), the beauty sector, including, besides the usual mesons, the B^0_s, beautiful and strange, measured in **$B^0_s \rightarrow \mu\mu$** (see details on this topic in Chapter 8), as well as baryons like Λ^0_b.

Considering CP violation in B_d and B_s mixing, using $B_d \rightarrow \psi K_s$ and $B_s \rightarrow \psi\phi$, respectively, and studying the time evolution of these decays, let us single out the determination of the CP-violating phase ϕ_{B_s} of the $B_s \rightarrow \psi\phi$ decay by three LHC experiments (Fig. 14-3).

$$\phi_{B_s}^{SM} = -\arg\frac{(V_{tb}^* V_{ts})^2}{|V_{tb}^* V_{ts}|^2} \approx -0.035.$$

An aside: BaBar, BELLE and LHC found many **multiquark states**, already quoted and reviewed in Chapter 28.

14.2 Any new physics?

LHCb has given evidence of **possible violations of lepton flavour universality**, which after reanalysis have essentially disappeared (Fig. 14-4). R(D*) was recently given at 1 σ of the SM (Fig. 14-5).

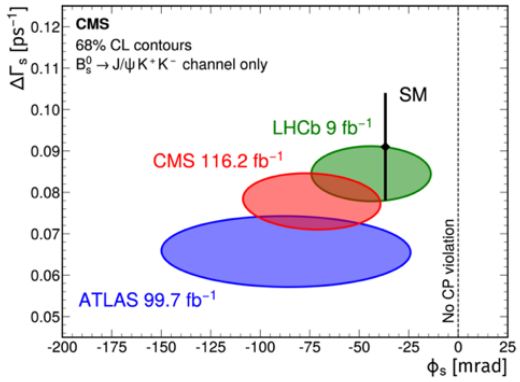


Fig. 14-3: ϕ_{B_s} obtained from the time evolution of the $B_S \rightarrow \psi\phi$ decay ($\Delta\Gamma_s = \Gamma_{sL} - \Gamma_{sH}$) [341].

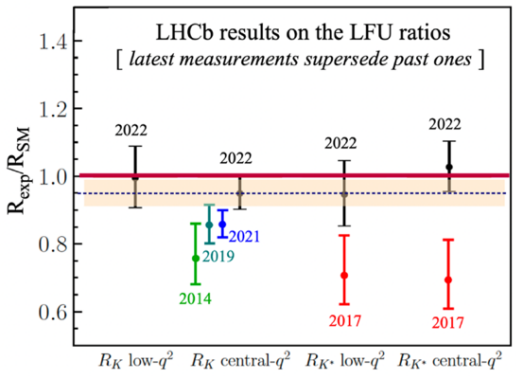


Fig. 14-4: The LHCb R_{K,K^*} measurement [342].

[339] J. Brodzicka, CP Violation and CKM Matrix Measurements. https://cds.cern.ch/record/2678400/files/JolantaBrodzicka_FFK19_v1.pdf

[340] J. P. Lees, Observation of Time-Reversal Violation in the B^0 Meson System. *Phys. Rev. Lett. 109, 211801 (2012),* https://journals.aps.org/prl/pdf/10.1103/PhysRevLett.109.211801
BaBar makes first direct measurement of time-reversal violation.
https://physicsworld.com/a/babar-makes-first-direct-measurement-of-time-reversal-violation/

[341] CMS collaboration, Evidence for CP violation and measurement of CP-violating parameters in $B^0 \rightarrow J/\psi\,\phi(1020)$ decays in pp collisions at $\sqrt{s}$ = 13 TeV. https://arxiv.org/abs/2412.19952

[342] From P. Ferrari, Experimental summary Moriond, QCD 2024. https://moriond.in2p3.fr/QCD/2024/Sunday/Ferrari.pdf

We recall that $R(D^*) = \frac{B\,(B^0 \to D^{*-}\,\tau^+\,\nu_\tau)}{B\,(B^0 \to D^{*-}\,\mu^+\,\nu_\tau)}$.

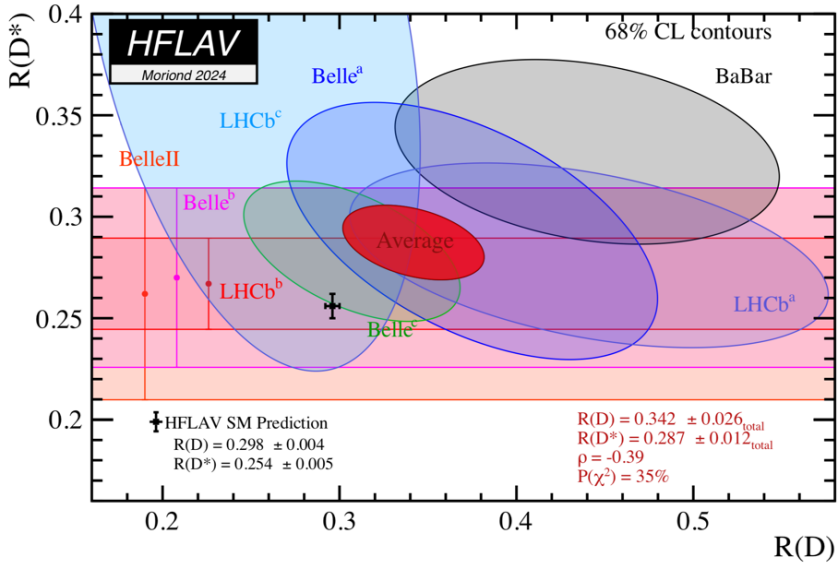


Fig. 14-5: R(D*) measurements [343].

Nevertheless, a better agreement with the SM does not put an end to these measurements and their verification by the BELLE II experiment is eagerly awaited. For more details see Ref. [344] and Fig. 14-6.

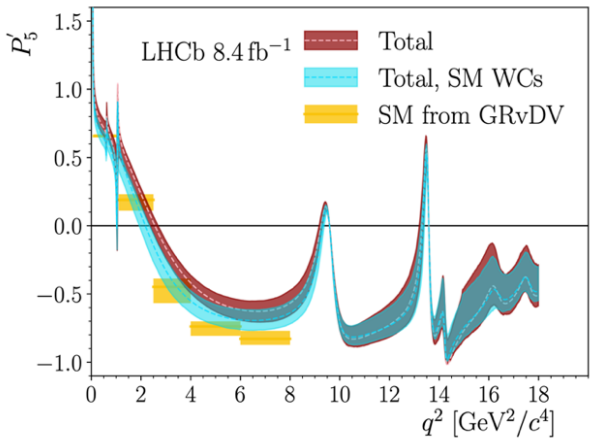


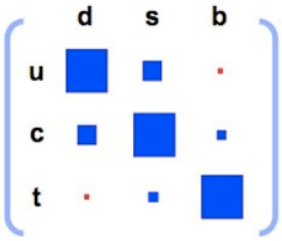
Fig. 14-6: One of the slight discrepancies left. P'_5 is an optimized variable appearing in the b → sμμ angular analysis [345].

[343] From M. Kado, ICHEP 2024: Conference Summary and Highlights.
https://indico.cern.ch/event/1291157/contributions/5958406/attachments/2903497/5123335/ICHEP-Summary.pdf
[344] B. Clerbaux, Experimental Summary, Electroweak Interaction & Unified Theories. Moriond 2024,
https://arxiv.org/abs/2409.07120
[345] LHCb Collaboration: Comprehensive analysis of local and nonlocal amplitudes in the $B^0 \to K^{*0}\mu^+\mu^-$ decay.
https://arxiv.org/abs/2405.17347

14.3 The present status

The current state of the CKM matrix is given visually and numerically in Fig. 14-7. Figure 14-8 shows the summary of the determination of the unitary triangle offered by the **CKMfittter**.

Clearly a huge amount of work has been done in the CP domain. The main findings [346] are that the **K– M mechanism is the dominant source** of observed CP violation. But CP violation in the quark sector is very **insufficient to explain baryogenesis**.



$$V_{\mathrm{CKM}} = \begin{pmatrix} 0.97401 \pm 0.00011 & 0.22650 \pm 0.00048 & 0.00361^{+0.00011}_{-0.00009} \\ 0.22636 \pm 0.00048 & 0.97320 \pm 0.00011 & 0.04053^{+0.00083}_{-0.00061} \\ 0.00854^{+0.00023}_{-0.00016} & 0.03978^{+0.00082}_{-0.00060} & 0.999172^{+0.000024}_{-0.000035} \end{pmatrix},$$

$$\eta = 0.355^{+0.012}_{-0.011}$$

Fig. 14-7: The CKM matrix.

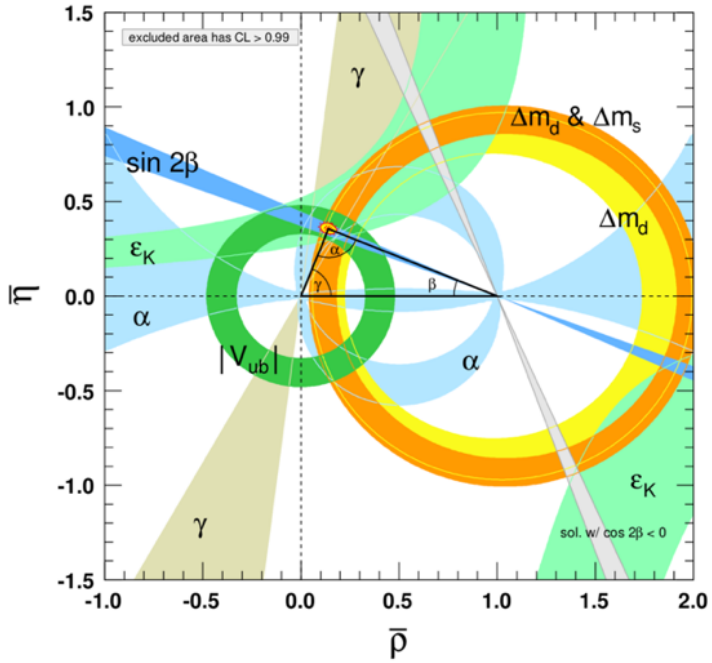


Fig. 14-8: Unitarity Triangle from CKM Fitter; $\gamma = (66.3^{+0.7}_{-1.9})^{o}$.

A slight tension (3 σ) called **Cabibbo anomaly** concerns the first line of the matrix: the Cabibbo angle deduced from K, π, D and τ decays disagrees slightly from the one from super-allowed beta decays (Fig. 14-9) [347].

[346] Y. Nir, Flavour physics and CP violation. *CERN Yellow Rep.School Proc.* 5 (2020) 79-128, https://e-publishing.cern.ch/index.php/CYRSP/article/view/1121/925
G. Isidori, Flavour Physics and CP Violation. https://arxiv.org/abs/2503.14042
[347] E. Passemar, Cabibbo Anomaly and Universality Tests. Moriond EW 2023, https://indico.in2p3.fr/event/29681/contributions/122506/attachments/76502/111031/03-EPassemar-v1.pdf

	Fit result, no constraint	
$\|V_{ud}\| = 0.97373(31)$ $\|V_{us}\| = 0.2231(6)$ $\|V_{us}\| / \|V_{ud}\| = 0.2311(5)$	$V_{ud} = 0.97365(30)$ $V_{us} = 0.22414(37)$ χ^2 / ndf = 6.6 / 1 (1.0%) $\Delta_{CKM} = -0.0018(6)$ -2.7σ	$\|V_{ud}\|^2 + \|V_{us}\|^2 + \|V_{ub}\|^2 = 1 + \Delta_{CKM}$ $\|V_{ub}\|^2$: negligible: ~ 2 $\times 10^{-5}$ (B decays)

Fig. 14-9: Cabibbo anomaly.

14.4 Perspective

The sector is on the way to increased precision. Super KEKB attains 2 fb^{-1} per day but has still a factor of 10 to gain. Belle + Belle II, run 1 accumulated 1.42 ab^{-1}. For the progress of SuperKEKB see Ref. [348]. With the LHCb upgrade, extremely rare and forbidden decays lead to multiple constraints on non-SM contributions. Electroweak penguins and radiative *B* decays offer multiple opportunities to search for new physics. One can hope to solve the long-standing discrepancy between inclusive and exclusive determinations of parameters through semi-leptonic decays.

As a prospect see Fig. 14-10 [349], showing the projections at LHC on the statistical uncertainty of the CPV phase ϕ_S from $B^0{}_S \to J/\psi K^+ K^-$.

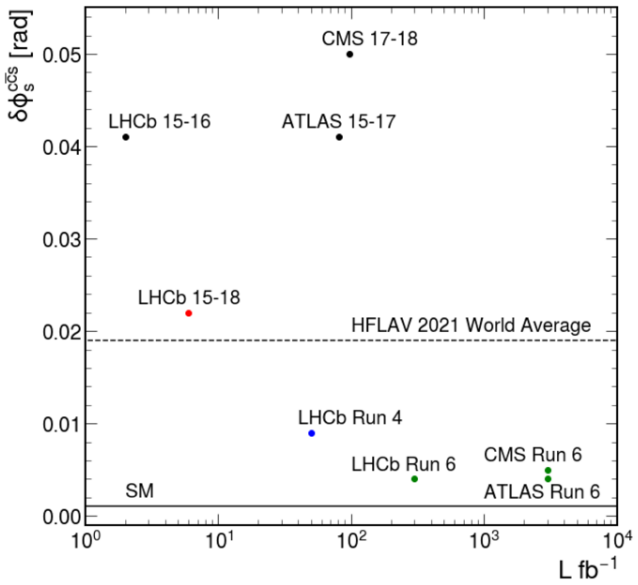


Fig. 14-10: Potential progress on CPV phase.

On a giga Z-factory one can hope to consider also the flattest of the unitary triangles (Fig. 14-11) and measure its α angle exploiting decays $\bar{B}_d \to \phi \bar{K}^{(*)0}$, $\bar{B}_s \to \phi \bar{K}^{(*)0}$, see Ref. [350].

[348] Y. Ohnishi, Recent Progress of SuperKEKB Project and Future Prospect.
https://inspirehep.net/files/ebaceb777fa2ed56df1de76d71ccdf45

[349] V. Lukashenko, New CP-violation measurements at LHC.
https://cds.cern.ch/record/2860687/files/FPCP2023_CPV_VLukashenko%200106.pdf

[350] R. Aleksan *et al.*, Measuring the angle α_{ds} of the flattest Unitary Triangle with $\bar{B}_d \to \phi \bar{K}^{(*)0}$, $\bar{B}_s \to \phi \bar{K}^{(*)0}$
https://arxiv.org/abs/2402.09987

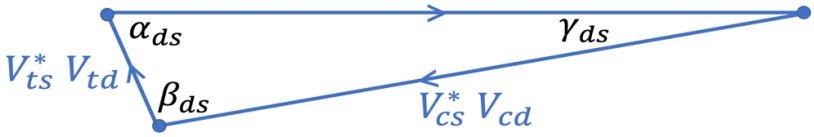


Fig. 14-11: The flattest UT.

A possible summary

In the FCNC part of Chapter 8 we met the B^0 and B^0_s direct decays to dimuons $B_s \rightarrow \mu^+\mu^-$ and $B_d \rightarrow \mu^+\mu^-$ with Standard Model BRs of about 4×10^{-9} and 10^{-10}.

In Chapter 13 we mentioned the first > 3 σ evidence for $K^+ \rightarrow \pi^+ \nu\ \bar{\nu}$ decay by NA62, to which one can add the measurement of $K_L \rightarrow \pi^0 \nu\ \bar{\nu}$ by the KOTO collaboration at J-PARC in Japan. The branching ratios for these decays are predicted to be in the ballpark of 8×10^{-11} and 3×10^{-11}, respectively. Finally let us consider $B \rightarrow K\ \nu\bar{\nu}$ and $B^* \rightarrow K\ \nu\bar{\nu}$ at BELLE II and at KEK.

According to Ref. [351], these measurements, with foreseeable improvements, are the most promising to observe deviations from the SM expectation due to new physics, which could be identified by studying correlations between them.

However, the SM predictions need to use elements of the CKM matrix which must be measured using K and B-mesons decays. The problem lies with V_{cb}, whose **exclusive and inclusive measurements disagree** as stated previously, a problem likely due to QCD evaluations. The angle γ also plays a role.

The above quoted reference discusses a possible way out, replacing the CKM dependence of the BR with independent observables for which QCD is under control. These observables are indicated in Fig. 14-12, with their intersection when γ changes, suggesting the actual value of the imprecise parameters V_{cb} and γ.

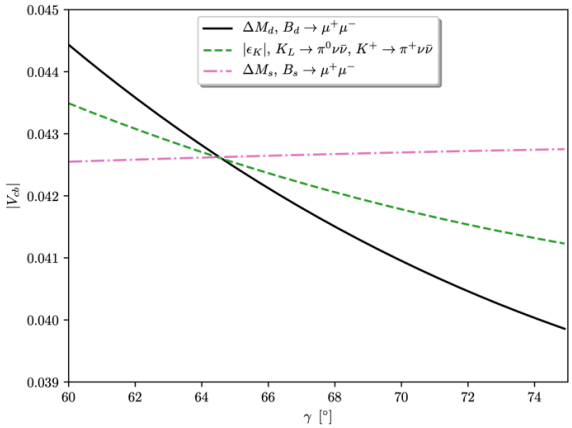


Fig. 14-12: Independent observables ΔM_s, ΔM_d and ε_K intersect in the $V_{cb} - \gamma$ plane. No new physics is required to fit them simultaneously. Uncertainties are not shown [352].

[351] A. Buras, Six Rare Decays at the Energy Frontier. In CERN Courier, July/ August 2024, p. 30, https://cerncourier.com/wp-content/uploads/2024/07/CERNCourier2024JulAug-digitaledition.pdf

[352] A. Buras, On the Superiority of the |Vcb| – γ Plots over the Unitarity Triangle Plots in the 2020s. https://arxiv.org/abs/2204.10337

14.5 Note on non-separability

In 1935, Albert Einstein, Boris Podolsky and Nathan Rosen (EPR) [353] pointed out that, in situations involving specially-prepared pairs of particles in a singlet state, the orthodox formulation of QM conflicted with **locality**. Or, assuming locality, each particle must carry a pre-existing information encoded in the so-called "hidden variables".

In 1964 John Bell [354] showed that the hypothesis of such hidden variables leads to **inequalities**, built from the results of proper sets of measurements performed on pairs of particles prepared in the **singlet state**, e.g. measurements of their spin. These inequalities must be respected. **Bell's theorem** states that the predictions of QM for such measurements cannot be accounted for by any local theory and lead to violation of the inequalities.

A question was whether predictions of QM are correct. It could only be answered by experiments. A class of these measured the polarizations of pairs of photons emitted, in some decay, in a state of total angular momentum zero, analogous to the singlet state mentioned above. Correlations between the outcomes of the two polarization measurements were monitored for different axes along which the polarizations were measured. In Alain Aspect's experiment the settings of the polarizer's axes were set while particles were already in flight.

The results were consistent with the QM predictions, proving with high statistical significance the violation of Bell-type inequalities. A series of experiments [355] of increasing complexity, to avoid more and more possible loopholes, were realized, concluding the same. This activity was recognized by the 2022 Nobel Prize [356]. It is likely that the premature death of John Bell deprived him from a Nobel Prize.

If two particles are entangled, the state of one particle cannot be described independently from the other. It has been observed in a wide variety of systems, ranging from photons or atoms to macroscopic diamond structures, and over distances from the nanoscale to hundreds of kilometres. Until now, however, entanglement has remained largely unexplored at the high energies accessible at colliders, such as the LHC.

But recently ATLAS, then CMS, reported a measurement of entanglement using **top-quark pairs** [357]. This showed that high-energy processes (for instance gg $\rightarrow$ t-pair or h $\rightarrow \tau$-pair) can lead to new tests of Bell's inequalities [358], however without Aspect's trick of "fast changing" the detector.

Belle has measured neutral B pairs from $\Upsilon(4S)$ decay and determined the time-dependent asymmetry due to flavour oscillations. QM reproduces results well, while local realistic models considered are disfavoured [359].

---

[353] A. Einstein, B. Podolsky and N. Rosen, Can Quantum-Mechanical Description of Physical Reality be Considered Complete? *Phys. Rev.* 47, 777 (1935)

[354] J. Bell, On the Einstein Podolsky Rosen Paradox. https://inspirehep.net/files/67578c1d19ace842e25198fa5675442e , J. Bell, On the Problem of Hidden Variables in Quantum Mechanics. https://inspirehep.net/files/90b70d2ed9fa199ef95ed3da417c6b5a

[355] A. Aspect, Testing Bell's Inequalities. https://inspirehep.net/files/facc14902a58a8f493db39dbbf86c70f

[356] Nobel Prize in 2022: https://www.nobelprize.org/prizes/physics/2022/prize-announcement/

[357] ATLAS Collaboration, Highest-energy observation of quantum entanglement. ATLAS-CONF-2023-069, https://cerncourier.com/a/highest-energy-observation-of-entanglement/

[358] A. J. Barr *et al.,* Quantum entanglement and Bell inequality violation at colliders. https://arxiv.org/abs/2402.07972

[359] A. Bay, Measurement of EPR-type flavour entanglement in $\Upsilon(4S) \rightarrow B^0\overline{B^0}$ decays. https://indico.in2p3.fr/event/151/contributions/20270/attachments/16441/20174/epr_moriond.pdf

14.6 The strong CP problem

The strong CP problem [360] is a major topic of the CP problematic. To the usual terms of the QCD Lagrangian, one should add one more term, namely, what was announced in Section 7.4.5, $\theta \frac{g_s^2}{32\pi^2} G^a_{\mu\nu} \widetilde{G}^{a\mu\nu}$, where $G^a_{\mu\nu}$ are the gluon field-strength tensors and $\widetilde{G}^{a\mu\nu}$ their dual (see Table 7-2, sum on a from 1 to 8 implied).

This term, a 4-divergence, including an angle θ, only contributes a surface term to the QCD action. However, surface terms may produce non-perturbative (NP) quantum effects which can be important in the strong coupling regime. In QCD, NP effects are associated with the existence of now familiar **colour instantons/sphalerons** introduced in Chapter 7 (see also Chapter 24), Yang–Mills configurations describing quantum-mechanical tunnelling between inequivalent vacua of QCD. **Such effects exist and hence the physics of QCD is θ-dependent**.

The physics of QCD does not change if one applies the transformations:
$q_j \rightarrow \exp^{i\alpha_j\gamma_5} q_j \qquad m_j \rightarrow \exp^{-2i\alpha_j} m_j \quad$ for j = 1,….., N_f , no sum $\quad \theta \rightarrow \theta - 2\sum_{j=1}^{n} \alpha_j$

This result and the change of θ follow from the chiral anomaly [361] in chiral currents:
$\partial_\mu(\bar{q}_j\gamma^\mu\gamma_5 q_j) = 2im_j\bar{q}_j\gamma_5 q_j \; - \frac{g_s^2}{16\pi^2} G_{a\mu\nu}\widetilde{G}^{a\mu\nu}$, sum over a implied, a = 1, 8. No sum on j implied.

Furthermore, if one includes the weak interaction, the **quark mass matrix m_q** is generally complex. One must diagonalize it to go to a physical basis and this performs a chiral transformation which changes θ by arg (det m_q).

The above implies that QCD is periodic in θ with period 2π and that QCD depends on θ only through the combination [362] $\bar{\theta} = \theta - \arg(\det m_q)$.

$\bar{\theta}$ is the parameter that sets the amount of P and CP violation in QCD.

But **no such effect was ever observed**. $\bar{\theta}$ is close to zero, with the best constraint ($\bar{\theta} < 0.6 \times 10^{-10}$) provided by the measured upper limit on the **neutron electric dipole moment** (see Section 32.2).

The strong CP problem is **why $\bar{\theta}$ is so small.** Since the quark masses originate from the EW sector (which violates P and CP), the SM does not explain **why arg (det m_q) should exactly cancel θ**. With CP violation *à la* Kobayashi–Maskawa, the Yukawa couplings are arbitrary complex numbers and $\bar{\theta}$ is expected to be of order one.

More on instantons and sphalerons in Chapter 24, and on the **axion solution to the strong CP problem** in Section 31.3.

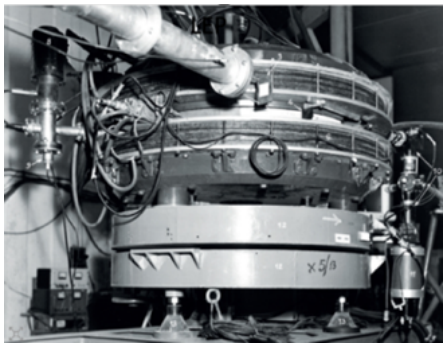
[360] P. Sikivie, The strong CP problem.
https://comptes-rendus.academie-sciences.fr/physique/item/10.1016/j.crhy.2011.10.002.pdf
R. Peccei, The Strong CP Problem and Axions. https://arxiv.org/abs/hep-ph/0607268
[361] Chiral anomaly: https://en.wikipedia.org/wiki/Chiral_anomaly
[362] The dependence of QCD upon θ would disappear if one of the quark masses vanishes, which is not favoured.

15. The e^+e^- colliders

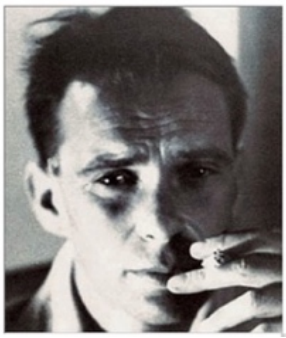
15.1 Historical comments

The dream of colliding beams stored in a ring took long to materialize. The first plans were to collide electrons in tangent rings [363]. Then the conviction that one could collide particles and antiparticles, possibly stored in a single ring, gave impetus to the field.

The small AdA e^+e^- ring (1964), inspired by Bruno Touschek [364], was built in Frascati and operated at the LAL Orsay linac by a Franco-Italian team including Pierre Marin and Jaques Haissinski [365] (Fig. 15-1). AdA detected interactions and launched the long series of these e^+e^- colliders, up to LEP. In France came ACO, then DCI and their series of studies on vector mesons ρ, ω, ϕ, and others. One can regret that a multi-GeV project like COPPELIA (proposed in Orsay in 1969) [366] was not carried out. For an historical account of the competition between Orsay and Novosibirsk on this sector, see Section 10.14.2 and its references.



The AdA ring



B. Touschek



J. Haissinski and P. Marin

Fig. 15-1: The AdA story [367].

ADONE [368] in Frascati, with 3 GeV CM energy, reached in 1969 a luminosity near the design value.

But it was in the US where the **November 1974 revolution** happened (Fig. 15-2), the discovery of the J/ψ [369], at the SPEAR (Stanford) e^+e^- collider and at the Brookhaven fixed-target experiment, soon interpreted by some authors as hidden charm (Chapter 8), but a real surprise due to its very small

[363] G. K. O'Neill, Storage Rings for Electrons and Protons.
https://s3.cern.ch/inspire-prod-files-f/faa296308222a4506a3e04d0c54615b6
[364] L. Bonolis, L. Maiani and G. Pancheri (Editors), Bruno Touschek 100 Years.
https://inspirehep.net/files/6a245d443e27e0149ec10dd1509cf3e2
[365] Hommage to J. Haissinski: his talk at the first Moriond meeting:
https://inspirehep.net/files/967e4a6050e7abf98865cce2e81f807c
[366] P. Marin, Souvenirs.
https://lpnhe.in2p3.fr/IMG/pdf/marin09.pdf?946/331e9f154e82fe77d72010774f54d737ebd28801
[367] AdA – the small machine that made a big impact.
https://cerncourier.com/a/ada-the-small-machine-that-made-a-big-impact/
J. Haissinski, AdA at Orsay. https://inspirehep.net/files/95fe8dc10ef532a513cf50c5ebfefb84
[368] C. Pellegrini, The Making of ADONE. https://inspirehep.net/files/836a708e226fb23eb2e9539e7fe500d1
[369] A. Khare, The November (J/Ψ) Revolution: Twenty-Five Years Later. https://arxiv.org/abs/hep-ph/9910468

width that no one had fully anticipated [370]. This discovery started much activity in "onia" spectroscopy [371].

An aside: it is difficult to retrospectively draw a judgement, but one may nevertheless regret that a bi-spectrometer set-up proposed as LoI in 1971 and exploiting the PS at CERN could not be realized before 1974, after the similar Brookhaven set-up discovered the J/ψ. Reference [372] gives an idea of the sequence of events.

Then came TRISTAN (Japan) and DORIS in Hamburg, followed by PETRA, where the TASSO experiment first discovered the gluon (1979), shortly afterwards similar three-jet event topologies were also announced by JADE, MARK J and PLUTO. CESR at Cornell (USA) observed the first e^+e^- collisions in 1979 and finally the asymmetric B factories became available [373] , as illustrated in Chapter 14.

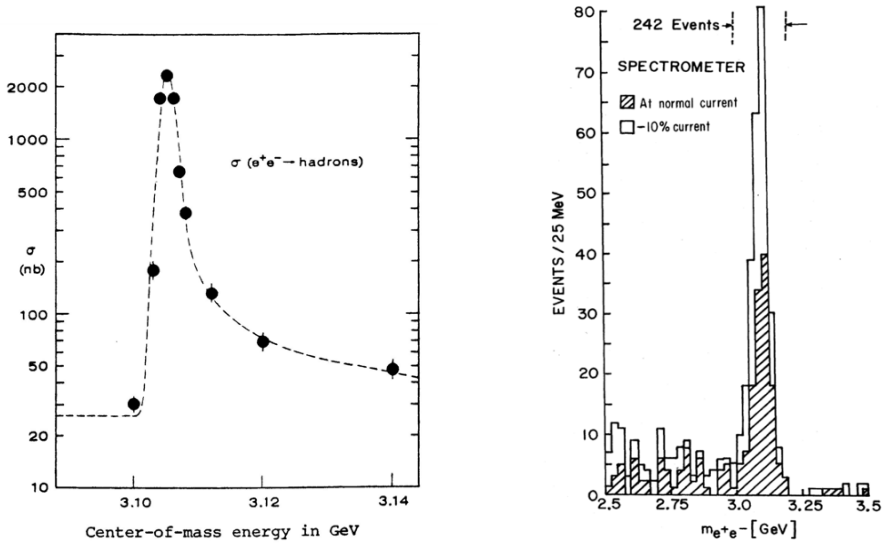


Fig. 15-2: The 1974 revolution: SPEAR (left) Brookhaven (right) [374].

Table 15-1 gives the list of all e^+e^- colliders ever built.

The machines presently in operation are DAΦNE in Frascati, VEPP-4M and VEPP-2000 in Russia, SuperKEKB [375] in Japan and BEPC II in China. The last two are double-ring machines. SuperKEKB5-11

[370] M. K. Gaillard *et al.,* Search for Charm. https://inspirehep.net/files/72841c7ee51952738bd58e4da82ff72d , and addendum: https://inspirehep.net/files/cadbe7db8812a032de4221afd6ae74ce
The first reference, just before the J/ψ discovery, predicts a width of 2 MeV and a BR into e^+e^- of 1%. The right numbers are: 92.6±1.7 keV and 5.97%.
[371] For a most vivid record of this period and others see A. de Rujula, Fifty years of Yang–Mills Theories: a phenomenological point of view. https://arxiv.org/abs/hep-ph/0404215
[372] LoI: Development of Layout of the Bi-Spectrometer.
https://cds.cern.ch/record/2880742/files/MPS-MU-EP-Note-74-24.pdf?version=1
[373] J. Seeman, Commissioning of the PEP-II Asymmetric B Factory.
https://www.slac.stanford.edu/pubs/beamline/29/2/29-2-seeman.pdf ,
R. Aleksan, CP Violation in the $B\bar{B}$ System at an Asymmetric e^+ e^- Collider.
https://inspirehep.net/files/347a9475bd6ed34e4205d806eaea23d3
[374] M. Breidenbach, J/ψ @50 SLAC Perspective.
https://indico.slac.stanford.edu/event/8587/contributions/9648/attachments/4349/11948/SSI2024%20Psi%20Discovery.pptx%20(1).pdf
S. C. C. Ting, The discovery of the J particle: A personal recollection.
https://cds.cern.ch/record/977942/files/RevModPhys.49.235.pdf
[375] M. Tobiyama, Status of SuperKEKB and Experience with Nonlinear Collimation.
https://inspirehep.net/files/a59cdd0dc4e8c22db50841ce56014a20

has now the world's highest instantaneous luminosity (4.7×10^{34} $cm^{-2}s^{-1}$), with however still some problems to understand. It may be worth quoting some machines which, besides COPPELIA, were considered, studied and did not (yet) realize.

A tau-charm factory was and still is such a machine in Spain, Italy, Russia/China [376]. The Chinese Super Tau-Charm Facility (STCF) seems to be well supported.

A high luminosity B factory in Europe was also studied for Hamburg [377], PSI [378] and CERN (in the ISR tunnel) [379].

Location	Name (type[a])	Beam Energy[b] (GeV)	Luminosity[b] ($cm^{-2}s^{-1}$)	Operation Period
Stanford/SLAC, USA	CBX[c] (e^-e^- DR)	0.5	2×10^{28}	1963-1968
	SPEAR (SR)	4	1.2×10^{31}	1972-1988
	PEP (SR)	15	6×10^{31}	1980-1990
	SLC (LC)	49	2.5×10^{30}	1989-1998
	PEP-II (DR)	9 (e^-) 3.1 (e^+)	1.2×10^{34}	1998-2008
Frascati, Italy	AdA (SR)	0.25	5×10^{25} [d]	1961-1964
	ADONE (SR)	1.5	6×10^{29}	1969-1993
	DAΦNE (SR)	0.51	2.4×10^{32} 4.5×10^{32} [e]	1999-present
BINP, Russia	VEP-1 (e^-e^- DR)	0.16	5×10^{27}	1964-1968
	VEPP-2 (SR)	0.67	4×10^{28}	1966-1970
	VEPP-2M (SR)	0.7	5×10^{30} (@0.511)	1974-2000
	VEPP-3 (SR)	1.55	2×10^{27}	1974-1975
	VEPP-4M (SR)	6	2×10^{31}	1984-present
	VEPP-2000 (SR)	1	5×10^{31}	2010-present
Cambridge, USA	CEA Bypass (SR)	3	8×10^{27}	1971-1973
Orsay, France	ACO (SR)	0.54	1×10^{29}	1965-1975
	DCI (DR)	1.8	1.7×10^{30}	1977-1985
DESY, Germany	DORIS (SR)	5.6	3.3×10^{31}	1973-1993
	PETRA (SR)	23.4	2.4×10^{31} (@17.5)	1978-1986
CERN, Europe	LEP (SR)	104.5	1×10^{32}	1989-2000
Cornell, USA	CESR (SR)	5.5	1.3×10^{33}	1979-2008
KEK, Japan	TRISTAN (SR)	32	4.1×10^{31}	1986-1995
	KEKB (DR)	8 (e^-) 3.5 (e^+)	2.1×10^{34}	1998-2010
	SuperKEKB (DR)	7 (e^-) 4 (e^+)	8×10^{35} [f]	2016-present
IHEP, China	BEPC (SR)	2.4	1×10^{31} (@1.84)	1988-2004
	BEPC II (DR)	2.47	1×10^{33} (@1.89)	2009-present

Table 15-1: List of all e^+e^- colliders in the world (all are e^+e^- unless marked as e^-e^-) [380]. References in Table [a] DR: Double ring, SR: Single ring, LC: Linear collider. [b] Highest achieved. [c] Princeton-Stanford Colliding Beam Experiment. [d] Collisions achieved when operated in Orsay. [e] Using a detector with no solenoid field. [f] Design goal.

[376] A. Pich, Tau physics opportunities at the super tau-charm facility. https://arxiv.org/abs/2405.19955 ,
M. E. Biagini, Design of a high luminosity tau/charm factory.
https://inspirehep.net/files/e4e45c7ad496a7729e908df14bf44a0f
M. Achasov *et al.*, Super τ-Charm facility (STCF). https://arxiv.org/abs/2303.15790
https://arxiv.org/abs/2509.11522
[377] HELENA, a Beauty Factory in Hamburg. https://cds.cern.ch/record/236722/files/cer-000151570.pdf
[378] R. Eichler, T. Nakada, K. R. Schubert, S. Weseler and K. Wille, Motivation and Design Study for a B-Meson Factory with High Luminosity. https://lib-extopc.kek.jp/preprints/PDF/1986/8612/8612288.pdf
[379] Y. Baconnier and R. Eichler. A B-factory in the CERN ISR Tunnel.
https://inspirehep.net/files/df7325dbca0cb546fbe14310331b3537
[380] CEPC Technical Design Report – Accelerator. https://arxiv.org/abs/2312.14363 p. 27
Particle Data Group, *Phys. Rev. D 54, 128 (1996).*
Particle Data Group, https://pdg.lbl.gov/2021/reviews/contents_sports.html
List of accelerators in particle physics. https://en.wikipedia.org/wiki/List_of_accelerators_in_particle_physics

15.2 The Stanford Linear Collider and beyond

The Stanford Linear Collider (SLC) [381], built upon the SLAC linac, was an inexpensive way to explore the physics of the Z boson while providing a valuable experience for future linear colliders. One can praise the efforts made in the operation of the arcs to follow the local terrain [382]. Developing precision diagnostics for beam characterization, refined feedback systems, new techniques for optical matching, beam-based alignment and wakefield control, the SLC finally reached near design luminosity (Fig. 15-3). The beam size at IP reached the micron level (Fig. 15-4). The availability of electron longitudinal polarization [383] made the SLC physics program a great success (Chapter 18).

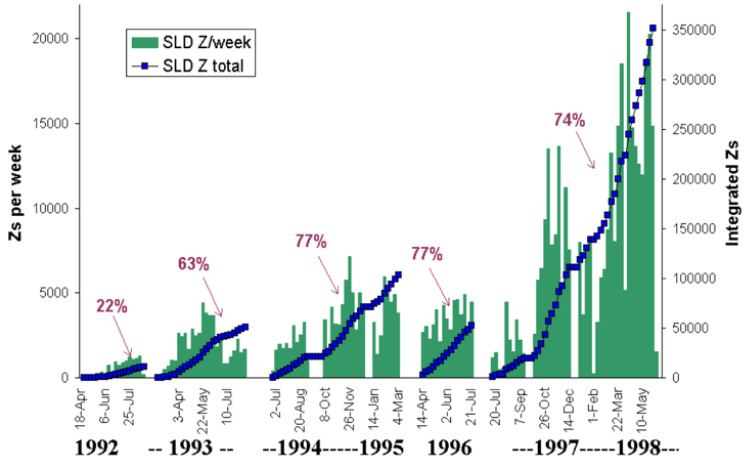


Fig. 15-3: SLD luminosity showing the improvement from 1992-1998.

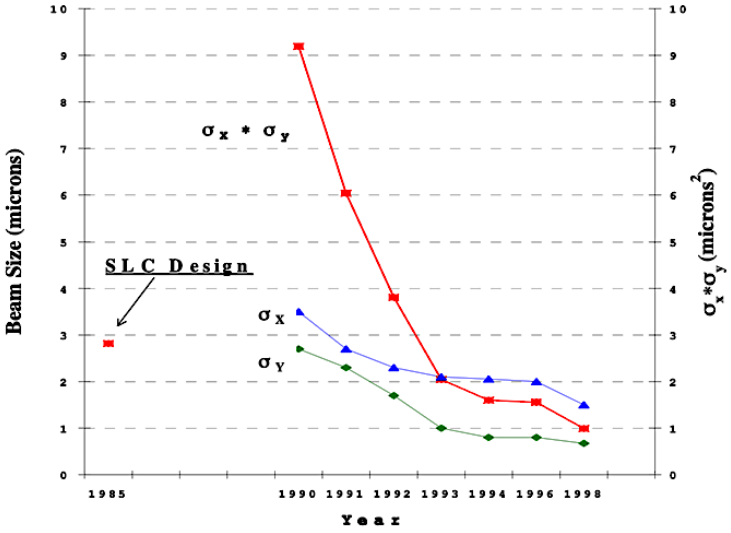


Fig. 15-4: Evolution of beam size at the SLC interaction point.

[381] N. Phinney, SLC Final Performance and Lessons. https://arxiv.org/abs/physics/0010008
[382] J. Haissinski *et al.*, Phasefix-Correcting the Tunes of the SLC Arcs.
https://inspirehep.net/files/81802a0d274ee955961e07d686bf946e ,
T. Fieguth *et al.,* Tuning the Arcs of the SLAC Linear Collider. https://accelconf.web.cern.ch/e88/PDF/EPAC1988_0272.PDF
[383] M. L. Swartz, Polarization at SLC. https://cds.cern.ch/record/190512/files/163.pdf

About Linear Colliders

The linear collider e^+e^- idea has a long history, well told for instance by Ugo Amaldi, Ref. [384]. After the SLC several projects were studied.

The projects considered in the last few decades are [385]:

- The **Next Linear Collider (NLC)**, a U.S.-based proposal developed at SLAC.
- The **Compact Linear Collider (CLIC),** proposed at CERN, using a novel "drive-beam" technology to achieve higher accelerating gradients. Several test facilities were exploited over the years (CTF1, CTF2, CTF3). The Conceptual Design Report (CDR) was published in 2012.
- The **Teraelectronvolt Energy Superconducting Linear Accelerator (TESLA)**, a German-led proposal centred at DESY. The TESLA Technical Design Report (TDR) was published in 2001.
- **The Global Linear Collider (GLC)**, name for the Japanese proposal.
- **The International Linear Collider (ILC)** merged several earlier regional proposals into one global effort in 2004. The choice of **"cold" (superconducting) technology for** the ILC was recommended by an international panel primarily due to its significant **energy efficiency** and operational advantages over the "warm" (normal-conducting) alternative. The ILC Technical Design Report (TDR) was published in June 2013.
- More recent, **the C3 (Cool Copper Collider)** is a proposed compact e^+e^- linear collider designed primarily as a Higgs factory, using novel cryogenically cooled copper accelerator technology.

The CM energies considered are 380 GeV, 1.5 and maybe 3 TeV for CLIC, 250 to 550 GeV, possibly 1 TeV for ILC.

The key of their luminosity is the vertical size of **1 to a few nanometres** of their beams at collision. Ref. [386] gives information about the R&D on this topic.

It is envisaged that the beam is delivered in parallel to two experiments which share the luminosity.

The polarization of electrons, and possibly of positrons, is a valuable asset for physics.

15.3 The Large Electron Positron Collider at CERN

Let's come to the Large Electron Positron Collider (**LEP**) [387, 388, 389]. Figure 15-5 left shows its location, between Jura mountains and Geneva airport, and its 27 km in circumference. Figure 15-5 right displays the four experiments, which quickly combined their data under the **ADLO** acronym, a welcome and beneficial move.

---

[384] U. Amaldi, Evolution of the Concepts and the Goals of Linear Colliders.
https://lib-extopc.kek.jp/preprints/PDF/1992/9206/9206285.pdf

[385] S. Stapnes, Future Linear Colliders.
https://indico.cern.ch/event/1462067/contributions/6155451/attachments/3032036/5353186/linear-colliders-CAS-2025%20.pdf

[386] A. Faus-Golfe, https://cds.cern.ch/record/2913174?ln=en

[387] K. Hübner, Designing and building LEP, *Phys.Rept. 403-404 (2004) 177-188*
E. Picasso, A few memories from the days at LEP. *Eur.Phys.J.H 36 (2012) 551-562*

[388] T. Taylor and D. Treille, The Large Electron Positron Collider (LEP): Probing the Standard Model.
https://inspirehep.net/files/d8317e2490824c0916b765874b74d84b

[389] R. Assmann *et al.,* A brief history of the LEP collider.
https://lib-extopc.kek.jp/preprints/PDF/2002/0210/0210055.pdf

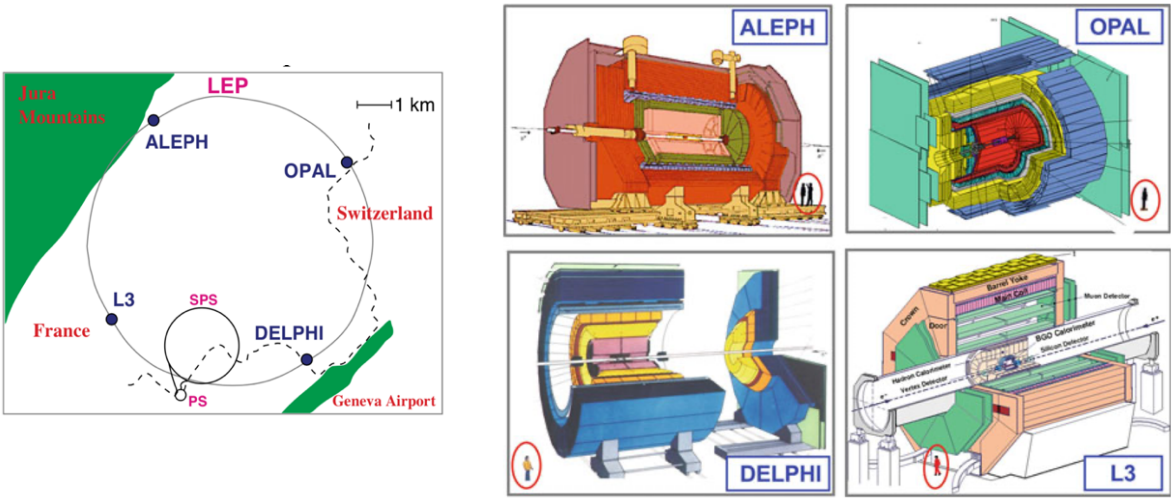


Fig. 15-5: The LEP ring (left), its four experiments (right).

As we saw in Chapter 9, in his seminal 1976 paper advocating LEP, Burt Richter, assuming a Z Boson at 100 GeV (Fig. 9-13), was not far from the truth.

The design of a linear collider was not yet mature and the idea of hosting the LHC in the same tunnel was already present (Chapter 10). The choice of a circular machine was therefore obvious.

References [390] give the evolution of the LEP design along the years. In the 1984 LEP design report, the "green book", the circumference was 26.7 km and the maximum beam energy was 125 GeV, with the prospect of installing accelerating radio-frequency cavities in the eight straight sections of the machine (a prospect that, it seems, was quickly abandoned).

The excavation of the LEP tunnel, the largest European construction site before the Channel Tunnel, required three tunnel boring machines, working in parallel. The excavation of the tunnel started in February 1985 and the ring was completed three years later. LEP consisted of 5176 magnets and, in its first phase, of 128 warm copper accelerating cavities.

Emilio Picasso [391] was the LEP project manager. The planning foreseen by John Adams in 1979 (Fig. 15- 6) [392] was well respected. The Director General Herwig Schopper played a major role in the LEP success [393].

LEP still is the largest e^+e^- collider ever built. In 1983, the first ground-breaking was inaugurated by François Mitterrand (French president) and Pierre Aubert (Swiss President). On July 14, 1989, the first

[390] K. Johnsen *et al*., (eds.), Design Concept for a 100 GeV e^+e^- Storage Ring (LEP). CERN-1977- 014 (CERN, Geneva, 1977). http://dx.doi.org/10.5170/CERN-1977-014
LEP Study Group, Design Study of a 15 – 100 GeV e^+e^- Colliding Beam Machine (LEP), "Blue Book", ISR-LEP 78/17 (CERN, Geneva, 1978). http://cds.cern.ch/record/101331
LEP Study Group, Design Study of a 22 – 130 GeV e^+e^- Colliding Beam Machine (LEP), "Pink Book", ISR-LEP 79/33 (CERN, Geneva, 1979). http://cds.cern.ch/record/101333
LEP design report ("The green book"), Vol. II, The LEP main ring, CERN-LEP/84-01 (1984). http://cds.cern.ch/record/102083?ln=en.
[391] E. Picasso, Superconducting Acceleration System for LEP. https://accelconf.web.cern.ch/srf84/papers/srf84-17.pdf
[392] J. B. Adams, Steering the LEP Project. Proceedings of LEP Summer Study, Les Houches, France, Sept 1978, CERN-79-01-V-2 (1979), https://cds.cern.ch/record/134730/files/271.pdf
[393] H. Schopper, LEP – The lord of the collider rings at CERN 1980-2000. Springer, 2016.

particle beam circulated. The first collisions were recorded on August 13, 1989, and on October 13, 1989, the first LEP results were published.

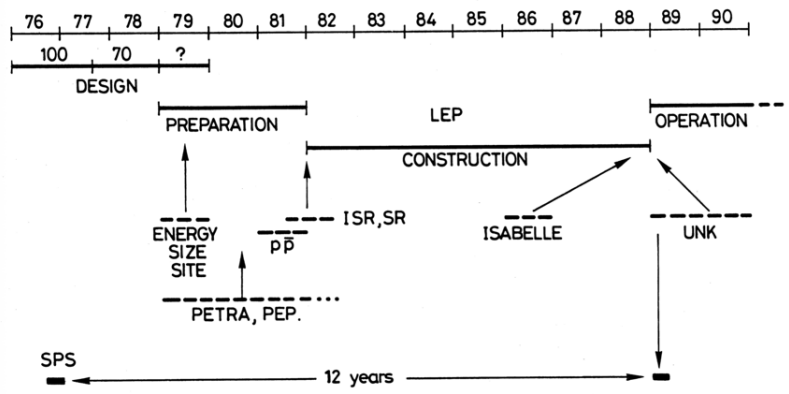


Fig. 15-6: LEP planning.

The initial centre-of-mass energy of LEP was close to the mass of the Z. In the first phase (LEP1) seven years were spent on the Z. The **first challenge was to obtain an ever-higher luminosity** [394]. LEP1 confirmed that there are only 3 families of neutrinos and thoroughly tested the SM, as we will see in detail in Chapter 16.

In 1995, LEP2 began its **second battle,** against synchrotron radiation (Fig. 15-7)**,** for **the energy rise** [395] and reached the threshold of producing W^+W^- pairs, then Z pairs. Thanks to 288 superconducting copper accelerating cavities (Fig. 15-8) [396] with internal niobium deposit [397], whose accelerating field turned out to be better than expected (Fig. 15-9). The collider finally reached a centre-of-mass energy of 209 GeV (206-207 useful) in 2000. Concerning the cavities one can quote the major contributions of Philippe Bernard, Herbert Lengeler, Emilio Picasso, Chris Benvenuti and Enrico Chiaveri.

The LIL (LEP Injector Linac) was designed and built by LAL (Orsay).

The quality of the machine and the frequency measurements were outstanding. With the accelerating RF (of 352.20904 MHz frequency) timed to capture the circulating beam (with harmonic number = (orbit length / RF wavelength) = 31320), the closed orbit length is quasi perfectly known at a given momentum (or energy). An observed variation of path length Δl is linked to a variation of momentum by $\Delta l/l = \alpha_c \, \Delta p/p = -\alpha_c \, \Delta f_{rf} / f_{rf}$, where α_c is the so-called momentum compaction factor, $\alpha_c = (1.814 \pm 0.004) \times 10^{-4}$ at LEP [398] and Δf_{rf} is the change of frequency needed to ensure the capture of the

[394] S. Myers, LEP Present Performance and Future Upgrades.
https://inspirehep.net/files/1a6bf5c55db0ce91188569eee58ea82
[395] S. Myers, High Energy Operation of LEP2. https://lib-extopc.kek.jp/preprints/PDF/1999/9906/9906017.pdf
[396] On RF acceleration in Technology Meets Research. https://inspirehep.net/files/02de568d4897c555515de27f0b96af4d , p. 42 and p. 239
[397] C. Benvenuti *et al.*, Superconducting Niobium Sputter-coated Copper Cavity Modules for the LEP Energy Upgrade.
https://accelconf.web.cern.ch/p91/PDF/PAC1991_1023.PDF
C. Benvenuti, Superconducting Skin Boosts Accelerator Cavity Performance. In Technology Meets Research, p. 238 of https://inspirehep.net/files/d8317e2490824c0916b765874b74d84b
The long march of niobium on copper: https://cerncourier.com/a/the-long-march-of-niobium-on-copper/
[398] L. Torino *et al.,* Momentum Compaction Measurement Using Synchrotron Radiation.
https://accelconf.web.cern.ch/ibic2018/papers/mopa17.pdf

circulating beam. This made it possible to detect very subtle effects [399], but significant, given the extreme precision aimed for, e.g. concerning the Z mass: the leaking currents due to the TGV Geneva-Paris and **the effects of the earth tides,** changing the path length. In November 1992, an energy variation of the beam of 4×10^{-4} was recorded over a 24-hour full moon period, consistent with tidal predictions [400].

In all aspects the LEP machine did better than expected (see Table 16-1 of Chapter 16) and one can only praise the team of machine experts [401] for these achievements.

On November 2, 2000, LEP was definitively shut down to install the LHC (Chapter 17).

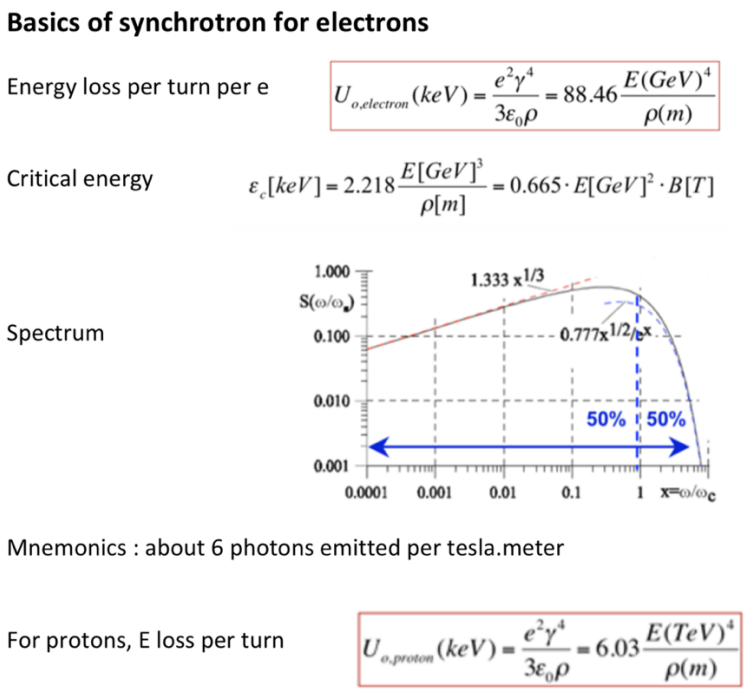


Fig. 15-7: Recap on synchrotron.

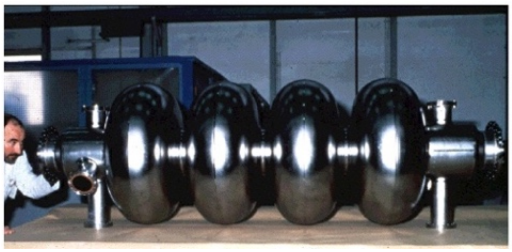


Fig. 15-8: LEP SC RF cavity.

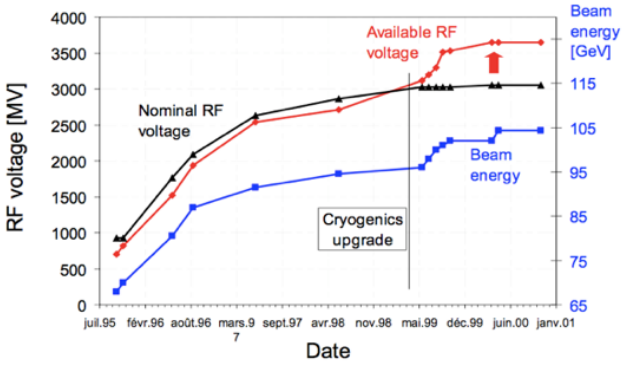


Fig. 15-9: LEP cavities accelerating voltage.

[399] A. Hofmann, Precise Energy Measurement: Heed the Moon, In Technology Meets Research: https://inspirehep.net/files/d59e7aaf7b366b4da3ed4a0798e7a8e9 , p. 244
M. Mayoud, Measuring the (Accelerator) World, In Technology Meets Research: https://inspirehep.net/files/d59e7aaf7b366b4da3ed4a0798e7a8e9 , p. 242

[400] L. Arnaudon *et al.*, *Nucl.Instrum.Meth.A 357 (1995) 249-252*

[401] R. Assmann *et al.*, A brief history of the LEP collider. https://lib-extopc.kek.jp/preprints/PDF/2002/0210/0210055.pdf

We will not describe the detectors in detail [402]. Figure 15-10 (courtesy Ugo Amaldi [403]) gives a list of their innovative elements that were later adopted by the LHC experiments. For some highlights see Ref. [404]. To the list we can add the change from the central mode of computing to the adoption of computing "farms" by individual experiments [405]. The needs of the LEP community to communicate in a new way and at a new scale were decisive in the advent of the WEB [406].

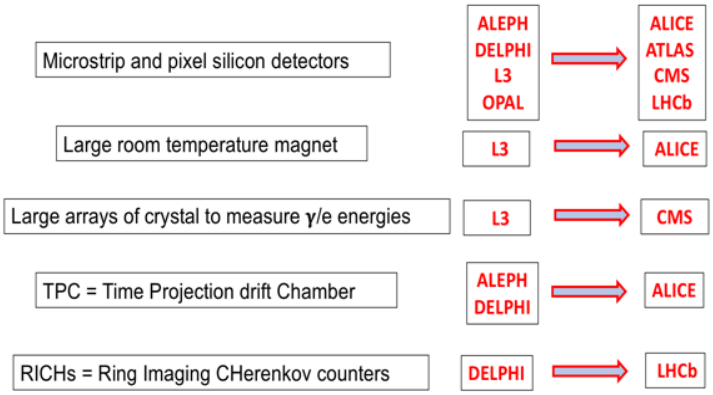


Fig. 15-10: Innovative items in LEP experiments.

Figure 15-11 shows a picture of the ALEPH experiment and some of its spokespersons.



Fig. 15-11: ALEPH and its état-major in full amusement.

---

[402] O. Callot and P. Charpentier, The LEP detectors.
https://comptes-rendus.academie-sciences.fr/physique/item/10.1016/S1631-0705(02)01394-4.pdf
[403] U. Amaldi, Detectors and Experiments at the Laboratory for Electro-Strong Physics: A Personal View.
https://inspirehep.net/files/f326403157ffa3993b5e86384d754293
[404] H. Dijkstra, The LEP Silicon Vertex Detectors: Right on Target, p. 246 in Technology Meets Research.
https://inspirehep.net/files/d8317e2490824c0916b765874b74d84b
P. Baillon, DELPHI RICH: The Luminous Footprint of Particles, ibid. p. 249
P. Lecoq, BGO for the L3 Experiment: Betting on Precision, ibid. p. 253
A. Hervé, The Magnetic Cavern of L3, ibid. p. 256
[405] The MUSCLE Report, https://cds.cern.ch/record/184457/files/CM-P00059881.pdf
S. Jarp, 25 years ago: the strategic move to PCs in high-energy physics.
https://home.web.cern.ch/news/news/computing/25-years-ago-strategic-move-pcs-high-energy-physics
[406] T. Berners-Lee, Information Management: A Proposal.
https://inspirehep.net/files/14010c49f3334997d3b6ad6617876d4e

LEP experiments achieved an excellent flavour tag (Fig. 15-12 left). Anticipating, Fig. 15-12 right shows the progress along years of ATLAS in c-jet and light-jet rejection for 70% b-jet tagging efficiency in $t\bar{t}$ jets.

LEP physics was prepared and followed by many studies and workshops associating closely theorists [407], experimentalists and machine physicists. Powerful programs to interpret data were built [408] (Chapter 16).

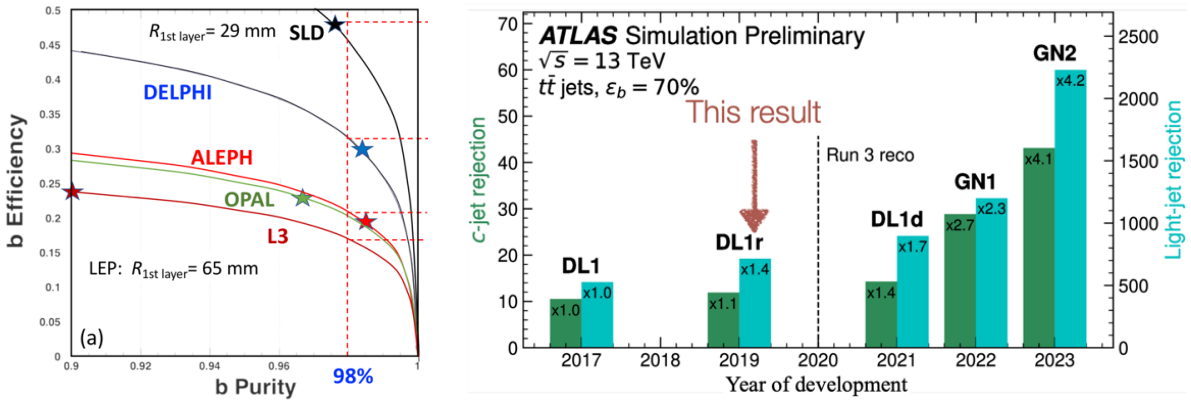


Fig. 15-12: Performances in heavy flavour tag at LEP (left) [409] and ATLAS at LHC (right) [410].

[407] J. Ellis *et al.*, A Phenomenological Profile of the Higgs Boson. *Nucl.Phys.B* 106 (1976) 292, https://cds.cern.ch/record/874049/files/CM-P00061607.pdf
G. Altarelli *et al.*, editors, Physics at LEP2. https://lib-extopc.kek.jp/preprints/PDF/1996/9606/9606016.pdf
Z physics at LEP1, https://inspirehep.net/files/be1fe991d2bf5ca1572f94d242a087ab
[408] D. Bardin *et al.*, The Zfitter program. https://arxiv.org/abs/hep-ph/9412201
[409] U. Amaldi, Detectors and Experiments at the Laboratory for Electro-Strong Physics: A Personal View. https://inspirehep.net/files/f326403157ffa3993b5e86384d754293
[410] P. Gadow, Heavy Flavour Jet Tagging Algorithms in ATLAS. https://indico.cern.ch/event/1274182/contributions/5458302/attachments/2690030/4667891/2023-07-25-CMS-BTV-Gadow-ATLAS.pdf

16. Florilège of LEP

LEP was an excellent machine, with four high-quality detectors, achieving clean, precise and subtle physics, which validated the SM at the "**level of the loop"** [411].

The machine worked wonderfully, offering e.g. a high-energy luminosity four times better than expected as illustrated in Table 16-1.

LEP: design and reality.

Parameter	Design (55/95 GeV)	Achieved (46/98 GeV)
Bunch Current	0.75 mA	1.00 mA
Total Beam Current	6.0 mA	8.4 mA/6.2 mA
Vertical Beam-beam parameter	0.03	0.045/0.083
Emittance ratio	4.0%	0.4%
Maximum Luminosity	$16/27\ 10^{30} cm^{-2} s^{-1}$	$34/100\ 10^{30} cm^{-2} s^{-1}$
Horizontal beta function at IP	1.75 m.	1.25 m.
Vertical beta function at IP	7.0 cm.	4.0 cm.

Table 16-1: Performances of the LEP machine [412].

The landscape of LEP is clear (Fig. 16-1): the peak of the Z (LEP1), then, a thousand times lower in cross-section, pairs of bosons (LEP2).

16.1 LEP1

At LEP1, 17 million Z were collected by ADLO (recap: acronym of the 4 experiments combining their results). It was quickly shown that there are 3 and only 3 families of low mass neutrinos [413] (Fig. 16-2).

In the field of precision measurements [414], LEP always did better, sometimes much better, than expected (Table 16-2) and took the lead in this field, with a few exceptions, such as the **SLC A_{LR} measurement** and the W mass of the Tevatron (± 16 MeV), a measurement revived by a new value, quite discrepant, presented by the CDF experiment (Chapter 18). For the most recent W mass measurements see Section 24.4.5.

Without producing the top quark, LEP, exploiting the effect of the loop (Fig. 16-3), gave information on its mass. Before LEP and the top discovery at Fermilab (see end of this chapter) there were only lower limits on M_{top}.

[411] For an elementary introduction to the Loops World: https://inspirehep.net/files/02de568d4897c555515de27f0b96af4d p. 145 and p. 227

[412] R. Assmann *et al.*, A Brief History of the LEP Collider. https://lib-extopc.kek.jp/preprints/PDF/2002/0210/0210055.pdf

[413] A key of this fast result was G. Feldman's suggestion. On the Possibility of Measuring the Number of Neutrino Species to a Precision of 1/2 Species with Only 2000 Z Events. https://slac.stanford.edu/pubs/slacreports/reports04/slac-r-315.pdf p. 169

[414] D. Treille, LEP/SLC: what did we expect? What did we achieve? *Nucl Phys. B Proc. Suppl.109 (2002) 1.* https://inspirehep.net/files/afcfc18e1f43e0e74a25184c9c32d189

As early as Moriond 1989, M_{top} was considered "very likely > 60 GeV". The current direct measurement [415] is M_{top} = 172.52 ± 0.33 GeV, the indirect one is M_{top} = 176.5 ± 2.1 GeV. See LHC physics in Chapter 24.

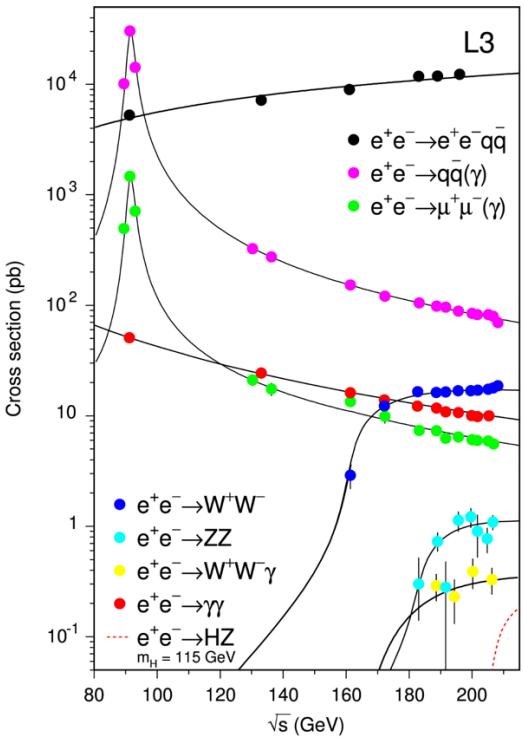


Fig. 16-1: LEP landscape [416].

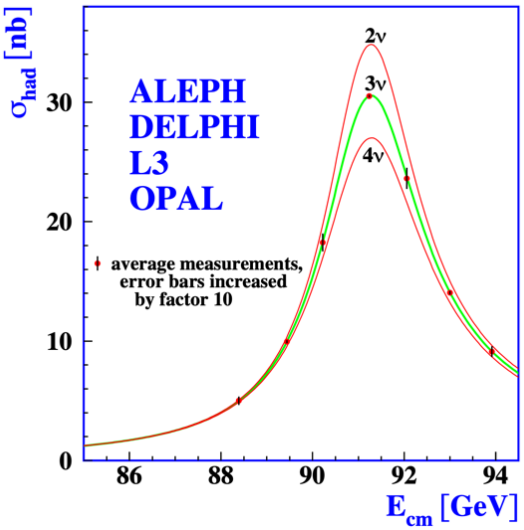


Fig. 16-2: The number of light neutrinos [417].

Quantity	*Expected error*	*Achieved*
m_Z	50 to 20 MeV	**2.1** MeV
m_W	100 MeV	**39** MeV
N_ν	0.3	**0.008**
$A_{FB}^{0,\mu}$	0.0035	**0.0013**
$A_{FB}^{0,b}$	0.0050	**0.0017**
$\mathcal{A}_\tau$	0.0110	**0.0043**

Table 16-2: Always better than expected [418].

[415] J. Bendavid, Recent Standard Model Measurements. https://indico.in2p3.fr/event/33627/contributions/153147/attachments/95164/145653/EPSSMExp-Jul9-2025-3.pdf
On the definition of the top mass: G. Corcella, The top-quark mass: challenges in definition and determination. https://arxiv.org/abs/1903.06574

[416] Values of the cross-sections measured by L3 and corresponding distributions predicted by the Standard Model (courtesy of CERN). See also A. Blondel *et al.*, LEP's electroweak leap. https://cerncourier.com/a/leps-electroweak-leap/

[417] ADLO Collaboration, Precision Electroweak Measurements on the Z Resonance. https://arxiv.org/abs/hep-ex/0509008

[418] J. Drees, Review of Final LEP Results or a Tribute to LEP. *Int.J.Mod.Phys. A17 (2002) 3259-3283,* https://arxiv.org/abs/hep-ex/0110077

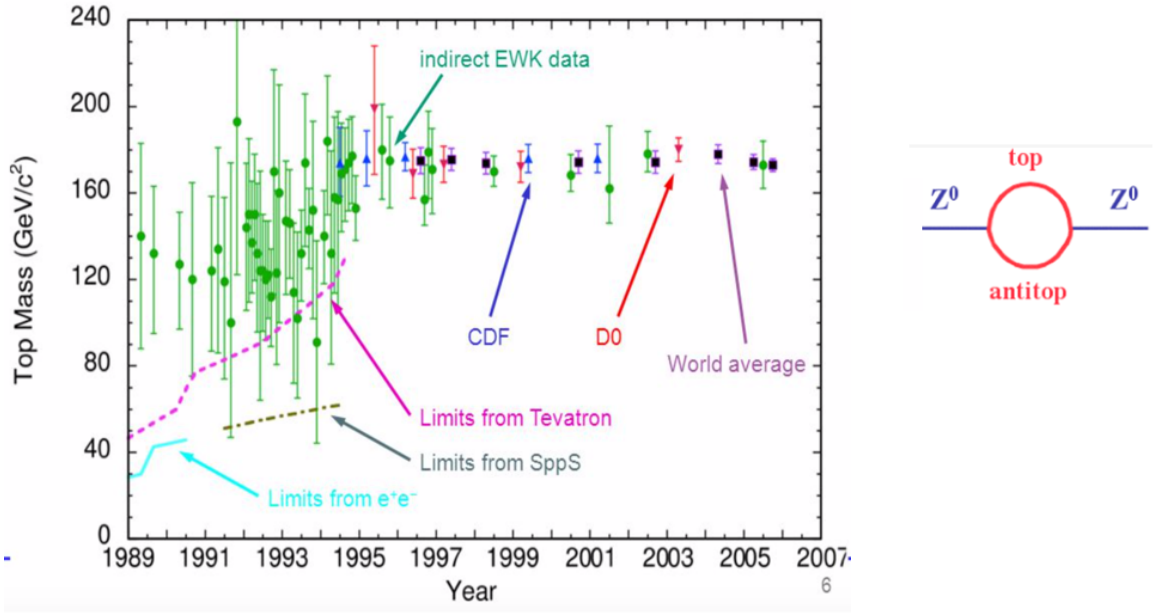


Fig. 16-3: Information on M_{top} determinations, courtesy Chris Quigg (left), the top loop at the Z (right).

The top problem solved [419], LEP gave an indication of M_{Higgs} (Fig. 16-4), but the Higgs is only logarithmically sensitive to it via the loop, also shown in Fig. 16-4. Much tribute is due to ZFITTER [420], the program from which these results come.

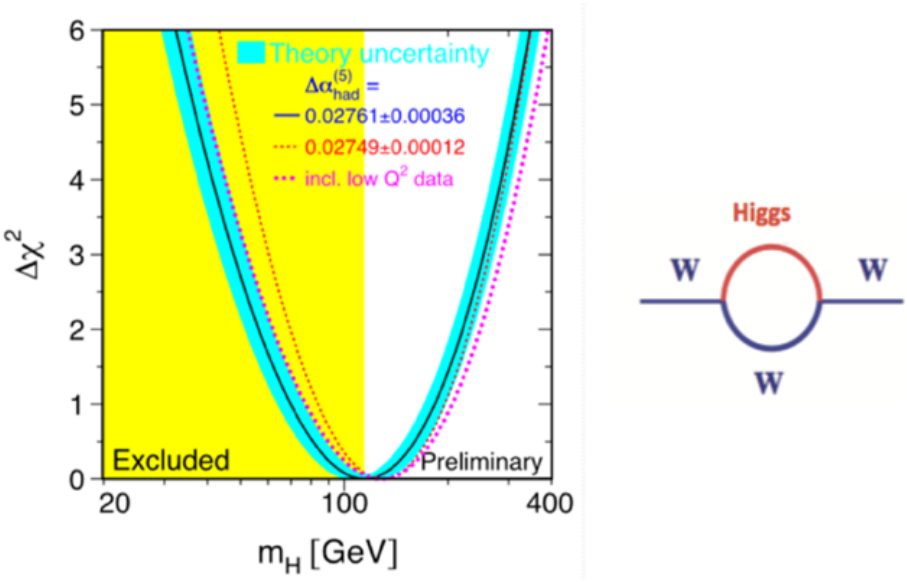


Fig. 16-4: Indication of the SM M_H value.

[419] A nice image from Guido Altarelli: "*Tracking the Higgs boson alongside the top quark would be like a* ***bush hunter****, with his ear to the ground, trying to spot the steps of a lion, while an elephant is trampling the ground nearby*".
[420] A. Akhundov *et al.*, The ZFITTER Project. https://arxiv.org/abs/1302.1395

LEP highlighted the role of loops, beyond the trivial variation of the $\alpha_{e.m.}$ coupling with scale. It measured $\Delta\rho = 0.005 \pm 0.001$ [421]. From M_W, M_Z, α, G_μ, one found $\Delta r = 0.032 \pm 0.002$, and by subtracting $\Delta\alpha$, $\Delta r_W = \Delta r - \Delta\alpha = -0.025 \pm 0.002$, **12σ from zero** (with the M_W of that time, $M_W = 80.450 \pm 0.034$ GeV, which seems to be confirmed by LHC). More in Section 18.3.

As illustrated by the following figures, LEP brought a lot to QCD [422].

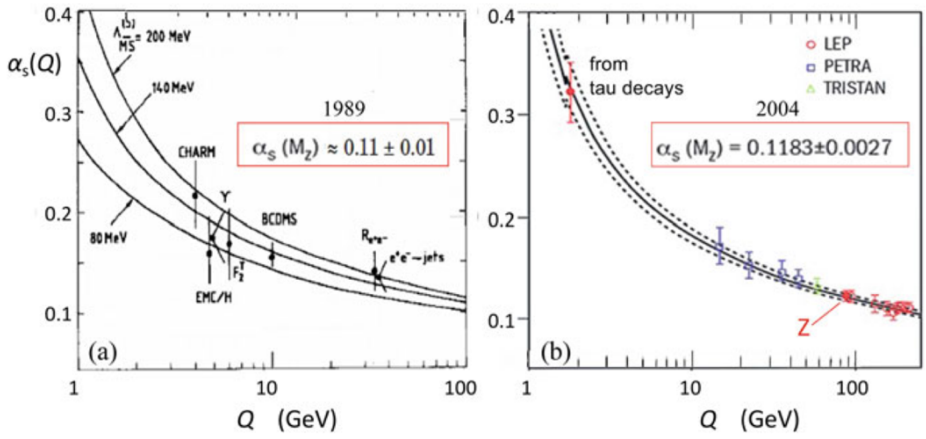


Fig. 16-5: The situation of the strong coupling before and after LEP [423].

Reference [424] gives the contributions to the strong coupling measurement of the various methods:

from event shapes and jets: $\alpha_S(M_Z) = 0.1196 \pm 0.0036$ (in NNLO)
from tau decays: $\alpha_S(M_Z) = 0.1192 \pm 0.0018$ (in N^3LO)
from electroweak precision fits: $\alpha_S(M_Z) = 0.1196 \pm 0.0030$ (in N^3LO)

A key parameter of QCD is the gluon self-coupling, which was studied in angular correlations and energy distributions of 4-jet events. Figure 16-6 [425] compares the distribution of the azimuthal angle between the planes defined by the two highest and the two lowest energetic jets in 4-jet events measured at LEP, to QCD predictions and to an Abelian theory where this self-coupling does not exist.

Figure 16-7 [426] shows the determination of the gauge structure functions [427] through the analysis of 4-jet angular correlations and fits to hadronic event shapes. The results $C_A = 2.89 \pm 0.01$ (stat) $\pm$ 0.21 (syst) and $C_F = 1.30 \pm 0.01$ (stat) $\pm$ 0.09 (syst) agree well with those of QCD ($C_A \equiv N_C = 3$, $C_A = 4/3$ and $T_R = 1/2$) and rule out an Abelian vector gluon model ($C_A = 0$, $C_F = 1$ and $T_R = 6$).

---

[421] F. Teubert, Precision tests of the electroweak interactions at LEP/SLC. https://arxiv.org/abs/hep-ph/0209163
[422] S. Bethke, Precision Physics at LEP. https://arxiv.org/abs/1712.03035
[423] U. Amaldi, Detectors and Experiments at the Laboratory for Electro-Strong Physics: A Personal View. https://inspirehep.net/files/f326403157ffa3993b5e86384d754293
G. Dissertori, The Determination of the Strong Coupling Constant. Contribution to The Standard Theory up to the Higgs discovery - 60 years of CERN, https://arxiv.org/abs/1506.05407
S. Bethke, QCD studies at LEP, *Phys.Rep.404 (2004) 203.16-5*
[424] S. Bethke, ibid.
[425] L3 Collaboration, B. Adeva *et al.,* A test of QCD based on 4-jet events from Z decays. *Phys. Lett. B248 (1990) 227*
[426] S. Kluth, Jet physics in e^+e^- annihilation from 14 to 209 GeV. https://arxiv.org/abs/hep-ex/0309070
[427] For a pedagogical introduction see M. Thomson: https://www.hep.phy.cam.ac.uk/~thomson/lectures/QCD.pdf
G. Heinrich, https://indico.in2p3.fr/event/16354/contributions/59530/attachments/49431/62853/QCD_partI_GH.pdf
C_F and C_A are the eigenvalues of the quadratic Casimir operator in the fundamental and adjoint representation, respectively. $C_F = T_R(N_c^2 - 1)/N_c$, $C_A = 2T_R N_c$.

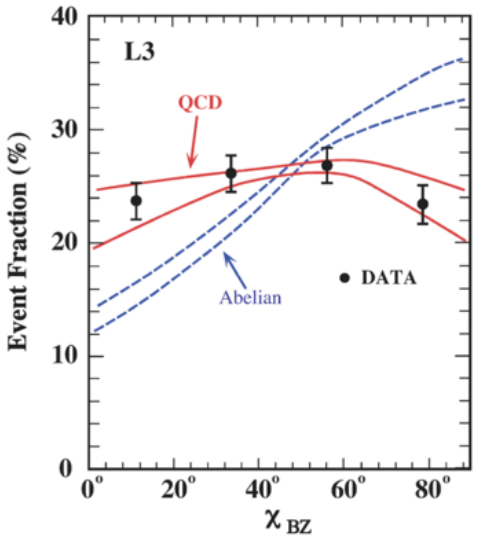


Fig. 16-6: Azimuthal angle between the planes defined by the two highest and the two lowest energetic jets in 4-jet events.

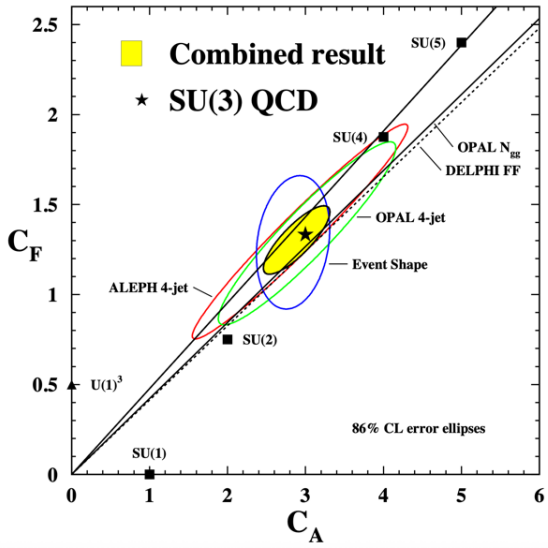


Fig. 16-7: Determination of the gauge structure functions by LEP experiments.

LEP showed that, in addition to the coupling constants, the masses of the quarks, like that of the b quark (Fig. 16-8), also "run" and decrease when energy and resolving power increase. See Section 24.4.6.

LEP also indirectly proved CP violation in the B sector. Figure 16-9 shows the tip of the unitary triangle (Chapter 14) in summer 2000, in the SM frame, due to results from LEP and other experiments, before results of asymmetric B factories (Chapter 14) and the measurements of angles became available.

LEP1, together with BES and CESR, settled a confuse situation about the τ, showing that it behaves as a normal lepton (Fig. 16-10). Being "normal", the τ can then be used as a most interesting laboratory for low energy hadronic physics and QCD.

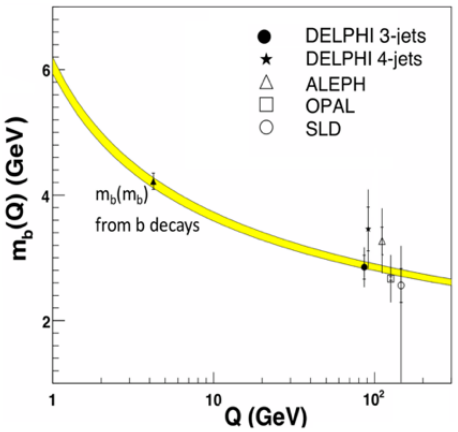


Fig. 16-8: The variation of m_b with energy [428].

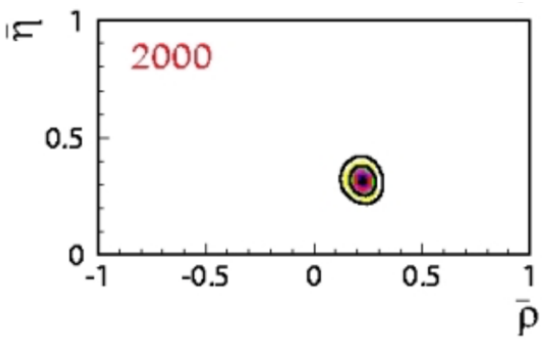


Fig. 16-9: Evidence of CP violation in B sector [429].

[428] U. Amaldi, Detectors and Experiments at the Laboratory for Electro-Strong Physics: A Personal View. https://inspirehep.net/files/f326403157ffa3993b5e86384d754293 , and ref. therein

[429] P. Roudeau, Ten years of b-physics at LEP and elsewhere. https://lib-extopc.kek.jp/preprints/PDF/2003/0302/0302014.pdf

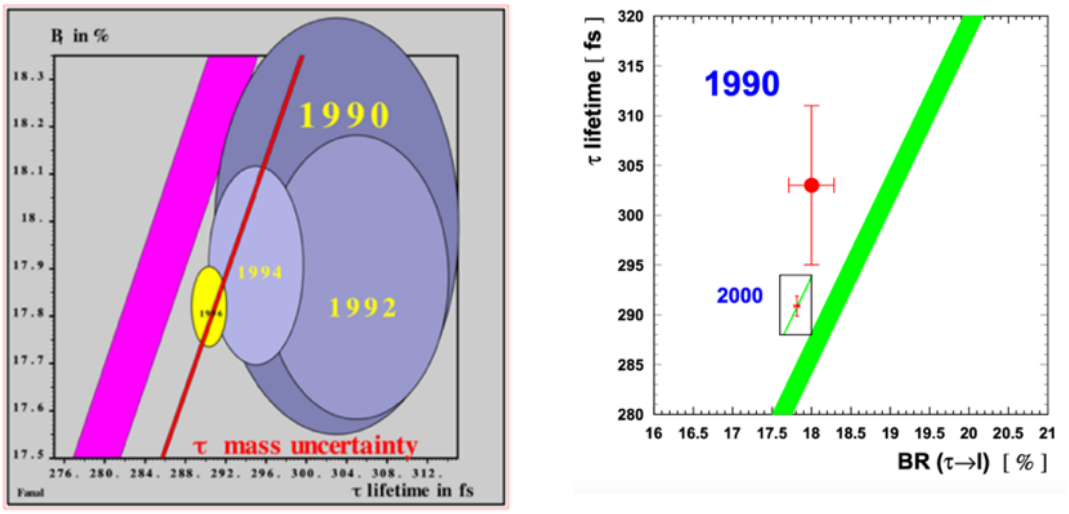


Fig. 16-10: The τ is a normal lepton. Left: courtesy H. Videau. Right: from Ref. [430].

By precisely measuring the couplings of the three forces at the Z scale, LEP was able to show their perfect triple convergence at O (10^{16} GeV) in the SUSY scenario (Fig. 16-11). This result caused a stir [431], but cannot constitute proof of SUSY.

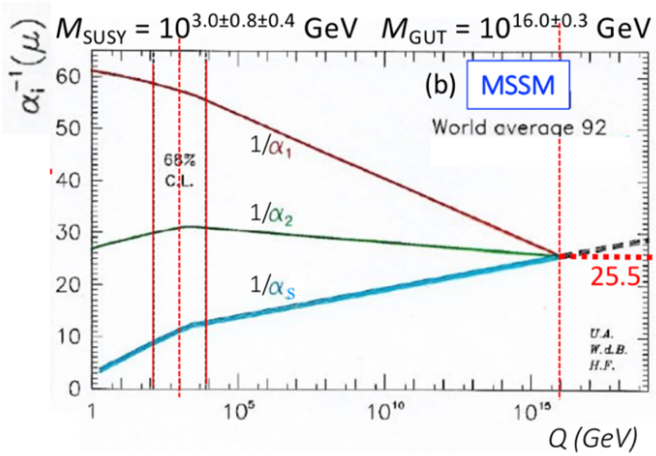


Fig. 16-11: The convergence of couplings at high energies in the MSSM.

16.2 LEP2

After four years spent on the Z resonance, the program turned to LEP2 at increasingly higher centre-of-mass energies. The key to the accelerating ramp-up required was the fleet of SC RF cavities described in Chapter 10. In 1999 their accelerating field reached 7.5 MV/m, a value better than initially expected, and the final useful beam energy reached at LEP2 was 103 GeV.

The W pair production cross-section (Fig. 16-12) clearly showed that the 3 bosons interact with each other, with the expected strength, proof of the **non-abelian character** of the electroweak interactions.

[430] ibid, W. Venus, A LEP Summary. https://inspirehep.net/files/64a04e13d6f5ec34d5f27e669cd45c1e
[431] U. Amaldi, Detectors and Experiments at the Laboratory for Electro-Strong Physics: A Personal View. https://inspirehep.net/files/f326403157ffa3993b5e86384d754293 , and ref. therein

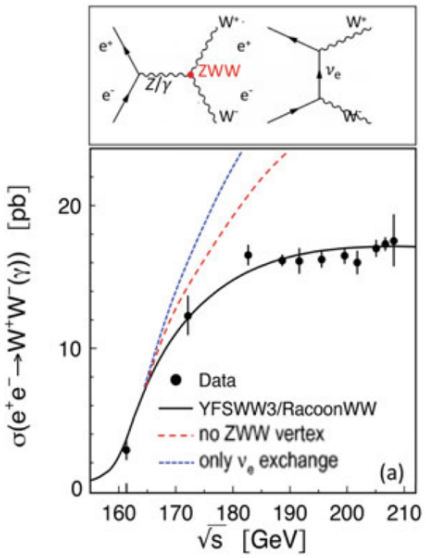


Fig. 16-12: The 3 bosons interacted with each other [432].

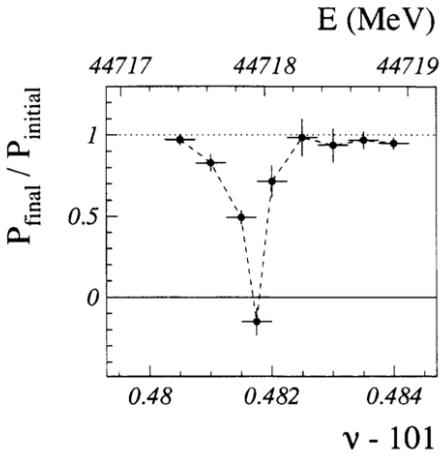


Fig. 16-13: Resonant depolarization [433].

16.3 Two brave attempts

One can add that at LEP a lot of work was devoted to two aspects:

- **obtaining and using transverse polarisation** [434]:
  In a circular machine there is a natural build-up of transverse polarization, due to the **Sokolov–Ternov effect** [435]. However, this is a slow process and various depolarization mechanisms counteract it. One must therefore speed up the rate of its growth and maintain the degree of polarization achieved.

  The full priority given to the energy rise at LEP finally led to discard an eventual longitudinal polarization program, which would have required to rotate it [436]. LEP left thus the **A_{LR} asymmetry** to be measured by SLC. As we mentioned already, the SLAC program was a great success (Chapter 18).

  However, **resonant depolarization** at LEP1 (Fig. 16-13) was the key of the ultraprecise determination of the Z mass. And speculations on polarization led to the invention of the Blondel scheme [437].
- **high luminosity at LEP** by increasing the number of bunches ("Pretzel" scheme) [438]. This option was only partly exploited.

---

[432] ibid, W. Venus, A LEP Summary, and ref. therein
U. Amaldi, Detectors and Experiments at the Laboratory for Electro-Strong Physics: A Personal View. https://inspirehep.net/files/f326403157ffa3993b5e86384d754293 , and ref. therein
[433] L. Arnaudon *et al.*, Accurate Determination of the LEP Beam Energy by Resonant Depolarization. https://lib-extopc.kek.jp/preprints/PDF/1994/9410/9410284.pdf
ADLO collaboration, Precision Electroweak Measurements on the Z Resonance. https://arxiv.org/abs/hep-ex/0509008
[434] Polarization at LEP: CERN-88-06-V-1, CERN-YELLOW-88-06-V-
[435] Sokolov–Ternov effect: https://en.wikipedia.org/wiki/Sokolov–Ternov_effect
[436] R. Schwitters and B. Richter, A Method for Producing Longitudinal Beam Polarization at PEP. https://inspirehep.net/files/fe04bfa8c40f31d456a57b132fcb9492
[437] A. Blondel, A scheme to measure the polarization asymmetry at the Z pole in LEP. https://cds.cern.ch/record/183640/files/198801022.pdf
[438] Report of the working group on high luminosities at LEP, CERN-91-02, CERN-Yellow-91-02.

16.4 More on the top story

Let us tell more on the top story described in Fig. 16-3. It shows the unambiguous limits set by the e^+e^- colliders that preceded LEP. Those set by the UA experiments have evolved: after a possible evidence by UA1 at M_{top} = 40 ± 10 GeV, unsupported afterwards, UA2 in 1990 gave the limit M_{top} > 69 GeV.

In 1995, the electroweak measurements performed at LEP and other measurements resulted in

$$M_{top} = 169\,^{+16\ +17}_{-18\ -20} \text{ GeV}.$$

The discovery of the top at Fermilab announced in 1995 [439] gave first

$$\text{D0} \quad M_{\text{top}} = 199^{+19}_{-21}\ (\text{stat}) \pm 22\ (\text{syst})\ \text{GeV}$$
$$\text{CDF} \quad M_{\text{top}} = 176\ \pm 8\ (\text{stat}) \pm 10\ (\text{syst})\ \text{GeV}.$$

Then Ref. [440] established

$$\text{D0} \quad M_{\text{top}} = 170\ \pm 15(\text{stat}) \pm 10\ (\text{syst})\ \text{GeV}$$
$$\text{CDF} \quad M_{\text{top}} = 176\ \pm 6\ (\text{stat}) \pm 7\ (\text{syst})\ \text{GeV},$$

resulting in a combined top mass value of M_{top} = 175 ± 8 GeV.

We recall the up to date value of the top mass: M_{top} = 172.52 ± 0.33 GeV.

16.5 A four-jet story

When LEP2 was running at $\sqrt{s}$ = 130–140 GeV, the ALEPH Collaboration reported a significant excess in the rate of four-jet production and a sharp structure in the invariant mass spectrum [441]. ALEPH confirmed this observation during the runs of LEP at $\sqrt{s}$ = 161 and 172 GeV. The di-jet mass sum distribution ΣM for the smallest ΔM distribution showed an accumulation around 105 GeV of 9 events for 0.6 events expected, a probability of ∼ 0.01%.

No significant evidence was found by the three other LEP experiments.

A LEP working group was convened to study the subject. Several checks did not show differences of performance between the four LEP experiments. It was thus decided to combine the results. The outcome is summarized in Fig. 16-14. The left plot shows the combined mass spectrum for DELPHI, L3 and OPAL (DLO) exhibiting a good agreement with SM expectations. A 95% CL upper limit on the cross-section of a hypothetical pair-produced signal cross-section derived using Poisson statistics was $\sigma_{95\%}$ ∼ 0.6 pb assuming no CM energy dependence of the cross-section. The right plot of the figure presents the ALEPH mass spectrum showing clearly an excess in two bins. If one interprets this excess as a signal, it corresponds to a cross-section of 2.3 ± 0.6 pb.

This story, maybe resulting from a huge statistical fluctuation, illustrates the importance of cross-checks between experiments on a given topic.

---

[439] P. K. Sinervo for CDF, The discovery of the top quark. FERMILAB-Conf-95/371-E, https://inspirehep.net/files/42fb1a8848efe5913487b784a1517865

[440] C. Campagnari and M. Franklin, The Discovery of the top quark. https://arxiv.org/abs/hep-ex/9608003

[441] M. A. Bizouard, 4-jet events at LEP. https://cds.cern.ch/record/2299547/files/C97-03-22_P7.pdf
R. Faccini. The LEP four-jets puzzle.
https://www.sciencedirect.com/science/article/abs/pii/S0920563297010165

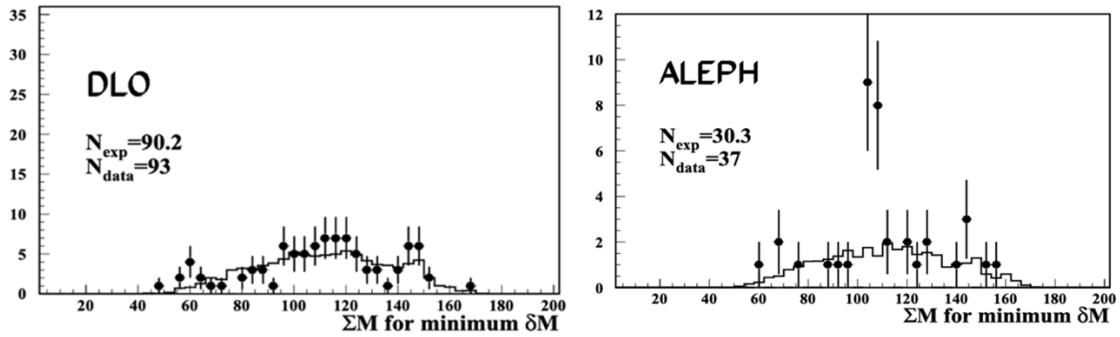


Fig. 16-14: Distribution of the sum of the dijet masses for the smallest mass difference at 133–172 GeV. Left: combination of DELPHI + L3 + OPAL (= DLO), right: for ALEPH.

16.6 A comment on LEP costs

The LEP collider (tunnel and LEP1) cost 1131 million Swiss Francs (1981 prices), compared to the initial estimate of 890 million [442]. The experiments cost 480 million Swiss Francs, of which CERN paid 140 million. The remaining 340 million came from outside institutes and universities. Furthermore, North America, Russia, China and Japan all contributed to the construction of the experiments. The cost of LEP200 was a further 400 million Swiss Francs. It is estimated that 2000 man-years have been invested in the whole project.

[442] R. Bailey, C. Benvenuti, S. Myers and D. Treille, The LEP collider. *C. R. Physique 3 (2002) 1107–1120*, https://comptes-rendus.academie-sciences.fr/physique/item/10.1016/S1631-0705(02)01402-0.pdf

17. LEP2 and its fate

The Feynman diagram of Fig. 17-1 shows the mechanism of Higgs production at LEP2.

At the Aachen LEP200 Workshop in 1986 [443], it was, for experimental reasons, still considered impossible to explore the Higgs mass range in the vicinity of the W mass, and a fortiori of the Z mass.

In 1989, however, one started to realize that with a good b-tag one would probably be able to "*break the Z wall*".

On the basis of simple estimates, a rule of thumb was proposed for a Higgs mass reach of: $M_H \sim \sqrt{s} - 100$ GeV, indicating a discovery potential per experiment.

Introducing more sophistication in the analysis and statistical methods and combining the four experiments led in the early nineties to the final $M_H \sim \sqrt{s} - M_Z$ GeV reach estimate, which was indeed obtained at each LEP energy. For a summary of this evolution see Ref. [444].

In the year 2000, the LEP CM energy was at its maximum near $2E_{beam} = 207$ GeV [445]. The allocated quota of accelerating RF cavities was fully in use.

Figure 17-2 shows the LEP2 landscape. The cross section of the H_{125}, the "*treasure island*", was not on the maps 30 years ago. On the other hand, the MSSM, which obsessed most minds (see e.g. Fig. 16-11), imperatively required the presence of a **light SM-type Higgs boson** [446].

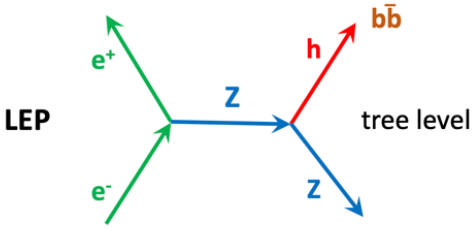


Fig. 17-1: Higgs production at LEP2.

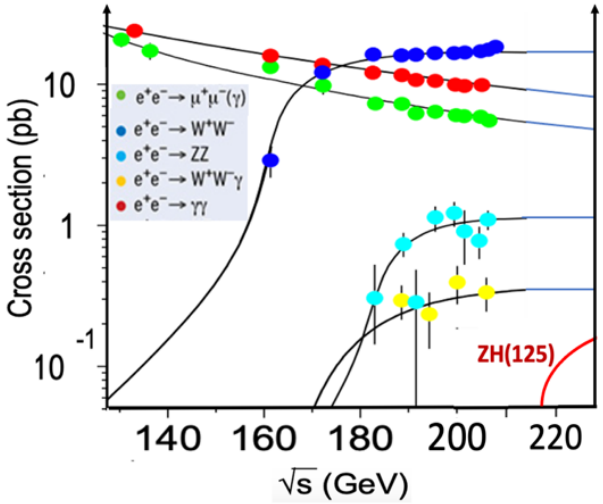


Fig. 17-2: The boson pairs cross-sections and the ZH (M_H = 125 GeV) cross section. Adapted from Fig. 16-1.

[443] S. L. Wu *et al.,* Search for neutral Higgs at LEP200. ECFA Workshop on LEP200, Aachen, 1986, Vol.II, p. 312, https://cds.cern.ch/record/180188/files/CERN-87-08-V-2.pdf

[444] D. Treille, LEP/SLC: What did we expect? What did we achieve? A very quick historical review. Nucl.Phys.B Proc.Suppl. 109 (2002) 1-16, https://www.sciencedirect.com/science/article/abs/pii/S0920563202900046 https://inspirehep.net/literature?sort=mostrecent&size=25&page=1&q=a%20treille%20and%20t%20achieve

[445] LEP could deliver, but with low luminosity, data up to 209 GeV E_{CM}.

[446] In SUSY the Higgs quartic coupling is not a free parameter but is related to the electroweak couplings, g and g'. Then the tree level mass of the lightest boson is < M_Z. To get the actual mass one needs to evaluate **radiative corrections** which depend on M^4_{top} and more mildly on the SUSY breaking mismatch between top and stop masses. For a stop in the TeV region, Fig. 17- 3 and its reference give the expected upper limit.

After radiative corrections were computed [447] and the top mass was known, the mass of this boson was expected below 130 GeV, as Fig. 17-3 and Fig. 17-7 show. It seemed natural to go and see…

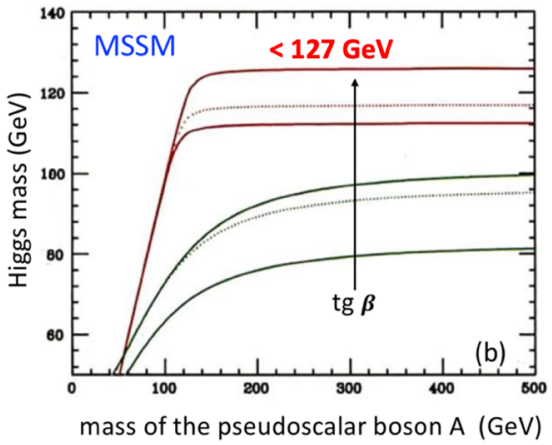


Fig. 17-3: Limit of the lightest MSSM boson mass [448].

Reaching **220 GeV CM energy** to explore up to 130 GeV [449] would have required 1/3 more RF cavities, namely to fill the acceleration areas equipped to host them [450]. A long series of attempts were made to convince the CERN management to go that way [451]. Unfortunately, for various reasons, this increase was not accepted.

The "treasure island" now appears on the maps. Let's hope Particle Physics will land there sometime. The treasure is that one event out of ~ 100 is a Higgs boson.

Quoting a 2004 statement [452]: *"The maximum energy of LEP2 was determined by the decision in 1996 to discontinue the industrial production of the superconducting cavities. Whether the potential of LEP should have been better fully exploited up to* ***its reasonable limit of 220 GeV*** *in the centre-of-mass and whether this would have led to the discovery of the Higgs particle as a number of models seemed to suggest … is a matter of speculation? The quest for the Higgs particle will hopefully end with the results obtained by the Tevatron and the LHC. In any case, LEP will stand as a landmark in the development of particle accelerators"*.

One year at 220 GeV with the luminosity delivered by LEP in 2000 would have given 21 Higgs events per experiment and a discovery. Scenarios reaching 220 GeV CM would have required spending about 40 to 70 MCHF.

---

[447] Y. Okada, M. Yamaguchi and T. Yanagida, *Prog.Theor.Phys. 85 (1991)*, H. E. Haber and R. Hempfling, *PRL. 66 (1991) 1815*, J. Ellis, G. Ridolfi and F. Zwirner, *Phys.Lett.B 257 (1991) 83.*

[448] M. Carena *et al., Phys. Lett. B 355 (1995) 209.*

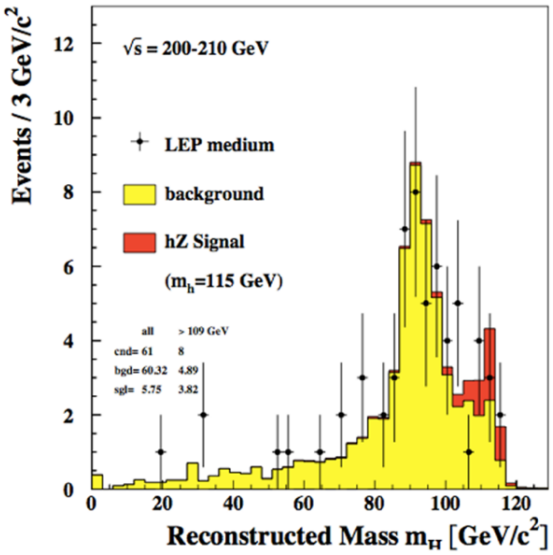
[449] D. Treille, Searches for New Particles. *Rep.Prog.Phys.57 p. 1137 (1994),* https://iopscience.iop.org/article/10.1088/0034-4885/57/11/002/pdf

[450] S. Myers and C. Wyss, Prospects for Energy and Luminosity at LEP. CERN 96-01 vol.1, p.23, https://cds.cern.ch/record/300671/files/CERN-96-01-V1.pdf

[451] D. Treille, LEP/SLC: What did we expect? What did we achieve? A very quick historical review. Nucl.Phys.B Proc.Suppl. 109 (2002) 1-16, https://inspirehep.net/files/afcfc18e1f43e0e74a25184c9c32d189
U. Amaldi, Detectors and Experiments at the Laboratory for Electro-Strong Physics: A Personal View. https://inspirehep.net/files/f326403157ffa3993b5e86384d754293
S. Myers, CERN: Fifty years of CERN Colliders. https://indico.ijclab.in2p3.fr/event/11336/contributions/36636/

[452] K. Hübner, Designing and Building LEP. *Phys. Rep.403-404 (2004),* https://cds.cern.ch/record/806279/files/ab-2004-099.pdf

Let us briefly recall the "115" interlude, with 115 GeV + M_Z = 206 GeV, effect observed close to the ultimate CM energy, especially in 4-jet events and mostly in a single experiment. It contained some nice events, with b-tag – as the Z likes (Fig. 17-4). Finally, given the overall low significance, a lower limit on M_H was set at 114.4 GeV. This signal was not confirmed at the LHC. The real boson was 10 GeV heavier. A near miss.



	EXP	$\sqrt{s}$(GeV)	Channel	M (GeV)	s/b	w
1	ALEPH	206.7	4-jet	114.3	4.6	1.73
2	ALEPH	206.7	4-jet	112.9	2.4	1.21
3	ALEPH	206.5	4-jet	110.0	0.9	0.64
4	L3	206.4	E-miss	115.0	0.7	0.53
5	OPAL	206.6	4-jet	110.7	0.7	0.53
6	DELPHI	206.7	4-jet	114.3	0.6	0.49
7	ALEPH	205.0	Lept	118.1	0.6	0.47
8	ALEPH	208.1	Tau	115.4	0.5	0.41
9	OPAL	205.4	4-jet	112.6	0.5	0.40
10	ALEPH	206.5	4-jet	114.5	0.5	0.40

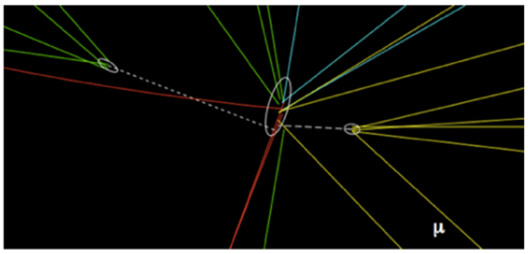


Fig. 17-4: About the effect in the year 2000. The signal (left), the candidates (top right) and bottom right, showing one event at the vertex (from ALEPH).

A possible explanation of what happened in the year 2000 is that for a 4-jet event, as in Fig. 17-5 (a ZZ event from DELPHI), roughly planar, if √s is attributed as overall energy and if 2 jets are **mass-constrained to M_Z**, as it was done, then the other two jets are **bound to have $\sqrt{s} - M_Z$ as mass**. At the phase space limit, in constraint physics, one must take care not to leave **physics for math.** As long as the E increased the new collected data excluded a possible mistake.

At 220 GeV CM a 125 GeV Higgs boson would have been comfortably far from the kinematic limit, allowing to avoid the problem just described.

At the end of LEP the only machine left on the Higgs topic was the Tevatron. But its program could only give a 3 σ indication of the 125 GeV boson, indication which came after its discovery (Fig. 17-6) [453].

As for the LHC, one knew that the discovery would request exploiting rare but visible decay modes, as $h \rightarrow \gamma\gamma$ (a BR of 2.3 per mille) and to $ZZ \rightarrow 4$ leptons (a BR of about 10^{-4}), as we shall see later.

Figure 17-7 illustrates the situation at the end of LEP operation concerning the expectations for the lightest SUSY Higgs and Fig. 17-8 summarizes the actual situation, with the Higgs cross-section and the maximal energy reached by LEP.

[453] Tevatron scientists announce their final results on the Higgs particle:
https://news.fnal.gov/2012/07/tevatron-scientists-announce-final-results-higgs-particle/

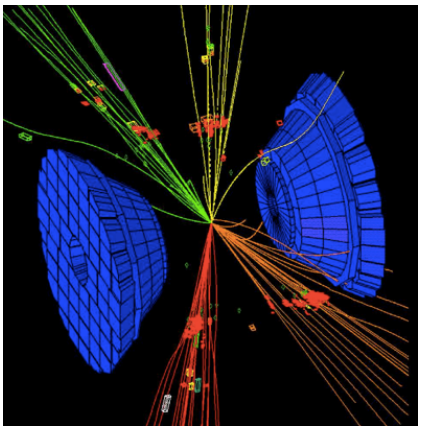


Fig. 17-5: A 4-jet Delphi event, probably a Z pair.

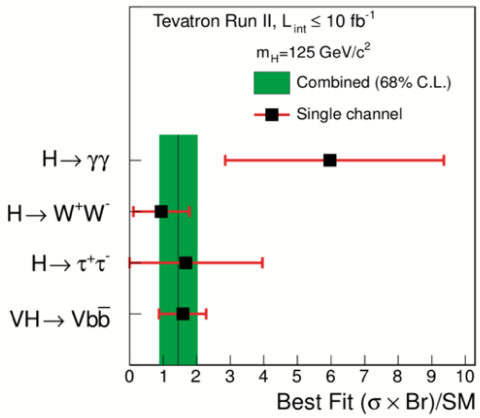


Fig. 17-6: The Tevatron indication in 2012.

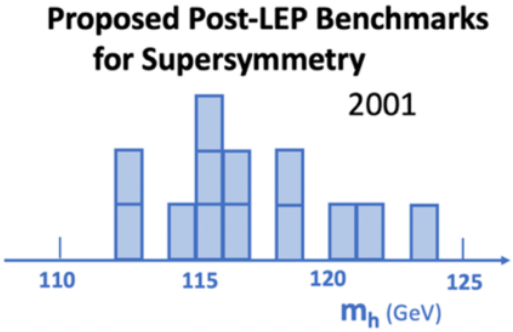


Fig. 17-7: Higgs mass values for the 13 benchmark scenarios proposed in Ref. [454] to span the post-LEP range of constrained mSUGRA possibilities (figure by D. Treille).

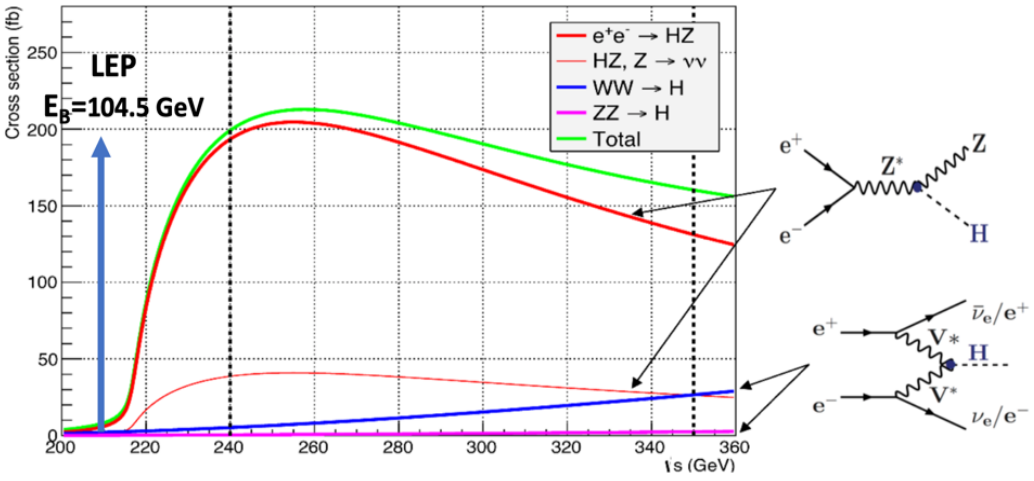


Fig. 17-8: The 125 GeV Higgs production cross section (courtesy P. Janot).

[454] M. Battaglia *et al.*, Proposed Post-LEP Benchmarks for Supersymmetry. https://arxiv.org/abs/hep-ph/0106204

18. Final message from LEP/SLC

18.1 Combined results

ADLO at LEP and SLD at SLC results were finally combined.

The final message of LEP on the Higgs boson (Fig. 18-1) was an indication of mass between the lower limit thus established and the upper limit inferred from the EW measurements within the framework of the SM, a limit evolving with the arrival of new data (value of α, results of the Tevatron, etc.).

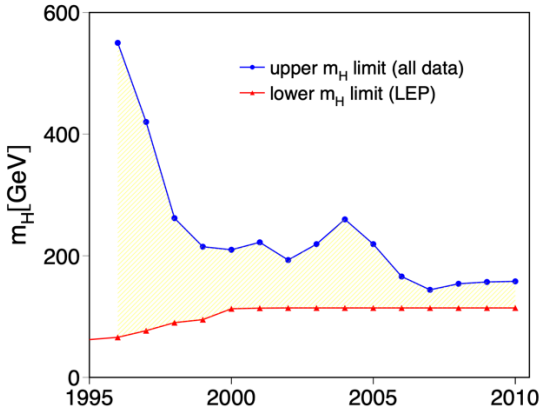


Fig. 18-1: Indication of Higgs mass from LEP [455].

Are the limits of LEP/SLD consistent? Should one be disturbed by the disagreement (Fig. 18-2) between the weak angle values obtained from the A_l spin asymmetry of SLD (based on an outstanding but single measurement of polarization at 0.5% precision) [456], and from the charge asymmetry of LEP $A_{FB}^{0,b}$, largely **dominated by statistics** (Fig. 18-3)? Subsequent LHC measurements also shown in Fig. 18-2, anticipating Chapter 24, would suggest that the situation is healthy.

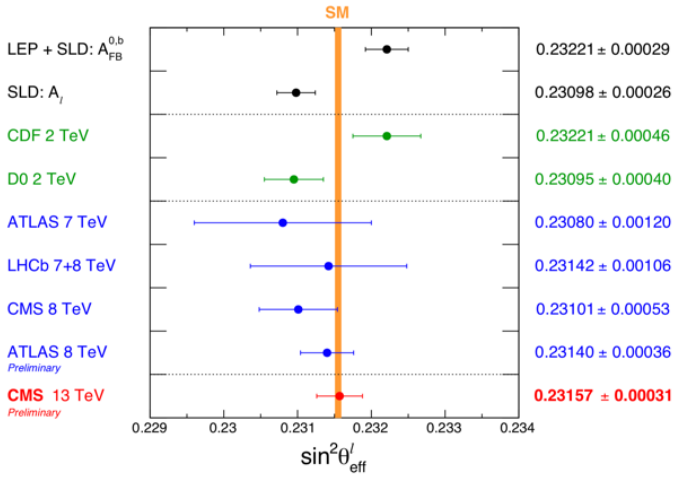


Fig. 18-2: The weak angle [457] (see also Fig. 24-33).

[455] A. Akhundov, *et al.,* The ZFITTER Project. https://arxiv.org/abs/1302.1395
[456] T. Abe for SLD Collaboration, The final SLD results for A_{LR} and A_{lepton} . https://arxiv.org/abs/hep-ex/0102021
[457] J. Bendavid, Recent Standard Model Measurements. EPS-HEP 2025, https://indico.in2p3.fr/event/33627/contributions/153147/attachments/95164/145653/EPSSMExp-Jul9-2025-3.pdf

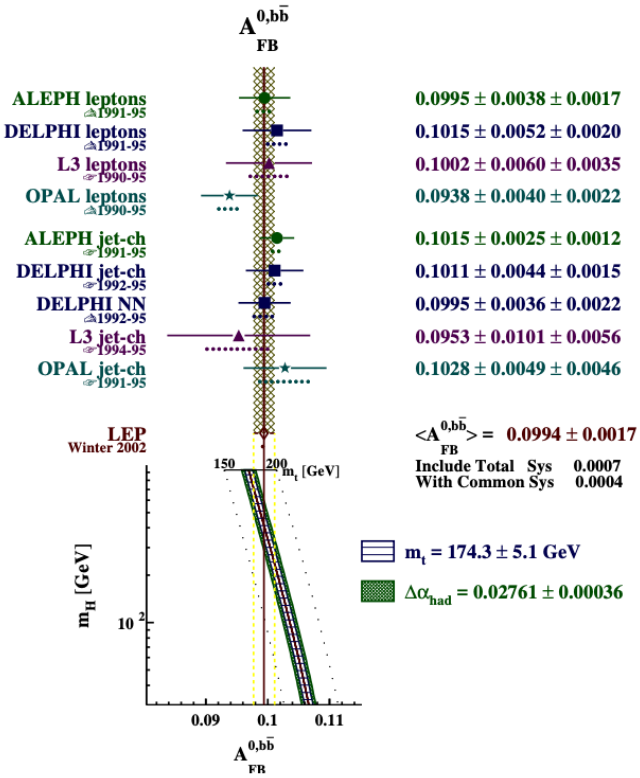


Fig. 18-3: LEP results on $A_{FB}^{0,bb}$, see Ref. [458].

Similar concerns about top-antitop asymmetries have arisen at the Tevatron but have faded away.

The weak angle measurements of LEP and followers (we anticipate on Chapter 24) are in relatively good agreement (Fig. 18-2). The global coherence illustrated in Fig. 18-4 (again tribute to ZFITTER) looks perfect.

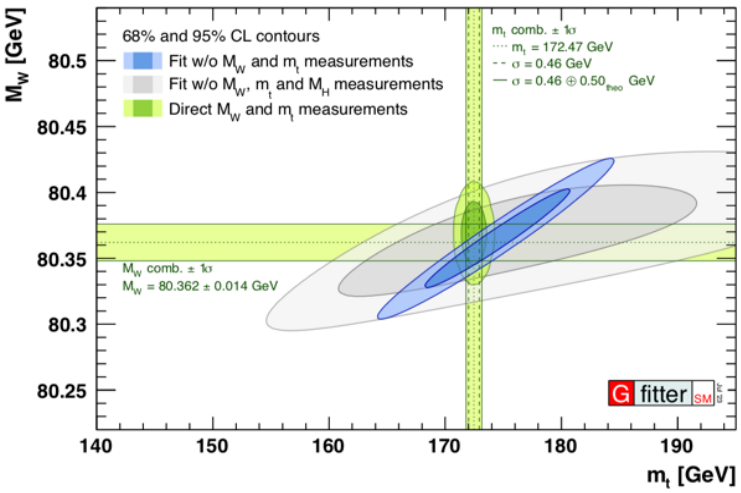


Fig. 18-4: The global coherence [459].

[458] W. Liebig, Precision measurements of the b forward-backward asymmetry at the Z pole from LEP. https://www.sciencedirect.com/science/article/abs/pii/S0920563202019680?via%3Dihub

[459] Y. Fischer *et al.*, The global electroweak fit in the SM and SMEFT. https://inspirehep.net/files/9edfb468cd0fa1c72de3e248ce82db1e

However, we may have still two stones in the shoe. The W mass of CDF (Fig. 18-5), now single outlier. And, maybe, the g–2 of the muon (Chapter 26).

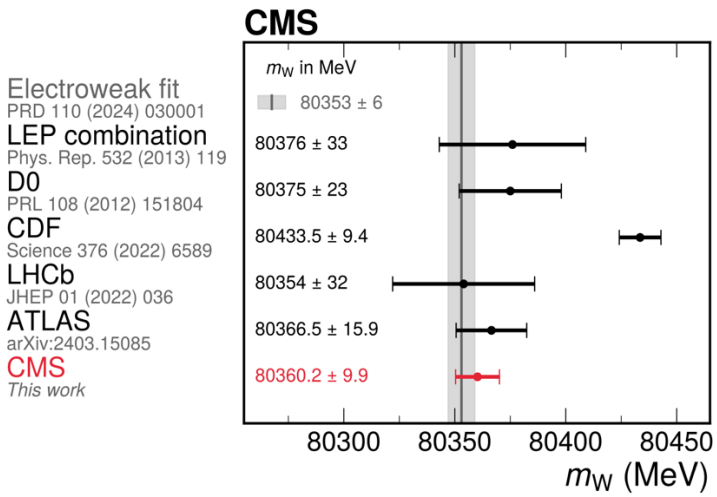


Fig. 18-5: All measured M_W values [460].

Figure 18-6, anticipating LHC results, gives the status of the Higgs mass expected from various measurements.

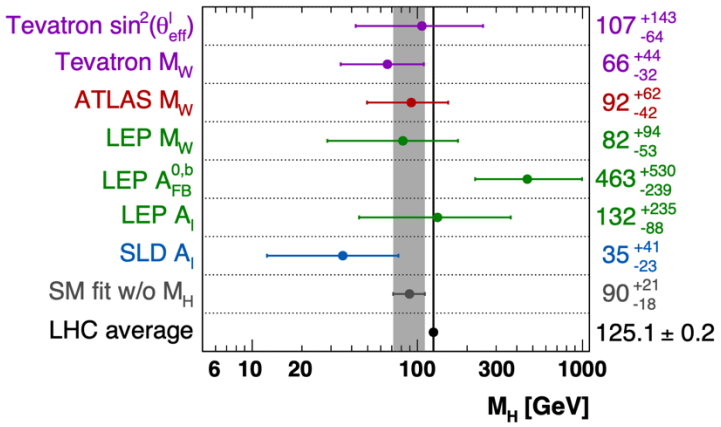


Fig. 18-6: M_H from various sources [461].

18.2 The 97/98 GeV hint at LEP

Let us tell the story of **the 97/98 GeV hint** [462], still often referred to. Figure 18-7 shows it was observed only at $2E_b$ = 189 GeV. Since 189 = 98 + M_Z, one may suspect a problem similar to the 115 GeV one (Fig. 18-7: the 206 GeV box).

[460] CMS Collaboration, High-precision measurement of the W boson mass with the CMS experiment at the LHC. https://arxiv.org/abs/2412.13872

[461] J. Haller *et al.,* Update of the global electroweak fit and constraints on two-Higgs-doublet models. https://arxiv.org/abs/1803.01853

[462] ADLO Collaboration, Search for the standard model Higgs boson at LEP. https://arxiv.org/abs/hep-ex/0107029
P. Janot, The infamous 95 GeV $b\bar{b}$ excess at LEP: Two b or not two b? https://arxiv.org/abs/2407.10948

Indeed, the paper says: "*In the 189 GeV data, an excess at m = 97 GeV has indeed been observed … (see the large negative value of −2lnQ close to the signal+background prediction) which was due mainly to small excesses in ALEPH and OPAL data compatible with $e^+e^- \rightarrow ZZ$, the dominant background in the vicinity of that mass. This excess still has a significance of about two standard deviations when LEP data from all energies are combined, and one cannot exclude a physics interpretation beyond the SM (e.g. MSSM with several neutral Higgs bosons). However, there is no evidence for a systematic effect at threshold in the data collected at the other energies below 206 GeV.*"

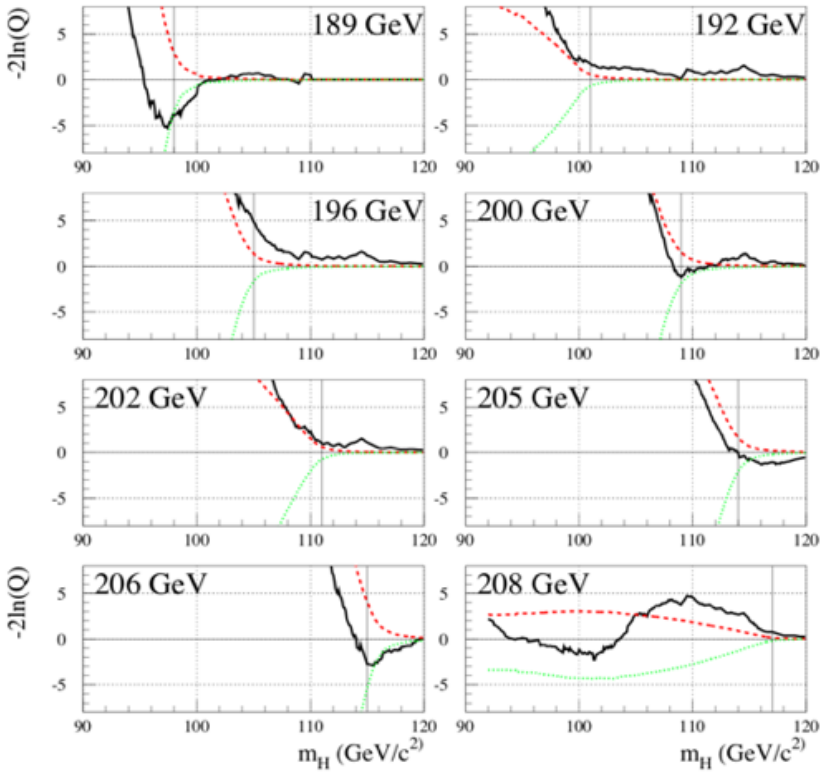


Fig. 18-7: −2lnQ as a function of m_H at each LEP CM energy.

18.3 The LEP/SLC global variables

Given the plethora of variables measured at LEP in the EW sector it was convenient to define a few global ones, capturing the essence of the results. The **epsilon variables** [463] are zero when only tree level SM plus pure QED and pure QCD effects are considered. They are built from 4 observables containing the key points of radiative corrections. **The S, T, U variables** [464] are built from 4 vacuum polarization functions, self-energies of γ, W, Z bosons and γ – Z mixing induced by loop diagrams. They have a clear physical meaning. Figures 18-8 to 18-10 summarize the key features.

[463] G. Altarelli, R. Barbieri and F. Caravaglios, Electroweak Precision Tests: A Concise Review. https://arxiv.org/abs/hep-ph/9712368

[464] M. Peskin and T. Takeuchi, Estimation of Oblique Electroweak Corrections. https://inspirehep.net/files/c82f9c672e89b81716fe429f5e75c85e

Following Ref. [465], let us briefly show how the epsilon global variables allow to present simply the effects of loops in the SM. The situation described here correspond to a period where, besides LEP1/SLD results, a consensus existed on the values of α, α_S and M_t.

One starts from the basic observables $\boldsymbol{m_W/m_Z}, \boldsymbol{\Gamma_\ell}, \boldsymbol{A_{FB}^\ell}$ and $\boldsymbol{\Gamma_b}$.
From these four quantities one can isolate the corresponding dynamically significant corrections

$$\boldsymbol{\Delta r_w}, \boldsymbol{\Delta\varrho}, \boldsymbol{\Delta\kappa} \text{ and } \boldsymbol{\epsilon_b},$$

which contain the small effects one is trying to disentangle and are defined from the previous ones as shown in Fig. 18-8.

$$(1-\frac{m_W^2}{m_Z^2})\frac{m_W^2}{m_Z^2} = \frac{\pi\alpha(m_Z)}{\sqrt{2}G_F m_Z^2(1-\Delta r_W)}$$

$$1-\Delta r = (1-\Delta\alpha)(1-\Delta r_W)$$

$$g_A = -\frac{\sqrt{\rho}}{2} \sim -\frac{1}{2}(1+\frac{\Delta\rho}{2})$$

$$s_0^2 c_0^2 = \frac{\pi\alpha(m_Z)}{\sqrt{2}G_F m_Z^2}$$

$$\frac{g_V}{g_A} = 1-4\sin^2\theta_{eff} = 1-4(1+\Delta k)s_0^2$$

$$g_{bA} = -\frac{1}{2}(1+\frac{\Delta\rho}{2})(1+\epsilon_b)$$

Fig. 18-8: Recap of some basic EW formulae. Masses and $\alpha(M_Z)$ define Δr_W, then Δr. $\rho \equiv \frac{M_W^2}{M_Z^2 cos^2\theta_W}$ is the Veltman parameter [466]. Relations between couplings g_V, g_A, g_{bA} and parameters are given. $c_0^2 = 1 - s_0^2$ ($s_0^2 = 0.231095$ for $m_z = 91.188$ GeV).

These quantities being all dominated by quadratic terms in M_t, one then trades Δr_W and $\Delta\kappa$ for two quantities exempt of such contributions and define the epsilons given in Fig. 18-9 (top), as well as their SM "large" asymptotic contributions (bottom).

The linearized relations between the ε_i, the four basic observables $\boldsymbol{m_W/m_Z}, \boldsymbol{\Gamma_\ell}, \boldsymbol{A_{FB}^\ell}$ and $\boldsymbol{\Gamma_b}$ and their Born approximations are:

$$\frac{m_W^2}{m_Z^2} = \frac{m_W^2}{m_Z^2}\Big|_B (1+1.43\varepsilon_1 - 1.00\varepsilon_2 - 0.86\varepsilon_3)$$

$$\Gamma_l = \Gamma_l|_B(1+1.20\varepsilon_1 - 0.26\varepsilon_3)$$

$$A_{FB}^\mu = A_{FB}^\mu|_B(1+34.72\varepsilon_1 - 45.15\varepsilon_3)$$

$$\Gamma_b = \Gamma_b|_B(1+1.42\varepsilon_1 - 0.54\varepsilon_3 + 2.29\varepsilon_b)$$

Defining $\delta\alpha_S = \frac{\alpha_S(M_Z)-0.118}{\pi}$ and $\delta\alpha = (\alpha(M_Z) - \frac{1}{128.97})/\alpha$, the Born approximations are:

$$\frac{m_W^2}{m_Z^2}|_B = 0.768905(1-0.40\delta\alpha)$$

$$\Gamma_l|_B = 83.563(1-0.19\delta\alpha)\text{MeV}$$

$$A_l^{FB}|_B = 0.01696(1-34\delta\alpha)$$

$$\Gamma_b|_B = 379.8(1+1.0\delta\alpha_s - 0.42\delta\alpha)$$

[465] G. Altarelli, R. Barbieri and F. Caravaglios, The epsilon variables for electroweak precision tests: a reappraisal. *Physics Letters B 349 (1995) 145-154*

[466] K. Gaemers and B. De Wit, M. J. G. Veltman 1931–2021. https://cerncourier.com/a/martinus-j-g-veltman-1931-2021/

$$
\begin{aligned}
\epsilon_1 &= \Delta\rho, && \Delta r_W,\ \Delta\rho,\ \Delta k \text{ and } \epsilon_b \\
\epsilon_2 &= c_0^2\Delta\rho + \frac{s_0^2\Delta r_W}{c_0^2 - s_0^2} - 2s_0^2\Delta k, \\
\epsilon_3 &= c_0^2\Delta\rho + (c_0^2 - s_0^2)\Delta k.
\end{aligned}
$$

$$
\begin{aligned}
\epsilon_1 &= \frac{3G_F m_t^2}{8\pi^2\sqrt{2}} - \frac{3G_F m_W^2}{4\pi^2\sqrt{2}} \tan^2\theta_W \ln\frac{m_H}{m_Z} + ..., \\
\epsilon_2 &= -\frac{G_F m_W^2}{2\pi^2\sqrt{2}} \ln\frac{m_t}{m_Z} + ..., \\
\epsilon_3 &= \frac{G_F m_W^2}{12\pi^2\sqrt{2}} \ln\frac{m_H}{m_Z} - \frac{G_F m_W^2}{6\pi^2\sqrt{2}} \ln\frac{m_t}{m_Z} ...., \\
\epsilon_b &= -\frac{G_F m_t^2}{4\pi^2\sqrt{2}} + ...
\end{aligned}
$$

Fig. 18-9: Details about the global epsilon variables.

As we said, the epsilon variables are defined in such a way that **they are zero in the approximation when only effects from the SM at tree level plus pure QED and pure QCD corrections are taken into account**, a simple version of improved Born approximation independent of m_t and m_H. In fact, the whole m_t and m_H dependence arises from weak loop corrections and therefore is **only contained in the epsilon variables**, extracted from the data without need of specifying m_t and m_H. All improvements, as computations of higher-loop effects, related to vacuum polarization diagrams or the $Z \to b\bar{b}$ vertex, simply affect the theoretical predictions of the ε_i in the SM but **do not invalidate their basic property**.

Values of the **ε** in the SM as functions of m_t and m_H are obtained from ZFITTER and TOPAZ0.

In terms of the **ε**, other precision observables as the total width Γ_T, the R ratio $\frac{\Gamma_h}{\Gamma_l}$, the hadronic cross-section σ_h, $R_{bh} = \frac{\Gamma_b}{\Gamma_h}$, $x = \frac{g_v}{g_a}$ obtained from A_{FB}^{μ} have similar expressions in the SM. Actually, besides the defining quantities, other LEP and SLC data, as well as other sets of high energy or low energy variables, can be used in the epsilon procedure.

Table 18-1 [467] gives the experimental values of the epsilons in the SM from different sets of data.

ϵ 10^3	Only def. quantities	All asymmetries	All High Energy	All Data
ϵ_1 10^3	4.0 ± 1.2	4.3 ± 1.2	4.1 ± 1.2	3.9 ± 1.2
ϵ_2 10^3	-8.3 ± 2.3	-9.1 ± 2.2	-9.3 ± 2.2	-9.4 ± 2.2
ϵ_3 10^3	2.9 ± 1.9	4.3 ± 1.4	4.1 ± 1.4	3.9 ± 1.4
ϵ_b 10^3	-3.2 ± 2.3	-3.3 ± 2.3	-3.9 ± 2.1	-3.9 ± 2.1

Table 18.1: Experimental values of the epsilons in the SM from different sets of data. These values (in 10^{-3} units) are obtained for $\alpha_s(m_Z) = 0.119 \pm 0.003$, $\alpha(m_Z) = 1/128.90 \pm 0.09$, the corresponding uncertainties being included in the quoted errors.

[467] G. Altarelli, R. Barbieri and F. Caravaglios, Electroweak Precision Tests: A Concise Review. https://arxiv.org/abs/hep-ph/9712368

As shown in Fig. 18-10, following Ref. [468], *"there is by now a solid evidence for departures from the "improved Born approximation", defined as including the predictions from the tree level Standard Model plus pure QED and pure QCD corrections only, where all the epsilons vanish. Such evidence comes from ε_1 and ε_3, both measured with an absolute error below 2×10^{-3} and shown to be different from zero at more than the 2σ level for each of them. In this way one has obtained a strong evidence for pure weak radiative corrections, thus fulfilling one of the explicit goals of the precision electroweak tests. LEP and SLC are now measuring the different components of the radiative corrections."*

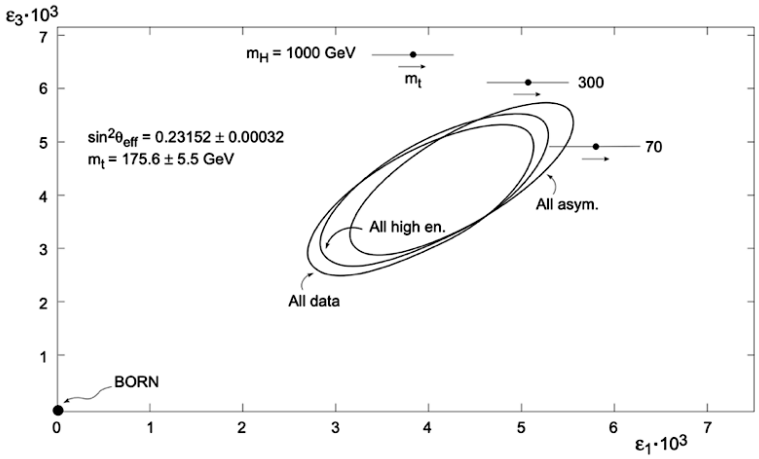


Fig. 18-10: LEP results in epsilon global variables. This is one of the many possible figures, ε_3 versus ε_1.

The use of global variables has a link to the EFT version of LHC physics (Chapter 24).

Finally, Fig. 18-11 deals with the S, T variables, their definition and properties (left) and the LEP/SLC results expressed that way (right).

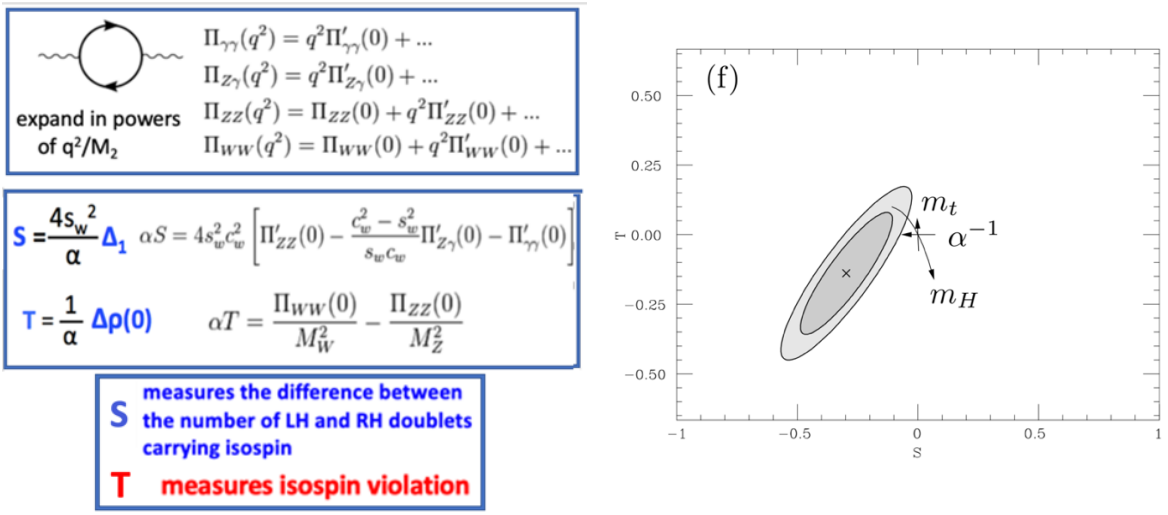


Fig. 18-11: Left: properties of the global variables S, T: The $\prod$ are vacuum polarization functions. Figure built from Ref. [469]. Right: LEP results seen in the S-T plot [470].

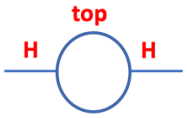
[468] G. Altarelli *et al.*, Electroweak precision tests: a concise review. https://arxiv.org/abs/hep-ph/9712368
[469] T. Takeuchi *et al.,* Precision Tests of Electroweak Physics. https://arxiv.org/abs/hep-ph/9904207
[470] ibid

The numerical results found are: S = −0.30 ± 0.13, T = −0.14 ± 0.15, U = 0.15 ± 0.21, depending on the values of M_t, M_H, and $\alpha^{-1}(M_Z)$ used as input to calculate the SM predictions.

The values of the global variables obtained from LEP and SLD Z–pole data, as well as the ρ parameter value, will be used as precious constraints that any new model of physics beyond the SM must satisfy.

18.4 The LEP paradox

This outcome of LEP results had much weight and led to a lot of brainstorming, but not to any discovery. The paradox [471] is that LEP indicates a heavy top and a light SM Higgs (Fig. 16-4) but gives also very high lower mass values for operators contributing to the precision EW observables. It points therefore to a problem of **hierarchy and naturalness** of the Fermi scale. The problem starts with the top itself, which a priori contributes (quadratically!) to a dramatic increase of M_H^2.



$$\rightarrow \delta M_H^2(\text{top}) \approx G_F M_{\text{top}}^2 \Lambda^2 \approx (0.3\Lambda)^2 \simeq 2\text{TeV}^2$$

This led to a multitude of theories dealing with the hierarchy problem, as shown for amusement in Fig. 18-12 [472].

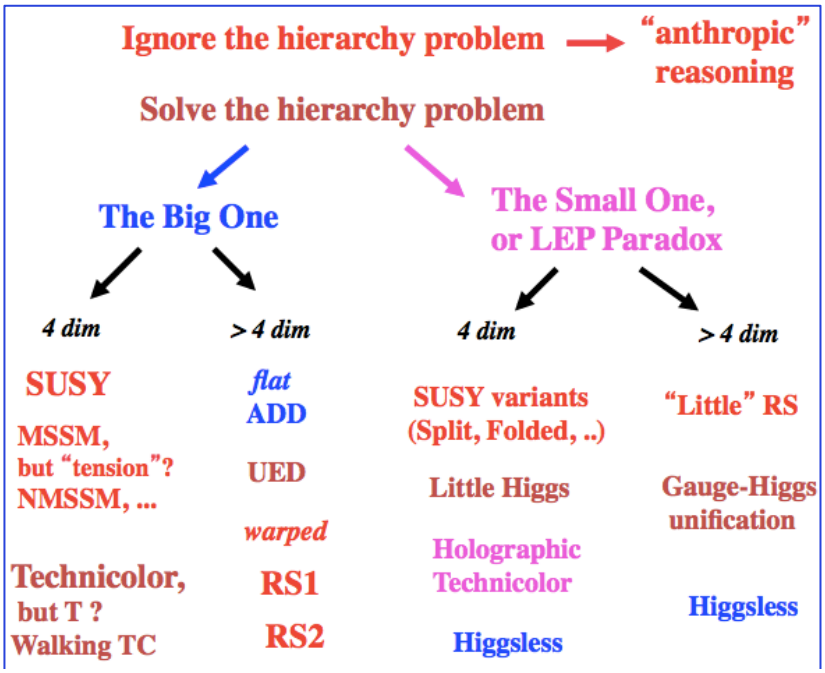


Fig. 18-12: Let hundred flowers blossom. About the hierarchy problem (figure by D. Treille).

[471] R. Barbieri and A. Strumia, The 'LEP paradox'. https://arxiv.org/abs/hep-ph/0007265

[472] D. Treille, Higgs and other searches at LEP. https://indico.cern.ch/event/858488/contributions/3620395/attachments/1953108/3243083/LEP30_Talk_DT.pdf

18.5 Digression on SUSY

Anticipating a bit, the 125 GeV Higgs boson, missed at LEP (Chapter 17) and discovered in 2012 at LHC (Chapter 24), is, as shown in Figs. 17-3 and 17-7, in the mass range as expected since more than 30 years, for the lightest Higgs in the MSSM [473]. It also looks SM-like as expected.

It's fun to recall the numerous predictions of the Higgs mass [474] (Fig. 18-13). One can note that nearly all those which appear in the vicinity of the correct mass were predicted **in the name of the MSSM (little arrows),** which relates its mass at tree level to the EW coupling constants (for the radiative corrections see Ref. [475]).

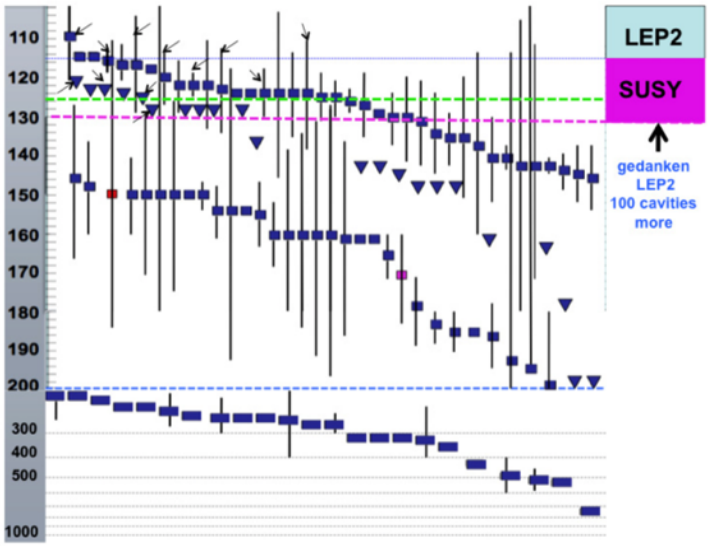


Fig. 18-13: The many predictions of M_H. The mass scale is on the left (log above 200 GeV) in GeV. The spectrum shows just the predictions (squares) or lower limits (triangles) in increasing order of mass with the quoted uncertainty. Plot from D. Treille using the compilation of Ref. [476].

A notable exception to the previous statement is Ref. [477], that we comment at the end of this chapter, although in the years preceding the discovery, given all indications available, it became difficult to speak of a prediction.

---

[473] For an elementary introduction to Supersymmetry (SUSY): Th. Taylor and D. Treille, The Large Electron Positron Collider (LEP): Probing the Standard Model. In Technology meets Research, https://inspirehep.net/files/02de568d4897c555515de27f0b96af4d p. 229

[474] T. Schucker, Higgs mass predictions. https://arxiv.org/abs/0708.3344

[475] Y. Okada, M. Yamaguchi and T. Yanagida, Upper Bound of the Lightest Higgs Boson Mass in the Minimal Supersymmetric Standard Model. *Prog.Theor.Phys. 85 (1991),* https://academic.oup.com/ptp/article/85/1/1/1856061?login=false
H. E. Haber and R. Hempfling, Can the mass of the lightest Higgs boson of the minimal supersymmetric model be larger than m_Z? *PRL. 66 (1991) 1815,* https://journals.aps.org/prl/abstract/10.1103/PhysRevLett.66.1815
J. Ellis, G. Ridolfi and F. Zwirner, Radiative corrections to the masses of supersymmetric Higgs bosons. *Phys.Lett.B 257 (1991) 83,* https://www.sciencedirect.com/science/article/abs/pii/037026939190863L

[476] T. Schucker, Higgs mass predictions. https://arxiv.org/abs/0708.3344

[477] M. Shaposhnikov and C. Wetterich, Asymptotic safety of gravity and the Higgs boson mass. *Phys. Lett. B 683, 196 (2010)*

At the difference of the boson, very light SUSY partners, as gauginos, expected by some physicists at LEP, without strong arguments, did not show up. None has appeared yet at LHC [478]. However, if the LSP is at the TeV scale [479], the LHC exclusions are not valid. Some benchmarks are still considered [480]. As for **fine-tuning**, its definition and meaning are ambiguous [481]: if variables are more correlated than expected, fine-tuning may disappear. More in Chapter 24.

So, paraphrasing Mark Twain, SUSY could say: **"The announcement of my death is very exaggerated".** Let us recall that SUSY was born from very deep mathematical considerations [482]. Concerning its phenomenology, from an early innovative paper [483] to elaborate considerations at LEP time [484] and up to now, a long list of papers appeared, dealing in particular with the various ways of **breaking SUSY.**

For amusement, Fig. 18-14 shows an old attempt to illustrate the complexity of SUSY phenomenology! Up to now *"much ado (already) about nothing (yet)* [485] *"*.

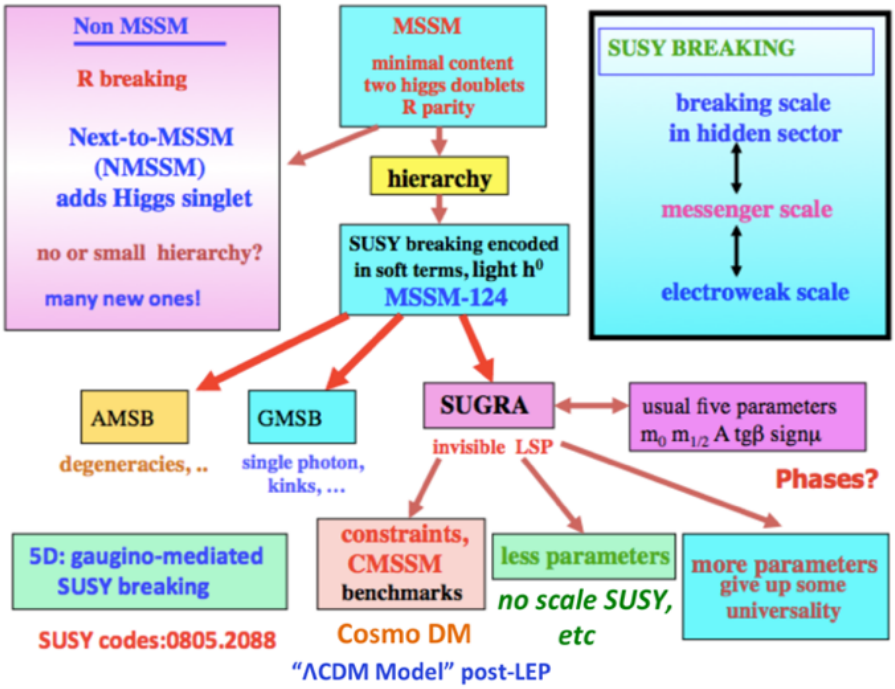


Fig. 18-14: An old attempt, by D. Treille, to grasp the SUSY world.

---

[478] See however M. Chakraborti *et al.,* Consistent Excesses in the Search for $\tilde{\chi}_2^0\tilde{\chi}_1^+$: Wino/bino vs. Higgsino Dark Matter. https://arxiv.org/abs/2403.14759

[479] H. Fukuda *et al.*, How Heavy can Neutralino Dark Matter be? https://arxiv.org/abs/1812.02066

[480] T. Cheng *et al.,* Supersymmetry with a Heavy Lightest Supersymmetric Particle. https://arxiv.org/abs/1407.0888
H. Baer *et al.,* Mini-review: Expectations for supersymmetry from the string landscape. https://arxiv.org/abs/2202.11578
N. Mahmoudi, Low energy SUSY and H boson studies.
https://indico.in2p3.fr/event/29681/contributions/122561/attachments/76683/111282/01-NMahmoudi-V1.pdf

[481] M. van Beekveld *et al.,* The current status of fine-tuning in supersymmetry. https://arxiv.org/abs/1906.10706

[482] See the preamble of J. L. Gervais: https://arxiv.org/abs/hep-th/9911008.pdf

[483] G. Farrar and P. Fayet, Phenomenology of the Production, Decay, and Detection of New Hadronic States Associated with Supersymmetry. https://lib-extopc.kek.jp/preprints/PDF/1978/7805/7805202.pdf

[484] V. Barger and R. J. N. Phillips, Supersymmetry Phenomenology. https://arxiv.org/abs/hep-ph/9306279.pdf
J. F. Gunion *et al.,* The Higgs Hunter guide, Front.Phys. 80 (2000) 1-404,
https://www.taylorfrancis.com/books/mono/10.1201/9780429496448/higgs-hunter-guide-john-gunion
S. P. Martin, A Supersymmetry Primer. https://arxiv.org/abs/hep-ph/9709356

[485] L. Pape and D. Treille, Supersymmetry facing experiment: Much ado (already) about nothing (yet). *Rept.Prog.Phys.* 69 (2006) 2843-3067, https://iopscience.iop.org/article/10.1088/0034-4885/69/11/R01/meta

18.6 A different track?

Let us go back to an interesting prediction of M_h quoted previously [486].

Knowing M_{top}, one could simply require stability of the EW vacuum: however, a heavier Higgs improves stability (see Fig. 24-18 of Chapter 24), thus this simple consideration does not lead to an upper limit for M_h.

A general prediction from **asymptotically safe quantum gravity** [487] is the approximate vanishing of all **quartic scalar couplings** at the UV fixed point beyond the Planck scale. A vanishing Higgs doublet quartic coupling near the Planck scale translates into a **prediction for the ratio between M_H and M_t.** If only the SM particles contribute to the **running of couplings below the Planck mass**, the observed $M_H \sim 125$ GeV results in the prediction for the top quark mass $M_t \sim 171$ GeV, or vice-versa. However, this may be affected by possible physics at an intermediate scale, as RH ν (Chapter 19), whose Yukawa couplings may cancel the issue of vacuum stability (Chapter 24). In 2010, assuming this was not so, a 126 GeV for M_H was announced [488].

A somewhat related and very humorous paper is Ref. [489].

18.7 After LEP

Anticipating on the spectacular results of LHC, and in spite of some precipitation in the LEP-LHC transition, one can only praise the sequence of these large colliders in the same tunnel with much infrastructure in common and understand the desire to reiterate such an operation in a tunnel of much larger circumference.

The Future Circular Collider (FCC) project is such an ambitious programme for the long-term future of CERN, proposing a new circular tunnel with a circumference of about 90 km. This project foresees a two-stage programme: FCC-ee followed by FCC-hh.

The p-p option will gain in energy from both the larger radius and the progress in available magnetic field (Section 10.10). Concerning the e^+e^- option it is clear that the gain in energy will be limited by synchrotron radiation, but modern collider lattices offer a gain in luminosity of more than two orders of magnitude compared to LEP. One must acknowledge the huge and unprecedented amount of studies and R&D which led to the FCC Conceptual Design Report (CDR) [490], aiming at O(100 TeV) p-p collisions, with their vast discovery and measurement potential, and an e^+e^- program covering all physics from the Z to Higgs and $t\bar{t}$ production at maximal luminosity and thus ultimate measurement precision.

The other possible options for future linear e^+e^- colliders are discussed in Section 15.2.

---

[486] M. Shaposhnikov and C. Wetterich, Asymptotic safety of gravity and the Higgs boson mass. *Phys. Lett. B 683:196 (2010),* https://arxiv.org/abs/0912.0208

[487] Asymptotic safety in quantum gravity: https://en.wikipedia.org/wiki/Asymptotic_safety_in_quantum_gravity

[488] M. Shaposhnikov and C. Wetterich, Asymptotic safety of gravity and the Higgs boson mass. *Phys.Lett.B683:196-200,2010*

[489] H. Nielsen *et al,* F(750), We Miss You as a Bound State of 6 Top and 6 Antitop Quarks, Multiple Point Principle. https://arxiv.org/abs/1705.10749

[490] Future Circular Collider Conceptual Design Report. https://fcc-cdr.web.cern.ch/

19. About neutrinos

Thirty years elapsed between Wolfgang Pauli's **"neutron" hypothesis** of 1930 [491], a new particle needed by energy conservation to explain the continuous energy spectrum of electrons in β-decays, and the observation of the first (anti)neutrino-induced interaction (Clyde Cowan and Frederick Reines, 1956 [492], Frederick Reines 1995 Nobel Prize, Clyde Cowan died in 1974).

In 1930, only electron, proton and photon were known. But in 1932 James Chadwick's neutron and Carl Anderson's positron were added. Enrico Fermi called **neutrino (ν)** Pauli's "neutron".

At the Solvay conference 1933, W. Pauli presented his idea the first time in public. Using this information, Fermi formulated a **quantum theory of β decay** with the e-ν pair acting as a field coupled to the charge-changing p-n current. Parity conservation was tacitly assumed. Two decades later came the V-A theory (1957).

A fundamental question was, and still is: **are ν's their own antiparticles**? If so, they are called **Majorana neutrinos, otherwise Dirac neutrinos**. We will come back to this major problem in Section 32.1.

In a series of experiments more and more stringent upper limits on the neutrino mass were derived from the **Fermi–Kurie plot** [493].

When parity violation was found, weak interaction theory was formulated as $H_{int} = \frac{1}{\sqrt{2}} G_F J^{\mu} J_{\mu}^{\dagger}$.
The weak current consists of a vector and an axial vector contribution and G_F is the universal weak coupling. This theory described all known low energy weak phenomena. As understood later, it was an **effective field theory** (Chapter 24), used before inventing the term and discovering the W.

Up to then, nuclear β-decays were the only possibility to study weak interactions. The newly discovered strange mesons and the muon decay $\mu^- \rightarrow e^- \nu_\mu \bar{\nu}_e$ offered new possibilities.

19.1 Accelerator neutrino physics

A very interesting old story is the **race for 2 neutrinos**, told in particular by Dieter Haidt [494] and showing (Table 19-1) how CERN has missed the discovery, which was made at Brookhaven in 1962.

Regarding the neutrino interaction, the main question concerned the existence of the **Intermediate Vector Boson W**. Possible candidates appeared in BC and spark chamber experiments. An upper limit of a few GeV for the W, if it existed, was published. The search continued by looking for a deviation from linearity in the total neutrino cross section, indicating a propagator effect, as illustrated in Fig. 19-1(a) and (b). The existence of the W was strongly suspected, but at that time its high mass was not anticipated.

Then came the events previously discussed: discovery of **Neutral Currents** (Chapter 9), development of the **Standard Model** (Chapter 7), discovery of the **Electroweak Bosons** (Chapter 12). It is worth following the progress in testing **quantum corrections.** Figure 9-18 summarizes the impact of all NC measurements at low E and illustrates the role of LEP/SLC.

---

[491] W. Pauli's letter of 4th of December 1930. https://www.pp.rhul.ac.uk/~ptd/TEACHING/PH2510/pauli-letter.html
[492] Cowan–Reines neutrino experiment: https://en.wikipedia.org/wiki/Cowan–Reines_neutrino_experiment
C. Sutton, Ghosts in the Machine. https://cds.cern.ch/record/2232603/files/vol56-issue6-p017-e.pdf
[493] Beta decay: https://en.wikipedia.org/wiki/Beta_decay
[494] D. Haidt, The Neutrino's 50th Birthday. https://www.desy.de/~haidt/nove06.pdf ,
F. W. Stecker, Neutrino Physics and Astrophysics Overview. https://arxiv.org/abs/2301.02935

Early 1960	CERN initiates feasibility study : ν flux and shielding (Krienen, Steinberger, Salmeron) bubble chambers (EP and NPA) and counter-cloud chamber (Faissner)
May 1960	SPC: very promising
Summer 1960	AGS at BNL completed : Lederman, Schwartz and Gaillard propose 10 t spark chamber
November 1960	CERN decides to carry out ν experiment in 2 stages: (#1) quick 2-3 weeks run in June 1961 with 2 bubble chambers and counter cloud chamber, (#2) long term program
April 1961	CERN Seminar : T.D.Lee's lecture on neutrino questions
May 1961	Alarm : v.Dardel measures secondary π flux and concludes that ν flux was overestimated by factor 10
June 1962	BNL finds two ν species

Table 19-1: The 2-neutrino story as told by D. Haidt.

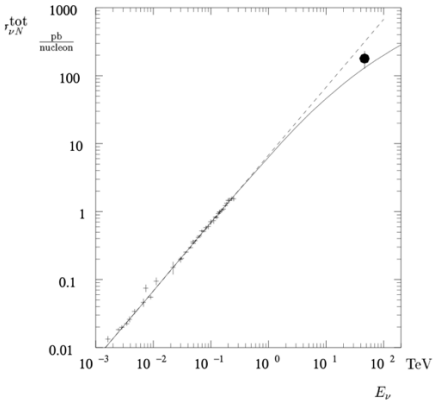


Fig. 19-1(a): The total ν cross-section: Data until 1993 [495].

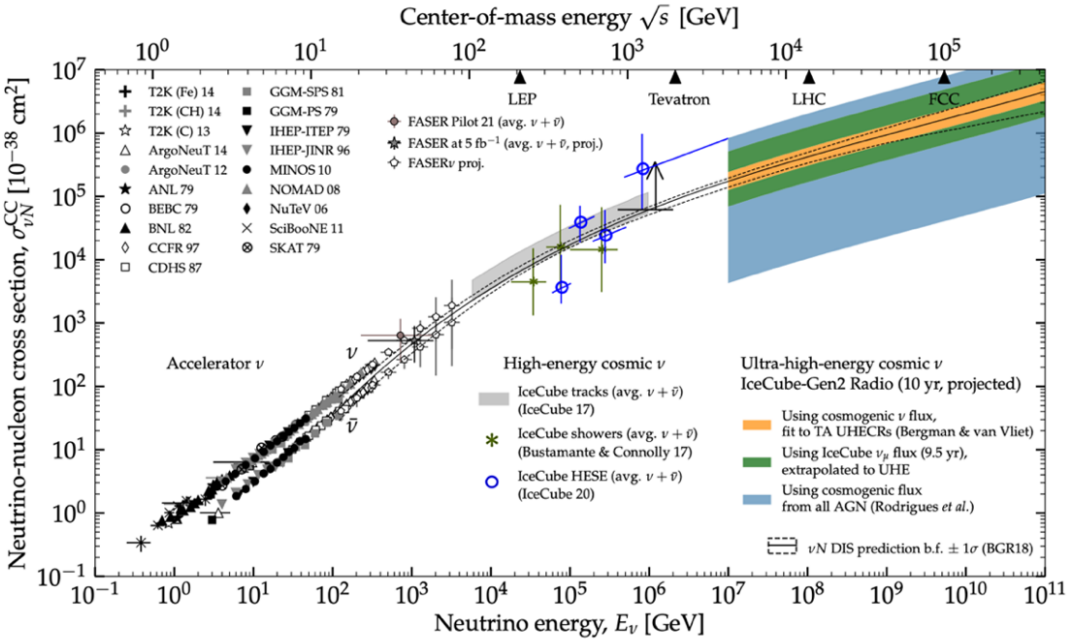


Fig. 19-1(b): Overall data of νN CC cross section measurements [496].

[495] ibid, The cross section of the purely weak process $e^+ + p \rightarrow \nu_e$ + anything, if interpreted as inverse ν fixed target experiment corresponding to a projectile energy of O (50 TeV), could be compared with the ν data and manifested the W propagator effect.

[496] V. B. Valera *et al.,* Comprehensive Measurement Forecasts of the EeV Neutrino-Nucleon Cross Section with Cosmic Neutrinos at IceCube-Gen2. https://arxiv.org/abs/2307.11050

See also V. B. Valera *et al.,* The ultra-high-energy neutrino-nucleon cross section: measurement forecasts for an era of cosmic EeV-neutrino discovery. https://arxiv.org/abs/2204.04237

C. Hill, EW Moriond 2025, Examining the High-Energy Neutrino Cross Section with the IceCube Neutrino Observatory. https://indico.in2p3.fr/event/35965/contributions/152528/attachments/91531/139512/6_CHill-v1.pdf

19.2 The number of neutrinos

After the discovery of the τ lepton, study of $e^+e^- \rightarrow \tau^+\tau^-$ showed that the τ belongs to an iso-doublet, hence inferring the existence of the ν_τ. In 2000 the DONUT Collaboration reported its first observation [497].

Before LEP, it was thus known that the number of families with a light neutrino was at least 3, but more was not excluded: $N_\nu \leq 4$ from astrophysics, < 5.5 from W and Z, quoted in the late 1980's.

LEP1 quickly answered the question, giving, from the Z resonance, $N_\nu = 2.9841 \pm 0.0083$ (Fig. 16-2 and Fig. 19-2), assuming light neutrinos (< 40 GeV). This measurement used the one of a cross section and therefore implied an excellent **absolute normalization.** Its precision is the result of a good collaboration/competition between theory and experiment, concerning respectively the estimate and the measurement of the Bhabha scattering, process used for the normalization (Fig. 19-3), the former involving the calculation of higher order diagrams, the latter a gradual increase in the accuracy of the luminometers [498].

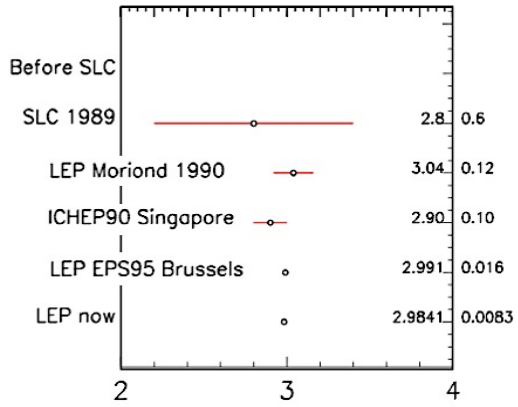


Fig. 19-2: The number of neutrinos [499].

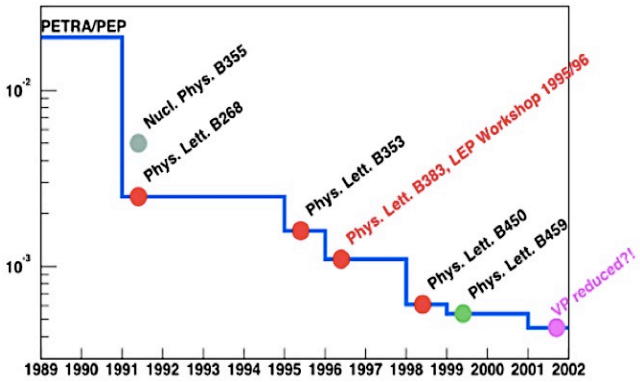


Fig. 19-3: Evolution of the precision of the luminosity measurement.

The number found was slightly less than 3 and pleased Cecilia Jarlskog, a major actor of ν physics [500], since she had deduced that the existence of other sterile neutrinos would penalize the 3 active ones. But a recent (2019) correction of the LEP number [501] gave 2.9963 ± 0.0074, cancelling all discrepancy.

Measuring radiative return to the Z (through single gamma events) gave $N_\nu = 3.00 \pm 0.08$, not competitive with the LEP method, but which could be quite interesting in a future Giga or Tera-Z factory [502].

---

[497] K. Kodama *et al.*, A first measurement of the interaction cross section of the tau neutrino. https://arxiv.org/abs/0711.0728.pdf

[498] S. Jadach, Theoretical calculations for LEP luminosity measurement. http://sfb-tr9.ttp.kit.edu/veranstaltungen/bhabha-talks/jadach.pdf

[499] W. Venus, A LEP Summary. https://inspirehep.net/files/64a04e13d6f5ec34d5f27e669cd45c1e

[500] C. Jarlskog, co-recipient of the EPS High Energy and Particle Physics Prize: https://cerncourier.com/a/eps-high-energy-and-particle-physics-awards-2023/

[501] S. Jadach and P. Janot, Improved Bhabha cross section at LEP and the number of light neutrino species. *Physics Letters B 803 (2020) 135319,* https://arxiv.org/abs/1912.02067 , Hommage to S. Jadach.

[502] A. Freitas *et al.,* Theoretical uncertainties for electroweak and Higgs-boson precision measurements at FCC-ee. https://arxiv.org/abs/1906.05379

19.3 The advent of neutrino astrophysics

It started with **solar neutrinos**, pioneered by Raymond Davis, relying on important theoretical work on energy production of stars and calculation of the solar ν-flux.

The chlorine experiment ($\nu_e + {}^{37}Cl \rightarrow e^- + {}^{37}Ar$) in the Homestake mine [503] in 1968 gave for the flux $\Phi(meas)/\Phi(calc) \approx 0.3 \neq 1$. This was the start of the **solar neutrino problem**. Was it a problem in measurement, in the solar processes or in particle physics?

The chlorine experiment is only sensitive to a very small high energy fraction of the solar neutrino flux. But later GALLEX/GNO and SAGE, sensitive to the pp cycle of the sun, confirmed the deficit (see Section 19.10 and references there).

After the discovery of two species of neutrinos, the possibility of neutrino mixing was systematically considered. However, K^0 mixing had already inspired Bruno Pontecorvo (1957–1958) to come up with the idea of **neutrino oscillations** [504].

The mass eigenstates and the weak eigenstates are related by a unitary mixing matrix U analogous to quark mixing. Not massless, neutrinos are evolving superpositions of at least **three mass eigenstates with distinct energies**. Neutrinos being always ultra-relativistic, the energies of the mass eigenstates differ only by tiny mass contributions of $m^2/2E$.

As the mass eigenstates propagate, **phase differences** develop between them proportional to the squared-mass splitting Δm^2 (Table 19-2).

Propagation of mass eigenstates $|\nu_j\rangle$ can be described by plane wave solutions as

$$|\nu_j(t)\rangle = e^{-i\left(E_j t - \vec{p}_j \cdot \vec{x}\right)} |\nu_j(0)\rangle \quad \text{with} \quad E_j = \sqrt{p_j^2 + m_j^2} \simeq p_j + \frac{m_j^2}{2p_j} \approx p_j + \frac{m_j^2}{2E}$$

Using $t \approx L$, where L is the distance traveled and dropping the phase factors, the wavefunction becomes

$$|\nu_j(L)\rangle = e^{-i\left(\frac{m_j^2 L}{2E}\right)} |\nu_j(0)\rangle$$

Table 19-2: Propagation of mass eigenstates.

The oscillation length λ from mass eigenstates 1 to j is defined as $\lambda = 4\pi \frac{E}{\Delta m_{j1}^2} = 2.5\ km \frac{E}{GeV} \frac{eV^2}{\Delta m_{j1}^2}$.

Thus, the sensitivity to Δm_{j1} depends on L/E, where L is the flight length. For ν oscillations one looks therefore for ranges from a few meters to the Earth diameter.

In the early eighties the story told in Chapter 9 about the weak angle motivated searches for **proton decay.** Several underground experiments were built: NUSEX, IMB, Kamioka, Frejus, Soudan, HPW (Section 32.4.1).

[503] B. Cleveland *et al.,* Results from the Homestake Solar Neutrino Observatory. https://inspirehep.net/files/27495c4d852a1a2f261471cb660137bd

[504] S. M. Bilenky, B. Pontecorvo and Neutrino Oscillations. https://inspirehep.net/files/6a148a1b89a4bf56f07c3d9cffdbb95d

The Japanese group at Kamioka pioneered a new technique and built a water Cherenkov detector. In 1998 the **Kamioka/Superkamioka** group was able to claim **evidence of neutrino oscillations** [505], for which the observation of the zenith angle distribution of the atmospheric ν_μ fluxes [506] gave a compelling argument (Fig. 19-4).

In 2001 came the results from the **Sudbury Neutrino Observatory** experiment SNO [507] and their combination with SuperKamiokande. SNO was designed to measure three processes, charged current (**CC**), elastic scattering on e^- (**ES**) and neutral current (**NC**) processes:

$$\text{CC: } \nu_e + d \rightarrow e^- + p + p \qquad \text{ES: } \nu + e^- \rightarrow \nu + e^- \qquad \text{NC: } \nu + d \rightarrow \nu + p + n$$

$$\text{with} \qquad \Phi_{CC} = \Phi(\nu_e) \qquad \Phi_{ES} = \Phi(\nu_e) + 0.1559\,\Phi(\nu_{\mu\tau}) \qquad \Phi_{NC} = \Phi(\nu_e) + \Phi(\nu_{\mu\tau})\,.$$

The factor of 0.1559 being the ratio of the ES cross sections for $\nu_{\mu\tau}$ and ν_e above T_{eff} = 5.0 MeV.

Figure 19-5 illustrates the results. It gives the flux of ^{8}B solar neutrinos which are of μ or τ flavour versus the flux of electron neutrinos deduced from the three neutrino reactions occurring in SNO.

This shows the crucial role of the neutral current contribution which enables to disentangle the ν_e component from the other contributions. An active oscillation component is established in agreement with the Standard Solar Model. The solar neutrino problem is solved.

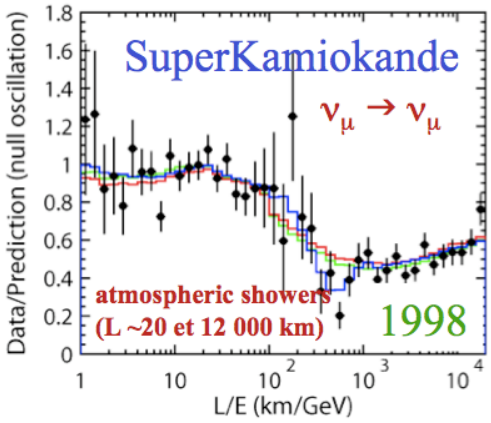


Fig. 19-4: Zenith angle distribution of the atmospheric ν_μ.

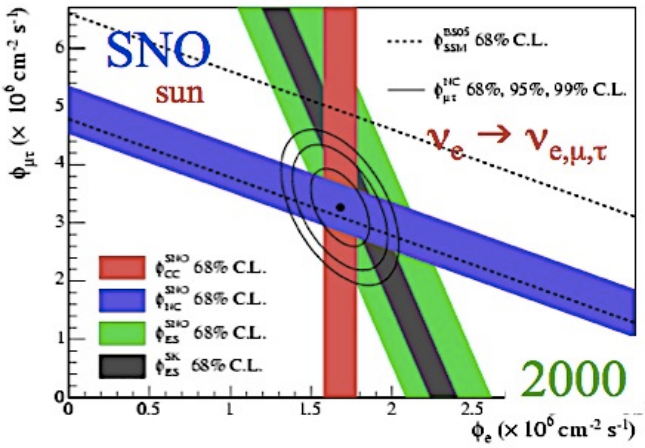


Fig. 19-5: Results from SNO.

19.4 Present status of oscillations

Neutrino oscillations [508] tell that leptons mix, as quarks do. It implies that ν have non-vanishing masses. At least one new particle species exists that the SM does not account for correctly.

None of these oscillations were within the scope of previous accelerator research, such as NOMAD's. This changed when long baseline experiments like Minos and T2K were implemented.

Since then the activity consisted of measuring the **PMNS matrix** [509], (Fig. 19-6, see values later) with major contributions made by SNO (2000–2004), Kamland, Daya Bay (2012), T2K, etc.

---

[505] Y. Fukuda *et al.,* Evidence for oscillation of atmospheric neutrinos. https://arxiv.org/abs/hep-ex/9807003.pdf

[506] Neutrinos produced by cosmic rays hitting the Earth atmosphere at about 20 km and having an energy above 100 MeV.

[507] A. Bellerive *et al.,* The Sudbury Neutrino Observatory. https://arxiv.org/abs/1602.02469

[508] M. S. Athar *et al.*, Status and Perspectives of Neutrino Physics. https://arxiv.org/abs/2111.07586

[509] J. Bernabeu, On the history of the PMNS Matrix... with today's perspective. https://arxiv.org/abs/1312.7451

Figure 19-6 summarizes the current situation and retains its mystery, especially compared to its equivalent for quarks. Rather, it suggests that a non-abelian discrete symmetry is at work [510].

Neutrino oscillations were observed because mixing angles are large and mass-squared differences are small. This is theoretically a surprise, since the charged leptons and the quarks have very large mass differences, while quarks mix with small to tiny angles. The lepton mixing pattern is now clear, with one close-to-maximal, one large, one small mixing angle. But a lot of work remains ahead.

Figure 19-7 gives the current information concerning the mass of the ν's, according to their hierarchy, normal ordering (NO) or inverted ordering (IO), depending on the sign of Δm^2_{31}. The tapers show the uncertainty due to CP violation.

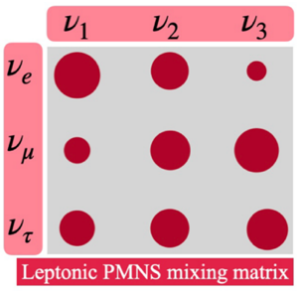


Fig. 19-6: Relative magnitude of the PMNS matrix elements.

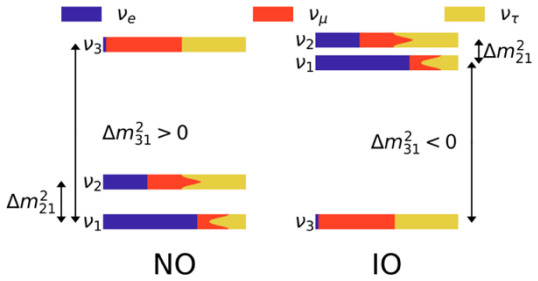


Fig. 19-7: Possible ordering of the neutrino mass spectrum [511].

Tests of the absolute neutrino mass scale and the nature of the ν mass are currently being pursued by three avenues [512]: **neutrinoless double beta decay** experiments (Fig. 19-8, see also Section 32.1), **kinematic measurements** (Fig. 19-9) [513] and **cosmological measurements** (Fig. 19-10) [514]. These approaches are complementary in the sense of testing different combinations of neutrino mass eigenstates depending on the parameter space they can access.

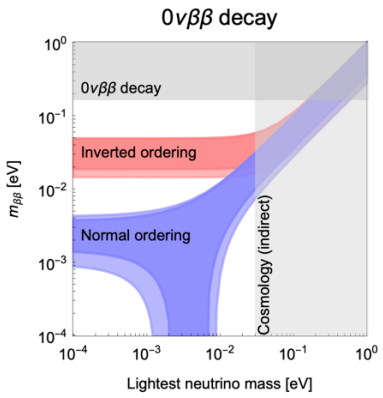


Fig. 19-8: $m_{\beta\beta}$ versus lightest ν mass from 0νββ.

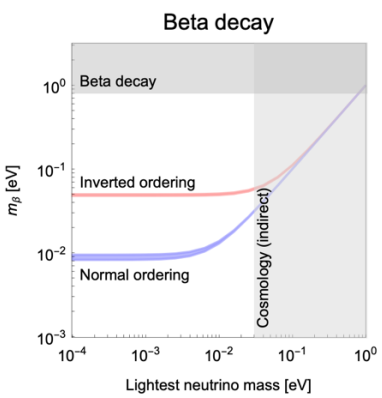


Fig. 19-9: m_β versus lightest ν mass from β decay.

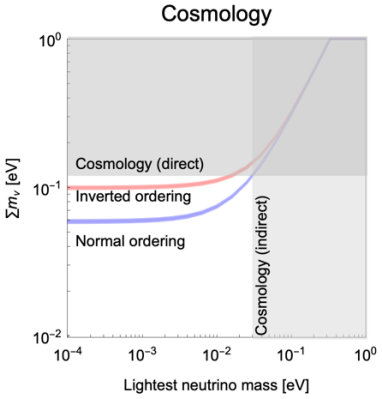


Fig. 19-10: $\sum m_\nu$ versus lightest ν mass from cosmology.

[510] P. F. Harrison *et al.*, Tri-Bimaximal Mixing and the Neutrino Oscillation Data. *Phys.Lett.B530:167,2002* ,
G. Altarelli and F. Feruglio, Discrete Flavour Symmetries and Models of Neutrino Mixing. https://arxiv.org/abs/1002.0211
[511] P. Martinez-Miravé *et al.*, Neutrino Physics. https://pos.sissa.it/406/321/pdf
[512] M. Sajjad Athar *et al.*, Status and Perspectives of Neutrino Physics. https://arxiv.org/abs/2111.07586
[513] M. Rayner, Tuning in to neutrinos. https://cerncourier.com/a/tuning-in-to-neutrinos/
[514] M. Archidiacono *et al.,* What will it take to measure individual neutrino mass states using cosmology? https://arxiv.org/abs/2003.03354
S. Gariazzo, Neutrino mass in cosmology. https://arxiv.org/abs/2401.11976

One may ask whether the lightest mass eigenstate can still be zero, whether upper bounds or lower ones on its value have been proposed. Reference [515] includes a set of possible answers.

The KATRIN experiment [516] presently gives $m_\nu < 0.3$ eV (90% CL). We will come back to $0\nu\beta\beta$ decay in Section 32.1.

19.5 Present activities

The remaining open problems are well known: ν mass hierarchy? CP violation? Long baseline experiments should provide some answers. Nature of the neutrino, Dirac or Majorana, the key being the search for ν-less double β-decay, existence or not of sterile ν in the domain eV, keV, GeV, etc., and their possible roles? With so many crucial questions, ν physics will certainly occupy us for a long time.

The excellent Fig. 19-11 [517] summarizes all ν physics activities related to machines and reactors.

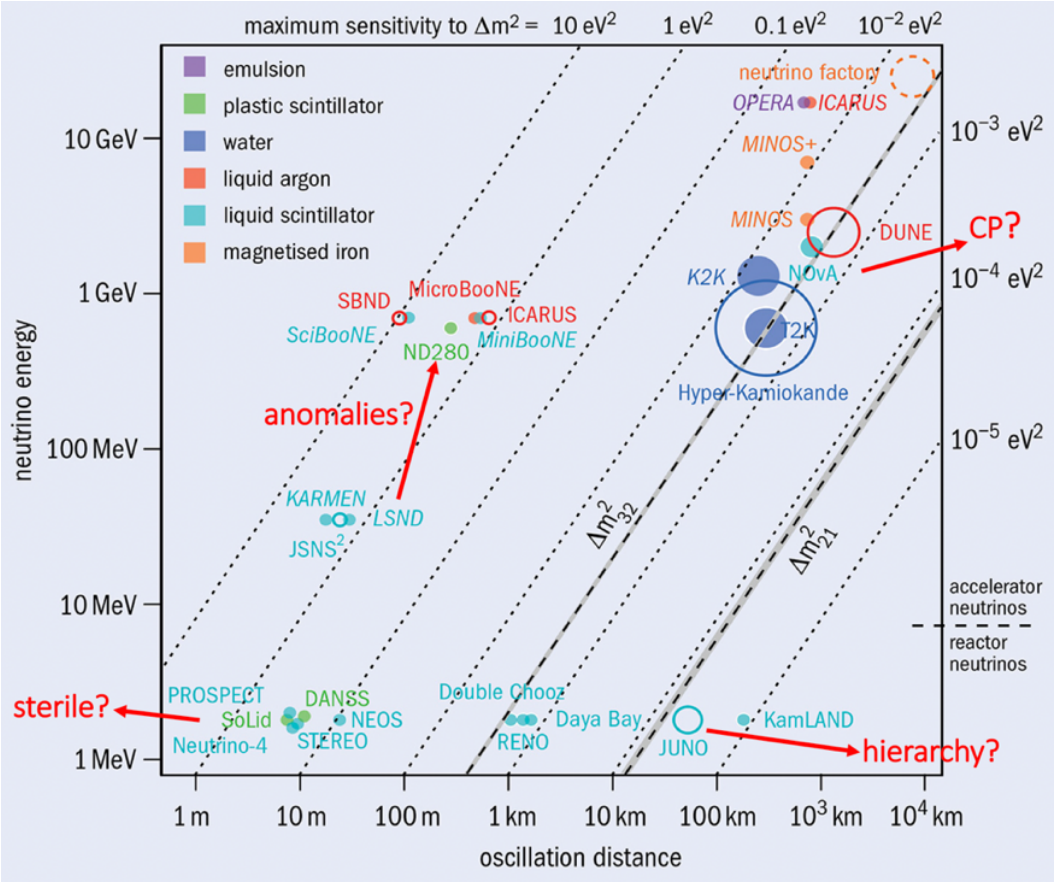


Fig. 19-11: All ν physics activities related to machines and reactors.

[515] GAMBIT Cosmology Workgroup. Strengthening the bound on the mass of the lightest neutrino with terrestrial and cosmological experiments. https://arxiv.org/abs/2009.03287
S. Zhou, The smallest neutrino mass revisited. https://arxiv.org/abs/2104.09050
S. Davidson *et al.,* The smallest neutrino mass. *Phys.Lett.B646:100-104,2007*
[516] M. Aker *et al.,* KATRIN: Status and Prospects for the Neutrino Mass and Beyond. https://arxiv.org/abs/2203.08059
S. Mertens, $0\nu\beta\beta$ and direct neutrino mass measurements. ICHEP 2024, https://indico.cern.ch/event/1291157/contributions/5958324/attachments/2901872/5089559/Mertens_ICHEP_final.pdf
[517] M. Rayner, Tuning in to neutrinos. https://cerncourier.com/a/tuning-in-to-neutrinos/

A first group of experiments, sensitive to the large mass splitting Δm_{23}, include both current (such as T2K and NOvA, and their joint analysis) and future (such as DUNE, HyperK) accelerator-neutrino experiments with long baselines and high energies, as well as a trio of reactor-neutrino experiments (Daya Bay, RENO and Double Chooz) with a baseline of about a km, operating just above the threshold for inverse beta decay.

A second group is a pair of long-baseline reactor-neutrino experiments (KamLAND and JUNO), which, as experiments with solar neutrinos, have sensitivity to the smaller squared-mass splitting Δm^2_{21}.

A third group includes short-baseline accelerator-neutrino experiments and very-short-baseline reactor neutrino experiments looking for hints of a **"sterile" neutrino**, split from the others by a squared-mass splitting of the order of 1 eV^2. The results are negative up to now [518].

The OPERA experiment (2008–2012), fed by the CNGS ν_μ beam (Chapter 10), observed ten ν_τ candidates and confirmed the discovery of ν_τ appearance with a significance level of 6.1 σ [519].

A spike in the number of entries in the INSPIRE data base on OPERA (Fig. 19-12) recalls a "famous incident" [520].

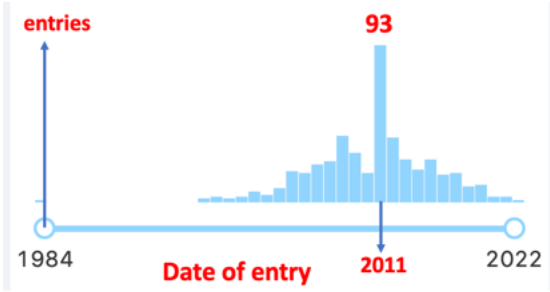


Fig. 19-12: A "famous incident" resulting in many citations of the OPERA publication. Figure by D. Treille.

Leptonic CP violation (δ_{CP}) [521], relevant for the unknown origin of the matter–antimatter asymmetry in the Universe, can only be observed if all three of the angles in the PMNS matrix are non-zero. From atmospheric and solar oscillations, this was clear for two of them. Concerning the third, which leads to a coupling between ν_3 and ν_e, after hints from T2K (appearance of ν_e from ν_μ) and Double Chooz (deficit of anti-ν_e), Daya Bay and RENO showed with 5σ evidence that it was non-zero.

To the content of Fig. 19-11 one should add other activities:

- Getting best physics out of DUNE and HyperK requires ancillary measurements: precise knowledge of hadron production in the target, measurement of **neutrino cross-sections** and neutrino energy response functions for all species (remembering that electron neutrinos are only about 1% of the beams). This requires exploiting near detectors of the long baseline experiments and using dedicated facilities, as HARP, NA61/SHINE.
- A systematic search for **sterile (or RH) neutrinos** which we describe in Section 19.6. Such objects can lie from eV to 10^{10} GeV. Between 100 MeV and a few GeV they can be produced in the decays

[518] B. Dasgupta and J. Kopp, Sterile neutrinos. https://arxiv.org/abs/2106.05913
[519] OPERA concludes on tau appearance. https://cerncourier.com/a/opera-concludes-on-tau-appearance/
OPERA Collaboration, Erratum: Final Results of the OPERA Experiment on ν_τ Appearance in the CNGS Neutrino Beam , Phys. Rev. Lett. 120, 211801 (2018), *Phys. Rev. Lett. 121, 139901 (2018)*
[520] The OPERA Experiment and the Value of High-Profile Scientific Blunders.
https://thereader.mitpress.mit.edu/when-science-fails-opera-neutrinos/
[521] Hyper-Kamiokande Design Report, https://arxiv.org/abs/1805.04163

of heavy flavours. One needs to combine high intensity production and large decay volume. Besides reactor experiments, quoted above, dedicated beam-dump experiments, opportunities at LHC of experiments in the forward region of its interaction regions and near detectors of the long baseline experiments offer many possibilities.

Figure 19-13 shows CP violation effect on the neutrino/antineutrino probability of detection for a set of parameters typical of those of HyperK. Figure 19-14 gives the expected significance of exclusion of sin $\delta_{CP} = 0$ in case of normal hierarchy.

The present indication on CP from the two main present players (NOvA, Off Axis, Fermilab to Ash River, and T2K, slightly off axis, J-PARC to SuperK) combined results is shown in Fig. 19-15 [522]. The two experiments prefer different regions of δ_{CP} in the NO case and strongly favour CP violation in the IO scenario. Present hints are not sufficient to conclude on CP violation. And with more statistics from NOvA the situation evolves rapidly [523].

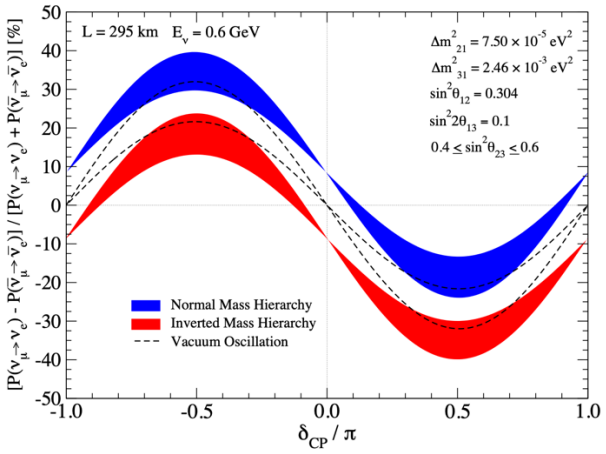


Fig. 19-13: Effect on the neutrino/antineutrino rate difference [524].

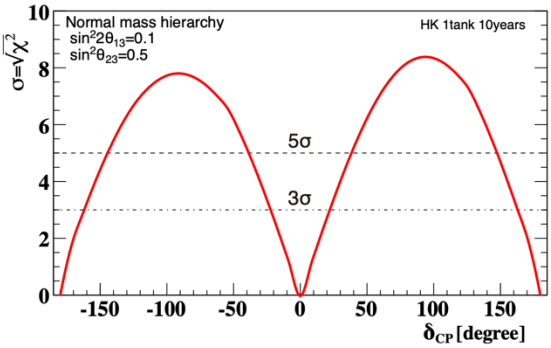


Fig. 19-14: Expected significance of exclusion of sin $\delta_{CP} = 0$ [525].

[522] J. P. Ochoa-Ricoux, Neutrino Oscillation and CP Violation: Status and Prospects. https://indico.cern.ch/event/1291157/contributions/5958323/attachments/2901877/5091041/NuOsc_Ochoa_ICHEP2024.pdf
[523] M. Maltoni, Neutrino masses and mixing. https://indico.cern.ch/event/1335188/contributions/6137452/attachments/2952939/5194256/seminar-maltoni.pdf
[524] K. Abe *et al.,* The Hyper-Kamiokande Proto-Collaboration, Hyper-Kamiokande Design Report. https://arxiv.org/abs/1805.04163
[525] ibid

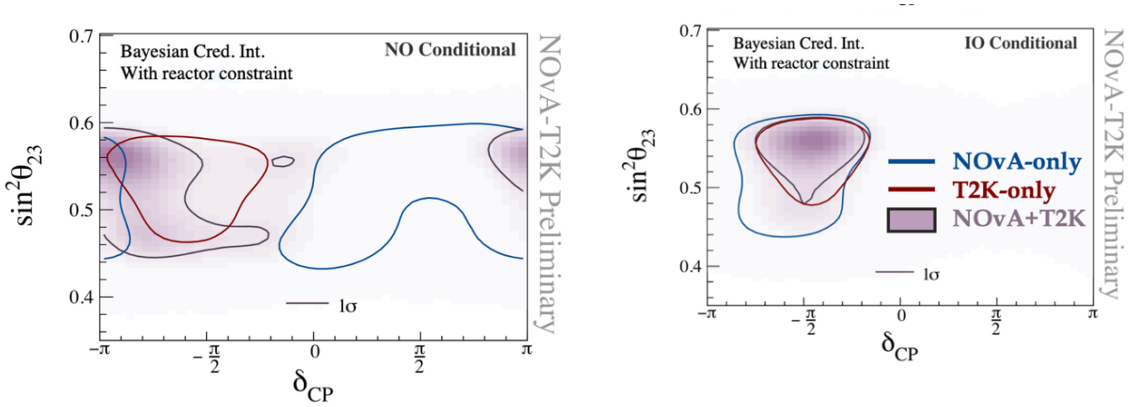


Fig. 19-15: NOVA and T2K results [526]: Left: mild preference for Inverted Ordering but influenced by θ_{13} constraint. Right: CP-conserving points are outside 3σ intervals if ordering is inverted.

19.6 Heavy Neutral Leptons

The very small masses of active neutrinos and their peculiar features, first sign of physics beyond the SM, call for an explanation, which necessarily requires some **extension of the SM** [527].

A popular one is to consider **Heavy Neutral Leptons (HNLs)** and more precisely **right-handed (RH) neutrino partners ν_R** to the SM LH active neutrinos [528].

HNLs, interacting through weak interaction via their **mixing with ordinary neutrinos**, are much studied as one of the portals to hidden sectors ("neutrino portal"). Non-minimal HNLs, which have additional interactions besides mixing, are also proposed [529].

The physical motivation for considering such objects is multiple:

- they can be associated with the generation of light neutrino masses via the type-I **seesaw mechanism**;
- they can also explain the observed **baryon asymmetry of the Universe (BAU)** via **leptogenesis** [530]. See Section 32.4.2;
- they can be considered as **Dark Matter** candidates (Chapter 31).

Currently, most searches assume that a single HNL flavour couples exclusively to one SM generation ("single flavour mixing"). This offers a well-defined benchmark for searches and sensitivity studies but does not fit with the observed light neutrino properties. One can therefore consider benchmark scenarios with couplings to more than one generation, effectively describing phenomenological aspects of realistic neutrino mass models [531].

The **seesaw mechanism** [532] is a model used to understand the relative sizes of observed LH ν masses, compared to those, much heavier, of quarks and charged leptons. There are several types of models,

[526] Z. Vallari, NOvA-T2K Joint Analysis Results. https://indico.fnal.gov/event/62062/contributions/279004/attachments/175258/237774/021624_NOvAT2K_JointFitResults_ZV.pdf
[527] A. de Gouvêa, The neutrino mass puzzle. https://cerncourier.com/a/the-neutrino-mass-puzzle/
[528] A. M. Abdullahi *et al.*, The Present and Future Status of Heavy Neutral Leptons. https://arxiv.org/abs/2203.08039
[529] M. Drewes *et al.,* New Benchmark Models for Heavy Neutral Lepton Searches. https://arxiv.org/abs/2207.02742
[530] D. Bödeker and W. Buchmüller, Baryogenesis from the weak scale to the grand unification scale. https://arxiv.org/abs/2009.07294
[531] M. Drewes *et al.,* New Benchmark Models for Heavy Neutral Lepton Searches. https://arxiv.org/abs/2207.02742
[532] M. R. Francis, From Symmetry: Neutrinos on a seesaw. https://sciencesprings.wordpress.com/2016/02/10/from-symmetry-neutrinos-on-a-seesaw/
S. King, Neutrino mass and mixing in the seesaw playground. *Nuclear Physics B 908 (2016) 456–466.*

each assuming an extension of the SM. The simplest assumes two or more additional right-handed ν_R, inert under the EW interaction, and the existence of a very high mass scale, possibly linked to the scale of **grand unification**. Figure 19-16 left gives a sketch of the basic idea of the seesaw type 1 and the key mass matrix, and Fig. 19-16 right [533] presents the three types of the seesaw scenarios.

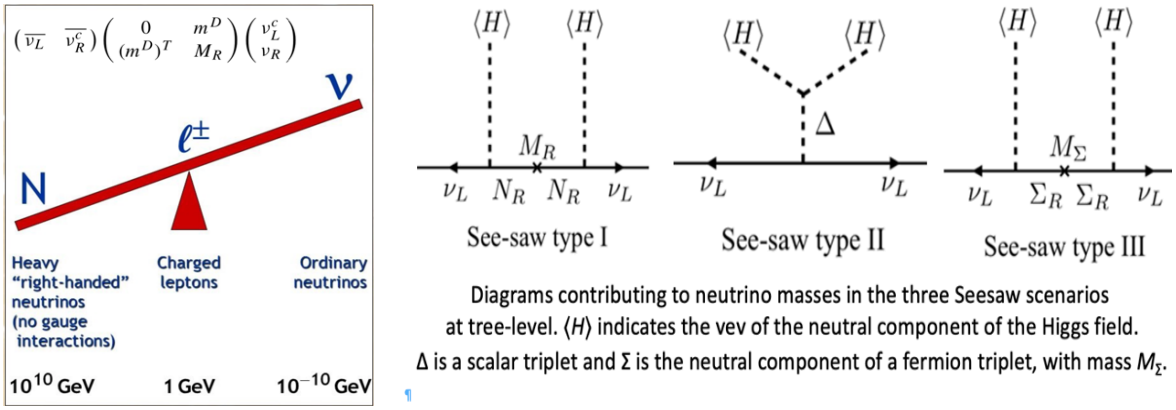


Fig. 19-16: Left: sketch of the see-saw. Right: the three see-saw scenarios.

A second motivation for the existence of HNLs with sub-TeV masses (besides explaining the light ν masses) lies in the possibility to explain the observed baryon asymmetry of the Universe **through low scale leptogenesis** [534].

Anticipating Chapter 31, a last merit of HNL is the possibility to link the existence of a sterile ν in the keV domain to the **warm DM problem**.

As Fig. 19-17 shows, across the allowed domain one can **trade coupling strength against mass** [535]: the mass of these hypothetical particles is thus unknown, between a fraction of an eV up to the GUT scale.

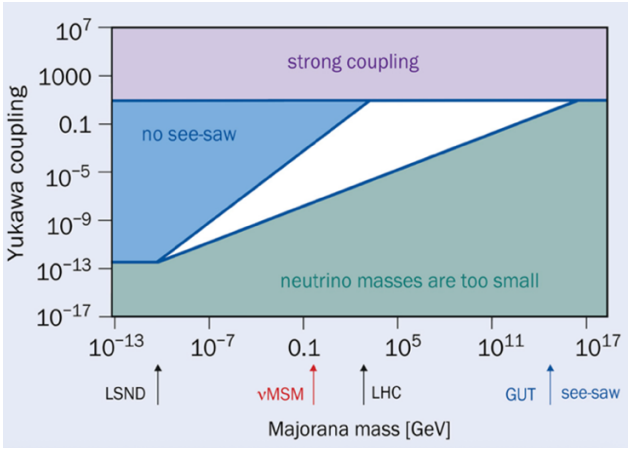


Fig. 19-17: Trading coupling against mass [536].

[533] A. M. Abdullahi, *et al.,* The Present and Future Status of Heavy Neutral Leptons. https://arxiv.org/abs/2203.08039
[534] J. Klaric *et al.,* Uniting Low-Scale Leptogenesis Mechanisms. 2008.13771, *Phys. Rev. Lett. 127, 111802 (2021)*
[535] Changing the Yukawa couplings of HNLs to ν by x and the HNL masses by x^2, and the active ν masses and their oscillations remain intact.
[536] A. Boyarsky and M. Shaposhnikov, Turning the screw on right-handed neutrinos. https://cerncourier.com/a/turning-the-screw-on-right-handed-neutrinos/

19.7 The νMSM

One can illustrate these points by a minimal extension of the SM, the **Neutrino Minimal Standard Model (νMSM)** [537], introducing three sterile ν_R (Fig. 19-18). The lightest one N_1 [538] at keV scale possibly accounts for cosmic DM (Fig. 19-19), while mass-degenerate N_2 and N_3 with mass in the 100 MeV/1 GeV region "give" masses to neutrinos and produce **baryon asymmetry of the Universe** (BAU) (Fig. 19-20).

Properties of Sterile ν Dark Matter, production of such keV-scale DM in the Early Universe and its laboratory searches for keV-scale Sterile ν are described in Ref. [539].

Neutrino masses are evidence of new physics beyond the SM and the theory of HNLs requires novel features.

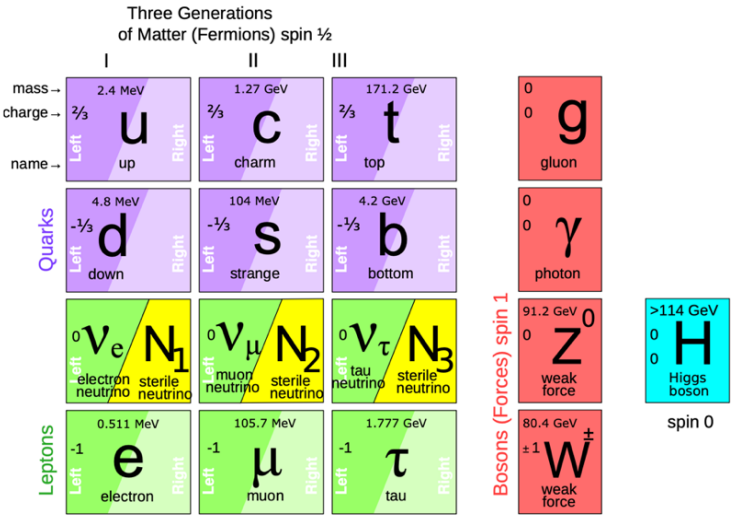


Fig. 19-18: The minimal addition of $N_{1,2,3}$ to the SM [540].

In brief, following Ref. [541]:
Neutrinos, being neutral, can be **Dirac or Majorana particles** (Section 32.1), corresponding to the conservation or not of the leptonic number symmetry L. Majorana neutrino satisfy $\nu = \nu^c \equiv C\bar{\nu}^T$, where C is the charge-conjugation matrix and ν^c the $\mathrm{charge-conjugate\ of}\ \nu$.

Neutrino masses can be of different types, leading to the Dirac or Majorana nature.

A Dirac mass term $\bar{\nu} m_D \nu = \bar{\nu}_L m_D \nu_R + \mathrm{h.c.}$ requires introducing RH ν_R. It is analogous to that of the SM charged fermions, it conserves L and gives the same L to both chiral components. It remains invariant under a $U(1)_L$ transformation $\nu_{L,R} \to e^{in}\nu_{L,R}$.

/

[537] T. Asaka *et al.,* The νMSM, Dark Matter and Neutrino Masses. https://arxiv.org/abs/hep-ph/0503065
[538] We keep the notations of the νMSM model
[539] A. Boyarsky *et al.,* Sterile Neutrino Dark Matter. https://arxiv.org/abs/1807.07938
[540] S. N. Gninenko, D. S. Gorbunov and M. E. Shaposhnikov, Search for GeV-scale sterile neutrinos responsible for active neutrino oscillations and baryon asymmetry of the Universe. https://onlinelibrary.wiley.com/doi/10.1155/2012/718259
[541] A. M. Abdullahi *et al.,* The Present and Future Status of Heavy Neutral Leptons. https://arxiv.org/abs/2203.08039
B. Kayser, Heavy Neutrinos and the Majorana vs. Dirac Question.
https://indico.cern.ch/event/800930/contributions/3557170/attachments/1921667/3181089/BorisKayser1910-1.pdf

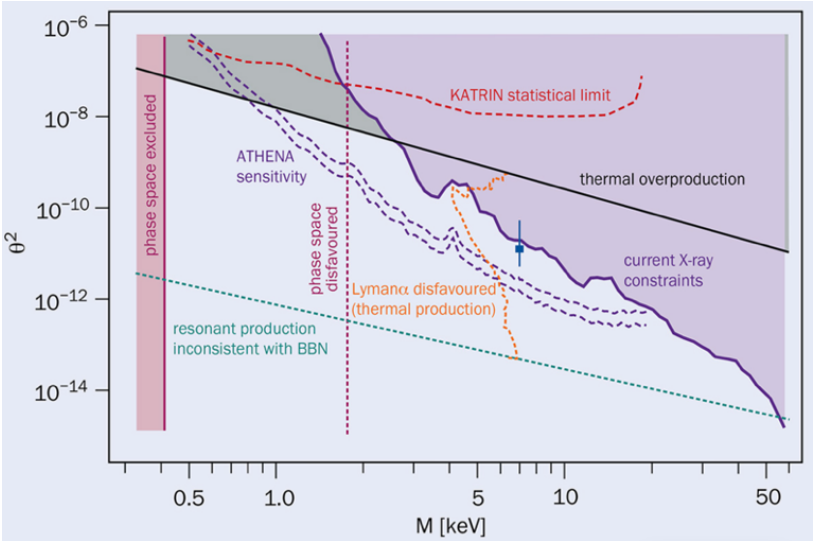


Fig. 19-19: Constraints imposed by DM. Blue square: interpretation of the 3.5 keV excess [542] as decaying sterile-ν DM [543].

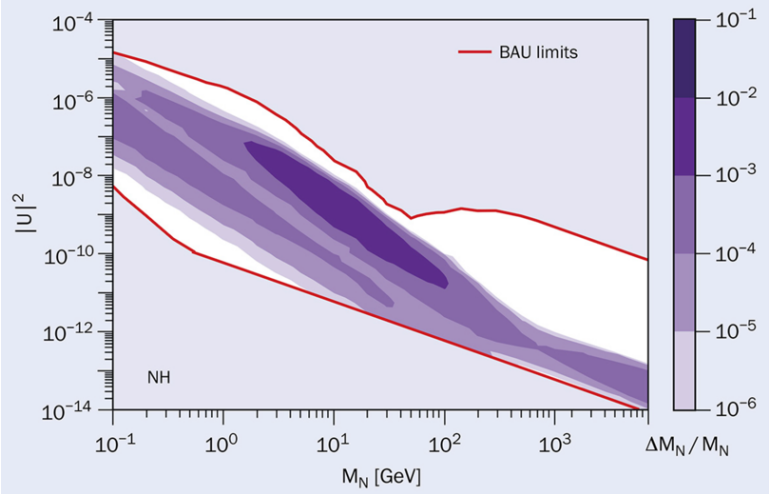


Fig. 19-20: Sketch of the limits imposed on mass and mixing angle by the observed value of BAU [544].

Majorana masses require only one Weyl spinor [545] ν_L as

$$-L_{Majorana} = \frac{1}{2}\overline{\nu^C} m_M \nu = -\frac{1}{2}\nu_L^T C^\dagger m_M \nu_L + h.c.$$

This term breaks lepton number by two units. It is also possible to have Majorana masses for ν_R. If the theory contains also ν_R, it is possible to have Dirac mass term and both Majorana ones for ν_L and ν_R. In this case, the resulting massive ν are of Majorana type and overall the Lagrangian does not conserve L.

[542] However, see C. Dessert *et al.,* Was There a 3.5 keV Line? https://arxiv.org/abs/2309.03254
[543] A. Boyarsky and M. Shaposhnikov, Turning the screw on right-handed neutrinos. https://cerncourier.com/a/turning-the-screw-on-right-handed-neutrinos/
[544] ibid
[545] A. M. Abdullahi *et al.,* The Present and Future Status of Heavy Neutral Leptons. https://arxiv.org/abs/2203.08039

In a full theory with 3 ν_L and N ν_R, there will be 3 light Majorana neutrinos and a number N of massive neutrinos that, if heavy, are denoted as HNLs and will be nearly-sterile.

A Majorana mass term using only ν_L violates the SM gauge invariance. Thus, the SM does not allow for ν masses.

19.8 The hunt for HNLs

Let us describe the hunt for HNLs, present and in the next decades, which will hopefully cover the keV to TeV mass range [546].

A first type of searches exploits **energy-momentum conservation in nuclear reactions**, which will allow to explore the full keV HNL mass range. If a HNL, as a keV-scale sterile neutrino, mixes with the electron neutrino/antineutrino, by reconstructing the kinematics of the nuclear decay products, one can obtain sensitivity to its existence, setting upper limits on mixing coefficients $|U_{e4}|^2$ as a function of the heavy mass m_4.

This method involves searches on Nuclear Decay, Beta Decay (Fig. 19-21), Electron Capture, Reactor searches, Neutrinoless Double Beta Decay searches (Section 30.5).

Short baseline ν experiments have a window to improve the sensitivity for HNL searches in the mass region of 1–10 MeV: **S**hort-**B**aseline **N**ear **D**etector (SBND), MicroBooNE, ICARUS, the DUNE near detectors at FNAL.

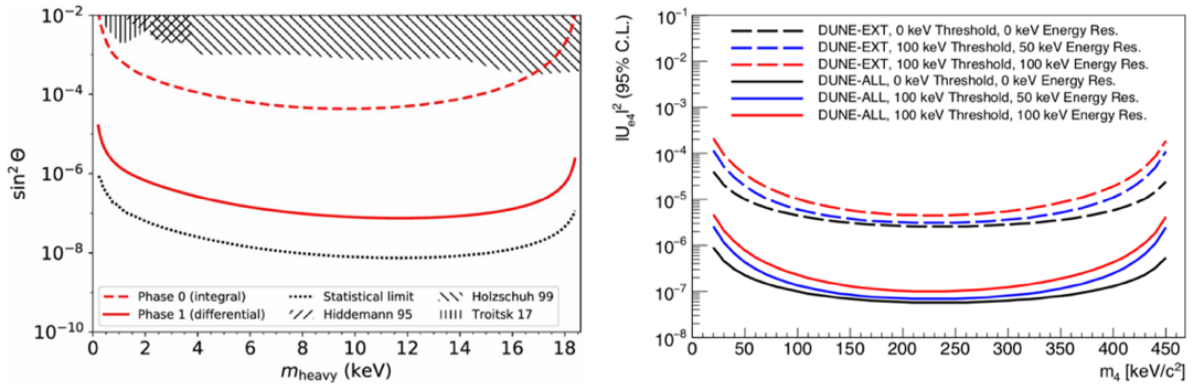


Fig. 19-21: Projected upper limits (95% CL) for $\sin^2\theta = |U_{e4}|^2$ as a function of heavy neutral lepton mass $m_{heavy} = m_4$ for KATRIN/TRISTAN (left) through β decays of tritium (^{3}H) and DUNE (right) using ionization charge measurements of ^{39}Ar β decays in the detector [547].

Searches at **extracted beamlines** have opportunities at FNAL (DarkQuest), J-PARC, PSI (PIONEER) and at CERN, where search of the **νMSM RH neutrinos was the initial motivation of the SHiP programme** [548]. The challenge for these experiments will be to have good handles on the **background control.**

The models quoted above can offer signatures at **e^+e^- colliders**, e.g. BaBar, Belle, Belle II and BESIII, using in particular a monophoton trigger (covering the $e^+e^- \rightarrow \bar{\chi}\chi\gamma$ process with χ invisible).

[546] ibid
[547] ibid
[548] W. Bonivento *et al.,* Proposal to Search for Heavy Neutral Leptons at the SPS. https://arxiv.org/abs/1310.1762

The capabilities of these searches are illustrated in some of the following figures.

The **LHC and possible future HE colliders** will offer excellent opportunities to search for HNLs. With the high luminosity, CMS and ATLAS can potentially reach in the minimal HNL model on active-sterile mixings $|V_{eN}|^2$ and $|V_{\mu N}|^2$ values of couplings $\leq 10^{-7}$–10^{-8}, in the mass region m_N of 5–20 GeV. LHCb will extend the range for lower mass values. The problem to reach smaller couplings at small masses is the decreasing acceptance of the central detectors due to the increasing HNL lifetimes.

For low values of the neutrino mixing angles, the decay length of the HNLs can be significant, leading to most discriminating **long-lived signatures** (Fig. 19-22). An example is an original search in B decays performed at CMS [549].

Let us end with the welcome initiative of searches in existing or foreseen detectors located in the **forward region of the LHC** collision points [550] : FASER, SND@LHC, MATHUSLA, CODEX-b, AL3X, ANUBIS, MAPP, the Forward Physics Facility, FACET. It is in particular satisfactory that $\boldsymbol{\nu}$ **physics** is now performed in the **forward region of an LHC interaction** point, e.g. by the SND@LHC experiment, with an accent put on the ν_τ species [551]. Their potential for HNL can be read from Fig. 19-23 and Fig. 19-24.

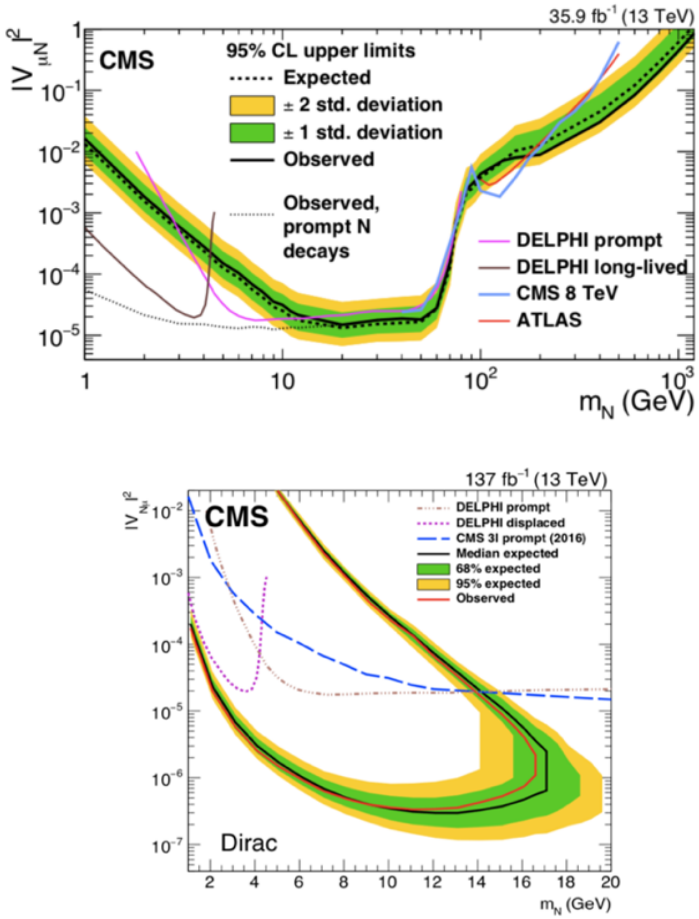


Fig. 19-22: Up: HNL exclusion region at 95% CL by the CMS experiment in the $|V_{\mu N}|^2$ vs. m_N plane. Down: The 95% CL limits by the CMS experiment on $|V_{\mu N}|^2$ as functions of mass m_N for a Dirac HNL [552].

[549] A. M. Lyon, Review of searches for new physics at CMS. https://moriond.in2p3.fr/QCD/2024/WednesdayMorning/Lyon.pdf

[550] A. M. Abdullahi *et al.,* The Present and Future Status of Heavy Neutral Lepton. https://arxiv.org/abs/2203.08039

[551] SND@LHC, https://snd-lhc.web.cern.ch

[552] A. M. Abdullahi *et al.,* The Present and Future Status of Heavy Neutral Lepton. https://arxiv.org/abs/2203.08039

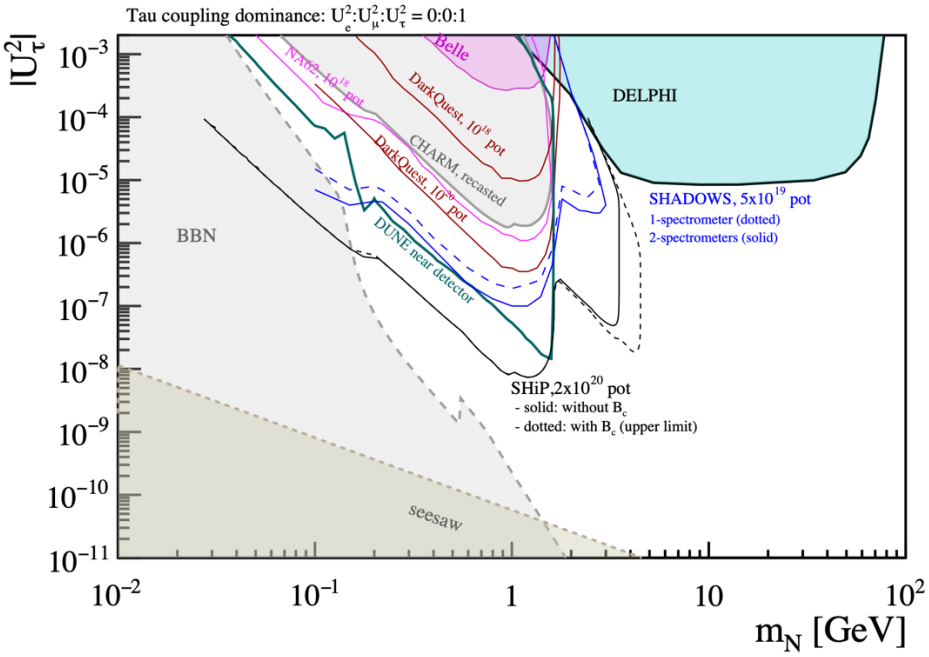


Fig. 19-23: HNL with coupling to the 3rd lepton generation [553]. Filled areas are existing bounds. Colored curves are projections.

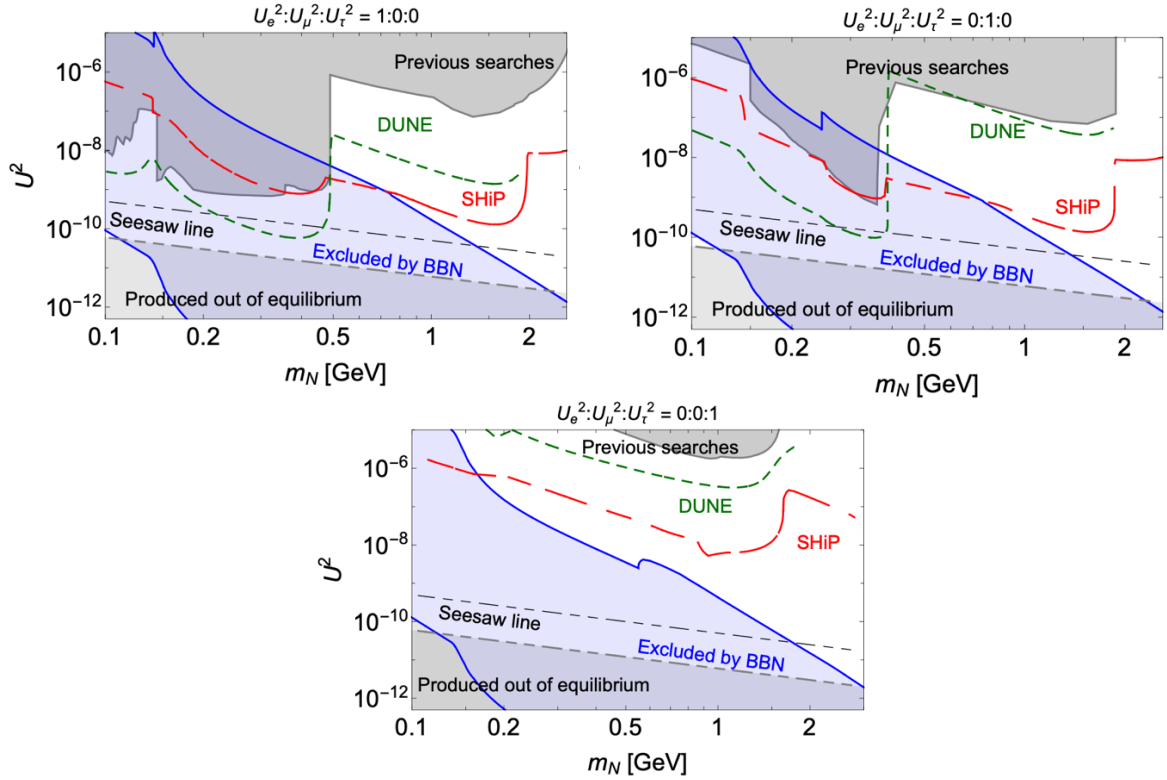


Fig. 19-24: BBN bounds on GeV scale HNL of the pure *e* (top left), μ (top right), and τ mixing (bottom) [554].

[553] ibid In previous plots the typical protruding oblique shape of the exclusion regions is due to a combination of (i) mass reach, (ii) sensitivity (lower limit), (iii) lifetime and acceptance of the object searched for (upper limit).
[554] ibid

19.9 HNL as DM

HNL may be produced in the early Universe at high T and then decay. But these processes should not impact the success of the **BB nucleosynthesis** (see Section 30.3). This sets limits, as shown in Fig. 19- 25.

Neutrinos as dark matter are usually considered as being "too light" and "too abundant". However, HNLs may cure these drawbacks [555] and provide potentially testable DM candidate from sub-keV range to MeV or even GeV. As we saw, the νMSM introduced three sterile RH ν, the lightest one possibly accounting for cosmic DM. Details on properties, production and searches of such keV scale DM sterile ν are described in [556] and constraints on sterile ν DM in Fig. 19-19.

The possible role of neutrinos in solving the **baryon asymmetry through leptogenesis** will be considered in Section 32.4. Figure 19-25 illustrates the exclusion regions in the U_μ^2 versus mass plane, where regions consistent with both seesaw and leptogenesis are shown (see also Fig. 19-20) HNL with coupling to the first (second) lepton generation are shown in Fig. 19-26 (Fig. 19-27).

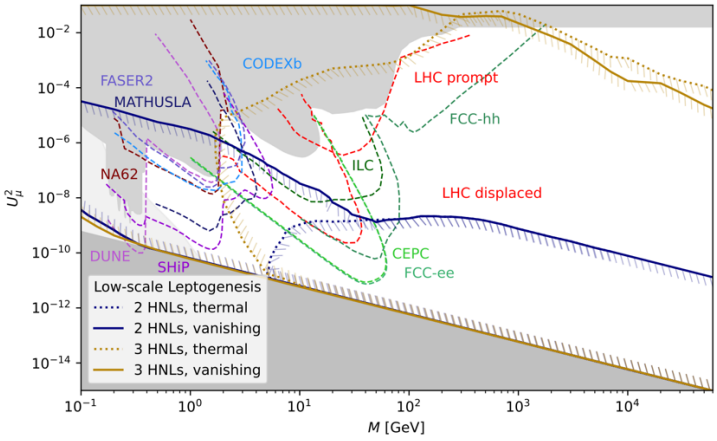


Fig. 19-25: Range consistent with both see-saw and leptogenesis [557].

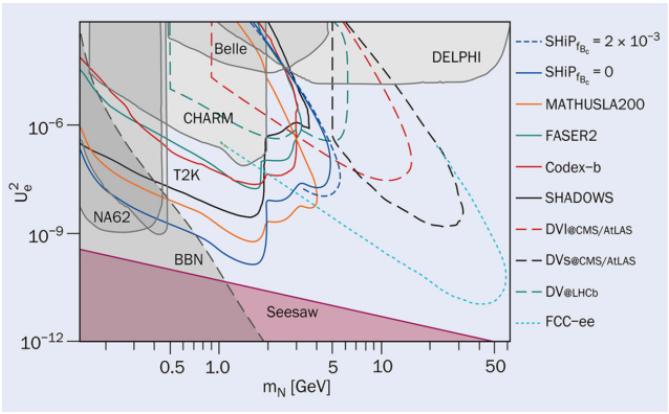


Fig. 19-26: Projected sensitivities to HNL coupled to electrons [558].

[555] M. Shaposhnikov, Dark Matter: The Case of Sterile Neutrino. https://arxiv.org/abs/astro-ph/0703673
[556] A. Boyarsky *et al.,* Sterile Neutrino Dark Matter. https://arxiv.org/abs/1807.07938
[557] A. M. Abdullahi *et al.,* The Present and Future Status of Heavy Neutral Lepton. https://arxiv.org/abs/2203.08039 and references therein.
[558] A. Boyarsky and M. Shaposhnikov, Turning the screw on right-handed neutrinos. https://cerncourier.com/a/turning-the-screw-on-right-handed-neutrinos/

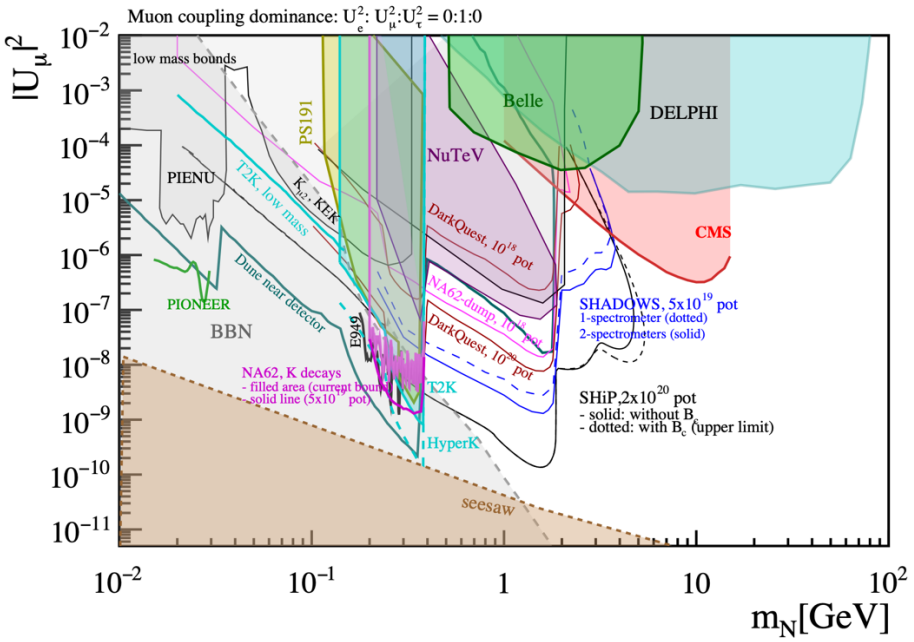


Fig. 19-27: HNL with couplings to the 2nd generation. Filled areas are existing bounds. Coloured curves are projections [559].

19.10 The gallium anomaly

A definition of the gallium anomaly [560]: the measurements of the charged-current **capture rate of neutrinos on ^{71}Ga** from strong radioactive sources have yielded results below those expected, based on the strength of the principal transition according to theory.

The anomaly appeared in calibration tests of two radiochemical detectors, GALLEX and SAGE [561], designed to probe low-energy components of the solar neutrino flux and studying the reaction ^{71}Ga (ν_e , e$^-$) ^{71}Ge (234 keV threshold, 11.43 d half-life of ^{71}Ge), with two possible approaches to the chemistry of the detector, one employing gallium as a $GaCl_3$ solution and the other as a metal.

For instance, the GALLEX underground 54 m^3 detector tank was filled with 101 tons of gallium trichloride-hydrochloric acid solution, containing 30.3 tons of gallium. The produced ^{71}Ge was chemically extracted from the detector, converted to $^{71}GeH_4$. Its decay was detected by counters. Each detected decay corresponded to one detected neutrino.

Exposing the gallium to a known source of ν_e and then carrying out the routine procedures of ^{71}Ge extraction and counting provides an end-to-end cross-check of all experimental procedures, including the reaction cross section.

No simple explanation for the anomaly has been found.

---

[559] A. M. Abdullahi *et al.,* The Present and Future Status of Heavy Neutral Lepton. https://arxiv.org/abs/2203.08039 and ref. therein.

[560] S. R. Elliott *et al.,* The Gallium Anomaly. https://arxiv.org/abs/2306.03299

[561] F. Kaether *et al.*, Reanalysis of the Gallex solar neutrino flux and source experiments. https://arxiv.org/abs/1001.2731
J. N. Abdurashitov *et al.*, Results of measurements of the solar neutrino capture rate in gallium metal by the Russian-American Gallium Experiment SAGE. https://arxiv.org/abs/astro-ph/0204245

This long-lasting anomaly deepened with recent results from the dedicated Baksan Experiment on Sterile Transitions (BEST) [562], utilizing a neutrino source of unprecedented intensity (intense ^{51}Cr sources) and a detector providing some information on counting rate as a function of distance from the source.

The BEST results, when combined with previous measurements (Fig. 19-28), yield a Ga anomaly of conservatively about 4σ significance.

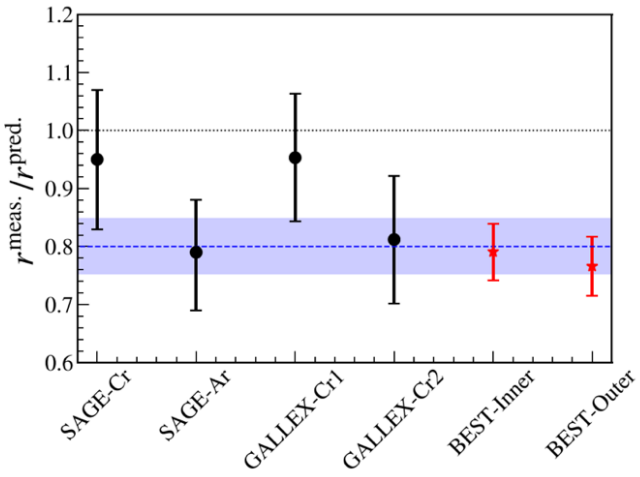


Fig. 19-28: The ratio of the measured ^{71}Ge production rate to the predicted rate for all 6 measurements. The dotted blue line (shading) is the best fit (uncertainty) to all 6 results [563].

The lack of more conventional explanations for the anomaly has led to suggestions that new physics might intervene, as an oscillation into a fourth sterile neutrino $\nu_e \rightarrow \nu_s$. The BEST and SAGE/GALLEX calibration results are consistent with such a possibility for a broad range of $\Delta m^2 \gtrsim 1$ eV^2 and large mixing angles in the range $\sin^2 2\theta \sim 0.3$–0.4.

But BEST found no evidence of distance dependence and thus no explicit sign of new physics. And oscillation parameters indicated by BEST are in conflict with various short-baseline null experiments.

Possibilities to use even more intense and higher energy sources are under study.

19.11 Neutrino detectors at accelerators

Table 19-3 [564] gives the list of detectors for accelerator-based neutrino beams.

Combined, the four far detector modules of DUNE [565] will hold nearly 70 000 tons of ultrapure liquid argon. The 800 tons argon ProtoDUNE detectors were constructed to test DUNE technologies at CERN.

[562] V. V. Barinov *et al.*, Results from the Baksan Experiment on Sterile Transitions (BEST). https://arxiv.org/abs/2109.11482
[563] S. R. Elliott *et al.*,The gallium anomaly. https://arxiv.org/abs/2306.03299
[564] Particle Detectors at Accelerators. https://pdg.lbl.gov/2022/reviews/rpp2022-rev-particle-detectors-accel.pdf
[565] DUNE at LBHF. https://lbnf-dune.fnal.gov/how-it-works/detectors-and-computing/
ProtoDUNE's argon filling underway. https://home.cern/news/news/experiments/protodunes-argon-filling-underway

Name	Type	Target	Total Mass (fiducial) [t]	$\langle E_\nu \rangle$ [GeV]	Location	Dates
Lederman et al.	Spark	Al	10	[0.2-3]	BNL	1962
CERN-spark.	Spark	Al	20	1.5	CERN	1963
Serpukhov	Spark	Al	20	[3-30]	IHEP	1974-82
Aachen-Padova	Spark	Al	40(20)	1.4	CERN	1976-77
Gargamelle	Bubble	Freon	12	[1-10]	CERN	1970-79
BEBC	Bubble	H,D,Ne-H	2-42	[50-150] & 20	CERN	1977-84
SKAT	Bubble	Freon	8	7	IHEP	1976-1987
ANL-12ft	Bubble	H,D	1-2	0.5	ANL	1970
BNL-7ft	Bubble	HD	0.4-0.9	1.3,3	BNL	1976-82
Fermilab-15ft	Bubble	D, Ne	1,20	[50-180] & [25-100]	FNAL	1973-92
CITF	Iron	Fe	92	[50-180]	FNAL	1974-83
CDHS	Iron	Fe	1250(520)	10-200	CERN	1976-84
MINOS	Iron	Fe	980(23.7), 5.5k (4.2k)	3	FNAL, SUL	2005-2012
MINOS+	Iron	Fe	980, 5.5k	4-10	FNAL, SUL	2013-2016
INGRID	Iron	Fe	160	0.6-3	J-PARC	2010-
Super-Kamiokande	Cherenkov	H_2O	50k (22.5k)	0.6	Kamioka	1996-
HyperK	Cherenkov	H_2O	260k(190k)	0.6	Kamioka	2027-
K2K-1kt	Cherenkov	H_2O	25	0.8	KEK	1998-2004
HWPF	Scintillation	CH_2, Fe	160	[50-180]	FNAL	1974-78
LSND	Scintillation	CH_2	167	0.003-0.06	LANL	1993-1998
NOvA	Scintillation	CH_2	300, 14k	2	FNAL,Ash River	2014-
SciBar	Scintillation	CH	15(9.5)	0.6	KEK	2003-2004
SciBooNE,	Scintillation	CH	15(9.5)	0.8	FNAL	2007-08
ICARUS	LArTPC	Ar	760(476)	17	LNGS	2006-12
ICARUS	LArTPC	Ar	760(476)	0.8	FNAL	2020-
Argoneut	LArTPC	Ar	0.025	3	FNAL	2009-10
MicroBooNE	LArTPC	Ar	170(85)	0.8	FNAL	2014-
DUNE	LArTPC	Ar	70(40)	3	FNAL	2026-
FNAL-E-531	Emulsion	Ag, Br	0.009	22	FNAL	1984
CHORUS	Emulsion	Ag, Br	0.8	27	CERN	1994-97
DONuT	Emulsion	Fe	0.26	53	FNAL	1997
OPERA	Emulsion	Pb	1.25k	17	LNGS	2008-12
NINJA	Emulsion	Fe	0.002(0.001)	0.6	J-PARC	2015-
CHARM	Hybrid	$CaCO_3$	(27),156(122)	20	CERN	1978-84
CHARM-II	Hybrid	glass	692	20	CERN	1984-91
BNL-E-734	Hybrid	CH_2	172	1.3	BNL	1981-86
BNL-E-776	Hybrid	concrete	240	1.4	BNL	1986
NOMAD	Hybrid	CH	2.9(2.7)	27	CERN	1995-98
CCFR	Hybrid	Fe	690	[30-260]	FNAL	1985-88
NuTeV	Hybrid	Fe	690	[70-180]	FNAL	1996-97
MINERvA	Hybrid	CH,H_2O,Fe,Pb,C,He	8	3.8	FNAL	2010-19
T2K-ND280	Hybrid	CH,H_2O	2	0.6	J-PARC	2010-

Table 19-3: Detectors for accelerator-based neutrino beams.

19.12 Astrophysical domain of ν physics

Let us briefly quote major set-ups in the astrophysical domain of ν physics. Clearly the detectors already listed can do ν astrophysics in the MeV energy domain and did so. Conversely the huge detectors quoted below, focusing on the highest energies, can also perform the basic measurement of ν oscillations (atmospheric ν, etc.). These are:

— **under wate**r ν telescopes: KM3NeT/ARCA (Sicily) [566], KM3NeT/ORCA [567] (near Toulon, France), Baikal-GVD [568];

[566] KM3NeT Collaboration, Astronomy potential of KM3NeT/ARCA. https://arxiv.org/abs/2402.08363
[567] D. Vivolo, First Results from the KM3Net Experiment. la Thuile 2024, https://agenda.infn.it/event/38205/contributions/219666/attachments/117010/168895/LaThuile24_dv.pdf
[568] V. M. Aynutdinov *et al.,* Large neutrino telescope Baikal-GVD: status 2023. https://inspirehep.net/files/e8ed1750e4496fd90ad74ac3bf719312

— a km^3-scale telescope **under ice**, IceCube [569];
— set-ups for radio detection of ultra-high-E ν with hundreds of km^3 of **ice target** as ARA [570].

The first two exploit grids of optical modules that detect **Cherenkov radiation** induced in the medium by charged secondary particles created in neutrino interactions. See more in Chapter 35.

The main goals are the study of **diffuse astrophysical ν flux** and searches for **point-like ν sources**. IceCube made the first ν observation of the Galactic Plane, the first observation of a steady emission neutrino point source NGC1068, new analyses of the cosmic ray flux from PeV to EeV and its secondary particles, and better measurements of the energy spectrum of the diffuse astrophysical flux.

We now turn to various added information, both historical and technical.

19.13 Details on oscillations

$\nu_{eL}(x)$, $\nu_{\mu L}(x)$ and $\nu_{\tau L}(x)$ are the fields describing the left-handed neutrinos **proper states of flavour**, defined as the ν's which couple by weak charged current to electron, muon, tau, respectively, and $\nu_{1L}(x)$, $\nu_{2L}(x)$ and $\nu_{3L}(x)$ describe neutrinos left-handed **proper states of mass** with masses m_1, m_2 and m_3 (Table 19-4). The unitary transform linking the two types of states, or **leptonic mixing matrix** is the PMNS matrix (Pontecorvo–Maki–Nakagawa–Sakata matrix) [571].

$$\begin{pmatrix} \nu_e(x) \\ \nu_\mu(x) \\ \nu_\tau(x) \end{pmatrix}_L = U \begin{pmatrix} \nu_1(x) \\ \nu_2(x) \\ \nu_3(x) \end{pmatrix}_L = \begin{pmatrix} U_{e1} & U_{e2} & U_{e3} \\ U_{\mu 1} & U_{\mu 2} & U_{\mu 3} \\ U_{\tau 1} & U_{\tau 2} & U_{\tau 3} \end{pmatrix} \begin{pmatrix} \nu_1(x) \\ \nu_2(x) \\ \nu_3(x) \end{pmatrix}_L \qquad \nu_{\alpha L}(x) = \sum_i U_{\alpha i} \nu_{iL}(x)$$

Table 19-4: Relations between the different fields.

It can also be described as the product of three rotations of angle θ_{ij}, the second of which depends of a phase δ_{CP} and of a diagonal matrix of phases P. The PMNS matrix numerical status is given in Table 19-5 [572].

Figure 19-29 gives visually the status of oscillations [573]. The 90 and 99% CL (2 d.o.f.) allowed regions are shown in the different plots.

Table 19-6 gives very close versions of the relevant numbers of the oscillations [574] .

[569] IceCube Collaboration, Highlights from the IceCube Neutrino Observatory. https://arxiv.org/abs/2310.12840
[570] K. Hoffman (ARA Collaboration), A Decade of the Askaryan Radio Array. https://inspirehep.net/files/2692cbeaa85ae1330476fee2c926e6d3
[571] C. Giganti *et al.,* Neutrino oscillations : the rise of the PMNS paradigm. https://arxiv.org/abs/1710.00715
P. F. de Salas *et al.,* 2020 Global reassessment of the neutrino oscillation picture. *J. High Energ. Phys. 2021, 71 (2021),* https://arxiv.org/abs/2006.11237
[572] Three-neutrino fit based on data available in November 2022. http://www.nu-fit.org/?q=node/256
[573] P. F. de Salas *et al.,* 2020 Global reassessment of the neutrino oscillation picture. *J. High Energ. Phys. 2021, 71 (2021),* https://arxiv.org/abs/2006.11237
[574] C. A. Ternes, Global analysis of neutrino oscillation experiments. https://inspirehep.net/files/e8276507d023a06bf54432ea787f6399

$$U = \begin{pmatrix} 1 & 0 & 0 \\ 0 & c_{23} & s_{23} \\ 0 & -s_{23} & c_{23} \end{pmatrix} \begin{pmatrix} c_{13} & 0 & s_{13}e^{-i\delta_{\rm CP}} \\ 0 & 1 & 0 \\ -s_{13}e^{i\delta_{\rm CP}} & 0 & c_{13} \end{pmatrix} \begin{pmatrix} c_{12} & s_{12} & 0 \\ -s_{12} & c_{12} & 0 \\ 0 & 0 & 1 \end{pmatrix} P$$

$$= \begin{pmatrix} c_{12}c_{13} & s_{12}c_{13} & s_{13}e^{-i\delta_{\rm CP}} \\ -s_{12}c_{23} - c_{12}s_{13}s_{23}e^{i\delta_{\rm CP}} & c_{12}c_{23} - s_{12}s_{13}s_{23}e^{i\delta_{\rm CP}} & c_{13}s_{23} \\ s_{12}s_{23} - c_{12}s_{13}c_{23}e^{i\delta_{\rm CP}} & -c_{12}s_{23} - s_{12}s_{13}c_{23}e^{i\delta_{\rm CP}} & c_{13}c_{23} \end{pmatrix} P \,.$$

$c_{ij} \equiv \cos\theta_{ij},\ s_{ij} \equiv \sin\theta_{ij}$

Atmospheric (+Accelerator) | Reactor (+Accelerator) | Solar (+Reactor)

$$|U| = \begin{bmatrix} |U_{e1}| & |U_{e2}| & |U_{e3}| \\ |U_{\mu 1}| & |U_{\mu 2}| & |U_{\mu 3}| \\ |U_{\tau 1}| & |U_{\tau 2}| & |U_{\tau 3}| \end{bmatrix} = \begin{bmatrix} 0.803 \sim 0.845 & 0.514 \sim 0.578 & 0.142 \sim 0.155 \\ 0.233 \sim 0.505 & 0.460 \sim 0.693 & 0.630 \sim 0.779 \\ 0.262 \sim 0.525 & 0.473 \sim 0.702 & 0.610 \sim 0.762 \end{bmatrix}$$

Table 19-5: The PMNS matrix including the numerical values.

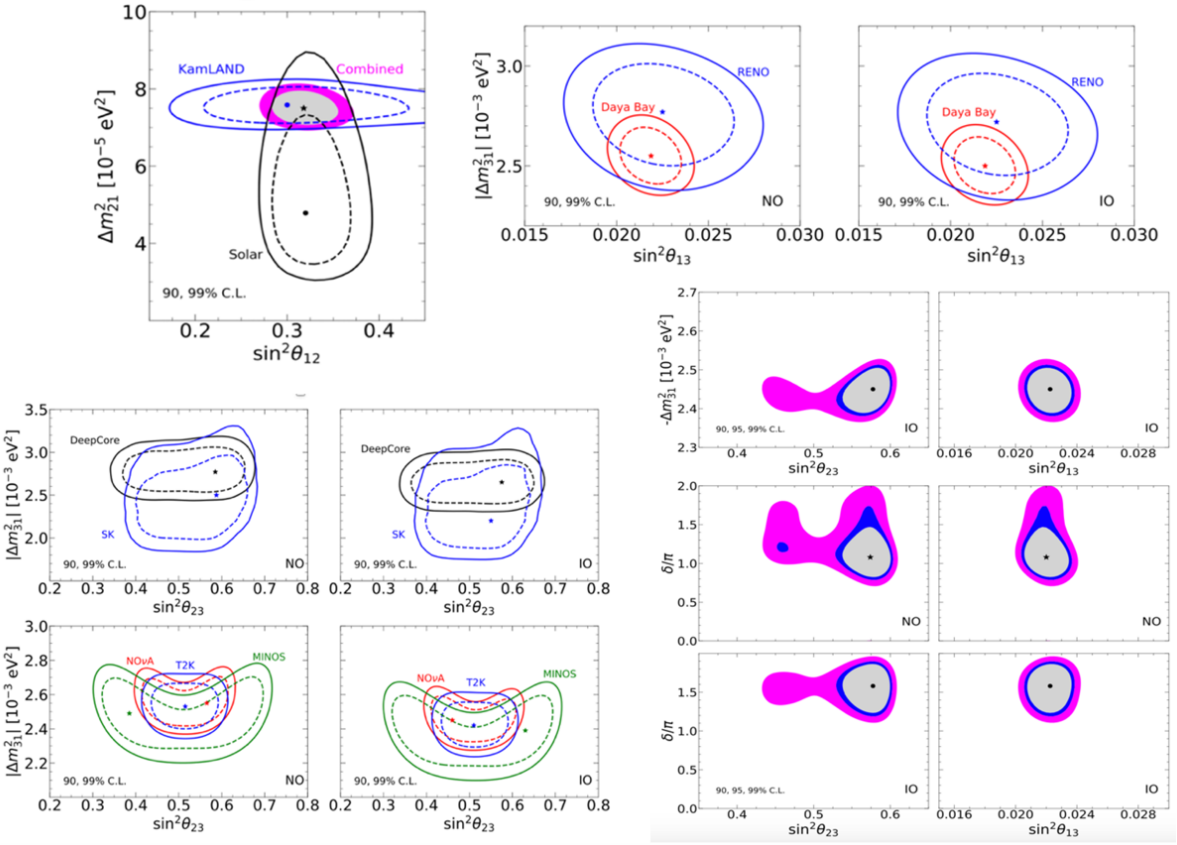


Fig. 19-29: The status of oscillations (visual).

parameter	best fit ± 1σ	2σ range	3σ range
Δm^2_{21} [10^{-5}eV^2]	$7.50^{+0.22}_{-0.20}$	7.12–7.93	6.94–8.14
$\lvert\Delta m^2_{31}\rvert$ [10^{-3}eV^2] (NO)	$2.55^{+0.02}_{-0.03}$	2.49–2.60	2.47–2.63
$\lvert\Delta m^2_{31}\rvert$ [10^{-3}eV^2] (IO)	$2.45^{+0.02}_{-0.03}$	2.39–2.50	2.37–2.53
$\sin^2\theta_{12}/10^{-1}$	3.18 ± 0.16	2.86–3.52	2.71–3.69
$\sin^2\theta_{23}/10^{-1}$ (NO)	5.74 ± 0.14	5.41–5.99	4.34–6.10
$\sin^2\theta_{23}/10^{-1}$ (IO)	$5.78^{+0.10}_{-0.17}$	5.41–5.98	4.33–6.08
$\sin^2\theta_{13}/10^{-2}$ (NO)	$2.200^{+0.069}_{-0.062}$	2.069–2.337	2.000–2.405
$\sin^2\theta_{13}/10^{-2}$ (IO)	$2.225^{+0.064}_{-0.070}$	2.086–2.356	2.018–2.424
δ/π (NO)	$1.08^{+0.13}_{-0.12}$	0.84–1.42	0.71–1.99
δ/π (IO)	$1.58^{+0.15}_{-0.16}$	1.26–1.85	1.11–1.96

$\sin^2(\theta_{12}) = 0.307 \pm 0.013$
$\Delta m^2_{21} = (7.53 \pm 0.18) \times 10^{-5}$ eV^2
$\sin^2(\theta_{23}) = 0.539 \pm 0.022$ (S = 1.1) (Inverted order)
$\sin^2(\theta_{23}) = 0.546 \pm 0.021$ (Normal order)
$\Delta m^2_{32} = (-2.536 \pm 0.034) \times 10^{-3}$ eV^2 (Inverted order)
$\Delta m^2_{32} = (2.453 \pm 0.033) \times 10^{-3}$ eV^2 (Normal order)
$\sin^2(\theta_{13}) = (2.20 \pm 0.07) \times 10^{-2}$
δ, *CP* violating phase $= 1.36^{+0.20}_{-0.16}\ \pi$ rad

PTEP 2022, 083C01 (2022)

Precision

From PDG 2024

$\sin^2(\theta_{12})$	0.307 ± 0.013	4.2 %
Δm^2_{21}	$(7.53 \pm 0.18) \times 10^{-5}$ eV^2	2.4 %
$\sin^2(\theta_{23})$	$0.558^{+0.015}_{-0.021}$	3.2 %
Δm^2_{32}	$(2.455 \pm 0.028) \times 10^{-3}$ eV^2	1.1 %
$\sin^2(\theta_{13})$	0.0219 ± 0.0007	3.2 %

Table 19-6: The status of oscillations (numbers).

19.14 Summary

Neutrino properties are not explained by the SM and oscillations, main source of quantitative information on them are a precious **window on BSM physics** [575]. Their measurements have entered the precision era. The data obtained up to now can be explained by the **3-neutrino model**. The sterile neutrino oscillations are not fully ruled out, but evidence has weakened. All types of oscillations will be more deeply studied and **sub-percent precision** will be reached for some of their parameters. The determination of the **mass ordering** will be obtained, hopefully this decade. If Nature is kind, one will observe leptonic CP violation. Hopefully the key answer about the nature of the neutrino, Dirac or Majorana, will be obtained, but this is a difficult challenge. We will come back to this point in Section 32.1 and on the role of neutrinos in the cosmology part.

19.15 Some synoptic plots

Finally comes a set of interesting figures which offer synoptic views of various aspects on the rich neutrino physics: DAYA Bay results (Fig. 19-30), the improvement of oscillations parameters along years (Fig. 19-31), the global neutrino scenery as a function of energy (Fig. 19-32), the principle of reactor measurements (Fig. 19-33), the neutrino scene in Asia and Juno's contribution (Figs. 19-34 to 19-36). The overall cosmic ray scenery (Fig. 19-35) can be compared to the neutrino scenery (Fig. 19-32). Figure 19-37 indicates the part of neutrinos in the total energy of the Universe along the scale factor evolution. Figure 19-38 gives the neutrino and antineutrino spectra generated by various natural phenomena.

And with even more details two beautiful figures concerning the neutrino world (Figs. 19-37 and 19-38).

[575] J. P. Ochoa-Ricoux, Neutrino Oscillation and CP Violation: Status and Prospects. ICHEP 2024, https://indico.cern.ch/event/1291157/contributions/5958323/attachments/2901877/5091041/NuOsc_Ochoa_ICHEP2024.pdf

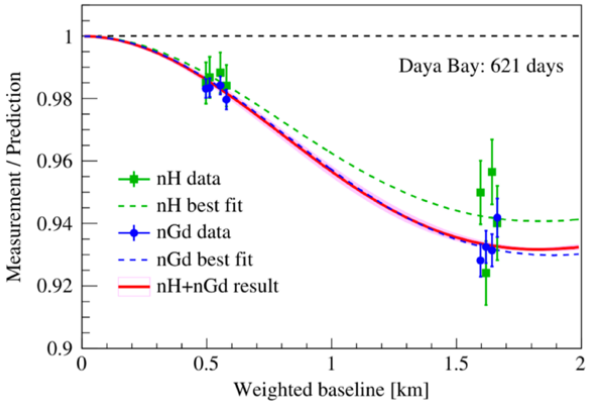


Fig. 19-30: DAYA Bay accuracy of measurement [576].

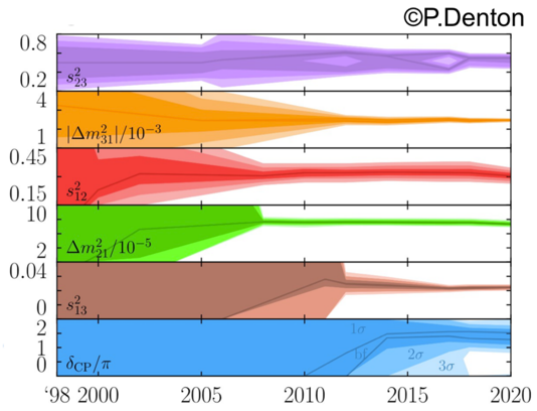


Fig. 19-31: Improved measurements as a function of time [577].

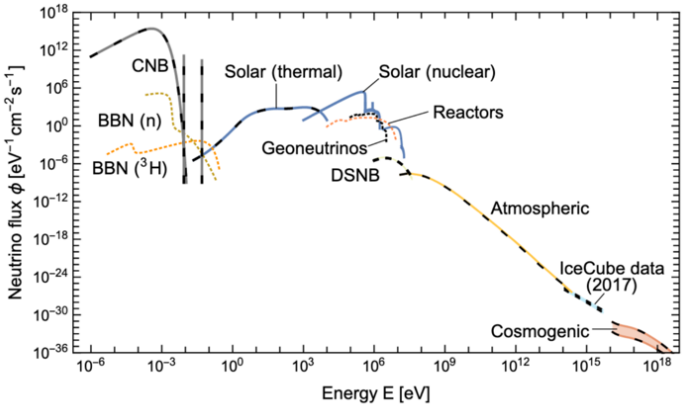


Fig. 19-32: The neutrino scenery [578].

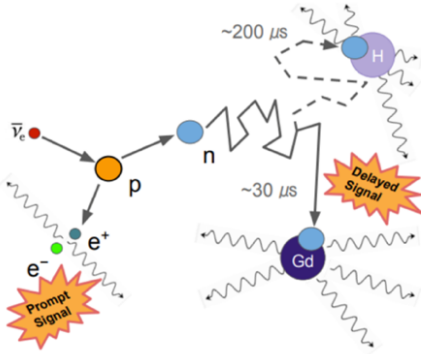


Fig. 19-33: Principle of reactor measurement [579].

[576] J. Li, Latest oscillation results from Daya Bay. EPS-HEP23, https://arxiv.org/abs/2409.14523

[577] P. B. Denton *et al.*, Snowmass Neutrino Frontier: NF01 Topical Group Report on Three-flavour Neutrino Oscillations. https://arxiv.org/abs/2212.00809

[578] E. Vitagliano *et al.,* Grand Unified Neutrino Spectrum at Earth: Sources and Spectral Components. https://arxiv.org/abs/1910.11878
M. S. Athar *et al.,* Status and Perspectives of Neutrino Physics. https://arxiv.org/abs/2111.07586

[579] J. Li, Latest Neutrino Oscillation Results from Daya Bay. https://indico.cern.ch/event/1291157/contributions/5899080/attachments/2899032/5083564/LastestResultDayaBay-ICHEP2024_169.pdf

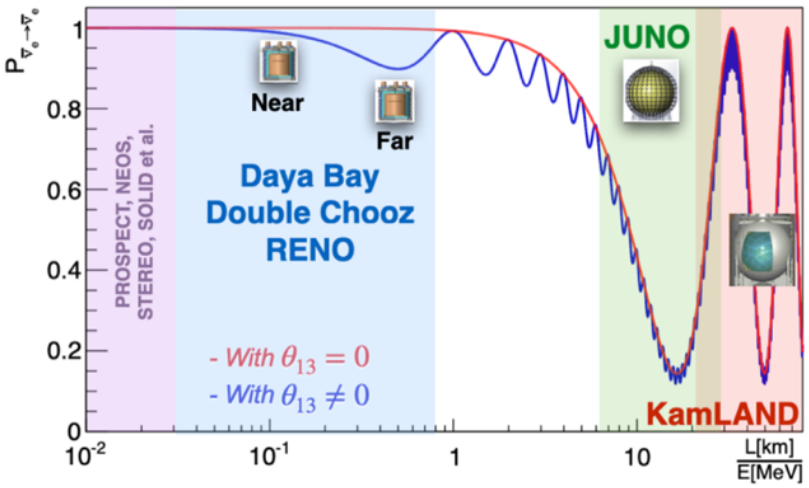


Fig. 19-34: The Asiatic neutrino scene [580].

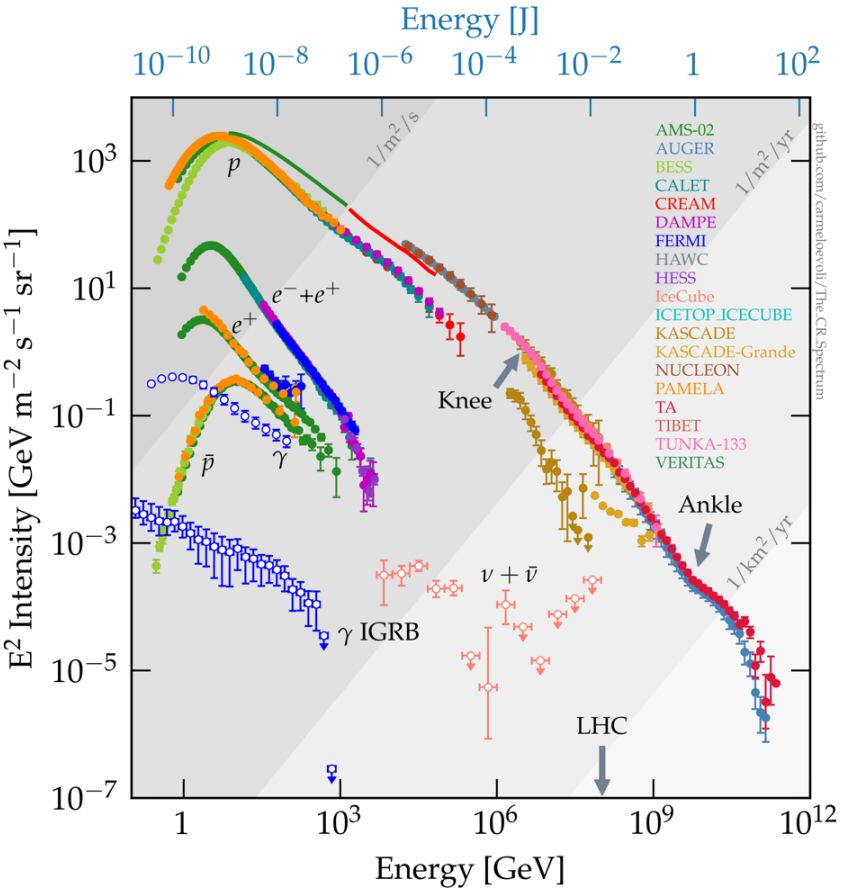


Fig. 19-35: The overall cosmic ray scenery [581].

[580] ibid

[581] F. Calore, Multi-messenger astroparticle physics.
https://indico.desy.de/event/34916/contributions/142222/attachments/84410/111842/EPS-HEP23_FCalore.pdf
and https://github.com/carmeloevoli/The_CR_Spectrum/blob/master/figures/The_CR_Spectrum_2024.png

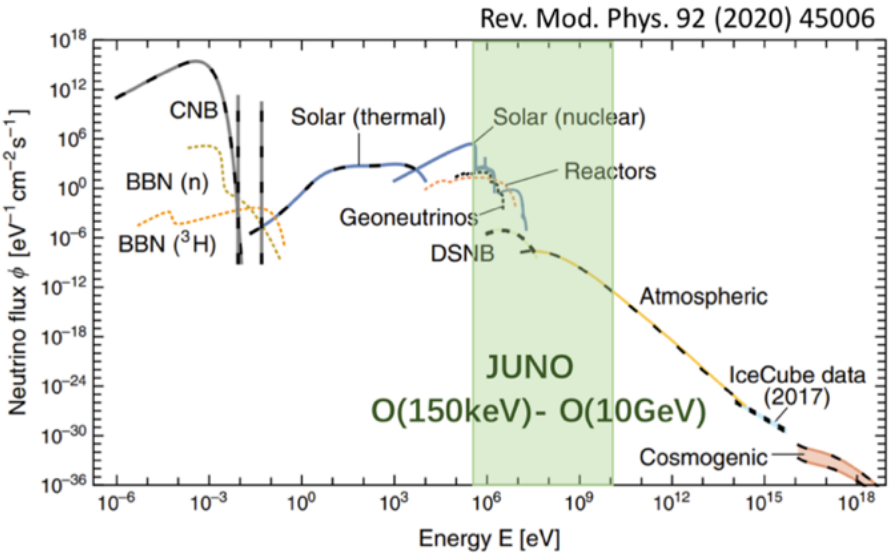


Fig. 19-36: JUNO in the neutrino scenery [582].

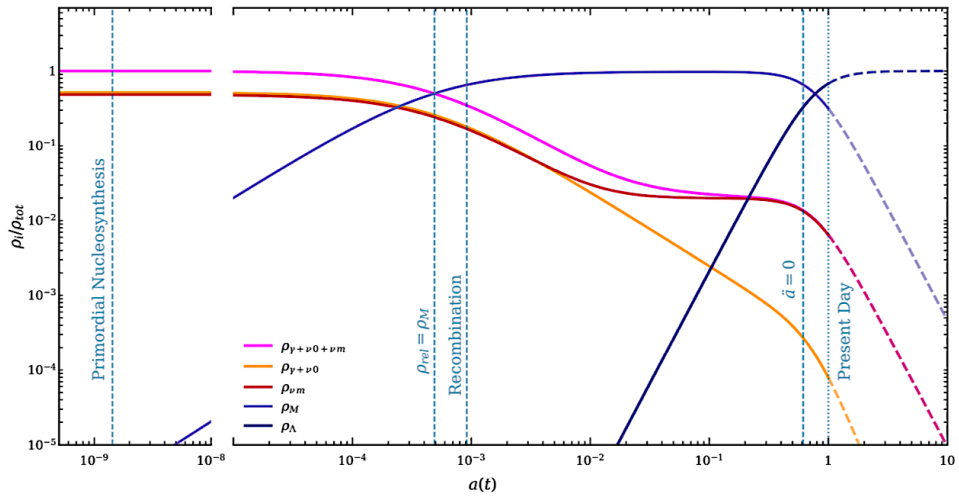


Fig. 19-37: The contributions to the total energy density of the Universe from different components as a function of the scale factor a(t) [583].

[582] E. Vitagliano *et al.,* Grand Unified Neutrino Spectrum at Earth: Sources and Spectral Components. *Rev.Mod.Phys. 92 (2020) 45006*, https://arxiv.org/abs/1910.11878

[583] A. V. Ivanchik *et al.,* Neutrino at different epochs of the Friedmann Universe. https://arxiv.org/abs/2404.07081

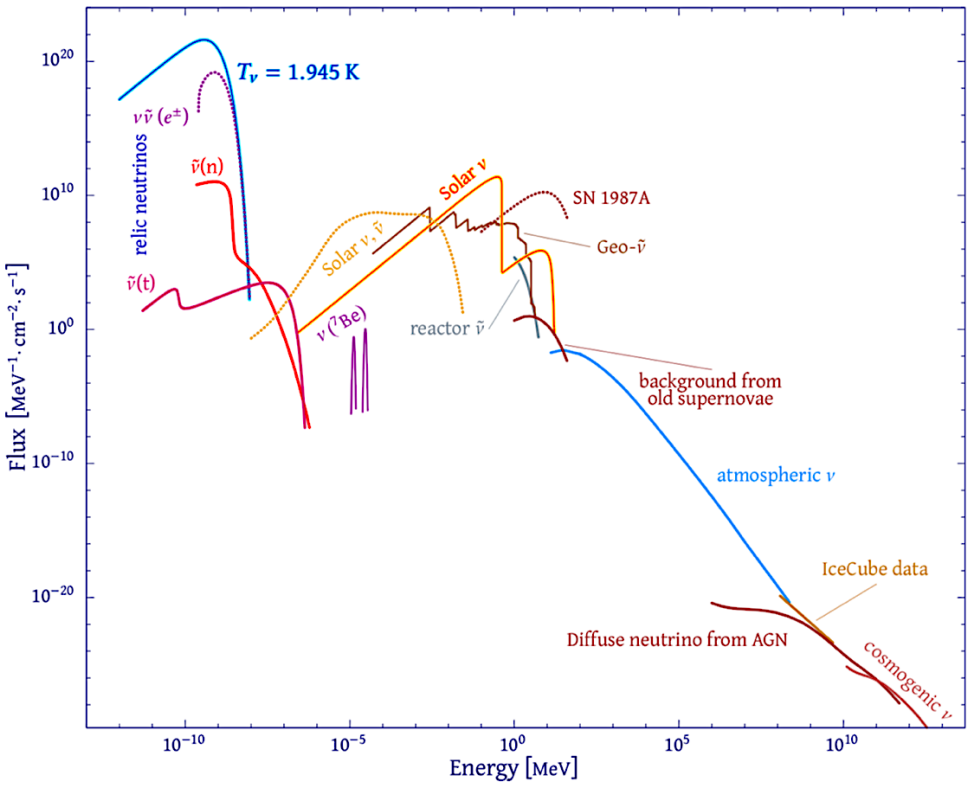


Fig. 19-38: Observed and theoretically calculated spectra of neutrinos and antineutrinos generated by various natural phenomena (local and cosmological) [584].

[584] ibid

20. Heavy ions

20.1 The scenery

An ultra-relativistic Heavy Ion (HI) collision has the following stages [585] (Fig. 20-1):

1. **initial collision**, occurring during the crossing of the Lorentz contracted nuclei;
2. **creation and thermalization** of the Quark Gluon Plasma (**QGP**) for 0.1–1 fm;
3. **expansion, collective movement and cooling** of the QGP;
4. **hadronization** when the temperature drops below the critical temperature T_C;
5. after 5–10 fm, **chemical freeze**: end of inelastic collisions, hadron production settles;
6. the **kinetic freezing** occurs: the elastic collisions stop, and the momenta no longer change.

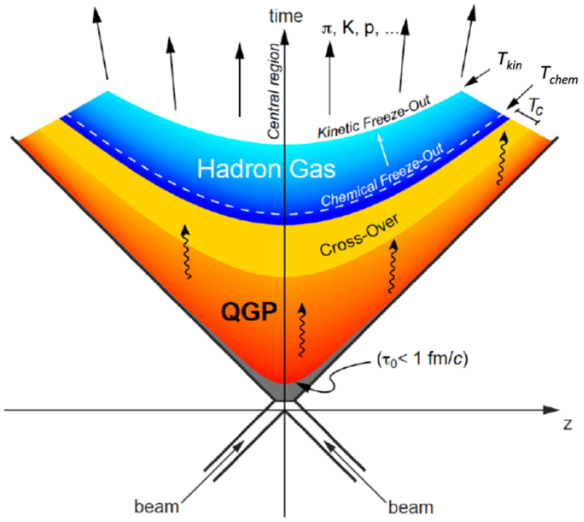


Fig. 20-1: The successive stages [586].

The effects of the hot medium are quantified by the **nuclear modification factor** R_{AA}, the ratio of the p_T distributions measured in AA and in pp collisions:

$$R_{AA} = (1/\langle N\text{coll}\rangle)\ (dN_{AA}/dp_T)\ /\ (dN_{pp}/dp_T),$$

where dN_{AA}/dp_T and dN_{pp}/dp_T are the differential rates in p_T of a given particle species in AA and pp collisions, respectively, and $\langle N\text{coll}\rangle$ is the average number of nucleon-nucleon binary collisions in the overlap region of the colliding nuclei. If medium effects are absent and cold nuclear matter effects are small, R_{AA} = 1 in the region where particle production by hard scattering processes dominates ($p_T \geq 2$ GeV).

The azimuthal distribution of the particles can be described well by a Fourier cosine series, dominated by the second harmonic, characterised by the parameter v_2, due to the rotationally asymmetric ellipsoidal shape of the nuclear overlap region.

---

[585] Y. Pachmayer, Heavy Ions, Experimental Overview. https://arxiv.org/abs/2012.08832 . Most figures below are borrowed from this reference.
See also A. Ohlson, Heavy-ion physics, past, present and future.
https://cerncourier.com/a/heavy-ion-physics-past-present-and-future/

[586] P. Braun-Munzinger and B. Dönigus, Loosely-bound objects produced in nuclear collisions at the LHC. https://arxiv.org/abs/1809.04681 (Figure courtesy of Boris Hippolyte).

Results are best described by models where the QGP obeys hydrodynamic equations, and thus behaves as low viscosity liquid exhibiting a “collective flow”, whose properties can be investigated using “hard probes”, products of hard scatterings occurring in the early stages of the collision.

20.2 Summary of results at ultra-relativistic energies

Some important results of heavy ion collisions at ultra-relativistic energies are summarized here.

20.2.1 The measurements of the EW probes and the parton distribution functions

The measurements of the EW probes constrain both the initial geometry of the collision and the parton distribution functions (Fig. 20-2).

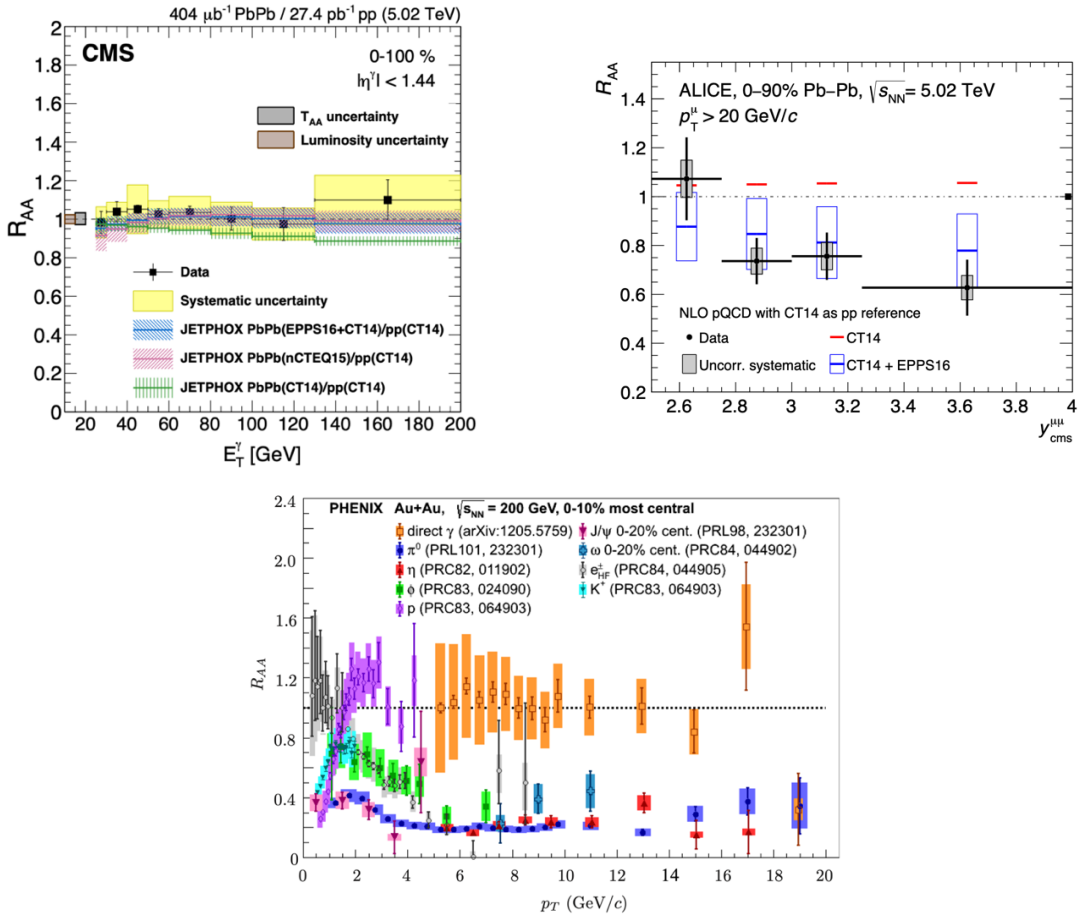


Fig. 20-2: Nuclear modification factor of single photons (top left) as a function of their transverse energy [587] and of Z bosons (top right) vs the rapidity in Pb–Pb collisions [588]. Bottom: R_{AA} for most central Au-Au collisions for a variety of particles as a function p_T [589].

[587] Y. Pachmayer, Heavy Ions, Experimental Overview. https://arxiv.org/abs/2012.08832
CMS Collaboration, The production of isolated photons in PbPb and pp collisions at $\sqrt{s_{NN}}$ = 5.02 TeV. https://arxiv.org/abs/2003.12797

[588] Y. Pachmayer, Heavy Ions, Experimental Overview. https://arxiv.org/abs/2012.08832
ALICE Collaboration, Z-boson production in p-Pb collisions at $\sqrt{s_{NN}}$ = 8.16 TeV and Pb – Pb collisions at $\sqrt{s_{NN}}$ = 5.02 TeV. https://arxiv.org/abs/2005.11126

[589] J. C. Hill, Highlights from the 17-Year Heavy Ion Program at the PHENIX Experiment at RHIC. https://ntse.khb.ru/files/uploads/2016/proceedings/Hill.pdf

20.2.2 Soft particle production

Soft particle production results show that the abundance of light flavour hadrons,^{3}He and p can be described by a **universal temperature** and that these particles participate in the **collective motion of the system** (Figs. 20-3 and 20-4).

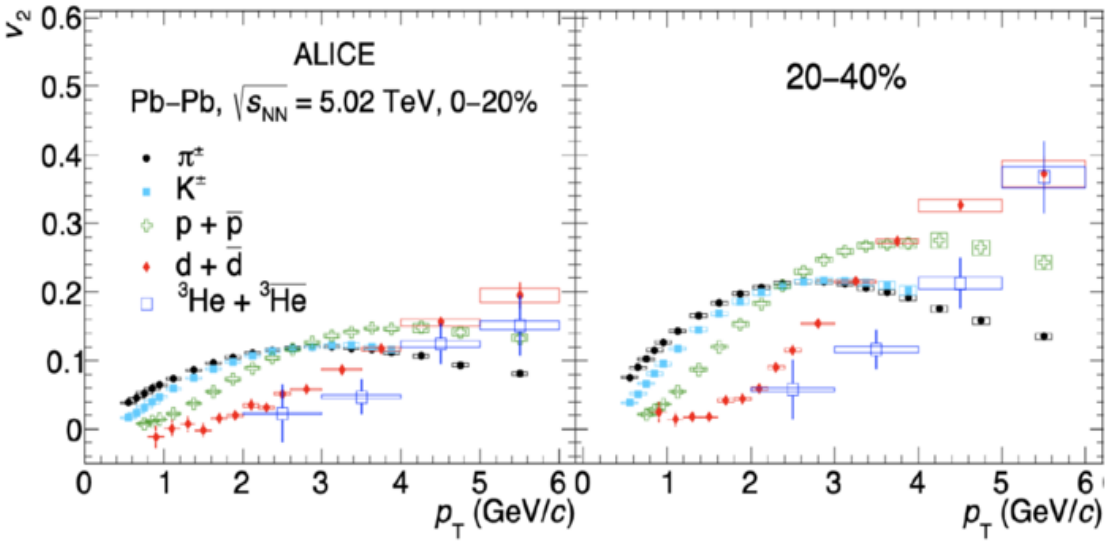


Fig. 20-3: Elliptical flux as a function of p_T for various species of particles [590].

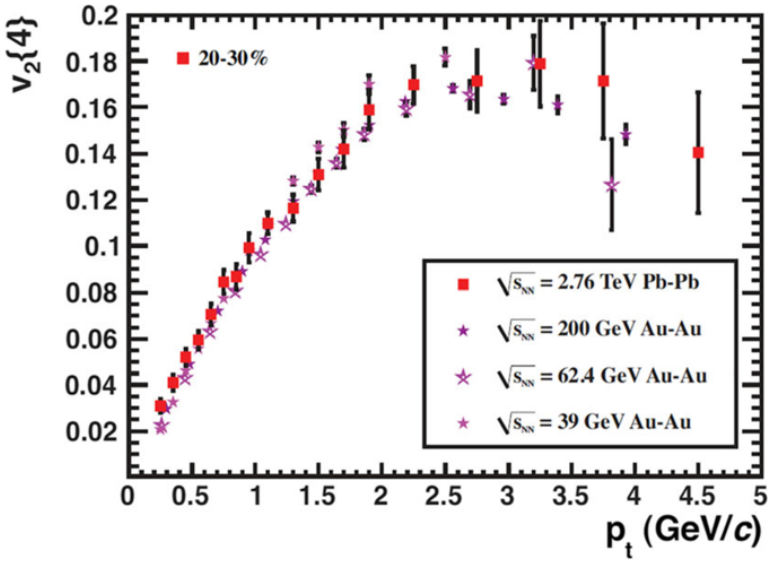


Fig. 20-4: Elliptic flow at various energies [591].

[590] ALICE Collaboration Measurement of the (anti-)^{3}He elliptic flow in Pb–Pb collisions at$\sqrt{}$ s_{NN} = 5.02 TeV. https://arxiv.org/abs/1910.09718
ALICE Collaboration, Elliptic and triangular flow of (anti)deuterons in Pb-Pb collisions at$\sqrt{}$ s_{NN} = 5.02 TeV https://arxiv.org/abs/2005.14639

[591] J. W. Harris and B. Müller, "QGP Signatures" revisited. *Eur.Phys. J.C (2024) 84-247,* https://link.springer.com/article/10.1140/epjc/s10052-024-12533-y

20.2.3 Studies of hard probes

Studies of hard probes, such as heavy quarks and jets, show that the **loss of parton energy** plays an important role in heavy ion collisions.

Heavy quarks (charm and beauty) are created in initial hard scattering processes and thus experience the whole spatial and temporal evolution of a HI collision (Fig. 20-5).

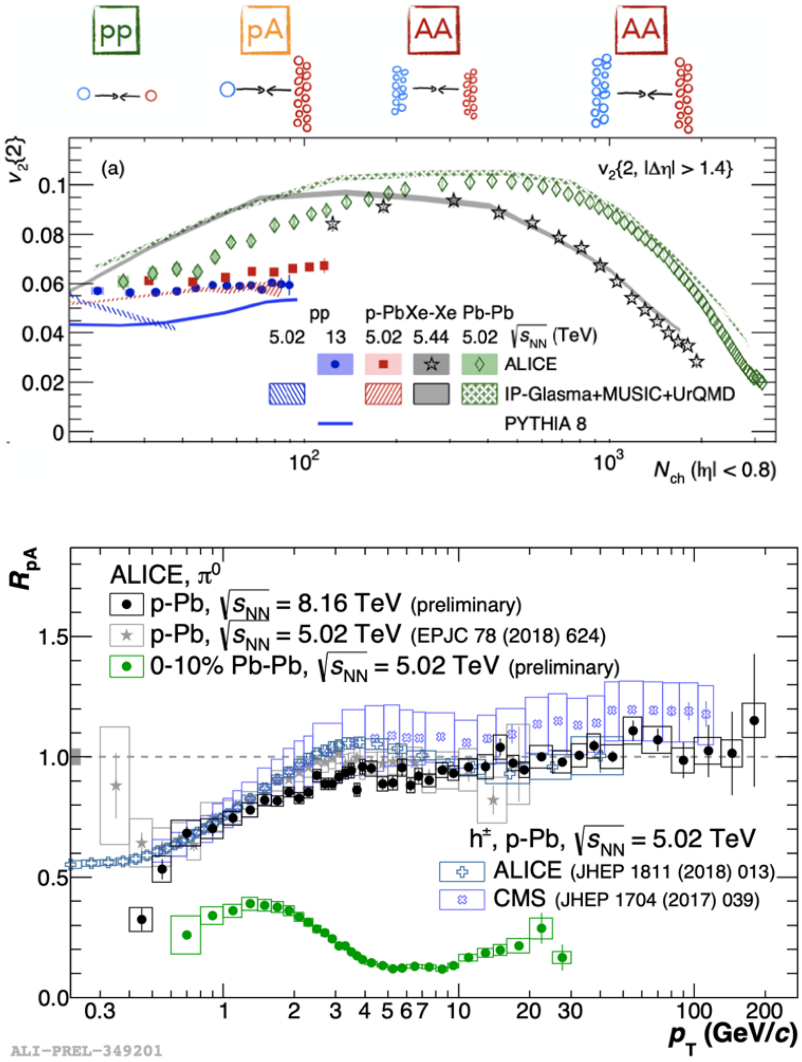


Fig. 20-5: Top: Elliptical flux coefficient v_2 as a function of charged multiplicity in pp, p–Pb, Xe–Xe and Pb–Pb collisions [592]. Bottom: Nuclear modification factor of π^0 mesons and charged hadrons in p–Pb and Pb–Pb collisions [593].

One expects $\Delta E_{\text{gluon}} > \Delta E_{\text{charm}} > \Delta E_{\text{beauty}}$, resulting in an expected ordering: $R^{\pi} \leq R^{D} \leq R^{B}$ for pions (mostly originating from gluons), D, and B mesons (Fig. 20-6 left). Figure 20-6 right shows that heavy quarks participate in the collective motion.

[592] Y. Pachmayer, Heavy Ions, Experimental Overview. https://arxiv.org/abs/2012.08832
ALICE Collaboration, Investigations of Anisotropic Flow Using Multiparticle Azimuthal Correlations in pp, p-Pb, Xe-Xe, and Pb-Pb Collisions at the LHC. https://journals.aps.org/prl/abstract/10.1103/PhysRevLett.123.142301
[593] ibid, https://arxiv.org/abs/2012.08832

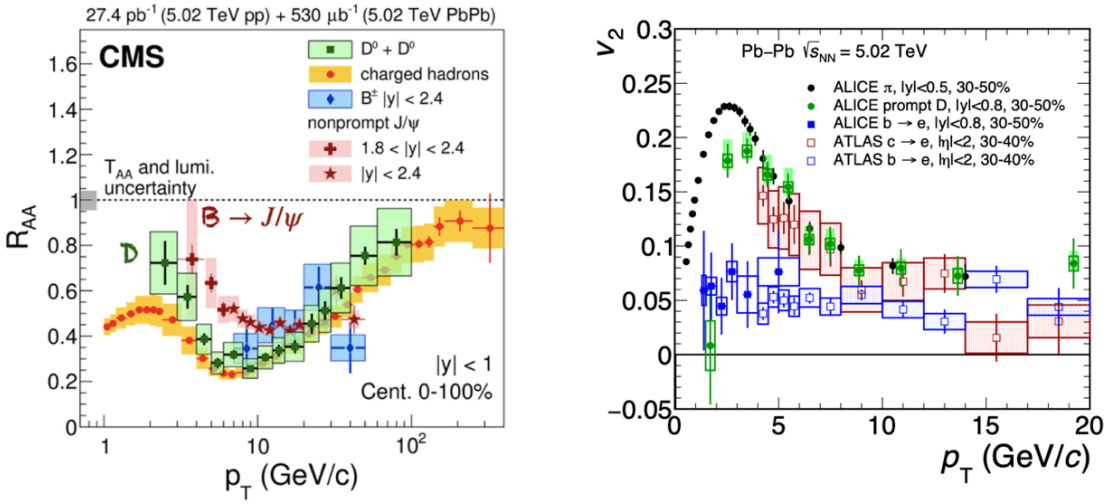


Fig. 20-6: Left: Nuclear modification factor R_{AA} of charged hadrons (mainly pions), prompt D mesons and $B^{\pm}$, non-prompt J/ψ versus p_T at 5.02 TeV [594]. Right: Elliptic flow v_2 of pions, prompt D mesons and electrons from charm and beauty-hadron decays in the same collision system [595].

20.2.4 Differential measurements of onia and evidence of deconfinement

Differential measurements of J/ψ mesons elucidate their mechanism of production, including regeneration, and provide evidence of deconfinement in Pb-Pb collision at full LHC energy [596] (Figs. 20-7 and 20-8).

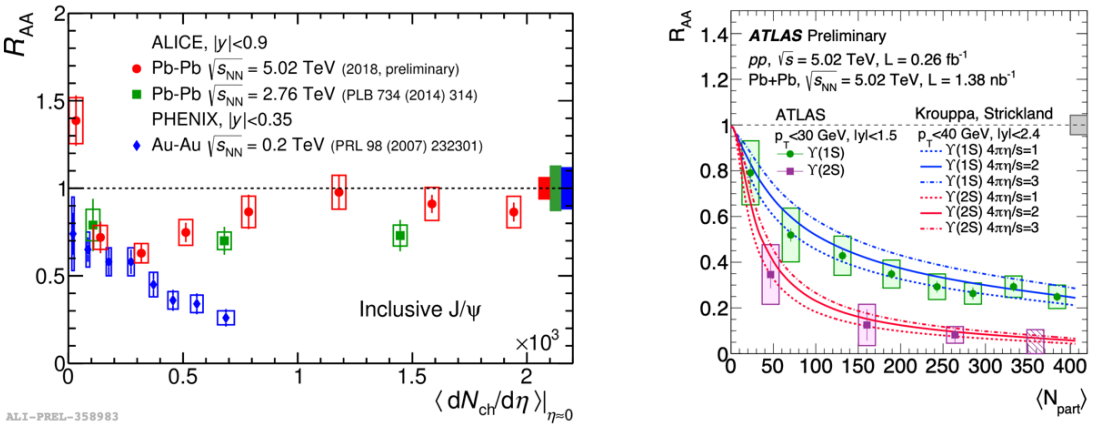


Fig. 20-7: R_{AA} of J/ψ (left) and Υ (right) as a function of charged particle density and average number of participants, respectively [597].

[594] CMS Collaboration, Nuclear modification factor of D^0 mesons in PbPb collisions at $\sqrt{s_{NN}}$ = 5.02 TeV. https://arxiv.org/abs/1708.04962

[595] ALICE Collaboration, Transverse-momentum and event-shape dependence of D-meson flow harmonics in Pb–Pb collisions at $\sqrt{s_{NN}}$ = 5.02 TeV. https://arxiv.org/abs/2005.11131

ATLAS Collaboration, Measurement of azimuthal anisotropy of muons from charm and bottom hadrons in Pb+Pb collisions at $\sqrt{s_{NN}}$ = 5.02 TeV with the ATLAS detector. https://arxiv.org/abs/2003.03565

Y. Pachmayer, Heavy Ions, Experimental Overview. https://arxiv.org/abs/2012.08832

[596] P. Faccioli and C. Lourenço, The fate of quarkonia in heavy-ion collisions at LHC energies: a unified description of the sequential suppression patterns. https://arxiv.org/abs/1809.10488

[597] Y. Pachmayer, Heavy Ions, Experimental Overview. https://arxiv.org/abs/2012.08832

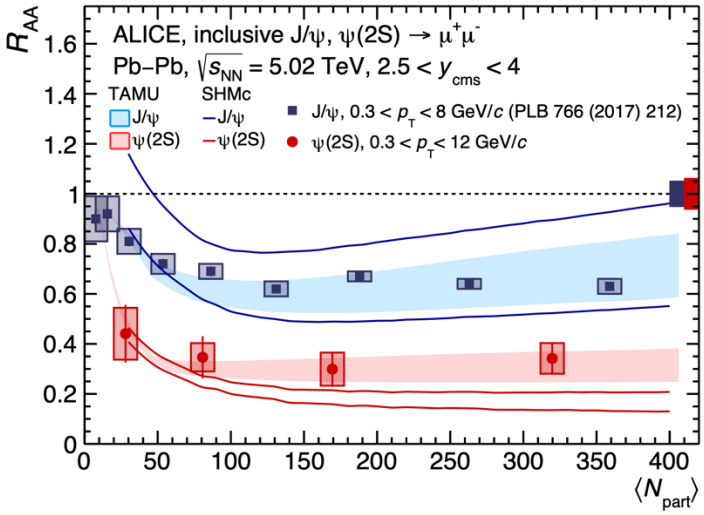


Fig. 20-8: R_{AA} for ψ(2S) and J/ψ versus centrality [598].

20.2.5 Study of rare probes

The abundance of data at the LHC makes it possible to study **rare probes** such as $\chi_{c1}(3872)$ and top-antitop production. $\chi_{c1}(3872)$ shows properties different from a conventional quark-antiquark bound state and is thus a candidate for an exotic structure. Measurements of antinuclear cross sections serve as information for searches for dark matter.

20.3 Conclusion

In brief, the expected features described at the start of this Chapter have been confirmed by decades of HI collisions at all energies. Following the conclusions of the excellent Ref. [599]:

In the most central HI collisions the initial energy density reached ***exceeds the threshold for QGP formation above*** $\sqrt{s_{NN}}$ ***= 10 GeV****. In the high energy range, this is shown by the measured charged-particle multiplicity* dN_{ch}/dy *and the brief time of hydrodynamization deduced from* ***elliptic flow****.*

From ***interferometry*** *of identical particles, one infers that the source of emitted hadrons is a* ***fireball of nuclear transverse size and a lifetime of 4–10 fm****, depending on the collision energy.*

Study of the ***collective flow patterns*** *allowed to* ***determine fluid properties of the QGP****. From the value of its shear viscosity (resistance to flow) one can consider QGP as* ***the most "perfect" fluid known.***

There is strong evidence that the collective flow is generated ***at the level of quarks not confined in hadrons.***

The enhancement of ***strange hadron production*** *compared to pp collisions and the behaviour of light hadrons give strong evidence for the* ***transition from hadronic matter to a deconfined QGP*** *at a temperature* $T_c \approx 155$ ***MeV****, as expected from lattice-QCD simulations.*

---

[598] J. Bielcikova, Experimental results from heavy ion collisions. https://inspirehep.net/files/a5d6d375b82cceaf84e6344fa5c3f36f ,
A. Dainese *et al.,* (ALICE Collaboration), Measurement of heavy-flavour production in proton–proton collisions at √s = 7 TeV with ALICE. PoS(ICHEP2022)008, https://arxiv.org/abs/1012.4036

[599] J. W. Harris and B. Müller, QGP Signatures revisited. https://doi.org/10.1140/epjc/s10052-024-12533-y and https://arxiv.org/abs/2308.05743

*The measured suppression pattern of **heavy quarkonium states,** especially the Υ states, and their sequential melting confirm the deconfinement of quarks and gluons in the QGP, with however a more complex behaviour than originally thought, as the reduced suppression at LHC of J/ψ, by **regeneration** at the phase boundary, showing that **charm quarks are deconfined in the QGP**.*

*Measurements of the spectrum of direct photons and the invariant mass spectrum of dileptons have yielded lower bounds for the temperature at which the QGP initially thermalizes. An unambiguous detection **of chiral symmetry restoration** [600] will require high-precision measurements of the lepton pair spectrum in the mass region $1 < M_{l^+l^-} < 2$ GeV.*

*The behaviour of **energetic quarks and gluons**, born from early hard scatters in the nuclear collision, informs on the energy loss of the primary parton on its path through the QGP, beginning with the suppression of the inclusive yield of high p_T hadrons in A+A collisions. The first observation as **a strong suppression of the high-p_T hadrons opposite in azimuth to a high-p_T trigger hadron was** extended to jets and di-jets, where a similar quenching of jets attributable to parton energy loss was observed.*

*The current understanding tells that the energy loss of the primary parton and the redistribution of its momentum within the jet is controlled by just **a few parameters** characterizing the medium. In a dense, thick medium, the **jet quenching parameter** encodes the transverse scattering power per unit length of the medium. The suppression factor R_{AA} of inclusive hadrons provides its direct measurement assuming that the energy loss of the primary parton is dominated by **gluon radiation** induced by scattering in the medium.*

20.4 Brief historical overview

The program started using ion-ion collisions, with for instance the NA35 experiment, putting the emphasis on 2-pion interferometry, NA36 and WA75 on strangeness production and WA80 on direct photons. A pioneering experiment was NA38, studying $\mu\mu$ production and J/ψ and ψ' suppression in p-Cu, p-U, 0-Cu, 0-U, S-U collisions at 200 GeV per nucleon [601]. A summary is given in Fig. 20-9 [602]. Early reviews of HI physics are presented in Ref. [603].

At CERN the lead beam programme started in 1994. A lead ion source was linked to the Proton Synchrotron (PS) and the SPS. The following large experiments measured various aspects of lead-lead and lead-gold collisions. They were NA44, NA45, NA49, NA50, NA52, NA57, NA60, NA61/SHINE, WA97, and WA98. Some were multipurpose detectors to measure and correlate several observable phenomena. Others were dedicated experiments focusing on rare signatures with high statistics. This co-ordinated and complementary effort was very successful.

Figure 20-10 [604], showing the yield of hyperons (left) and the evolution of J/ψ production (right), demonstrates that the SPS experiments were already well in the game.

---

[600] Before its restauration let us see its definition and breaking: D. Tong: Lectures on Gauge Theory, http://www.damtp.cam.ac.uk/user/tong/gaugetheory.html , see also Chapter 7. Chiral Symmetry Breaking. https://www.damtp.cam.ac.uk/user/tong/gaugetheory/5chisb.pdf , p. 243

[601] L. Kluberg, 20 years of J/ψ suppression at CERN SPS. *Eur.Phys.J.C 43 (2005) 145-156*

[602] https://upload.wikimedia.org/wikipedia/commons/c/c2/CERNSPSExp.pdf

[603] P. Sonderegger, Ultrarelativistic Heavy Ion Physics. https://lib-extopc.kek.jp/preprints/PDF/1994/9405/9405612.pdf W. J. Willis, The birth of relativistic heavy ion physics. CERN-EP/81-21 18 March 1981; https://indico.bnl.gov/event/572/contributions/14957/attachments/13279/16220/ZajcWillisSymposiumNew.pdf C. Lourenço, Heavy flavour production in heavy ion collisions: present status and future prospects, *156 AIP Conf.Proc. 459 (1999) 1, 147-156*

[604] J. W. Harris and B. Müller, "QGP Signatures" revisited. *Eur. Phys. J. C* 84, 247 (2024), https://doi.org/10.1140/epjc/s10052-024-12533-y

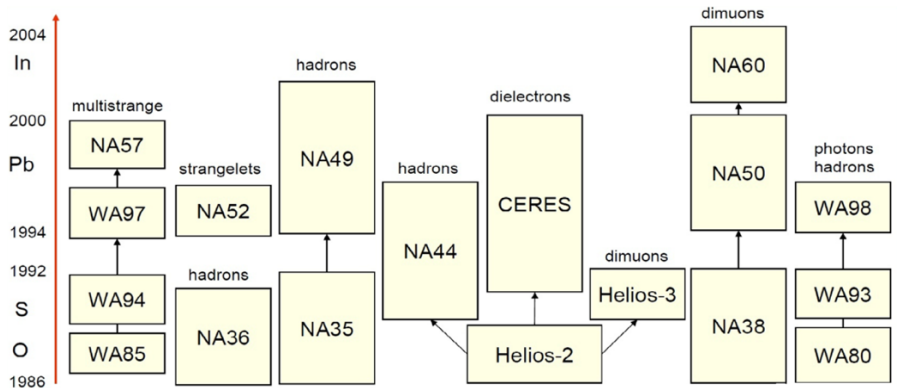


Fig. 20-9: The early HI experiments at CERN (figure by C. Lourenço).

.

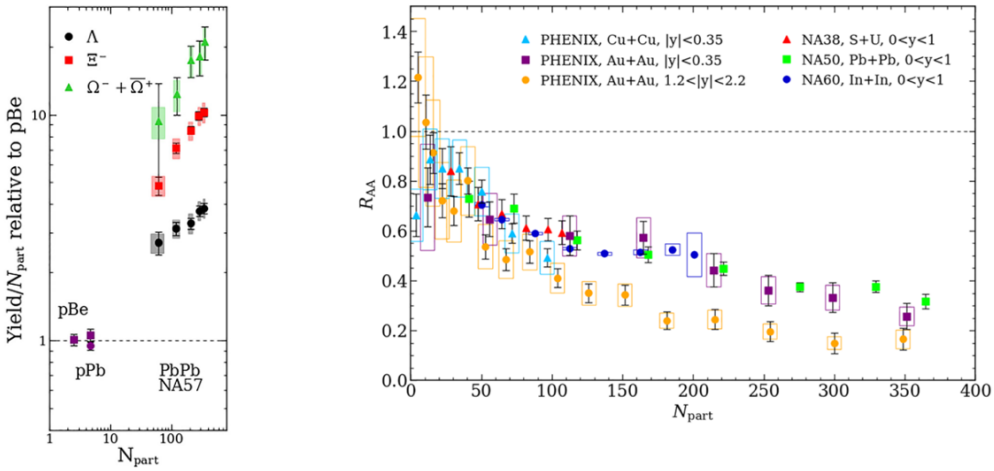


Fig. 20-10: Yield of hyperons (left) and the evolution of J/ψ production (right).

As said previously, a "*New State of Matter created at CERN*" was announced on 10 Feb 2000.

"The combined data coming from the seven experiments on CERN's Heavy Ion programme have given a clear picture of a new state of matter. This result verifies an important prediction of the present theory of fundamental forces between quarks. It is also an important step forward in the understanding of the early evolution of the Universe. We now have evidence of a new state of matter where quarks and gluons are not confined. There is still an entirely new territory to be explored concerning the physical properties of quark-gluon matter. The challenge now passes to the Relativistic Heavy Ion Collider at the Brookhaven National Laboratory and later to CERN's Large Hadron Collider."

The aim was then to study this newly produced matter at higher and lower temperature in order to fully characterize its properties and definitively confirm the quark gluon plasma interpretation. The focus indeed moved to **RHIC** [605] **and to LHC**, with in particular a dedicated heavy ion experiment, ALICE.

[605] Relativistic Heavy Ion Collider: https://www.bnl.gov/rhic/rhic.php and https://www.bnl.gov/rhic/spin.php
J. C. Hill, Highlights from the 17-Year Heavy Ion Program at the PHENIX Experiment at RHIC. https://inspirehep.net/files/86baa62622e9c44aea35bf9dfbc1199c
S. Kabana, Highlights from the STAR experiment at RHIC. https://arxiv.org/abs/1203.1814

The goal of RHIC Au-Au collisions program at $\sqrt{s_{NN}}$ = 200 GeV with initially 4 detectors was to identify the existence of the QGP by using "bulk probes", the majority of produced particles at low p_T, and "penetrating probes", less frequently produced particles such as heavy flavour, jets and identified particles at high p_T RHIC also run as a polarized proton collider [606], achieving a spin program with much impact on our understanding of the nucleon's spin structure (Chapter 5).

At LHC, the LHCb and CMS/ATLAS experiments are complementary. ALICE is unique for physics at low p_T and fully optimised (measurement, identification) for HI physics. LHCb is unique for its covering of the forward region and its capability of heavy flavour measurement. CMS/ATLAS have an angular covering complementary of ALICE and are better in reconstructing jets.

20.5 Searches with HI at colliders

Concerning these interesting searches, as for axion-like particles (ALPs), Ref. [607] illustrates them in Figs. 20-11 and 20-12 (see also Section 31.3).

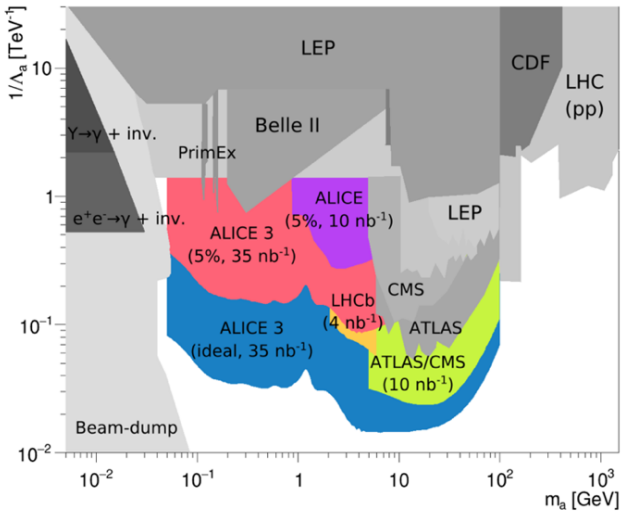


Fig. 20-11: Bounds in the (m_a, $1/\Lambda_a$) plane from existing (grey) and future (coloured, with HI at LHC) ALP searches. This figure will also be shown in Section 31.3 as Fig. 31-38.

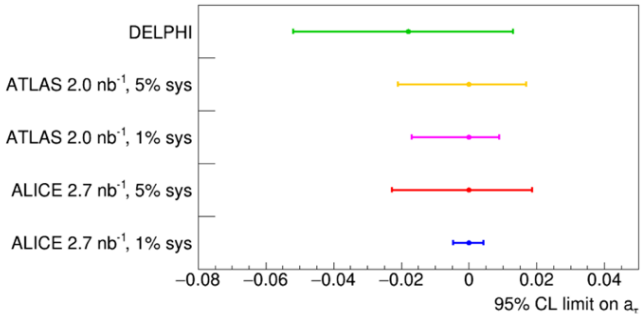


Fig. 20-12: Expected 95% CL limits on the anomalous e.m. moments of the tau, a_τ, by measurements from Pb Pb → Pb Pb ττ, through γγ, compared to DELPHI.

[606] A. Bazilevsky and for the RHIC Spin collaboration 2016, The RHIC Spin Program Overview. *J. Phys.: Conf. Ser. 678 012059,* https://iopscience.iop.org/article/10.1088/1742-6596/678/1/012059/pdf

[607] D. d'Enterria *et al.,* Opportunities for new physics searches with heavy ions at colliders. https://arxiv.org/abs/2203.05939

Let us close this section on HI with a spectacular fact [608] in off-centre collisions *"fast-moving positive charges should generate a very strong magnetic field, predicted to be 10^{18} gauss*". By comparison, neutron stars have fields of "only" about 10^{14} gauss.

20.6 On the ridges

A "ridge" in multiparticle final states of hadronic collisions is a positive correlation between two particles produced at similar azimuthal angles ϕ, spanning a large range in rapidity η.

More precisely, for **peripheral** heavy ion (HI) collisions the 2- particle correlation function (2PC) shows a sharp peak centred at (Δϕ, Δη) = (0, 0) and a broad structure (in Δη) at Δϕ ≈ π, referred to as "recoil", both predominantly originating from non-flow effects. In **high-multiplicity** collisions, in addition to the structure observed in low-multiplicity collisions, the 2PC reveals a broad structure (in Δη) at Δϕ ≈ 0, called the **"near-side ridge".** The distribution at Δϕ ≈ π is also broadened relative to peripheral collisions, consistent with the presence of a long-range component (the **"away-side ridge"**).

This was first observed in 2005 in HI collisions at the Relativistic Heavy-Ion Collider (RHIC) at Brookhaven (Fig. 20-13) [609] and since then at LHC. The observation in collisions other than HI collisions was made in 2010 by the CMS collaboration in **"high-multiplicity" proton-proton collisions** (Fig. 20-14) [610]. Soon after, CMS, ALICE and ATLAS observed the phenomenon also in collisions of p-lead nuclei.

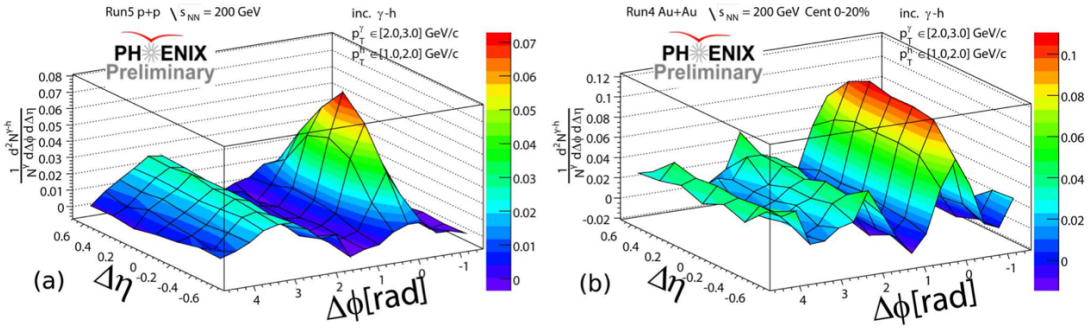


Fig. 20-13: Per trigger conditional yields for inclusive photons, $2 < p_T^{\gamma} < 3$ GeV, paired with charged hadron partners, $1 < p_T^{h} < 2$ GeV, in p+p and Au+Au collisions, (a) and (b) respectively.

This long-range correlation in η with a typically dominant cos(2Δϕ) modulation in azimuth is understood in HI collisions as a **signature of collectivity**. It corresponds to a sinusoidal modulation of the single-particle azimuthal angle distributions [611], believed to *"emerge from **fluctuating initial transverse collision geometries** varying weakly with rapidity and leading to anisotropic final particle distributions via the almost **perfect fluid evolution of the medium**".*

---

[608] Super Strong Magnetic Fields Leave Imprint on Nuclear Matter: Brookhaven Newsroom, https://www.bnl.gov/newsroom/news.php?a=121694

[609] M. P. McCumber, for the PHENIX Collaboration, The "Shoulder" and the "Ridge" in PHENIX. https://arxiv.org/abs/0804.4319
V. S .Pantuev, "Jet-Ridge" effect in heavy ion collisions as a back splash from stopped parton. https://arxiv.org/abs/0710.1882

[610] D. Velicanu, for the CMS collaboration, Ridge correlation structure in high multiplicity pp collisions with CMS. https://arxiv.org/abs/1107.2196

[611] For an event the ellipsoidal shape of the nuclear overlap region is rotationally asymmetric. One must then assume that from the event properties one can define a ϕ = 0 orientation, e.g. through the trigger (on jet, hard probes, etc.).

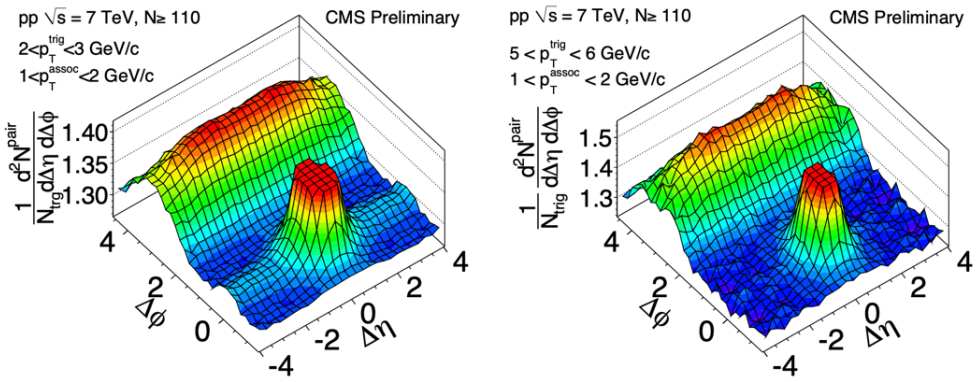


Fig. 20-14: Two-dimensional (2-D) per-trigger-particle associated yield of charged hadrons as a function of Δη and Δϕ with jet peak cut-off for better demonstration of the ridge from high multiplicity (N ≥ 110) pp collisions at √s = 7 TeV, for (a) $2 < p_T^{trig} < 3$ GeV and $1 < p_T^{assoc} < 2$ GeV and (b) $5 < p_T^{trig} < 6$ GeV and $1 < p_T^{assoc} < 2$ GeV.

However, the surprise is that two particle correlation measurements in **small systems like proton-proton** or proton-lead collisions show strikingly similar features to those in HI collisions, in particular this double ridge, and this asks for explanation, either similar or different.

Is the ridge still a collective phenomenon involving all of the particles in the event, or does it arise merely from contributions from a few of them, such as resonance decays, jets, or multi-jet production (so-called "non-flow")? Non-collective correlations in small systems are large and need special methods to be suppressed. ATLAS [612] was able to progress in that direction and Figs. 20-15 and 20-16 give evidence for the need of a sinusoidal component in the template fitting the data.

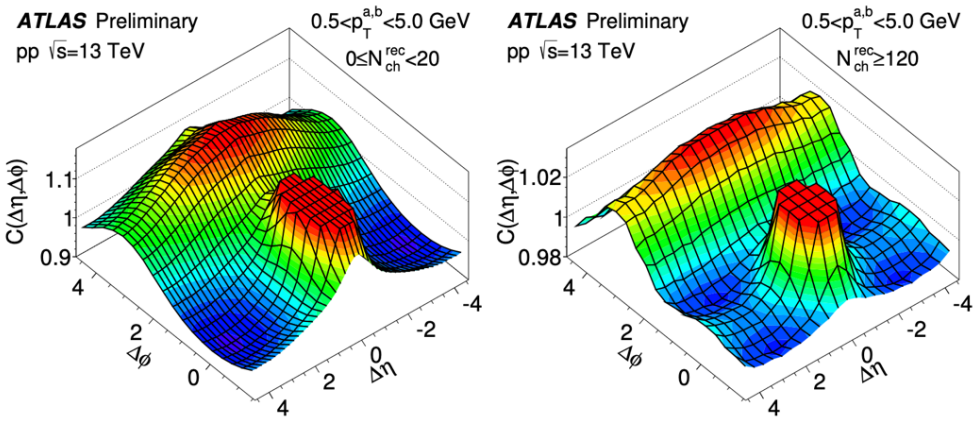


Fig. 20-15: Two-particle correlation function C (Δη, Δϕ) in 13 TeV pp collisions. With N_{chrec} > 120, the ridge is seen as the enhancement at Δφ near zero that extends over the full range of Δη.

A few facts seem to appear. For instance, the integrated near-side yield as a function of multiplicity seems independent of the collision energy.

[612] A. Trzupek, for the ATLAS Collaboration, Measurement of the ridge in pp and p+Pb collisions with the ATLAS detector at the LHC. https://cds.cern.ch/record/2214865/files/ATL-PHYS-PROC-2016-139.pdf?version=2
ATLAS Collaboration, New insight into the proton-proton ridge.
https://atlas.cern/updates/briefing/new-insight-proton-proton-ridge

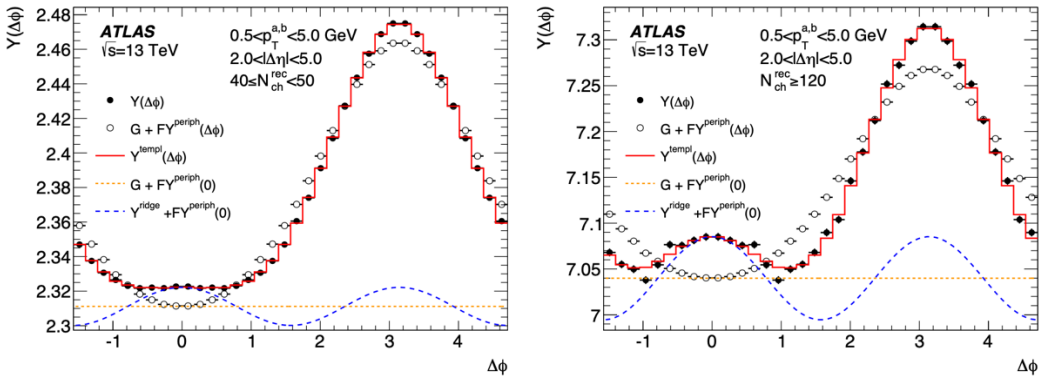


Fig. 20-16: Per-trigger-particle yields, Y(Δϕ), for $0.5 < p_T^{a,b} < 5.0$ GeV in different N_{ch}^{rec} intervals in 13 TeV pp data. Results are shown for $40 \le N_{ch}^{rec} < 60$ (left) and for $N_{ch}^{rec} \ge 120$ (right). The open points and curves show components of the template.

It is then quite natural to try to **relate the observations to a model of the proton**, more precisely of high energy colliding protons. Following theoretical developments, several phenomenological models of the proton structure were proposed, from which the anisotropy coefficients could be calculated.

A proposal made in Ref. [613] is that the origin of these events is due to *the inelastic collisions of **aligned gluonic flux tubes** that underlie the colour confinement of the quarks in each proton* (Fig. 20-17). Then one could expect that high-multiplicity hadronic ridges may also appear in the high energy γ–γ collisions in ultra-peripheral p-p LHC collisions or at a high energy e^+e^- collider.

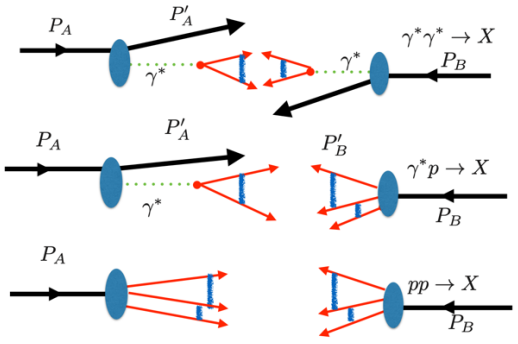


Fig. 20-17: Collisions of flux tubes in γ–γ, γ–p and p–p reactions at the LHC.

More radically, according to Ref. [614], one should recourse to the **colour glass condensate (CGC) effective theory of high-energy QCD** [615]. Two hadrons in HE collision are then visualized as **sheets of**

[613] S. J. Brodsky *et al.,* Ridge Production in High-Multiplicity Hadronic Ultra-Peripheral Proton-Proton Collisions. https://arxiv.org/abs/1708.07173 ,
J. D. Bjorken *et al.,* Possible multiparticle ridge-like correlations in very high multiplicity proton-proton collisions. SLAC-PUB-15352, https://arxiv.org/abs/1308.1435

[614] L. McLerran, A Brief Introduction to the Color Glass Condensate and the Glasma. https://arxiv.org/abs/0812.4989
A. Dumitru *et al.,* The ridge in proton–proton collisions at the LHC.
https://www.sciencedirect.com/science/article/abs/pii/S0370269311000487

[615] J. Schukraft, Heavy Ion Physics at the LHC: What's new? What's next? https://arxiv.org/abs/1311.1429
The CGC is a 'first principles' classical field theory approximation to QCD which is applicable to very dense (high occupation number) parton systems like those found at small-x and small Q^2 in the initial state wave function of hadrons.

coloured glass. These classical fields, prior to the collision, are **transverse** to the direction of motion and confined to the region of thin sheets (Fig. 20-18, left). *"In the time it takes light to travel across the thin sheets, the sheets become charged with colour electric and colour magnetic charge. This results in **longitudinal** colour electric and colour magnetic fields between the sheets."* (Fig. 20-18, right)



Fig. 20-18: Left: classical fields, prior to the collision, are transverse to the direction of motion. Right: longitudinal colour electric and colour magnetic fields between the sheets [616].

That the integrated near-side yield as a function of multiplicity is independent of collision energy could result naturally from the fact that *"multiparticle production is driven by a **single semihard saturation scale** in the colour glass condensate framework"* [617].

But one could also imagine that some BSM effect is at play. For instance, Ref. [618] considers the possibility *that a new stage of matter, stemming from hidden/dark sectors beyond the Standard Model, to be formed in pp collisions at the LHC, can significantly modify the correlations among final-state particles.*

Adding pA results, the situation is not settled. But one can say, as Ref. [619], that the LHC ridge discovery in pp and pA is important. If a Quark Gluon Plasma (**QGC-like**) state can be created and studied in smaller systems than foreseen, comparing pp, pA and AA may reveal precious information on correlation lengths and relaxation time scales. On the contrary, if the answer rests on initial state effects and saturation physics, another new state of matter, **the colour glass condensate**, has been observed.

[616] L. McLerran, A Brief Introduction to the Color Glass Condensate and the Glasma. https://arxiv.org/abs/0812.4989
[617] K. Dusling *et al.,* Energy dependence of the ridge in high multiplicity proton-proton collisions. https://doi.org/10.1103/PhysRevD.93.014034
[618] M. A. Sanchis-Lozano and E. K. Sarkisyan-Grinbaum, Signatures of new physics versus the ridge phenomenon in hadron–hadron collisions at the LHC. https://arxiv.org/abs/1808.01463
[619] J. Schukraft, Heavy Ion Physics at the LHC: What's new ? What's next ? https://arxiv.org/abs/1311.1429

21. The LHC challenges

The physical landscapes of an e^+e^- collider and a hadronic collider are very contrasted. In the first the projectiles are elementary. Besides electromagnetic radiation, the total CM energy is available for the collision. In the second, interesting collisions take place between elementary objects, quarks and gluons, distributed in momentum according to their structure functions (Chapter 5), with an average energy substantially lower than the nominal energy of the machine, E_{beam} = 7 TeV, typically by an order of magnitude, but with higher energy tails. Nevertheless, the much higher energy accessible to protons, a factor of 70 between LHC and LEP nominal energies, offers higher energy collisions at reduced luminosity and at the cost of an unavoidable and intense rate of interactions. This high rate imposes drastic conditions to the detectors.

The usual motto that the former is a measuring machine and the latter a discovery machine is only a partial truth, not supported by history. The e^+e^- collider**, a threshold machine**, can discover if it has sufficient energy. The hadronic collider, to discover in spite of the background, may need to resort to very discriminating but rare modes. However, it has also proven that, at the cost of complex analyses to master systematics, it can provide high-precision measurements of key quantities.

In 1984, a year after the discovery of the W and Z bosons, a workshop was held in Lausanne [620] where the first ideas were discussed on a possible proton-proton collider and the associated experiments to search for the Higgs boson. The aim was to re-use the LEP tunnel after the end of the LEP programme. Among the main protagonists were the scientists of the UA1 and UA2 experiments. An exploratory machine was needed to cover the wide range of possible SM Higgs boson mass values, its various production mechanisms and decay signatures, and to discover any new high-mass particles at a centre-of-mass energy ten times higher than previously explored.

A hadron (proton-proton) collider is such a discovery machine as long as energy and instantaneous luminosity, L, measured in $cm^{-2}s^{-1}$, are large enough. We recall that the event rate of a given process is determined by $L \times \sigma$ where σ is its production cross-section, measured in units of cm^2.

The most interesting and easily detectable final states at a hadron collider involve **charged leptons** (Chapter 12) and **photons** and have low $\sigma \times BR$, where BR is the branching ratio in the decay mode of interest.

Elucidating the mechanism of EW symmetry breaking was therefore a major objective of LHC. It was also clear that new physics at the TeV energy scale had to be sought for because the SM is incomplete.

The LHC and its experiments were designed to find new particles, new forces and new symmetries which could include the Higgs boson(s), supersymmetric particles, Z' bosons or evidence of spatial extra dimensions [621]. A "general purpose" experiment that could detect all these hypothetical particles gave the best opportunity to discover anything that could be produced at LHC [622]. Two of them were needed for an **imperative mutual cross-checking.**

The many orders of magnitude existing between the cross-section of the most interesting processes and the total pp cross-section dictate drastic conditions for the LHC and its detectors (Fig. 21-1) [623].

---

[620] Workshop on the Feasibility of Hadron Colliders in the LEP Tunnel, Organized under the Joint Sponsorship of ECFA and CERN. https://inspirehep.net/files/8ac1885184c4fbb6e217a9431aa6dc86 , (1984)

[621] F. Pauss, Beyond the Standard Model in pp collisions. ECFA LHC-Workshop, Aachen, Oct. 1990, https://cds.cern.ch/record/215072/files/cer-000127371.pdf

[622] F. Pauss and M. Dittmar, Experimental Challenges at the LHC. https://arxiv.org/abs/hep-ex/9901018

[623] J. M. Campbell, J. W. Huston and W. J. Stirling, Hard interactions of quarks and gluons: a primer for LHC physics. https://arxiv.org/abs/hep-ph/0611148

For the detector design [624], the LHC challenges could be summarized by the following numbers:

- ~ 4×10^7 bunch crossings/s
- ~ 25 interactions/crossing
- ~ 10^9 events /s
- ~ 100 particles /event
- ~ 1MB / event

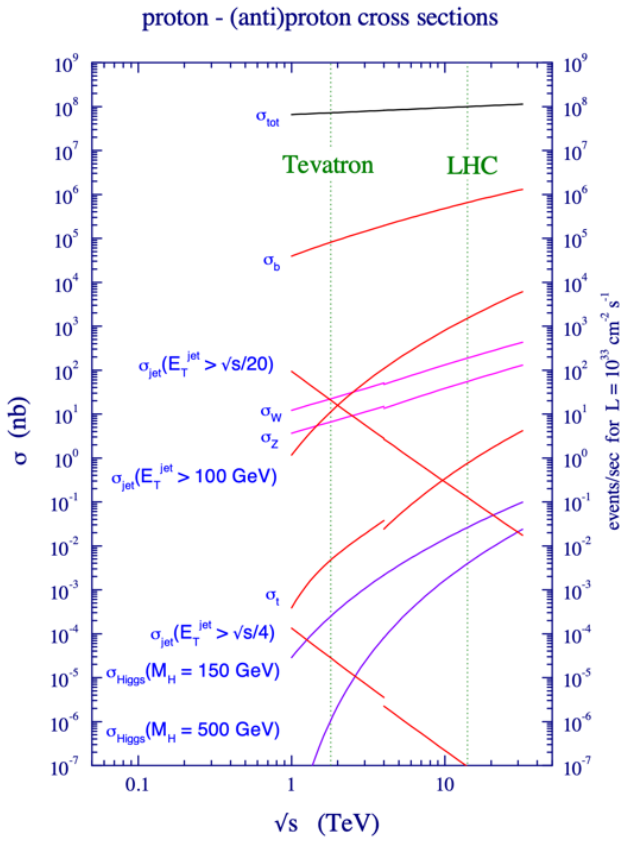


Fig. 21-1: Standard Model cross sections at the Tevatron and LHC colliders as function of √s.

Hence the four challenges for detectors are these:

- a high number of independent channels;
- a very strong irradiation;
- a very selective triggering performed in two levels: $10^9 \rightarrow 10^5$, then $10^5 \rightarrow O(10^3)$ events recorded;
- a very large volume of information at all levels.

In the machine (Fig. 21-2) there are ~ 3000 bunches of ~ 10^{11} protons in each bunch, despite the infinitesimal energy of each proton [625], match to the one of a TGV. Hence a lot of precautions and collimations are needed to avoid any possible damage to machine and detectors.

[624] Some of these numbers have been largely exceeded

[625] The kinetic energy of a little mosquito localized in a domain of Fermi size results in a **huge energy density,** about the one of our U-128niverse at a picosecond of age.

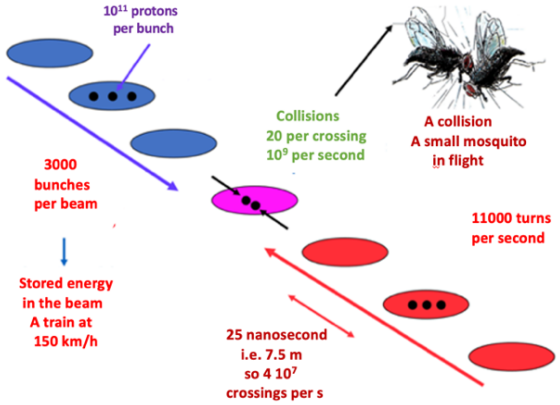


Fig. 21-2: The pattern of bunch crossing.

Concerning the region of interaction: at each bunch crossing, a few cm long by 10 to 15 microns transversely (Fig. 21-3), a high number of collisions occur, each creating many particles (Fig. 21-4, artist view from ATLAS). The high performance of vertex detectors has overcome the problem of disentangling this complex situation. But, in addition to the **spatial resolution**, the current attempt is to improve the **time resolution**, a challenging goal because one must aim for a resolution of 15–20 ps (Fig. 21-5).

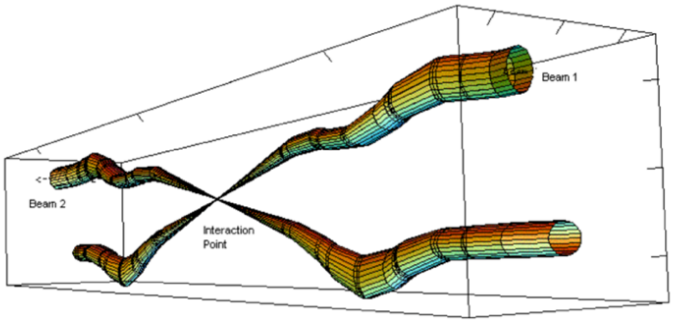


Fig. 21-3: Beams interacting: relative beam sizes around interaction point at collisions.

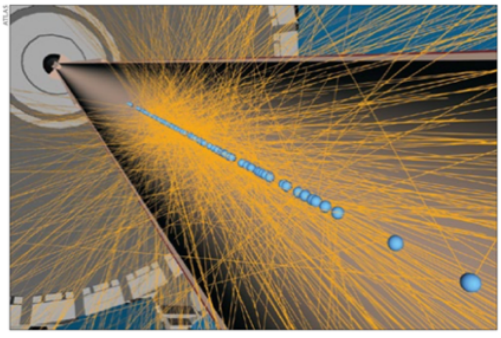


Fig. 21-4: Crowd in interaction region [626].

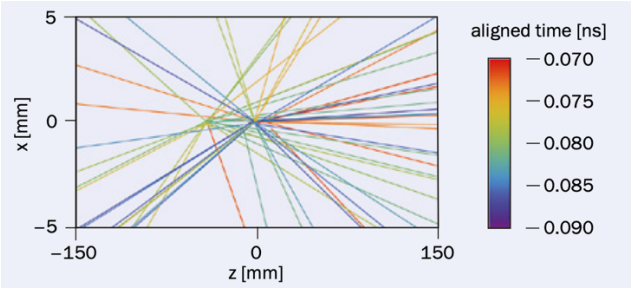


Fig. 21-5: The time window needed [627].

[626] Artist view from ATLAS, https://atlas.cern/Updates/Feature/High-Luminosity-ATLAS
[627] LHCb Looks Forward to the 2030s, CERN Courier 63 no 2 p. 23:
https://cds.cern.ch/record/2857133/files/CERNCourier2023MarApr-digitaledition.pdf

Figure 21-6 shows under which luminosity and pile up conditions data were taken in 2023 [628]. Figure 21-7 illustrates the mean number of interactions per crossing during the data taking period 2011 to 2025 as observed by ATLAS [629].

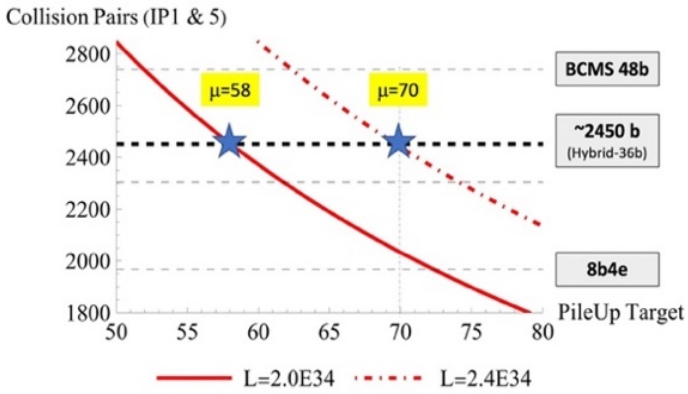


Fig. 21-6: Number of bunches versus pile up.

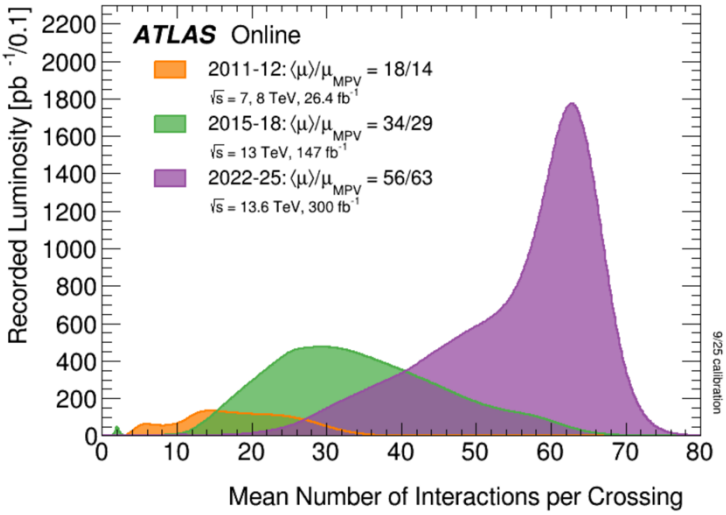


Fig. 21-7: Beam conditions for ATLAS: luminosity-weighted distribution of the mean number of interactions per crossing as measured by ATLAS. the mean μ value, and the most probable (MPV) μ value are given for data taking periods from 2011 till 2025.

[628] F. Moortgat, private communication
[629] ATLAS Collaboration, https://twiki.cern.ch/twiki/bin/view/AtlasPublic/LuminosityPublicResultsRun3

22. LHC: from doubts to confidence

At the LHC Lausanne meeting in 1984 [630], Christopher Llewellyn Smith showed a certain pessimism concerning the visibility of the Higgs boson: *"Extensive studies of Higgs boson production were reported at Lausanne, which lead to the conclusion that discovering a conventional heavy Higgs boson will be difficult even at 20 TeV, the energy we assume in the following discussion."*

But things improved: M_{top} turned out to be higher (see Chapter 24 for explanation) than expected, in La Thuile 1987 [631] the bold decision to **aim at a luminosity of 10^{34} $cm^{-2}s^{-1}$** was suggested (10 times more than first considered) and LEP indicated indirectly a rather **light Higgs Boson**. A massive R&D program started, led by the Detector Research and Development Committee (DRDC) [632].

"Politically", let us recall that the LHC had to face the competition of the US SSC (Section 10.13) until, in October 1993, the US Congress officially cancelled the project [633]. One can underline the major role of the Council President Hubert Curien concerning the arrival of the LHC.

Nevertheless, doubts about the ability to face such a luminosity in open detectors existed. A quote [634]: *"An extreme case… would be that of a special intersection region with a luminosity of 5 × 10^{34} $cm^{-2}s^{-1}$, 50 times larger than the standard LHC luminosity. In this high-luminosity region, only a "beam-dump" experiment with muon detection would probably survive."*

Figure 22-1 shows in its first incarnation what would become CMS. Figure 22-2 illustrates the doubts existing about the exploitation of the huge luminosities foreseen.

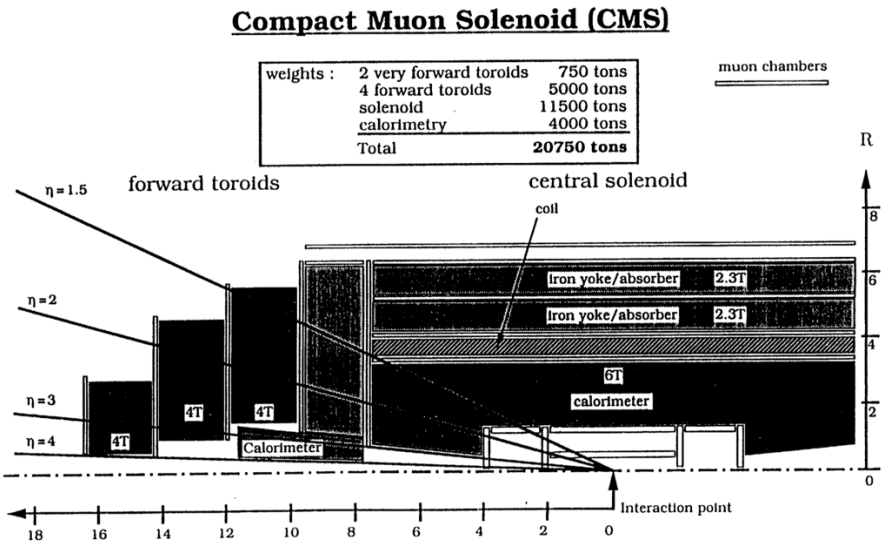


Fig. 22-1: First appearance of what CMS will be [635].

[630] C. Llewellyn Smith, The Physics Case: Physics with a multi TeV hadron collider. *Conf.Proc.C 840321 (1984) 27-48,* ECFA 84/85 CERN 84-10 p. 38: https://cds.cern.ch/record/397209
CERN-87-07-V-1, CERN-YELLOW-87-07-V-1, https://cds.cern.ch/record/179654?ln=de
[631] The feasibility of experiments at high luminosity at the Large Hadron Collider (1988): https://cds.cern.ch/record/187254
[632] C. Llewellyn Smith, Genesis of the Large Hadron Collider.
https://royalsocietypublishing.org/doi/pdf/10.1098/rsta.2014.0037
[633] D. Appell, The Supercollider That Never Was.
https://www.scientificamerican.com/article/the-supercollider-that-never-was/
[634] D. Froidevaux, Experimental Studies in the Standard Theory Group. https://cds.cern.ch/record/371343/files/61.pdf
[635] M. Pimia, Compact Muon Solenoid. HU-SEFT-1990-03, http://cds.cern.ch/record/215207/files/p547.pdf ,
https://cds.cern.ch/record/215207

ANSWERS TO PROFESSOR LORENZO FOA

QUESTION 0:
General question that concerns all experiments: What can your e.m. calorimeter do in a "stand alone" mode, I mean if you have to switch off your inner tracking because of excessive rate ?

We would like to distinguish between two scenarios, namely:

i) all inner tracking fails. We consider this to be an unlikely scenario.

ii) tracking is still possible in the area close to the calorimeters i.e. the last four points are still measurable. We would like to stress that the 4 T field considerably reduces the density of charged tracks in the outer regions of the tracking cavity. Even if we have underestimated the minimum bias background by a factor of 10 the occupancies in this region will remain below a few percent. We do not believe that beam related backgrounds would drastically affect this region which is ≥ 1.2 m from the beam-line in the barrel.

Fig. 22-2: Picturesque exchange in the LHCC [636].

Undertaking the LHC required a complete vision of the situation of technologies **and their derivatives with time**: Figure 22-3 shows the future as seen from 1997, assuming realizing LHC in 2004. We see for example that the needed bandwidth of the switching network was considered as a critical point.

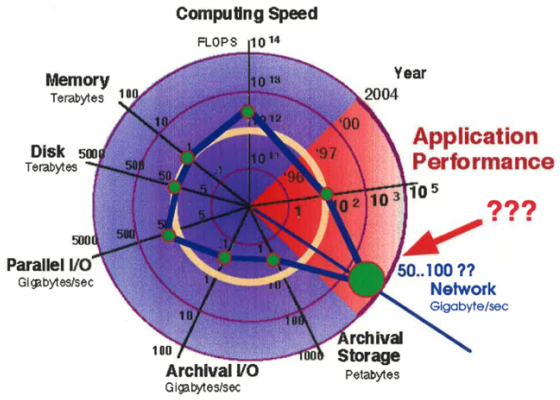


Fig. 22-3: "Rose des vents" of data acquisition system (DAS) technologies, from Sergio Cittolin [637].

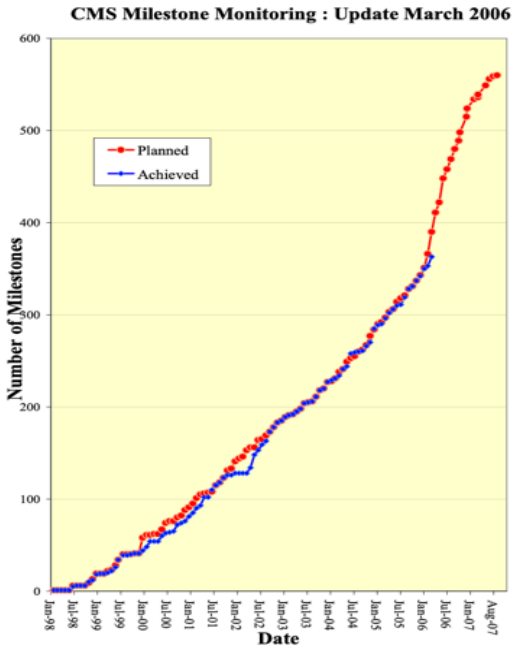


Fig. 22-4: A continuous progress monitoring!

[636] In P. Sphicas, CMS@30 celebration, 2022. CMS Week 2022 12. https://indico.cern.ch/event/1180059/contributions/5131626/attachments/2561693/4416364/CMSWeek-2022-12-Sphicas.pdf

[637] ibid

The realization of the large multipurpose detectors was a progressive and extremely **carefully monitored** process with many milestones to pass (Fig. 22-4) and a few hard choices to make. The actual LHC planning was not exactly what was foreseen in the early nineties (Fig. 22-5).

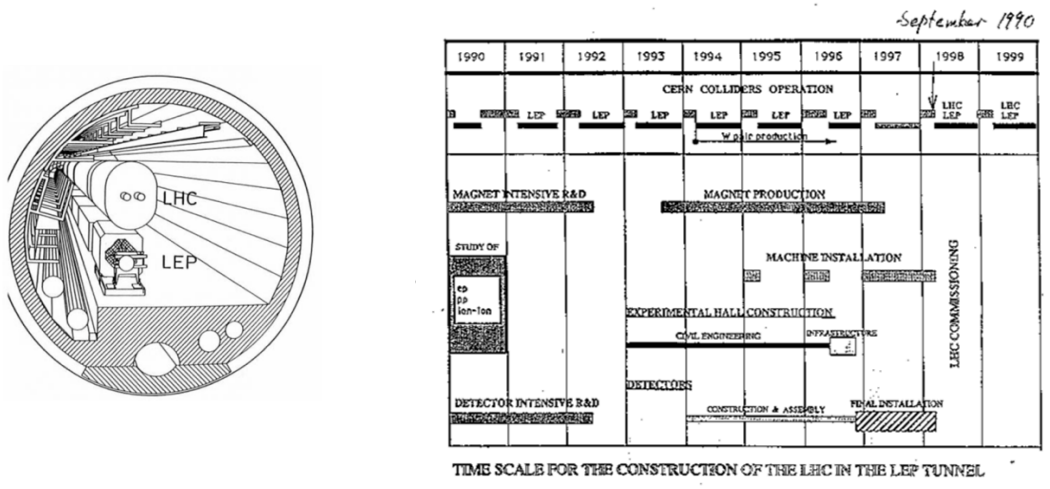


Fig. 22-5: The 1990 planning of LHC coexisting with LEP [638]. The left figure is from Ref. [639].

But it was worth waiting: what a great machine!

Not only the 10^{34} $cm^{-2}s^{-1}$ luminosity was reached and exploited, but bolder steps are on the way (Fig. 22-6), which will culminate with **the High Luminosity LHC (HL-LHC)** in about 2029. This new challenge obviously implies major upgrades and changes for the machine and for the detectors [640].

What an impressive landscape the LHC detectors offer! Besides the boson discovery, many measurements were performed. A subtle spectroscopy of low mass states performed at full luminosity (Fig. 22-7, see Chapter 28) swept all doubts about the performance of detectors. Another impressive example is shown in Figs. 22-8 and 22-9.

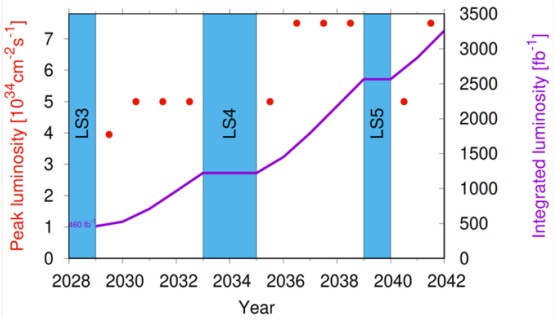


Fig. 22-6: Prospects for the peak and integrated luminosity for LHC [641].

[638] P. Jenni, The Story of the LHC Project, the Higgs Discovery and Beyond. https://indico.in2p3.fr/event/12358/attachments/7333/9006/P.Jenni.CPPM.LHCproject.13Nov2015.pdf

[639] The Future of CERN. https://cds.cern.ch/record/1950870/files/36-39%20en.pdf

[640] M. Mlynarikova for the ATLAS and CMS Collaborations, Higgs Physics at HL-LHC. https://arxiv.org/abs/2307.07772
G. Apollinari *et al.,* High Luminosity Large Hadron Collider (HL-LHC). https://arxiv.org/abs/1705.08830
Z. Citron for the ATLAS Collaboration, The ATLAS Upgrade Program.
https://inspirehep.net/files/abad4e22b52db6c48ed0c82e217a7839
M. Mannelli, The CMS HL-LHC Phase II upgrade program: Overview and selected highlights.
https://inspirehep.net/files/f3ba83db06d10af8e5a9563c5346ab2e
M. Zerlauth and O. Brüning, Status and Prospects of the HL-LHC Project.
https://inspirehep.net/files/8f6dffee31ce7227fb9528ae7137692e

[641] O. Brüning and M. Zerlauth, LHC Status – 2023. https://inspirehep.net/files/a1a8018a00cc629573a4a80d1017549f

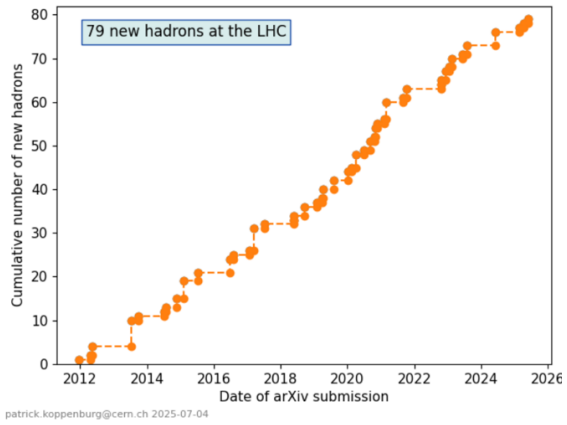


Fig. 22-7: An avalanche of new hadrons [642].

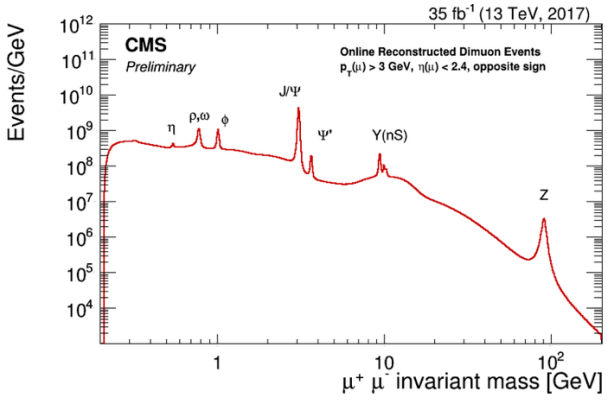


Fig. 22-8: The full dimuon scenery in one picture [643].

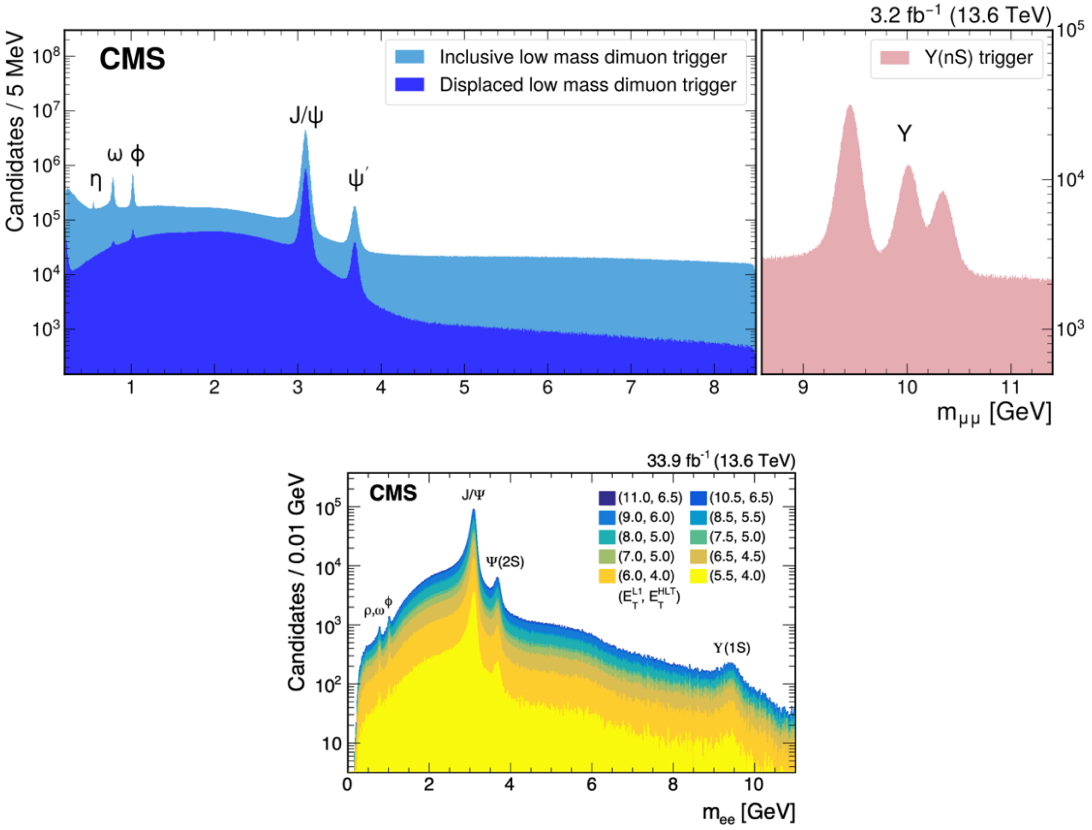


Fig. 22-9: CMS two lepton mass spectrum: Top: dimuon mass spectra obtained from data recorded in 2022. Bottom: The invariant mass distribution for pairs of oppositely charged electrons originating from a common vertex [644].

[642] P. Koppenburg, New particles discovered at the LHC. https://www.koppenburg.ch/particles.html
[643] CMS Collaboration: https://twiki.cern.ch/twiki/bin/view/CMSPublic/HLTDiMuon2017and2018
CMS Collaboration, Enriching the Physics Program of the CMS Experiment via Data Scouting and Data Parking. https://arxiv.org/abs/2403.16134
[644] ibid

23. Instrumental highlights of LHC

The role of physicists, builders and leaders of the LHC experiments has been rightly acknowledged and praised. One could also focus attention on the key contribution of **technical coordinators** of these huge detectors and **experts** in instrumentation who contributed to various highlights. The same is also obviously true **on the machine side**, in all aspects, magnets, radiofrequency, cryogeny, ultravacuum, etc., as illustrated in Section 23.2.

23.1 Images of some instrumental breakthroughs

Some major instrumental breakthroughs are shown in Figs. 23-1 and 23-2. An overview of these achievements can be found in Ref. [645] and [646]. New forward detectors as FASER (Fig. 23-3), etc., are now at work [647].

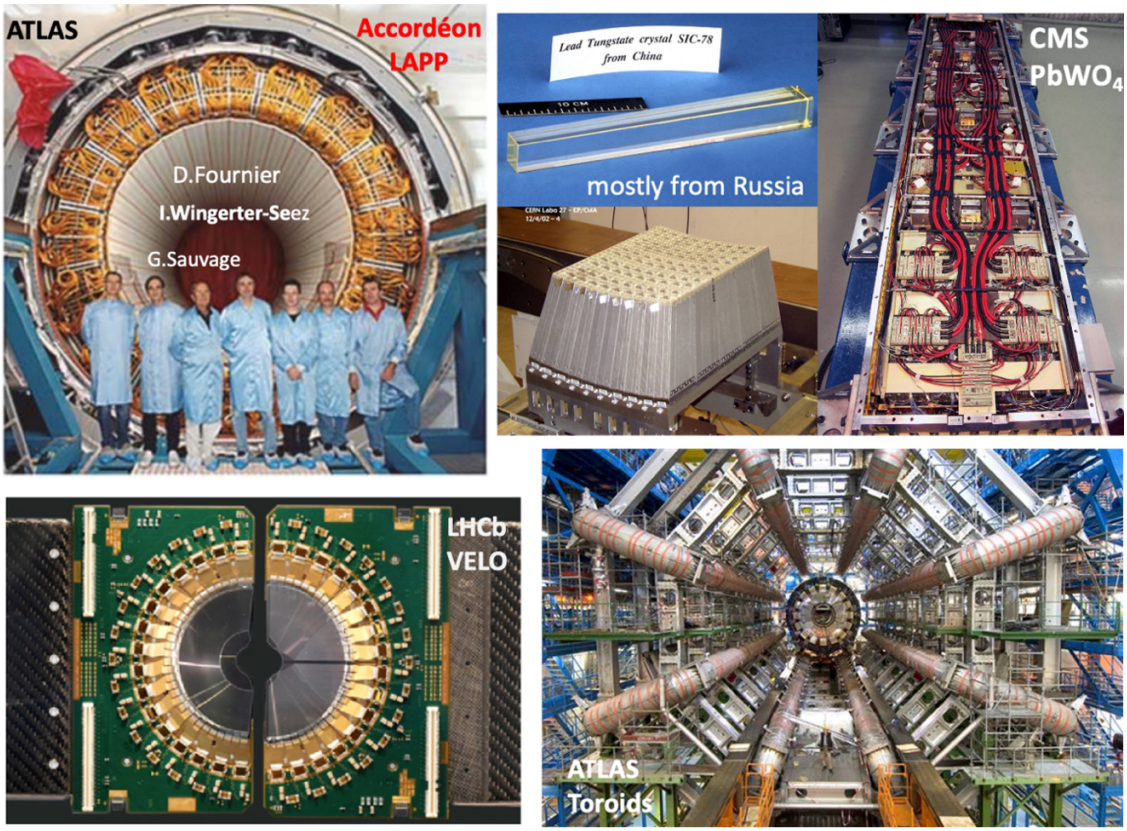


Fig. 23-1: Major instrumental breakthroughs [648].

[645] D. Froidevaux, Integration of Detectors into a Large Experiment: Examples from ATLAS and CMS. https://inspirehep.net/files/f2ad7fa061e17fdef13533e2883dd3fa

[646] G. Brianti and P. Jenni, The Large Hadron Collider (LHC): The Energy Frontier. In Technology Meets Research: https://inspirehep.net/files/d59e7aaf7b366b4da3ed4a0798e7a8e9 , p. 263

[647] L. A. Anchordoqui, Looking forward to forward physics at the CERN's LHC. https://arxiv.org/abs/2205.12413

[648] For the large calorimeters: T. Virdee, Two Approaches to High Resolution Electromagnetic Calorimetry. In Technology Meets Research: https://inspirehep.net/files/d59e7aaf7b366b4da3ed4a0798e7a8e9 , p. 300
For the large LHC magnets: A. Hervé, P. Jenni. T. Taylor, Giant Magnets for Giant Detectors. ibid p. 318
For the Si detectors: L. Rolandi, Large Silicon Trackers: Fast, Precise, Efficient. ibid p. 296

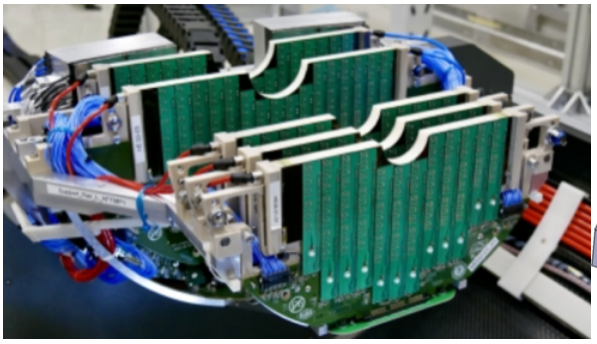


Fig. 23-2: ALICE muon spectrometer.

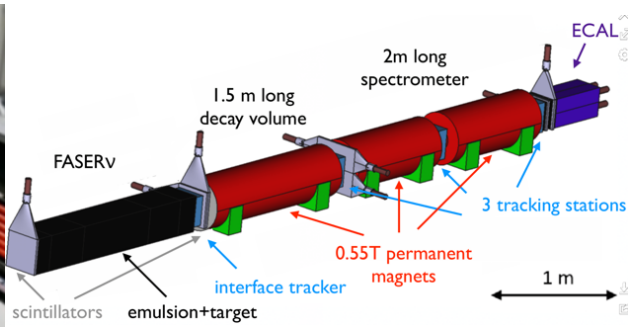


Fig. 23-3: The FASER proposal.

23.2 Details about the main highlights

Without much text, the next pages show much more details about the main highlights and refer to major experts (Figs. 23-4 to 23-12). This is borrowed from the book *Technology meets Research*, in free access at [649]. Concerning CCT (canted cosine theta) magnets and their prototyping see Ref. [650].

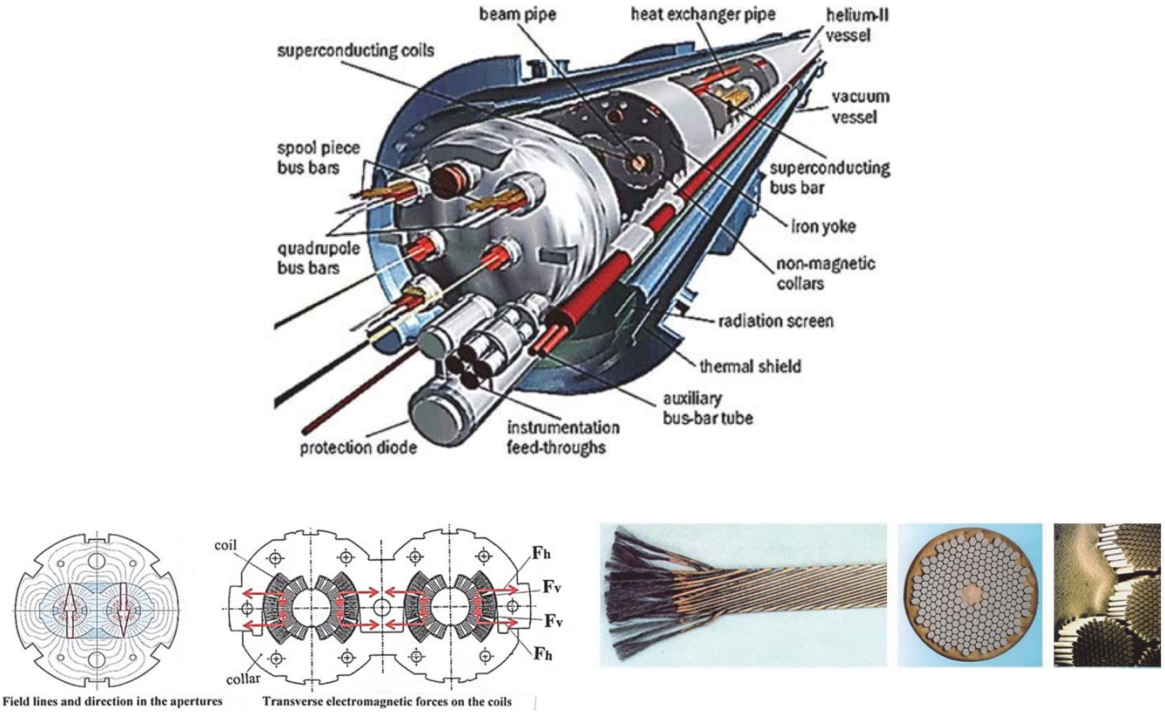


Fig. 23-4: The LHC magnets [651]. Top: cut-away view of the 15 m long superconducting dipole. Bottom left: field and forces in the twin aperture magnet. Bottom right: a flat LHC cable, a strand and groups of Nb-Ti filaments in a strand.

[649] Technology meets Research: https://inspirehep.net/files/02de568d4897c555515de27f0b96af4d
[650] L. N. Brouwer, Canted-Cosine-Theta Superconducting Accelerator Magnets for High Energy Physics and Ion Beam Cancer Therapy. https://escholarship.org/uc/item/8jp4g75g
M. Koratzinos, HTS variant to QC1 magnet. https://agenda.infn.it/event/37720/contributions/212723/
[651] R. Perin, Superconducting Magnets: Powerful, Precise, Plentiful. In Technology meets Research: https://inspirehep.net/files/d59e7aaf7b366b4da3ed4a0798e7a8e9 p. 278



Fig. 23-5: Beam screen and vacuum tube coating [652].

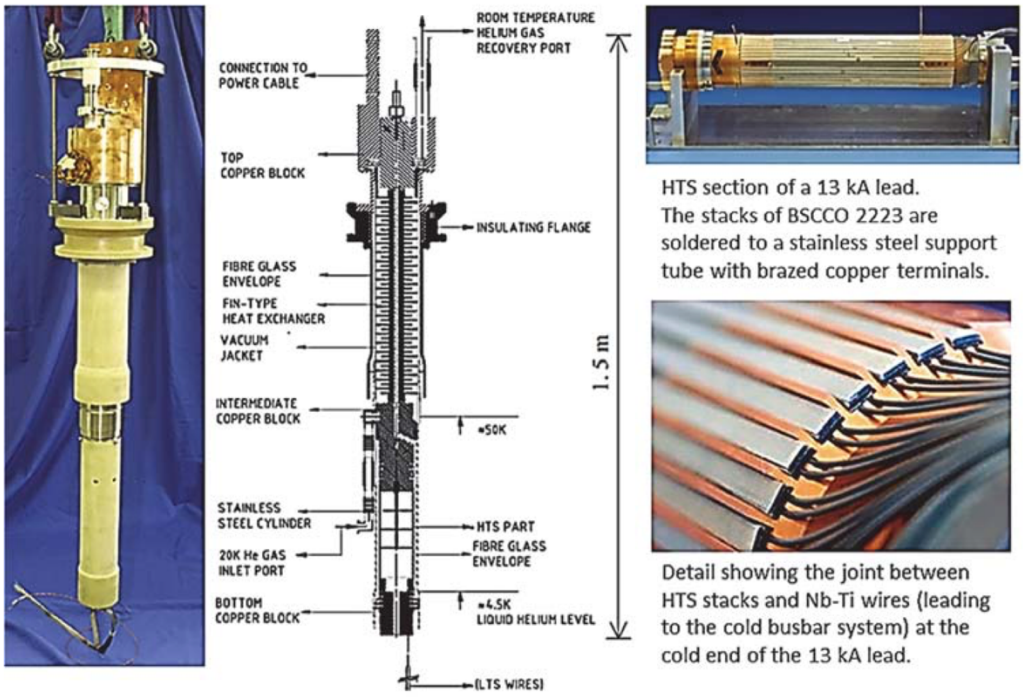


Fig. 23-6: Details on the warm superconducting current entries, a major achievement [653].

[652] C. Benvenuti, A Pumping Vacuum Chamber: Ultimate Simplicity. ibid p. 290

[653] A. Ballarino, Current Leads: High Temperature Superconductors to the Fore. In Technology meets Research: https://inspirehep.net/files/d59e7aaf7b366b4da3ed4a0798e7a8e9 p. 287

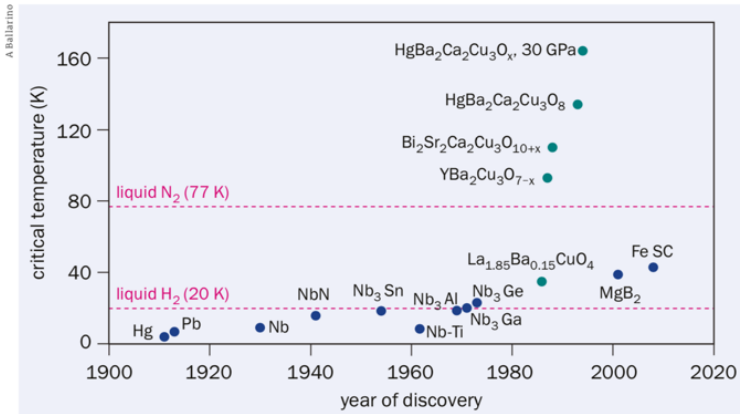


Fig. 23-7: Discovery of HT superconductors versus year [654].

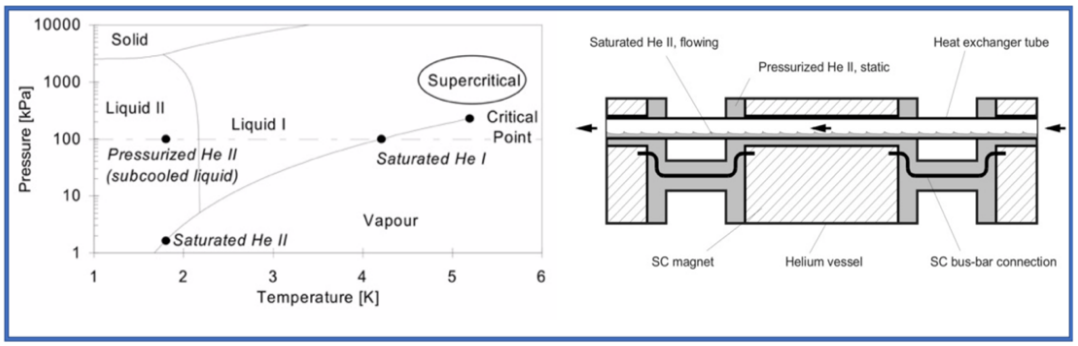


Fig. 23-8: The LHC cryogeny [655].

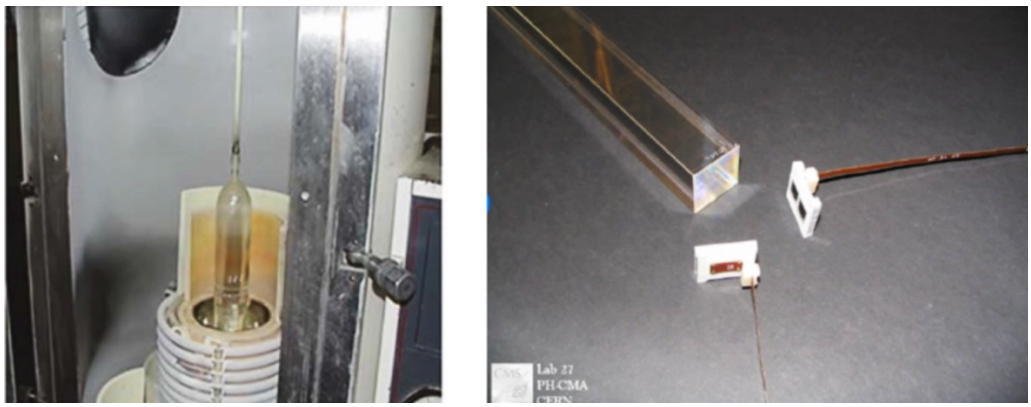
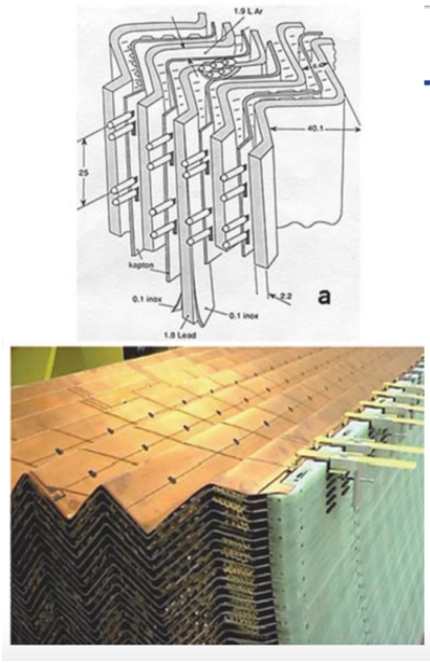


Fig. 23-9: CMS crystal. Drawing a crystal of lead-tungstate (left). The avalanche photodiodes for its read-out used in CMS (right) [656].

[654] A. Ballarino, New Superconducting Technologies for the HL-LHC and Beyond. CERN Courier May/June 2023, p. 37, https://cerncourier.com/wp-content/uploads/2023/05/CERNCourier2023MayJun-digitaledition2.pdf

[655] P. Lebrun, LHC Cryogenics : Quantum Fluids at Work. In Technology meets Research: https://inspirehep.net/files/d59e7aaf7b366b4da3ed4a0798e7a8e9 p. 283

[656] P. Lecoq *et al.,* Two Examples of Recent Crystal Development. https://inspirehep.net/files/e5fb2700d826902c9846e664e24bb240
F. Nessi-Tedaldi, Response evolution of the CMS ECAL and R&D studies for electromagnetic calorimetry at the High-Luminosity LHC. https://arxiv.org/abs/1211.3885



LAr EMB: exemple de découpage en tâches

$,Euros,CHF
~30% FR
~30% US
~20% CERN
~20% IT,S,...

OBJET	Dessin/Specs	Realisation	Commentaire
Cryostat (40 m³ LAr)	US	KHI/Japon	Financé/US
Cryogénie	CERN/FR	GB/Norvege/FR	Financé/FR
Traversées étanches	US/FR/Canada	US	200000 traversées -0 probleme
PLOMB	FR	Allemagne	Contrôle usine FR
INOX	FR	US/teledyne	Sans concurrent
Prepreg	FR	FR/Structil	
Machine a former les accordéons	CERN	CERN	Trop compliqué→industrie
Presse de collage	FR	FR (Deshors/Brive)	Haute precision
Barreaux anisotropes	CERN	Suisse	Contrat/ES cassé –
Electrodes/matiere polyimide	Grande largeur	Japon	Dupont a renoncé (dimensions)
Electrodes/réalisation	CERN	Suisse	Abandon FR (cout)
Electrodes/machine test	FR	FR	Installé et opéré en usine
Séparateurs nid d'abeille	FR	B/FR	« sous-produit » aviation
Presampler	FR/S	FR/S/B	Partie des tests/Maroc
Cables froids microcoax	FR	FR/Axon	Tests en usine/appareillage labo
Preamplis hybrides	FR/US	US/Italie	
ASIC Amplis/formeurs	FR	Aut/AMS	
Memoires analogiques	FR	FR/DMILL	
Cartes	US/FR	US	Moins cher/Europe. Tests US/FR
Assemblage modules→roue	FR	FR/Sacsum	Sur site au CERN

Fig. 23-10: The ATLAS accordion: its structure and the organisation of its construction [657].

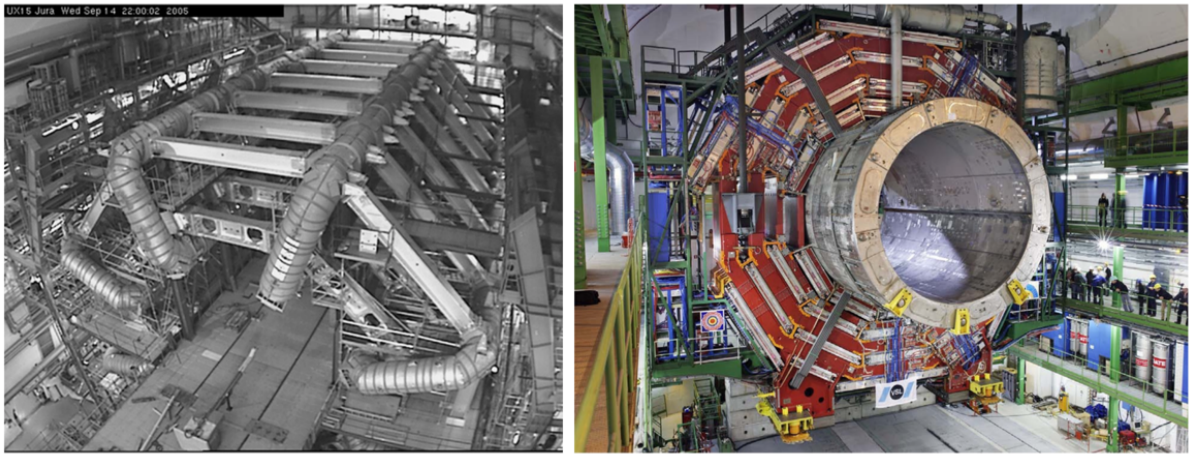


Fig. 23-11: LHC giant magnet: ATLAS toroid (left), CMS solenoid (right) [658].

[657] ATLAS EM Barrel Liquid Argon Calorimeter Group, Construction, assembly and tests of the ATLAS electromagnetic barrel calorimeter. https://cds.cern.ch/record/883909/files/phep-2005-034.pdf
D. Fournier, Le Défi des Détecteurs.
https://indico.in2p3.fr/event/8302/contributions/44880/attachments/36471/45104/Fournier_24Avril.pdf
Le Prix Lagarrigue 2023 est décerné à Daniel Fournier :
https://www.ijclab.in2p3.fr/actualite/le-prix-lagarrigue-2023-est-decerne-a-daniel-fournier/
[658] A. Hervé, P. Jenni and T. Taylor, Giant Magnets for Giant Detectors. In Technology meets Research:
https://inspirehep.net/files/d59e7aaf7b366b4da3ed4a0798e7a8e9 p. 318

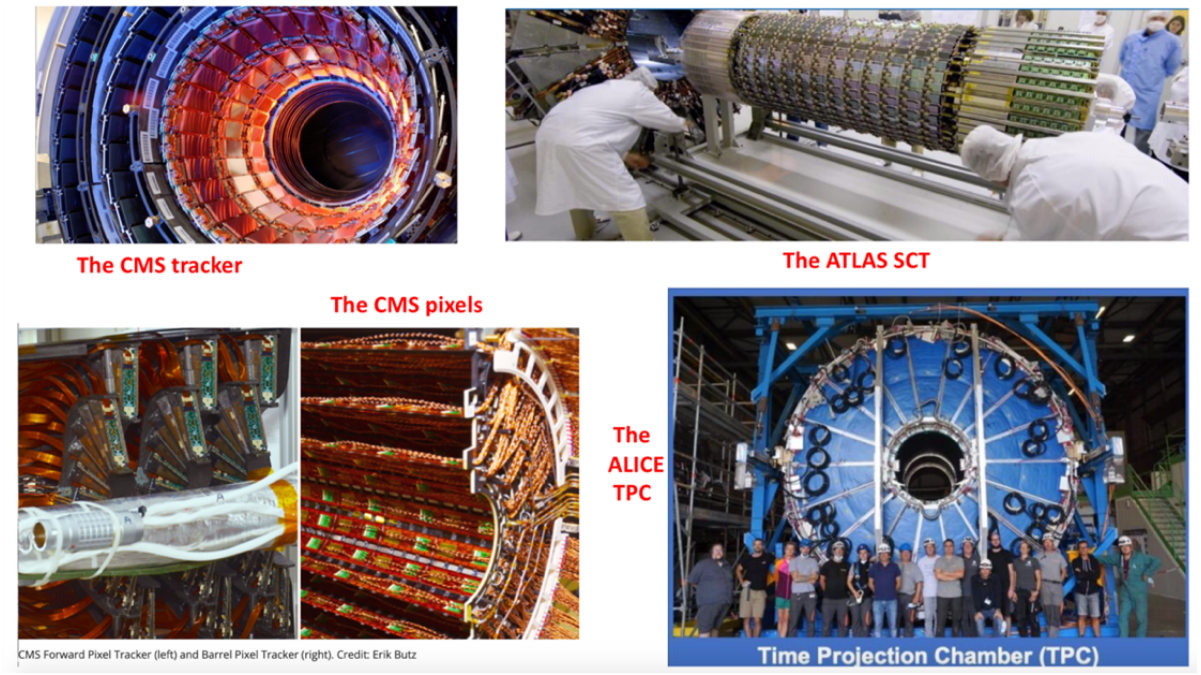


Fig. 23-12: The LHC trackers [659].

For general considerations and examples about **Managing the Laboratory and Large Projects,** see Ref. [660].

23.3 Particle flow

By using tracking and calorimetry, the main goal of the experiments is the careful elaboration and exploitation of the **particle flow** (**PF**, following what ALEPH started [661]). Combined calorimetry is part of it. An improved PF gives better jet mass resolution and in particular better estimate of **Missing Energy Transverse (MET)**, offering thus for instance **better searches for BSM physics involving MET,** as SUSY, etc. Figure 23-13 shows the quality of MET achieved at LHC.

Particle Flow (PF) allows to deal with **tracks only**, or with **tracks plus photons** (electromagnetic calorimeter), or with **everything** (thus adding neutrals in the hadron calorimeter). Ideally one should look for plots showing the corresponding gradual improvement when you include more, as in Fig. 23-14. Useful references to the PF achievements can be found in Ref. [662].

---

[659] L. Rossi, Vertex Detectors at LHC: In Search of Beauty. In Technology meets Research: ibid p. 292
G. Rolandi, Large Silicon Trackers. In Technology meets Research: ibid p. 296
https://www.researchgate.net/figure/Barrel-Toroid-structure-in-ATLAS-cavern-completed-Sep-05_fig10_3313169
The ALICE TPC: https://alice-collaboration.web.cern.ch/menu_proj_items/tpc
ATLAS-PHO-ach-2015-029-1 Workers assembling the ATLAS SemiConductor (SCT) Tracker:
https://cds.cern.ch/record/2047419?ln=en

[660] P. Lebrun and T. Taylor, Managing the Laboratory and Large Projects. In Technology meets Research:
https://inspirehep.net/files/648e1e370385824b5c9939cebc8db32f p. 393.

[661] P. Janot, Particle-Flow Event Reconstruction from LEP to LHC.
https://indico.cern.ch/event/96989/contributions/2124494/attachments/1114188/1589704/ParticleFlow.pdf

[662] CMS Collaboration: Particle-Flow Event Reconstruction in CMS and Performance for Jets, Taus, and MET.
https://cds.cern.ch/record/1194487 , MET performance in 8 TeV data.
https://cms-results.web.cern.ch/cms-results/public-results/preliminary-results/JME-12-002/index.html ,
Particle-flow reconstruction and global event description with the CMS detector. https://arxiv.org/abs/1706.04965

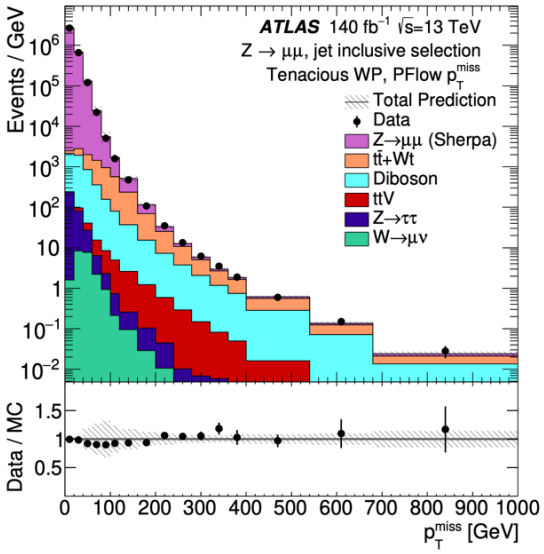


Fig. 23-13: Distributions of p_T^{miss} in MC simulation and data. Events satisfy a $Z \rightarrow \mu\mu$ selection and p_T^{miss} is built, using Particle Flow jets [663].

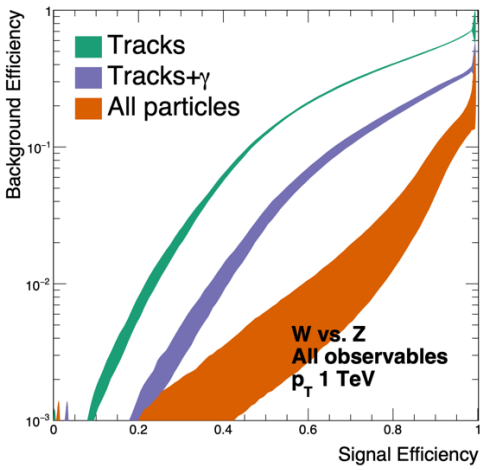


Fig. 23-14: Progressive improvement in W/Z separation when more kinds of objects are added [664].

23.4 Aspects of LHC computing

Before electronic computers were available at CERN, Wim Klein performed astonishing feats of mental arithmetic to help his colleagues with their calculations. On 27 August 1976, Klein calculated the 73rd root of a 500-digit number in 2 minutes and 43 seconds, a feat recorded by the Guinness Book of Records. He became known as "the human computer" (Fig. 23-15).

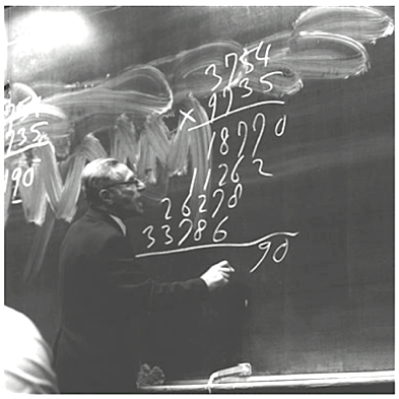


Fig. 23-15: Wim Klein, computer-man [665].

[663] ATLAS Collaboration, The performance of missing transverse momentum reconstruction and its significance with the ATLAS detector using 140 fb^{-1} of √s = 13 TeV pp collisions. https://arxiv.org/abs/2402.05858
[664] E. Coleman *et al.,* The importance of calorimetry for highly-boosted jet substructure. https://arxiv.org/abs/1709.08705
[665] W. Klein, CERN's first computer: https://timeline.web.cern.ch/wim-klein-cerns-first-computer
https://en.wikipedia.org/wiki/Willem_Klein

Tim Berners-Lee invented the World Wide Web (WWW) in 1989 (Fig. 23-16), while working at CERN [666]. The WEB was originally conceived and developed to meet the demand for automated information-sharing between scientists in universities and institutes around the world. On 30 April 1993, CERN put the World Wide Web software **in the public domain**. Later, CERN made a release available with an open license, a more reliable way to maximize its dissemination. This allowed the web to flourish.

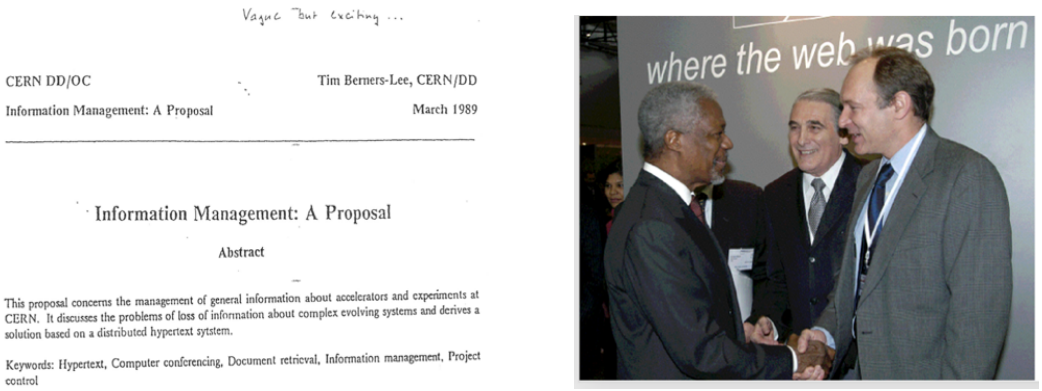


Fig. 23-16: Left: "*Vague but exciting*", first comment on WEB-Idea. Right: Few years after, the consecration of WEB, Tim Berners-Lee and Kofi Annan during the WSIS in 2003 [667].

Figure 23-17 illustrates a fast travel through the computing means at CERN, see also Ref. [668].



Fig. 23-17: left: IBM709 (1960), middle: CRAY (1968), right: Now

An interesting number: performance CPU/cost × 80 000 000 in 40 years and external connectivity: from kbps near 1980 to probably 100 Gbps at LHC time (from David Williams).

23.5 Evolution of data analysis

At the beginning of the seventies, only big BC packages existed, managed by HYDRA (Julius Zoll, Luc Pape), fitting package (MINUIT) and histogramming (SUMX). For electronic experiments, every group used its own programs, but René Brun created many easy-to-use general programs: histogramming package (HBOOK), memory manager (ZBOOK) and simulation program (GEANT 1).

[666] The birth of the Web: https://www.home.cern/science/computing/birth-web
[667] CERN hosts major policy conference: https://cerncourier.com/a/cern-hosts-major-policy-conference/
[668] F. Hemmer and P. G. Innocenti, Data Handling and Communication. In Technology meets Research: https://inspirehep.net/files/87110a239677f4cf66a65ff562b7586d

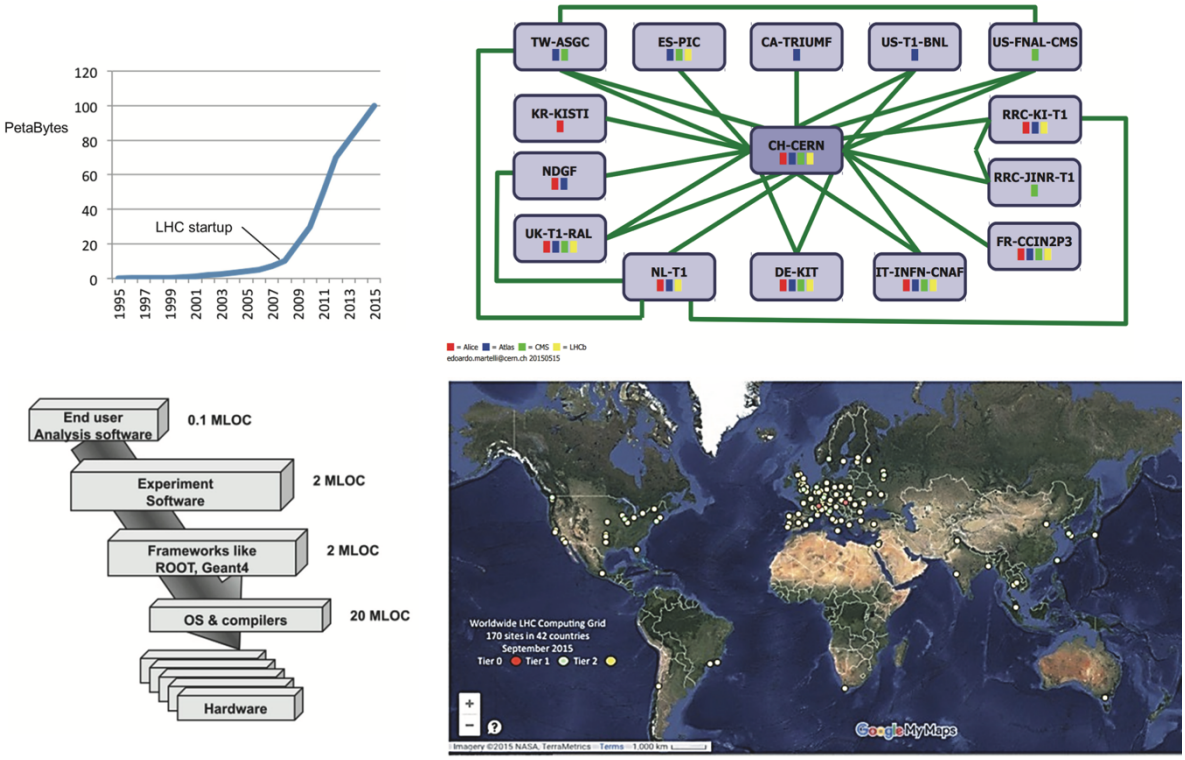


Fig. 23-18: Aspects of LHC computing. Top left: mass storage usage at CERN; top right: LHC Optical Private Network; bottom left: the software hierarchy (MLOG = Million Lines Of Code); bottom right: a grid of 170 interconnected computing clusters [669].

It would be beyond the scope of this document to describe in detail the evolution of all sectors of the field which followed. Let us list some major changes and highlights :

- A complete change occurred of machine and operating systems, leading to the present role of Linux.
- Languages and compilers changed from FORTRAN to C++. The actual move to OO programming happened between 1995 and 2005.
- GEANT 3 appeared in 1980, GEANT 4 in C++ in 2000.
- The major steps were the advent of PAW (René Brun 1985), used until 2005, and of ROOT (René Brun 1994), with Root version 2.25/02 available in 2000, used also for data taking at Fermilab, then at CERN.
  Thus, data structures, management systems went from ZBOOK and HYDRA to ZEBRA, and then to ROOT, histogramming from HBOOK to ROOT. As for the key sector of interactive data analysis systems, it went from none in early times to PAW and to ROOT afterwards.
- And obviously the WEB revolution between 1989 and 1992 had a big impact.

Among the actors of this major evolution, a few emerge, starting with René Brun and his pioneering role in the main big steps [670].

[669] F. Hemmer and P. G. Innocenti, Data Handling and Communication. In Technology meets Research: https://inspirehep.net/files/87110a239677f4cf66a65ff562b7586d p. 327

[670] René Brun received the 2017 Special Prize of the EPS high-energy and particle-physics division and the 2022 Aldo Menzione prize for his exceptional contributions to the development of innovative detection techniques.

24. LHC Physics

24.1 Higgs Boson physics at LHC

24.1.1 Discovery and properties

Excellent reviews about ten years of Higgs Boson physics at LHC can be found in Ref. [671].

The two modes of discovery of the Higgs Boson are spectacular [672] (Figs. 24-1 and 24-2). Its production from gluons goes through the **top loop.** It decays into 2 γ through a loop involving top and W. The Boson was thus discovered through **quantum effect**s and from a **tiny fraction of its decays** (Fig. 24-3).

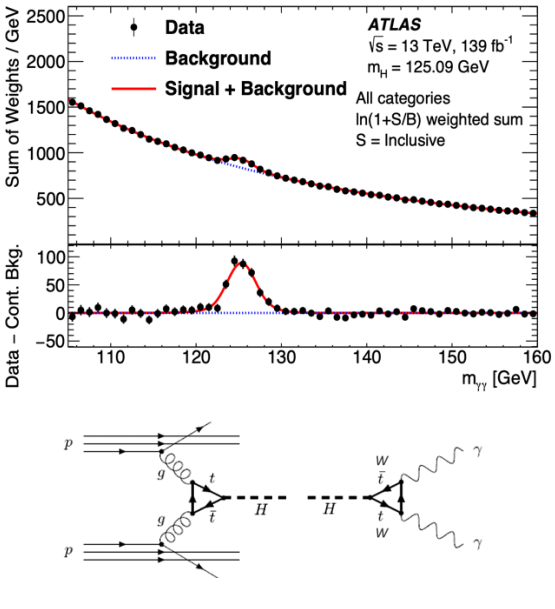


Fig. 24-1: The 2-photon mass spectrum [673].

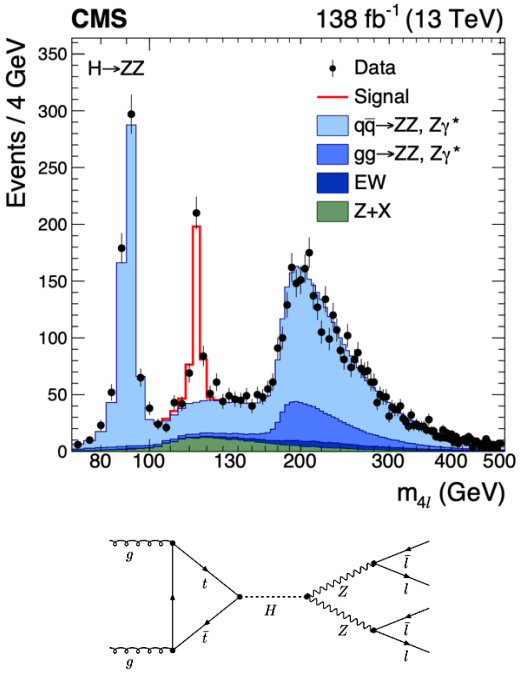


Fig. 24-2: The 4-lepton mass spectrum [674].

The Higgs Boson mass is measured at the 0.1% level.

ATLAS: m_H = 125.11 ± 0.11 GeV CMS: m_H = 125.08 ± 0.10 (stat) ± 0.05(syst) GeV

Its width was determined indirectly by measuring its contribution outside the mass-shell.

ATLAS: $\Gamma_H = 4.3^{+2.7}_{-1.9}$ MeV CMS: $\Gamma_H = 3.0^{+2.0}_{-1.5}$ MeV. Thus, about 50% precision.

---

[671] ATLAS Collaboration, A detailed map of Higgs boson interactions by the ATLAS experiment ten years after the discovery. *Nature 607 (2022) pp.52–59,* https://arxiv.org/abs/2207.00092
CMS Collaboration, A portrait of the Higgs boson by the CMS experiment ten years after the discovery. *Nature 607 (2022) 60,* https://arxiv.org/abs/2207.00043
Y. Nir, The three jewels in the crown of the LHC. https://arxiv.org/abs/2010.13126
G. Salam *et al.,* The Higgs boson turns ten. https://arxiv.org/abs/2207.00478

[672] Both experiments have similar discovery plots in both channels.

[673] ATLAS Collaboration, A detailed map of Higgs boson interactions by the ATLAS experiment ten years after the discovery. *Nature 607 (2022) pp.52–59,* https://arxiv.org/abs/2207.00092

[674] CMS Collaboration, A portrait of the Higgs boson by the CMS experiment ten years after the discovery. *Nature 607 (2022) 60,* https://arxiv.org/abs/2207.00043

Figure 24-3 gives the Higgs Boson decay modes, illustrating the fact that it was indeed discovered through channels of very small branching fraction, thanks to their visibility.

Decay channel	Branching Fraction (%)
bb	57.63 ± 0.70
WW	22.00 ± 0.33
gg	8.15 ± 0.42
ττ	6.21 ± 0.09
cc	2.86 ± 0.09
ZZ	2.71 ± 0.04
γγ	0.227 ± 0.005
Zγ	0.157 ± 0.009
ss	0.025 ± 0.001
μμ	0.0216 ± 0.0004

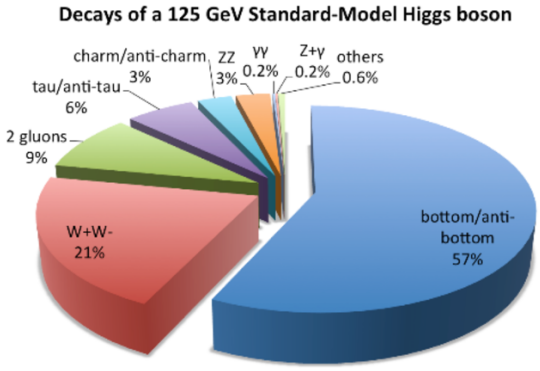


Fig. 24-3: Branching fraction of the Higgs decay channels (rounded in the figure).

More work and statistics are needed. Figure 24-4 shows results for the dominant beauty-antibeauty decay mode, and Fig. 24-5 for the tau pair mode.

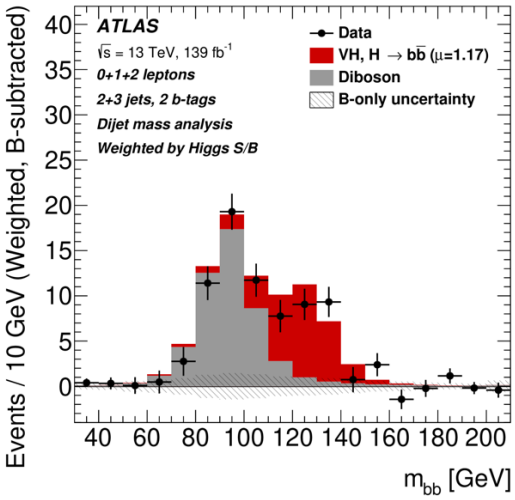


Fig. 24-4: The Higgs boson in its channel of highest decay branching fraction [675].

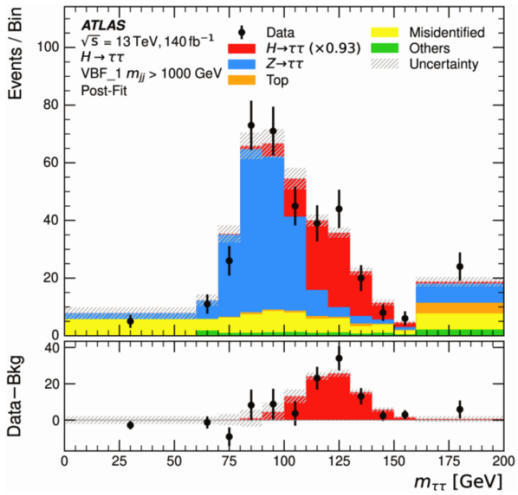


Fig. 24-5: The Higgs boson decay to a tau pair [676].

The upper limit on the Higgs invisible mode BR is still 10–15% (e.g. ATLAS < 10.7 %, 95% CL [677]).

However, modes with high visibility progress: a collaborative effort led to the first evidence of the Higgs decay into **Z-γ**, with a significance of 3.4 σ. The measured signal rate relative to the SM prediction was 2.2 ± 0.7. ATLAS alone [678] has now a significance of 2.5 σ (1.9 σ expected) with $\mu = 1.3^{+0.6}_{-0.5}$.

[675] ATLAS Collaboration, Measurements of WH and ZH production in the H → bb̄ decay channel in pp collisions at 13 TeV with the ATLAS detector. https://atlas.web.cern.ch/Atlas/GROUPS/PHYSICS/PAPERS/HIGG-2018-51/

[676] ATLAS Collaboration, Unveiling Higgs-boson production properties using tau-lepton pairs. https://atlas.cern/Updates/Briefing/Higgs-Tau-Pairs

[677] ATLAS Collaboration, Combination of searches for invisible decays of the Higgs boson using 139 fb^{-1} of proton-proton collision data at √s = 13 TeV collected with the ATLAS experiment. https://arxiv.org/abs/2301.10731

[678] ATLAS Collaboration, Search for the Higgs boson decay to a Z boson and a photon in pp collisions at √s = 13 TeV and 13.6 TeV with the ATLAS detector. https://cds.cern.ch/record/2937635/files/ATLAS-CONF-2025-007.pdf

24.1.2 Higgs interactions

Let us move to the processes governing Higgs physics at LHC. Figure 24-6 shows the Feynman diagrams for the leading Higgs boson interactions: **Higgs boson production** in (a) gluon-gluon fusion (ggH), (b) vector boson fusion (VBF), (c) associated production with a W or Z (V) boson (VH), (d) associated production with a top or bottom quark pair (ttH or bbH), (e, f) associated production with a single top quark (tH); with **Higgs boson decays** into (g) heavy vector boson pairs, (h) fermion-antifermion pairs, and (i, j) photon pairs or Zγ; Higgs boson pair production: (k, l) via gluon-gluon fusion, and (m, n, o) via vector boson fusion. The different Higgs boson interactions are labelled with the **coupling modifiers** κ, shown in red for Higgs-fermion interactions, in blue for Higgs-gauge-boson interactions and in green for multiple Higgs boson interactions. A particle and its antiparticle are not distinguished.

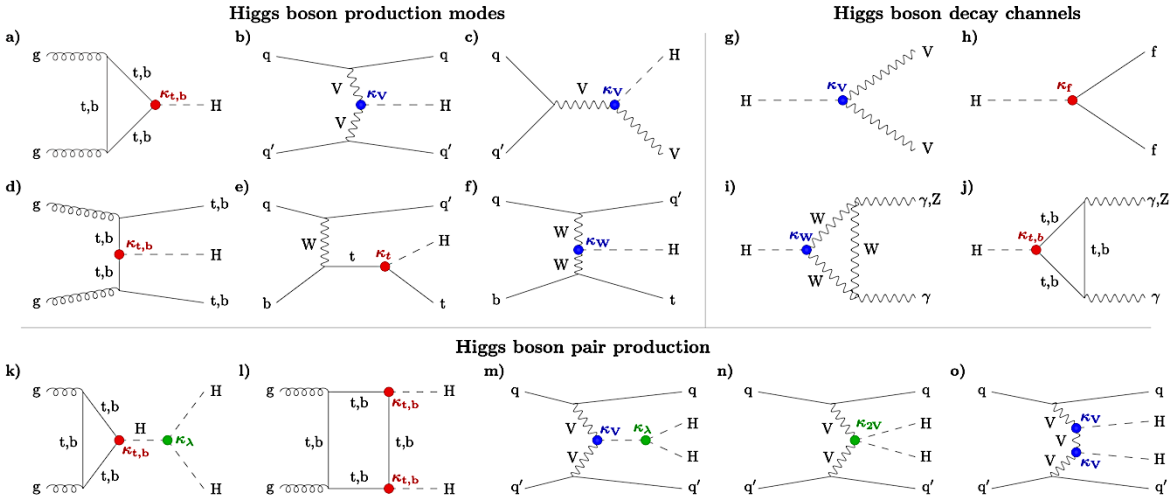


Fig. 24-6: The Feynman diagrams for the leading Higgs boson interactions. See text for explanations [679].

The μ-framework for signal strengths.

For a "***i → H → f***" process, the **signal strengths** for individual production channels, μ_i, and decay modes, μ^f, are defined as $\mu_i = \sigma_i / (\sigma_i)_{SM}$ and $\mu^f = B^f / (B^f)_{SM}$, where σ is the **production cross section** and B is the **branching fraction.** Perfect agreement with SM expectations would correspond to **all μ equal to one**. Fitting all production and decay modes with a common μ gives

$$\mu_{if} = \frac{(\sigma_i \times B_f)}{(\sigma_i^{SM} \times B_f^{SM})} = 1.023 \pm 0.028\ (\text{stat.})\ ^{+0.026}_{-0.025}\ (\text{exp.})\ ^{+0.039}_{-0.036}\ (\text{sig. theo.})\ \pm 0.012\ (\text{bkg. theo.})$$

Relaxing this assumption and introducing different μ_i and μ^f, measurements are shown in Fig. 24-7 [680] for decay channels in CMS. Similar results are obtained for production modes and for ATLAS.

The κ-framework for coupling modifiers.

To probe BSM deviations from the predictions of the SM, the κ-framework is used. Quantities, as σ_i, Γ^f, and Γ_H, computed from the corresponding SM predictions, are scaled by κ_j^2, as shown by the labels in Fig. 24-6. In the SM **all κ are equal to 1.**

[679] CMS Collaboration, A portrait of the Higgs boson by the CMS experiment ten years after the discovery. *Nature 607 (2022) 60,* https://arxiv.org/abs/2207.00043
[680] ibid

A first fit to Higgs couplings involves **two parameters, κ_V and κ_f**, which scale the Higgs couplings to massive gauge bosons and to fermions, respectively. Both coupling modifiers are found to agree, within 10%, with the SM.

With a second fit one extracts the **coupling modifiers κ** for the Intermediate Vector Bosons (κ_W, κ_Z) and the fermions probed in the analyses (κ_t, κ_b, κ_τ and κ_μ). Predictions for processes occurring in the SM via **loops of intermediate virtual particles**, e.g. Higgs production via ggH, or Higgs decay to a pair of gluons, γ, or to Zγ, are computed in terms of the κ_i above. ATLAS results are shown by Fig. 24-8 [681], as a function of the probed particle mass.

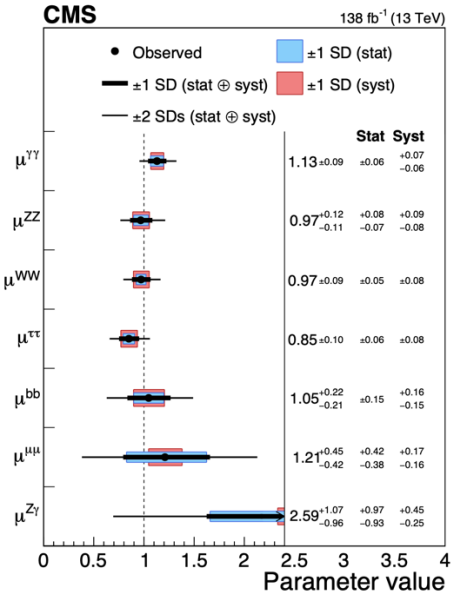


Fig. 24-7: Agreement with SM predictions for the different decay channels.

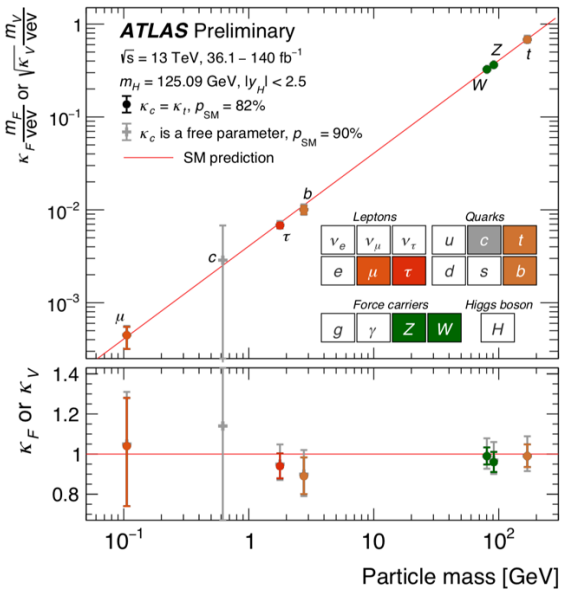


Fig. 24-8: Measured Higgs couplings modifiers as a function of the particle mass.

So far, the boson behaves as expected: Figure 24-8 shows the **proportionality to the mass (mass²)** of its coupling to the **fermions (bosons).** We therefore see for τ and μ, that the Yukawa couplings do not at all respect the universality of lepton flavour.

Actually, the situation is clear for the heaviest objects, EW bosons and third generation (Table 24-2).

For the second generation, results are appearing and LHC will answer [682] (Tables 24-1 and 24-2). Figure 24-9 shows the ATLAS signal of $H \rightarrow \mu\mu$ (left) and the status of $H \rightarrow c\bar{c}$ in CMS (right).

The present accuracies [683] of the effective Higgs couplings are: to W: 4%, Z: 5%, γ: 7%, Zγ: 31%, gluon: 7%, top: 9%, bottom: 12%, τ: 7%, μ: 21% (all assuming $B_{BSM} = 0$, $\kappa_c = \kappa_t$). For the overall agreement with the SM, the combined production and decay mode p-values are: ATLAS/CMS = 0.85/0.006 (all categories).

---

[681] ATLAS Collaboration, A detailed map of Higgs boson interactions by the ATLAS experiment ten years after the discovery. *Nature 607 (2022) pp.52–59,* https://arxiv.org/abs/2207.00092

[682] Y. Nir and P. P. Udhayashankar, Lessons from ATLAS and CMS measurements of Higgs boson decays to second generation fermions. https://arxiv.org/abs/2404.16545

[683] A. Hoecker, EPS-HEP 2025 — Conference Highlights. summary talk at EPS Marseille 2025. https://indico.in2p3.fr/event/33627/contributions/153160/attachments/95391/146107/EPS-HEP-Highlights-Jul2025.pdf

However, it will be most difficult to answer concerning **the first generation** since for instance the SM BR of $H \rightarrow e^+e^-$ is 5×10^{-9}. The question is crucial and will deserve all efforts to reach or at least set limits on the electron-Higgs coupling [684], first with HL-LHC. The fact that the Higgs boson gives mass to e, u and d may stay as a conjecture. On the other hand, a good surprise from BSM physics is still possible.

$\mu_{\mu^+\mu^-} = 1.21^{+0.45}_{-0.42}$ (CMS)	$\mu_{c\bar{c}} = 7.7^{+3.8}_{-3.5}$ (CMS)
$\mu_{\mu^+\mu^-} = 1.2 \pm 0.6$ (ALTAS)	$\mu^{Vh}_{c\bar{c}} = -9 \pm 15$ (ATLAS)
$\mu_{\mu^+\mu^-} = 1.21 \pm 0.35$ (average)	$1.1 < \lvert\kappa_c\rvert < 5.5$ (CMS)
$0.92 \leq \kappa_\mu \leq 1.25$	$\left\lvert\frac{\kappa_c}{\kappa_b}\right\rvert < 4.5$ (ATLAS)
	$\kappa_c = 3.1 \pm 1.0$ (CMS, 1 sigma)

"For the muon, $\mu_{\mu^+\mu^-}$ measurement now strongly supports that the muon acquires mass through the Yukawa interaction with the field of the observed scaler h.
For the charm quark, the $\mu_{c\bar{c}}$ measurement still leaves open the possibility that this is not the case."

Table 24-1: Second generation couplings [685].

	Current	HL-LHC	FCC (ee)	FCC (hh)
κ_γ	6%	1.8%	3.9%	
κ_g	7%	2.5%	1%	
$\kappa_{Z\gamma}$	30%	9.8%		
$\kappa_{W,Z}$	6%	1.5%, 1.7 %	0.4%, 0.2 %	
κ_t	11%	3.4%	-	1%
κ_b	11%	3.7%	0.7%	-
κ_τ	8%	1.9%	0.7%	-
κ_μ	20%	4.3%	8.9%*	

Table 24-2: Status of incertitude on coupling measurements [686].

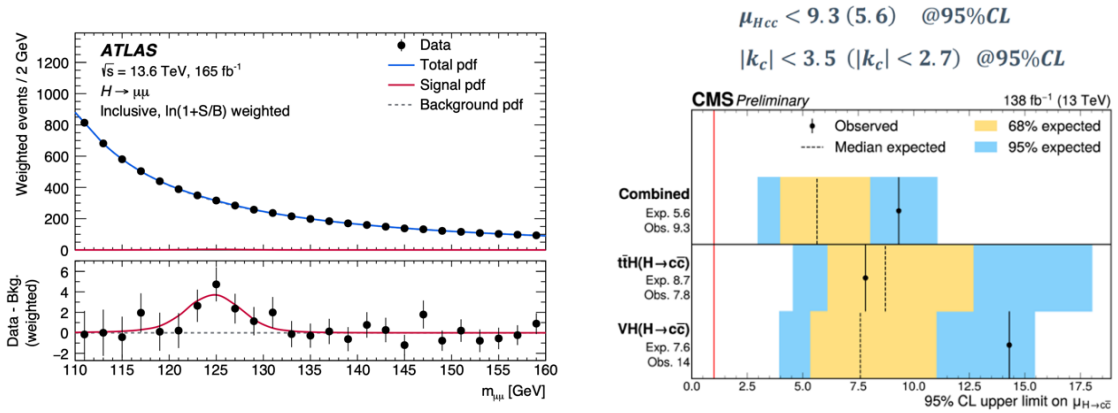


Fig. 24-9: Left: ATLAS results on $H \rightarrow \mu\mu$ [687]; right: CMS upper limit on $H \rightarrow c\bar{c}$ [688].

---

[684] D. d'Enterria *et al.,* Measuring the electron Yukawa coupling via resonant s-channel Higgs production at FCC-ee. https://arxiv.org/abs/2107.02686
This prospective idea is to consider an exposure at a high luminosity e^+e^- collider, as FCC-ee, at $E_{CM} = M_H$ to exploit the s-channel Higgs production. The key points are to obtain a CM energy width not much larger than the Higgs width of 4 MeV, a very good knowledge of the beam energy, to avoid missing the signal, and a very performing analysis, since the signal $H \rightarrow e^+e^-$ is 0.57 fb while the Drell–Yan $e^+e^- \rightarrow q\bar{q}$ background is about 100 pb. For preliminary estimates see:
Z.-J. Zhang *et al.,* Optimized physics performance evaluation of monochromatization interaction region optics for direct ss-channel Higgs production at FCC-ee. https://inspirehep.net/files/f0d06a84e72ae36605fca297b5c6882e . For instance, achieving a CM energy spread ($\delta_{\sqrt{s}}$) = 29.59 MeV and L_{int} = 1.45 ab^{-1} would lead to an upper limit (95% CL) on the Higgs–electron coupling of $|y| < 4.2\ |y^{SM}|$.
[685] Numbers extracted from Y. Nir and P. P. Udhayashankar, Lessons from ATLAS and CMS measurements of Higgs boson decays to second generation fermions. https://arxiv.org/abs/2404.16545 . μ is the ratio BR /$(BR)_{SM}$
[686] From M. Kado, Concluding talk of ICHEP 2024.
https://indico.cern.ch/event/1291157/contributions/5958406/attachments/2903497/5123335/ICHEP-Summary.pdf
[687] M. Cepeda, Experimental Summary. 15th Higgs Hunting Conference 2025,
https://indico.ijclab.in2p3.fr/event/11484/contributions/36644/attachments/26056/39320/HHExperimentalSummary.pdf
[688] ibid

24.1.3 Higgs self-interaction

The direct evidence of Higgs self-coupling is one of the major missing pieces of the Standard Model. Let us thus consider the natural and naïve question concerning the **Higgs self-interaction** and prospects to measure its **self-coupling parameter (SC)**. The Higgs potential in the SM broken phase is parameterized as (h is the CP-even neutral component of the Higgs doublet) [689].

$$V(h) = \frac{1}{2} m_h^2 h^2 + \frac{1}{3!}\lambda_{hhh} h^3 + \frac{1}{4!}\lambda_{hhhh} h^4 .$$

The SM trilinear and quadrilinear Higgs SCs are $\lambda_{hhh}^{SM} = \frac{3m_h^2}{v} \simeq 190$ GeV and $\lambda_{hhhh}^{SM} = \frac{3m_h^2}{v^2} \simeq 0.77$.

Focusing on the trilinear self-coupling λ_{hhh}, let us call **κ_λ the ratio of its value to the SM value.**

A crucial question is whether a strong enough **first-order EW phase transition may lead to EW baryogenesis** [690]. Can adequate modifications of the Higgs potential lead to such a phase transition and could these be linked to the **Higgs self-coupling** that LHC offers to study [691]? See Sections 24.1.5 and 24.1.6.

Obviously **double Higgs production** will be the process *de choix* to provide information on this parameter. Figure 24-10 [692] lists the reactions involving the appearance of two bosons.

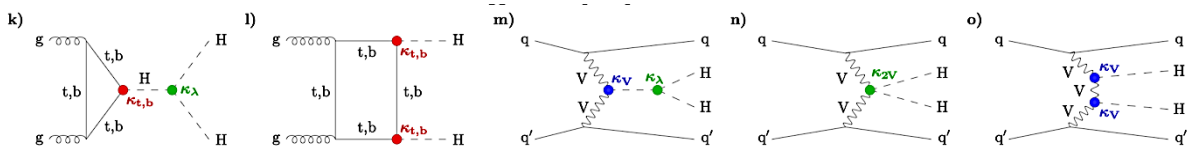


Fig. 24-10: Higgs boson pair production. See also Fig. 24-6 for explanations.

Both **gluon-gluon** (gg) and **Vector Boson Fusion** (VBF) processes contribute, and, besides the Higgs **self-interaction coupling modifier κ_λ ,** others intervene, as **the quartic VVHH coupling modifier κ_{2V}**.

Interference between subprocesses changes the expected cross sections and the kinematics of the two Higgs bosons, affecting much the efficiency for detecting signal events. In particular, processes k and l of Fig. 24-10, similar in magnitude, have opposite signs and **interfere destructively**. The overall Higgs pair production rate is thus small, ≈ 33 fb, three orders of magnitude below the single Higgs cross-section (Fig. 24-11) and challenging to observe (except if BSM physics destroys the interference).

Figure 24-11 shows the present limits on the Higgs pair production cross-section, obtained by combining Higgs boson candidates reconstructed from different final states (Fig. 24-12). The bottom left plot of Fig. 24-11 shows an observed HH SM significance of 0.8 σ for an expected one of 1.0 σ.

---

[689] An alternative is V(H) = ½ m_H^2 H^2+ $\lambda_3 v H^3$ + ¼ $\lambda_4 H^4$

[690] The problem is involved. For the conditions of baryogenesis (Sakharov) see V. Rubakov, Cosmology. https://arxiv.org/abs/1804.11230
For the idea and role of sphalerons/instantons see https://en.wikipedia.org/wiki/Instanton and https://en.wikipedia.org/wiki/Sphaleron
For the transition itself see E. Senaha, Overview of Electroweak Baryogenesis. https://arxiv.org/abs/1305.1563

[691] M. Reichert *et al.,* Probing Baryogenesis through the Higgs Self-Coupling. https://arxiv.org/abs/1711.00019
C. Wagner, Electroweak Baryogenesis and Higgs Physics. https://arxiv.org/abs/2311.06949

[692] CMS Collaboration, Stairway to discovery: a report on the CMS programme of cross section measurements from millibarns to femtobarns. https://arxiv.org/abs/2405.18661 p. 90

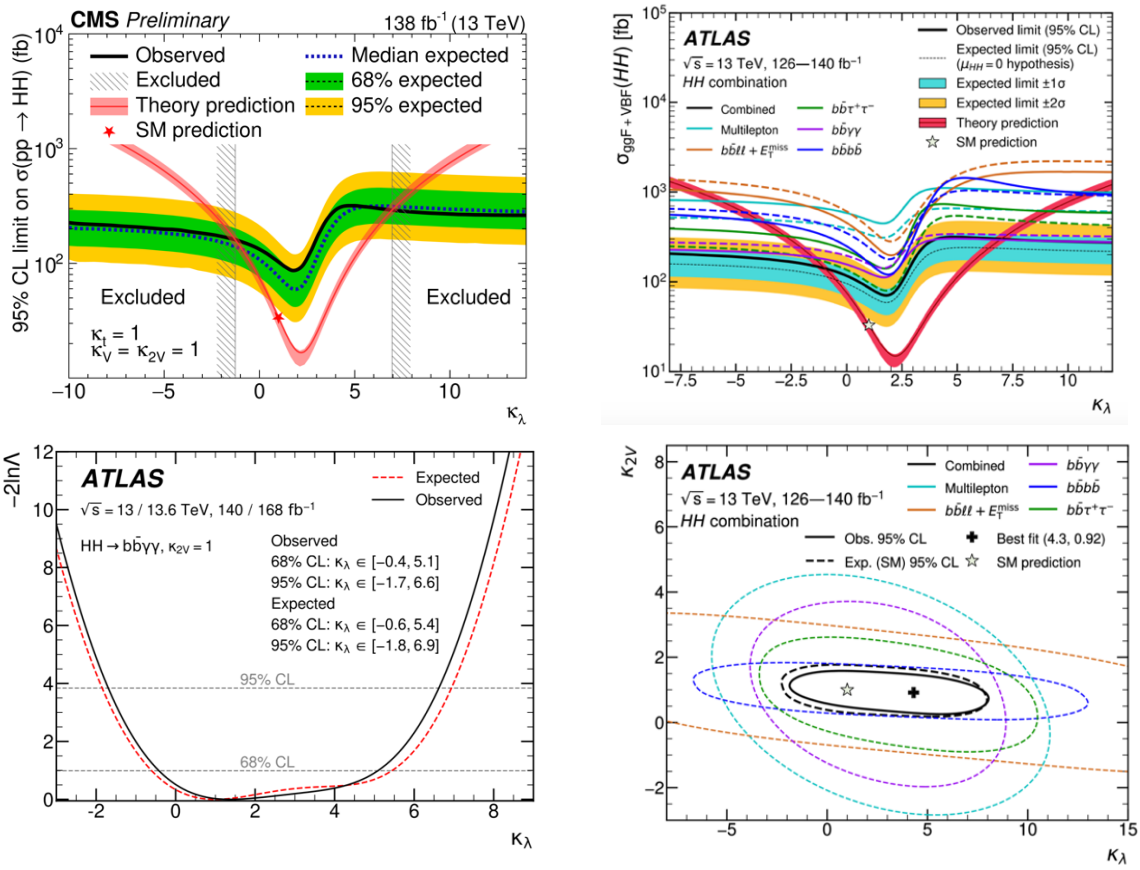


Fig. 24-11: The plots show the CMS and ATLAS present limits on HH cross-section versus κ_λ (top) [693], the ATLAS limits on κ_λ in $b\bar{b}\gamma\gamma$, run 2 + part run 3 (bottom left) and the result on modifiers (bottom right) [694].

Figure 24-12 [695] shows the effect of the "silver channels" bbγγ, 4b, bbττ. The current upper limit on σ(HH) is about three times the SM cross section from both ATLAS and CMS. Figure 24-13 [696] suggests what the HL-LHC should achieve for the self-interaction coupling modifier κ_λ.

Figure 24-14 brings a small correction to the overwhelming role of the HH channel: actually, **single Higgs (H) processes** are sensitive to λ_{hhh} through NLO EW corrections and give some information on this self-coupling, as suggested by the bottom diagram (left) and shown by the plot (right) [697], giving

[693] CMS Collaboration, A portrait of the Higgs boson by the CMS experiment ten years after the discovery. *Nature 607 (2022) 60,* https://arxiv.org/abs/2207.00043. All parameters and couplings are set to their SM values except for κ_λ. That the prediction minimum is not at the SM value comes from features of the selection procedure.
CMS Collaboration, Combination of searches for nonresonant Higgs boson pair production in proton-proton collisions at √s = 13 TeV. https://cms-results.web.cern.ch/cms-results/public-results/preliminary-results/HIG-20-011/
ATLAS Collaboration, Combination of Searches for Higgs Boson Pair Production in pp Collisions at √s = 13 TeV with the ATLAS Detector. *Phys. Rev. Lett. 133 (2024) 101801* https://journals.aps.org/prl/pdf/10.1103/PhysRevLett.133.101801
[694] ATLAS Collaboration, Shedding light on Higgs-boson self-interactions. https://atlas.cern/Updates/Briefing/Di-Higgs-Run2
L. Shchutska, Experimental Summary, Moriond QCD 2025,
https://indico.cern.ch/event/1480248/contributions/6419614/attachments/3046263/5382526/ExpSummary.pdf
[695] Combination of searches for nonresonant Higgs boson pair production in proton-proton collisions at √s = 13 TeV. CMS-PAS-HIG-20-011, https://cms-results.web.cern.ch/cms-results/public-results/preliminary-results/HIG-20-011/
[696] Higgs physics at the HL-LHC and HE-LHC. CERN Yellow Report, doi.org/10.23731/CYRM-2019-007.221,
https://e-publishing.cern.ch/index.php/CYRM/article/view/952
[697] CMS Collaboration, A portrait of the Higgs boson by the CMS experiment ten years after the discovery. *Nature 607 (2022) 60,* https://arxiv.org/abs/2207.00043
CMS Collaboration, The Higgs Boson, as it interacts with itself. https://cms.cern/news/higgs-boson-it-intracts-itself

constraint on the Higgs boson self-coupling modifier κ_λ from single and pair production of Higgs boson(s).

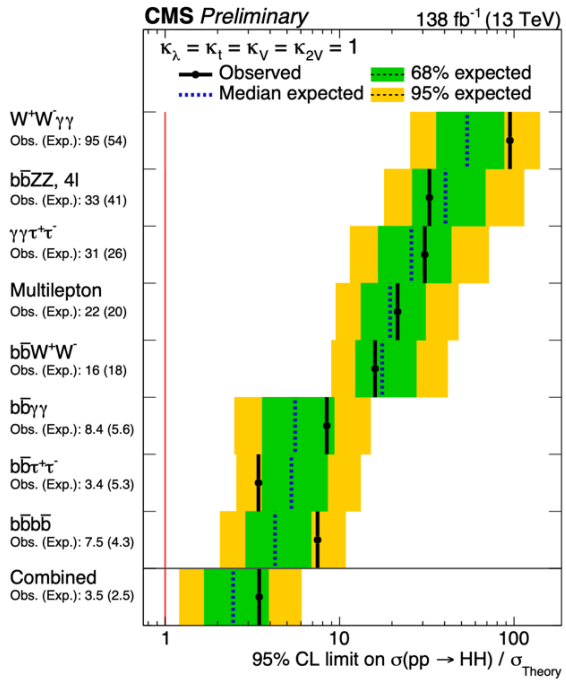


Fig. 24-12: The 95% CL upper limits on the inclusive signal strength r = $\sigma_{HH}/\sigma_{HH}^{SM}$ for each channel and their combination. It suggests the path remaining to narrow the window [698].

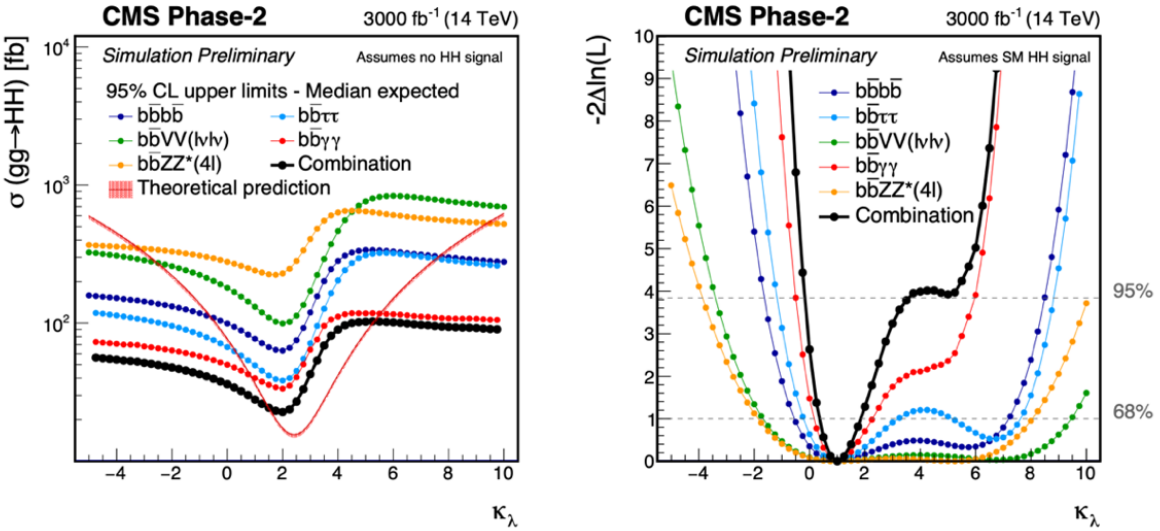


Fig. 24-13: It suggests what the HL-LHC will bring for the self-interaction coupling modifier κ_λ. Asymmetric shapes are explained by previous remarks in the text [699].

[698] CMS Collaboration, Combination of searches for nonresonant Higgs boson pair production in proton-proton collisions at $\sqrt{s}$ = 13 TeV. https://cds.cern.ch/record/2917252/files/HIG-20-011-pas.pdf

[699] Higgs physics at the HL-LHC and HE-LHC. CERN Yellow Report, doi.org/10.23731/CYRM-2019-007.221 https://e-publishing.cern.ch/index.php/CYRM/article/view/952

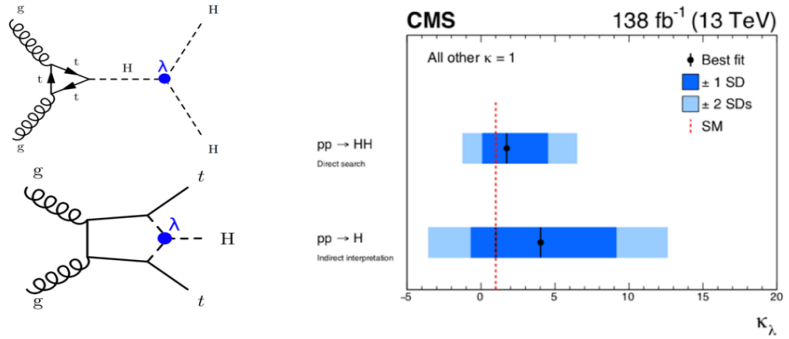


Fig. 24-14: Some information from single Higgs (H) processes on Higgs self-coupling modifier κ_λ, as suggested by the bottom diagram (left) and shown by the plot (right).

As shown by the upper plot of Fig. 24-15, all present CMS results on the pp → HH cross-section show a slight excess compared to expectation [700]. The lower plot shows that HL-LHC should give the answer.

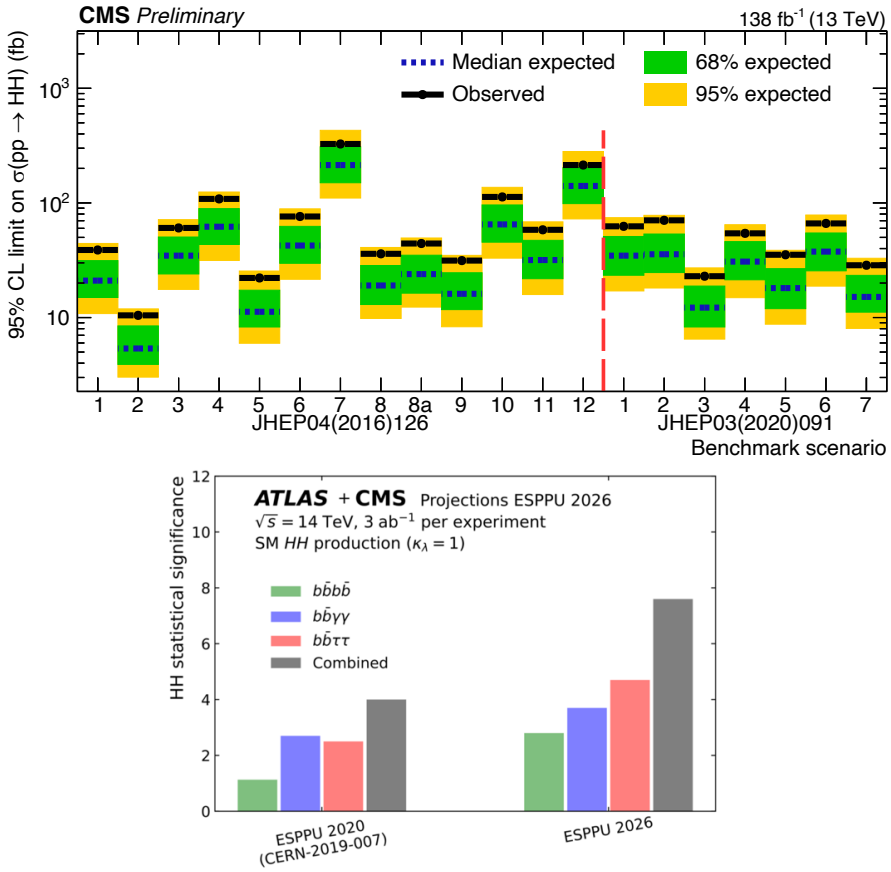


Fig. 24-15: Top: Upper limits on the HH production cross section at 95% CL for the two sets of HEFT (Higgs and Effective Field Theory) benchmarks. One benchmark is JHEP04(2016)126 (there were 12 benchmarks) the other is JHEP03(2020)091 (7 benchmarks). No significant deviations from expectations are observed, but there is an overall excess in all benchmarks, between 68% and 95% CL. Bottom: this overall excess will be checked at HL-LHC: combined (ATLAS+CMS) projections show an expected sensitivity of 7.6 σ [701].

[700] CMS Collaboration, Combination of searches for nonresonant Higgs boson pair production in proton-proton collisions at $\sqrt{s}$ = 13 TeV. https://cms-results.web.cern.ch/cms-results/public-results/preliminary-results/HIG-20-011/index.html

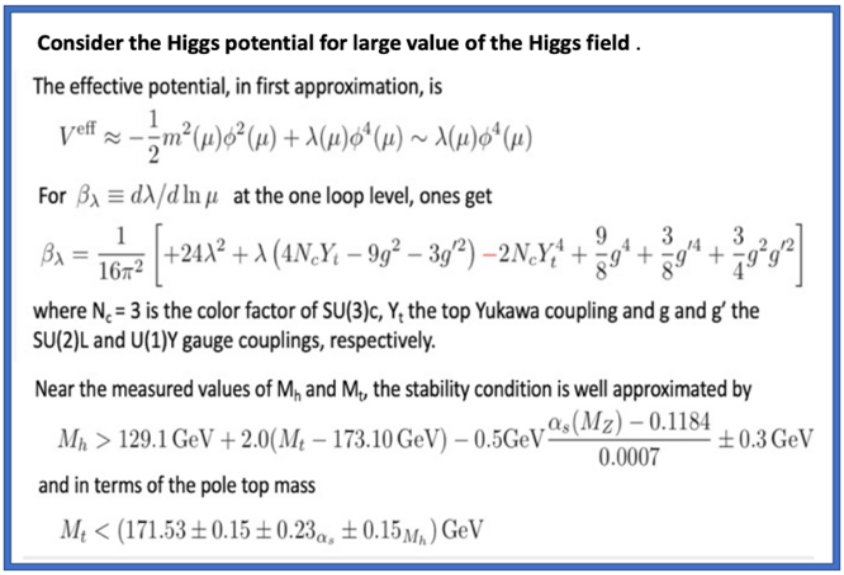
[701] L. Shchutska, Experimental Summary, Moriond QCD 2025, https://indico.cern.ch/event/1480248/contributions/6419614/attachments/3046263/5382526/ExpSummary.pdf

24.1.4 A deep mystery

Changing perspective, the Higgs boson is **an object of a totally new type**: a scalar which so far seems elementary. More than an end, as was said too often, its discovery is a beginning. **Precision first**: we will have to refine our knowledge of its properties. But the existence of elementary scalars being suggested by fundamental theories, such as superstrings, and appearing in other fields of physics, e.g. in cosmology, it is interesting to **enlarge the field of speculation**. For example, could the Higgs field be responsible for **cosmological inflation**?

With M_h known, all the SM parameters are measured, and we can extrapolate the behaviour of λ using the **renormalization group equations (RGE).** Some maths illustrating this point appear in Fig. 24-16.

A feature of what we observe is the cooperation of the top quark and the Higgs boson to put the EW vacuum in a situation of **metastability** [702], linked to the Higgs quartic coupling, here called λ, turning negative at high scale (see Fig. 24-17, giving two different versions of this property), and opening a kind of cosmic *detective story* (Fig. 24-18).



Consider the Higgs potential for large value of the Higgs field .

The effective potential, in first approximation, is

$$V^{\text{eff}} \approx -\frac{1}{2}m^2(\mu)\phi^2(\mu) + \lambda(\mu)\phi^4(\mu) \sim \lambda(\mu)\phi^4(\mu)$$

For $\beta_\lambda \equiv d\lambda/d\ln\mu$ at the one loop level, ones get

$$\beta_\lambda = \frac{1}{16\pi^2}\left[+24\lambda^2 + \lambda\left(4N_cY_t - 9g^2 - 3g'^2\right) - 2N_cY_t^4 + \frac{9}{8}g^4 + \frac{3}{8}g'^4 + \frac{3}{4}g^2g'^2\right]$$

where $N_c = 3$ is the color factor of SU(3)c, Y_t the top Yukawa coupling and g and g' the SU(2)L and U(1)Y gauge couplings, respectively.

Near the measured values of M_h and M_t, the stability condition is well approximated by

$$M_h > 129.1\,\text{GeV} + 2.0(M_t - 173.10\,\text{GeV}) - 0.5\text{GeV}\frac{\alpha_s(M_Z) - 0.1184}{0.0007} \pm 0.3\,\text{GeV}$$

and in terms of the pole top mass

$$M_t < (171.53 \pm 0.15 \pm 0.23_{\alpha_s} \pm 0.15_{M_h})\,\text{GeV}$$

Fig. 24-16: Sketch of the relation between M_h and M_{top} [703].

The Higgs is light enough to allow this extrapolation and the SM may remain consistent up to the Planck scale. However, our Universe is not located at the global minimum of the Higgs potential: a much deeper vacuum exists at large field values. This situation is called **metastability**. Our vacuum is not in immediate danger! But one would like to understand how cosmology put the Universe in that state.

Moreover, the evolution of the Universe went probably through violent periods, as **inflation and reheating,** where the Higgs field may have experienced large fluctuations, and one must understand why the vacuum did not decay into the true value, without assuming that some BSM physics is guaranteeing its stabilization [704].

---

[702] G. Degrassi *et al.,* Higgs mass and vacuum stability in the Standard Model at NNLO. https://arxiv.org/abs/1205.6497
F. Bezrukov *et al.,* Living beyond the edge: Higgs inflation and vacuum metastability. https://arxiv.org/abs/1412.3811
G. Degrassi, The role of the top quark in the stability of the SM Higgs potential. https://arxiv.org/abs/1405.6852

[703] G. Degrassi, ibid

[704] M. Zatta, The Higgs Boson and the Cosmos.
https://helda.helsinki.fi/server/api/core/bitstreams/a5bf308f-3c1e-42b7-b76f-5d94dae03ee8/content

Coming back to inflation (more in Section 30.10), it is well known that the scalar supposed to drive it needs a **flat effective potential** at high field value to ensure a "slow-roll" evolution. A priori the Higgs potential evolves approximatively as the 4th power of the field value, which is inadequate. A possible way to restore flatness is to allow the existence of **Higgs-inflaton couplings or non-minimal coupling with gravity**, see Ref. [705]. Figures 24-19 and 24-20 illustrate this possibility in the two different scenarios.

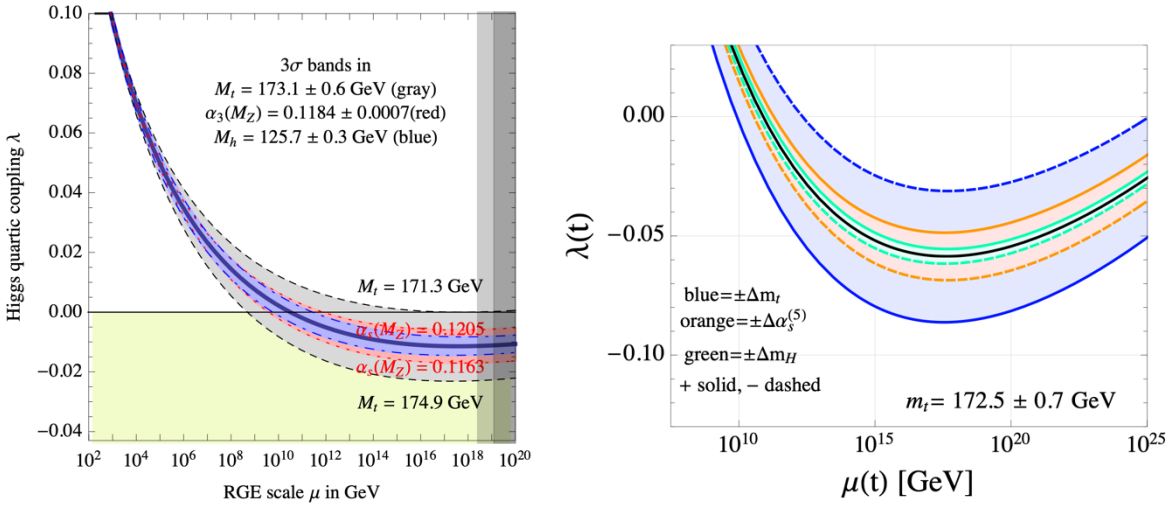


Fig. 24-17: Evolution of the quartic coupling with RGE scale: left from Ref. [706], right from Ref. [707].

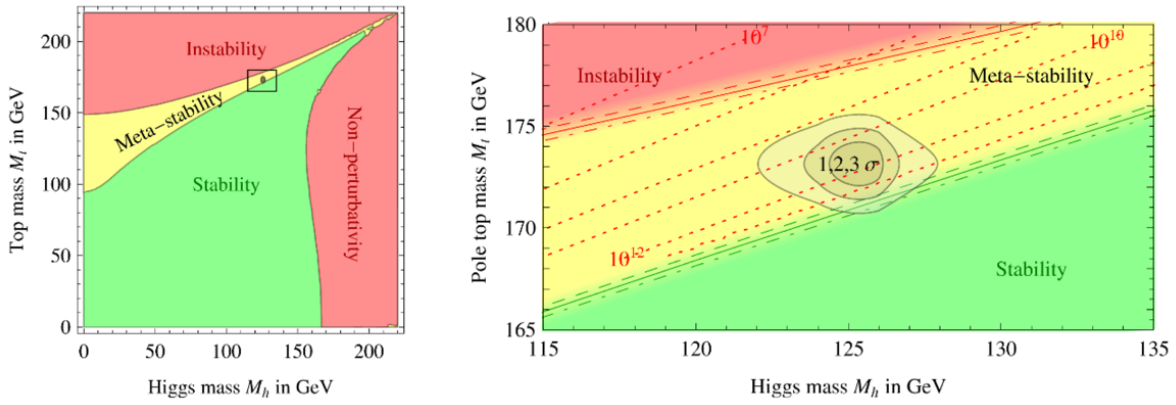


Fig. 24-18: Regions of stability, meta-stability and instability of the SM vacuum in the M_t – M_h plane (left). Right: zoom in the region of the preferred experimental range of M_h and M_t (the grey areas denote the allowed region at 1, 2, and 3 σ) [708].

[705] F. L. Bezrukov and M. E. Shaposhnikov, The Standard Model Higgs boson as the inflaton. https://arxiv.org/abs/0710.3755
[706] G. Degrassi *et al.,* Higgs mass and vacuum stability in the Standard Model at NNLO , https://arxiv.org/abs/1205.6497
[707] I. Masina and M. Quiros, EW instability and Higgs inflation. https://arxiv.org/abs/2403.02461
[708] G. Degrassi *et al.,* Higgs mass and vacuum stability in the Standard Model at NNLO. https://arxiv.org/abs/1205.6497

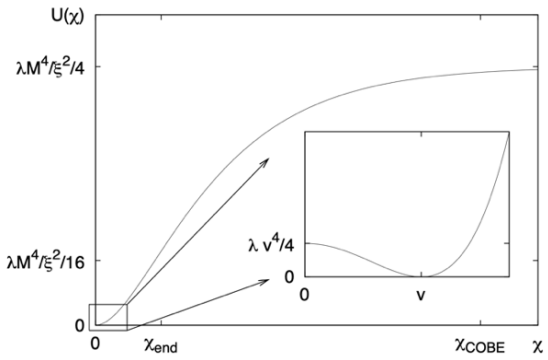


Fig. 24-19: A possible full effective potential of Higgs inflation (χ is related to h, χ ~h for small h). It is the near flatness of the potential at $\chi \gg M_P$ which makes the inflation possible [709].

About Fig. 24-20: extrapolating the SM Higgs potential at high field value, this work studies the barrier between the EW and Planck scale minima, arising by taking the central values of the relevant experimental inputs (α_S, M_t, M_H). It then extends the SM by including **a non-minimal coupling to gravity** and explore the phenomenology of the Higgs inflation model. The critical configuration shown corresponds to two degenerate minima. Even configurations that would be metastable in the SM may become viable for inflation.

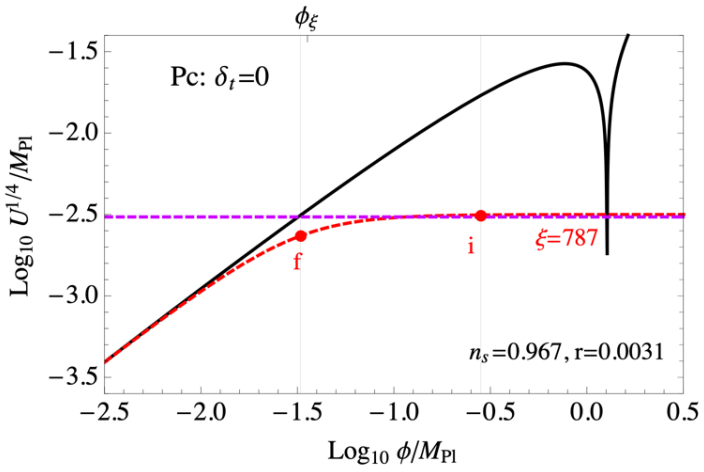


Fig. 24-20: This plot shows how the effective potential at high energies (black) is made flat (red) by introducing a non-minimal gravitational coupling between the Higgs and the Ricci scalar [710].

Let us summarize (see Ref. [711]). The measurement of M_h has determined the last unknown parameter of the SM, fixing the **Higgs quartic coupling λ**. It is most important to try to interpret it and understand whether it contains information about physics at shorter distances. The extrapolation of λ at high energies has revealed an unexpected and intriguing feature of the SM: assuming its validity up to very high energy scales, the measured value of M_h places the EW vacuum at the border between absolute stability and metastability. This calls for still better precision on the relevant key quantities, especially M_{top}.

[709] F. L. Bezrukov and M. E. Shaposhnikov, The Standard Model Higgs boson as the inflaton. https://arxiv.org/abs/0710.3755
[710] I. Masina and M. Quiros, EW instability and Higgs inflation. https://arxiv.org/abs/2403.02461
[711] J. Rubio, Higgs inflation. https://arxiv.org/abs/1807.02376
D. Buttazzo *et al.,* Investigating the near-criticality of the Higgs boson. https://arxiv.org/abs/1307.3536
A. Mantziris, On the cosmological implications of the electroweak vacuum instability. https://arxiv.org/abs/2111.02497

Metastability has important cosmological implications because large fluctuations in the Higgs field could trigger vacuum decay in the early Universe. Another fascinating possibility is that the Higgs field itself could **lead to inflation**, provided a non-minimal coupling to the Ricci scalar is added to the SM action. If substantiated, **Higgs inflation** would offer an unexpected relation between the SM parameters and the Universe at large scales.

24.1.5 More on baryogenesis

Bis repetita placent…

As we saw in Section 7.4.3, baryon and lepton numbers are not conserved in the SM, because of the **axial anomaly**, which connects them to **the integer-valued change of axial charge ΔQ_A** of the weak gauge field (see Section 7.4.4).

To conform to the literature, it is usual to introduce here the **Chern–Simons number N_{CS}** [712], the integral over $\partial_\mu J^\mu = [g^2/(16\pi^2)]\ \mathrm{Tr}[F_{\mu\nu}\tilde{F}^{\mu\nu}]$, so, as underlined in Section 7.4.5 quite similar to the axial charge and the winding number.

Baryogenesis at the EW scale is possible because of the chiral anomaly which relates the baryon number of fermions to the topological N_{CS} of the EW SU(2) gauge fields.

Vacua in the **EW theory** are labelled by an integer-valued N_{CS}. In the early Universe, for $T > 100$ GeV, it is possible to move from one vacuum to another over the potential barrier through **instanton/sphaleron** transitions, thus changing N_{CS} and B and L (but not B—L).

The change is $\Delta N_{cs}(t) = [g^2/(16\pi^2)] \int_0^t dt' \int d^3x\ \mathrm{Tr}[W_{\mu\nu}\tilde{W}^{\mu\nu}]$

$W^{\mu\nu} = \frac{\sigma^a}{2} W^{a\mu\nu}$, where σ^a are the Pauli matrices and $W^{a\mu\nu}$ the EW field strength. Sum over a, a = 1,3.

This change over time leads to $B(t)-B(0) = L(t)-L(0) = 3(N_{CS}(t) - N_{CS}(0))$.

Repeating what was said in Chapter 7, the key is **topology:** mappings from the 3-sphere S_3 to the gauge group G. If G is compact, as the EW $SU(2)_L$, which has the **topology of a sphere**, the mappings are classified by an **integer winding number** or topological charge, counting the number of times G can be wrapped around S_3. B violation is caused by the "winding" of the fields from one equilibrium to another.

The **sphaleron** [713] of Chapter 7, non-perturbative process, time-independent solution to the SM EW field equations, is involved in such B and L numbers violating processes. Since a sphaleron may change B, if the density of sphalerons was at some stage high enough, they could **wipe out any net excess of quarks over antiquarks.**

---

[712] This is our first (and nearly last) encounter of the Chern–Simons theory. However, the close relationship of the Chern–Simons number to the winding number of Section 7.4.4 is clear**.** In words, the Chern–Simons number transforms under a (large) gauge transformation as $N_{CS} \rightarrow N_{CS} + N$, where N is the winding number of the gauge transformation. The change in B and L is thus an integral multiple of the number of families N_F=3.
See R. Jackiv, Topological Aspects of Gauge Theories. https://arxiv.org/abs/hep-th/0501178 .
As said repeatedly, topology is the key. In math terms: not all gauge transformations can be generated by infinitesimal gauge transformations in general. An example is when the base manifold is a compact manifold without boundary such that the **homotopy class** of mappings from that manifold to the Lie group is nontrivial.
See also Parts I-6 and II-4 of J. C. Baez and J. P. Muniain, Gauge fields, knots and gravity. World scientific publishing, http://home.ustc.edu.cn/~zcj12138/reference/Gauge%20Fields,%20Knots%20and%20Gravity.pdf

[713] P. Arnold and L. McLerran, The Sphaleron Strikes Back. Fermilab-Pub-87/120-T, *Phys.Rev.D37, 1020,* https://lib-extopc.kek.jp/preprints/PDF/1987/8709/8709325.pdf

In the **EW Baryogenesis** scenario, the Universe B number is supposed to be generated **during** the EW phase transition**.** But this scenario does not work in the SM: it requires **stronger CP violation** (Chapter 14) and a **first order phase transition**, whereas the SM seems to have a smooth crossover.

However, knowing m_H, it is very useful, by simulating the effective EW theory on the lattice, to determine the sphaleron rate in the energy range of the EW crossover (see below). This is in particular relevant for Baryogenesis **via Leptogenesis**, which was evoked in Chapter 19 in relation with eventual **right-handed neutrinos**: if the lepton asymmetry is generated just before or during the EW phase transition, one must know the effect of the sphaleron rate on the generated B number.

This may suggest changes to bring to the SM, which could lead to an effective EW baryogenesis. For instance, including **additional multiplets of scalars to the SM Higgs sector**, accounting for the finite-temperature corrections, may change the sphaleron energy and its rate in comparison with the Hubble expansion rate. The exploration at LHC of an eventual extended Higgs sector will be the subject of Section 24.2.

We will come back to baryogenesis in Sections 27.2 and 32.4.2.

24.1.6 More on the sphaleron and the search for it

The particular sphaleron solution found in Ref. [714] in the Weinberg–Salam theory is identified as **the barrier between neighbouring vacua** for the following reasons:

(1) it is a static, unstable solution to the equations of motion;

(2) there exists a path through configuration space from one vacuum to the next for which the sphaleron is the point of maximum potential energy;

(3) moving from one vacuum to the sphaleron changes baryon number by exactly one half the amount of moving from one vacuum to the next.

The last point is determined by computing the Chern–Simons charge (see Ref. [715]) of the sphaleron $Q = N_F\, g^2/(32\,\pi^2)\int d^3x\, K^0$, where the Chern–Simons current is

$$K^\mu = \epsilon^{\mu\nu\rho\sigma}\left(F^a_{\nu\rho}\, W^a_\sigma - \frac{2}{3} g\, \epsilon_{abc}\, W^a_\nu\, W^b_\rho\, W^c_\sigma\right),$$

N_F is the number of families and a sum over a, a = 1,3 is made. This charge is related to **baryon number violation** by $\Delta B = \Delta Q$.

The sphaleron is studied in pure SU (2) theory with the Weinberg angle treated as a perturbation. The size of the sphaleron is $\mathbf{r \approx 1/M_W}$ and its energy is $E_{sp} = 2\, M_W\, A\, (\lambda/g^2)/\alpha_W$ where A varies between 1.8 and 3, hence E_{sp} between 8 and 14 TeV at zero T, depending on the quartic Higgs self-coupling λ. With its measured value for the 125 GeV Higgs, one expects $\mathbf{E_{sp} \sim 9\ TeV}$, as an estimate of the energy required for the sphaleron transitions to overcome the potential barrier.

Using a Boltzmann factor, the rate per unit volume for crossing the barrier might be of the order

$$R \sim T^4\, e^{-E_{sp}(T)/T},$$

[714] F. R. Klinkhamer and N. S. Manton, A Saddle-Point Solution in the Weinberg-Salam Theory. https://inspirehep.net/files/4af12e146ead230707ecf306e4b7b7dd

[715] P. Arnold and L. McLerran, The Sphaleron Strikes Back. https://libextopc.kek.jp/preprints/PDF/1987/8709/8709325.pdf J. Zanelli and L. Huerta, Introduction to Chern–Simons Theory. https://www.researchgate.net/publication/323460123_Introduction_to_Chern-Simons_Theory , and https://inspirehep.net/files/9c82fb4d04fcefa94c2e4cbc534e13b5

where M_W is replaced by the effective temperature-dependent mass $M_w(T)$ of finite-temperature field theory. As one approaches the critical temperature T_C of Weinberg–Salam, the size of the sphaleron becomes infinite, the classical energy barrier becomes zero and the R estimate becomes of order 1.

It has been claimed that tunnelling between topologically distinct vacua is negligible in the weak interactions. But this argument only applies to a virtual quantum process. If there were **sufficient real energy available**, more than the sphaleron energy E_{sp}, the tunnelling process might be enhanced.

According to Ref. [716], "*the sphaleron appears to provide a viable baryon-number changing mechanism, and in a range of temperatures, $M_w(T) \ll T \ll M_w(T)/\alpha_W$, the rate of baryon-number change may be reliably computed in a weak coupling limit*."

There seem to be two situations, at least, where this could happen.

i. HE collisions of particles

The first is in **HE collisions of particles**, with as signature of the process the **violation of baryon and lepton number conservation** [717].

Within perturbative SM physics, one globally conserved current exists for each of the 12 fundamental LH fermions doublets. An anomaly breaks this conservation because the integral of the anomalous term, **namely** the Chern–Simons (or winding) number $\mathbf{N_{CS}}$, is nonzero. The anomaly exists for each fermion doublet, so the lepton number L changes by $\Delta L = 3\,\Delta\mathbf{N_{CS}}$ (3 leptons produced, each has L = 1). The baryon number change ΔB is the same (each quark has B = 1/3 and there are 3 colours and 3 generations of quarks produced). Then $\Delta(B + L) = 6\,\Delta\mathbf{N_{CS}}$ and $\Delta(B - L) = 0$, key relations for the role of sphalerons.

The sphaleron would thus involve 12 left-handed fermions doublets: 3 quarks doublets for each generation and one lepton doublet for each generation. A schematic diagram of flavour structure of the process related to a unit change in Chern–Simons number, $\mathbf{\Delta N_{CS}} = 1$, is shown in Fig. 24-21 [718]. Hence possible events as $q + q \rightarrow 7\,\bar{q} + 3\bar{l} + n_B$W/Z/$\gamma$/H, where n_B is the total number of gauge and Higgs bosons.

Such a **search for EW sphaleron** was performed by CMS [719]. An upper limit of 0.021 is set at 95% confidence level on the fraction of all quark-quark interactions above the nominal threshold energy of 9 TeV resulting in the sphaleron transition.

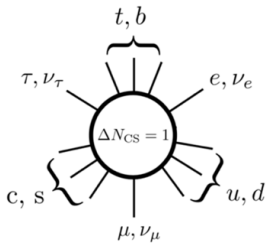


Fig. 24-21: The diagram of flavour of the process related to a unit change in Chern–Simons number, $\Delta N_{CS} = 1$.

[716] P. Arnold and L. McLerran, The Sphaleron Strikes Back. https://libextopc.kek.jp/preprints/PDF/1987/8709/8709325.pdf
[717] A. Papaefstathiou *et al.,* On the phenomenology of sphaleron-induced processes at the LHC and beyond. Here one considers QCD sphalerons. https://arxiv.org/abs/1910.04761
J. Ellis and K. Sakurai, Search for Sphalerons in Proton-Proton Collisions.
https://cds.cern.ch/record/2124347/files/arXiv:1601.03654.pdf
[718] Ibid, https://arxiv.org/abs/1910.04761
[719] CMS collaboration, Search for black holes and sphalerons in high-multiplicity final states in proton-proton collisions at $\sqrt{s}$ = 13 TeV. https://arxiv.org/abs/1805.06013. Transitions searched for were somewhat simpler than the 12 LH fermions doublets one and included missing E_T for undetected ν.

ii. System at very high temperature

The other situation is for a system at **very high temperature** ($kT > E_{sp}$). Thermal fluctuations might then produce the baryon number violating process via the sphaleron at a substantial rate. This could be important in the **Universe at early times**. Large-scale lattice simulations give the rate of baryon number violating processes (the sphaleron rate). Figure 24-22 shows the SM sphaleron rate as a function of temperature [720] across the EW phase transition temperature. Although the cross-over is rather sharp, with a "pseudocritical" temperature T_C = 159 ± 1 GeV, there is **no true phase transition in the SM**. Such studies in BSM scenarios are thus welcome.

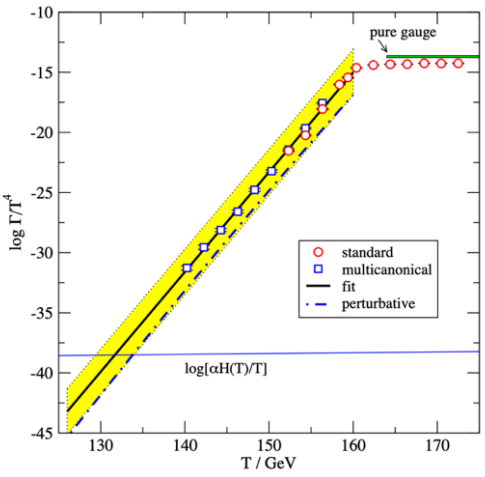


Fig. 24-22: The SM sphaleron rate as a function of temperature.

24.2 Exploration of an eventual extended Higgs sector

One important field of research is obviously **the Higgs sector**. Are there, beyond the 125 GeV object, other scalar or pseudoscalar particles hiding? It is known that, respecting existing EW results, e.g. keeping the ρ parameter (see Section 18.3) close to one, one can perform additions to the unique doublet of the SM and introduce singlets and doublets. The **2 Higgs-doublet** is familiar, e.g. in SUSY. It is also possible to introduce triplets, for instance one real and one complex in the Georgi–Machacek (GM) model, offering more states, as a doubly-charged Higgs [721]. One can even consider still richer possibilities, as a Higgs septet [722].

Benchmarks of such scenarios are considered, sometimes fed by hints of modest fluctuations observed in some LHC data (e.g. Fig. 24-23), calling a confrontation with the same data of the other experiment (Fig. 24-24). Such fluctuations, as in Fig. 24-25, up to now, are not coined as significant by the experiments, who should give an exact definition of them [723] and keep control on their eventual combination.

---

[720] M. d'Onofrio *et al.,* The Sphaleron Rate in the Minimal Standard Model. https://arxiv.org/abs/1404.3565

[721] An extreme case is a supersymmetric version of the GM model, L. Cort *et al.,* Supersymmetric Custodial Triplets. https://arxiv.org/abs/1308.4025

[722] J. Hisano and K. Tsumura, The Higgs boson mixes with an SU(2) septet representation. https://arxiv.org/abs/1301.6455

[723] A good model is a review of ATLAS published results of searches for possible additional scalar particles and exotic decays of the Higgs boson using up to 140 fb^{-1} of 13 TeV proton–proton collision. ATLAS Collaboration, ATLAS searches for additional scalars and exotic Higgs boson decays with the LHC Run 2 dataset. https://arxiv.org/abs/2405.0491

In such matters care is required: the late "750 GeV" object detains the record of INSPIRE entries (Fig. 24-26). Another concern is the status of the 95.4 GeV two-photon excess [724], often linked to the probably fake "97/98 GeV excess" of LEP (Chapter 18).

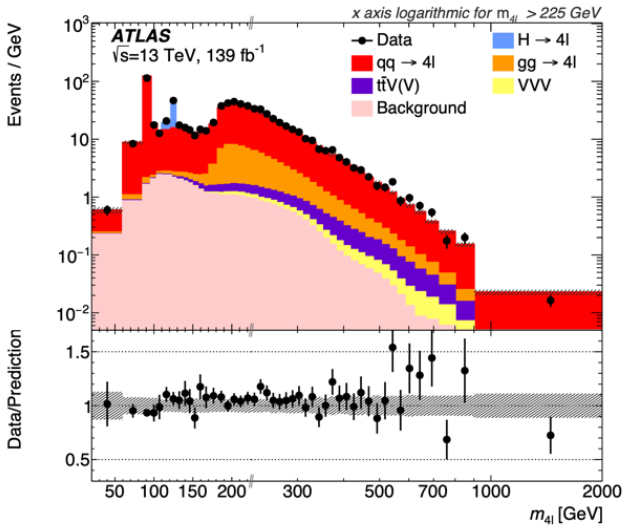


Fig. 24-23: The ATLAS 4-lepton spectrum, which stirred some turmoil [725].

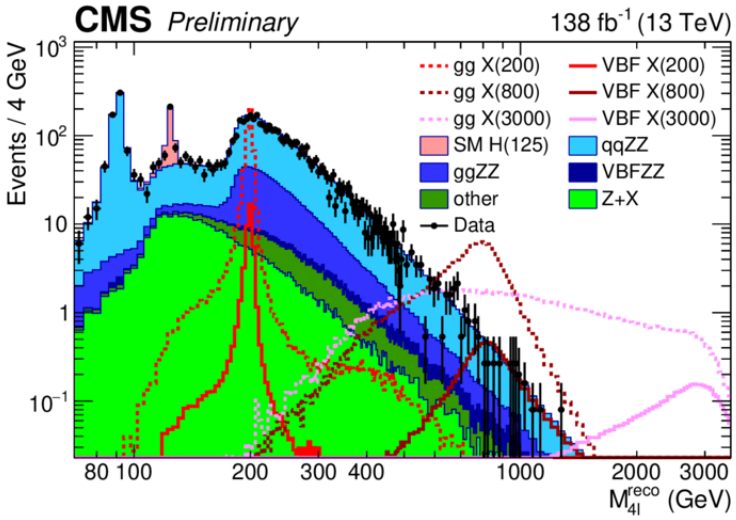


Fig. 24-24: The same spectrum, from CMS [726].

As shown elsewhere, adding objects to the SM may solve some of the puzzles left. In Chapter 19 the see-saw solution to the neutrinos tiny masses was considered. Extra states completing the SM Higgs

[724] ATLAS Collaboration, Measurement of the H → γγ fiducial cross-section in *pp* collisions at √s = 13.6 TeV with the ATLAS detector. ATLAS-CONF-2023-03, https://inspirehep.net/files/263d630ef8c7191eb42f5e29bfa4bb8e , CMS observes an excess of local (global) significance of 2.9σ (1.3σ) at 95.4 GeV. ATLAS observes a local significance of 1.7σ at 95.4 GeV.
[725] ATLAS Collaboration, Measurements of differential cross-sections in four-lepton events in 13 TeV proton-proton collisions with the ATLAS detector. https://arxiv.org/abs/2103.01918
[726] CMS Collaboration, Search for heavy scalar resonances decaying to a pair of Z bosons in the 4-lepton final state at 13 TeV. CMS-PAS-HIG-24-02, https://cms-results.web.cern.ch/cms-results/public-results/preliminary-results/HIG-24-002/

sector could change the **nature of the EW transition** in such a way that EW baryogenesis could be considered [727], as discussed previously.

The potential complexity of Higgs searches in the di-top final state is described in Ref. [728]. See also Fig. 24-38.

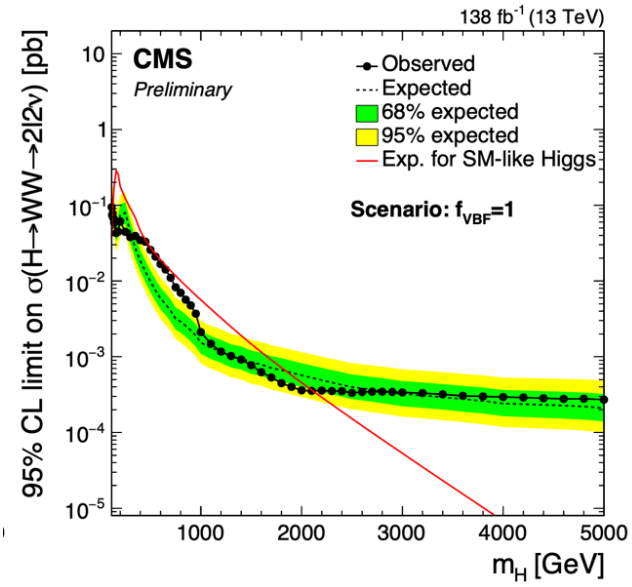


Fig. 24-25: A still existing anomaly in the H → WW search [729].

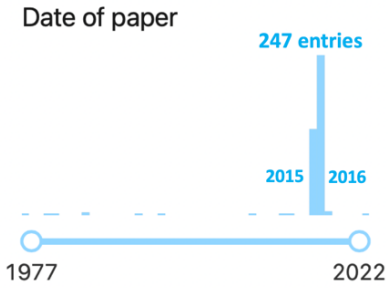


Fig. 24-26: The "750 GeV", 247 entries in the INSPIRE data base in 2015 and 2016.

The importance of the Higgs sector, still illustrated in Fig. 24-27 [730], calls obviously for a careful and thorough study at LHC, HL-LHC and machines to come. As discussed previously the Higgs self-interaction, hence double Higgs production, is a most crucial topic. The excellent agreement of the 125 GeV Higgs production cross-sections and decay branching ratios allows to make fair predictions at higher energies.

Higgs production cross-sections are given in Fig. 24-28 [731] for pp and e^+e^- collisions at diverse energies and in Fig. 24-29 [732] for e^+e^- as a continuous function of energy.

---

[727] M. J. Ramsey-Musolf, The electroweak phase transition : a collider target. https://arxiv.org/abs/1912.07189

[728] H. Bahl *et al.,* Impact of interference effects on Higgs-boson searches in the di-top final state at the LHC. https://arxiv.org/abs/2503.02705

[729] CMS Collaboration, Search for high mass resonances decaying into W^+W^- in the dileptonic final state with 138 fb^{-1} of proton-proton collisions at $\sqrt{s}$ = 13TeV. CMS PAS HIG-20-016, https://cds.cern.ch/record/2803723/files/HIG-20-016-pas.pdf

[730] S. Dawson *et al.,* Report of the Topical Group on Higgs Physics for Snowmass 2021: The Case for Precision Higgs Physics. https://arxiv.org/abs/2209.07510

[731] U. Amaldi *et al.,* Charting the European Course to the High-Energy Frontier. https://arxiv.org/abs/1912.13466
pp cross-sections from R. Contino *et al.,* Physics at a 100 TeV pp collider: Higgs and EW symmetry breaking studies. https://arxiv.org/abs/1606.09408 and J. Baglio *et al.,* Prospects for Higgs physics at energies up to 100 TeV. https://arxiv.org/abs/1511.07853
e^+e^- cross sections from The Compact Linear Collider (CLIC) 2018 Summary Report. https://arxiv.org/abs/1812.06018
P. Roloff *et al.,* The Compact Linear e^+e^- Collider (CLIC): Physics Potential. https://arxiv.org/abs/1812.07986
A. Robson and P. Roloff, Updated CLIC luminosity staging baseline and Higgs coupling prospects. https://arxiv.org/abs/1812.01644
$\mu^+\mu^-$ *cross sections* from J. P. Delahaye *et al.,* Muon Colliders (The Muon Collider Working Group). https://arxiv.org/abs/1901.06150 .
Double beam polarization can increase the HHZ and HHνν cross-sections by a factor of 1.5 to 2.

[732] ibid for e^+e^-

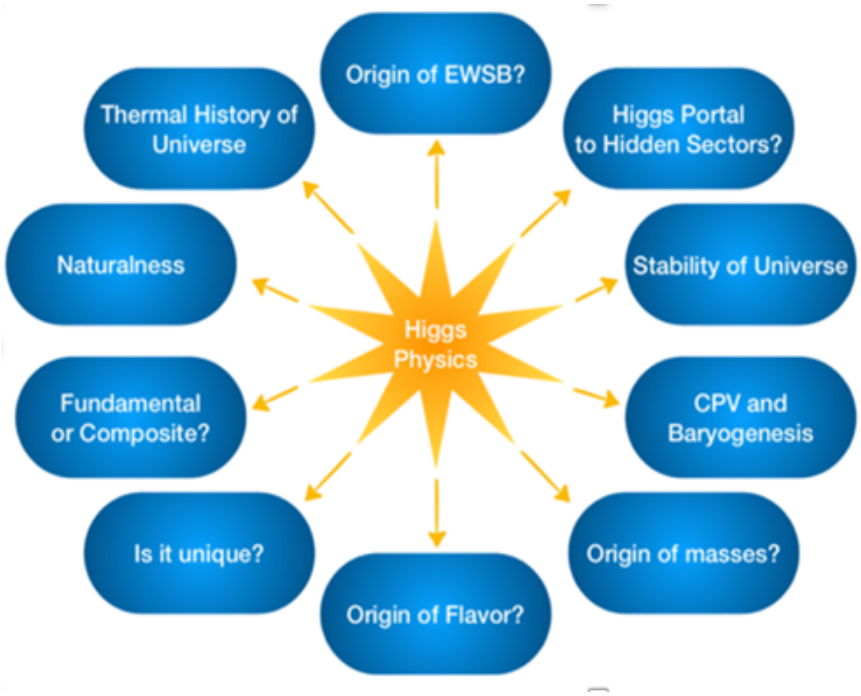


Fig. 24-27: Questions raised by the Higgs sector.

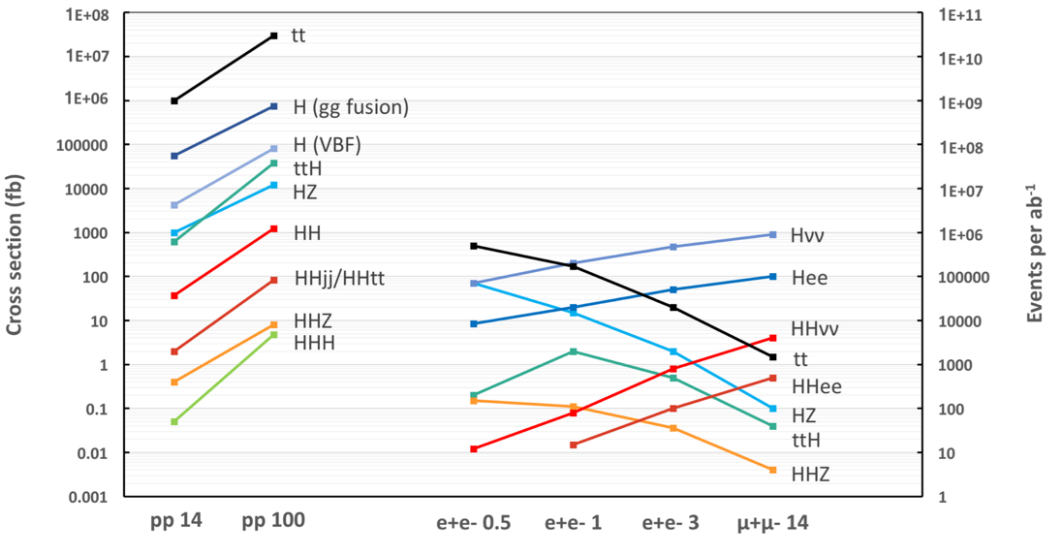


Fig. 24-28: Cross-section of key Higgs channels at different considered energies of pp and e^+e^- collisions.

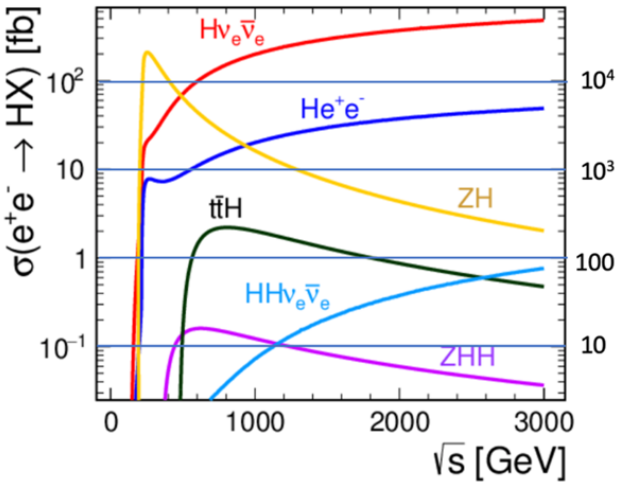


Fig. 24-29: Higgs cross-section in e^+e^- collisions as function of $\sqrt{s}$. At right, number of events per year (10^7 efficient seconds per year) at 10^{34} $cm^{-2}s^{-1}$ luminosity and 100% acceptance.

24.3 Other searches at LHC

24.3.1 The scenarios

At the end of Chapter 18, Fig. 18-12 illustrated the proliferation of theories invented to try to solve, at different depths, the problem of **hierarchy**. All these theories have led to domains of searches. The confirmation of a light and apparently SM-like Higgs boson has closed or weakened some possibilities. However, it started searches for an extended Higgs sector. Being at the right mass for SUSY it entertained searches for superpartners.

The ATLAS, CMS and LHCb experiments have thus performed many searches beyond Standard Model (BSM) physics [733] with LHC Run 2 data, covering a wide variety of models and signatures: generic searches, SUSY searches, extended Higgs sector, new fermions and bosons. So far, none of these searches have shown any significant deviation from SM expectations. The results of the analyses have been interpreted in terms of various models, and lower bounds on new particle masses or upper bounds on cross sections have been reported.

The quest continues with the design of more searches, using more refined techniques. In the meantime, preparations are underway for the **High-Luminosity LHC**, exploring innovative research methods that would allow to exploit at best this huge luminosity [734].

We have seen or will see in various chapters covering different topics, which are the corresponding searches at LHC and elsewhere.

Basic searches for new high-mass resonances decaying to fermions at the LHC are summarized in Ref. [735].

Searches for **Flavour Changing Neutral Currents** (Chapter 9 and Section 30.8) are pursued in all sectors and extended to top and Higgs decays.

---

[733] S. Sekmen on behalf of the ATLAS, CMS et LHCb Collaborations, Highlights on Supersymmetry and Exotic Searches at the LHC. https://arxiv.abs/abs/2204.03053

[734] ibid

[735] B. Clervaux and C. Gwilliam, Searches for New High-Mass Resonances Decaying to Fermions at the LHC. https://arxiv.org/abs/2311.09824

All kinds of searches for **Heavy Neutral Leptons (HNLs)** are carried out at the LHC, covering a variety of signatures and theoretical models [736] (Chapter 19).

If **Dark Matter** interacts weakly with the SM it could be produced at the LHC. Chapter 31 will give more details. In particular **Axion Like Particles (ALPs)** (Section 31.3) are searched for at LHC in a wide range of masses [737] **from 0.5 GeV to a few TeV** with various analysis strategies and advanced analysis techniques improving the sensitivity.

Unfortunately, a common point to all these searches is **the absence, up to now, of any discovery.**

However, in spite of the huge luminosity, the quality of LHC detectors allowed the exploration of a rich **low mass spectroscopy**, with the discovery of close to hundred new objects. This is described in detail in Chapter 28.

Another positive fact is that new and relatively modest experiments installed in the **forward regions of the LHC interaction points** will bring a most important complement to LHC physics (Chapter 31).

24.3.2 Back to Supersymmetry

We already briefly discussed the status of Supersymmetry in Chapter 18. Presently, most LHC analyses are performed within the context of **simplified models** [738]. For arguments calling for more contact with deep theoretical ideas, as Strings, the Landscape, etc., see for instance Ref. [739].

The absence, up to now, of SUSY partners at the LHC has started a **naturalness crisis** within the HEP community. Before the LHC advent, it was widely expected that superparticles would exist with mass values comparable to $m_{weak} \sim 100$ GeV. There was already a concern in some minds after the non-appearance of charginos at LEP2.

On the contrary, the observed Higgs mass $M_h = 125$ GeV is well within (albeit on the upper side) the predictions of the Minimal Supersymmetric SM (MSSM). Let us recall that in SUSY the quartic coupling of the Higgs potential is related to the gauge couplings of the electroweak sector. Therefore, in the MSSM, the lightest Higgs mass deviates from the Z mass only through **radiative corrections**, which lead to an upper mass bound of 130 GeV (Chapter 17).

Besides the Higgs boson mass value and LHC direct bounds, the constraint having by far the strongest impact on the parameter space of the MSSM is the **relic density**.

A scan of soft SUSY breaking terms over "a friendly landscape" (Ref. [740]) predicts that $m_h \simeq 125$ GeV is favoured along with no signs yet of sparticles, which is what LHC has told up to now.

An estimate of plausibility of a SUSY model is largely based on **naturalness**. The impression may have been given that it is somewhat subjective. It is therefore essential to define what one means by naturalness and to provide a quantitative measure of what can be called natural or not (Chapter 18). **The definition** and meaning of fine-tuning may indeed be ambiguous: if variables are more correlated than expected, fine-tuning may disappear.

So, SUSY could repeat, as Mark Twain: **"The announcement of my death is very exaggerated".**

---

[736] J. M. Vizan Garcia, Heavy Neutrino Searches at LHC. https://www.researchgate.net/publication/380750227_Heavy_Neutrino_Searches_at_LHC

[737] M. Gallinaro, Axion-like particle searches at the LHC. https://www.researchgate.net/publication/378889710_Axion-like_particle_searches_at_the_LHC

[738] For a good status report see I. Vivarelli, Supersymmetry and the LHC Run 2. http://www.scholarpedia.org/article/Supersymmetry_and_the_LHC_Run_2

[739] H. Baer *et al.,* Prospects for supersymmetry at high luminosity LHC. https://arxiv.org/abs/2502.10879

[740] ibid

Concerning hopes, Fig. 24-30 [741] shows for instance the expected range of sparticle and Higgs masses from the non-universal Higgs model NUHM3 as realized from the string landscape. The expected range of masses is shown by the blue histogram, the orange histogram shows the reach of HL-LHC.

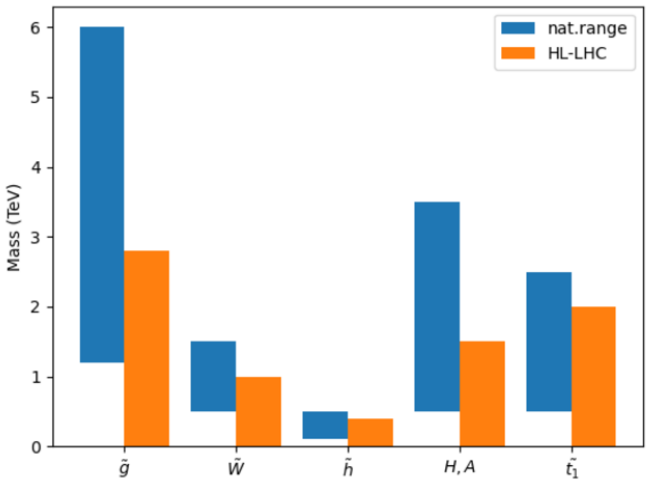


Fig. 24-30: Expected range of sparticle and Higgs masses from the non-universal Higgs model NUHM3.

As an example of actual searches, combinations of ATLAS SUSY searches for charginos and neutralinos using various decay channels are presented in Ref. [742]. For electroweak-inos and sleptons [743], ATLAS/CMS observed limits are in all cases weaker than the expected ones: the significance is small but, according to some theorists, the effects are crudely similar (Fig. 24-31 left). The limits are displayed in the **$m(\tilde{\chi}_2^0)$ – Δm, Δm = $m(\tilde{\chi}_2^0) - m(\tilde{\chi}_1^0)$ plane**. For one of the scenarii (higgsino), the observed limits for ATLAS (CMS) are shown in black (brown), where the bands indicate the 1σ theory uncertainties. The authors say: "*the ATLAS excess is most pronounced at Δm ∼ 30 GeV, while CMS shows an excess of events in the range Δm = 20–30 GeV".* Obviously more data are needed.

Figure 24-31 right illustrates that, as the experiments improve their reconstruction, **compressed EW SUSY models** including degenerate neutralinos / charginos (higgsinos) can be tested at LHC. The traditional sport in SUSY, closing "holes" left in the domains of parameters, is systematically pursued.

For the possible impact of SUSY on the very precise measurements that a Z giga-factory could offer, see Ref. [744].

---

[741] ibid

[742] ATLAS Collaboration, Statistical Combination of ATLAS Run 2 Searches for Charginos and Neutralinos at the LHC. https://arxiv.org/abs/2402.08347

[743] ATLAS Collaboration, Search for chargino–neutralino pair production in final states with three leptons and missing transverse momentum in √s = 13 TeV pp collisions with the ATLAS detector. https://arxiv.org/abs/2106.01676
ATLAS Collaboration, Searches for electroweak production of supersymmetric particles with compressed mass spectra in √s = 13 TeV pp collisions with the ATLAS detector. https://arxiv.org/abs/1911.12606
CMS Collaboration, Combined search for electroweak production of winos, binos, higgsinos, and sleptons in proton-proton collisions at √*s* = 13 TeV. CMS-PAS-SUS-21-008, https://cds.cern.ch/record/2853345?ln=en
CMS Collaboration, Search for supersymmetry in final states with two or three soft leptons and missing transverse momentum in proton-proton collisions at √s = 13 TeV. https://arxiv.org/abs/2111.06296
Comments from U. Ellwanger *et al.,* NMSSM explanation for excesses in the search for neutralinos and charginos and a 95 GeV Higgs boson. https://arxiv.org/abs/2404.19338
D. Agin *et al.,* Seeking a coherent explanation of LHC excesses for compressed spectra. https://arxiv.org/abs/2404.12423

[744] S. Knapen *et al.,* Imprints of supersymmetry at a future Z factory. https://arxiv.org/abs/2407.13815

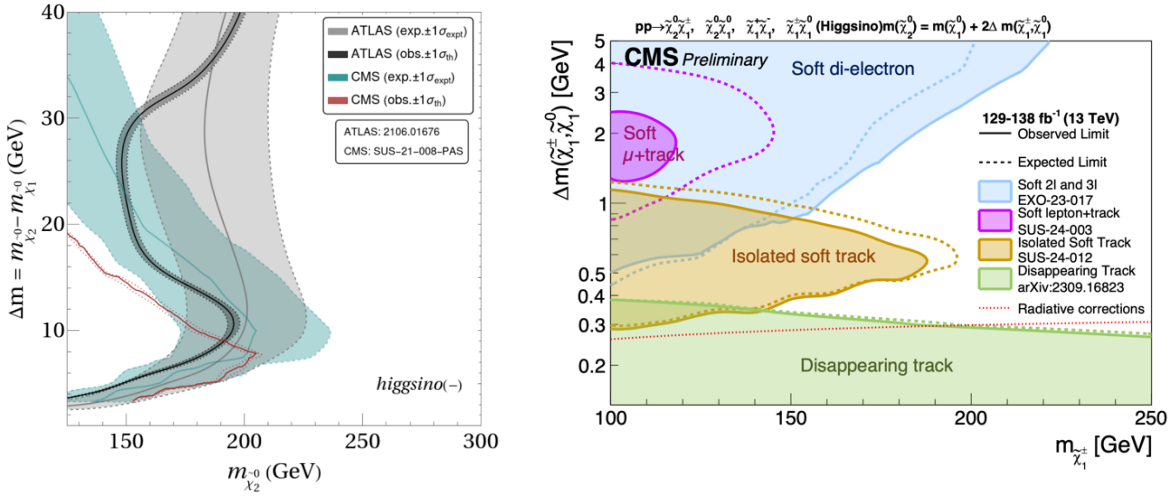


Fig. 24-31: Left: observed and expected limits with ±1σ uncertainty in higgsino search [745]. Right: excluded regions in $\Delta m - m_{\tilde{\chi}_1^\pm}$ plane [746].

24.3.3 Effective field theory

The absence so far of discoveries other than the BEH boson has led to turn to **effective field theories** (EFT). The idea is that "*things become **simpler seen from afar** because the details escape*". For the SM, this means that the experiments carried out at energy E (the long distance) do not require precise knowledge of the physics involved at a scale $\Lambda \gg E$, the short distance.

As for the SM the Lagrangian is built of gauge invariant operators involving the fermions, gauge and Higgs fields, but the difference is that the interactions with arbitrarily high **mass dimensions D** are introduced in the Standard Model EFT (SMEFT), organized in an **expansion in inverse power D-4 of Λ**. The SM is of dimension 4. In dimension 5 there is a single operator which only concerns neutrinos. Those of interest for LHC physics are of dimension 6. For an excellent introduction to EFT and its illustration with Fermi theory see Ref. [747]. A pioneering work is described in Ref. [748]. A complete and non-redundant list of operators in SMEFT exists now, called the Warsaw basis [749].

The SMEFT Lagrangian can be written as

$$L_{SMEFT} = L_{SM} + \frac{1}{\Lambda}\sum_i c_i^{(5)} O_i^{D=5} + \frac{1}{\Lambda^2}\sum_i c_i^{(6)} O^{D=6} + \frac{1}{\Lambda^3}\sum_i c_i^{(7)} O^{D=7} + \frac{1}{\Lambda^4}\sum_i c_i^{(8)} O^{D=8}$$

where each O_i^D is a gauge invariant operator of canonical dimension D constructed from the SM fields, and the parameters $c^{(D)}$ are called **the Wilson Coefficients** (WC).

Considering for instance the EW fit (see Fig. 18-5), besides probing the SM, implementing BSM parameters into the fit allows to search directly for new physics by adding coefficients of a SMEFT to the EW fit [750]. Getting a compatibility with zero for the WCs proves the validity of the SM.

---

[745] M. Chakraborti *et al.,* Consistent Excesses in the Search for $\tilde{\chi}_2^0\tilde{\chi}_1^\pm$: Wino/bino vs. Higgsino Dark Matter. https://arxiv.org/abs/2403.14759

[746] A. Hoecker, EPS-HEP 2025 — Conference Highlights. https://indico.in2p3.fr/event/33627/contributions/153160/attachments/95391/146107/EPS-HEP-Highlights-Jul2025.pdf

[747] A. Falkowski, Lectures on Effective Field Theories. https://indico.in2p3.fr/event/22195/contributions/86017/attachments/59873/81148/eftlectures.pdf

[748] W. Buchmüller and D. Wyler, Effective Lagrangian Analysis of New Interactions and Flavour Conservation. https://lib-extopc.kek.jp/preprints/PDF/1985/8510/8510273.pdf

[749] B. Grzadkowski *et al.,* Dimension-Six Terms in the Standard Model Lagrangian. https://arxiv.org/abs/1008.4884

[750] Y. Fischer *et al.,* The global electroweak fit in the SM and SMEFT. https://inspirehep.net/files/9edfb468cd0fa1c72de3e248ce82db1e

The problem is that a complete basis of operators of dimension D = 6 is characterized by 2499 independent parameters. It is imperative to make a selection, and from this point of view the symmetries of flavour offer an effective principle of organization in this vast set of parameters.

An example is given in Ref. [751]. The $U(2)^5 = U(2)_q \times U(2)_u \times U(2)_d \times U(2)_l \times U(2)_e$ symmetry is a global symmetry, acting on each of the five SM fermion species with independent gauge quantum numbers (q, u, d, l, e). Within each of these species, the two lightest generations transform as a doublet under a specific subgroup of $U(2)^5$, whereas the third generation is a singlet. The question motivating this asymmetry is: are present data compatible with the hypothesis of new dynamics **primarily coupled to the 3rd generation** of fermions near the TeV scale and, if so, under which UV conditions?

The d = 6 SMEFT operators in the exact $U(2)^5$ symmetric limit, in the CP-conserving limit, consist of "only" 124 independent terms. The effective Lagrangian can thus be decomposed as $L = L_{SM}^{(d=4)} + \sum_i C_i Q_i$, where the first term is the SM Lagrangian, Q_i are operators and C_i their WC.

To constrain the $U(2)^5$ symmetric SMEFT, a combination of bounds stemming from EW, flavour and collider observables was performed. Once observables have been expressed in terms of SMEFT WCs at the right scale Λ_{NP}, the $U(2)^5$ symmetry is imposed. Theory expressions then depend on WCs of the $U(2)^5$-symmetric SMEFT.

The results tell that with the hypothesis of exact $U(2)^5$ symmetry, and additional simple assumptions, such as the mild suppression of all operators involving light fields at the high scale, all present bounds can be reconciled **with an effective scale as low as 1.5 TeV**. This result is particularly encouraging in light of ongoing experimental searches for NP, both at the low- and high-energy frontier. Concerning EW observables, a future Giga Z / Higgs factory program would bring a major progress.

Reference [752] explores the leading directions in the SMEFT and classifies all possible irreducible representations under $U(3)^5$ flavour symmetry of new heavy spin-0, 1/2, and 1 fields integrating out to dimension-6 operators at the tree level. Experimental constraints are derived with the existing global SMEFT fits, using top, Higgs boson and EW measurements along with various constraints. The set of obtained bounds summarises the present knowledge from indirect searches of flavour-blind new physics mediators.

CMS [753] gives a combined EFT interpretation of Higgs, EW vector boson, top quark, and multijet measurements.

---

[751] L. Allwicher *et al.,* New Physics in the Third Generation: A Comprehensive SMEFT Analysis and Future Prospects. https://arxiv.org/abs/2311.00020 .This symmetry results from $U(3)^5 = U(3)_q \times U(3)_u \times U(3)_d \times U(3)_l \times U(3)_e$, the flavour symmetry corresponding to the independent rotation of each SM fermion field, the $SU(2)_L$ doublets called q and l (for all the quarks and leptons) and the $SU(2)_L$ singlets called u (for all the 2/3 quarks), d (for all the –1/3 quarks) and e (for all the charged leptons), **by singularizing the 3rd family with respect to the light ones.**

[752] A. Greljo and A. Palavric, Leading directions in the SMEFT. https://arxiv.org/abs/2305.08898 $U(2)^5$ of L. Allwicher *et al.,* New Physics in the Third Generation: A Comprehensive SMEFT Analysis and Future Prospects. https://arxiv.org/abs/2311.00020 is derived from $U(3)^5$ of A. Greljo and A. Palavrić, Leading directions in the SMEFT. https://arxiv.org/abs/2305.08898 , whose structure is explained in the previous note.

[753] CMS Collaboration, Combined EFT interpretation of top quark, Higgs boson, electroweak and QCD measurements at CMS. https://arxiv.org/abs/2501.02957

24.4 Other LHC measurements and top physics

24.4.1 Overview

In addition to studying the Higgs boson, the LHC has performed **a large number of measurements.** Figure 24-32 gives substance to Fig. 21-1, illustrates the huge amount of work done on experimental and theoretical sides, and proves that a hadron collider can also be a great instrument for measurements.

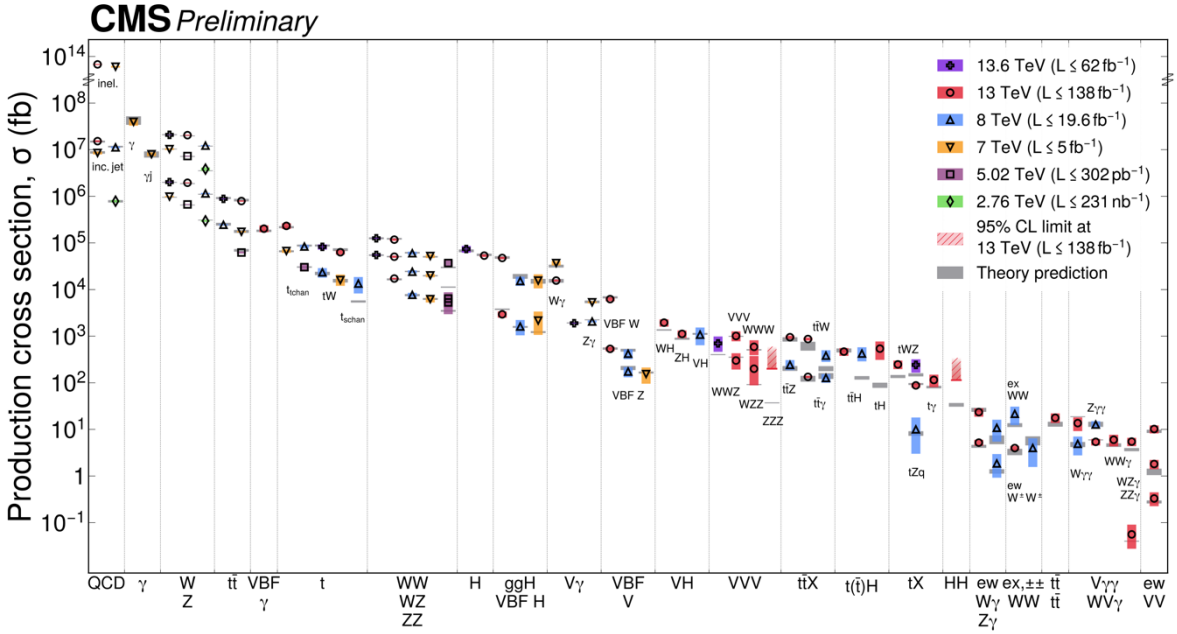


Fig. 24-32: Overview of CMS measurements (ATLAS has similar results) [754].

The production of **single, di- and tri-bosons** is a first sector of activity. The number of decades covered is impressive, as well as the agreement with theoretical expectations.

In basic EW measurements, LHC is now reaching and overtaking the accuracy of the LEP/SLD ones. For instance, Fig. 24-33 completes Fig. 18-4 with a CMS measurement giving for the weak angle a value in full agreement with the SM expectation, midway between the two former measurements of A_l at SLD and the statistically dominated LEP A_{FB}^b (Chapter 18).

24.4.2 Double parton scattering

At LHC a general topic needs much attention: **double parton scattering (DPS)** [755]. Its cross-section S_{AB}, for processes of cross-sections S_A and S_B is crudely given by $S_{AB} = S_A \times S_B / \sigma_{eff}$, with $\sigma_{eff} \sim 12$ mb. Table 24-3 gives the list of processes where DPS were evaluated and the values found for σ_{eff}.

[754] CMS Experiment, Stairway to discovery: a report on the CMS programme of cross section measurements from millibarns to femtobarns. https://arxiv.org/abs/2405.18661

[755] CMS Collaboration, Observation of same-sign WW production from double parton scattering in proton-proton collisions at $\sqrt{s}$ = 13 TeV. https://arxiv.org/abs/2206.02681
ATLAS Collaboration, Observation of double parton scattering in same-sign W boson pair production in pp collisions at $\sqrt{s}$ = 13 TeV with the ATLAS detector. https://arxiv.org/abs/2505.08313

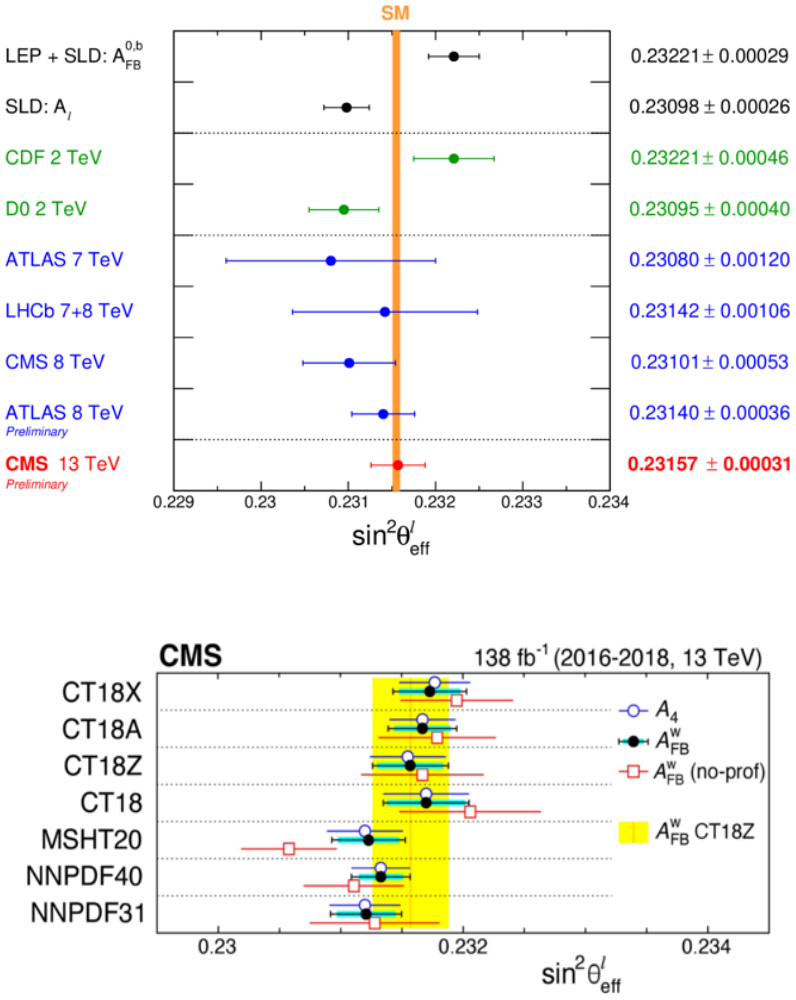


Fig. 24-33: Top: all measurements of the weak angle [756]. Bottom influence of PDF's choice on the result [757].

24.4.3 Top production and mass

The top quark is the heaviest SM particle and its mass plays a key role e.g. in the consistency fits of the electroweak sector and in our understanding of the stability of the Universe. It is the only quark decaying before hadronization, and its physics is a unique chance to study a bare quark.

At the LHC, top quarks are dominantly produced via the strong interaction, resulting in a top quark-antiquark pair. In the SM it decays almost 100% of the time to a b quark and a W boson.

The **top-antitop, alone or produced with an EW boson or a Higgs boson, and the 4-top production** are most important channels. The **single top production** is also of interest.

The next figures describe the situation.

---

[756] Measurement of the forward-backward asymmetry in Drell–Yan production and the effective leptonic electroweak mixing angle in p-p collisions at $\sqrt{s}$ = 13 TeV. CMS PAS SMP-22-010, https://cms-results.web.cern.ch/cms-results/public-results/superseded/SMP-22-010/CMS-PAS-SMP-22-010_Figure_010.png . For the definition of Collins–Soper frame see E. Richter-Was and Z. Was, Separating Electroweak and Strong interactions in Drell–Yan processes at LHC: leptons angular distributions and reference frames. https://arxiv.org/abs/1605.05450

[757] J. Bendavid, Recent Standard Model Measurements. EPS-HEP 2025, Marseille, France. https://indico.in2p3.fr/event/33627/contributions/153147/attachments/95164/145653/EPSSMExp-Jul9-2025-3.pdf

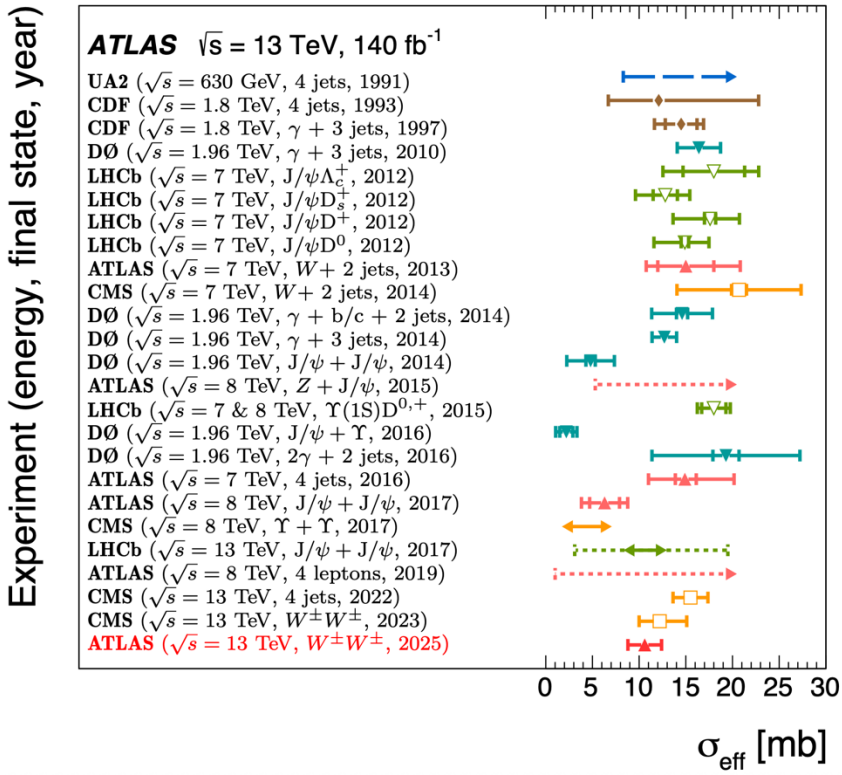


Table 24-3: The values found for σ_{eff} [758].

The top-antitop production cross-section (Fig. 24-34) is huge, close to a nb at 13.6 TeV, and, besides its own interest, may represent a large background for searches. Figure 24-35 list the graphs of the processes we will meet in top physics.

A basic problem is **how to interpret the top mass measurements**. Indeed, in quantum field theory quantum corrections affect the meaning of the mass. To come to a physically relevant definition, one must absorb divergent high-energy corrections into the mass definition, using renormalisation techniques. For these, several schemes exist, and the mass parameter is thus scheme-dependent. Masses in various schemes can be related to each other through a perturbative series. The so-called pole mass, m_t^{pole}, contains corrections from all energy scales down to zero momentum. Because of large corrections from QCD at low energies, m_t^{pole} contains an intrinsic ambiguity of 110–250 MeV.

So-called short-distance masses do not take into account contributions from energy scales below some scale and therefore depend on that scale. It is taken to be larger than ΛQCD ∼ O(200 MeV), the characteristic scale of confinement in QCD.

The most precise top quark mass measurements rely on kinematic reconstruction of the top quark from its decay products. Various techniques exist to extract the top quark mass from the decay products, implying different sources of systematic uncertainties. They rely on the simulated distributions of observables sensitive to the top quark mass parameter in the MC generator. The direct measurements are thus limited by the accuracy of the MC generator for modelling these distributions and the conceptual meaning of the top mass parameter used in this generator, m_t. The CMS and ATLAS Collaborations have measured m_t with a precision of about 500 MeV.

[758] ATLAS Collaboration, Observation of double parton scattering in same-sign W boson pair production in pp collisions at $\sqrt{s}$ = 13 TeV with the ATLAS detector. https://arxiv.org/abs/2505.08313

The present value of the top mass is $m_{top} = 172.52 \pm 0.14(\text{stat}) \pm 0.30(\text{syst})$ GeV (Table 24-4).

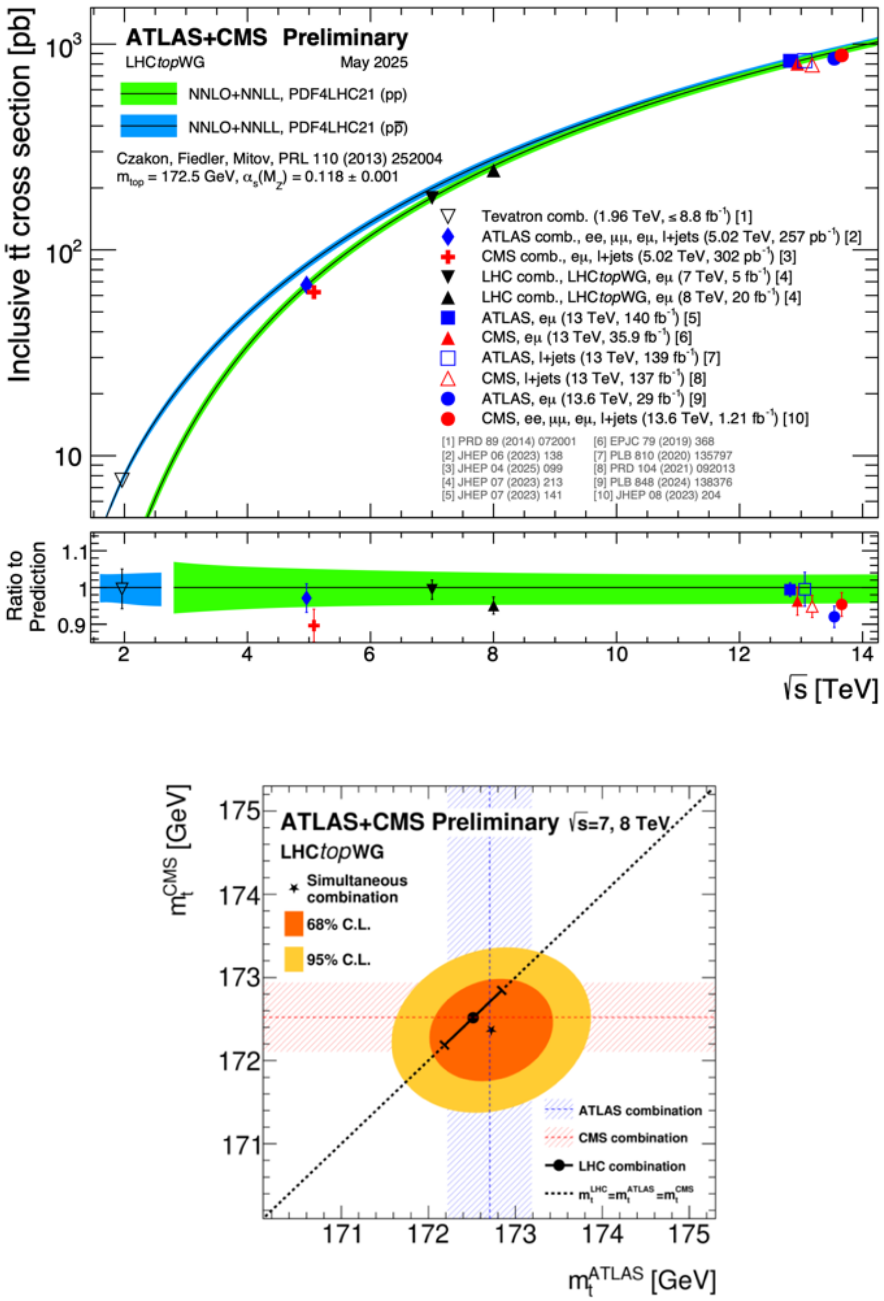


Fig. 24-34: Top: the top-antitop cross section. Bottom: the top mass [759].

[759] L. Skinnari, Top Measurements ATLAS/CMS, la Thuile 2024, https://agenda.infn.it/event/38205/contributions/219717/attachments/117202/169224/skinnari_TopMeasurements_LaThuile2024.pdf
J. Bendavid, Recent, SM measurements. EPS-HEP 2025, Marseille, France. https://indico.in2p3.fr/event/33627/contributions/153147/attachments/95164/145653/EPSSMExp-Jul9-2025-3.pdf
https://cds.cern.ch/images/ATLAS-PHOTO-2023-067-2
https://twiki.cern.ch/twiki/bin/view/AtlasPublic/TopPublicResults
https://twiki.cern.ch/twiki/bin/view/CMSPublic/PhysicsResultsTOP
D. Dobur, Standard Model top results overview. IHEP 2024, Prague, https://indico.cern.ch/event/1291157/contributions/5958357/attachments/2902259/5091115/ICHEP_2024_Dobur.pdf

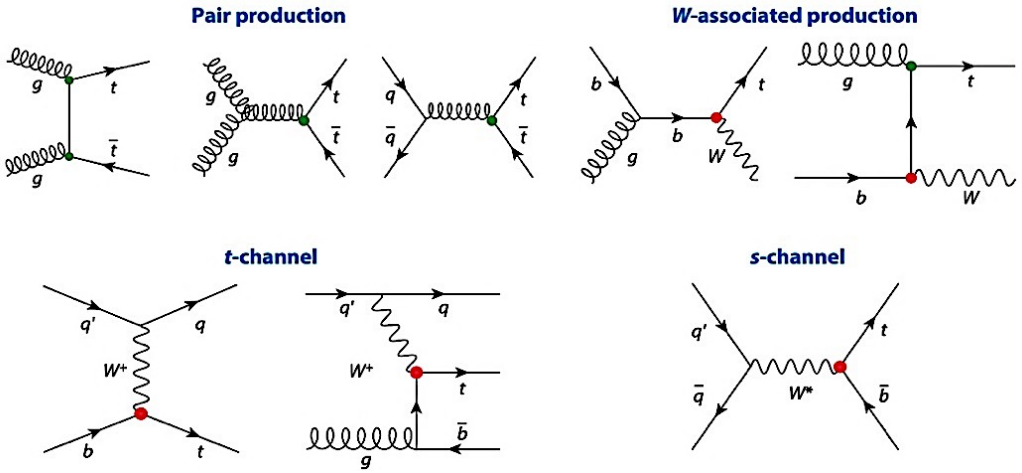


Fig. 24-35: The processes leading to top pairs and single top final states [760].

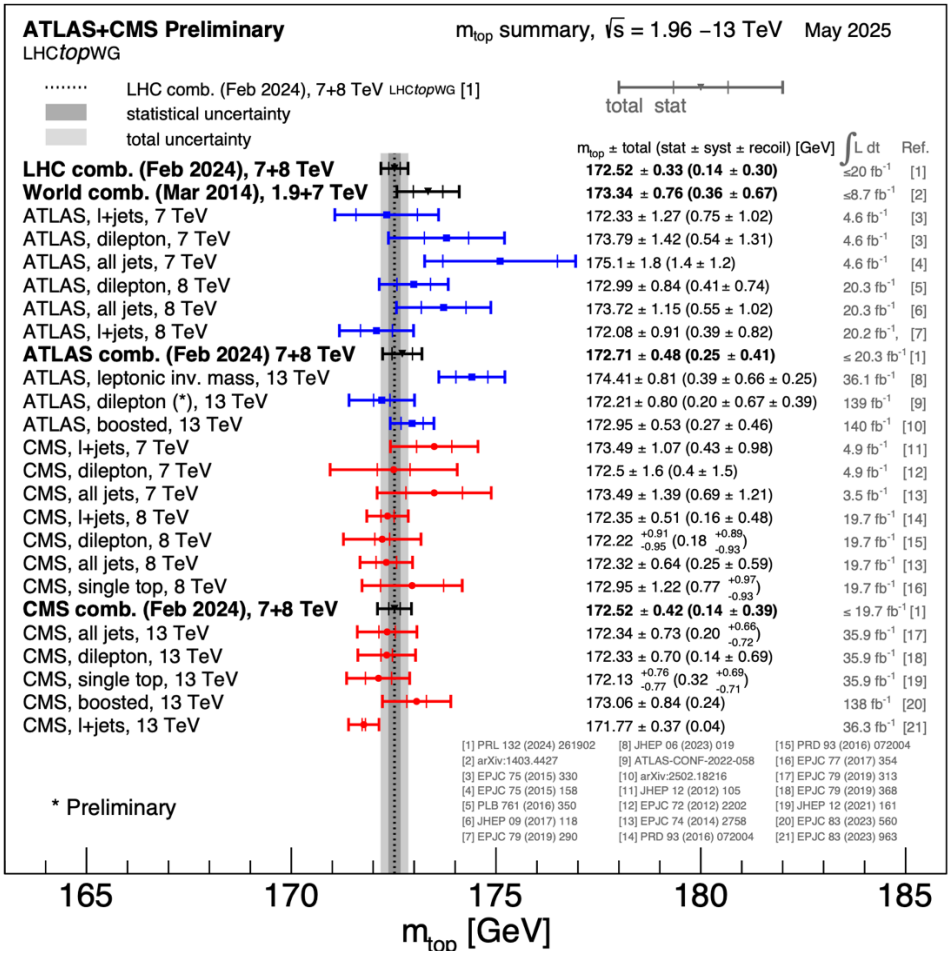


Table 24-4: The set of all top quark mass measurements [761].

[760] P. Ferreira da Silva, Physics of the Top Quark at the LHC: An Appraisal and Outlook of the Road Ahead. *Annu. Rev. Nucl. Part. Sci. 2023. 73:255–84,* https://doi.org/10.1146/annurev-nucl-102419-052854

[761] J. Bendavid, Recent Standard Model Measurements. EPS-HEP 2025, Marseille, France. https://indico.in2p3.fr/event/33627/contributions/153147/attachments/95164/145653/EPSSMExp-Jul9-2025-3.pdf https://twiki.cern.ch/twiki/bin/view/LHCPhysics/TopMassHistory

Figure 24-36 gives an overview of the cross-sections of all processes involving the top.

The associated production of top quarks (single or in pair) and bosons (γ, W, Z, H) has sensitivity to BSM physics. They are high-mass states and involve typically weaker couplings. The cross sections are **therefore small (< 1 pb).** Nearly all processes in which a single boson is produced in association with top quarks have already been established experimentally.

$t\bar{t}W$ is an irreducible source of same-sign dilepton pairs. It is also a background for the measurement of the $t\bar{t}h$ and four-top production. It is important to have precise theoretical predictions of this process, as was done by Ref. [762].

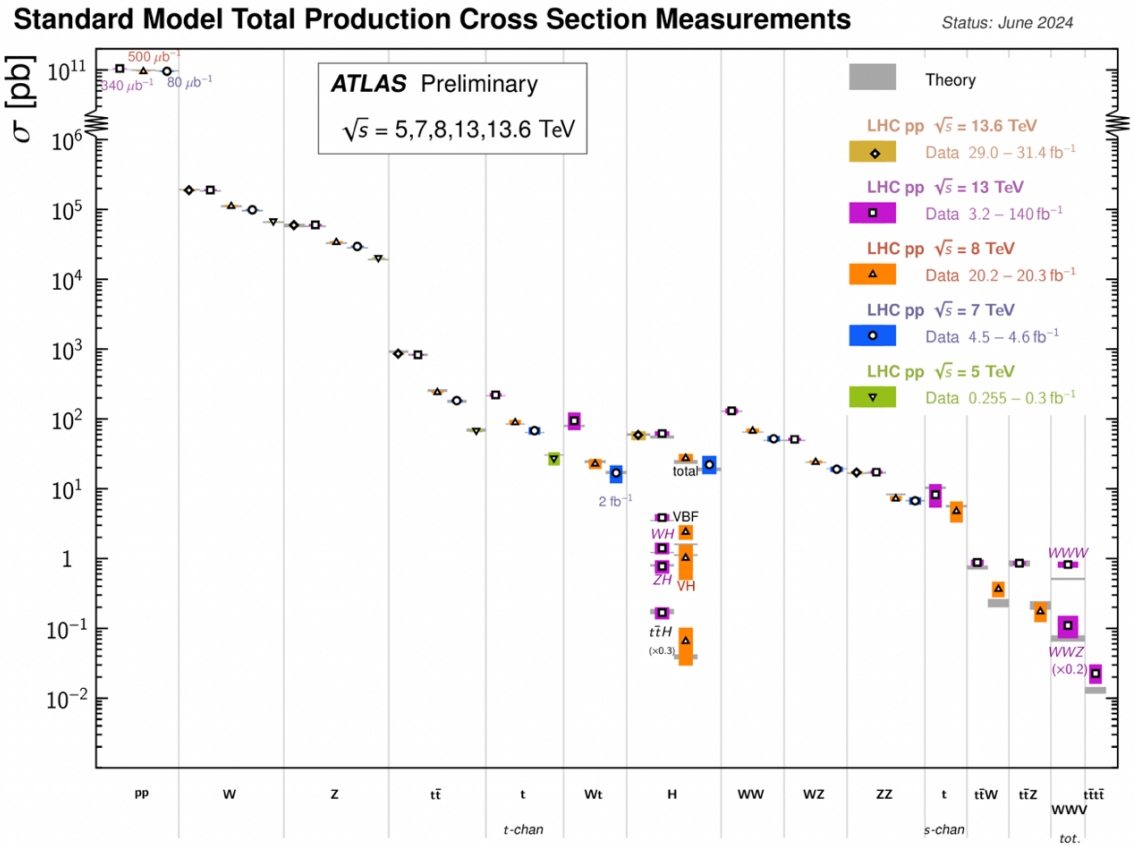


Fig. 24-36: Top quark production cross-section measurements [763].

Of these let us focus first on top pairs produced in association with an IVB or a Higgs boson.

Figure 24-37 shows the ATLAS result for $t\bar{t}W$ and Fig. 24-38 compares the expected cross-section to the measurement performed by the CMS and ATLAS. A tension remains at the 1 sigma to 2 sigma level. As for $t\bar{t}h$ production, it is a direct probe of the top-Higgs coupling, hence a primary objective of Higgs physics. Figure 24-39 presents LHC results for $t\bar{t}h$ compared to the expected cross-sections at various orders, and Fig. 24-40 shows the first observation by CMS of a top + 2 IVB production process.

[762] L. Buonocore *et al.*, Precise Predictions for the Associated Production of a W Boson with a Top-Antitop Quark Pair at the LHC. *Phys. Rev. Lett. 131, 231901 (2023),* https://journals.aps.org/prl/pdf/10.1103/PhysRevLett.131.231901

[763] J. Andrea and N. Chanon, Single-Top Quark Physics at the LHC: From Precision Measurements to Rare Processes and Top Quark Properties https://arxiv.org/abs/2307.14044
P. Berta, in la Thuile 2024, ATL-PHYS-PUB-2023-038,
https://atlas.web.cern.ch/Atlas/GROUPS/PHYSICS/PUBNOTES/ATL-PHYS-PUB-2024-011/

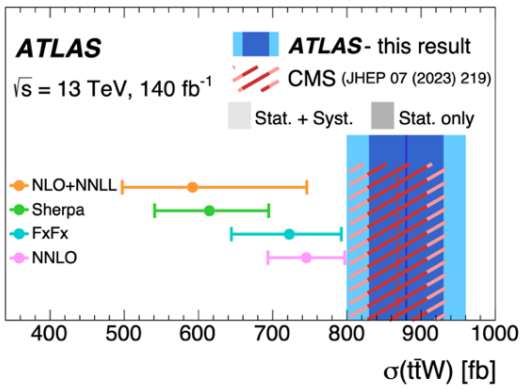


Fig. 24-37: Top-antitop produced with a W boson [764].

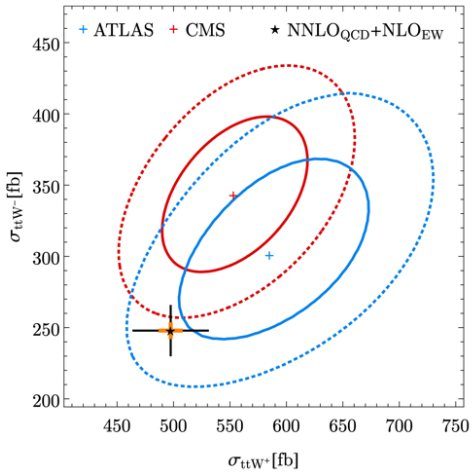


Fig. 24-38: Comparison of $NNLO_{QCD}$ + NLO_{EW} result to the measurement of CMS (red) and ATLAS (blue) [765].

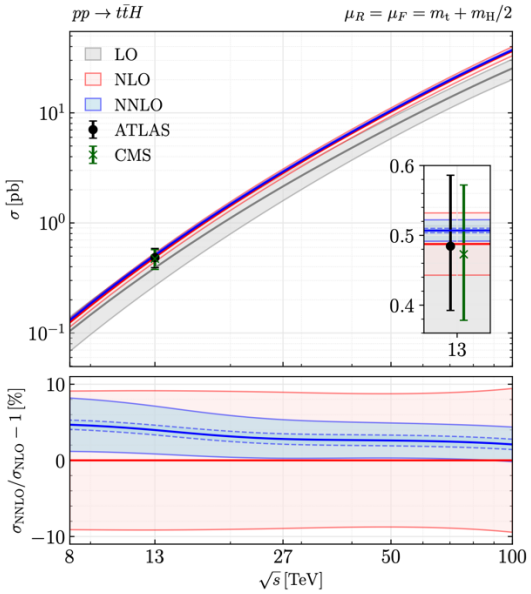


Fig. 24-39: LO, NLO and NNLO cross sections for pp → tt̄h with their perturbative uncertainties as functions of the centre-of-mass energy [766].

Single top

Top can be singly produced through EW interactions (Fig. 24-41). Thanks to the EW V–A structure, the single-top quark (STQ) production has specific sensitivities to PDFs, the V_{tb} element of the CKM matrix, BSM Wtb coupling and top quark polarization. Measuring STQ processes test perturbative QCD. STQ associated production with a boson B, complementing the $t\bar{t}B$ process, informs on the B-top coupling.

The three main production modes for STQ processes are production via the exchange of a virtual W boson in the *t*- and *s*-channels and the associated production with a W boson (tW production), as illustrated in Fig. 24-35.

[764] ATLAS Collaboration; Measurement of the total and differential cross-sections of $t\bar{t}W$ production in *pp* collisions at $\sqrt{s}$ = 13 TeV with the ATLAS detector. https://arxiv.org/abs/2401.05299

[765] L. Buonocore *et al.,* Precise predictions for the associated production of a W boson with a top-antitop quark pair at the LHC. https://arxiv.org/abs/2306.16311

[766] S. Catani *et al.,* Higgs boson production in association with a top–antitop quark pair in next-to-next-to leading order QCD. https://arxiv.org/abs/2210.07846

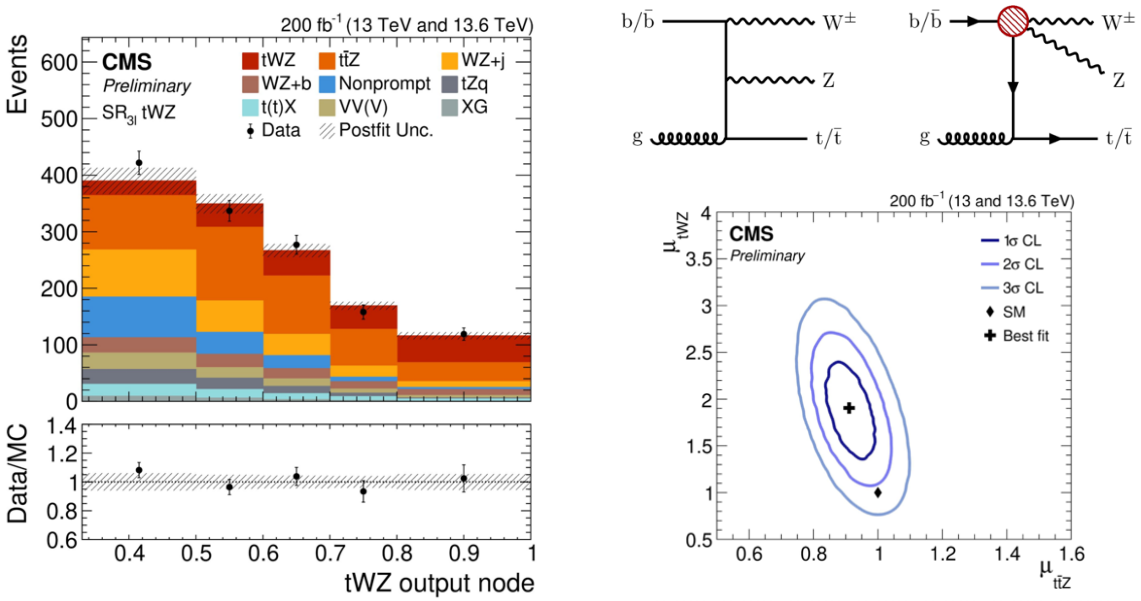


Fig. 24-40: First observation of tWZ production by CMS [767].

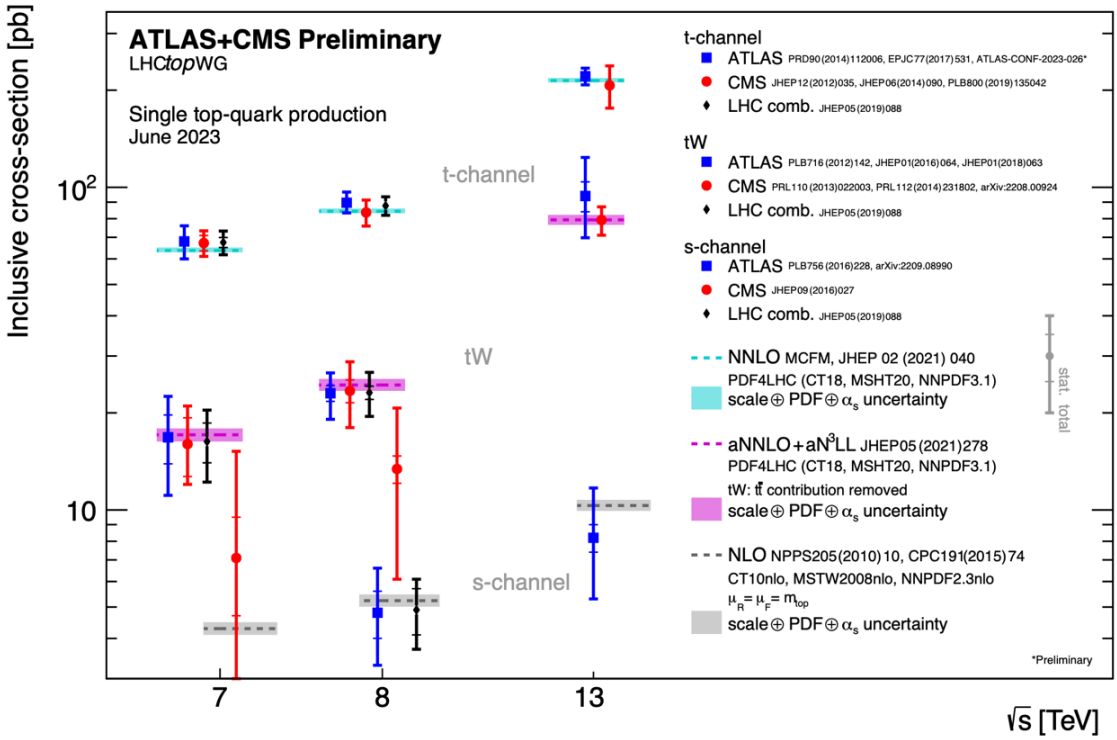


Fig. 24-41: Summary of single-top quark cross-section measurements by ATLAS and CMS in the *t*-channel, *tW* production, and *s*-channel, as functions of the CM energy, compared with theoretical predictions [768].

[767] CMS Collaboration, Observation of tWZ production at the CMS experiment. CMS-PAS-TOP-24-009, https://cms-results.web.cern.ch/cms-results/public-results/preliminary-results/TOP-24-009/
J. Bendavid, Recent Standard Model Measurements, EPS-HEP 2025, https://indico.in2p3.fr/event/33627/contributions/153147/attachments/95164/145653/EPSSMExp-Jul9-2025-3.pdf

[768] J. Andrea and N. Chanon, Single-Top Quark Physics at the LHC: From Precision Measurements to Rare Processes and Top Quark Properties. https://arxiv.org/abs/2307.14044

Multi-tops

Four top quark production [769] is a rare process. The SM prediction for Its cross section is $13^{+1.0}_{-1.8}$ fb at $\sqrt{s}$ = 13 TeV. New massive bosons can dramatically enhance it and the process may provide a precious probe for new physics. It can also serve as a probe of the top-Higgs Yukawa coupling, complementary to other measurements of this SM parameter. Figure 24-42 presents the LHC results.

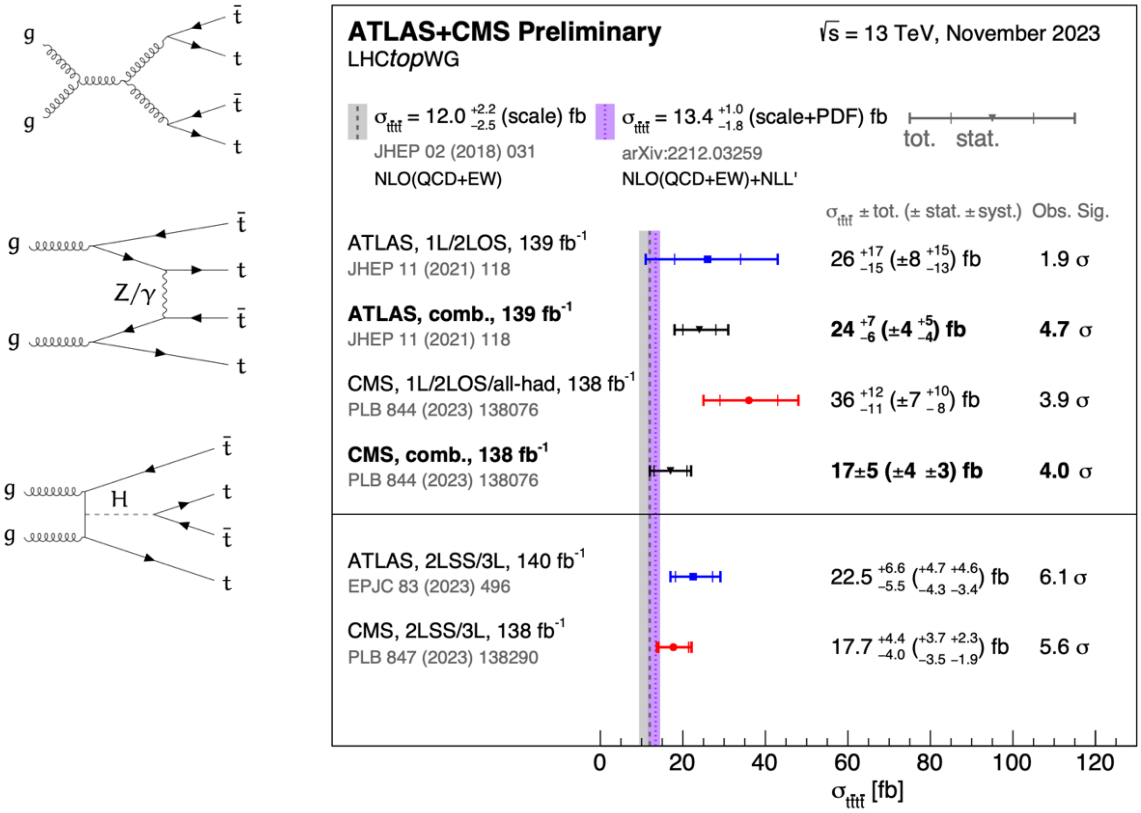


Fig. 24-42: Representative Feynman diagrams for the 4-top signal in the SM. The mediator connecting two top quarks can be a gluon, a γ or Z, or a Higgs boson (left). ATLAS and CMS 4 top production cross-section (right) [770].

On a speculative side, the idea that Higgs exchange between t quarks produces enough attraction to generate their multiple bound states. The humorous Ref. [771] claimed that the system of 6 t and 6 $\bar{t}$ quarks is bound so strongly that it may be very light, possibly linked to the late 750 GeV hint (Fig. 24-26). Reference [772] discusses the possibility of such a bound state.

---

[769] ATLAS Collaboration, Observation of four-top-quark production. *Eur. Phys. J. C 83 (2023) 496*, https://link.springer.com/article/10.1140/epjc/s10052-023-11573-0
CMS Collaboration, Observation of four top quark production in proton-proton collisions at $\sqrt{s}$ = 13 TeV. *Phys. Lett. B 847 (2023) 138290*, https://arxiv.org/abs/2305.13439

[770] D. Dobur, Standard Model top results overview. IHEP 2024, https://indico.cern.ch/event/1291157/contributions/5958357/attachments/2902259/5091115/ICHEP_2024_Dobur.pdf
LHCTopWG Summary Plots: Four Top Quark Production, https://twiki.cern.ch/twiki/bin/view/LHCPhysics/LHCTopWG , https://twiki.cern.ch/twiki/bin/view/LHCPhysics/LHCTopWGSummaryPlots#Four_Top_Quark_Production

[771] H. F. B. Nielsen *et al.,* F(750), We Miss You as a Bound State of 6 Top and 6 Antitop Quarks, Multiple Point Principle. https://arxiv.org/abs/1705.10749

[772] M. Y. Kuchiev *et al.,* On bound states of multiple t-quarks due to Higgs exchange. https://arxiv.org/abs/0808.3632

24.4.4 Toponium

The idea that toponium can lead to various effects near top-antitop threshold is also pursued [773]. Both ATLAS and CMS have by now observed top entanglement [774]. The two problems, possibly linked, are considered below and illustrated in Figs. 24-43 and 24-44.

In top–antitop quark events spin entanglement is detected by measuring an observable D, inferred from the angle between the charged leptons in their parent top- and antitop-quark rest frames. The measurement is done in a narrow interval around the top–antitop quark production threshold, where the detection of entanglement is expected to be significant.

ATLAS first measured the entanglement marker to be D = −0.547 ± 0.002 (stat) ± 0.021 (syst) for $340 < m_{t\bar{t}} < 380$ GeV. The result is more than five standard deviations from a scenario without entanglement and represents both the first observation of entanglement in a pair of quarks and the highest-energy observation of entanglement to date (Fig. 24-43 left).

CMS performed a similar measurement (Fig. 24-43 right) at a bit higher mass and under 2 different assumptions concerning the toponium (a PS maximally entangled of 343 GeV and σ = 6.43 ± 0.90 pb).

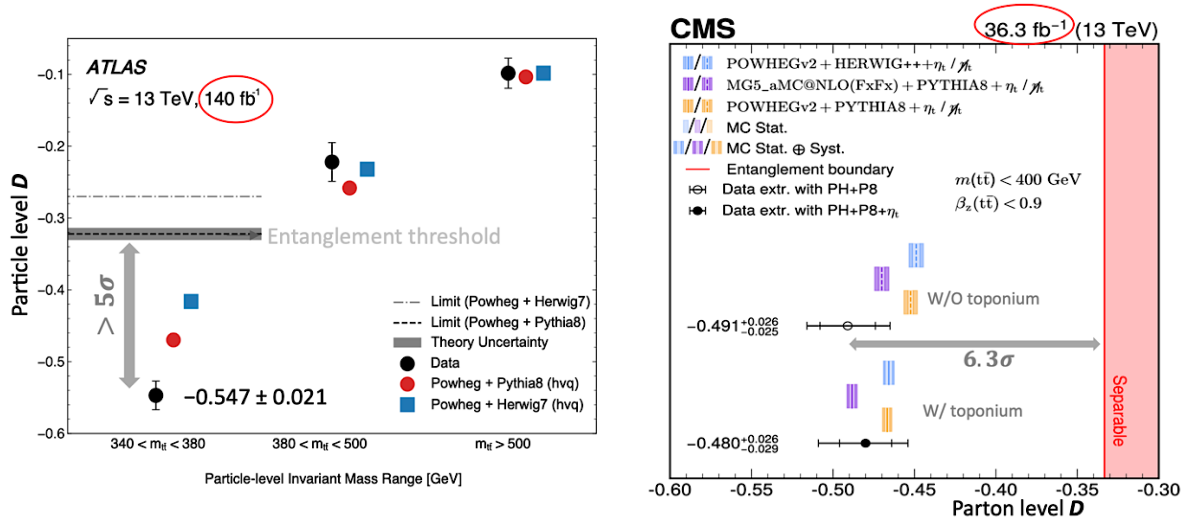


Fig. 24-43 Left: ATLAS evidence for entanglement [775]. Right: CMS measurement of the D parameter [776].

[773] B. Fuks *et al.,* Signatures of toponium formation in LHC run 2 data. https://arxiv.org/abs/2102.11281.pdf
See also B. Fuks *et al.,* Simulating toponium formation signals at the LHC. *Eur. Phys. J. C 85 (2025) 157,* https://arxiv.org/abs/2411.18962

[774] ATLAS Collaboration Observation of quantum entanglement with top quarks at the ATLAS detector. *Nature 633 (2024) 542*, https://arxiv.org/abs/2311.07288
CMS Collaboration, Observation of quantum entanglement in top quark pair production in proton-proton collisions at √s = 13 TeV. *Rep. Prog. Phys. 87 (2024) 117801*, https://iopscience.iop.org/article/10.1088/1361-6633/ad7e4d

[775] ATLAS Collaboration, Observation of quantum entanglement with top quarks at the ATLAS detector. https://arxiv.org/abs/2311.07288
D. Dobur, Standard Model top results overview. IHEP 2024, https://indico.cern.ch/event/1291157/contributions/5958357/attachments/2902259/5091115/ICHEP_2024_Dobur.pdf

[776] CMS Collaboration, Probing entanglement in top quark production with the CMS detector. CMS PAS TOP-23-001 https://inspirehep.net/files/3450bee9a43eb7906e34a8d5a9ffff8c

For amusement, Fig. 24-44 compares the modern view on toponium [777] to a hypothetical and most spectacular effect it could have led to (see Ref. [778]) in case of its degeneracy with the Z.

Actually CMS [779] observed a substantial effect at top threshold (Fig. 24-45 left) which is no more visible when a model of toponium is introduced (right). This new feature must be followed [780].

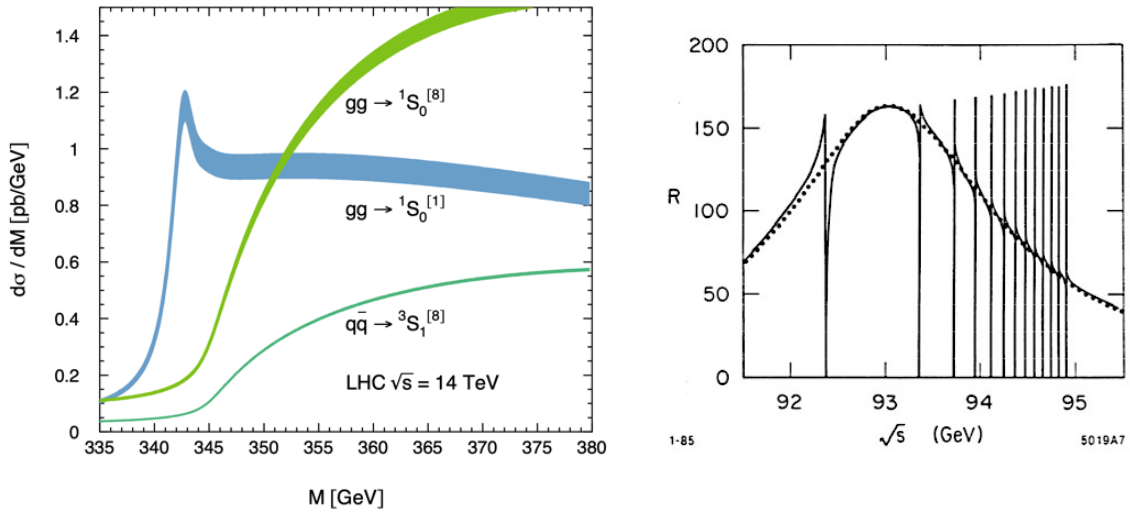


Fig. 24-44: Left: Invariant mass distributions for leading subprocesses: $gg \to {}^1S_0$ (blue and light green, respectively) and $q\bar{q} \to {}^3S_1$ (green) [781]. Right: long ago, when the top was thought much lighter, a possible manifestation of toponium superimposed on the Z boson [782].

The signal (Fig. 24-46 and Table 24-5) is compatible with the production of a ${}^1S_0\, t\bar{t}$ bound state (η_t), as proven in Fig. 24-47. Figure 24-48 proposes a nice position space picture of toponium.

[777] Y. Kiyo *et al.,* Top-quark pair production near threshold at LHC. https://arxiv.org/abs/0812.0919
Y. Sumino, *et al.,* Top-quark pair production near threshold. *Phys. Rev. D 47, 56 (1993)* ,
M. Jezabek, J. H. Kuhn and T. Teubner, Momentum distributions in t anti-t production and decay near threshold. *Z.Phys.C 56 (1992) 653-660* ,
F. Maltoni *et al.,* Quantum detection of new physics in top-quark pair production at the LHC. *J. High Energ. Phys. 2024, 99 (2024).* https://link.springer.com/article/10.1007/JHEP03(2024)099 ,
J.A. Aguilar-Saavedra, Toponium Hunter's Guide. https://arxiv.org/abs/2407.20330
L. Jeppe, Search for heavy scalar or pseudoscalar states in t anti-t events at CMS.
https://indico.cern.ch/event/1368706/contributions/6012506/attachments/2935624/5156184/TOP2024_LauridsJeppe_v7.pdf
CMS Collaboration, Search for heavy pseudoscalar and scalar bosons decaying to top quark pairs in proton-proton collisions at √s = 13 TeV. CMS-PAS-HIG-22-013,
https://cms-results.web.cern.ch/cms-results/public-results/preliminary-results/HIG-22-013/index.html
[778] W. Buchmüller et *al.,* Toponium Physics at LEP. https://lib-extopc.kek.jp/preprints/PDF/1986/8604/8604083.pdf
[779] L. Jeppe, Search for heavy scalar or pseudoscalar states in $t\bar{t}$ events at CMS. CMS-PAS-HIG-22-013,
https://indico.cern.ch/event/1368706/contributions/6012506/attachments/2935624/5156184/TOP2024_LauridsJeppe_v7.pdf
[780] The toponium is not an "onium", it decays because a t quark decays. It is however a bound state of physical matter density about 10^{12} times the nuclear density.
[781] Y. Kiyo *et al.,* Top-quark pair production near threshold at LHC. https://arxiv.org/abs/0812.0919
J. Bendavid, Recent Standard Model Measurements, EPS-HEP 2025,
https://indico.in2p3.fr/event/33627/contributions/153147/attachments/95164/145653/EPSSMExp-Jul9-2025-3.pdf
[782] S. Güsken, J. H. Kühn and P. M. Zerwas, Toponium production in e^+e^- collisions. *Nucl. Phys. B262 (1985) 393-438*

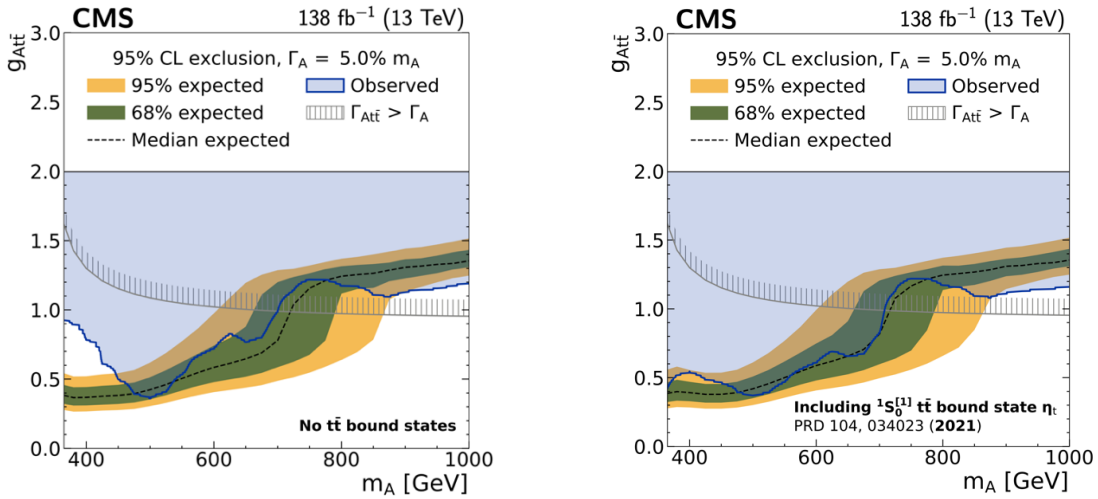


Fig. 24-45: Search for heavy scalar or pseudoscalar states in $t\bar{t}$ events at CMS. The effect at top threshold (left) is no more visible when a model of toponium is introduced (right) [783].

Experiment	Model	Cross section (pb)
ATLAS	NR-QCD	9.0 ± 1.2 (stat) ± 0.6 (syst)
ATLAS	Pseudoscalar	13.4 ± 1.7 (stat) ± 1.0 (syst)
CMS	Pseudoscalar	8.8 ± 0.5 (stat) ± 1.2 (syst)

Table 24-5: The cross-section obtained for the $t\bar{t}$ bound state [784].

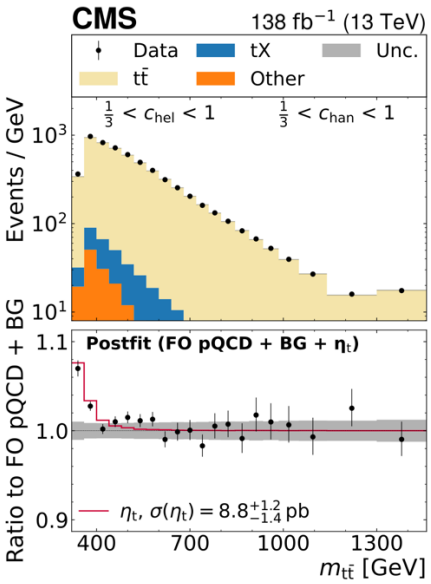


Fig. 24-46: The signal of a $^1S_0$ $t\bar{t}$ bound state [785].

[783] CMS Collaboration, Search for heavy pseudoscalar and scalar bosons decaying to a top quark pair in proton-proton collisions at $\sqrt{s}$ = 13 TeV. https://arxiv.org/abs/2507.05119

[784] J. Bendavid, Recent Standard Model Measurements, EPS-HEP 2025, https://indico.in2p3.fr/event/33627/contributions/153147/attachments/95164/145653/EPSSMExp-Jul9-2025-3.pdf

[785] ibid, and CMS collaboration, Observation of a pseudoscalar excess at the top quark pair production threshold. https://arxiv.org/pdf/2503.22382

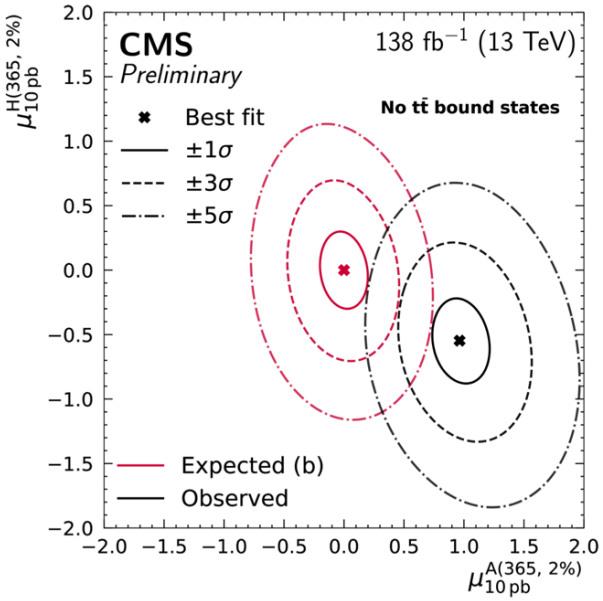


Fig. 24-47: The plot shows the local significance contours for the pair of A/H (365,2%) considering only the resonant signal components. The deviation looks significantly more pseudoscalar-like than scalar-like [786].

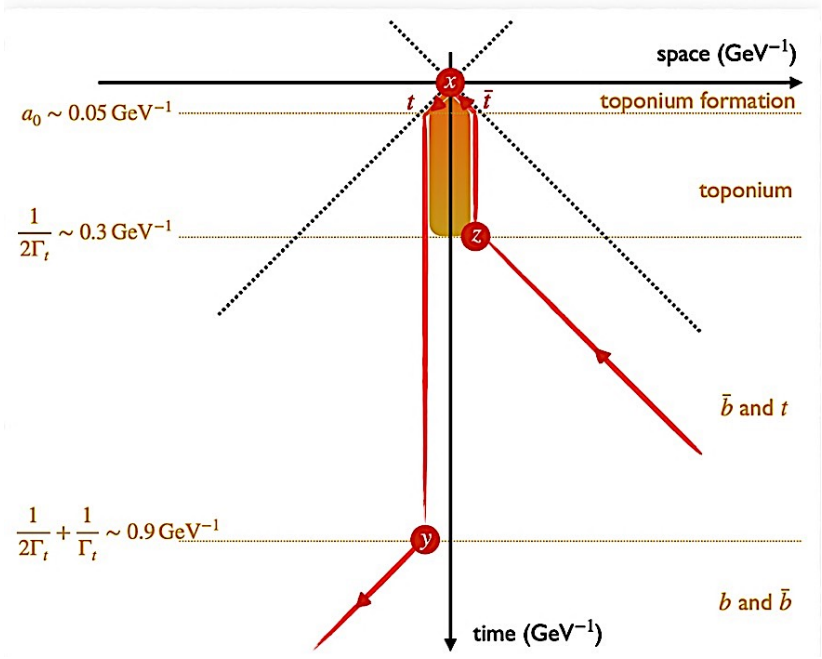


Fig. 24-48: A position space picture of toponium [787].

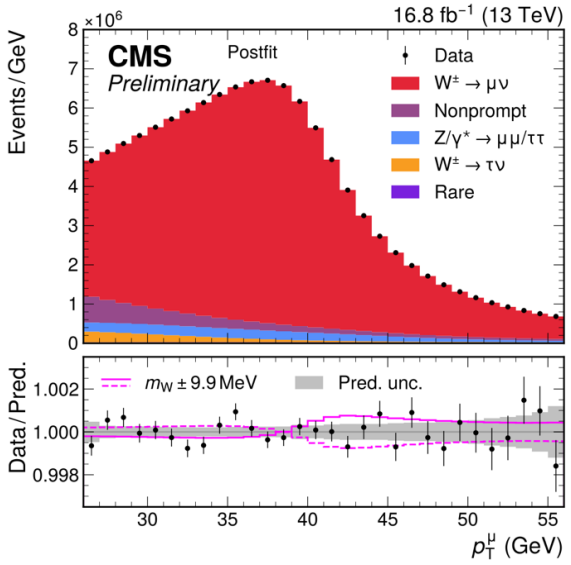
[786] CMS Collaboration, Search for heavy pseudoscalar and scalar bosons decaying to top quark pairs in proton-proton collisions at $\sqrt{s}$ = 13 TeV. CMS PAS HIG-22-013, https://inspirehep.net/files/5d8ec488cb1ea00470ee5c6ff6ea228c

C. Schwanenberger, Top quark production at the $t\bar{t}$ threshold at CMS.
https://indico.in2p3.fr/event/33627/contributions/154956/attachments/94073/144233/CMS_ttbar_threshold_CS_final.pdf

[787] B. Fuks, Toponium Physics at LHC.
https://indico.in2p3.fr/event/35965/contributions/152515/attachments/91681/139728/5_BFuks-v1.pdf

24.4.5 The M_W measurement by CMS

Let us end by this long-awaited result. Figure 24-49 [788] shows the μ p_T spectrum from W-decay including all backgrounds and a summary of all uncertainties.



Source of uncertainty	Impact (MeV) Nominal	Global
Muon momentum scale	4.8	4.4
Muon reco. efficiency	3.0	2.3
W and Z angular coeffs.	3.3	3.0
Higher-order EW	2.0	1.9
p_T^V modeling	2.0	0.8
PDF	4.4	2.8
Nonprompt background	3.2	1.7
Integrated luminosity	0.1	0.1
MC sample size	1.5	3.8
Data sample size	2.4	6.0
Total uncertainty	9.9	9.9

Fig. 24-49: The μ p_T spectrum (left) and table of all sources of uncertainties (right).

Figure 24-50 presents all measurements of the W mass. The CDF value is clearly an outlier.

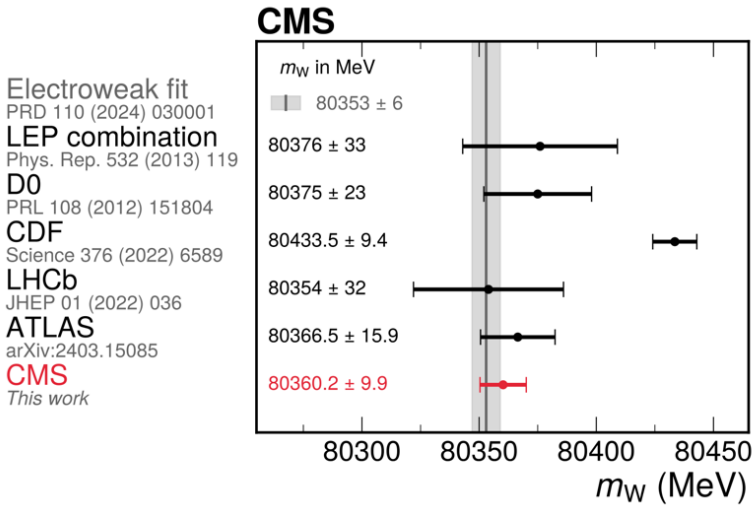


Fig. 24-50: Comparison of all measurements of the W mass and the EW fit prediction [789].

[788] J. Bendavid, A high precision measurement of the W mass at CMS.
https://indico.cern.ch/event/1441575/attachments/2928975/5142714/mWCERNSeminar-Sept17-2024.pdf
CMS Collaboration, High-precision measurement of the W boson mass with the CMS experiment at the LHC.
https://arxiv.org/abs/2412.13872
ATLAS Collaboration: New ATLAS result weighs in on the W boson.
https://atlas.cern/Updates/Briefing/2023-W-Mass-Measurement
[789] CMS Collaboration, High-precision measurement of the W boson mass with the CMS experiment at the LHC.
https://arxiv.org/abs/2412.13872

Finally, Figs. 24-51a and 25-51b give the resulting global status of EW data [790].

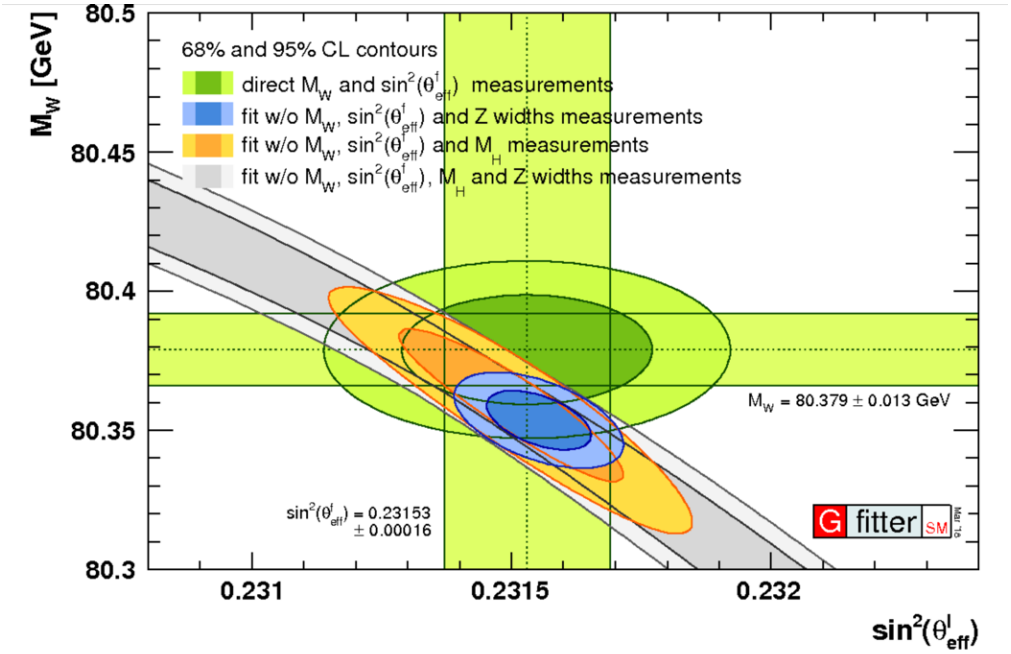


Fig. 24-51a: The confidence-level contours of the indirect determination of the W and $\sin^2(\theta^{\mathrm{l}}_{\mathrm{eff}})$ from the global EW fit compared to the measurements of M_W and $\sin^2(\theta^{\mathrm{l}}_{\mathrm{eff}})$.

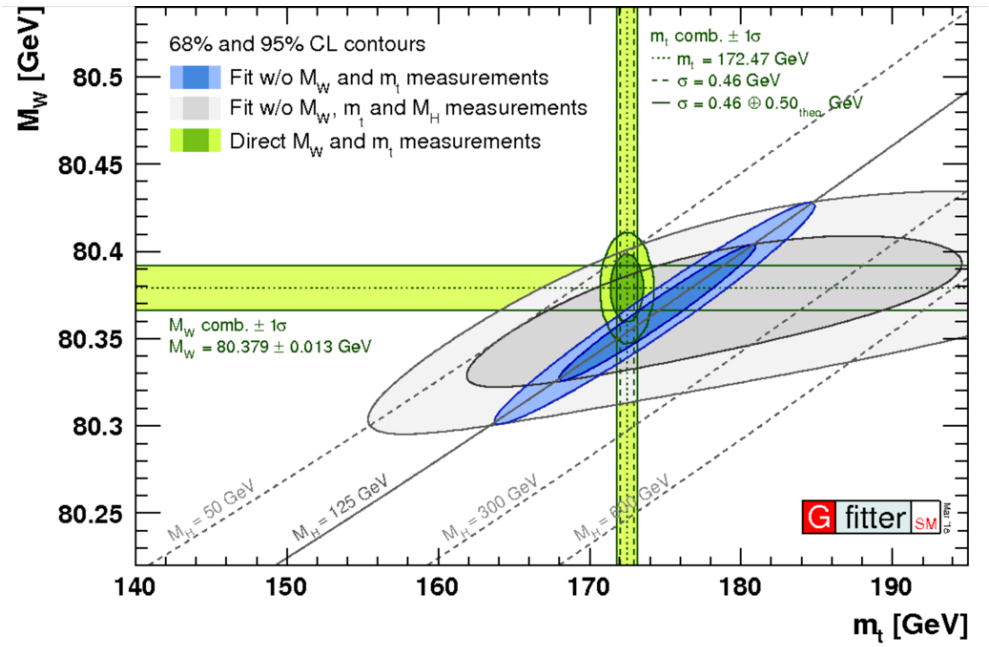


Fig. 24-51b: The confidence-level contours of the indirect determination of the W and top mass from the global EW fit compared to the measurements of M_W and M_{top}.

[790] Results for the Global Electroweak Standard Model Fit: https://project-gfitter.web.cern.ch/Standard_Model/
J. Bendavid, Recent Standard Model Measurements. EPS-HEP 2025,
https://indico.in2p3.fr/event/33627/contributions/153147/attachments/95164/145653/EPSSMExp-Jul9-2025-3.pdf

The LHC contributions to QCD are summarized in Figs. 24-52 and 24-53. Both figures are from Ref. [791].

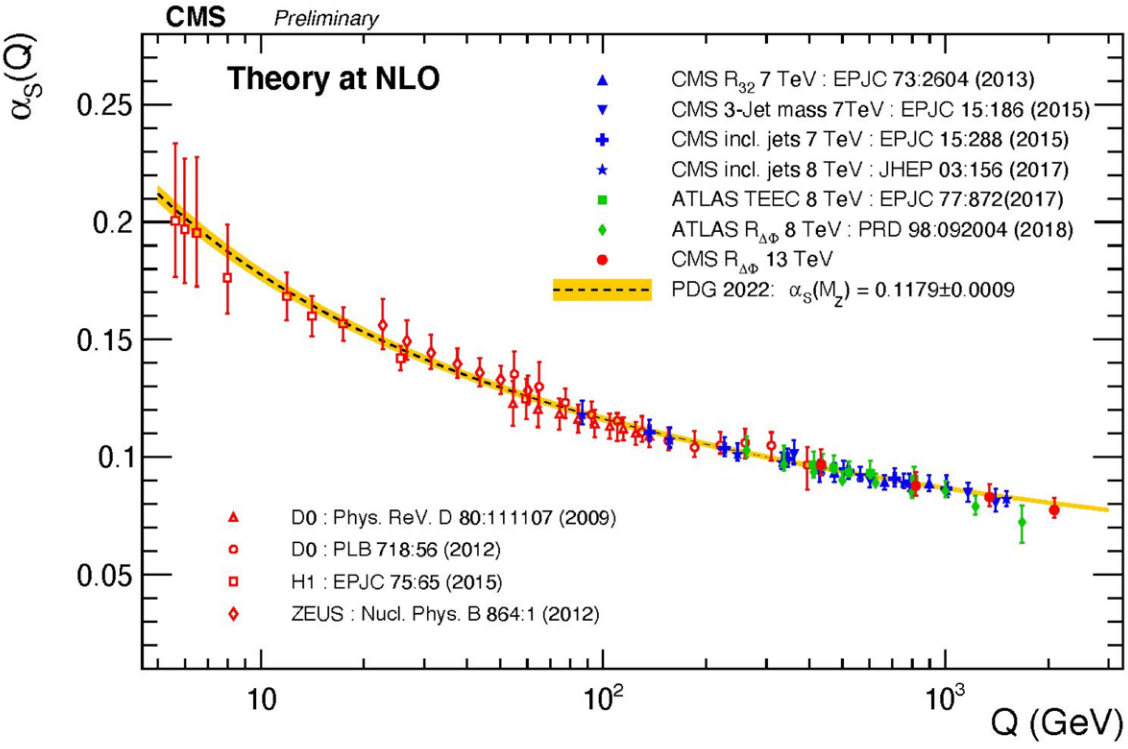


Fig. 24-52: CMS measurements of α_s as function of Q.

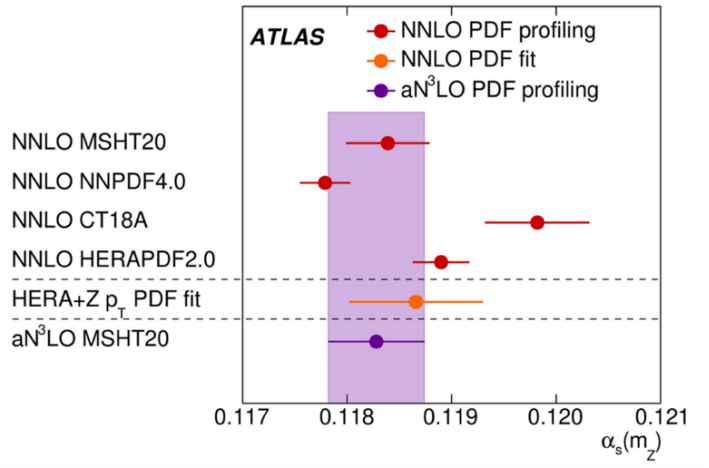


Fig. 24-53: ALTAS determination of α_s (m_Z).

[791] J. Bendavid, Recent Standard Model Measurements. EPS-HEP 2025, https://indico.in2p3.fr/event/33627/contributions/153147/attachments/95164/145653/EPSSMExp-Jul9-2025-3.pdf

24.4.6 About running masses

When considering couplings and masses in the EW theory or QCD, a problem arises due to the occurrence of loop diagrams [792], which are divergent and force to perform renormalization [793]. In this procedure one must introduce an arbitrary point of renormalization, μ, the energy scale at which one chooses to define the physical observables. Since these should not depend on μ, this leads to the renormalization group equations (RGE).

Thus, in quantum field theory, quantities like coupling constant and mass "run" with the energy scale of HE physics. The running mass of a fermion or massive boson depends on the energy scale at which the observation occurs, in a way described by a RGE and calculated by a renormalization scheme such as the minimal subtraction scheme ($\overline{\text{MS}}$) [794]. The running mass refers to a Lagrangian parameter whose value changes with the energy scale at which the renormalization scheme is applied. Actually, the running mass is not a fundamental parameter of the SM Lagrangian, but the product of the running Yukawa coupling y_b and the Higgs vacuum expectation value v. However, the agreement of the observed running with the SM expectation indicated that no BSM physics is implied.

Experiments have found evidence for the "running" of the charm quark at HERA and have studied the scale evolution of the top quark at the LHC (Fig. 24-54). The most precise measurements of the b mass are performed at relatively low energy. The "world average" is given by the PDG: $m_b(m_b) = 4.18 \pm 0.03$ GeV.

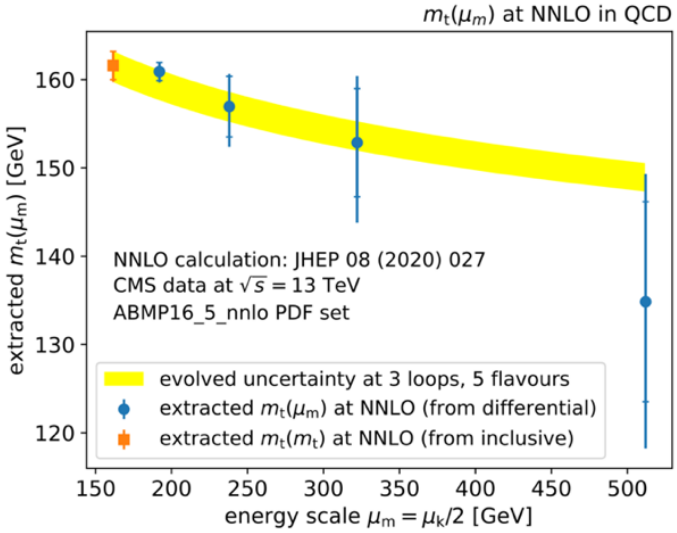


Fig. 24-54: Extracted $m_t(\mu_k/2)$ compared to $m_t(m_t)$ [795].

[792] Naively speaking, the quantum world does all what it is allowed to do by its specific basic laws. We look at it with different resolving powers, and thus see more or less the details. A quark as b dresses itself by emitting and reabsorbing gluons, giving ephemerous pairs of light quarks. The better the resolution, the more specific will be the image, and the lighter the mass.
[793] P. D. Collins, A. D. Martin and E. J. Squires, Particle Physics and Cosmology. Copyright © 1989 by John Wiley & Sons, Inc. ISBN: 0-471-60088-1, Ch 2
[794] In this scheme one absorbs into the counter terms the divergent part of the radiative corrections, plus a universal constant that always arises along with the divergence in Feynman diagram calculations.
[795] M. M. Defranchis *et al.,* Running of the top quark mass at NNLO in QCD. https://arxiv.org/abs/2208.11399
CMS Collaboration, Running of the top quark mass from proton-proton collisions at √s = 13TeV. https://arxiv.org/abs/1909.09193

The bottom quark mass was obtained at LEP [796] (see Fig. 16-8) by measuring the decay width of the Z into 2 and 3 jets containing the b-quark including complete quark mass effects. The 3-jet observables are very sensitive to the b-quark mass and well suited for its determination at LEP. The result was $m_b(m_Z) = 2.82 \pm 0.28$ GeV.

A new measurement of the b quark mass in the $\overline{\text{MS}}$ scheme at the renormalization scale of the Higgs mass came from measurements of Higgs boson decay rates at the LHC [797], giving: $m_b(m_H) = 2.60 \pm 0.36$ GeV. The measurement has a negligible theory uncertainty and excellent prospects to improve at the HL-LHC and a future Higgs factory.

These results give strong evidence for the "running" of the bottom quark mass (Fig. 24-55).

A different problem about M_{top} is to quantify the mismatches between the pole mass and the masses measured in different ways: reconstruction, giving M_t^{MC}, hence the pole mass a few hundreds of MeV away, or measurement of $t\bar{t}$+X cross-sections, giving $M_t^{\overline{\text{MS}}}$ near 163 GeV, to be related to the pole mass, etc.

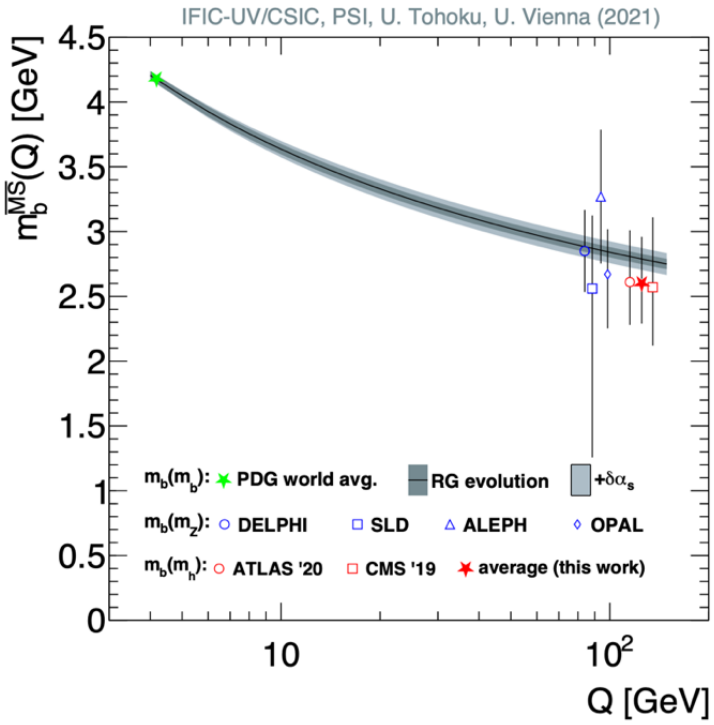


Fig. 24-55: The scale evolution of the b quark $\overline{\text{MS}}$ mass [798].

[796] M. S. Bilenky *et al.,* Three jet production at LEP and the bottom quark mass. https://arxiv.org/abs/hep-ph/9410258
G. Dissertori, Measurements of the Bottom Quark Mass. https://arxiv.org/abs/hep-ex/0010005
[797] J. Aparisi *et al.,* m_b at m_H: The Running Bottom Quark Mass and the Higgs Boson. https://arxiv.org/abs/2110.10202
[798] ibid

25. More on precision: Atomic parity violation

The idea of the Atomic parity violation (APV), see Fig. 25-1, and the first realizations of the domain are the work of Marie-Ann and Claude Bouchiat [799] (Fig. 25-2).

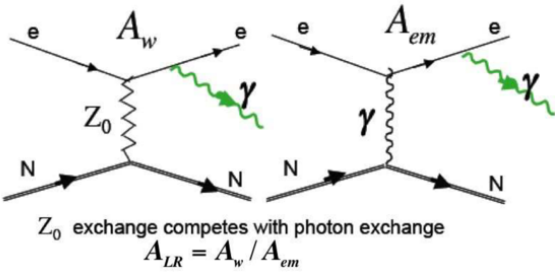


Fig. 25-1: The 2 interfering amplitudes.



Fig. 25-2: M.-A. and C. Bouchiat.

M.-A. Bouchiat [800]: *"Optical experiments have proven that the symmetry of the mirror could be broken during the absorption or emission of light by atoms. Such results, which conflict with the laws of quantum electrodynamics, support the electroweak unification. The interpretation of the experimental results calls upon the virtual exchanges of weak neutral bosons Z between the nucleus and the electrons of the atom. The progress made in the determination of the weak charge of the QW cesium nucleus (Cs) has succeeded in promoting Parity Violation experiments in Atoms to the rank of precision electroweak tests, complementary to tests carried out at high energies."*

The first measurements were made by M.-A. Bouchiat's team at the Laboratoire Kastler Brossel on cesium (Cs). Then they were taken up and improved elsewhere (Fig. 25-3) [801].

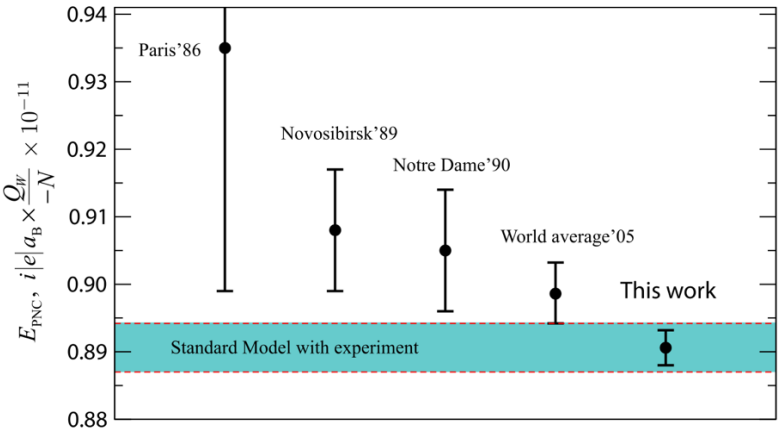


Fig. 25-3: Progress in evaluating the parity non-conserving (PNC) amplitude.

[799] M.-A. Bouchiat, Atomic Parity Violation. Early days, present results, prospects. *Il Nuovo Cimento C 35(4), 78-84 (2012),* https://arxiv.org/abs/1111.2172 , and Parity violation in atoms. *Rept.Prog.Phys. 60 (1997) 1351-1396*

[800] ibid

[801] S. G. Porsev *et al.,* Precision determination of electroweak coupling from atomic parity violation and implications for particle physics, https://arxiv.org/abs/0902.0335

Obviously, the interpretation of the results requires a very thorough knowledge of atomic physics [802].

Although belonging to Atomic Physics, APV has an impact on SM tests [803]. For example, concerning some possible heavy Z', the potential limits from APV are in competition with those of high energy colliders [804] (Table 25-1). About implications of the W-boson mass anomaly (if any) for APV, see Ref. [805].

Model	$Q_W(^{133}_{55}\mathrm{Cs})$ 0.48%	$Q_W(^{208}_{87}\mathrm{Fr})$ 0.1%
E_6 η	485	997
E_6 χ	969	1993
E_6 ψ	0	0
E_6 I	1083	2228
E_6 sq	1110	2283
E_6 N	593	1220
Left Right (LR)	1033	2117
Alternate LR (ALR)	741	1527
UUM	505	1012
SSM	1033	2117
TC1	520	1073
Littlest Higgs (LH)	505	1012
Simplest LH (SLH)	1589	3274
Anom. Free LH (AFLH)	1320	2718
331 2U1D	968	1993
331 1U2D	1589	3274
ETC	245	490
TC2	872	1800

Table 25-1: Limits on Z' boson masses in GeV.

The sensitivity of the measurements increases approximately as Z^3, the cube of the electric charge of the nucleus. Switching from Cs to the next alkaline, francium, would thus be very beneficial. Its longest-lived isotope only lives 23 minutes. However, this possibility may still be under consideration [806].

For the potential role of APV, among other probes, to search for new physics, see Ref. [807].

However, the simplest single e atom is hydrogen and APV in hydrogen is uniquely sensitive to the weak angle.

Can one hope to extract the proton weak charge from APV in a transition in hydrogen, as suggested by J. Li *et al.,* in Ref. [808] ?

[802] ibid

[803] C. Wieman and A. Derevianko, Atomic parity violation and the standard model. https://arxiv.org/abs/1904.00281

[804] R. Diener *et al.,* Constraining Extra Neutral Gauge Bosons with Atomic Parity Violation Measurements. https://arxiv.org/abs/1111.4566

[805] H. B. Tran Tan and A. Derevianko, Implications of W-Boson Mass Anomaly for Atomic Parity Violation. https://arxiv.org/abs/2204.11991

[806] G. Gwinner and L. A. Orozco, Studies of the weak interaction in atomic systems: towards measurements of atomic parity non-conservation in francium. 2022 Quantum Sci. Technology. 7 024001, https://iopscience.iop.org/article/10.1088/2058-9565/ac4424

[807] G. Arcadi *et al.* New physics probes: Atomic parity violation, polarized electron scattering and neutrino-nucleus coherent scattering. https://arxiv.org/abs/1906.04755

[808] J. Li *et al.,* Feasibility of extracting the proton weak charge from quantum-control measurements of atomic parity violation on the 2s−3s or 2s−4s transition in hydrogen. https://arxiv.org/abs/2310.14689

26. More on precision: the g–2 factor of the muon

"*g–2 is not an experiment: it's a way of life*", John Adams (CERN DG 1971–1975) once said. Indeed, some of the actors of its first version, in 1958, were still there 40 to 50 years later. This program is a superb piece of work, both theoretical and experimental, a "*game of tennis with well-matched players on either side of the net*" [809].

26.1 Basics of g–2

According to Dirac, g should be 2, but loops involving all three forces give a slight deviation from 2. The lowest order correction is $\alpha/2\pi \sim 0.00116$. Things complicate quickly: e.g. there are 12 672 5-loop diagrams.

A nonzero g–2 induces a beat between the frequency of rotation of the μ and the frequency of precession of its spin, measured by oscillation of the rate of e from μ decay at a point in the ring.

Figure 26-1 recalls the basics of g–2 and Fig. 26-2 gives details on the contributions to g–2.

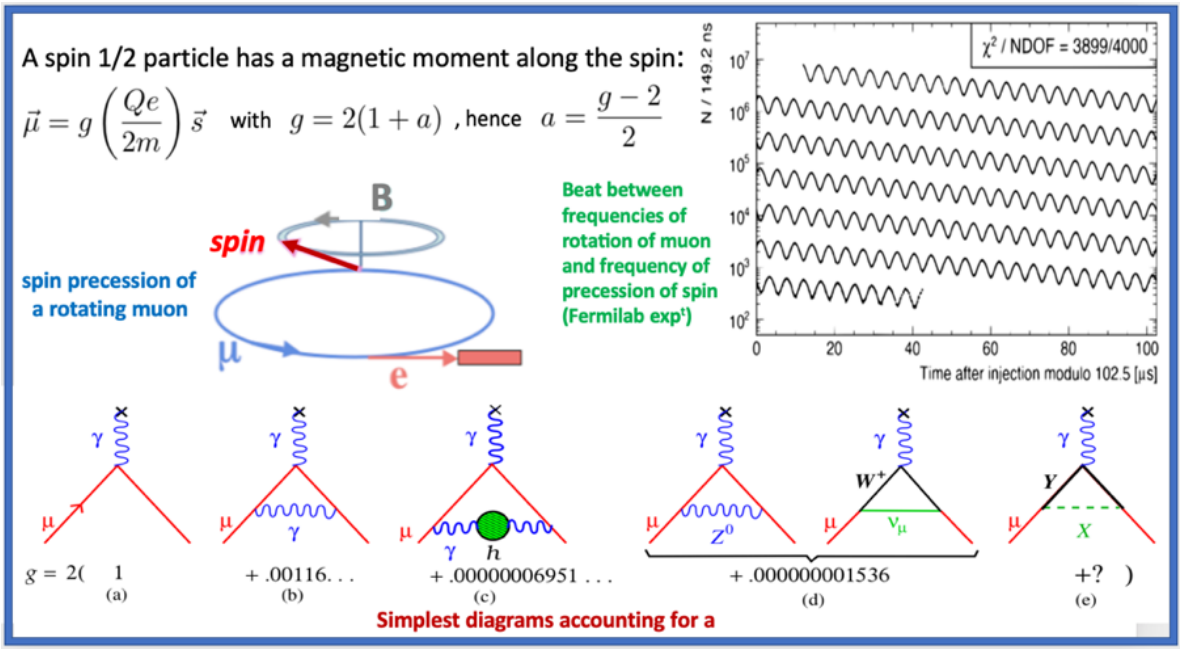


Fig. 26-1: Basics of g–2 [810].

CERN experiments were followed by the one in Brookhaven. The last experimental information came from the Fermilab experiment, using the Brookhaven ring [811].

---

[809] F. Farley and Y. K. Semertzidis, The 47 years of muon g–2. *Prog.Part.Nucl.Phys. 52 (2004) 1-83.*
B. Lee Roberts, The History of the Muon (g–2) Experiments. https://arxiv.org/abs/1811.06974
A. Keshavarzi *et al.,* Muon g–2: A review. https://arxiv.org/abs/2106.06723
[810] B. Lee Roberts, The History of the Muon (g–2) Experiments. https://arxiv.org/abs/1811.06974
[811] Muon g–2 announces most precise measurement of the magnetic anomaly of the muon.
https://news.fnal.gov/2025/06/muon-g-2-most-precise-measurement-of-muon-magnetic-anomaly/
G. Venanzoni, New results from the Muon g–2 Experiment. https://arxiv.org/abs/2311.08282

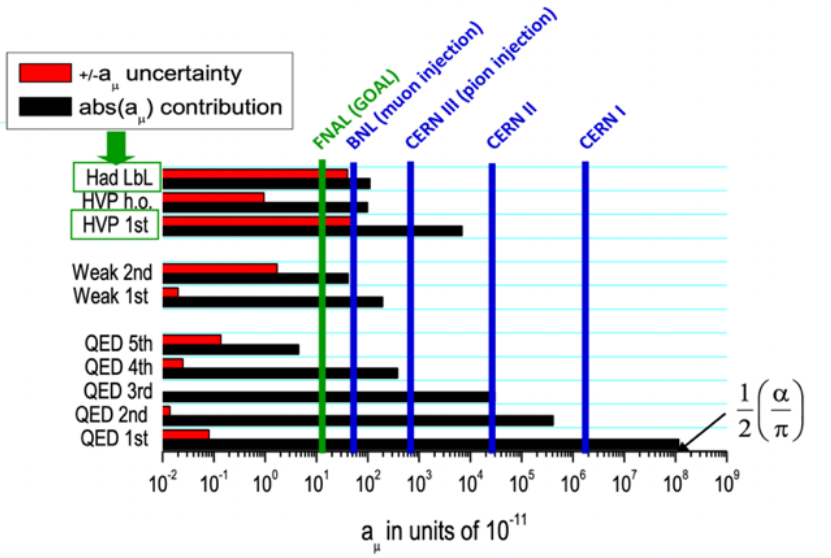


Fig. 26-2: List of the contributions to g–2. HVP: hadronic vacuum polarization; LbL: light by light [812].

26.2 Measurements and predictions

The measurement and the prediction agree at 10^{-6}, but there remains a discrepancy which reached 4.2 sigma (Fig. 26-3). New physics? Defect of measurement or estimate [813]?

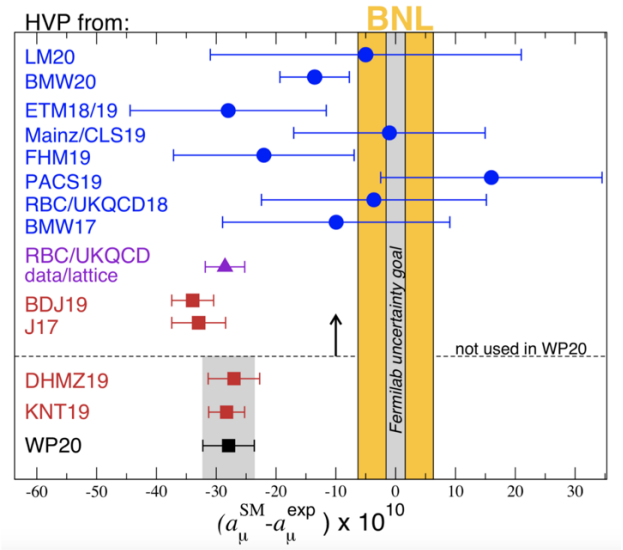


Fig. 26-3: A problem?

On the theory side, work in progress concerns the "photon box" diagram and especially the hadronic correction, needing experimental inputs: $e^+e^- \rightarrow$ low E hadrons (Fig. 26-4) and tau hadronic decays.

[812] Y. K. Semertzidise, The new muon g–2 results from Fermilab: Physics and High Precision implications. https://indico.global/event/8789/attachments/39256/73024/YkS_g2_INP_Demokritos_2021_0608(2).pdf
[813] M. Davier, The muon magnetic moment: a precision test shaking the Standard Model. https://inspirehep.net/files/84213e7ed30b838c0f26ac0b7e22c3da

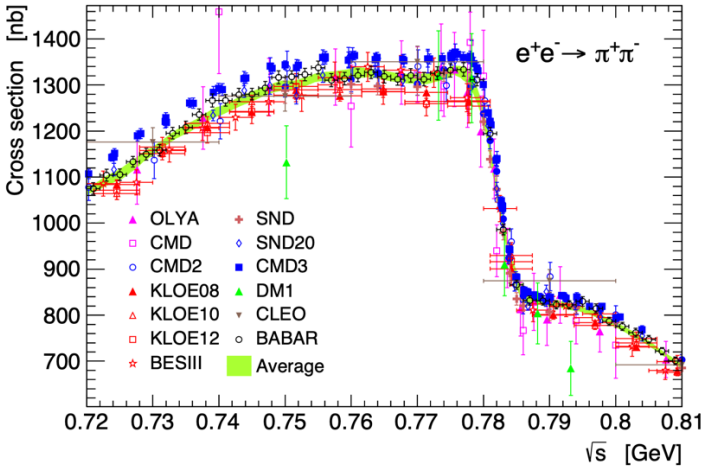


Fig. 26-4: $e^+e^- \to$ low E hadrons, the key energy region [814].

But a first new fact is that **lattice computing** has also entered the confrontation and some versions are less at odds with the experiment than the traditional theory (Fig. 26-5).

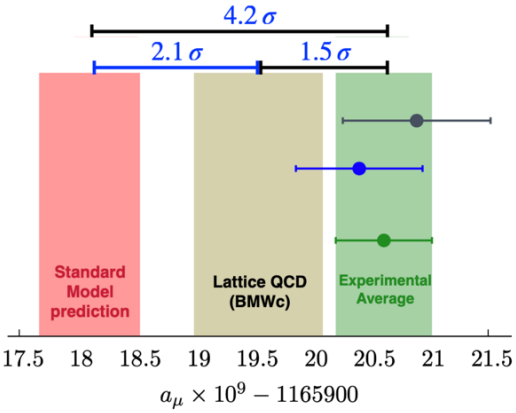


Fig. 26-5: Lattice QCD comes in Ref. [815].

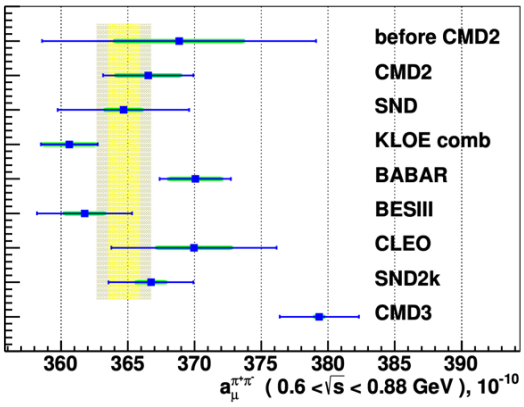


Fig. 26-6: CMD3 experiment comes in Ref. [816].

And the situation got more complex with the result of CMD3 on VEPP2000 (Fig. 26-6): *"The most significant difference to other energy scan measurements, including previous CMD-2 measurement, is observed at the left side of ρ-meson (√s = 0.6–0.75 GeV), where it reaches up to 5%, well beyond the combined systematic and statistical errors of the new and previous results* (Fig. 26-7). *The source of this difference is unknown at the moment".*

Figure 26-8 may suggest a tension between KLOE and others. For an in-depth review of the situation see Ref. [817] and Fig. 26-9.

---

[814] M. Davier *et al.*, Tensions in $e^+e^- \to \pi^+\pi^-(\gamma)$ measurements: the new landscape of data-driven hadronic vacuum polarization predictions for the muon g−2. Eur. Phys. J. C 84, 721 (2024), https://arxiv.org/abs/2312.02053

[815] M. Kado, Electroweak Experimental Summary and Highlights. Moriond EW 2023, https://indico.in2p3.fr/event/29681/contributions/122580/attachments/76723/111568/MKado-Summary.pdf

[816] F. V. Ignatov *et al.*, Measurement of the $e^+e^- \to \pi^+\pi^-$ cross section from threshold to 1.2 GeV with the CMD-3 detector. https://arxiv.org/abs/2302.08834

[817] M. Davier, The muon magnetic moment: a precision test shaking the Standard Model. https://inspirehep.net/files/84213e7ed30b838c0f26ac0b7e22c3da

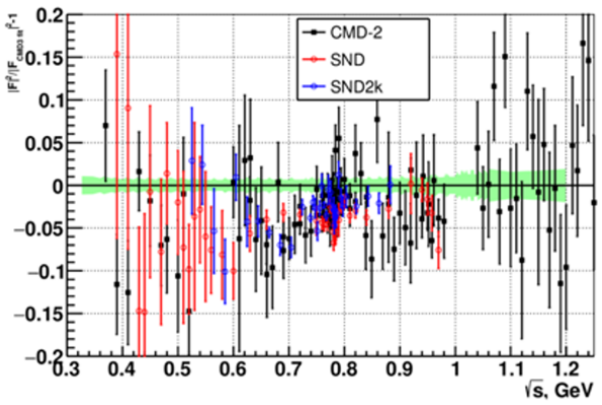


Fig. 26-7: The critical mass region.

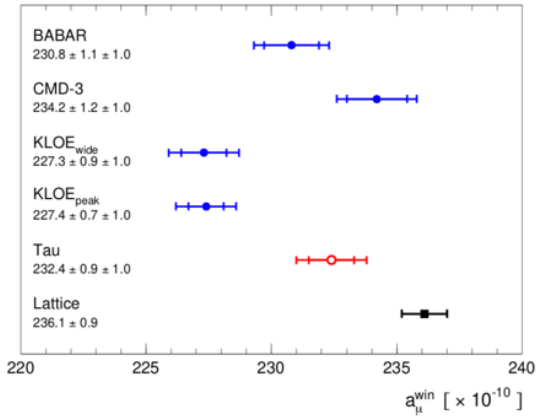
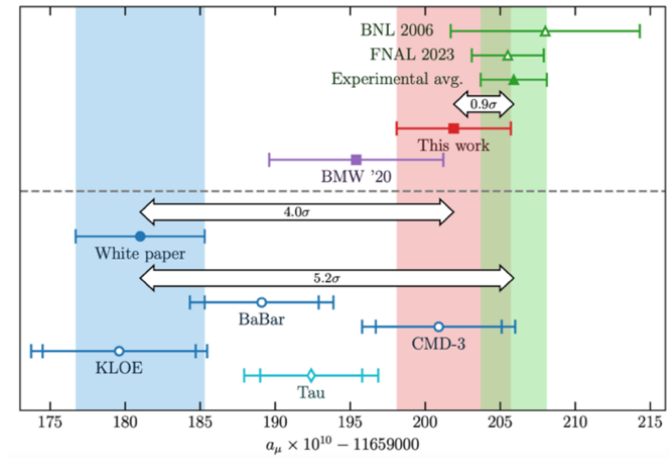


Fig. 26-8: Some tension between KLOE and other results [818]?



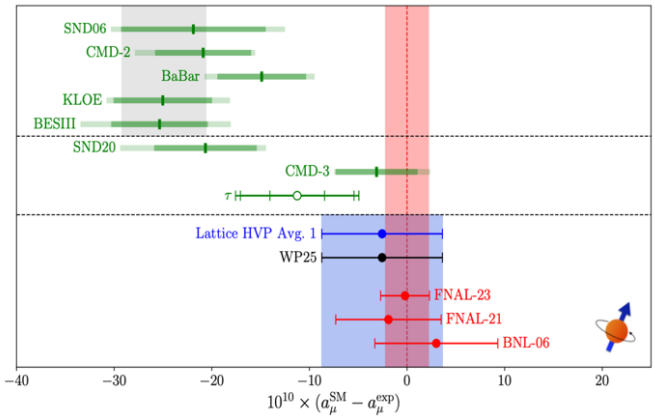


Fig. 26-9: The present situation, top see Ref. [819], bottom see Ref. [820].

[818] M. Davier *et al.,* Tensions in $e^+e^- \to \pi^+\pi^-(\gamma)$ measurements: the new landscape of data-driven hadronic vacuum polarization predictions for the muon g−2. Eur. Phys. J. C 84, 721 (2024), https://arxiv.org/abs/2312.02053

[819] A. Boccaletti *et al.,* High precision calculation of the hadronic vacuum polarization contribution to the muon anomaly. https://arxiv.org/abs/2407.10913

[820] P. Aliberti *et al.,* The anomalous magnetic moment of the muon in the Standard Model: an update. https://arxiv.org/abs/2505.21476

26.3 Some history of a_μ

In this section we discuss the muon anomaly $a_\mu = (g_\mu - 2)/2$ [821].

The first CERN experiment [822] used a long magnet (Fig. 26-10).

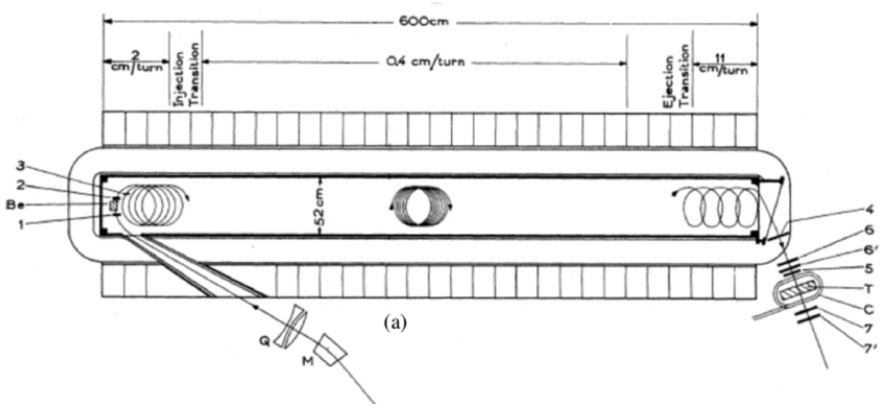


Fig. 26-10: The magnet of the first experiment.

The second one [823] used a 5-m diameter ring (Figs. 26-11 and 26-12).



Fig. 26-11: The team of the second g–2 experiment. Left: F. Farley; centre: G. Charpak; right: A. Zichichi.



Fig. 26-12: The ring of the 2nd experiment.

With the presence of both electric and magnetic fields, the spin rotation frequency [824] is

$$\vec{\omega}_S = -\frac{Qe}{m}\left[\left(\frac{g}{2} - 1 + \frac{1}{\gamma}\right)\vec{B} - \left(\frac{g}{2} - 1\right)\frac{\gamma}{\gamma+1}\left(\vec{\beta}.\vec{B}\right)\vec{\beta} - \left(\frac{g}{2} - \frac{\gamma}{\gamma+1}\right)\left(\frac{\vec{\beta}\times\vec{E}}{c}\right)\right].$$

[821] B. Lee Roberts, The History of the Muon (g−2) Experiments. https://arxiv.org/abs/1811.06974

[822] G. Charpak, F. J. M. Farley and R. L. Garwin, A New Measurement of the Anomalous Magnetic Moment of the Muon. *Phys. Lett. 1, 16 (1962)*

[823] J. Bailey *et al.,* Precision measurement of the anomalous magnetic moment of the muon. *Phys. Lett. B28, 287 (1968)*

[824] L. H. Thomas, The Kinematics of an electron with an axis. *Phil. Mag. Ser.7 3, 1 (1927),* https://www.tandfonline.com/doi/abs/10.1080/14786440108564170

V. Bargmann, L. Michel and V. L. Telegdi, Precession of the Polarization of Particles Moving in a Homogeneous Electromagnetic Field. *Phys. Rev. Lett. 2, 435 (1959)*

While a relativistic particle moving in an electric field will experience a motional magnetic field, the negative sign in the parentheses introduces a **cancellation at γ_m** = 29.3, p_μ = 3.09 GeV. The choice of this value for γ was the principle of the 3rd experiment [825] (Fig. 26-13).

CERN a_μ measurements reached respectively 5164 ppm, 266 ppm, 7.3 ppm precision. The 3rd experiment gave $a_\mu = (1\ 165\ 924 \pm 8.5) \times 10^{-9}$. Brookhaven reached 0.54 ppm and Fermilab 0.12 ppm. The third and final result from the Muon g–2 collaboration at Fermilab, based on the last three years of data, is in perfect agreement with the previous results, further solidifying the experimental world average, as illustrated in Fig. 26-14 [826]. The obtained value is:

$$a_\mu = 0.001\ 165\ 920\ 705 \pm 0.000\ 000\ 000\ 114(\text{stat}) \pm 0.000\ 000\ 000\ 091(\text{syst})\ .$$

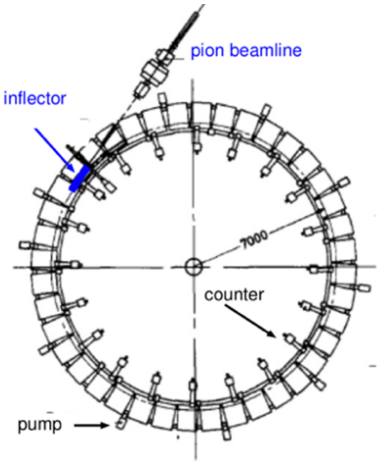


Fig. 26-13: CERN second ring.

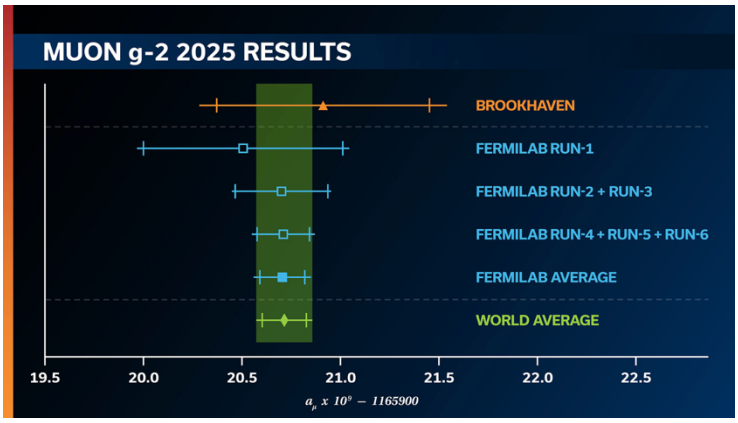


Fig. 26-14: Credit: Muon g–2 collaboration.

26.4 g–2 of the tau and electron

Preliminary measurements of the **g–2 of the tau** [827] are appearing, with substantial uncertainties. The result is still 3–4 orders of magnitude above sensitive corrections, as e.g. for the EW contribution (Fig. 26-15).

As for the **g–2 of the electron**, its measurement amounts to **a measurement of α**. The electron's a_e has recently been measured to a precision of 0.13×10^{-12} (see Ref. [828]).

But α is also measured by the ratio (h / atomic mass) (Fig. 26-16): $\alpha^2 = \frac{2R_\infty}{c}\frac{m_{atom}}{m_e}\frac{h}{m_{atom}}$.

Introducing α extracted from Cs and Rb atom interferometric experiments into the QED expansion for a_e gives an agreement to one part in 10^{12}.

---

[825] J. Bailey *et al.,* Final report on the CERN muon storage ring including the anomalous magnetic moment and the electric dipole moment of the muon, and a direct test of relativistic time dilatio. *Nucl. Phys. B150, 1 (1979)*

[826] Muon g–2: https://muon-g-2.fnal.gov/
D. P. Aguillard *et al.,* Measurement of the Positive Muon Anomalous Magnetic Moment to 127 ppb. https://arxiv.org/abs/2506.03069

[827] M. Pierini, CMS Highlights. ICHEP 2024, https://indico.cern.ch/event/1291157/contributions/5958001/attachments/2901064/5087563/CMSHighlights.pdf , https://cms-results.web.cern.ch/cms-results/public-results/publications/SMP-23-005/

[828] X. Fan *et al.* Measurement of the Electron Magnetic Moment. https://arxiv.org/abs/2209.13084

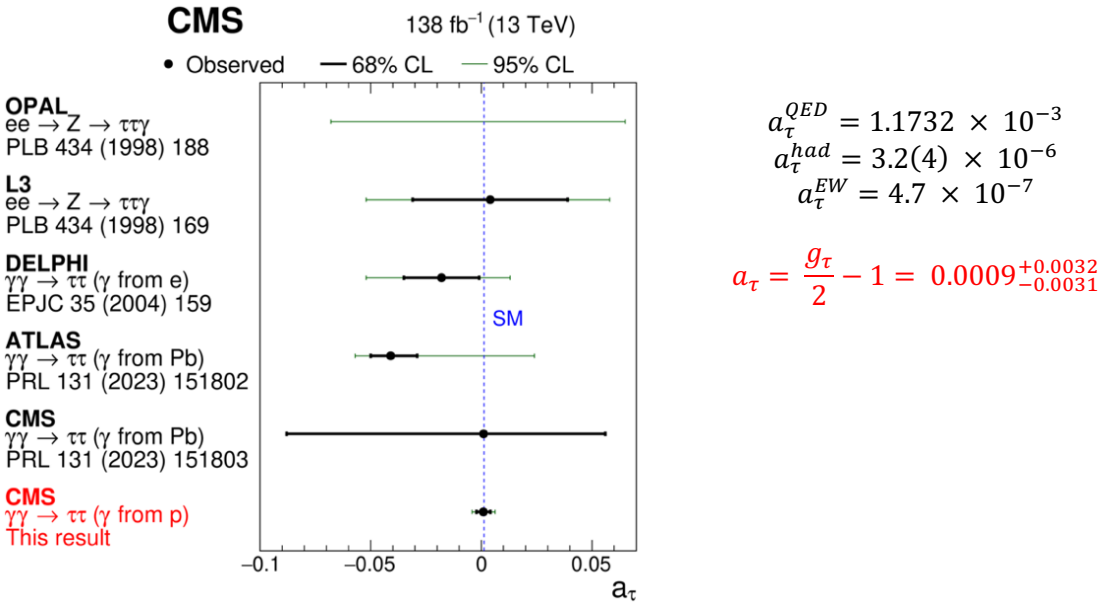


Fig. 26-15: g−2 of the tau (left), present measurement and expected components (right).

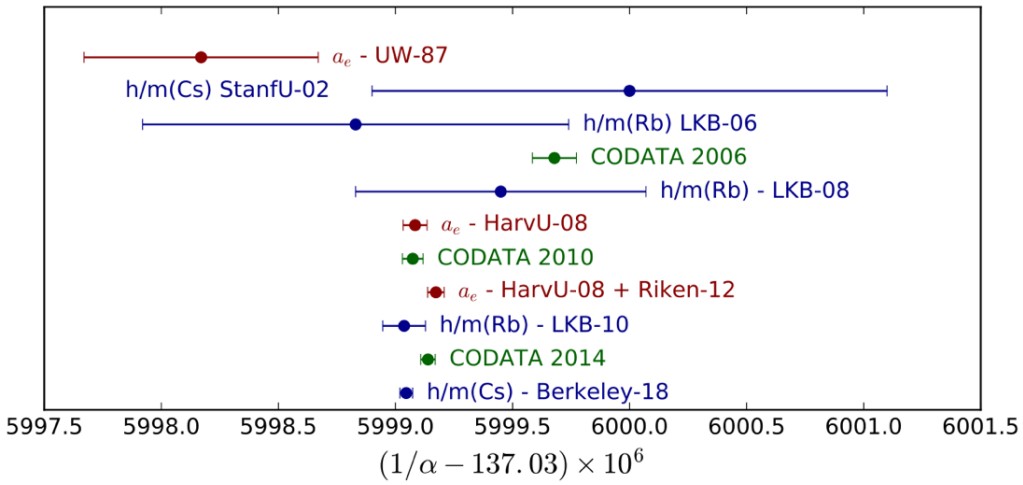


Fig. 26-16: α determination: Comparison of different determinations of α with uncertainties below 10^{-8}. In red, determinations from the magnetic moment of the electron, in blue from h/m_{At} and in green from the CODATA [829].

This agreement is not perfect (Fig. 26-17) [830], but the difference of 2.5 σ is not statistically sufficient to conclude that there is physics beyond the SM.

[829] P. Cladé *et al.,* State of the art in the determination of the fine structure constant and the ratio h/m_u. https://arxiv.org/abs/1901.01990
L. Morel *et al.,* Determination of the fine-structure constant with an accuracy of 81 parts per trillion, *Nature 588 (7836) (2020) 61–65*, https://doi.org/10.1038/s41586-020-2964-7
The h/m_{At} ratio comes from measuring the kinetic energy of an atom of mass m_{At} $(\hbar k)^2/(2m_{At})$ that recoils from scattering a photon of momentum $\hbar k$.
[830] Ibid

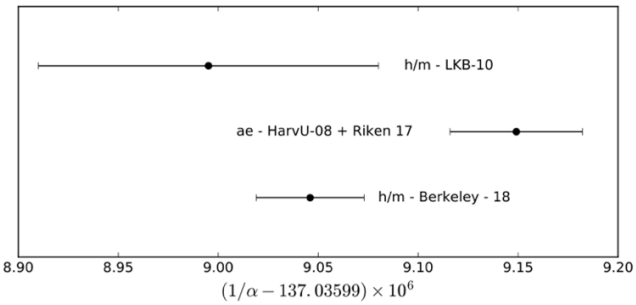


Fig. 26-17: Three best determinations of α from h/m and from a_e [831].

26.5 Another access to the hadronic vacuum polarisation: a^{HVP}

$$a^{HVP} = \frac{\alpha}{\pi}\int_0^1 dx(1-x)\Delta\alpha_{had}[t(x)]$$

The MuonE experiment's [832] goal is to provide an independent and innovative method to evaluate the hadronic vacuum polarisation (HVP) a^{HVP} based on the evaluation of the equation shown above, which depends on the **hadronic contribution to the running of the e.m. coupling** in the space-like region of momenta, $\Delta\alpha_{had}(t)$, a smooth function [833].

The process used for the measurement is the **μ – e elastic scattering** on light target, using the CERN muon beam at E_μ = 150 GeV. The CM energy is thus $s = m_e^2 + M_\mu^2 + 2m_eE_\mu \simeq (400\ \text{MeV})^2$. The momentum transfer *t* ranges from $t_{min} \simeq -(380\ \text{MeV})^2$ to zero. x and t variables are related by $t = x^2 M_\mu^2/(x—1)$.

The elasticity curve of Fig. 26-18, where $\theta_{e,\mu}$ are the scattering angles in lab, is **the basic constraint** for MuonE to discriminate elastic scattering events from the background of radiative events and inelastic processes. Figure 26-19 shows the relative importance of HVP in the μ – e scattering. The integrand of the integral is given in Fig. 26-20.

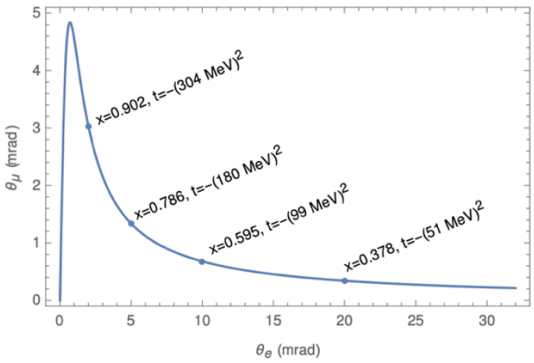


Fig. 26-18: Relation between the muon and the e scattering angles [834].

---

[831] α = 1/137.035999206(21) (CODATA 2022) by combining measurements of the $e^\pm$ g–2 with measurements of the Rydberg constant and atomic masses with interferometry of atomic recoil kinematics. For comparison in PP two well measured quantities are: M_Z = 91.1876(21) GeV from the Z line-shape. $G_F = 1.1663787(6) \times 10^{-5}$ GeV^{-2} from muon lifetime.

[832] P. Banerjee *et al.,* Theory for muon-electron scattering @ 10 ppm: A report of the MUonE theory initiative. *Eur. Phys. J. C (2020) 80: 591*, https://arxiv.org/abs/2004.13663
M. Rocco, Muon-electron scattering at NNLO with McMule. https://arxiv.org/abs/2309.06071

[833] T. San José *et al.,* The hadronic running of the electromagnetic coupling and electroweak mixing angle. https://arxiv.org/abs/2212.02366

[834] P. Banerjee *et al.,* Theory for muon-electron scattering @ 10 ppm: A report of the MUonE theory initiative. *Eur. Phys. J. C (2020) 80: 591*, https://arxiv.org/abs/2004.13663

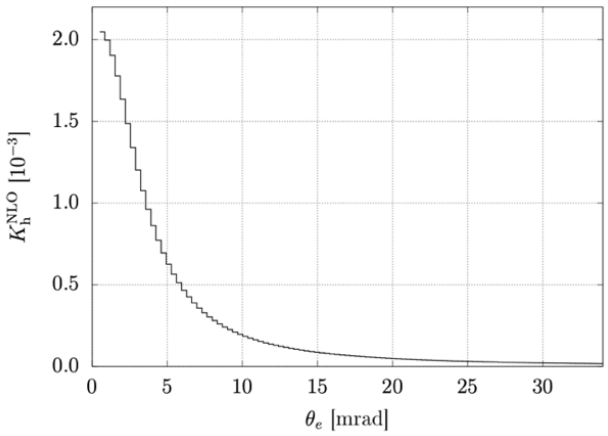


Fig. 26-19: Relative importance of the HVP at NLO in μ – e scattering [835].

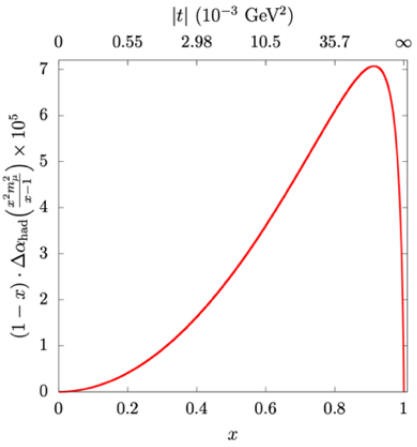


Fig. 26-20: The integrand as a function of x (bottom scale) or t (top scale) [836].

The HVP changes the differential cross section of μ-*e* scattering by up to O(10^{-3}), depending on θ_e. To obtain a^{HLO} with a relevant statistical error, one must extract HVP from μ – e data with **an uncertainty < 1%.**

One needs to calculate μ-e scattering at least up to NNLO in the perturbative expansion in α (Fig. 26-21). See the references for more details on the calculations at successive orders and the ways to deal with potential large logarithms. Achieved is "*a fully differential parton-level Monte Carlo program containing (i) the fully massive NLO QED (and EW) contributions; (ii) the fully massive (dominant) electronic contributions at NNLO; (iii) the fully massive NNLO hadronic contributions; (iv) the remaining contributions at NNLO in a massified approach, i.e. neglecting finite electron mass terms.*"

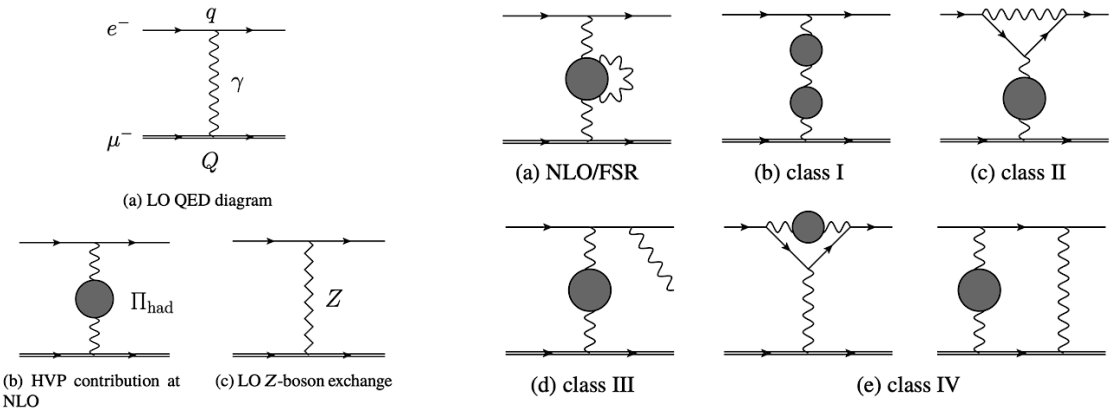


Fig. 26-21: Left: LO contributions; right: diagrams contributing at NLO (a) and NNLO (b-e) [837].

[835] ibid , The NLO K-factor is the ratio of the θ_e distributions of the hadronic contribution at NLO and the Born cross section.
[836] G. Abbiend *et al.,* Measuring the leading hadronic contribution to the muon g–2 via scattering. *Eur. Phys. J. C 77, 139 (2017)*, https://arxiv.org/abs/1609.08987
[837] P. Banerjee *et al.,* Theory for muon-electron scattering @ 10 ppm: A report of the MUonE theory initiative. *Eur. Phys. J. C (2020) 80: 591*, https://arxiv.org/abs/2004.13663

Defining $R_{had} \sim 1 + 2\Delta\alpha_{had}(t)$, Fig. 26-22 shows the expected result for the indicated luminosity. An approximate fit give $\Delta\alpha_{had}(t) \simeq -\frac{1}{15}Kt$, with K = 0.136 $\pm$ 0.026 in E^{-2}.

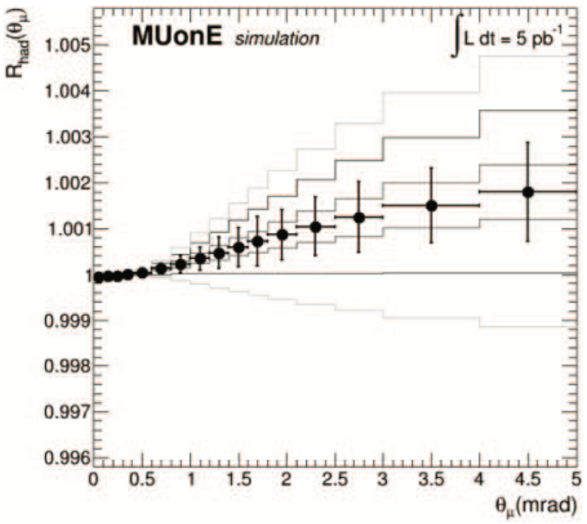


Fig. 26-22: Ratio R_{had} as a function of the muon scattering angle [838].

26.6 To conclude

Another measurement of a_μ is planned at J-PARC@KEK [839] using a very different technique with a compact magnetic ring and low momentum μ^+. Data-taking should start in 2028 and 2 years of running would give a result with about twice the uncertainty of Muon g–2.

At present, the current status of lattice calculation seems to agree with the evaluation using VEPP2000 e^+e^- hadron production measurements and with the experimental a_μ value. But persistent disagreements with other estimates have to be understood. Speculations as in Ref. [840] may not be over.

[838] R. N. Pilato, The MUonE experiment. https://cds.cern.ch/record/2824507/files/ncc12407.pdf
[839] M. Abe *et al.,* A New Approach for Measuring the Muon Anomalous Magnetic Moment and Electric Dipole Moment. https://arxiv.org/abs/1901.03047
[840] G. R. Farrar, The muon g–2 and lattice QCD hadronic vacuum polarization may point to new, long-lived neutral hadrons. https://arxiv.org/abs/2206.13460
P. Paradisi, On the old and new muon g–2 puzzle. https://inspirehep.net/files/67535471ce9b73d248031f3cfaabd113

27. Flashback, for the pleasure: the π meson

It is, for the pleasure, a return to the past …

27.1 History and studies of π^0

The existence of the π meson was postulated in 1935 by Yukawa to explain the characteristics of the nucleon-nucleon interaction. After some confusion with the muon, the charged pion was discovered in 1947 in cosmic rays, by César Lattes et al. The π meson was produced in 1948 at Berkeley for the first time in an accelerator and observed in the $\pi \to \mu\nu$ mode. Several searches for the $\pi \to e\nu$ mode were unsuccessful, and the absence of this mode at the expected value posed a big problem for Fermi's description of the weak interaction. In 1958 the first CERN accelerator, the Synchrocyclotron (SC) (Chapter 3), finally offered the discovery, as expected, of the **rare but precious $\pi \to e\nu$ decay** [841].

The π^0 was observed in 1950 by a series of experiments in its main mode in 2-gamma: at the 184-inch synchrocyclotron in Berkeley in proton-nucleus scattering and in $\pi^- p \to \pi^0 n$ with pions at rest, in cosmic rays as well as photoproduced at Berkeley.

Electromagnetic effects cause π^+ to be 4.6 MeV heavier than the neutral π^0.

One way to calculate the amplitude $\pi^0 \to \gamma\gamma$ (Fig. 27-1) was to use the PCAC condition (partially conserved axial-vector, isovector, current) which relates the pion field to the divergence of the axial current. But the lifetime thus found was too long by three orders of magnitude. Moreover, the amplitude vanished at the chiral limit of massless quarks and pions.

It was the discovery of **the chiral anomaly** (Chapter 7) that solved the problem. An additional term then appears in the divergence of the axial current and accounts for the observations. The triangle anomaly of Fig. 27-1 leads to a $\pi^0 \to \gamma\gamma$ amplitude that we give for curiosity:

$$M = \frac{Ae^2}{f_\pi}\frac{1}{4\pi^2}\epsilon_{\mu\nu\rho\sigma}p_1^\rho p_2^\sigma \varepsilon_1^{\mu *}\varepsilon_2^{\nu *} .$$

p_i and ε_i are the γ momenta and polarization vectors, f_π = 93 MeV is the π decay constant and A = 1.

The result of the axial anomaly calculation [842] is a width of 7.87 eV, in agreement with measurement and demonstrating the **key role of colour.**

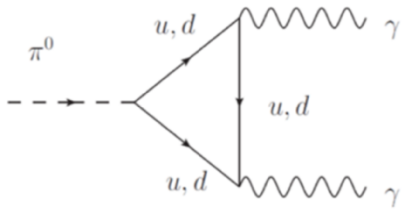


Fig. 27-1: Diagram of $\pi^0 \to \gamma\gamma$.

Another intriguing aspect of this particle is the extreme simplicity of one of its **lifetime measurements** in 1985 [843]: two thin sheets of tungsten that can be gradually separated exposed to a high-energy

[841] G. Fidecaro, Discovery of the $\pi \to e\nu$ Decay: Rare and Precious. In Technology Meets Research, https://inspirehep.net/files/53479a7bd7931662e81f61632e1e8c8f

[842] H.W. Atherton *et al.,* Direct measurement of the lifetime of the neutral pion. *Phys.Lett.B 158 (1985) 81-84,* https://www.sciencedirect.com/science/article/pii/0370269385907440?via%3Dihub

[843] ibid

beam. If the π^0 generated in the 1st step skips the second, this has no effect. If it decays before the second, the two photons convert in it (Fig. 27-2). You also need to know the π^0 energy. The lifetime found is

$$\tau_{\pi 0} = (0.897 \pm 0.022 \pm 0.017) \times 10^{-16} \text{ s, i.e. width } \Gamma_{\pi 0} = (7.34 \pm 0.18 \pm 0.11) \text{ eV.}$$

This is a good place to recall the **important role of the chiral anomaly** in basic problems [844], as baryogenesis (Chapters 7, 24 and Section 32.4).

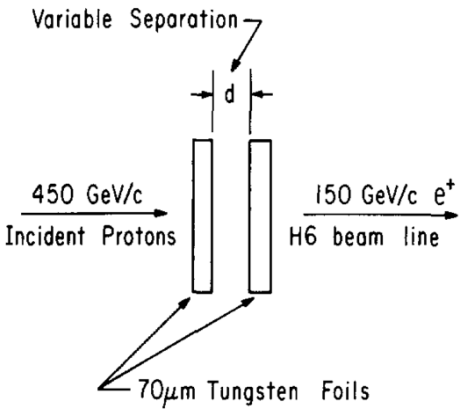
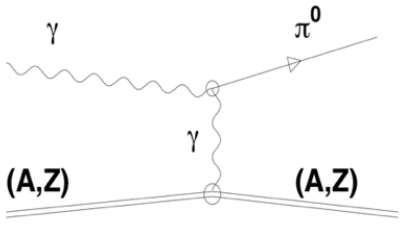


Fig. 27-2: A very simple set-up [845].

Let us also mention the classic measurements of the π^0 width made via the **Primakoff effect,** illustrated in Fig. 27-3.



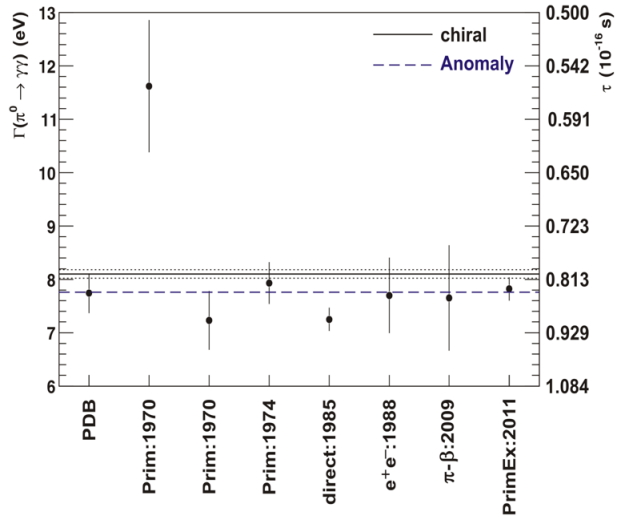


Fig. 27-3: Left: The Primakoff effect. Right: $\pi^0 \to \gamma\gamma$ decay width in eV (left scale) and $\tau(\pi^0)$, the mean π^0 lifetime in units of 10^{-16} s (right scale) measured by the most accurate experiments [846].

[844] D. Tong, Lectures on Gauge Theory. https://www.damtp.cam.ac.uk/user/tong/gaugetheory.html
[845] H. W. Atherton *et al.,* Direct measurement of the lifetime of the neutral pion. *Phys.Lett.B 158 (1985) 81-84,* https://www.sciencedirect.com/science/article/pii/0370269385907440?via%3Dihub
[846] A. M. Bernstein and B. R. Holstein, Neutral Pion Lifetime Measurements and the QCD Chiral Anomaly. *Reviews of Modern Physics, 85, 49(2013),* https://arxiv.org/abs/1112.4809

27.2 Recap about baryon number non-conservation

This short section, which can be skipped, repeats and summarizes what appeared in Chapters 7 and 24.

After the discovery of the **chiral anomaly** [847] (see also Chapters 7 and 24), thoughts and work made clear that the structure of the anomaly could be described mathematically more deeply [848] or, in physics language, in terms of **instantons**.

The EW Standard Model has all the necessary ingredients for successful **baryogenesis**, although these interactions may be insufficient to explain the total baryonic number of the observed Universe if the initial baryon number of the Universe at the time of the Big Bang is zero. Beyond C and CP violation, baryonic number (B) violation appears through the Adler–Bell–Jackiw anomaly of the group.

The baryonic number B is not conserved by the usual EW interactions due to the **quantum chiral anomaly**. The classic EW Lagrangian conserves baryonic number B. Quarks always enter in combinations such that a quark can disappear only by colliding with an antiquark. In other words, the classical baryonic current J^B_μ is conserved:

$$\partial^\mu J^B_\mu = \sum_j \partial^\mu(\bar{q}_j \gamma_\mu q_j) = 0$$

However, quantum corrections known as the sphaleron, that we met in Sections 7.7 and 24.1.5, destroy this conservation law, adding to the righthand side of this equation a non-vanishing quantum term, the QCD ABJ anomaly

$$\partial^\mu J^B_\mu = \frac{g_s^2}{16}\frac{C}{\pi^2} G^{\mu\nu a}\widetilde{G}^a_{\mu\nu}$$

where **C** is a numerical constant vanishing for $\hbar$ = 0. The gauge field strength is given by the usual expression (Table 7.1) $G^a_{\mu\nu} = \partial_\mu A^a_\nu - \partial_\nu A^a_\mu + g_s^2 f^a_{bc} A^b_\mu A^c_\nu$ and $\widetilde{G}^a_{\mu\nu} = \frac{1}{2}\epsilon_{\mu\nu\alpha\beta} G^{a\alpha\beta}$.

Electroweak sphalerons can only change the baryon and/or lepton number by 3 or multiples of 3 (collision of 3 leptons into 9 antiquarks or of 3 antileptons into 9 quarks, see Fig. 24-21).

Repeating what we said in Chapter 7, an important fact is that the anomalous current non-conservation is proportional to the **total derivative of a vector operator**.

We saw that the effect of this total derivative is non-vanishing due to **instanton configurations** of the gauge field, which are pure gauge at infinity.

---

[847] Chiral anomaly. https://en.wikipedia.org/wiki/Chiral_anomaly
R. Jackiv, Topological Aspects of Gauge Theories. https://arxiv.org/abs/hep-th/0501178

[848] For math-oriented minds: the math version considers bundles with a non-trivial **homotopy group.** An instanton is a local minimum of the action that mediates vacuum tunnelling. The sphaleron sits in-between the vacua, in a certain sense, it is the instanton "in the middle of tunnelling". The anomalous current K_μ is the Hodge dual of the Chern–Simons 3-form.

28. New spectroscopy from LHC and elsewhere

Let us come to this new avalanche of new particles announced in Chapter 4, which offers multiquark hadron candidates.

28.1 From expected to unexpected spectroscopy

After the quark conjecture, it was Richard Dalitz who developed the model, focusing first on the then more numerous baryons. With the invention of colour, linked to Pauli's principle, Chromodynamics was built, according to which physical states are “colour-blind” states, or colour singlets. But QCD said little about the non-perturbative sector and did not explain the pattern of quark states, consistent with the data.

With the arrival of charm and beauty came very rich spectroscopies, of “closed” flavour and “open” flavour, and the mesons regained the main role (Fig. 28-1).

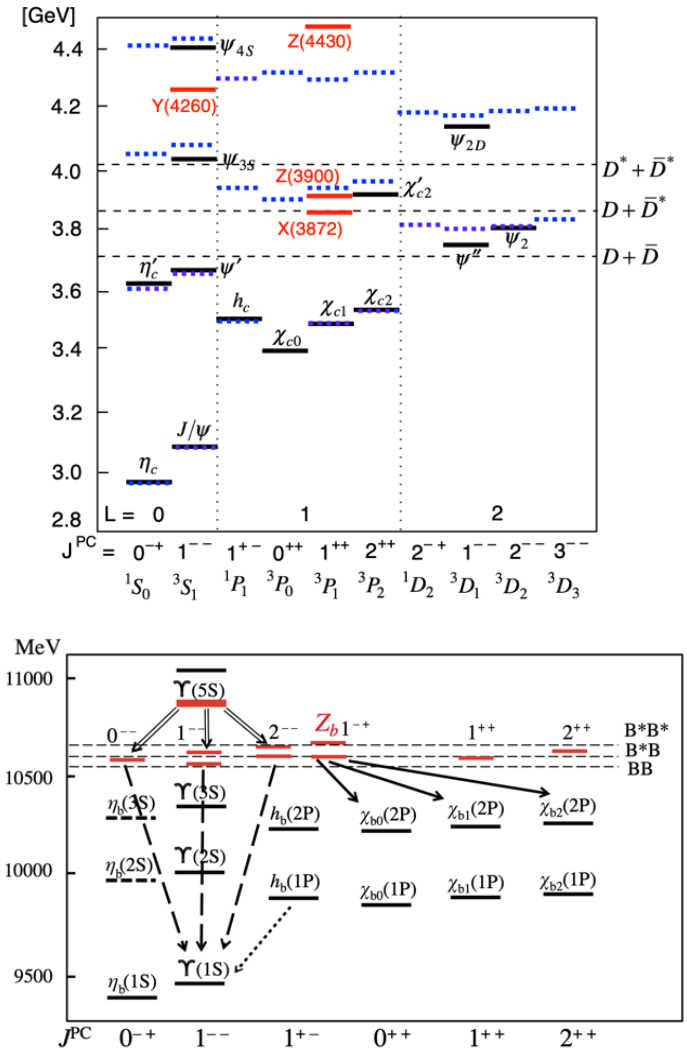


Fig. 28-1: Spectroscopies of charmonium (top) and bottomonium (bottom) [849].

[849] A. Hosaka *et al.,* Exotic hadrons with heavy flavors: X, Y, Z, and related states. https://arxiv.org/abs/1603.09229

It was soon realized that combinations more complex than the standard representation also offered colour singlet states. The guide to the quark model being well established, such states were called **exotic**.

QCD forces can be described in terms of oriented strings originating at a quark and ending at an antiquark [850]. The end of the string carries a 3 representation of $SU(3)_C$, so that the strings from the 3 quarks of a baryon can join at a point in an invariant way of $SU(3)_C$. New colour singlets can be obtained from mesonic or baryonic configurations by replacing an antiquark with a colour 3 diquark, forming an invariant 3-string junction (Fig. 28-2) [851].

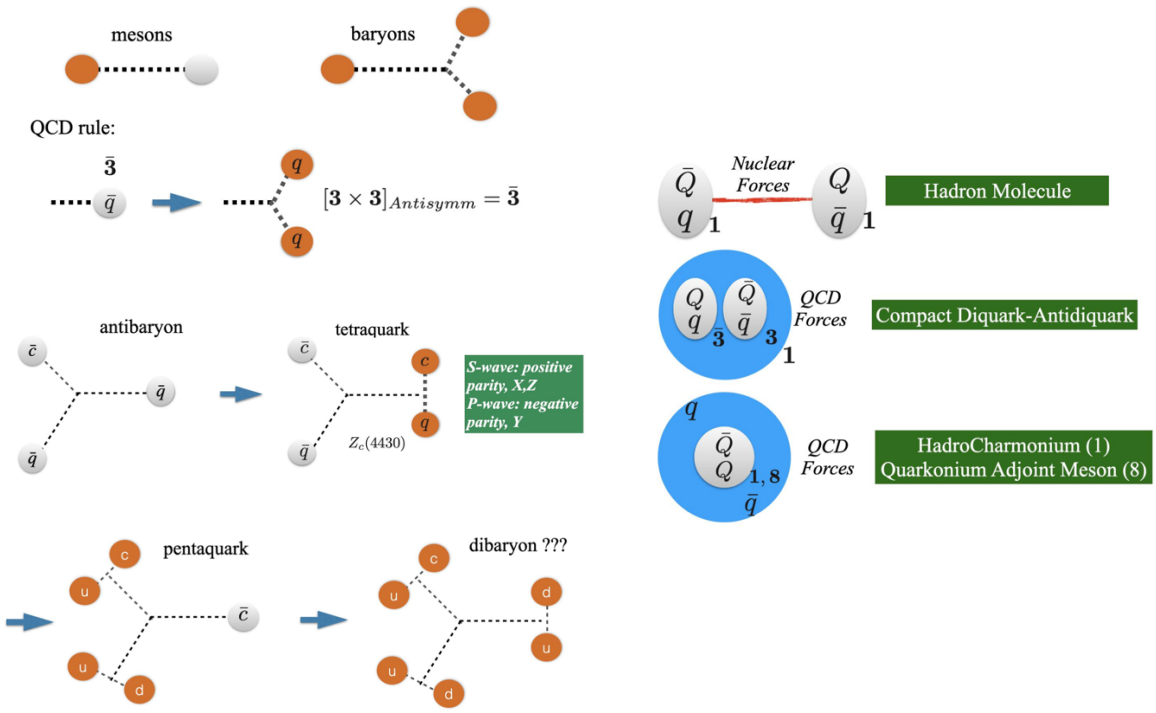


Fig. 28-2: How to make coloured singlets: colour strings in ordinary particles**,** colour strings in multiquark states (left) and scheme of hadronic molecules, compact tetraquarks, HadroCharmonium (right).

In recent years, many so-called exotic hadrons have been discovered: particles made up of four or five quarks instead of the usual two or three. Heavy quarks play an important role.

Figure 28-3 gives the map of “unexpected” states in relation to charmonium [852].

The X (3872) $\rightarrow$ J/ψ $\pi^+\pi^-$ was the first unexpected candidate with a mass of 3871.68 MeV/c which did not fit the classical scheme. Discovered in 2003 by BELLE, confirmed by other experiments, classified 1^{++}, it gave rise to several hypotheses, including that of a tetraquark [853].

[850] L. Maiani and A. Pilloni, GGI Lectures on Exotic Hadrons. https://arxiv.org/abs/2207.05141
[851] ibid
[852] ibid.
[853] X.-R. Lyu, Advances in (experimental) hadron physics, ICHEP 2024, https://indico.cern.ch/event/1291157/contributions/5958375/attachments/2902667/5091817/ICHEP2024_Hadron_LYU.pdf
There is a new strong indication of a sizeable charmonium or tetraquark compact component of the X(3872)!

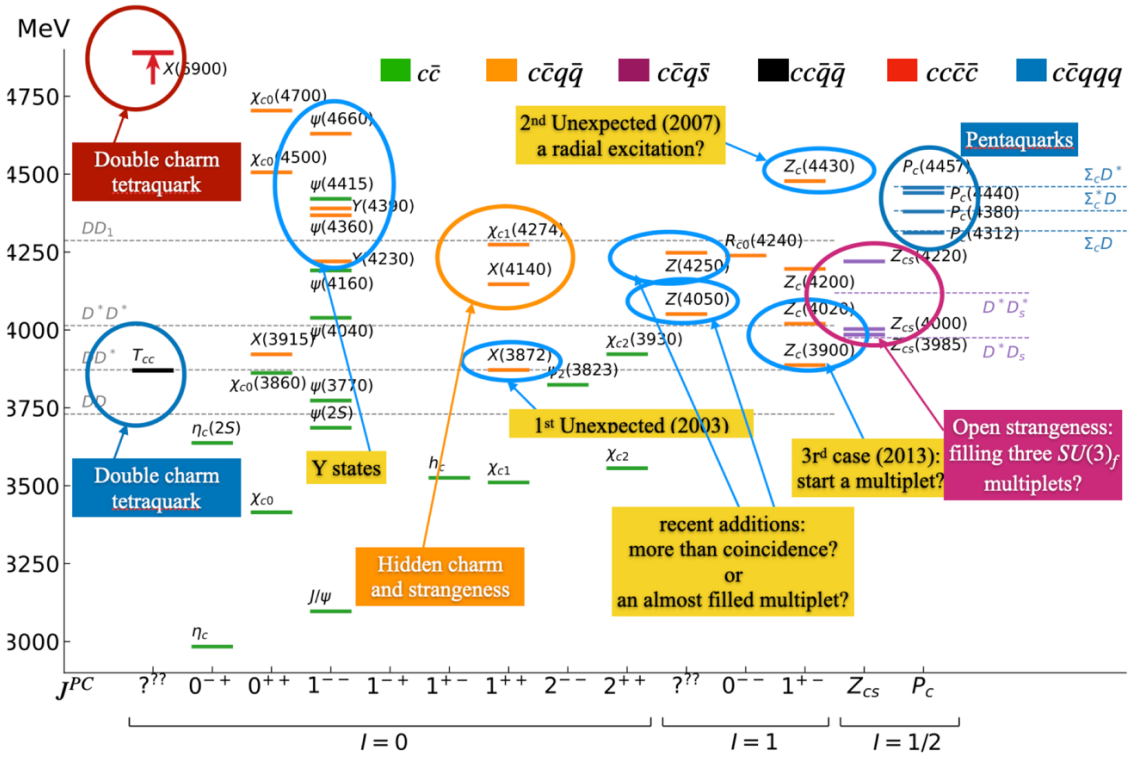


Fig. 28-3: Map of unexpected states in charmonium spectroscopy.

A pair of heavy quarks is difficult to create and destroy in a hadron. So, hadrons giving a J/ψ (or Y) in their decay are likely to contain a valence pair of heavy quarks. As the spectra of charmonia and bottomonia are theoretically well controlled, any state that does not satisfy their spectra is a good candidate for an exotic multiquark.

These are the X (neutral, typically seen in J/ψ + pions, JPC = 0++, 1+±, 2++) and Y (neutral, seen in annihilation $e^+e^- \rightarrow$ Y, so has $J^{PC} = 1^{--}$) mesons of the last decades, the first example of which is this X (3872) and the Y (4260) ($\pi^+\pi^-$J/ψ, BaBar 2005). This particle appears in B_S^0 decay in association with a ϕ meson [854] (Fig. 28-4).

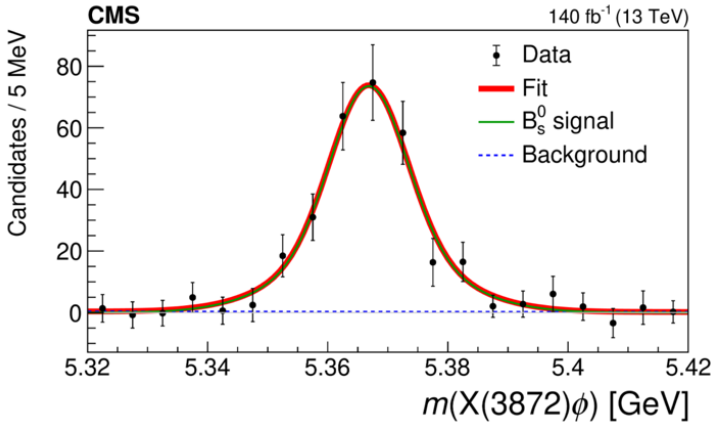


Fig. 28-4: Background-subtracted X(3872)ϕ invariant mass distributions.

[854] CMS Collaboration. Observation of the $B^0_s \rightarrow X(3872)\phi$ decay. https://arxiv.org/abs/2005.04764

Another class of exotic states are electrically charged states of charm and beauty. These unanticipated states are the particles called Z, the first of which was $Z_c(4430)$ ($\rightarrow \psi(2S)\,\pi^+$), Belle 2008, LHCB 2014).

A tetraquark species, Tcc+ (LHCb, 3875 MeV, seen in $D^0\,D^{*+}$) contains two c quarks as well as a u antiquark and a d antiquark. It is the first tetraquark to contain two c quarks, without a compensating c antiquark, therefore **two heavy quarks and two light antiquarks**, a category predicted in [855]. It is not yet known exactly how this object is assembled.

One can also speculate on possible **hexaquarks (or sexaquarks**), hypothetical particles consisting of 6 quarks or antiquarks of all flavours and colour charge 0. For example, an assembly of six quarks would look like 2 bound baryons. One can suspect such dibaryons to be relatively stable [856] and wonder if such objects, electrically neutral, could have escaped detection in the measurements of $e^+e^- \rightarrow$ hadrons, which would have an implication on the theoretical estimate of the g–2 of the muon.

The exact structure of these hadrons is still questionable.

In some cases, the familiar forces of nuclear physics play a role and the LHC makes it possible to reach all combinations of mesons of all flavours.

28.2 Exotic states

In general, the simple image of mesons seems robust as long as they are not close to hadron pair production channels in the S-wave channel. Exotic mesons and hadrons seem to be correlated with some S-wave channel having the same quantum numbers as a nominal $q\text{-}\bar{q}$ state and causing a state to appear near the corresponding S-wave threshold.

We can consider different levels of exoticism (Fig. 28-5):

- the less exotic flavoured hadrons would be **nucleus-like mesons**, with pion exchange between pairs of constituent meson;
- then come **"hybrids"** where the gluonic degrees of freedom are excited in the presence of quarks;
- finally, we can consider colour singlet states, combinations of **compact diquarks**, allowed in principle by QCD.

These exotic states must be studied in different production mechanisms and decay channels. A true resonant state should appear in several, otherwise a structure may suggest a dynamic effect rather than a resonance.

The following summarizes the states seen at the LHC (Fig. 28-6), gives a list of recent LHCb hadrons and their presumed nature (Fig. 28-7) [857]. Figure 28-7 gives another presentation of the exotic hadrons [858].

Needless to say, a unified way of naming all these new particles (the clearest if possible) would be much welcome.

---

[855] J. M. Richard, Fully heavy multiquarks. https://arxiv.org/abs/2106.07434
M. Karliner and J. L. Rosner, Discovery of doubly-charmed Ξ_{cc} baryon implies a stable $bb\bar{u}\bar{d}$ tetraquark. *Phys. Rev. Lett. 119, 202001 (2017),* https://arxiv.org/abs/1707.07666

[856] G. R. Farrar and Z. Wang, Constraints on long-lived di-baryons and di-baryonic dark matter. https://arxiv.org/abs/2306.03123

[857] P. Gandini, Reviewing a decade of spectroscopy at LHCb and the observation of new baryonic structures. https://indico.cern.ch/event/1231803/attachments/2634454/4557224/gandini_CERN_seminar_v2.pdf

[858] P. Koppenburg and M. Pappagallo. A bestiary of exotic hadrons. CERN Courier Nov/Dec 2024, https://cerncourier.com/a/a-bestiary-of-exotic-hadrons/

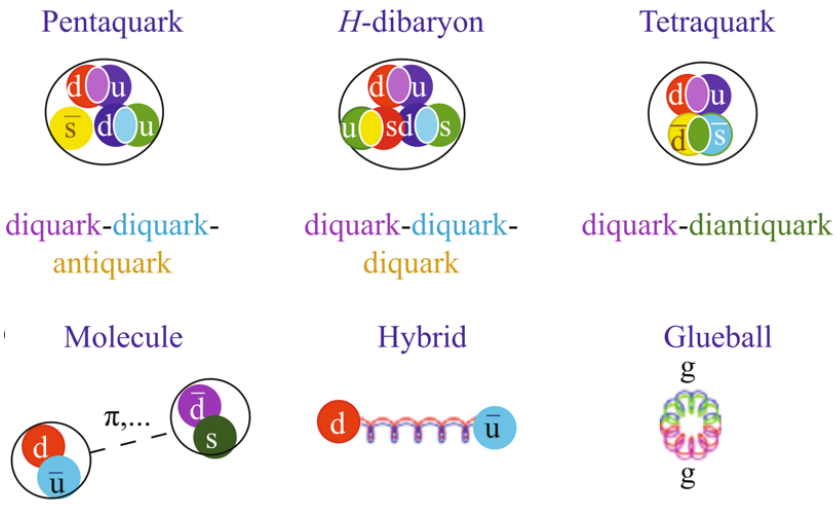


Fig. 28-5: The different levels of exoticism [859].

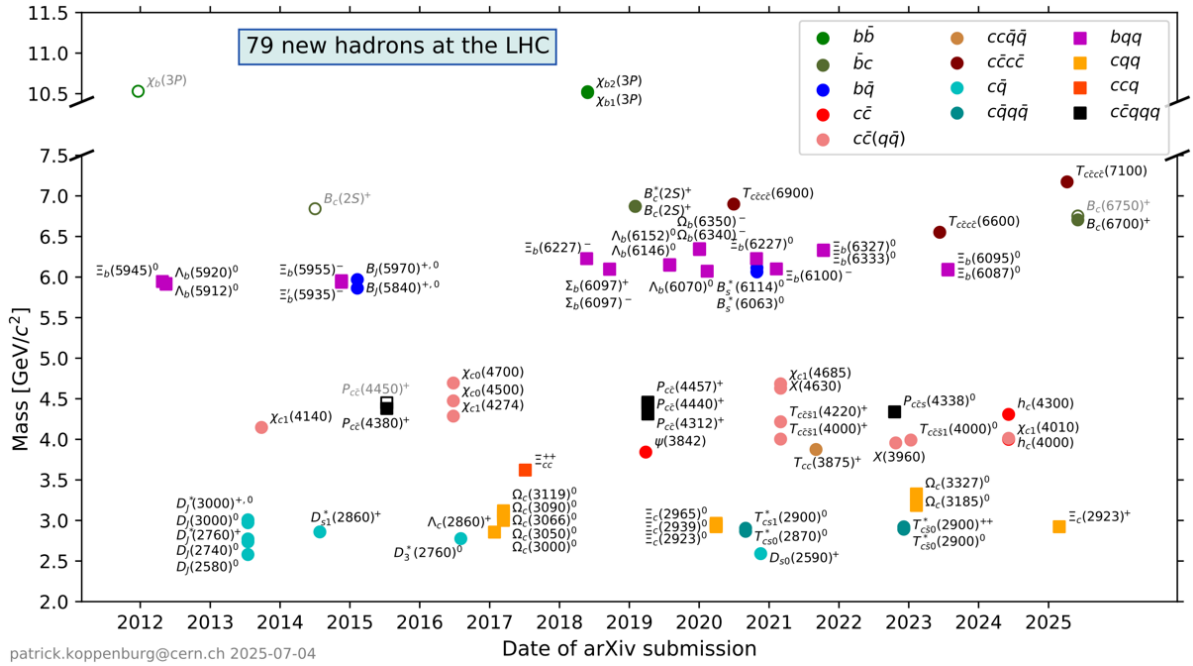


Fig. 28-6: The new hadrons at LHC**,** figure by P. Koppenburg [860].

[859] S. L. Olsen, A new hadron spectroscopy. *Front. Phys. 10, 121–154 (2015).* https://link.springer.com/article/10.1007/s11467-014-0449-6

[860] P. Koppenburg: https://www.koppenburg.ch/particles.html

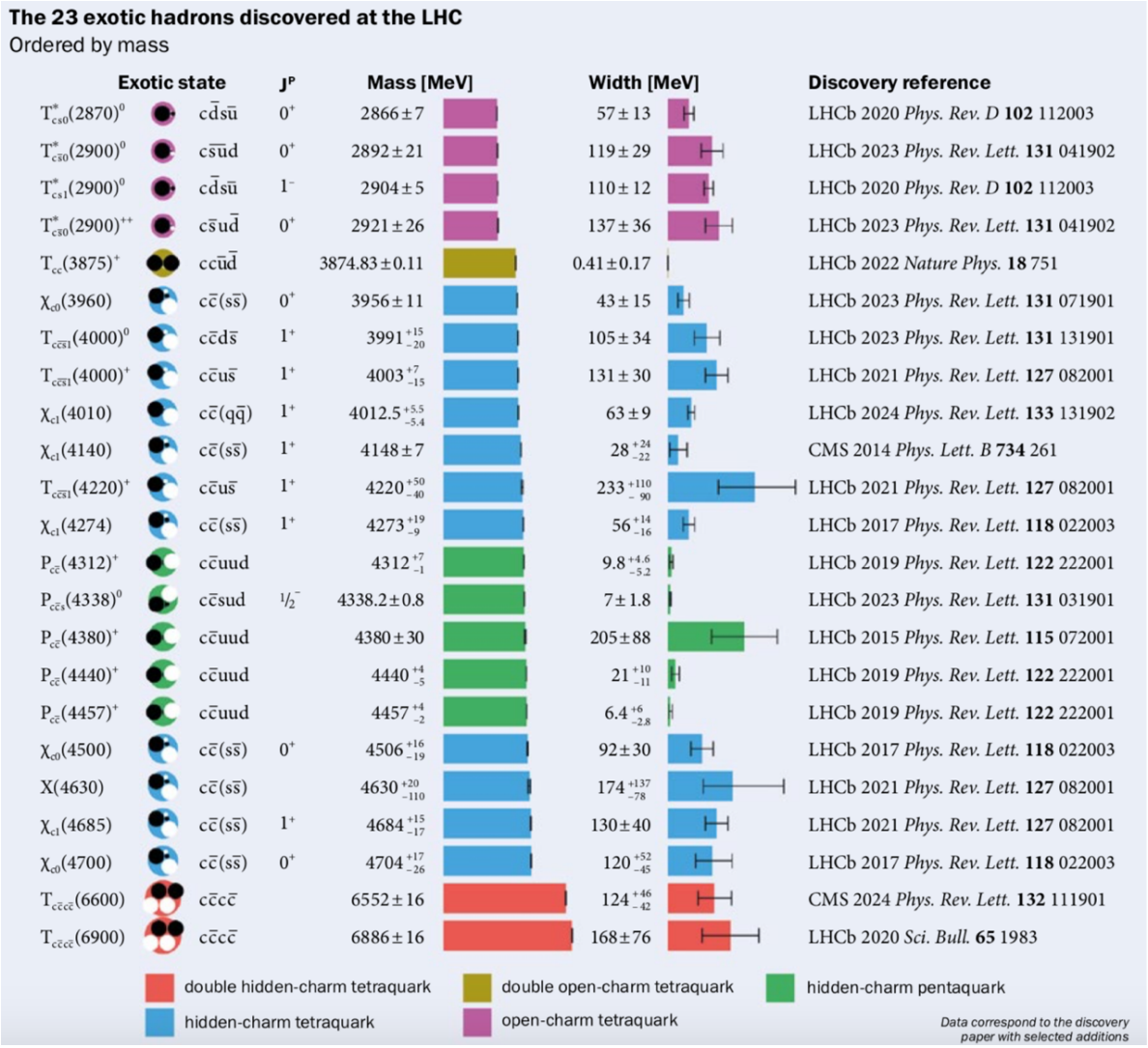


Fig. 28-7: Table and presumed nature of exotic hadrons found at LHC.

28.3 Diquark, all-charm tetraquarks, glueball?

Let us mention the role of an object which kept appearing in spectroscopy from early days to now: the **diquark.**

For instance, after their discovery in 1974, the new narrow resonances could be interpreted in the three-triplet model (see Chapter 5, Han–Nambu model) with integral baryon numbers as diquark colour excitations of the qq ± $\bar{q}\bar{q}$ type [861]. As we know, this interpretation was not maintained.

Presently, the possibility that some of the new resonances observed may involve **diquarks** is again considered. For instance, [862] the two nearby resonances, X(1840) and X(1880) into 3($\pi^+\pi^-$), observed

[861] Y. Nambu and M. Y. Han, Diquark Color Excitation and the Narrow Resonances.
https://lib-extopc.kek.jp/preprints/PDF/1976/7603/7603047.pdf
[862] M. Karliner and J. L. Rosner, Possible mixing of a diquark-antidiquark with a p$\bar{p}$ hadronic molecule.
https://arxiv.org/abs/2406.05920

by BESIII, partially below the $p\bar{p}$ threshold, might be due to mixing between two metastable states with the same $J^{PC} = 0^{-+}$ quantum numbers, but rather different internal structure. One is a $p\bar{p}$ hadronic molecule and the other a bound state of a light-quark diquark and an antidiquark, both with spin 1 and isospin 0, a composite color antitriplet and triplet, respectively.

One may quote the case of **all charm tetraquarks** discovered in several experiments and studied by CMS, 3 candidates in the 6 to 8 GeV range, $X \rightarrow J/\psi\, J/\psi \rightarrow 4\,\mu$ (Fig. 28-8) [863]. True tetraquark connecting two coloured objects (cc) and $(\overline{cc})$ through direct strong interaction or molecule, bound state of two mesons? An elaborate analysis, with J/ψ polarization, angular analysis, etc., performed all blinded, led to a consistent picture of 3 exotic tetraquarks with the same J^{PC}, very probably 2^{++}.

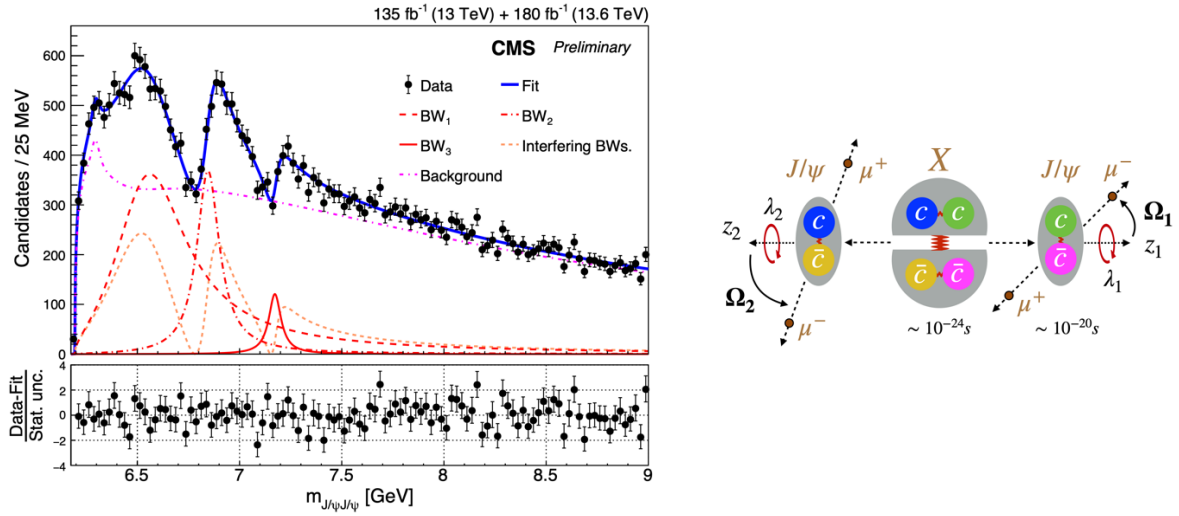


Fig. 28-8: All charm tetraquarks in the 6-8 GeV range, $X \rightarrow J/\psi\, J/\psi \rightarrow 4\,\mu$.

Let us conclude by a last piece of news about a long-sought-after particle [864] in radiative J/ψ decay (Fig. 5-24), the possible discovery of a Glueball-like particle X (2370) at BESIII in $K^0_S K^0_S \eta'$ (Fig. 28-9).

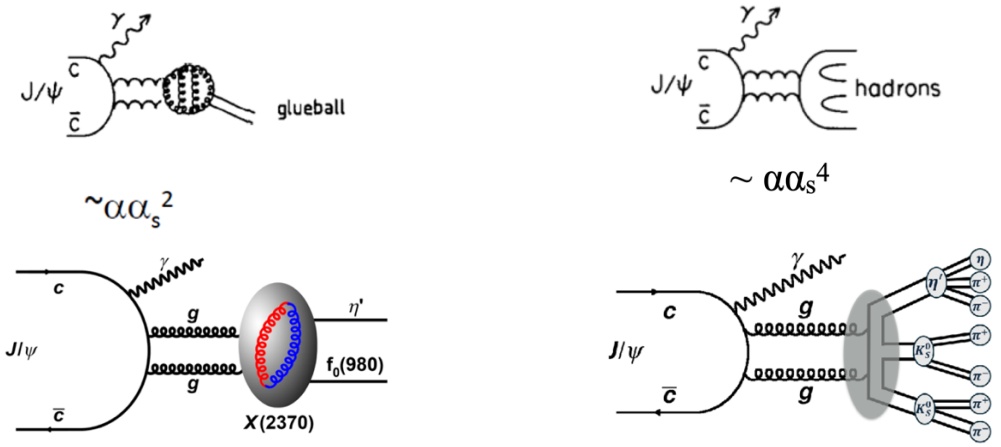


Fig. 28-9: The X(2370) candidate glueball.

[863] A. Gritsan, Spin and symmetry properties of all-charm tetraquarks with CMS. CERN LHC seminar, April 8 2025, https://indico.cern.ch/event/1533044/attachments/3046193/5385260/talk_CERN_seminar.pdf

[864] D. Vadacchino, A review on Glueball hunting. https://arxiv.org/abs/2305.04869

This particle has a mass of 2.395 GeV a spin of 0, a branching fraction of approximately 0.000013 and a statistical significance of 11.7 σ.

The J/ψ system can decay to a photon and two gluons, the two gluons can combine to create the X(2370) exotic particle.

Lattice computations predict the lightest glueball state should be a pseudoscalar with total spin 0, no electric charge, odd parity and a rest mass of between 2.3 and 2.6 GeV.

The nature of the X(2370) is still not fully certain, but its interpretation as a glueball is fairly compelling, and it could be the first glueball particle ever revealed by experiment.

29. Overview and timeline of discoveries

From the muon discovered [865] without being predicted to the Higgs Boson whose discovery came half a century after being invented (Fig. 19-1, from P. Rosnet), the contrast is striking…

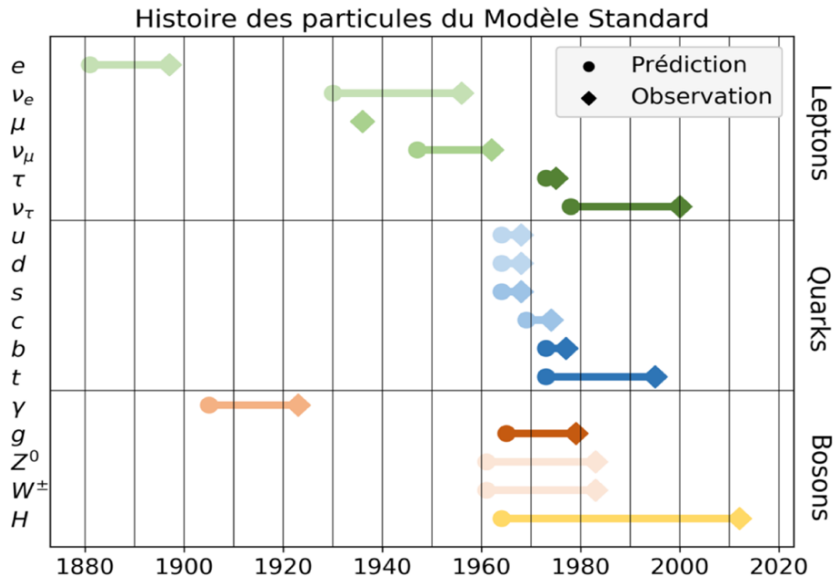


Fig. 29-1: History of prediction and observation of leptons, quarks and bosons of the SM.

In the following, some plots (Figs. 29-2 to 29-4), obtained from the INSPIRE data base, illustrate the time span between the appearance of basic ideas and their consideration by the scientific community.

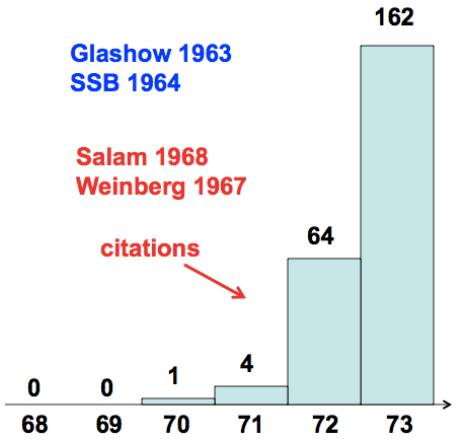


Fig. 29-2: Some delays in the minds (entries in the INSPIRE data base) concerning the SM.

Let us end with a beautiful timetable of our field, illustrated in Fig. 29-5.

[865] In 1936 Carl Anderson and Seth Neddermeyer at Caltech (US) discovered the muons in cosmic radiation.

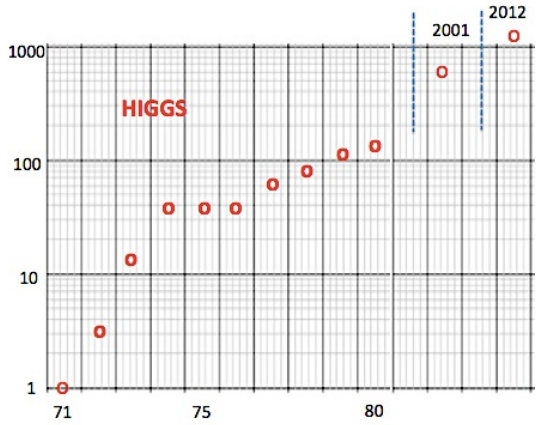


Fig. 29-3: Some delays in the minds (entries in the INSPIRE data base) concerning the Higgs boson, invented in 1964 and discovered in 2012 at CERN.

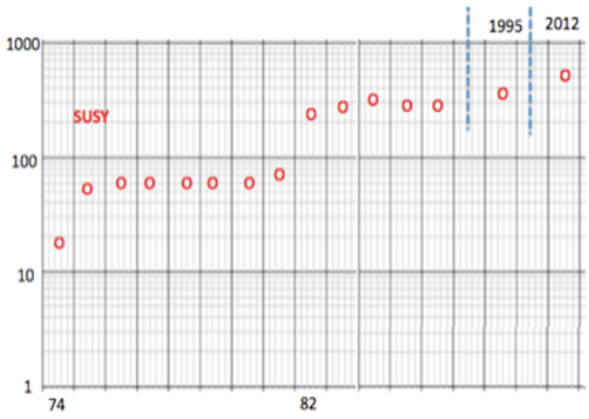


Fig. 29-4: Some delays in the minds (entries in the INSPIRE data base) concerning the idea of SUSY, idea born around 1974.

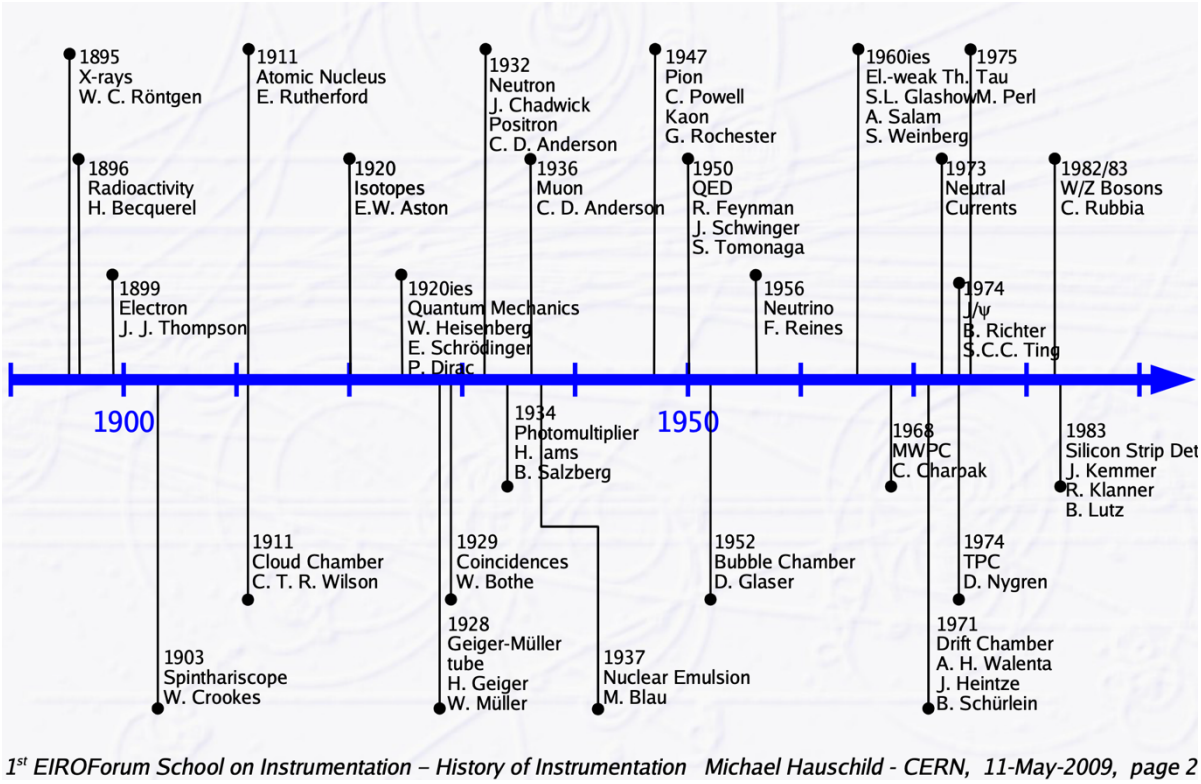


Fig. 29-5: Timeline of Particle Physics and Instrumentation [866].

[866] M. Hauschild, 1st EIROForum School on Instrumentation – History of Instrumentation. CERN, 11-May-2009, https://indico.cern.ch/event/43007/contributions/1065007/attachments/927852/1313685/DetectorHistory.pdf

30. Change of perspective: News from the sky

So far, the main focus was put on the high-energy frontier of PP. But other important subjects were and are treated at lower energy, exploiting either very luminous machines or **natural phenomena,** as radioactivity. And much information comes from the Cosmos.

Starting with a sketch of modern cosmology, let us first consider two "dark" topics that the SM of PP ignores, although, in our present view, they make 95% of the observed energy content of the Universe.

One can then try to link our PP SM with the cosmological model, now considered to be the **ΛCDM.** Λ refers to the so-called **dark energy (DE)**, source of the Universe acceleration. Figure 30-1 [867] gives its content, according to present understanding. Does DE correspond to a **Cosmological Constant (CC)?** This open question is discussed in Section 30.7. Ordinary matter, most of which is located outside galaxies, is only about 1/6 of all matter, hence the introduction of **dark matter (DM)** [868]. A fact: the observed Universe appears as **spatially-flat, i.e. Euclidean** [869].

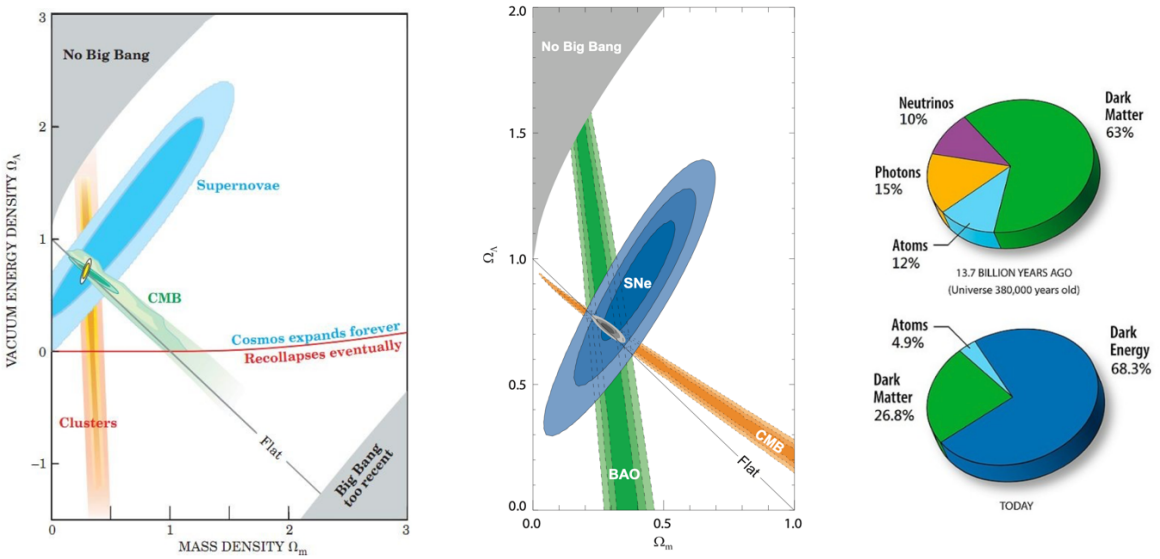


Fig. 30-1: The Universe location in the $\Omega_\Lambda - \Omega_m$ plot (dark energy versus matter) and its content (right plot) at two distant ages.

This presentation follows closely the prevailing vision of cosmology. However, it will also carefully account for its potential shortcomings, widening cracks appearing in the model, recent results suggesting a dark sector more complex than commonly assumed. For **problems and alternatives** see e.g. Ref. [870].

---

[867] C. Weniger, Dark matter – Evidence and Candidates. https://www.mpi-hd.mpg.de/lin/_isapp2019/talks/ISAPP2019-Weniger_1.pdf , M. Kowalski *et al.,* Improved cosmological constraints from new, old and combined supernova datasets, https://arxiv.org/abs/0804.4142

[868] A. M. Green, Dark Matter in Astrophysics/Cosmology. https://arxiv.org/abs/2109.05854

[869] G. Efstathiou and S. Gratton, The evidence for a spatially flat Universe. https://arxiv.org/abs/2002.06892
https://pdg.lbl.gov/2023/reviews/astro-cosmo.html
https://physicsworld.com/a/boomerang-backs-flat-universe/

[870] E. Abdalla *et al.,* Cosmology Intertwined: A Review of the Particle Physics, Astrophysics, and Cosmology Associated with the Cosmological Tensions and Anomalies https://arxiv.org/abs/2203.06142
A. Leauthaud and A. Riess, Looking beyond lambda. https://arxiv.org/abs/2509.00359
and more radically, J. Stenflo, Use of Redshifts as Evidence of Dark Energy, https://arxiv.org/abs/2506.12279

The SM and the **ΛCDM** can question each other: is dark matter (DM) made of particles, known or still unknown? This question is asked to particle physics (Chapter 31). Could cosmology and astrophysics hint at phenomena requiring the completion of the PP SM? In between them, a scientific domain called **astroparticle** is blooming (Chapter 35).

Let us first quote a famous problem. The **quantum vacuum energy** resulting from the zero-point fluctuations of the quantum fields, a consequence of the uncertainty principle, is a candidate for the CC. But the expectation is about 124 orders of magnitude larger than the critical density of the Universe [871]. Evidently, if quantum vacuum **energy** was gravitating, the Universe would not have survived. This is the **longstanding CC problem**. Assuming one can solve it, the discovery of the accelerating Universe brings a second one: after cancelling 124 orders of magnitude, how can one reintroduce a single one to make CC non-zero but tiny?

As an example, Ref. [872] proposes a solution to the problems by combining two existing ideas, first by invoking the **gauge theory of gravity as a substitute of GR** as the foundation of gravity theory and second by assuming **de Sitter symmetry** [873] as the underlying group property of the Universe. The huge radius of curvature of the de Sitter space and the CC smallness get linked. This faces challenges from quantum aspects, remedies are discussed.

Let us now summarize the main aspects of the **ΛCDM.**

30.1 The expanding Universe

The model of an **expanding Universe** [874] is now quasi unanimously recognized as the most credible one [875]. About this model, what one should keep in mind is the representation of an **expansion**, as the uniform expansion of the arms of Escher's lattice [876] would suggest (for references see Ref. [877]), rather than the confusing idea of an explosion (of what into what?). An inflating balloon can also be a useful image.

As key authors of the model, Einstein, with his **General Relativity (GR),** wrote the relevant equations. Alexander Friedmann got first the solution corresponding to an expanding Universe, an idea shared by Georges Lemaître, but which Albert Einstein first refused. Edwin Hubble brought the first experimental proof of the expansion (for an historical account see the very interesting Ref. [878]) by showing that galaxies recede from one another at a speed proportional to their distance, the **Hubble law** ($v = H_0 D$), first pillar of the model. Several other great names, Willem de Sitter, Hermann Weyl, Karl Schwarzschild, etc., played important roles in this construction. However, the precise value of the Hubble constant H is a long-lasting problem (see below).

---

[871] S. Weinberg, The cosmological constant problem. *Rev. Mod. Phys 61,1 (1989).*

[872] P. Chen, Gauge Theory of Gravity with de Sitter Symmetry as a Solution to the CC Problem and the Dark Energy Puzzle. https://arxiv.org/abs/1002.4275

[873] The notion that the physical laws are not invariant under the Poincare group but instead under the de Sitter group was first proposed by L. Fantappie in 1954 and reinvestigated in 1968 by H. Bacry and J-M. Levy-Leblond.
H. Bacry and J-M. Levy-Leblond, Possible Kinematics. *J. Math Phys. 9, 1605 (1968).*
See also https://en.wikipedia.org/wiki/De_Sitter_invariant_special_relativity

[874] V. A. Rubakov, Cosmology. https://arxiv.org/abs/1804.11230

[875] At the expense of major changes in basic laws one may conceive different cosmologies. For instance, C. Wetterich, A Universe without expansion. https://arxiv.org/abs/1303.6878 . He gets a **Universe without expansion** by assuming that Planck mass and the masses of particles change exponentially with time.

[876] https://www.wikiart.org/en/m-c-escher/cubic-space-division

[877] M. Pössel, The expanding Universe: an introduction. https://arxiv.org/abs/1712.10315

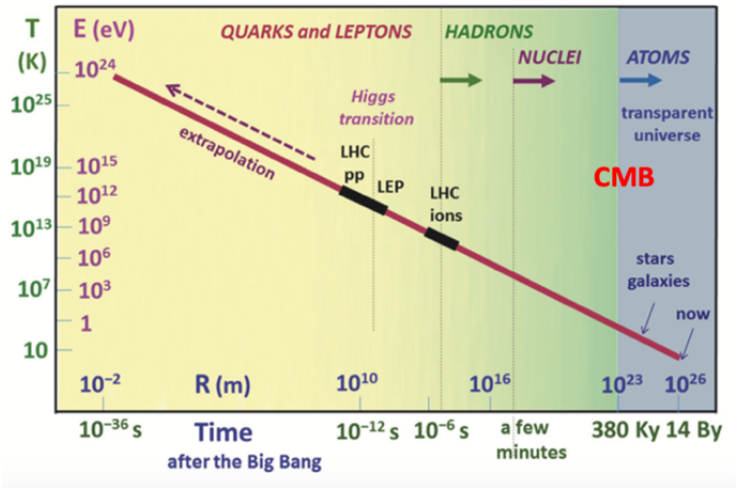
[878] E. Elizalde, Reasons in favor of a Hubble-Lemaître-Slipher's (HLS) law. https://arxiv.org/abs/1810.12416

Presently, the model is exploited in the simplifying frame of the **Cosmological Principle**, namely the assumption of a homogeneous and isotropic space. Expansion is encoded in the FLRW [879] space-time metric $ds^2 = dt^2 - a^2(t)\,dx^2$ where x is the comoving space coordinate and a(t) is the scale factor increasing in time. The basic equation governing the expansion rate of the Universe is the **Friedmann equation**, actually the (00)-component of the Einstein equations of GR, specified to the FLRW metric. In Fig. 30-2 $\dot{a}$ is derivative with respect to cosmic time, ρ is the total energy density in the Universe, Λ is the cosmological constant [880] and Euclidean 3-space is assumed.

While this view is probably valid at very large scales, the Universe is obviously not homogeneous at small and intermediate scales, since for instance voids of more than a billion light-years across are known [881]. It is always good therefore, before drawing conclusions, to **remember the simplification assumed** [882].

One learns about the Universe first by "looking" at it, as long as it is transparent to electromagnetic radiation, then, when it was opaque, by **"recreating" microscopic samples of its physics**, as PP does. But other messengers from the past, as **gravitational waves** (**GW**), which do not care about the transparency of the Universe, do and will bring further information (Chapter 34).

The expansion of the Universe expands the wavelength of radiation. The **z factor** or **red shift** measures this dilatation. For large values, z gives simply the ratio of the observed and emitted wavelengths. Visible light emitted at z = 1000 is thus detected at a millimetre wavelength. The relation between z and age is complex.



$$H^2 = \left(\frac{\dot{a}}{a}\right)^2 = \frac{8\pi}{3}G\rho + \frac{\Lambda}{3}$$

where $G = \frac{\hbar c}{M_{Pl}^2}$

Fig. 30-2: Left: the Universe timeline; right: the Friedmann equation with Euclidean 3-space.

Figure 30-2, same as Fig. 2-3, gives in logarithmic scales the timeline of the Universe in the expanding model. In abscissa is the age of the Universe. The log scale shrinks dramatically the domain of observation, although it covers nearly the full time-span, close to 14×10^9 years during which the force of gravity was at work, shaping the present universe. In ordinate is temperature, also in log scale. We indicate the typical energy of particles at a given time. With this choice of coordinates, the timeline is nearly exactly the straight line drawn, with an imperceptible (on the figure, not in numbers) change of

[879] https://en.wikipedia.org/wiki/Friedmann–Lemaître–Robertson–Walker_metric
[880] The value of Λ(PDG) is $1.088(30)\times10^{-56}\text{cm}^{-2}$
[881] https://en.wikipedia.org/wiki/Giant_Void
[882] About the effect of non-homogeneity: T. Buchert *et al.,* Is there proof that backreaction of inhomogeneities is irrelevant in cosmology? https://arxiv.org/abs/1505.07800

slope when the Universe changes from radiation to matter domination (z = 3500, t = 50 000 y), near the time of **recombination,** i.e. of **Cosmic Microwave Background (CMB**) and emergence of atoms, and the "recent" **acceleration** of the expansion. We give also an idea of what would have been, at the corresponding age, the radius R of the Universe observable now. These sizes illustrate the fact that, contrary to hasty statements, high energy PP is **not "re-doing the Big Bang".**

Before the recombination era, the important transitions are:

- the transition corresponding to **electroweak symmetry breaking,** at a picosecond or so. This is the time where elementary particles are supposed to have acquired their masses via the **Higgs mechanism** (Chapters 7 and 24). The exact nature of this **phase transition** is still under debate. An important question is to know whether an asymmetry between quarks and antiquarks, leading later to the **baryon number of the Universe,** could result from this time (Chapter 24);
- the **quark-hadron transition**, at 1–10 μs, when quarks, free until then, got trapped inside hadrons. This is the domain of hadronic physics, at a typical energy of a GeV (the mass of the nucleon) and, experimentally, of the heavy ion collisions performed at colliders, in particular at LHC (Chapter 20);
- the **nucleosynthesis** of light nuclei, in the first few minutes, when the Universe was acting as a thermonuclear reactor, and which is therefore the domain of nuclear physics.

30.2 The quark-hadron transition

Our first stop concerns the transition from quarks to hadrons [883], at 1–10 μs, where "quarks and gluons condense to form a gas of nucleons and light mesons, the latter decay subsequently".

Quarks and gluons will never be freed again. The question is whether one can, at least partly, observe the inverse process and get some evidence for a transient **quark–gluon plasma (QGP),** giving the proof of some deconfinement (see Chapter 20, which gives a positive answer). It is amusing that physics has now identified two **nearly perfect fluids**, one, the Bose–Einstein condensate of very cold atoms, close to the absolute zero at 10^{-7} K, and this one at 10^{12} K.

At a few μs of age the presently observable Universe had the size of the solar system, while the Hubble radius (i.e. ~ ct) was a few km. One does not know whether this transition created fluctuations of cosmic relevance, or wiped-out pre-existing ones. But the **emergence of the nucleon** was decisive!

One can ask whether the transition involved the full population of quarks and antiquarks, or only the left-over excess of quarks (by definition), one extra quark per about 10 billion quark–antiquark pairs, after massive annihilation. In other words,

i. did matter-antimatter annihilation occur between nucleons and antinucleons, or,
ii. did it occur previously, before the formation of nucleons, between quarks and antiquarks?

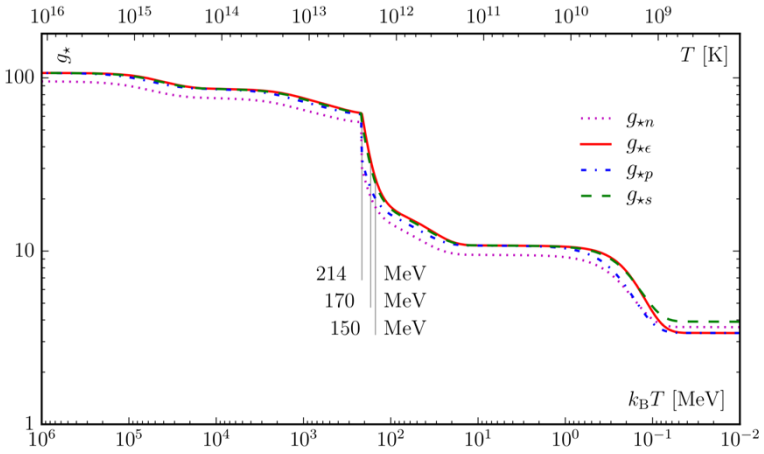
Was the Universe once briefly a ball of mesons? [884]

In the former case, naïvely speaking, the presently visible Universe must have been big enough to contain 10^{80} or so nucleons (i.e. R > few 10^{11} m). This seems compatible with what one can guess of the Universe at T = 214 MeV, with ~ 10^{89} γ and ν still dominating the energy content at that time [885].

Figure 30-3 [886] gives the **effective degrees of freedom, g*,** in the early Universe, from before the EW scale, a few femtoseconds after the BB, until the disappearance of last e^+ few minutes later. It shows

[883] D. Schwarz, The first second of the universe. https://arxiv.org/abs/astro-ph/0303574
[884] M. J. Fromerth and J. Rafelski, Hadronization of the Quark Universe. https://arxiv.org/abs/astro-ph/0211346
[885] These numbers are approximate and respect the baryon-to-photon ratio **$\eta = 6.12 \times 10^{-10}$**
[886] L. Husdal, On Effective Degrees of Freedom in the Early Universe. https://arxiv.org/abs/1609.04979.pdf

the fate of particle species, as their temperature cools down, from relativistic to non-relativistic, until they annihilate completely. One can express the Hubble parameter at radiation domination in terms of temperature through the Stefan–Boltzmann law $\rho_{rad} = \frac{\pi^2}{30} g_* T^4$.



Event	Temperature	$g_{\star n}$
		95.5
Annihilation of $t\bar{t}$ quarks	<173.3 GeV	
		86.5
Annihilation of Higgs boson	<125.6 GeV	
		85.5
Annihilation of Z^0 boson	<91.2 GeV	
		82.5
Annihilation of W^+W^- bosons	<80.4 GeV	
		76.5
Annihilation of $b\bar{b}$ quarks	<4190 MeV	
		67.5
Annihilation of $\tau^+\tau^-$ leptons	<1777 MeV	
		64.5
Annihilation of $c\bar{c}$ quarks	<1290 MeV	
		55.5
QCD transition †	150–214 MeV	
		15.5
Annihilation of $\pi^+\pi^-$ mesons	<139.6 MeV	
		13.5
Annihilation of π^0 mesons	<135.0 MeV	
		13.5
Annihilation of $\mu^+\mu^-$ leptons	<105.7 MeV	
		9.5
Neutrino decoupling	<800 keV	
		6.636
Annihilation of e^+e^- leptons	<511.0 keV	
		3.636

Fig. 30-3: Effective degrees of freedom in early Universe (left). The evolution of densities and pressure as functions of temperature. Fate of various particles (right). List of events which impact $g_{\star n}$.

30.3 Big Bang Nucleosynthesis

Our next stop will be at the first few minutes, when the Universe, a thermonuclear reactor as we said, was synthesizing light nuclei from protons and neutrons. This is a fairly well documented period [887].

To estimate the result of this transition, two "terrestrial" pieces of information are needed. Since the **neutron** is part of the game, an accurate knowledge of its **lifetime** is necessary (see Section 32.4.3). This accuracy is progressively improving, e.g. due to the availability of ultra-cold neutrons sources. One must also know **how many species of light active ν** participated at that time. LEP (Chapter 16) said three.

Then one can plot the expected rates of various light nuclei, starting with helium, as a function of the key parameter, the **density of ordinary matter relative to photons**, another most important result from the study of the CMB: a **baryon-photon ratio** of $6.12 \pm 0.04 \times 10^{-10}$. For this value obtained by WMAP, the expectation is 25% of ^{4}He (for mass abundance), which is exactly what astrophysicists measure.

Results on **Big Bang Nucleosynthesis** include the Planck likelihood distributions for the baryon density, progress in He abundance determinations and a recent cross section measurement for d(p,γ)^{3}He [888].

[887] D. Baumann, Cosmology. https://cmb.wintherscoming.no/pdfs/baumann.pdf , R. L. Workman *et al.,* Particle Data Group, https://pdg.lbl.gov/2023/reviews/astro-cosmo.html
T. Davis, and C. H. Lineweaver, Expanding confusion: common misconceptions of cosmological horizons and the superluminal expansion of the Universe. https://arxiv.org/abs/astro-ph/0310808
[888] K. A. Olive, Impact of Current Results on Nucleosynthesis. https://arxiv.org/abs/2105.04461

The success of primordial nucleosynthesis has been limited by the long-standing **Lithium problem**. Reference [889] concludes that the Lithium problem has most likely an astrophysical solution, while the Deuterium discrepancy provides a possible hint of new physics.

Let us recall that nuclei heavier than Be will be synthesized later in stars or created in cosmic collisions (e.g. mergers of neutron stars [890]), accrediting the fact that we are indeed "star dust". This primordial nucleosynthesis is the **3rd pillar of the expanding Universe model**. It even became a probe of physics/cosmology beyond the Standard Model: new hypothetical ingredients should not "spoil" its success.

30.4 The Cosmic Microwave Background

The first glimpse at the young Universe, at 379 000 years of age, when the atoms formed and after which photons could travel freely, is a pivotal information, because it is the oldest electromagnetic radiation in the Universe, dating to the epoch of recombination. We are indeed bombarded by microwaves coming from all directions of space, electromagnetic radiation which is a remnant from an early stage of the Universe, also known as "relic radiation". The **fossil Cosmic Microwave Background (CMB)** is faint cosmic background radiation filling all space. This is the **2nd pillar of our vision of the expanding Universe**. For a list of experiments studying the CMB see Ref. [891].

Corresponding to a perfect Planck spectrum of 2.725 K, it was emitted at 3 000 K at z = 1089, hence its present millimetre wavelength. It was predicted, approximately, in 1948 by Gamow and discovered in 1965 (Nobel Prize 1978). Its temperature is very homogeneous over the full sky and it took some time and effort to spot its **inhomogeneities** at the level of 10^{-5}, what the COBE satellite did first (Nobel Prize 2006), followed, with much better resolution, by WMAP and PLANCK.

Emitted at the time of recombination, the CMB shows temperature fluctuations, indicating density fluctuations, which are **the seeds of the large-scale structures** of the present Universe (Fig. 30-4 [892]).

It is also suspected that these fluctuations may themselves result from the **quantum fluctuations** of a field during a hypothetical very early phase of the Universe, called **inflation** [893]: a brief exponential growth of space, considered from a different angle in Chapter 24.

After the recombination time, one encounters the **Dark Ages of the Universe**, a time where the Universe was transparent but had no light emitted yet, since no source of light (galaxies, stars) already existed. The atomic hydrogen was then emitting its typical 21cm line, corresponding to an atomic transition between spin states. Emitted at a z of about 10, this radiation has now a 2m wavelength, in the domain of radio waves. When the first light sources occurred, they re-ionized progressively the hydrogen around them and stopped the emission. These important studies of the **re-ionization** period (Section 30.5) will be led in particular by the James Webb Space Telescope (JWST) [894] and giant radio telescopes like the distributed Square Kilometer Array (SKA) [895].

---

[889] M. Deal *et al.,* Primordial nucleosynthesis with varying fundamental constants - Solutions to the lithium problem and the deuterium discrepancy. https://arxiv.org/abs/2106.13989

[890] M.-H. Chen *et al.,* Neutron star mergers as the dominant contributor to the production of heavy r-process elements. https://arxiv.org/abs/2402.08214

[891] https://en.wikipedia.org/wiki/List_of_cosmic_microwave_background_experiments

[892] D. Baumann, Cosmology. https://cmb.wintherscoming.no/pdfs/baumann.pdf

[893] D. Baumann, TASI Lectures on Inflation. https://arxiv.org/abs/0907.5424
G. German *et al.,* Solution for cosmological observables in the Starobinsky model of inflation. https://arxiv.org/abs/2307.08257

[894] https://science.nasa.gov/mission/webb/

[895] https://en.wikipedia.org/wiki/Square_Kilometre_Array

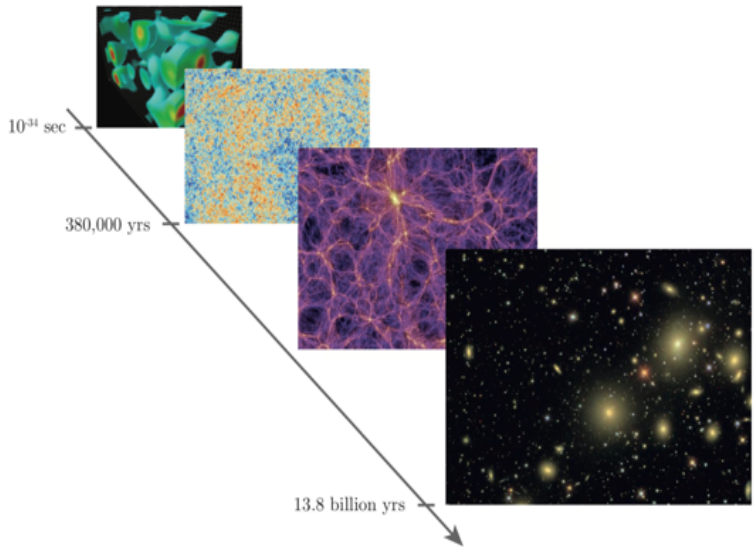


Fig. 30-4: From quantum fluctuations to large structures.

The CMB is also polarized and the study of its modes of **polarization** is the present focus of the observations, as well as its **"non-gaussian" behaviour**, not expected from the simplest versions of inflation, as encoded in 3-point correlations, instead of the 2-point ones studied so far.

The PLANCK satellite has accomplished its mission [896]. Figure 30-5 give the main results [897]. It allowed significant advances in many domains of astrophysics and cosmology. It revised the value of cosmological parameters, as composition and age of the Universe. It allowed to establish more firmly the **inflation paradigm**, to probe re-ionization and to check the validity of the **hierarchical scenario** of cosmic structures formation.

From the CMB, one learns first that the Universe is **spatially flat,** as already said, i.e. Euclidean. Indeed, the study of **acoustic peaks**, understood patterns of a known size at a known distance from the observer (Section 30.7), proves that the photons of the Last Scatter came to us along straight paths [898].

The need for DM, recognized since long, leads to the "cocktail" of the Universe content shown in Fig. 30-1, generally accepted and called the **Concordance Mode**l. Figure 30-1 tells where the information comes from.

Baryon acoustic oscillations (BAO) correspond to fluctuations in the density of visible baryonic matter caused by the **acoustic waves at the last scattering time** [899]. They provide another "standard ruler" (500 M light years in the present Universe) measured by looking at the large-scale structure of the Universe by astronomical surveys, as the spectrographic astronomical surveys of distant galaxies

[896] N. Aghanim *et al.,* Planck 2018 results. I. Overview and the cosmological legacy of Planck.
https://arxiv.org/abs/1807.06205v2.pdf
N. Aghanim and H. Dole, Les résultats cosmologiques de la mission Planck.
https://www.refletsdelaphysique.fr/articles/refdp/abs/2020/01/refdp202064p4/refdp202064p4.html?mb=0
However, see https://www.uniroma1.it/en/notizia/cosmological-revolution-universe-really-flat
[897] For a recap of acoustic peaks and polarization, see W. Hu, Ringing in the New Cosmology.
https://background.uchicago.edu/~whu/intermediate/intermediate.html
[898] Let us recall also the contribution of the Boomerang satellite, S. Masi *et al.,* The BOOMERanG experiment and the curvature of the Universe: https://arxiv.org/abs/astro-ph/0201137
[899] For a tutorial see: https://adh-sj.info/bao_cmb.php

conducted by the **Dark Energy Spectroscopic Instrument** (**DESI**) [900] (see Fig. 30-12). DESI results, shown later, bring new constraints on cosmological parameters, as a still controversial possible constraint on DE parametrization [901], which could deviate from a Cosmological Constant.

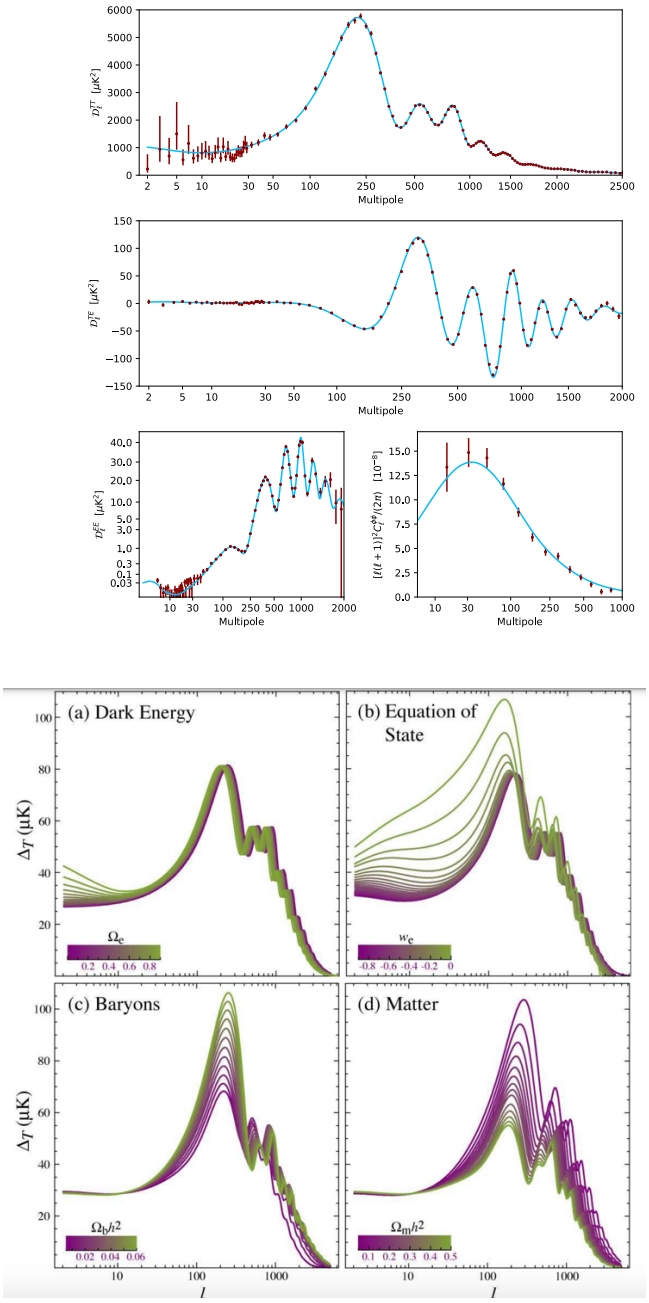


Fig. 30-5: Upper part: The Planck 2018 angular power spectra of the CMB (TT, TE, EE) and of the lensing potential (bottom right). The blue line is a best-fit model to temperature and polarization data. [July 2018] [902]. Lower part: Sensitivity of the temperature power spectrum to four fundamental cosmological parameters. All are varied around a fiducial flat model [903].

[900] https://en.wikipedia.org/wiki/Dark_Energy_Spectroscopic_Instrument
[901] M. Malekjani *et al.,* Cosmological constraints on dark energy parametrizations after DESI 2024: Persistent deviation from standard ΛCDM cosmology. https://arxiv.org/abs/2407.09767
[902] Planck Picture Gallery: https://www.cosmos.esa.int/web/planck/picture-gallery
[903] W. Hu, CMB Temperature and Polarization Anisotropy Fundamentals. https://arxiv.org/abs/astro-ph/0210696

Figure 30-6 [904] shows the combined results of Planck and the Atacama Cosmology Telescope (ACT) [905].

Measurements of the T and E-mode polarization angular power spectra of the CMB from observing 4% of the sky have been performed with SPT-3G, the camera on the South Pole Telescope (SPT) [906].

Combined **ground-based** (SPT+ACT) CMB data have reached Planck's constraining power on some parameters, a milestone for CMB cosmology. Combining these three CMB experiments yields the tightest CMB constraints to date [907]. CMB data alone show no evidence for physics beyond ΛCDM. We will see later how these compare to BAO results from DESI-DR2.

In the future ground-based data may be expected from China [908].

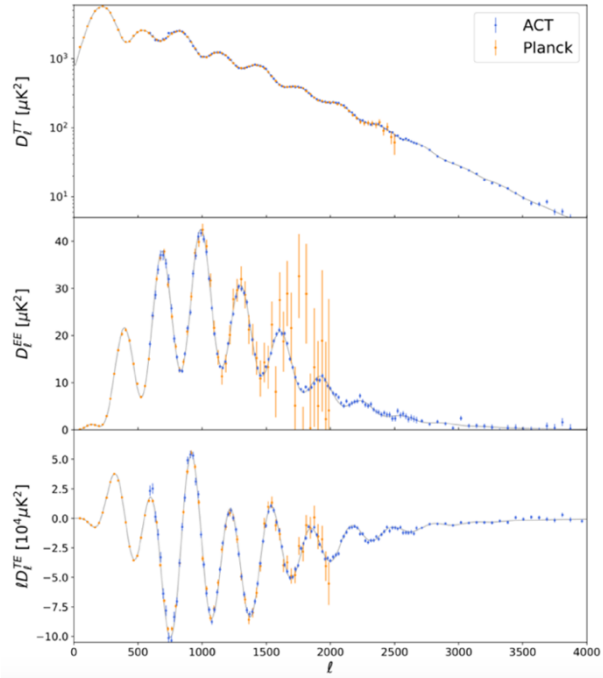


Fig. 30-6: ACT DR6 and Planck PR3 (Planck Collaboration 2020b) combined TT (top), EE (middle), and TE (bottom) power spectra. The full ACT multi-frequency spectra extend to ℓ = 8500. The grey lines show the joint ACT and Planck (P-ACT) ΛCDM best-fit power spectra. The ΛCDM model provides an excellent fit to both data sets.

The cocktail showed previously indicates that known forms of matter represent only a tiny part of it. One should however recall that "heretic" alternatives are still being considered, as a possible **modification of General Relativity** at very low acceleration (Section 31.1.2) or the effect of the non-homogeneity of the present Universe at intermediate scales already underlined.

For possible CMB anomalies see Ref. [909].

---

[904] The Atacama Cosmology Telescope: DR6 Power Spectra, Likelihoods and ΛCDM Parameters. https://arxiv.org/abs/2503.14452

[905] https://en.wikipedia.org/wiki/Atacama_Cosmology_Telescope

[906] E. Camphuis *et al.,* SPT-3G D1: CMB temperature and polarization power spectra and cosmology from 2019 and 2020 observations of the SPT-3G Main field. https://arxiv.org/abs/2506.20707

[907] ibid

[908] China-led consortium starts primordial gravitational wave detection experiment in Tibet. https://window-to-china.de/2025/08/06/china-led-consortium-starts-primordial-gravitational-wave-detection-experiment-in-tibet/

[909] D. J. Schwartz *et al.,* CMB anomalies after Planck. https://arxiv.org/abs/1510.07929
E. Gaztanaga, On the Interpretation of Cosmic Acceleration https://doi.org/10.3390/sym16091141

30.5 Re-ionization

The first phase change of hydrogen in the Universe was recombination, occurring at z = 1 089 (379 000 years after the BB), due to the cooling of the Universe to the point where the rate of recombination of e and p to form neutral hydrogen was higher than the re-ionization rate.

The second phase change occurred when objects started to condense in the early Universe and were energetic enough to **re-ionize neutral hydrogen**. As they formed and radiated energy, the Universe composed of neutral atoms started to contain again an ionized plasma. This occurred between 150 million and one billion years after the Big Bang (at a redshift $6 < z < 20$).

Re-ionization marks the end of the dark ages, with the first sources of ionizing photons lighting up. The CMB anisotropy pattern is a main source of information on the re-ionization process.

The Planck mission [910] could measure the opacity [911] of the Universe due to re-ionization. Its value (0.055 ± 0.009) indicates that re-ionization occurred at a red shift between 8 and 9. Planck data show that the re-ionization process was not very efficient before a shift of 15. There is an excellent agreement between Planck polarization indications and astrophysical data in determining the integrated optical depth. Figure 30-7 [912], giving the evolution with red-shift of ionized interstellar atomic hydrogen, show no evidence beyond **monotonic re-ionization histories.**

But, considering the subsequent rate of accretion of matter to form the earliest cosmic structures, recent data point at a possible problem. Observations by the JWST of objects present **much earlier as expected** after decoupling raised questions about the ΛCDM. It is wise to wait for more data [913] but one may also consider scenarios [914] allowing such features. Concerning re-ionization see also Ref. [915].

30.6 Supernovae and the acceleration

From the study, as a function of z, of the brightness of Supernovae (exploding stars) used as standard candles, the conclusion was that our Universe is not only expanding, but also in a phase of **accelerated expansion** [916] (Nobel Prize 2011 to Saul Perlmutter, Adam Riess and Brian Schmidt) (Figs. 30-8 to 30-10). The basic formulae of cosmology tell then that some kind of repulsive gravity, with **negative pressure**, is required. Lacking a better name, it was called **dark energy (DE)**.

---

[910] Planck Collaboration, Planck 2018 results. I. Overview and the cosmological legacy of Planck. https://arxiv.org/abs/1807.06205v2

[911] The opacity τ is a unitless quantity which provides a measure of the line-of-sight free-electron opacity to CMB radiation. https://lambda.gsfc.nasa.gov/education/graphic_history/taureionzation.cfm

[912] D. Paoletti *et al.,* Extended reionization in models beyond ΛCDM with Planck 2018 data. https://arxiv.org/abs/2005.12222

D. K. Hazra *et al.,* Joining Bits and Pieces of Reionization History. https://arxiv.org/abs/1904.01547

[913] A. D. Dolgov, James Webb Space Telescope: data, problems, and resolution. https://agenda.infn.it/event/33694/contributions/190205/attachments/102590/143361/05_Dolgov_JWST-data-solution.pdf

[914] E. Di Valentino *et al.,* In the Realm of the Hubble tension − a Review of Solutions. https://arxiv.org/abs/2103.01183

A. D. Dolgov, Tension between HST/JWST and ΛCDM Cosmology, PBH, and Antimatter in the Galaxy. https://arxiv.org/abs/2310.00671

[915] C. Cain *et al.,* Chasing the beginning of reionization in the JWST era. https://arxiv.org/abs/2409.02989

[916] A. G. Riess, The Case for an Accelerating Universe from Supernovae. https://iopscience.iop.org/article/10.1086/316624/pdf

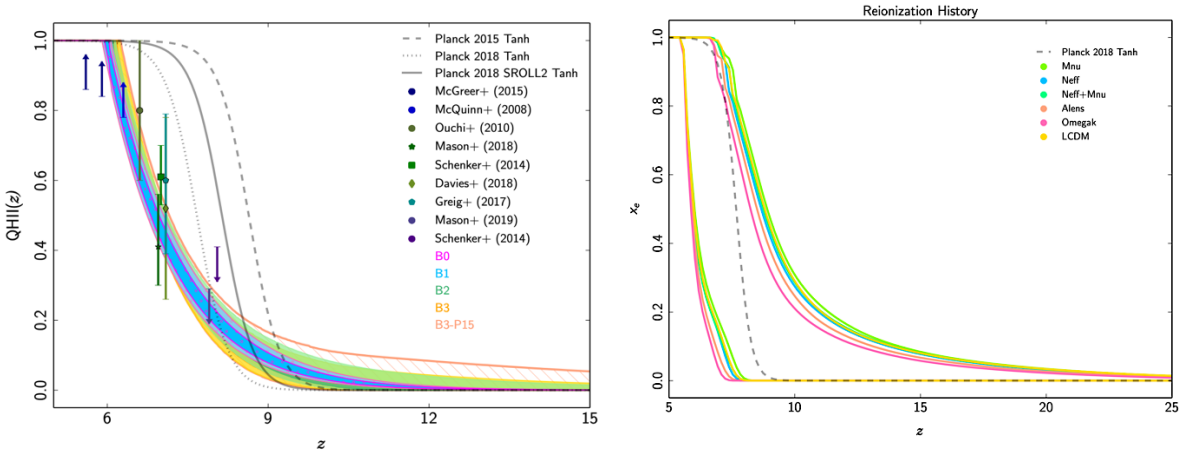


Fig. 30-7: The re-ionization history: left: 68.3% and 95% CL on QHII (fraction of ionized hydrogen) as a function of redshift in four different cases considered. Right: 95% CL bands for the ionization fraction as a function of redshift as reconstructed for a subset of the extensions to the ΛCDM.

Next come some curves showing the distances of supernovae versus red shift obtained in various surveys. To get an idea of the methods and care taken in the determination of this distance see for instance [917]. The curves show clearly the preference for a large value of Ω_Λ , the energy fraction of dark energy in Universe.

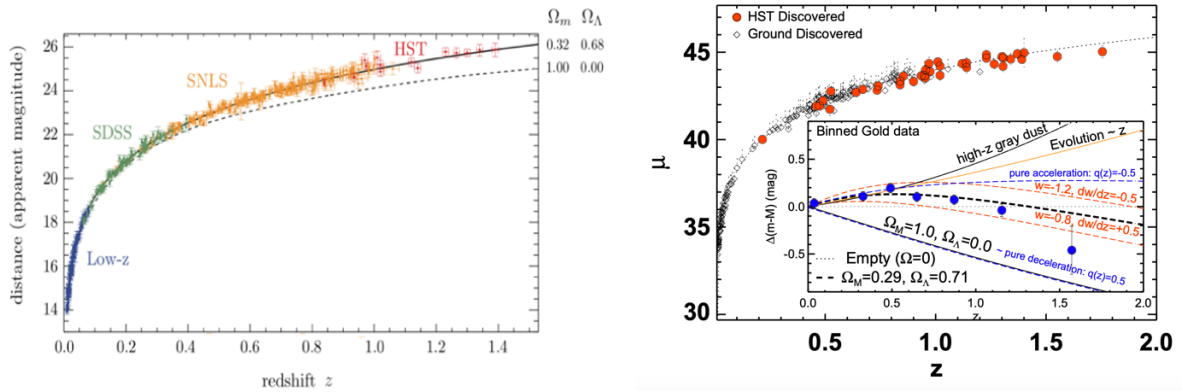


Fig. 30-8: Left: distance of supernovae versus z from various surveys [918]. Right: same, μ is related to the luminosity distance [919].

[917] SNLS SuperNova Legacy Survey. https://irfu.cea.fr/dphn/en/Phocea/Vie_des_labos/Ast/ast_technique.php?id_ast=2289 H. K. Fakhouri *et al.,* Nearby Supernova Factory Collaboration, Improving Cosmological Distance Measurements Using Twin Type Ia Supernovae. https://arxiv.org/abs/1511.01102

[918] D. Baumann, Cosmology. https://cmb.wintherscoming.no/pdfs/baumann.pdf

[919] A. G. Riess *et al.,* New Hubble Space Telescope Discoveries of Type Ia Supernovae at z ≥ 1: Narrowing Constraints on the Early Behavior of Dark Energy. https://arxiv.org/abs/astro-ph/0611572

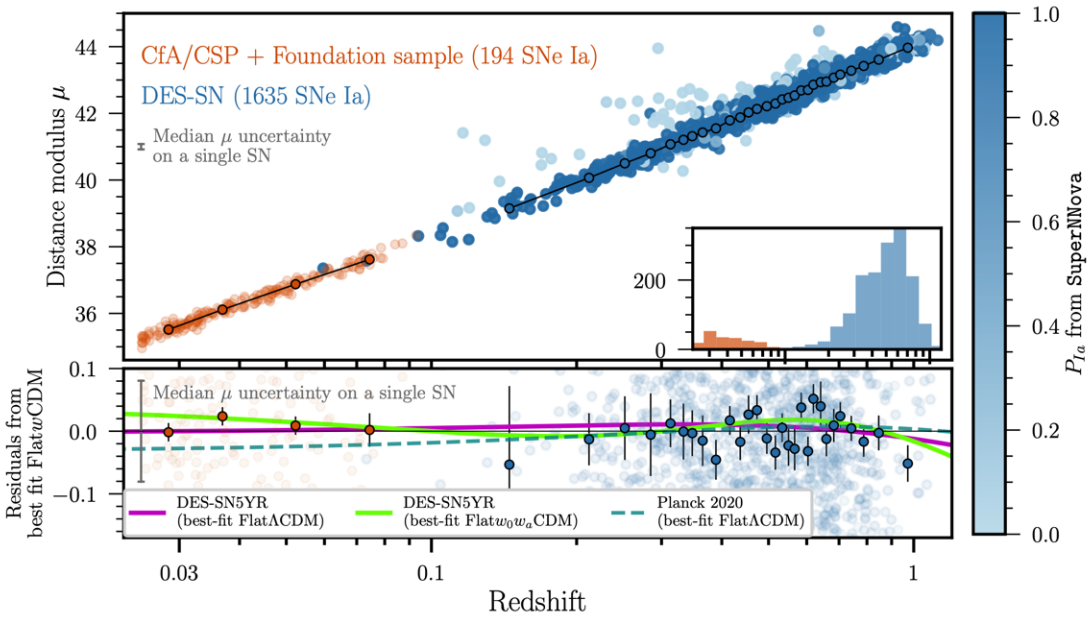


Fig. 30-9: Hubble diagram of DES-SN5YR [920].

Figure 30-10 shows the results of supernovae from JWST. For the moment the ΛCDM seems in good shape.

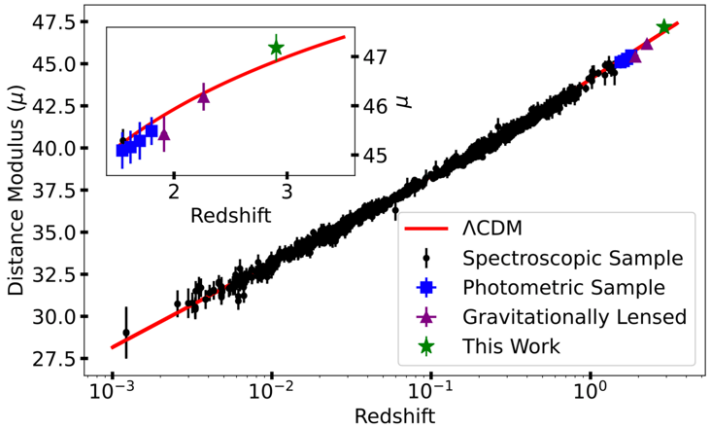


Fig. 30-10: Distance versus redshift from JWST [921].

Another long-lasting problem is the discrepancy of the **Hubble parameter** [922] (rate of expansion of the Universe) from the CMB (its first "photo" at z = 1 089) to exploration of galaxies at smaller z.

The Hubble constant discrepancy is illustrated in Fig. 30-11 [923].

---

[920] DES Collaboration, The Dark Energy Survey: Cosmology Results With ~1500 New High-redshift Type Ia Supernovae Using The Full 5-year Dataset. https://arxiv.org/abs/2401.02929

[921] J. D. R. Pierel *et al.,* Discovery of An Apparent Red, High-Velocity Type Ia Supernova at z = 2.9 with JWST. https://arxiv.org/abs/2406.05089

[922] D. Brout, The Hubble Constant Tension Problem: An Overview. https://inspirehep.net/files/cea50cdb8e317db58b4ce959d926fcd0

[923] L. Galbany *et al.,* An updated measurement of the Hubble constant from near-infrared observations of Type Ia supernovae. https://arxiv.org/abs/2209.02546

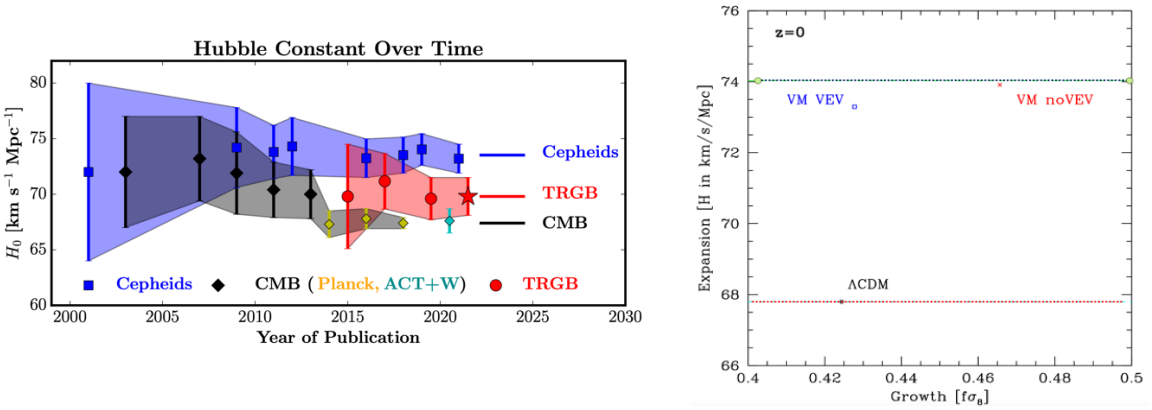


Fig. 30-11: Left: Hubble parameter problem [924]. Right, the data [925]: expansion and growth histories plotted simultaneously at z = 0. VM means vacuum "metamorphosis", a quantum gravity effect [926]. Growth characterizes how strongly clustered is all the matter in Universe. Green line: Cepheid value of H_0. Red: ΛCDM H_0.

30.7 Baryon Acoustic Oscillation

Figure 30-12 shows the BAO signal of DESI [927], caused, as said before, by the **acoustic waves at the last scattering time,** and another precious "standard ruler". Several following figures will describe the challenging DESI results in detail.

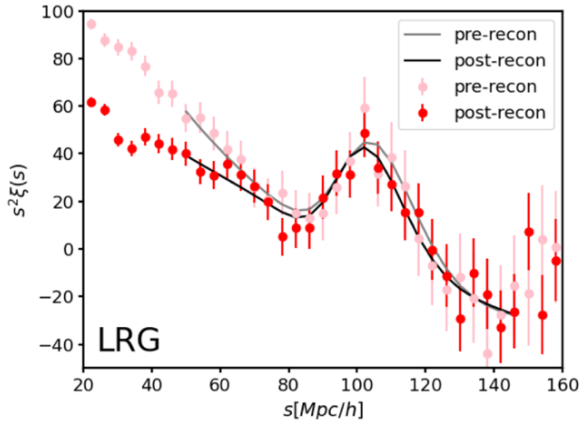


Fig. 30-12: BAO from DESI Luminous Red Galaxies sample. Two-point correlation function measurements versus separation *s* between two galaxies.

Figure 30-13 illustrates the results of DESI in terms of the evolution of BAO as a function of z.

[924] W. L. Freedman, Measurements of the Hubble Constant: Tensions in Perspective. https://arxiv.org/abs/2106.15656
M. S. Turner, The Road to Precision Cosmology. https://arxiv.org/abs/2201.04741 , W. L. Freedman and B. F. Madore, Progress in Direct Measurements of the Hubble Constant. https://arxiv.org/abs/2309.05618
A. R. Khalife *et al.,* Updated Constraints on Hubble Tension solutions. la Thuile 2024, https://agenda.infn.it/event/38205/contributions/219667/attachments/117048/168945/Khalifes-Updated_Constraints_H0_Tension.pdf and A. R. Khalife, Review of Hubble tension solutions with new SH0ES and SPT-3G data. https://arxiv.org/abs/2312.09814
[925] E. Linder, What is the Standard Cosmological Model? https://arxiv.org/abs/2105.02903
[926] L. Parker and A. Raval, Vacuum-driven Metamorphosis. https://arxiv.org/abs/gr-qc/9908069
[927] J. Moon *et al.,* First Detection of the BAO Signal from Early DESI Data. https://arxiv.org/abs/2304.08427

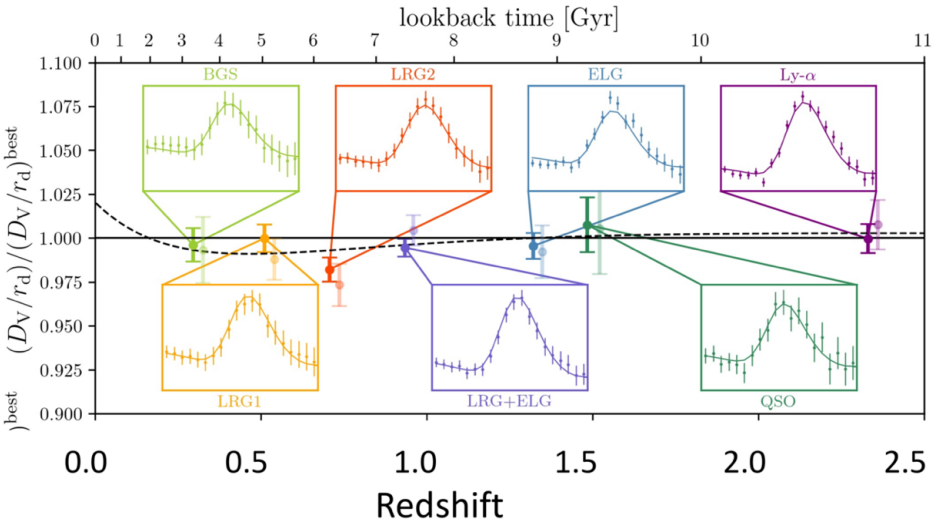


Fig. 30-13: The DESI BAO signal from various methods and different redshift. **ΛCDM** would be the horizontal black line. The LRG2 set (luminous red galaxies) is the main source of an eventual deviation [928].

Figure 30-14 offers another view of DESI results.

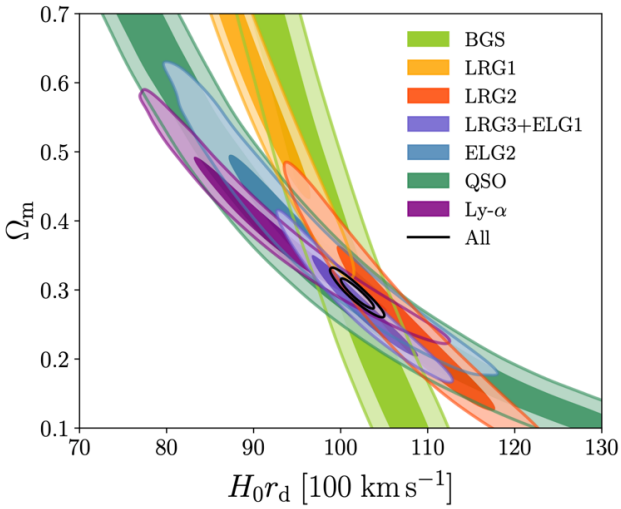


Fig. 30-14: 68% and 95% credible-interval contours for parameters Ω_m and $H_0 r_d$ obtained for a flat ΛCDM model from fits to BAO measurements from each DESI tracer type. r_d is the sound horizon [929].

We now summarize in Figs. 30-15 to 30-17 some of the potential **anomalies, now present in cosmological data.**

Figure 30-15 gives DESI BAO + CMB result in the w_0 - w_a plot where the DE parameterisation is:

$$\frac{P_{DE}}{\rho_{DE}} = w_0 + w_a \frac{z}{1+z}$$

[928] C. Yèche, DESI Year-1 Results.
https://indico.cern.ch/event/1335188/contributions/6137465/attachments/2954594/5194779/03_yeche.pdf
C. Yèche, DESI DR2 Results.
https://indico.in2p3.fr/event/35965/contributions/152493/attachments/91640/139672/6_CYeche-v1.pdf-short.pdf
[929] DESI collaboration, DESI 2024 VI: Cosmological Constraints from the Measurements of Baryon Acoustic Oscillations.
https://arxiv.org/abs/2404.03002

Figure 30-16 is still another view of the results and Fig. 30-17 gives the evolution of the deceleration parameter, q(z), as a function of redshift in the w_0w_aCDM model, showing a quite different behaviour than the ΛCDM model.

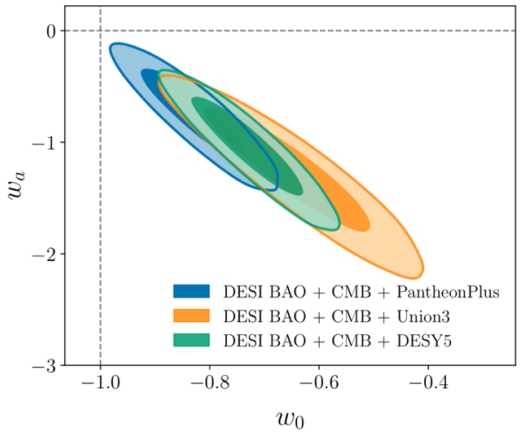


Fig. 30-15: Constraints from DESI BAO combined with CMB and other datasets. The significance of the tension with ΛCDM ($w_0 = -1$, $w_a = 0$) is 2.5 σ, 3.5 σ and 3.9 σ for the three different cases respectively [930].

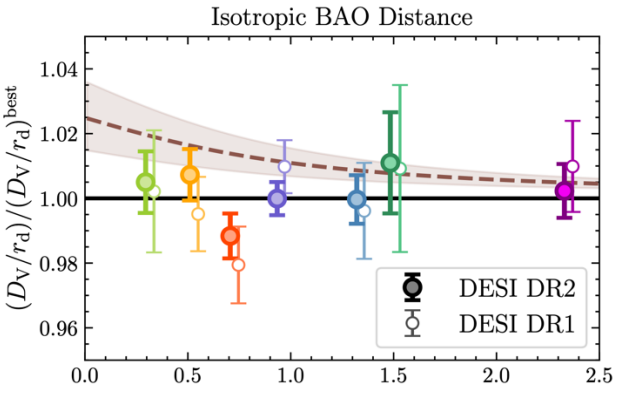


Fig. 30-16: DESI results: abscissa is the redshift; r_d is the scale of the pre-recombination sound horizon; D_V is the isotropic BAO distance [931].

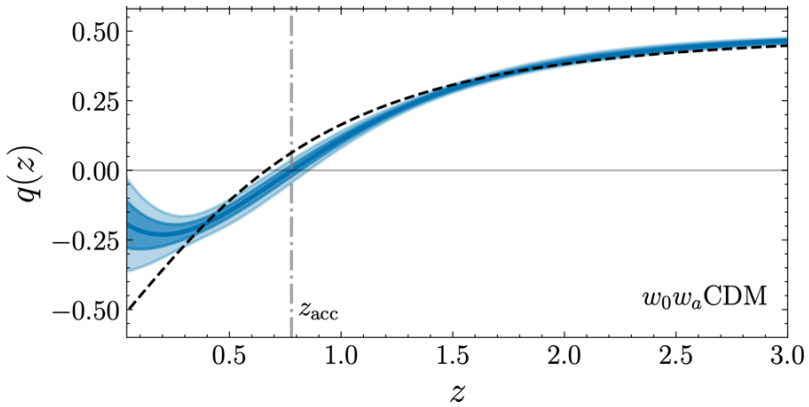


Fig. 30-17: Evolution of the deceleration parameter, q(z), as a function of redshift in the w_0w_aCDM model. The black dashed line depicts the best-fit ΛCDM for the same data combination. The grey vertical line shows the redshift (z_{acc}) corresponding to the onset of cosmic acceleration [932].

These results are quite striking. No surprise that argumented doubts and support are expressed. Examples are given in Ref. [933].

---

[930] ibid

[931] DESI collaboration, DESI DR2 Results II: Measurements of Baryon Acoustic Oscillations and Cosmological Constraints. https://arxiv.org/abs/2503.14738
https://indico.in2p3.fr/event/35965/contributions/152493/attachments/91640/139672/6_CYeche-v1.pdf-short.pdf

[932] DESI Collaboration, Extended Dark Energy analysis using DESI DR2 BAO measurements. https://arxiv.org/abs/2503.14743 See also CERN Courier May-June 2025 p. 11, https://cerncourier.com/wp-content/uploads/2025/05/CERNCourier2025MayJun-digitaledition.pdf

[933] S. Afroz and S. Mukherjee, Hint towards inconsistency between BAO and Supernovae Dataset: The Evidence of Redshift Evolving Dark Energy from DESI DR2 is Absent. https://arxiv.org/abs/2504.16868

The following figures give still more information on DESI results. Figure 30-18 [934] shows that DES-SNSYR, the Dark Energy Survey (DES) Supernova Program (see also Fig. 30-9) alone is not very informative on the DE question.

Figure 30-19 [935] gives the present information on the plot of the **sum of neutrino masses** information from cosmology **versus the Hubble constant.** The improvement over CMB is driven by the tighter constraint on H_0 from BAO.

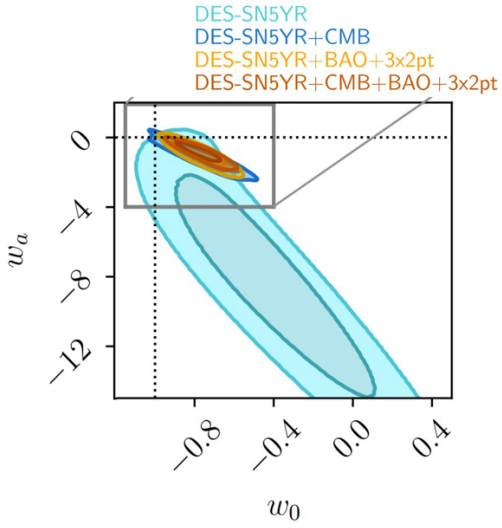


Fig. 30-18: Constraints for Flat-w_0w_a CDM model from the DES-SN5YR dataset only (cyan), combined with BAO (orange), SN5YR combined with CMB measurements (blue), and from all these combined (red). The dotted cross indicates the CC scenario.

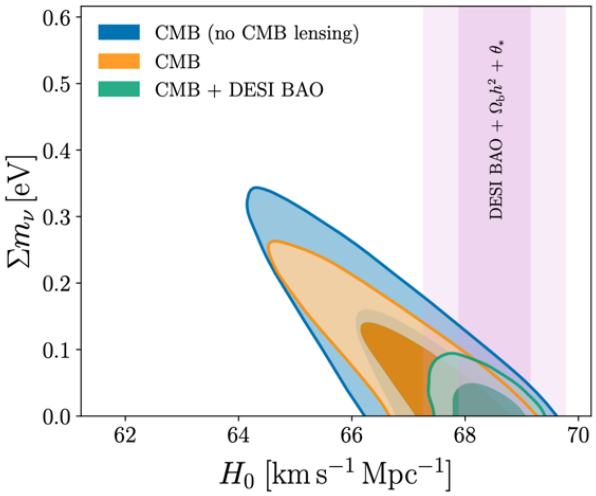


Fig. 30-19: 68% and 95% credible intervals on $\sum m_\nu$ and H_0 from Planck, CMB and DESI+CMB data, illustrating the degeneracy between these parameters from the CMB, and how DESI BAO data contribute to breaking it.

Figure 30-20 gives the same neutrino mass information plotted against the **lightest neutrino mass** with Planck and DESI BAO limits (red colour). Data prefer a sum of masses as small as possible, even negative.

Figure 30-21 [936] shows again the tension between late and early measurements of the Hubble constant.

D. Wang and D. Mota, Did DESI DR2 truly reveal dynamical dark energy? https://arxiv.org/abs/2504.15222
L. Huang *et al.,* The DESI DR1/DR2 evidence for dynamical dark energy is biased by low-redshift supernovae. https://arxiv.org/abs/2502.04212
G. Efstathiou, Evolving Dark Energy or Supernovae Systematics? https://arxiv.org/abs/2408.07175
A. Notari *et al.*, BAO vs. SN evidence for evolving dark energy. https://arxiv.org/abs/2411.11685
R. Brandenberger, Why the DESI results should not be a surprise. https://arxiv.org/abs/2503.17659

[934] In F. Andrade Oliveira, Observational Cosmology: Measuring the late Universe. ICHEP 2024. https://indico.cern.ch/event/1291157/contributions/5958352/attachments/2902275/5090759/2024_FA-O_ichep_v1p1.pdf
See also DES Collaboration, The Dark Energy Survey: Cosmology Results With~1500 New High-redshift Type Ia Supernovae Using The Full 5-year Dataset. https://arxiv.org/abs/2401.02929
R. Camilleri *et al.,* The Dark Energy Survey Supernova Program: Investigating Beyond-ΛCDM. https://arxiv.org/abs/2406.05048

[935] DESI collaboration, Cosmological Constraints from the Measurements of Baryon Acoustic Oscillations. https://arxiv.org/abs/2404.03002

[936] ibid

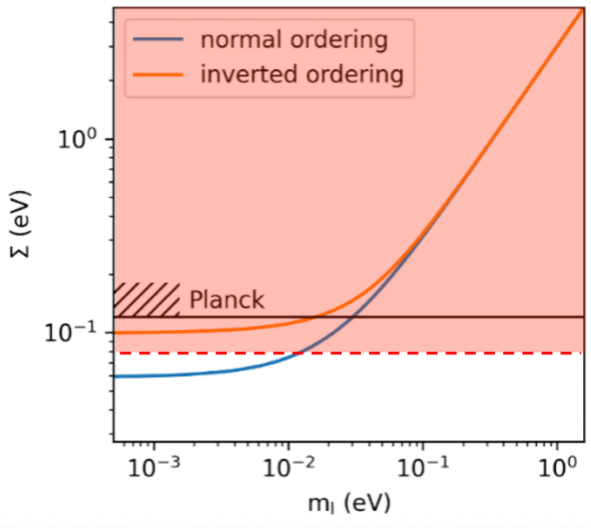


Fig. 30-20: Neutrino mass information plotted against the lightest neutrino mass [937].

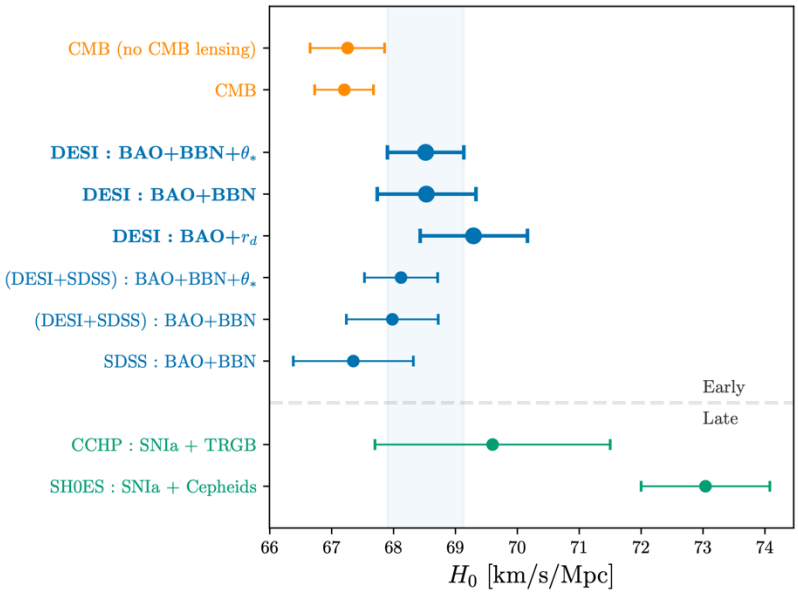


Fig. 30-21: 68% credible-interval constraints on the Hubble constant, assuming the flat ΛCDM model.

In summary, **DESI results and the Hubble problem** are presently the two main points where the otherwise very successful **ΛCDM may be in trouble**.

For curiosity, Ref. [938] shows a spectacular individual case of baryon acoustic oscillation.

[937] M. Kado, Conference Summary and Highlights. ICHEP 2024
https://indico.cern.ch/event/1291157/contributions/5958406/attachments/2903497/5123335/ICHEP-Summary.pdf
[938] R. B. Tully *et al.,* Ho'oleilana: An Individual Baryon Acoustic Oscillation? https://arxiv.org/abs/2309.00677

30.8 One more big problem?

A very recent publication forces us to come back to the world of Supernovae.

In Ref. [939] a significant bias in the way astronomers measure cosmic expansion using type Ia supernovae has been recently identified, suggesting that these supernovae are not as uniform as previously assumed: their brightness varies depending on the **age of their host galaxies**. The analyse of over 300 supernova-hosting galaxies showed a clear correlation of up to 5.5 σ between host age and Hubble residual (HR): *the younger the galaxy, the dimmer its supernovae*. *Distant galaxies, which are typically younger, therefore produce explosions that appear fainter—not necessarily because they are farther away, but because of this age effect.* See Fig. 30-22.

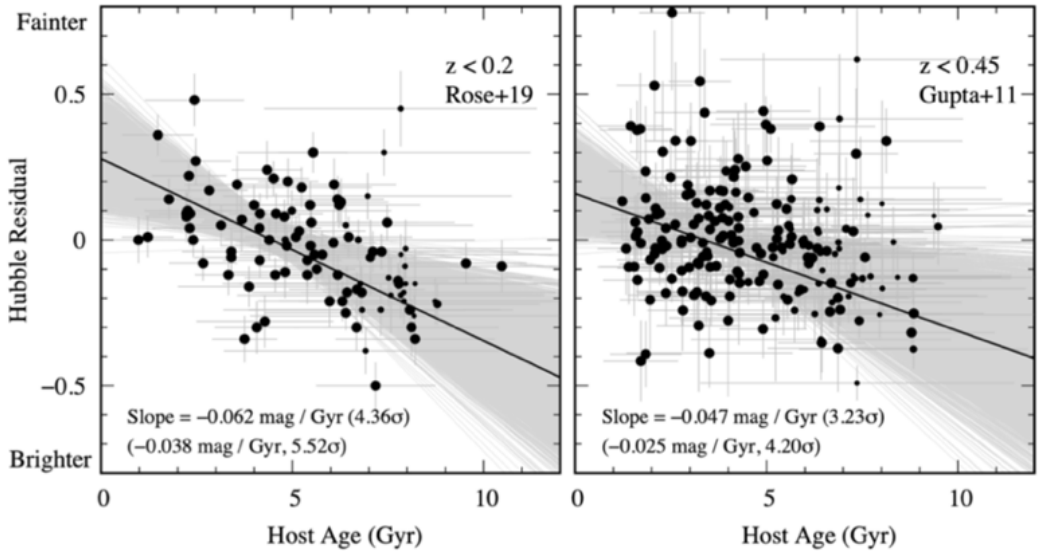


Fig. 30-22: Correlation between population age and HR for SN host galaxies. The Hubble Residual is a measure of relative luminosity when the SN sample is confined to a narrow redshift range. From Ref. [940].

Before the age-bias correction, the SN data are broadly consistent with the ΛCDM model, as shown by Fig. 30-23 top. After correcting for the age-bias, however, the SN dataset no longer supports the ΛCDM model, but aligns more closely with a time-varying dark energy equation-of-state model (flat-w_0w_aCDM), as recently suggested by the DESI BAO (DR2) project in a combined analysis of BAO and CMB and that we met in Section 30.7. See also Fig. 30-24, complementing Fig. 30-15.

The addition of SN data, after applying the age-bias correction, support the deviation from the ΛCDM model indicated by BAO-only measurements. Therefore, the revised standard candle (SNeIa) seems to be in agreement with the standard ruler (BAO). This, in turn, could substantially alleviate the Hubble tension quoted previously.

Then Fig. 30-25, reminiscent of Fig. 30-17, gives the evolution of the deceleration parameter q of the Universe, according to the various models quoted. The new analysis claims, in agreement with the BAO+CMB, that the present Universe would rather be in a slightly decelerating phase and that its future would be radically different from what the ΛCDM predicts.

[939] J. Son *et al.,* Strong Progenitor Age-bias in Supernova Cosmology. II. Alignment with DESI BAO and Signs of a Non-Accelerating Universe. https://arxiv.org/abs/2510.13121
[940] ibid

This new and iconoclast claim is [941] and will go on being [942] disputed. Possible flaws concern the issue of galactic ages used by the authors instead of galactic masses used previously, forcing them to exploit older databases. The second issue is the connection between galaxy age and progenitor age, the team using the former as a proxy to the latter, assuming that the progenitor formed when the galaxy formed. Studies suggest that Supernovae-Ia occur less than a billion years after the formation of their progenitor.

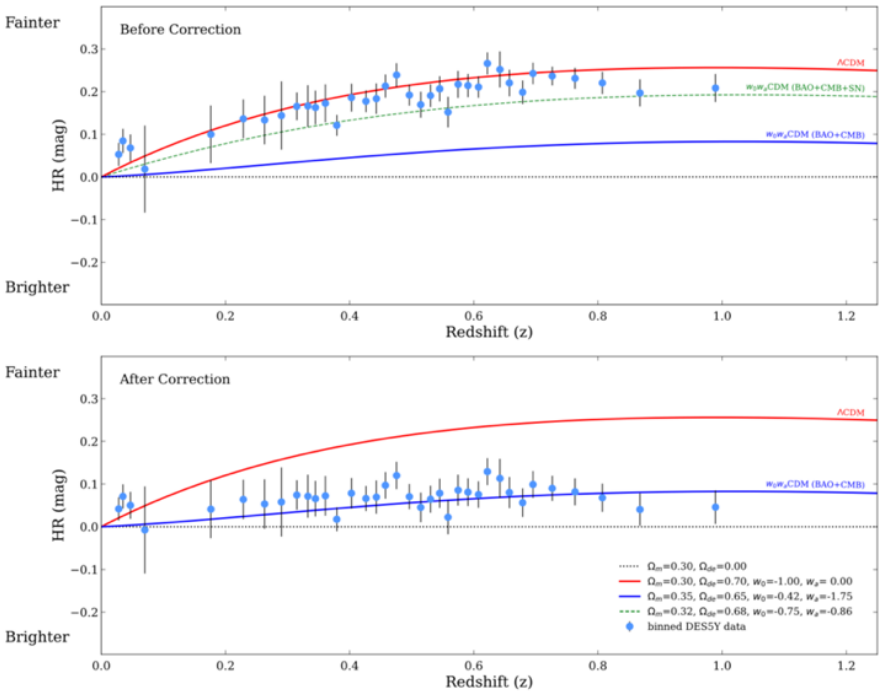


Fig. 30-23: The residual Hubble diagram before (top) and after (bottom) the age-bias correction.

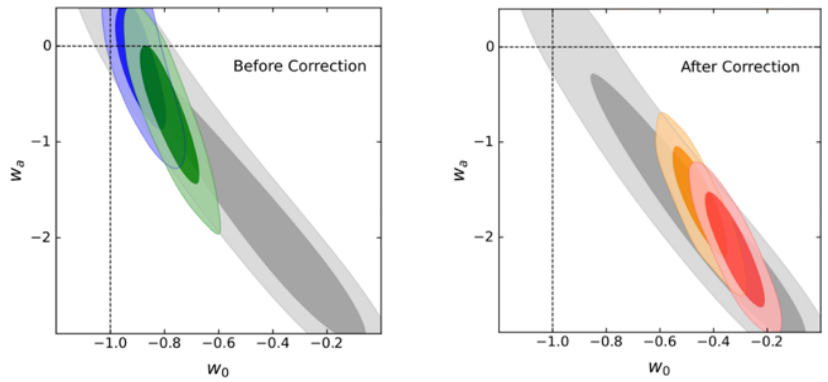


Fig. 30-24: Posterior distributions in the $w_0 - w_a$ parameter spaces for the flat-w_0w_a CDM model, before (left) and after (right) corrections.

[941] B. Koberlein, A. Riess communication to Universe Today.
https://www.universetoday.com/articles/remember-that-paper-claiming-the-universe-is-decelerating-heres-what-a-nobel-laureate-has-to-say-abo

[942] Last minute: here comes a documented answer to J. Son *et al*, https://arxiv.org/abs/2510.13121
by P. Wiseman *et al.,* Still Accelerating: Type Ia supernova cosmology is robust to host galaxy age evolution.
https://arxiv.org/pdf/2601.13785 . Referring to the argumentation of J. Son *et al*, they conclude that *"our analysis shows that these effects are both already accounted for, and highly exaggerated."*

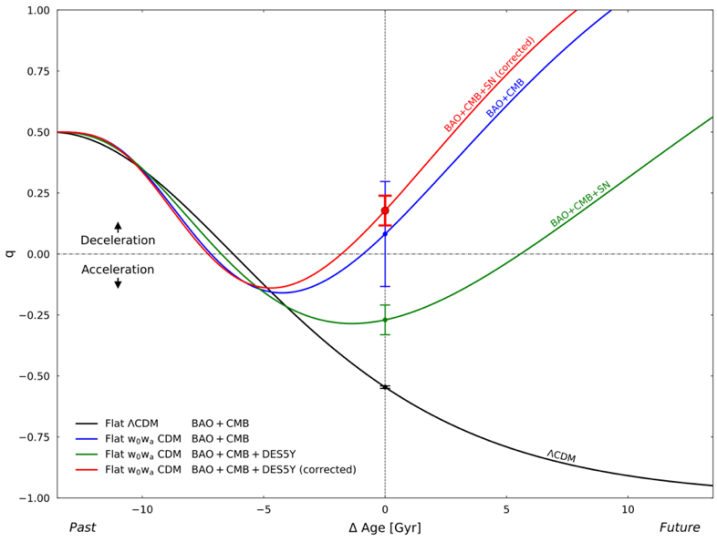


Fig. 30-25: Evolution of the deceleration parameter q, of the Universe. The vertical dotted line indicates the present age of the Universe. The black line shows the result from the BAO + CMB data under the assumption of the flat-ΛCDM model. The green and red lines represent the flat-w_0w_aCDM models derived from the combined datasets (BAO + CMB + DES5Y SN) before and after applying the age-bias correction to the SN dataset, respectively [943].

30.9 Towards the origin?

The previous pages delt with topics built from solid experimental evidences and data.

However a very legitimate and often asked question concerns scenarios accounting for **the origin of the content of matter, visible or dark, in the Universe**, giving more substance to the extrapolations suggested on the left side of Fig. 30-2. Needless to say one can not do more than offer **conjectures**.

The possibility of a **Grand Unification** (GU) can be delt with properly thanks to the **renormalisation group equations (RGE).** They can be used both ways, data obtained at the EW scale extrapolated to the GUT scale (see Fig. 16-11) or hypotheses made at the GUT scale implying features at the EW scale (e.g. in SUSY). A smoking gun of GUTs would be the observation of **proton decay** (Section 32.4).

In the next paragraphs, we will assume an **inflationary phase** of the Universe [944], a scenario resting on quite respectable arguments, but not the only possible one [945].

Inflation theory includes first a period of **exponential expansion**, explaining the observed spatial flatness of the Universe and involving some **inflaton** field ϕ [946]. The produced **density fluctuations** should agree with the CMB measurements (Section 30.4). Finally, one needs a **reheating phase** [947].

---

[943] J. Son *et al.,* Strong Progenitor Age-bias in Supernova Cosmology. II. Alignment with DESI BAO and Signs of a Non-Accelerating Universe. https://arxiv.org/abs/2510.13121

[944] A. H. Guth and D. I. Kaiser, Inflationary cosmology: Exploring the Universe from the smallest to the largest scales. https://arxiv.org/abs/astro-ph/0502328
D. Bauman, TASI Lectures on Inflation. https://arxiv.org/abs/0907.5424

[945] A. Ijjas and P. J. Steinhardt, Bouncing Cosmology made simple. https://arxiv.org/abs/1803.01961

[946] With possibly the Higgs boson playing a role, see Fig. 24-19 and its ref.

[947] D. J. H. Chung *et al.,* Production of massive particles during reheating. https://arxiv.org/abs/hep-ph/9809453
L. Kofman, A. Linde and A. Starobinski, Reheating After Inflation. https://arxiv.org/abs/hep-th/9405187
L. Kofman, A. Linde and A. Starobinski, Towards the Theory of Reheating After Inflation. https://arxiv.org/abs/hep-ph/9704452
L. Kofman, The Origin of matter in the universe: Reheating after inflation. https://arxiv.org/abs/astro-ph/9605155

The basic idea of reheating is **particle production by an oscillating scalar field**. In the simplest models, this field is the same **inflaton** field ϕ that drives inflation (see Fig. 24-18 for Higgs inflation). After inflation, the scalar field ϕ oscillates near the minimum of its effective potential and produces elementary particles. Interacting with each other, they eventually reach a thermal equilibrium.

The efficiency of reheating is highest when a **direct decay channel exists for the inflaton to** SM fields. At the end of inflation, **the inflaton decays** produce a bath of relativistic particles. The radiation density rapidly increases, reaching a **peak temper**ature, T_{max}, which then falls until the energy density in radiation becomes equal to that stored in the inflaton condensate, thus defining **the reheating temperature T_{RH}** directly related to the inflaton decay rate. T_{RH} must be of at least a few MeV, as required by Big Bang Nucleosynthesis (BBN, see above) and potentially higher or much higher (as necessary for baryogenesis).

A possibility [948] is that reheating is realized through a coupling between **the inflaton and the Higgs boson**, for instance inflaton ϕ decay to H through an interaction term $\mu\phi|H|^2$. One can determine the relative values of μ and m_ϕ such that the Higgs potential remains **stable and perturbative** at high energy. Taking into account the running of the Higgs quartic self-coupling (Section 24.1.4) and the experimental constraints from the LHC one can give limits on T_{RH} and the inflaton bare mass.

The **thermal bath** can generate very weakly coupled non-SM particles that do not reach thermal equilibrium. These might include **a dark matter** component. The **gravitino** is an example of such feebly interacting massive particle, **FIPs** (Section 31.2), whose relic density is determined by its production cross section from the thermal bath, sensitive to T_{RH} or T_{max}, depending on its coupling to the SM [949].

If a direct coupling between the inflaton and matter and dark matter exists, these can come directly from **inflaton decays or scatterings.** If not, DM can come from **inflaton radiative decays,** provided DM **has a** coupling to the SM particles.

When there is no direct coupling between dark matter and either the inflaton or SM particles, its production through **gravitational interactions** is still always present.

Reheating is a hard problem. As we said, it depends obviously on which particles the inflaton decays to, fermions or vector fields. Perturbation theory has limitations. One must consider the **expansion of the Universe** and the **backreaction of created particles**. Friction terms must be added to the equation of motion of the scalar field in order to simulate energy transfer from it to matter. Different stages of reheating have thus been identified, in particular early stages, occurring in a regime of a broad parametric resonance, the so-called **preheating phase.**

One may consult both founding papers, listed in the references, and more recent works, including suggestions of possible experimental evidences of reheating features.

30.10 More on inflation

Let us simply reproduce a couple of pedagogical texts on this topic.

- **Inflationary solution to the horizon problem**.
  Quoting from [950]: "*The comoving Hubble sphere shrinks during inflation and expands during the conventional Big Bang evolution (at least until dark energy takes over at a ≈ 0.5). Conformal*

M. A. G. Garcia *et al.,* Inflaton Oscillations and Post-Inflationary Reheating. https://arxiv.org/abs/2012.10756
K. Kaneta *et al.,* Gravitational production of spin-3/2 particles during reheating. https://arxiv.org/abs/2309.15146
[948] Y. Cado et al, Phenomenological Constraints on Higgs reheating. https://arxiv.org/abs/https://arxiv.org/abs/2508.13155
[949] E. Dudas *et al.,* Slow and Safe Gravitinos. https://arxiv.org/abs/2104.03749
[950] D. Baumann, TASI Lectures on Inflation. https://arxiv.org/abs/0907.5424

time during inflation is negative. The spacelike singularity of the standard Big Bang is replaced by the reheating surface, i.e. rather than marking the beginning of time it now corresponds simply to the transition from inflation to the standard BB evolution. All points in the CMB have overlapping past light cones and therefore originated from a causally connected region of space." (Fig. 30-26).

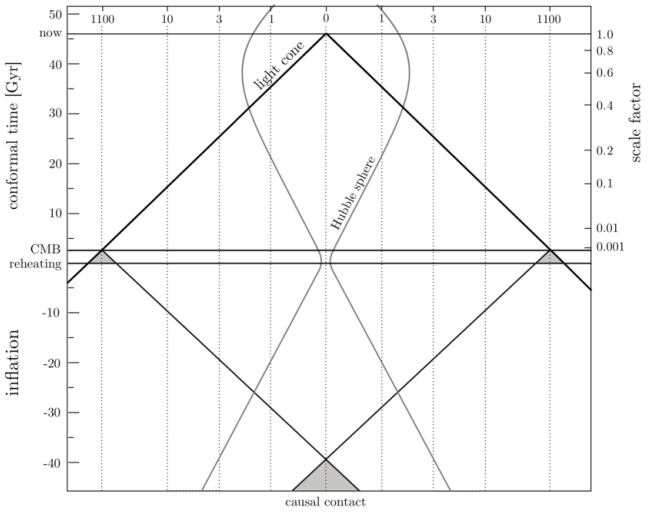


Fig. 30-26: See text for explanation [951].

- **Space-time sketch of inflationary cosmology**

  Quote from [952]: *"The Hubble radius (HR) separates **scales where microphysics dominates over gravity (sub-Hubble scales) from ones on which the effects of microphysics are negligible** (super-Hubble scales). Hence, a necessary requirement for a causal theory of structure formation **is that scales we observe today originate at sub-Hubble lengths in the early Universe**. The third length is the "horizon", the forward light cone of our position at the Big Bang. The horizon is the causality limit. Because of the exponential expansion of space during inflation, the horizon is exponentially larger than the HR. One should not confuse these scales, but HR and horizon are the same in Standard Cosmology. From the figure it is clear that, provided that the period of inflation is sufficiently long, all scales which are currently observed originate as sub-Hubble scales at the beginning of the inflationary phase. Thus, in inflationary cosmology it is possible to have a causal generation mechanism of fluctuations. The inflationary Universe scenario of structure formation is based on the hypothesis that **all current structure originated as quantum vacuum fluctuations.** To obtain exponential expansion of space in the context of Einstein gravity the energy density must be constant. Thus, during inflation the total energy [953] and size of the Universe both increase exponentially. In this way, inflation can solve the size and entropy problems of Standard Cosmology. To summarize the first crucial criterium which must be satisfied in order to have a successful theory of structure formation is that **fluctuation scales originate inside the Hubble radius**. In inflationary cosmology it is the accelerated expansion of space during the inflationary phase."* (Fig. 30-27) [954].

[951] D. Baumann, Cosmology. https://cmb.wintherscoming.no/pdfs/baumann.pdf
[952] R. H. Brandenberger, Introduction to Early Universe Cosmology. https://arxiv.org/abs/1103.2271
[953] But with a pressure equal to minus the energy density. $P + \rho = 0$
[954] R. H. Brandenberger, Introduction to Early Universe Cosmology. https://arxiv.org/abs/1103.2271

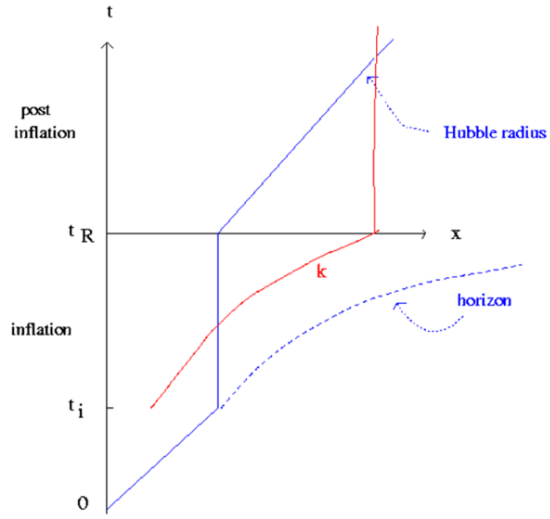


Fig. 30-27*:* Space-time sketch of inflationary cosmology. The vertical axis is time, the horizontal axis corresponds to physical distance. The solid line labelled k is the physical length of a fixed comoving fluctuation scale.

30.11 More on cosmology

Similarly, we reproduce a couple of pedagogical text-quotations on this topic.

- **Spacetime diagrams of our Universe**
  Quoting from [955]: "*Spacetime diagrams showing the main features of the general relativistic description of the expansion of the Universe for the* (Ω_M, Ω_Λ) = (0.3,0.7) *model with* H_0 = 70 km s^{-1} Mpc^{-1} (Fig. 30-28). *Dotted lines show the worldlines of comoving objects. We are the central vertical worldline. The current redshifts of the comoving galaxies shown appear labelled on each comoving worldline. The normalized scale factor,* $a = R/R_0$, *is drawn as an alternate vertical axis. All events that we currently observe are on our past light cone (with apex at t = now). All comoving objects beyond the Hubble sphere (thin solid line) are receding faster than the speed of light. Top panel (proper distance): The speed of photons relative to us (the slope of the light cone) is not constant but is rather* $v_{rec} - c$. *Photons we receive that were emitted by objects beyond the Hubble sphere were initially receding from us (outward sloping lightcone at* $t \leq 5$ *Gyr). Only when they passed from the region of superluminal recession* $v_{rec} > c$ *(gray crosshatching) to the region of subluminal recession (no shading) can the photons approach us. More detail about early times and the horizons is visible in comoving coordinates (middle panel) and conformal coordinates (lower panel). Our past light cone in comoving coordinates appears to approach the horizontal (t = 0) axis asymptotically. However, it is clear in the lower panel that the past light cone at t = 0 only reaches a finite distance: about 46 Glyr, the current distance to the particle horizon. Currently observable light that has been travelling towards us since the beginning of the Universe, was emitted from comoving positions that are now 46 Glyr from us. The distance to the particle horizon as a function of time is represented by the dashed line. Our event horizon is our past light cone at the end of time,* $t = \infty$ *in this case. It asymptotically approaches* $\chi = 0$ *as* $t \rightarrow \infty$. *The vertical axis of the lower panel shows conformal time. An infinite proper time is transformed into a finite conformal time so this diagram is complete on the vertical axis. The aspect ratio of* $\sim 3/1$ *in the top two panels represents the ratio between the radius of the observable Universe and the age of the Universe, 46 Glyr/13.5 Gyr.*"

[955] T. M. Davis and C. H. Lineweaver, Expanding Confusion: common misconceptions of cosmological horizons and the superluminal expansion of the Universe. https://arxiv.org/abs/astro-ph/0310808
T. M. Davis, Fundamental Aspects of the Expansion of the Universe and Cosmic Horizons.
https://arxiv.org/abs/astro-ph/0402278

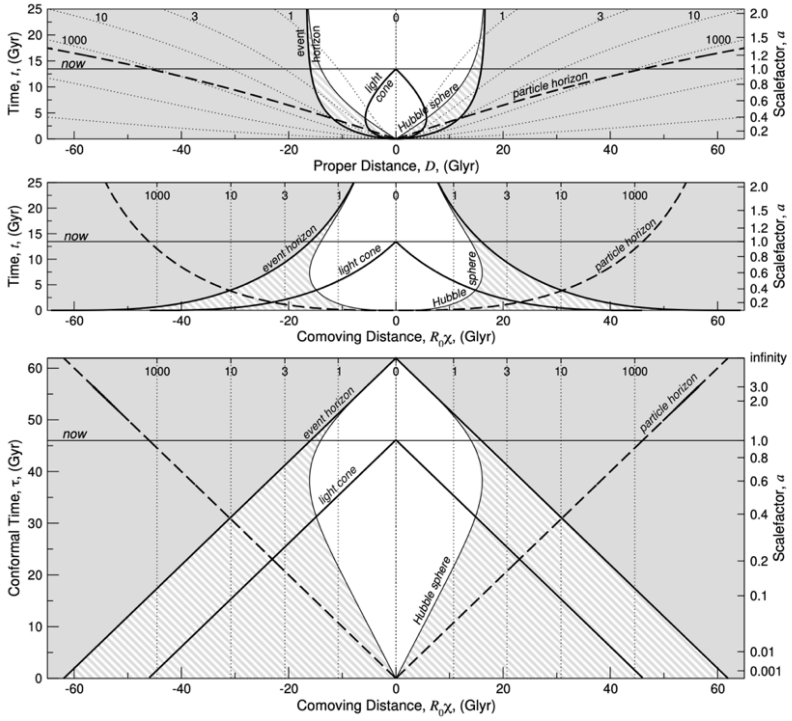


Fig. 30-28: Spacetime diagrams showing the main features of the general relativistic description of the expansion of the Universe. For more explanations see text.

Quoting Ref. [956]: "*Spacetime diagram for conformal time τ and co-moving cosmic distance r, in units of years and light-years, respectively, for a FLRW Universe with $\Omega_\Lambda = 0.7$, $\Omega_M = 0.3$, $H_0 = 70$ km/s Mpc^{-1} (Fig. 30-29). In the left half of the image, contour lines of **constant recession speed** are shown, expressed as fractions or multiples of the speed of light c. In the right half of the image, contour lines of **constant relative speed** (the magnitude of the radial relative velocity) are shown. Relative speed is between the event at which the value is displayed and the corresponding reception event on our own galaxy's world-line, with all values given as fractions of c.*"

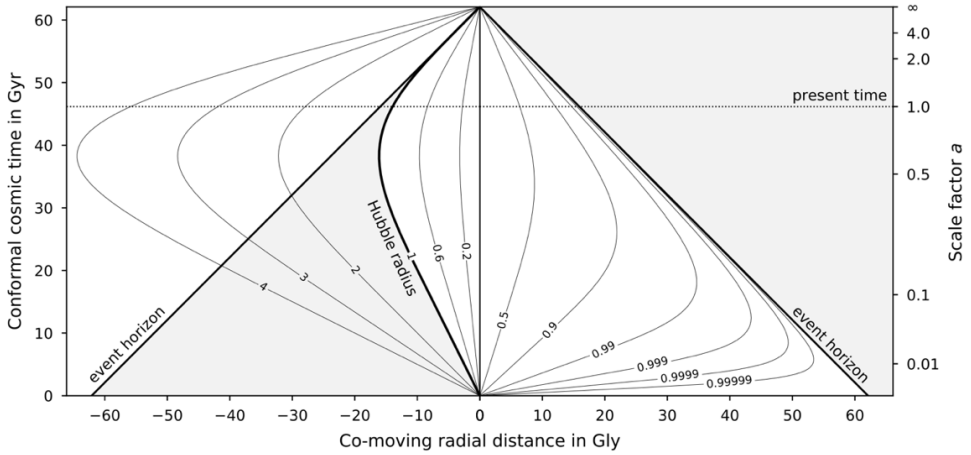


Fig. 30-29: Spacetime diagram for conformal time τ and co-moving cosmic distance r, in units of years and light-years. For more explanations see text.

[956] M. Pössel, Cosmic event horizons and the light-speed limit for relative radial motion. https://arxiv.org/abs/1912.11677

30.12 Digression 1: The Universe in logM-logR coordinates

Before discussing possible relations between the two SM, let us recall a well-known 2-D representation of the Universe in log M versus log R (Fig. 30-30). The triangle PUF is made of the Planck point, the Heisenberg line PF at – 45° and the Schwarzschild line PU at + 45°. Lines of slope 1/3 are isodensities. As the time is evolving, all the densities decrease except the Dark Energy density d_E which remains constant (Cosmological Constant).

The point U assumes the asymptotic victory of the CC at its present value and is located at the radius of the asymptotic de Sitter space [957] (1.65×10^{26} m). **Under this assumption** one can close the triangle by the line UF of DE energy density and call it "*eternal* ". This triangular representation is not new [958], but closing the triangle is assumption dependent (Fig. 30-30). Zooming into any point inside the triangle and describing our present understanding of the corresponding region is a rewarding attempt [959].

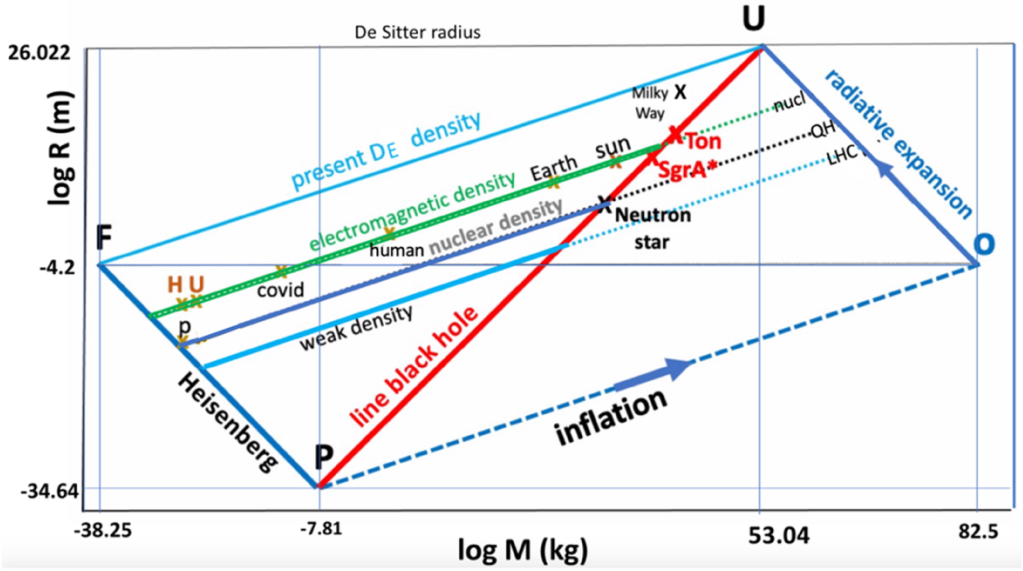


Fig. 30-30: The Universe in logM-logR coordinates. P is Planck. U is the Universe fate, as de Sitter, **if a CC wins** (the present Hubble radius is 83 % of the de Sitter radius. Besides Heisenberg and Schwarzschild lines, it shows isodensity lines (slope 1/3). The line at present DE density would close the triangle PUF. Inflation could look as the line PO at Planck density. The BB in O would start the radiative expansion of the Universe. Bekenstein–Hawking entropy in U is 1.65×10^{122}. Mass in O is 2×10^{91} M_P. Figure by R. Barate and D. Treille.

However, one could get bolder and imagine how to represent the trajectory we attribute to the **presently observable Universe**, which is not far from U (the present Hubble radius is 1.37×10^{26} m). Then inflation (if any), assumed (perhaps wrongly) to have occurred at Planck density, is represented by the line PO, where O, at reheating, is the **actual Big Bang** for our observable Universe today. The line OU of slope – 45° (i.e. R × M = constant) correctly accounts for the **radiative expansion** of our

[957] https://en.wikipedia.org/wiki/De_Sitter_space

[958] V. Weisskopf, *Science*, *New Series, Vol. 187, No. 4177 (Feb. 21, 1975), pp. 605-612,* http://www.jstor.org/stable/1739660
B. J. Carr and M. J. Rees, The anthropic principle and the structure of the physical world. *Nature278(1979)605–612*
See also A. Ianni *et al.*, A new approach to dark matter from the mass-radius diagram of the Universe. https://arxiv.org/abs/2112.03755

[959] R. Barate, TRIANGLE 2020, book in preparation.

Universe [960]. The exact treatment of the upper corner is involved and is treated in detail elsewhere [961]. The "eternal" Fig. 30-30 does not deal with the evolution in this region.

But e.g. the fact that nuclei appear at a time of electromagnetic density is correct and a mystery.

The mass of O is about 10^{91} Planck masses. This is a bit too large: one usually assumes rather 10^{89} fully relativistic objects, γ , ν , etc., in the visible Universe. The **Bekenstein entropy bound** [962] (in R x M) is already reached at point O. The **Hawking–Bekenstein entropy** [963] k_B area /(4 L_{Pl}^2) grows along OU and equals the Bekenstein bound in U, where area /4 $L_{Pl}^2 = 1.65 \times 10^{122}$.

30.13 Digression 2: An interesting but controversial topic

In Ref. [964] one reads: "*A major consequence of such inflationary theories is that, since k* ***and Λ are zero, the net energy of the Universe is zero:*** *the positive kinetic energy … is precisely balanced by the negative gravitational potential energy. Since the net amount of other conserved quantities such as charge and angular momentum is also found to vanish (at least to very high accuracy) this raises the fascinating possibility that the Universe was created "ex nihilo," perhaps by some sort of quantum fluctuation (see Barrow and Tipler (1986)). The properties that now produce its distinctive features, particularly the nonzero baryon and lepton number, have arisen (by hypothesis) because B and L are not precisely conserved (though B —L must be, to ensure that neutral atomic matter can result), and because CP invariance is slightly violated, too, … If so, many of the properties of the Universe are probably "accidental" consequences of its early evolution and not uniquely required by fundamental physical principles.*"

However, this was written before one knew that Λ is not zero.

Nevertheless, many authors [965], some presumably aware of the acceleration of the Universe, still defend this point of view. Since Nathan Rosen, NarayanBanerjee and several others until now (e.g. authors considering *creatable* Universes, born from a fluctuation), many knowledgeable people, using the energy/momentum complex (of Albert Einstein, Lev Landau, Steven Weinberg, etc.) or proceeding other ways (e.g. in teleparallel GR, ...), tend also to find **zero total energy**, say for:

$$E = \int (-g)^{\frac{1}{2}} (T_0^0 + t_0^0) d^3x \, .$$

---

[960] R. An and V. Gluscevic, Reconstructing the early-universe expansion and thermal history. https://arxiv.org/abs/2310.17195 , https://arxiv.org/html/2310.17195v2 Backward in time, the quasi flat a x T(a) curve is documented up to the BBN time (a about 10^{-9} of its present value, few minutes, 10^9 K). The EW transition is at 10^{15} K, few ps, a 10^{-15} of now. See Fig. 30-2.

[961] R. Barate, TRIANGLE 2020, book in preparation

[962] J. D. Bekenstein (2008), Bekenstein bound. Scholarpedia, 3(10):7374, http://www.scholarpedia.org/article/Bekenstein_bound

[963] J. D. Bekenstein (2008), Bekenstein–Hawking entropy. Scholarpedia, 3(10):7375, http://www.scholarpedia.org/article/Bekenstein-Hawking_entropy

[964] P. D. Collins, A. D. Martin and E. J. Squires, *Particle Physics and Cosmology* Copyright © 1989 by John Wiley & Sons, Inc. ISBN: 0-471-60088-1. See p. 404.

[965] N. Rosen The Energy of the Universe. *Gen Relat Gravit* 26, 319–321 (1994). https://doi.org/10.1007/BF02108013
V. B. Johri *et al.,* Gravitational Energy in the Expanding Universe. *Gen Relat Gravit* 27, 313–318 (1995). https://doi.org/10.1007/BF02109127
V. Faraoni and F. I. Cooperstock. On the total energy of open Friedmann–Robertson–Walker universes. https://arxiv.org/abs/astro-ph/0212574
S. S. Xulu, Total energy of the Bianchi type I universes. https://arxiv.org/abs/gr-qc/9910015
M. Mouland master thesis, The Total Energy of Friedmann-Robertson-Walker Universes 2009. https://www.duo.uio.no/bitstream/handle/10852/10952/makefile.pdf
I.-C. Yang, The energy of the universe in the Bianchi type-II cosmological model. https://arxiv.org/abs/1810.06193
J. J. Ferrando *et al.,* Creatable Universes. https://arxiv.org/abs/0705.1049

In Ref. [966] one reads: "*the total energy of the spatially closed FRW Universe is zero and so also* ***the total energy enclosed within any finite volume of the spatially flat FRW Universe*****.**" And this conclusion is repeated by several authors.

For instance, Ref. [967] finds that the energy-momentum vanishes for all class A models of the Bianchi classification, which includes our flat FRW Universe. They add: "*The physical interpretation is that the negative gravitational binding energy density exactly cancels the positive material energy density.*"

In Ref. [968] one reads: "*The results ... that the energy of the Universe is constant and zero for open or critically open FRW Universes, and for Bianchi models evolving into de Sitter spacetimes, should not be regarded as merely technical. Indeed, it is well to question why Universes that are so different all have zero total energy. One could speculate that this fact might be related to the problem of the origin of the Universe. Indeed, since the Universe is by definition an isolated system, the zero-energy result is compatible with the Universe emerging from a "system" with zero energy, be it quantum vacuum (M. Albrow 1973, E. P. Tryon 1973, A. H. Guth 1981), "nothing" (A. Vilenkin 1983), flat empty space (I. Prigogine et al. 1988, 1989, E. Gunzig et al. 2001a, 2001b), or something else. In such a picture, matter particles would have to be created at the expense of the gravitational field energy (e.g. I. Prigogine et al. 1988, 1989). It seems inconceivable that the cosmos could emerge from any physical system that has nonvanishing total energy. This would require an exchange of energy between the Universe and a third system, making a cosmological spacetime an open system from the thermodynamical point of view.*"

Such statements seem to go against some generally admitted facts in GR, and we are in the impossibility to draw any conclusion. At least, se non è vero, è ben trovato ….

Let us leave these digressions and come back to less speculative matters, such as the dark component.

[966] N. Banerjee and S. Sen, Einstein pseudotensor and total energy of the universe. *Pramana Vol. 49, No. 6, Dec.1997 pp. 609-615,* https://www.ias.ac.in/article/fulltext/pram/049/06/0609-0615

[967] J. M. Nester *et al.,* On the energy of homogeneous cosmologies (2008). https://arxiv.org/abs/0803.0181

[968] V. Faraoni and F. I. Cooperstock. On the total energy of open Friedmann-Robertson-Walker universes. https://arxiv.org/abs/astro-ph/0212574

31. Dark matter

31.1 Dark matter overview

31.1.1 Brief historical account

For a detailed history of Dark Matter (DM) see Ref. [969]. In the 1930s Fritz Zwicky found a large scatter in the apparent velocities of 8 galaxies belonging to the Coma cluster and applied the **virial theorem** [970] to estimate its mass. Anomalies were observed also in 1936 by Sinclair Smith [971] on the VIRGO cluster and by Horace Babcock in 1939 on Andromeda Nebula rotation [972]. Knut Lundmark evoked DM as early as 1930 [973].

In the 1970s Vera Rubin found that a large amount of matter in excess of the observable one was required to explain the rotation of ionised gas at the edge of large disks of the Milky Way or Andromeda. With others, like Albert Bosma [974], she played a key role in convincing the community of the presence of DM. Mid-seventies a common solution existed for the mass discrepancies observed in clusters and galaxies, the claim was that the galaxies mass had been until then **underestimated by a factor of ~ 10.**

To explain how stars orbit in galaxies (Figs. 31-1 to 31-3) and how galaxies orbit in clusters, a large variety of hypotheses have been considered as shown in Fig. 31-6.

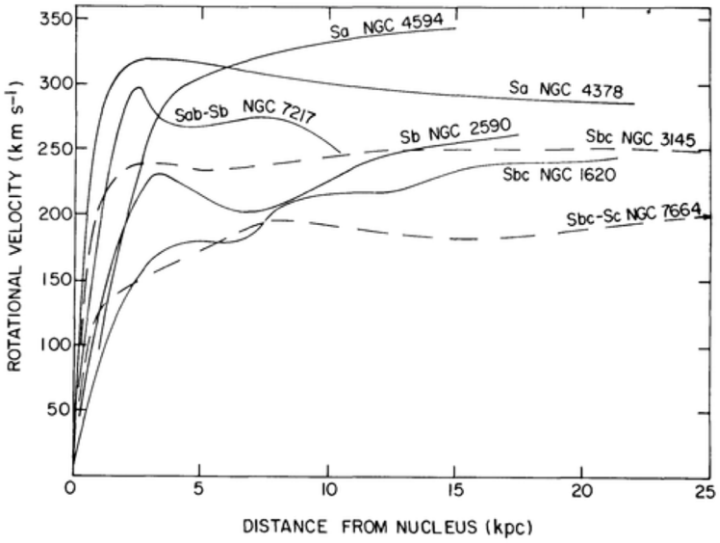


Fig. 31-1: Historical plot of Vera Rubin in 1978 [975].

[969] G. Bertone and D. Hooper, A History of Dark Matter. https://arxiv.org/abs/1605.04909
See also the entertaining article by A. de Rujula, The Dark Side of the Universe. https://arxiv.org/abs/2108.01691
[970] In statistical mechanics the **virial theorem** provides a general equation that relates the average over time of the **total kinetic energy** of a system of discrete particles in a stable configuration, bound by a conservative force with that of the **total potential energy** of the system.
[971] S. Smith, The Mass of the VIRGO Cluster. https://adsabs.harvard.edu/pdf/1936ApJ....83...23S
[972] H. Babcock, The rotation of the Andromeda Nebula. https://ui.adsabs.harvard.edu/abs/1939LicOB..19...41B/abstract
[973] https://en.wikipedia.org/wiki/Knut_Lundmark
[974] A. Bosma, Rotation curves and the dark matter problem. https://arxiv.org/abs/2309.06390
[975] V. C. Rubin: A Biographical Memoir by Neta A. Bahcall, ©2021 National Academy of Sciences.
https://www.nasonline.org/wp-content/uploads/2024/06/rubin-vera.pdf

Besides these, another major argument in favour of DM existence is the **growth of structures.**

Starting from the recombination time (see Fig. 30-4), where the fluctuations $\delta\rho_m/\rho_m$ are at the 10^{-5} level, and to reach for $\delta\rho_m/\rho_m$ a value of the order of 1 now, one must couple hadronic matter to a fluid as cold DM, feeling only the force of gravity, not opposed by any force, such as radiation pressure.

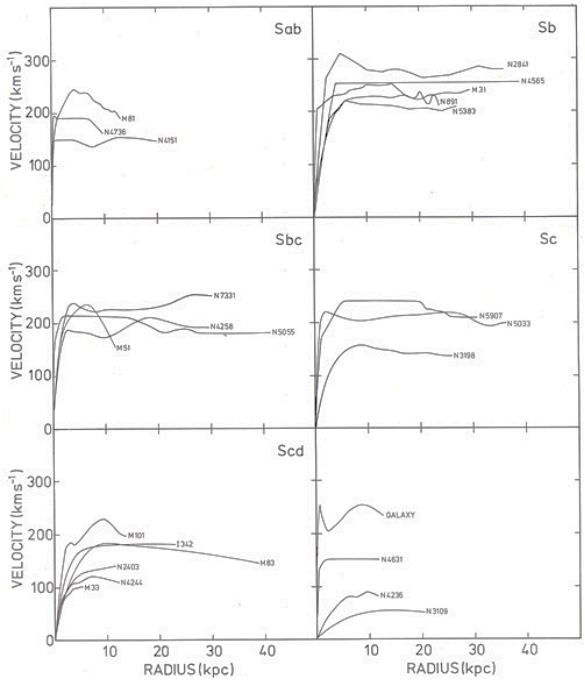


Fig. 31-2: Historical plots of rotational curves from different galaxies of A. Bosma [976].

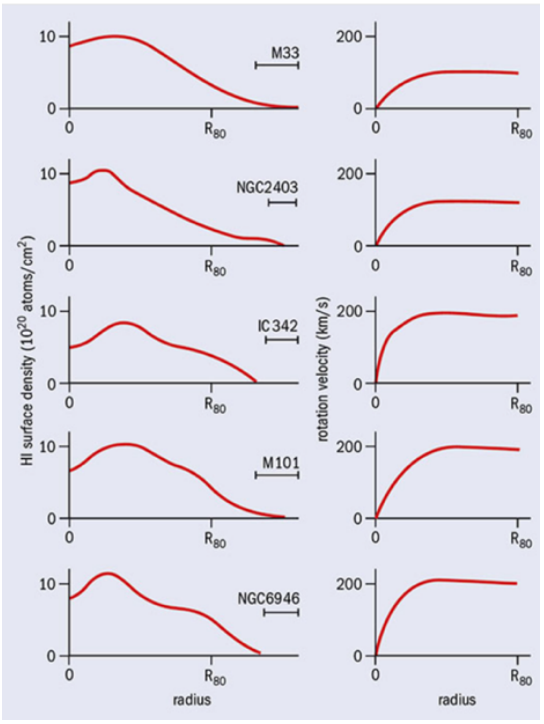


Fig. 31-3: Hydrogen surface density profile (left) and the rotation curves (right) of 5 galaxies obtained by D. H. Rogstad and G. S. Shostak in 1972 [977].

This is what explains the shape of the **matter power spectrum,** describing the density contrast of the Universe (Figs. 31-4 and 31-5). As a result, DM begins to collapse into a complex network of DM halos well before ordinary matter, which is impeded by pressure forces. Without DM, the epoch of galaxy formation would occur substantially later in the Universe than observed

More on Fig. 31-4. Left: once inflation ends all the lengths of interest are larger than the Hubble radius. The evolution of the density contrast then depends on the scale k^{-1}, the a_{cross} of it crossing of the Hubble radius and whether the Universe is then radiation- or matter- dominated. The evolved fluctuation and the matter power function at the present epoch have thus an expected "feature" around $k^{-1} = k^{-1}_{eq}$, of the order of 300 Mly.

V. C. Rubin *et al.,* Extended rotation curves of high-luminosity spiral galaxies. IV. Systematic dynamical properties, Sa → Sc. https://adsabs.harvard.edu/abs/1978apj...225l.107r

[976] A. Bosma, The Distribution and Kinematics of Neutral Hydrogen in Spiral Galaxies of Various Morphological Types. Ph.D. Thesis (1978), University of Groningen, Groningen, http://ned.ipac.caltech.edu/level5/March05/Bosma/frames.html

[977] G. Bertone and D. Hooper, How dark matter became a particle. https://cerncourier.com/a/how-dark-matter-became-a-particle/

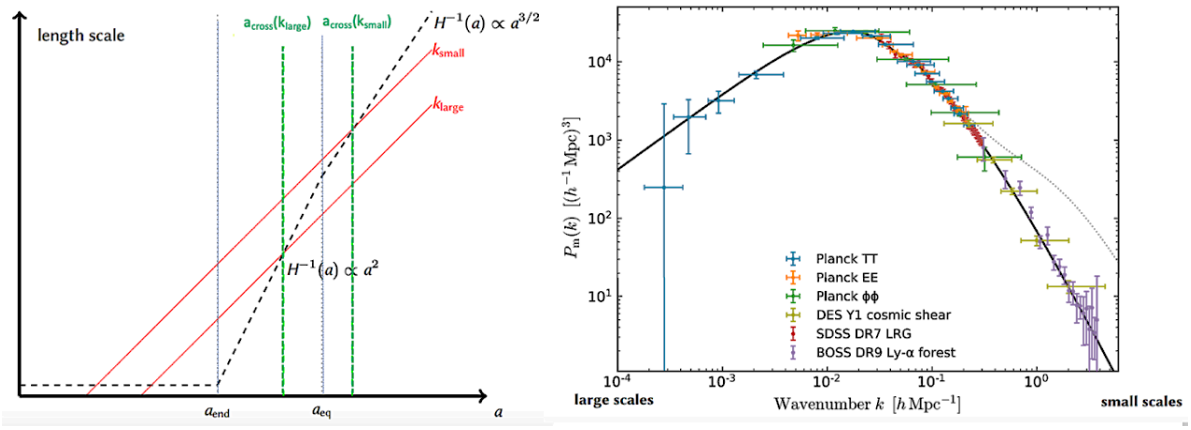


Fig. 31-4: Left: dependence of scales k^{-1} on their time a_{cross} of crossing the Hubble radius $H^{-1}(a)$. Right: the matter power spectrum [978].

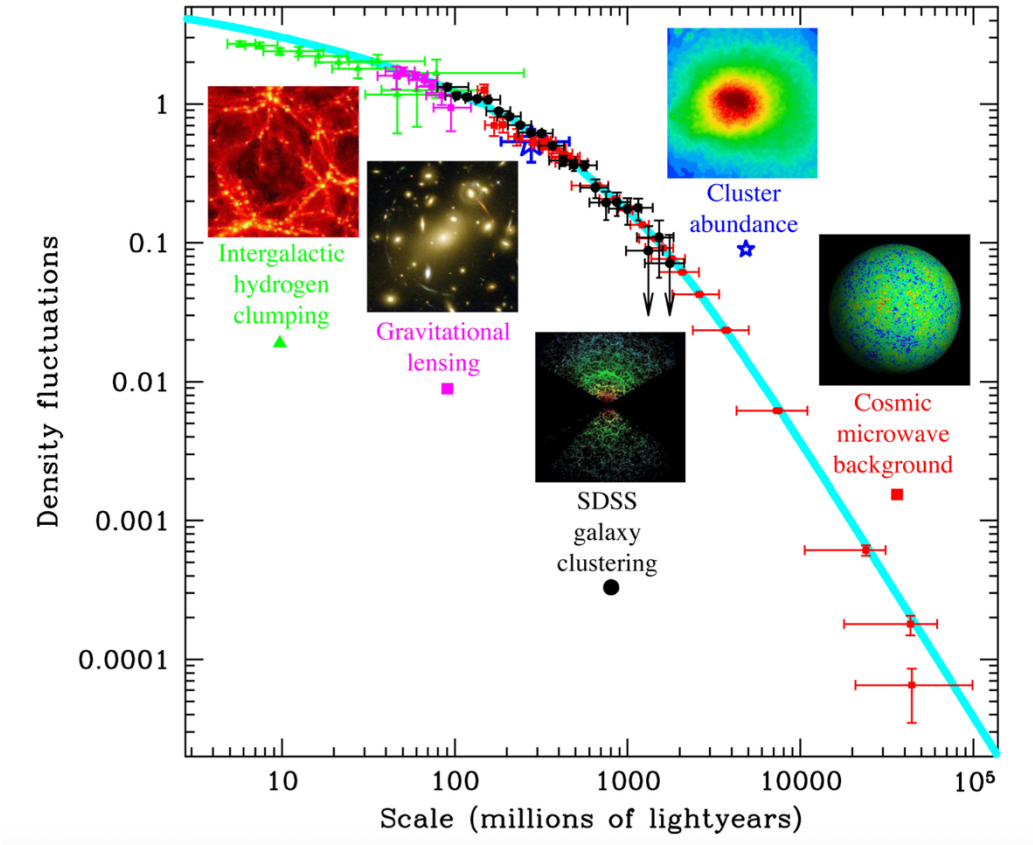


Fig. 31-5: Another view of the power spectrum of density fluctuations in the Universe [979]. The y-axis labelled "Density fluctuations", shows the power spectrum in dimensionless form, as the variance per logarithmic interval in k, $\Delta^2(k) \propto k^3P(k)$. The x-axis is the comoving scale (1 Mpc ~ 3.3 Mly). Different tracers of the density are used on different scales. The turquoise curve shows a fit to the data with the parameters of the standard ΛCDM cosmological model (Figure credit: M. Tegmark, MIT).

[978] T. R. Choudhury, Cosmology, Lecture 12.
http://www.ncra.tifr.res.in:8081/~tirth/Teaching/Cosmology-2021/Lectures/lecture-12-web.pdf
[979] M. Pettini. Large scale structure. https://people.ast.cam.ac.uk/~pettini/Intro%20Cosmology/Lecture14.pdf

31.1.2 Dark matter particles or MOND

But the main option has been and is still to assume **invisible "dark matter" particle**s [980] which accompany the ordinary matter. This assumption, very flexible, can explain a lot of what we observe. Here too the number of candidates considered is large, see Fig. 31-6 and Table 31-1.

However numerous experiments have all **failed to find evidence for such objects**. Negative results do not rule out this interpretation of DM. Maybe the interaction of DM particles with ordinary matter is less than originally thought, one can consider new forces and add more particle species than originally done. This proliferation of unseen particles is called the **"hidden sector**", which is described in next chapters.



Fig. 31-6: Visualization of possible solutions to the dark matter problem [981].

An alternative idea that extra matter **does not exist** and that the equations of gravity need some modification has received less attention. It is the theory of **Modified Newtonian Dynamics (MOND)**, valid at **very small accelerations** [982]. For its status and a list of references see [983], from its inventor.

Both solutions have strong and weak points. For instance, the extreme variety of galaxy species requires to adapt the DM hypothesis to each case, while MOND offers a general solution (Fig. 31-7) with a single parameter. The figure shows for 153 galaxies a correlation between the radial acceleration traced by rotation curves and that predicted by the observed distribution of baryons. *"This radial acceleration relation is tantamount to a natural law for rotating galaxies."*

Despite its many predictive successes, modified gravity has also serious problems. It works across a large range of different galaxy types but does not explain well the motion of **galaxy clusters**.

---

[980] G. Bertone and D. Hooper, How dark matter became a particle. https://cerncourier.com/a/how-dark-matter-became-a-particle/

[981] G. Gertone and T. M. P. Tait, A New Era in the Quest for Dark Matter. https://arxiv.org/abs/1810.01668

[982] This acceleration at which gravity departs from Newton is close to the acceleration of the universe, of the order of c^2/R_H

[983] M. Milgrom, MOND as manifestation of modified inertia. https://arxiv.org/abs/2310.14334

1976: Light Neutrinos

Zeldovich& Gershtein 1966 → Upper limit on neutrino masses 400 eV

Szalay & Marx 1976 → ~10 eV neutrinos might account for "missing mass"

White, Frenk & Davis 1983 → neutrinos (hot DM) excluded

1977: Heavy neutrinos

Hut; Lee & Weinberg; Sato & Kobayashi; Zeldovich 1977 → multi-GeV neutrinos are allowed

"Of course, if a stable heavy neutral lepton were discovered with a mass of order 1-15 GeV, the gravitational field of these heavy neutrinos would provide ***a plausible mechanism for closing the universe.*** (Lee & Weinberg 1977)

1977: Gravitinos

Hut 1977 → "cosmological gravitino problem"

Pagels & Primack 1982 → *"Gravitinos could also provide the* ***dark matter required in galactic halos and small clusters of galaxies****"*

1977: Axions

Wilczek; Weinberg 1977 → Peccei-Quinn mechanism implies Nambu-Goldstone boson

Abbott & Sikivie 1983 → Misalignment mechanism and cold DM

1983: Neutralinos

Weinberg & Goldberg 1983 → photino DM

Ellis, Hagelin, Nanopoulos, Olive & Srednicki → **neutralino DM**

1993: Sterile neutrinos

Dodelson & Lawrence 1993 → sterile neutrinos with masses above ~ keV as DM candidate

C. Weniger - Dark matter evidence & candidates

Table 31-1 The variety of particle candidates for DM [984].

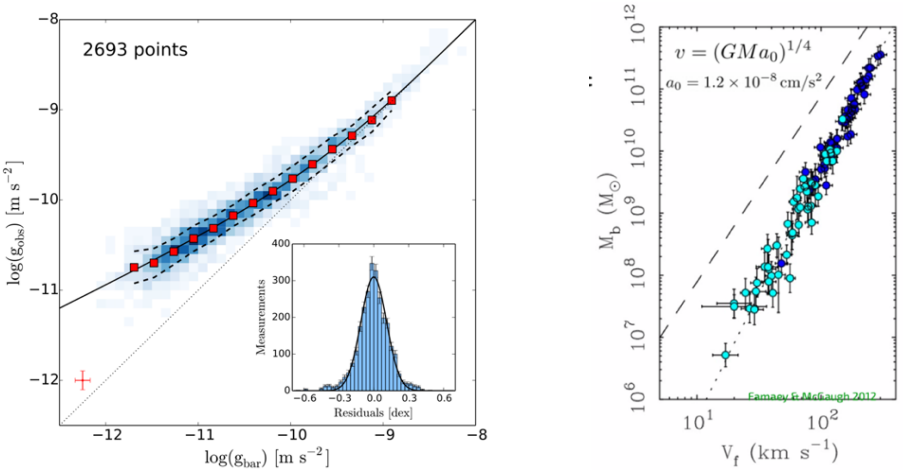


Fig. 31-7: A problem for DM? [985] Left plot: The centripetal acceleration observed in rotation curves, $g_{obs} = V^2/R$, is plotted against that predicted for the observed distribution of baryons, $g_{bar} = |\partial\Phi_{bar}/\partial R|$. The dotted line is the line of unity. The function $\boldsymbol{g_{obs} = F(g_{bar})} = g_{bar} / (1 - e^{-\sqrt{g_{bar}/g_\dagger}})$ gives a good fit with $g_\dagger = 1.20 \pm 0.02(\text{random}) \pm 0.24(\text{syst}) \times 10^{-10}$ ms^{-2}.
Right plot: **Tully-Fisher relation** showing a tight correlation between the angular velocity of spiral galaxies and their **baryonic mass**. **MOND** correctly accounts for normalization and slope of the correlation over four orders of magnitude in galaxy mass.

[984] C. Weniger, Dark matter – Evidence and Candidates. ISAPP School 2019 – The dark side of the universe, https://www.mpi-hd.mpg.de/lin/_isapp2019/talks/ISAPP2019-Weniger_1.pdf

[985] S. McGaugh *et al.,* The Radial Acceleration Relation in Rotationally Supported Galaxies. https://arxiv.org/abs/1609.05917
S. Hossenfelder and S. McGaugh, Is Dark Mater Real? https://www.scientificamerican.com/article/is-dark-matter-real/,
B. Famaey and S. McGaugh, Modified Newtonian Dynamics (MOND): Observational Phenomenology and Relativistic Extensions. https://arxiv.org/abs/1112.3960 ,
C. Weniger, Dark Matter – Evidence and Candidates. ISAPP School 2019 – The dark side of the universe. https://www.mpi-hd.mpg.de/lin/_isapp2019/talks/ISAPP2019-Weniger_1.pdf

In particular the pattern of **galaxies in collision** is a problem for this theory (Figs. 31-8 and 31-9). One finds that the major mass component (cluster scale-DM halos) is in spatial agreement with the galaxies and not with the X-rays gas, which could confirm the collision-less nature of dark matter [986]. The Bullet Cluster does not seem to present a challenge to the ΛCDM model. For a second similar cluster see Ref. [987].

MOND applied to rich clusters of galaxies has a deficit (by around 2) of predicted dynamical mass derived from the virial theorem (VT) with respect to observations. But approaching differently the VT, using the velocity dispersion of cluster members along the line of sight and applying pressure (surface) corrections for non-closed systems, one shows [988] that "*solutions existing for MOND in clusters give similar results to Newton+DM*".

For another type of comparison, coming from Gaia DR2, see Ref. [989], close to conclude the effective equivalence of DM and MOND on circum-galactic and galactic scales.

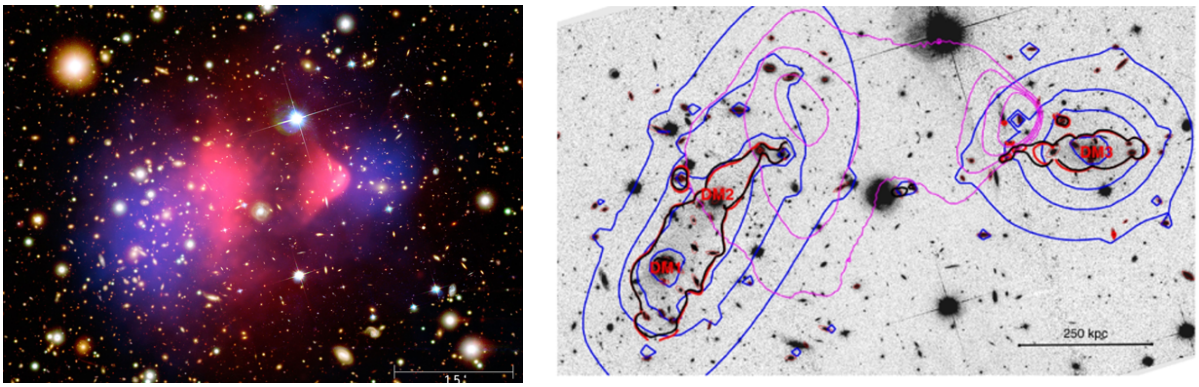


Fig. 31-8: A problem for MOND [990]? The bullet cluster left: artistic view. Gas SM interacting in the middle, DM in the outskirts. Right: as seen by CHANDRA X-rays [991]. In this image of the Bullet cluster, the blue contours show the projected mass density. The magenta lines show the contours of the Chandra X-rays brightness map. The dark matter and galaxies do not experience friction and do not lose velocity. Baryons in hot, X-ray-emitting gas do experience friction, get slowed down and lag behind DM and galaxies.

At this point, both particle dark matter and modified gravity have advantages and shortcomings. It would be prudent to keep open the possibility that gravity must be modified (Fig. 31-9) [992]. Some recent theoretical developments suggest that maybe the truth is in between: *"a type of particle dark matter that can masquerade as modified gravity"* [993].

---

[986] D. Paraficz *et al.,* The Bullet cluster at its best: weighing stars, gas and dark matter. https://arxiv.org/abs/1209.0384
[987] I. Bartalucci *et al.,* PSZ2 G282.28+49.94, a recently discovered analogue of the famous Bullet Cluster. https://arxiv.org/abs/2409.07290
[988] M. López-Corredoira *et al.,* Virial theorem in clusters of galaxies with MOND. https://arxiv.org/abs/2210.13961
[989] Y. Zhu *et al.,* How close dark matter haloes and MOND are to each other: three-dimensional tests based on Gaia DR2. https://arxiv.org/abs/2211.13153
[990] D. Kraljic and S. Sarkar, How rare is the Bullet Cluster (in a ΛCDM universe)? https://arxiv.org/abs/1412.7719
[991] D. Paraficz *et al.,* The Bullet cluster at its best: weighing stars, gas, and dark matter. https://arxiv.org/abs/1209.0384
[992] C. Weniger, Dark matter – Evidence and Candidates.
https://www.mpi-hd.mpg.de/lin/_isapp2019/talks/ISAPP2019-Weniger_1.pdf
https://physicsworld.com/a/cosmic-combat-delving-into-the-battle-between-dark-matter-and-modified-gravity/
[993] Y. Zhu *et al.,* How close dark matter haloes and MOND are to each other: three-dimensional tests based on Gaia DR2. https://arxiv.org/abs/2211.13153

A possible and radical line of thought, since DM manifestations are up to now purely gravitational, is to ask whether introducing **non-locality in General Relativity** (in the name of QM and accounting maybe for eventual loops in graviton exchange) can lead to a well-behaved theory which **fully mimics DM in all aspects**: the answer seems to be positive [994].

CDM vs MOND

	Cold Dark Matter	Modified Newtonian Dynamics
CMB: Magnitude of fluctuations	yes	no
CMB: Angular power spectrum	yes	no
Baryon acoustic oscillations in galaxy distribution	yes	no
Bullet cluster (DM / gas segregation)	yes	maybe*
Spiral galaxy rotation curves	yes	yes
Tully-Fisher	probably yes**	yes
Faber-Jackson	probably yes**	yes
Simultaneous explanation of DM in dwarf galaxies and clusters	yes	maybe

*could work in more complete theories of MOND (e.g. Israel & Moffat 2016)
** impact of baryons in galaxy formation is difficult to simulate a priori

Fig. 31-9: Dark matter and modified gravity advantages and shortcomings.

Anyway, the discovery of the CMB in 1965 and its measurement in 1973 made clear that Big Bang Nucleosynthesis tells that **a small part only of the critical density is due to baryons,** and one must draw consequences. A large variety of theoretical models try to address the problem, but on the experimental side most of the activity so far concentrated on the **search for new particles** with sizeable couplings to SM ones and masses above the EW scale. However, particles explaining phenomena may be at lower scale and too feebly interacting with SM ones to have offered their detection. They would belong to the so-called **hidden or dark sector** that we explore briefly in the next chapters.

31.1.3 Dark Matter: Hypotheses and classification

Let us assume that dark matter is a **cosmological reality** attributed to the existence of **new particles or objects.**

Figure 31-10 recalls the extreme variety of hypotheses considered as to its nature, covering nearly 20 orders of magnitude in mass, from 10^{-22} eV to primordial black holes of tens of solar masses [995].

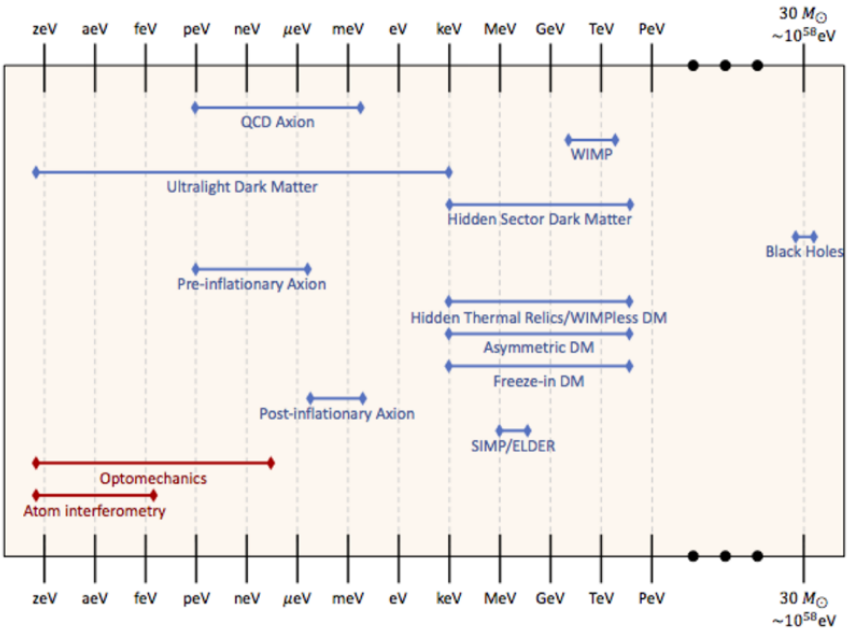
Our ignorance of **the properties of DM** is also extreme. However, it seems to be **non-self-interacting**.

A classification is provided by the **DM production mechanism** in the early Universe. Assuming a **thermal production**, through interactions with the SM in the early Universe, in standard or not standard cosmologies, the viable DM masses are restricted to the few keV to 100 TeV range (e.g. **WIMPS and hidden sector (HS) particles**). On the contrary **ultralight sub-eV particles** must be

[994] C. Deffayet and R. P. Woodard, The Price of Abandoning Dark Matter Is Nonlocality. https://arxiv.org/abs/2402.11716
R. P. Woodard, The case for non-local modifications of gravity. https://arxiv.org/abs/1807.01791
Nonlocal modifications of gravity may be seen not as new fundamental theories but rather as the gravitational vacuum polarization engendered by infrared quanta produced during primordial inflation.

[995] Lower limit to have a sufficiently short de Broglie wavelength to form dwarf galaxies.

produced non-thermally (e.g. **QCD axion and axion-like particles**) and allow for different cosmological histories. See Section 31.2.



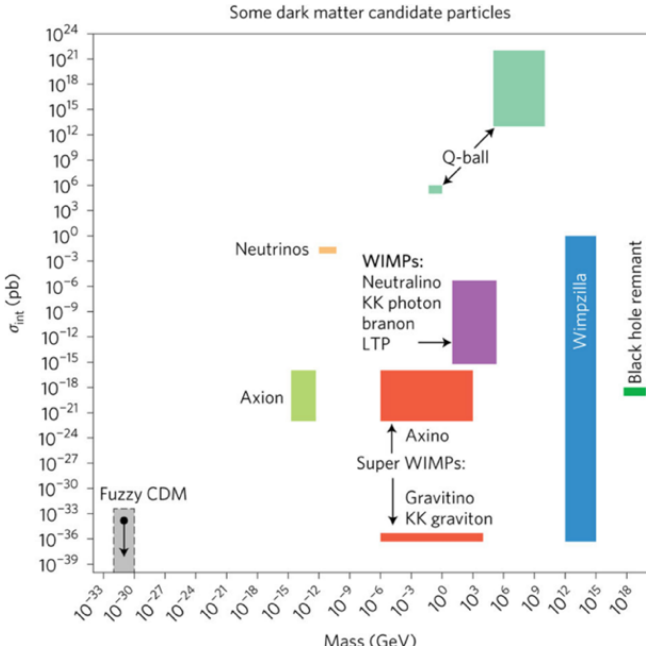


Fig. 31-10: The variety of hypotheses on the nature of DM. Top: Figure taken from Ref. [996]. Summary of some among the dark matter candidates and their mass compared to the range of parameters covered by atom interferometry and optomechanical set-ups, proposed to test light DM candidates. Bottom: Figure taken from Ref. [997].

[996] A. Belenchia *et al.,* Quantum physics in space. https://arxiv.org/abs/2108.01435
[997] S. Crépé-Renaudin, Dark matter search at ATLAS with top quarks. https://indico.in2p3.fr/event/18239/contributions/71544/attachments/53177/69107/topDM_topLHCFrance2019f.pdf

Concerning its interactions, DM, as part of a **dark sector** (**DS**), may interact only gravitationally with SM matter, or through new particles charged under the SM gauge group directly coupled to DM. It may also interact via **DS mediators** (neutral under the SM gauge group) **interacting/mixing with a SM operator**, called **a portal,** as, according to spin:

- the **Higgs Portal**: Dark Higgs,
- the **Fermions Portal**: Sterile Neutrinos (see Chapter 19),
- the **Pseudoscalar Portal**: Axions (and ALPS) which will be treated in Section 31.3,
- the **Vector Portal**: Dark photons.

It may be that DM itself carries SM charges, as part of an extended BSM sector with many new states carrying SM quantum numbers. Then a **preserved symmetry** distinguishing between SM and BSM particles makes **the DM particle stable** (as in SUSY). In such BSM theories, made to solve other problems, DM is usually referred to as **Weakly Interacting Massive Particles (WIMPs**) (see Section 31.2).

Given the range of possible masses for these objects, one can distinguish several regions, corresponding to different physics and search techniques. In decreasing mass:

- **massive compact objects** (Section 31.4),
- **WIMPs** (Section 31.2),
- **few keV-GeV dark matter** (FIMPs, Section 31.2),
- **very weakly coupled sub-eV particles, as Axions and ALPS** (Section 31.3).

31.1.4 The three types of Dark Matter searches

The three types of research performed are [998]: **direct and indirect research** of cosmic DM and possible **"human" production** of DM particles (Fig. 31-11). Direct detection uses collision of cosmic DM on a detector. Indirect detection includes indirect **astrophysical searches** for the annihilation products of DM (namely gamma-rays, neutrinos, antiparticles).

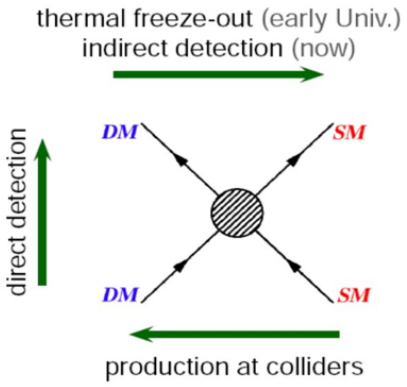


Fig. 31-11: The three types of DM searches [999].

[998] R. Cebrian, Review on dark matter searches. https://arxiv.org/abs/2205.06833
Physics Briefing Book: Input for the European Strategy for Particle Physics Update 2020. CERN-ESU-004, 1910.11775, chapter 9, and references therein. https://arxiv.org/abs/1910.11775
D. F. Jackson Kimball and K. van Bibber, The Search for Ultralight Bosonic Dark Matter.
https://link.springer.com/book/10.1007/978-3-030-95852-7
[999] C. Weniger, Dark matter – Evidence and Candidates. ISAPP School 2019 – The dark side of the universe,
https://www.mpi-hd.mpg.de/lin/_isapp2019/talks/ISAPP2019-Weniger_1.pdf

At present, **direct detection (DD)** searches have excluded spin-independent (spin-dependent) DM-nucleon cross sections as low as 10^{-46} cm^2 (10^{-41} cm^2). Figure 31-12 gives the exclusion limit from DD (we will see more in Section 31.2) and an example of **indirect detection (ID).**

Besides direct and indirect searches, present and future **colliders** offer a unique opportunity to **create DM in the laboratory**. DM can be produced directly in beam-beam collisions with other SM particle(s), or in the decays of SM particles or yet undiscovered BSM states.

The simplest collider process is the production of the **mediator particle**, which subsequently decays into DM. Final states from such processes offer $\mathbf{p_T^{miss}}$ **accompanied by at least one visible object**, such as a jet, lepton, photon (the so-called "mono-X" searches) or a larger system.

But the mediator, produced at colliders by the interaction of SM particles, can also decay back to those SM particles. Thus, one can search for DM indirectly, via visible resonances due to mediator production.

Simplified benchmark models [1000], used to guide searches, consist of a DM candidate and a mediator particle, the mediator being a new BSM state or a known object mixing with a new one.

Beyond simplified models, it is well known that **Extended Dark Sectors** of particles also exist, based on SUSY, Extra Dimensions, or extended scalar sectors, topics presented elsewhere in the document.

Besides colliders, DM and Dark Sectors searches are also performed at **beam-dump, fixed-target and LHC forward experiments,** as presented in Fig. 31-13, which shows the current limits and expected sensitivities of a list of experiments for dark photon mediators decaying to SM particles, as a function of ε (the mixing between the photon mediator and the SM photon that defines the SM-mediator coupling) and the mediator mass.

Ultralight DM (lighter that about 0.7 keV) must be **bosonic** and the effects of halo DM in terrestrial experiments are best described as **wavelike disturbances**. A particularly compelling candidate for ultralight DM is the **QCD axion**, see Section 31.2, whose mass can be in the range 10^{-12} to 10^{-3} eV.

31.1.5 Short overview of DM search techniques

For additional information, a few general plots shown in Figs. 31-14 to 31-16 provide an overview of the DM search techniques, from Ref. [1001].

Let us now focus more precisely on two sectors of all DM candidates:

i. Weakly Interacting Massive Particles (WIMPS) and FIPs, their extension towards low mass;
ii. Axions and similar objects, called ALPs.

[1000] CMS Collaboration, Dark sector searches with the CMS experiment. https://arxiv.org/abs/2405.13778
[1001] US Cosmic Visions: New Ideas in Dark Matter 2017: Community Report. https://arxiv.org/abs/1707.04591

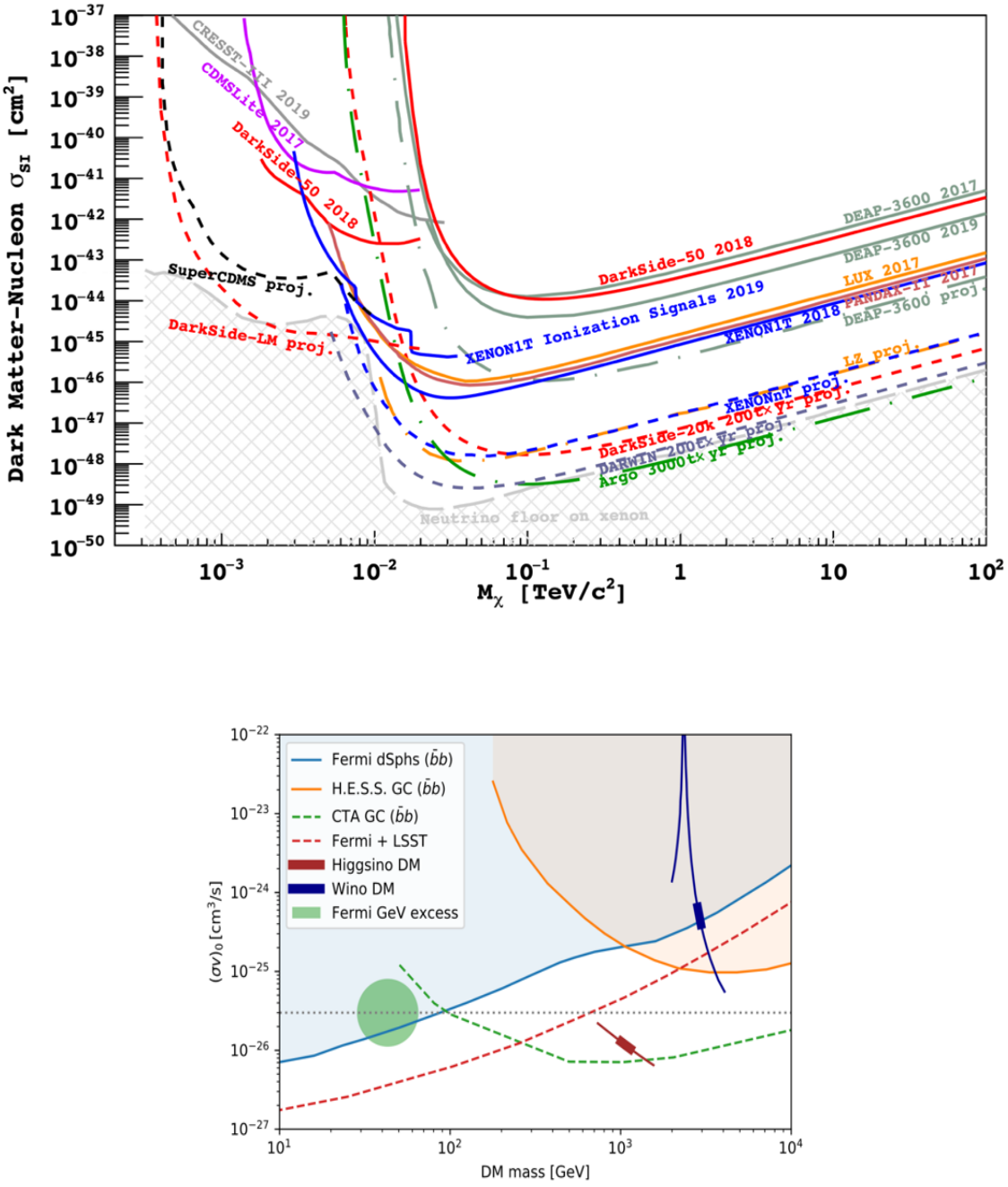


Fig. 31-12: Top: 90% CL exclusion limits showing leading results from **direct detection** (continuous lines) and the neutrino floor curve. Different types of detectors cover the low and high mass regions. Bottom: as an example of **indirect detection** from gamma-ray observations of dwarf spheroidal (dSph) galaxies, current constraints on the DM self-annihilation cross section into beauty-antibeauty from Fermi LAT (dSph, dwarf spheroidal satellite galaxies) and H.E.S.S. Galactic Centre (GC) and expected future reach with CTA [1002].

[1002] Physics Briefing Book: Input for the European Strategy for Particle Physics Update 2020. CERN-ESU-004, chapter 9, and references therein. https://arxiv.org/abs/1910.11775

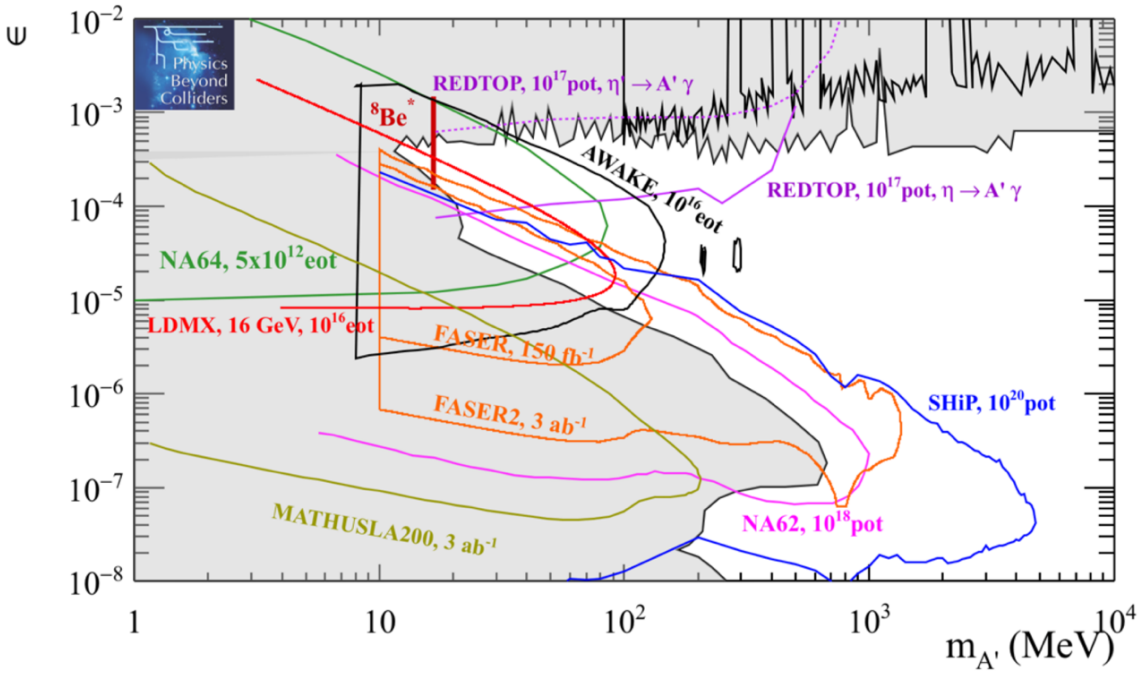


Fig. 31-13: Current limits and expected sensitivities of proposed experiments for dark photon mediator decaying to SM particles in the plane mixing strength ε versus mass $m_{A'}$. The figure lists Physics Beyond Colliders projects on a ~ 10 to 15-year timescale [1003].

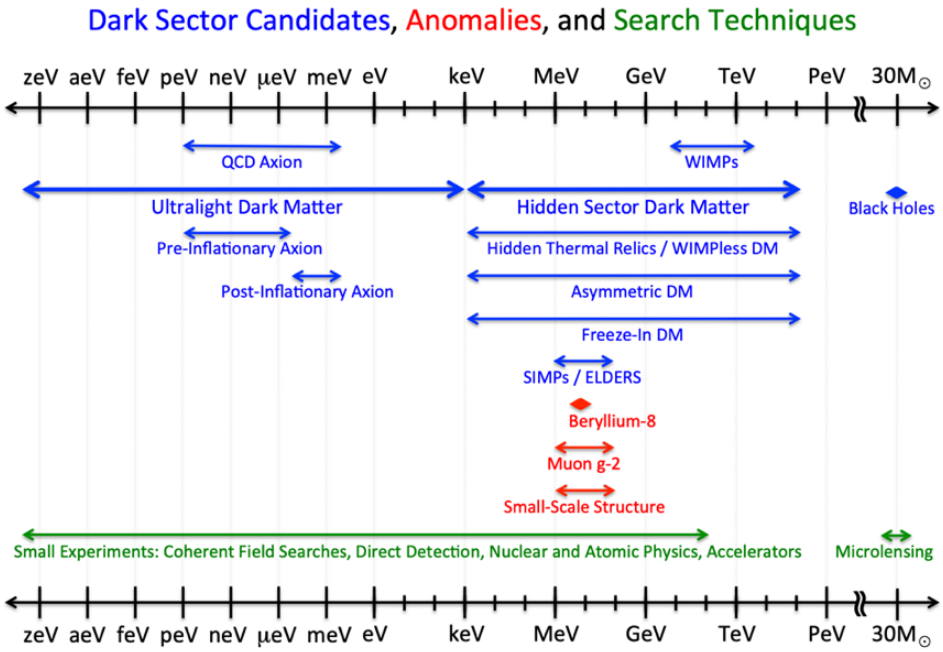


Fig. 31-14: Mass ranges for dark matter and mediator particle candidates, experimental anomalies, and search techniques.

[1003] Physics Briefing Book: Input for the European Strategy for Particle Physics Update 2020. CERN-ESU-004, chapter 9, and references therein. https://arxiv.org/abs/1910.11775

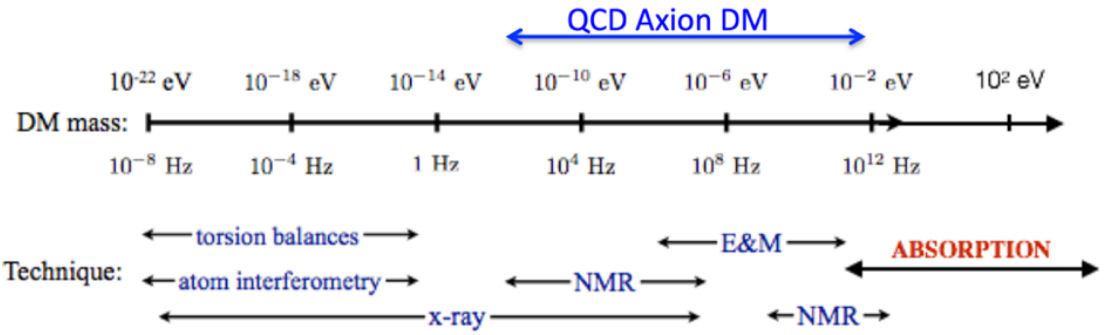


Fig. 31-15: Illustration of the complementarity of different types of experiments in exploring QCD axion DM and ultralight DM more generally. Indicative ranges of sensitivity for different techniques are shown.

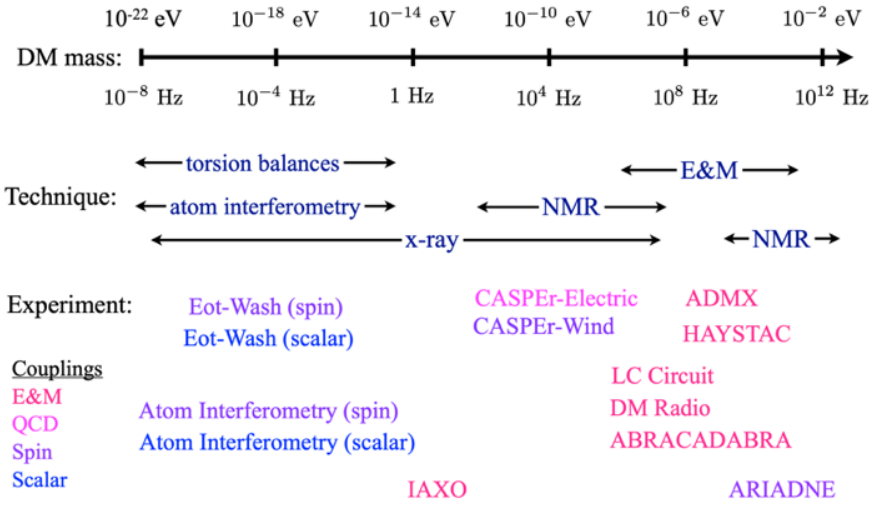


Fig. 31-16: Mass range for ultralight dark matter. Names of particular experiments and proposals.

31.2 Weakly Interacting Massive Particles and Feebly Interacting Particles

31.2.1 Characteristics of Weakly Interacting Massive Particles (WIMPs)

The so-called "**WIMP miracle**" means that "*the qualitative observation that particles with roughly weak scale O (100) GeV masses, and weak scale interactions with SM particles, will end up with about the observed thermal relic density after freeze out in standard Big Bang cosmology*".

WIMPS, candidate objects making DM, offer a simple explanation for its cosmic abundance ($\Omega_{DM} \sim 0.26$) and a connection to the EW scale. It is an ideal target via the detection of nuclear recoils and for colliders. Supersymmetry offers DM candidates up to masses of a TeV or more (see SUSY in Chapter 18).

Figure 31-17 locates WIMPS in the mass spectrum and Fig. 31-18 gives a simplified view of the expected WIMP-nucleon cross-section as a function of mass.

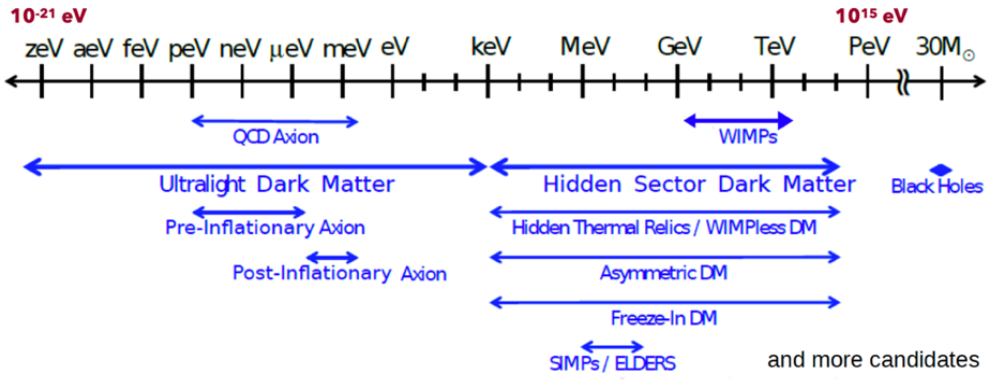


Fig. 31-17 WIMP location in mass [1004].

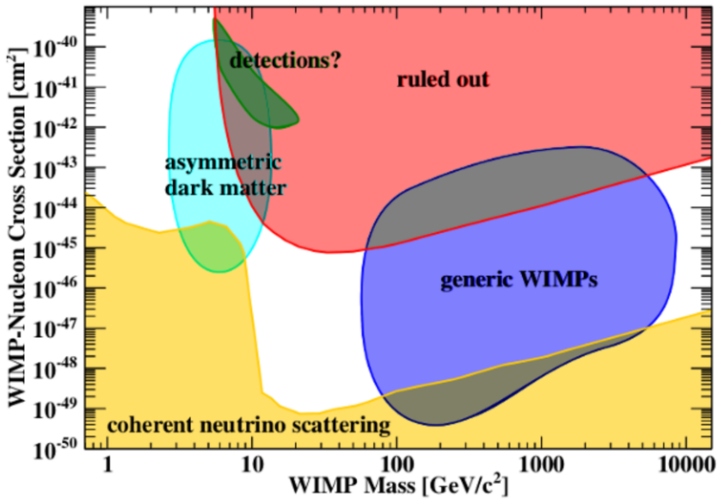


Fig. 31-18: WIMP-nucleon cross-section as function of the WIMP mass [1005].

31.2.2 WIMPs exclusion

Figure 31-19 gives, as a function of mass, the limits reached on their cross section of interaction with the nucleon. One sees a clear loss of sensitivity at low mass. Figure 31-20 illustrates the progress made on the Wimp exclusion, with a figure looking like an inverse Moore law.

[1004] B. von Krosigk, Direct Dark Matter Searches. 32nd Rencontres de Blois, France, 2021, https://indico.cern.ch/event/997281/contributions/4574201/attachments/2330505/3971353/von%20Krosigk.pdf
L. Hsu, Particle-like Dark Matter. ICHEP 2020 Prague/Virtual Conference, https://indico.cern.ch/event/868940/contributions/3905692/attachments/2084342/3501375/ichep2020_dm_plenary_hsu.pdf
A similar plot is presented in Direct Detection of Dark Matter – APPEC Committee Report 2021, https://arxiv.org/abs/2104.07634

[1005] R. F. Lang, Ups and Downs in the Search for Dark Matter. https://physics.aps.org/articles/v6/136#

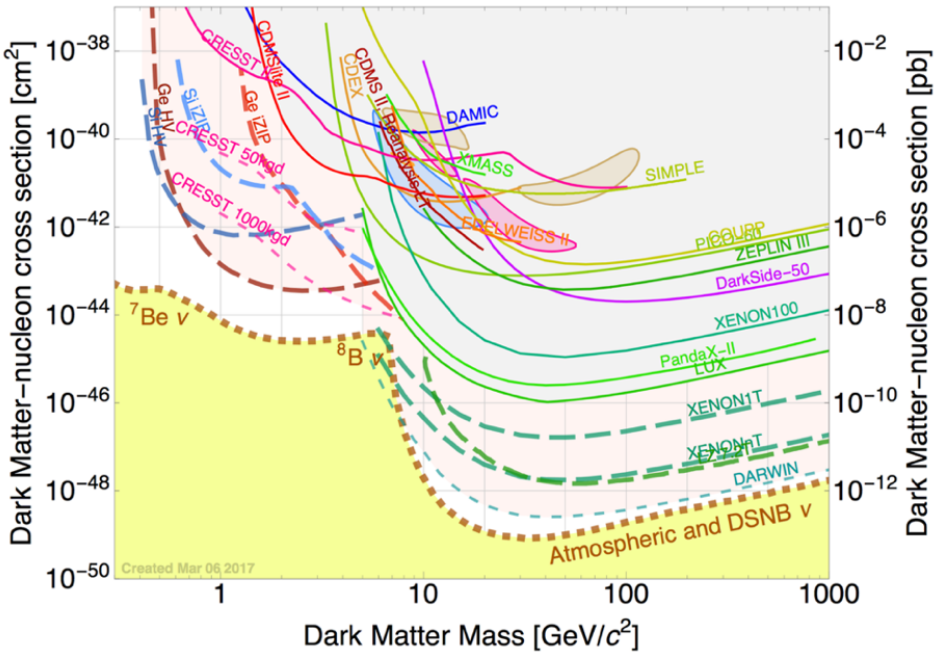


Fig. 31-19: DM-nucleon cross section as function of the DM mass. Exclusion limits reached [1006].

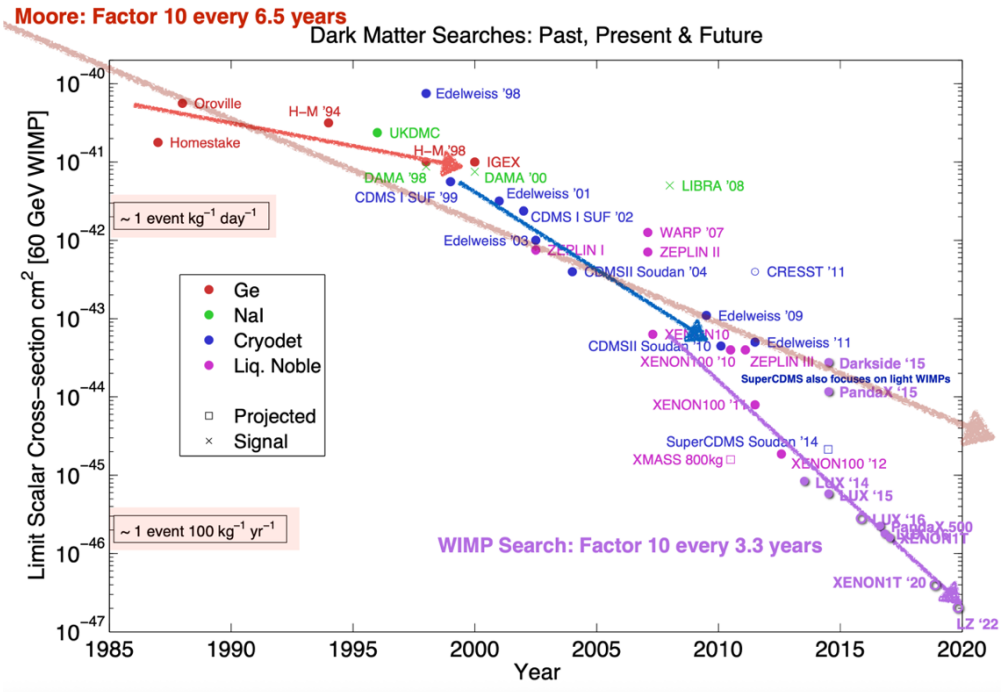


Fig. 31-20: Progress of the WIMP exclusion [1007].

[1006] R. Gaitskell, Understanding WIMP Searches.
https://indico.cern.ch/event/591895/contributions/2602723/attachments/1476295/2287042/170613_Invisibles_Zurich_WIMPS_DM_Gaitskell.pdf
[1007] ibid

Figure 31-21 shows a sketch of an **experiment of direct search,** the XENON1T Dark Matter Experiment, and its reach. Presently the largest ones are XENONnT at Gran Sasso National Laboratory (LNGS), PandaX-4t in China, LZ in the US and DEAP-3600 in Canada. The DarkSide-20k at LNGS (liquid argon) is to come in operation. The DARWIN/XLZD experiment [1008] is a next-generation DM detector with a multi-ten-ton liquid Xenon

time projection chamber. For the challenge that larger masses of Xenon would represent see Ref. [1009].

Solid-state detectors as CRESST and SuperCDMS, lowering their thresholds, aim at 100 MeV DM masses through nuclear recoils.

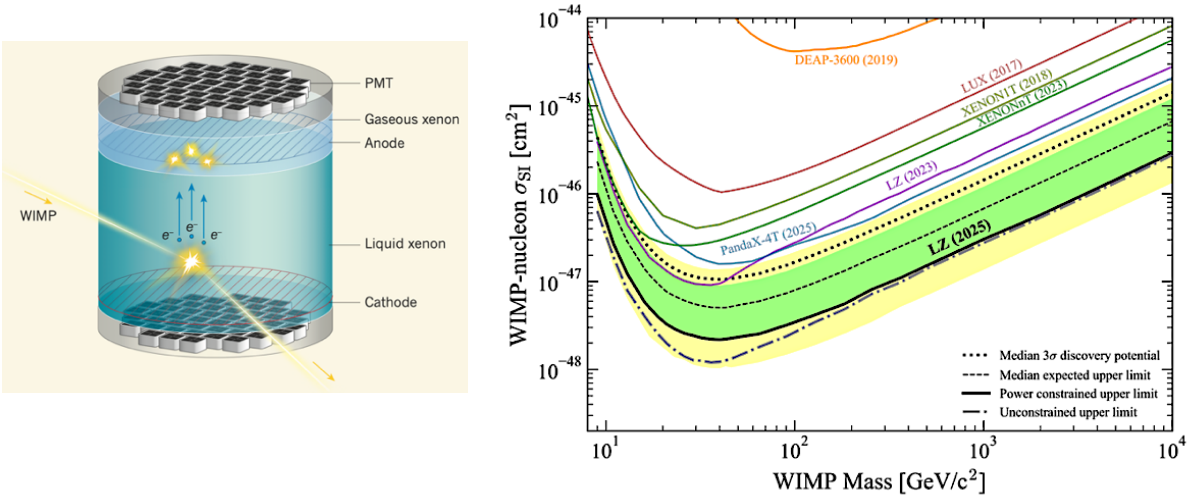


Fig. 31-21: Dual-phase Xenon detection technology (left) and present upper limits (90% CL) on the spin-independent WIMP-nucleon cross section as a function of WIMP mass from different experiments (right) [1010].

Figure 31-22, close variant of Fig. 31-19, gives an overview of the situation concerning Wimp direct searches. It shows that searches are approaching the **"neutrino floor"**, where background from astrophysical ν will swamp the signal of nuclear recoil from interactions of halo wimps. Together, the future experiments quoted aim to explore the WIMP parameter space in the neutrino background.

31.2.3 Complementarity with collider results

There is a nice complementarity between collider results and direct and indirect searches. The comparison of sensitivities is possible within given theoretical frameworks. Let us just offer a couple of examples. Figure 31-23 gives the comparison with direct detection in the context of a **Z'-like simplified model** and Fig. 31-24 for the Higgs boson decaying to **invisible Majorana DM**.

[1008] L. Baudis, DARWIN/XLZD: a future xenon observatory for dark matter and other rare interactions. https://arxiv.org/abs/2404.19524
[1009] A. Kopec, Design Challenges for a Future Liquid Xenon Observatory. https://arxiv.org/abs/2310.00722
[1010] E. Aprile *et al.,* The XENON1T Dark Matter Experiment. https://arxiv.org/abs/1708.07051.pdf
X. Ji, Dark matter remains elusive. *Nature 542, 172–173 (2017).* https://doi.org/10.1038/542172a
J. Aalbers *et al.,* Dark Matter Search Results from 4.2 Tonne-Years of Exposure of the LUX-ZEPLIN (LZ) Experiment. https://arxiv.org/abs/2410.17036
XENON Collaboration, Search for Light Dark Matter in the Neutrino Fog with XENONnT. *Phys. Rev. Lett. 134, 111802 (2025),* https://doi.org/10.1103/PhysRevLett.134.111802

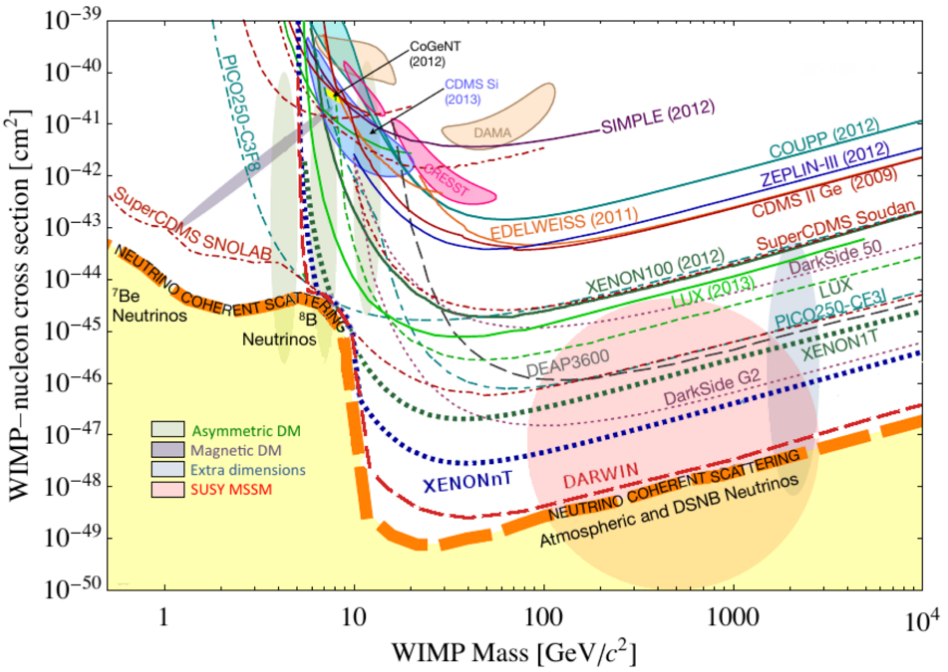


Fig. 31-22: A compilation of WIMP-nucleon spin-independent cross section limits [1011].

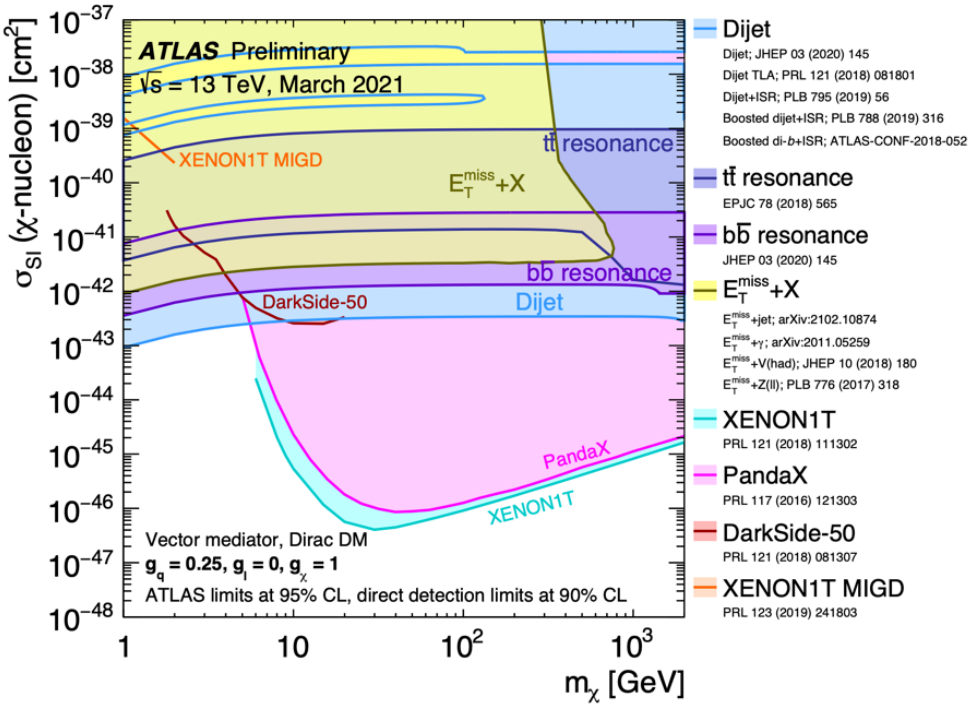


Fig. 31-23: Comparison of ATLAS limits with other experiments for direct detection limits on the spin-independent WIMP–nucleon scattering cross-section in the context of a Z'-like simplified model [1012].

[1011] L. Baudis, WIMP Dark Matter Direct-Detection Searches in Noble Gases. https://arxiv.org/abs/1408.4371
D. Bauer *et al.,* Snowmass CF1 Summary: WIMP Dark Matter Direct Detection. https://arxiv.org/abs/1310.8327
D. Buttazzo, Closing the window on wimps.
https://indico.in2p3.fr/event/29681/contributions/122536/attachments/76590/111139/05-DButtazzo-v2.pdf
[1012] ATLAS Collaboration, Dark matter summary plots for s-channel mediators. ATL-PHYS-PUB-2021-006,
https://cds.cern.ch/record/2758386/files/ATL-PHYS-PUB-2021-006.pdf

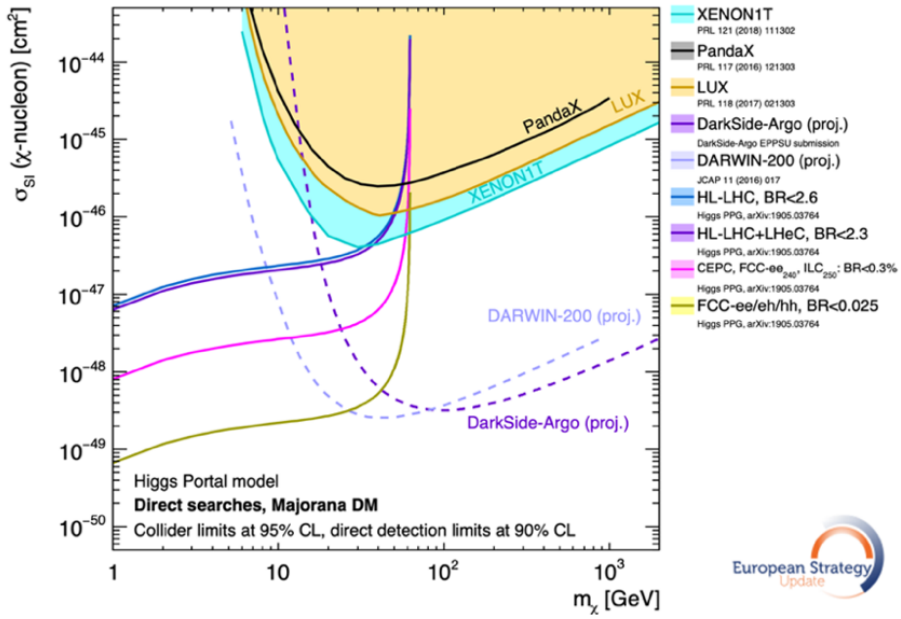


Fig. 31-24: Future colliders limits (direct searches for Higgs invisible decays) with constraints from current and future direct detection experiments on the spin-independent WIMP– nucleon scattering cross section for a simplified model with the Higgs decaying to invisible (DM) Majorana particles [1013].

The status of **SUSY searches for winos and higgsinos** at LHC has been summarized in Chapter 24 [1014] and the complementarity with indirect detection is most evident at high mass. Seen as thermal relics, their abundance fixes their mass (and mass splitting) to ~ 1.1 TeV for Higgsinos and 2.8–3.1 TeV for winos [1015].

31.2.4 Seasonal variation and directional detection

Concerning an eventual **seasonal variation of WIMP detection**, linked to the speed of Earth, Fig. 31-25 shows some tension (euphemism) between similar experiments: the left plot is from Ref. [1016], the right plot is from Ref. [1017].

The interest of a **directional detection of WIMPs** is based on the specific signature of galactic dark matter. Table 31-2 [1018] lists the corresponding programs and Figs. 31-26 and 31-27 present the results.

[1013] Physics Briefing Book: Input for the European Strategy for Particle Physics Update 2020. CERN-ESU-004, https://arxiv.org/abs/1910.11775 chapter 9, p. 149 and references therein

[1014] ATLAS Collaboration, Search for chargino–neutralino pair production in final states with three leptons and missing transverse momentum in √s = 13 TeV *pp* collisions with the ATLAS detector. https://arxiv.org/abs/2106.01676
CMS Collaboration, Combined searches for electroweak production of winos, binos, higgsinos, and sleptons in proton-proton collisions at √s = 13 TeV. *Phys. Rev. D 109 (2024) 112001*
https://journals.aps.org/prd/abstract/10.1103/PhysRevD.109.112001 For comments see https://arxiv.org/abs/2403.14759 and https://arxiv.org/abs/2404.19338

[1015] E. Bagnaschi *et al.,* Likelihood Analysis of the Minimal AMSB Model.
https://cds.cern.ch/record/2239331/files/arXiv:1612.05210.pdf
M. Beneke, R. Szafron and K. Urban, Sommerfeld-corrected relic abundance of wino dark matter with NLO electroweak potentials. https://arxiv.org/abs/2009.00640

[1016] S. Cebrián, Review on dark matter searches. https://arxiv.org/abs/2205.06833

[1017] G. H. Yu *et al.,* Limits on WIMP dark matter with NaI(Tl) crystals in three years of COSINE-100 data.
https://arxiv.org/abs/2501.13665

[1018] S. Cebrián, Review on dark matter searches. *2023 J. Phys.: Conf. Ser. 2502 012004,*
https://iopscience.iop.org/article/10.1088/1742-6596/2502/1/012004

Both plots are from Ref. [1019]. Figure 31-26 gives the flux of 100 GeV WIMPs with a speed greater than that required to give 25 keV of recoil to the Fluor nucleus.

Figure 31-27 shows an example of the discovery limit. Top curves: low threshold and mass detector (0.1 keV, 0.1 ton). Bottom curves: high threshold and mass detector (5 keV, 10^4 ton).

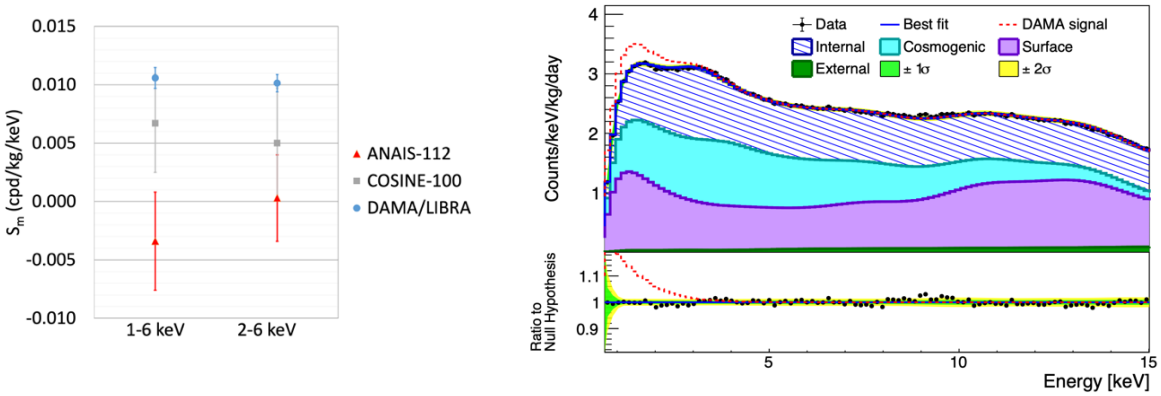


Fig. 31-25: Left: Results on modulation amplitudes obtained by DAMA/LIBRA, ANAIS-112 and COSINE-100 experiments in the energy regions of 1-6 keV_{ee} and 2-6 keV_{ee} (electron-equivalent energy). Right: COSINE-100 3-year data, the expected spectrum based on DAMA/LIBRA's observation is shown as a red dashed line.

Experiment	Technique	Laboratory	Size
DRIFT	TPC+MWPC	Boulky (UK)	1 m^3
MIMAC	TPC+Micromegas	LSM (France)	1 m^3 (in prep)
NEWAGE	TPC+μPIC	Kamioka (Japan)	31×31 cm^2, 41 cm drift
DMTPC	TPC+optical readout	WIPP (US)	1 m^3 (in prep)
CYGNO	TPC+optical readout	LNGS (Italy)	1 m^3 (in prep)
NEWS-dm	Emulsion+optical readout	LNGS (Italy)	10 g (prototype)

Table 31-2: Properties of current or beginning directional experiences.

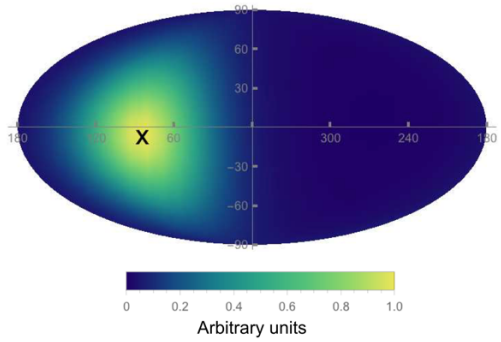


Fig. 31-26: Map of the WIMP flux in Galactic coordinates. The direction of v_{lab} is indicated as a cross on the map.

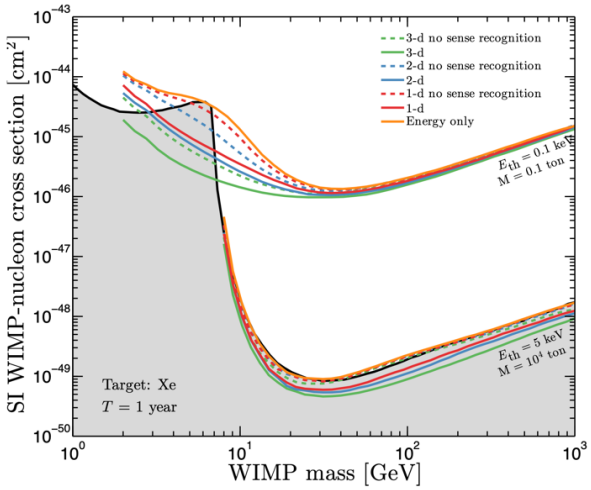


Fig. 31-27: Discovery limits with different detector scenarios.

[1019] F. Mayet *et al.,* A review of the discovery reach of directional Dark Matter detection. https://arxiv.org/abs/1602.03781

31.2.5 Feebly interacting particles: few keV – GeV light dark matter

Feebly interacting particles (**FIPs or FIMPs**) are defined by having extremely suppressed interactions with the SM. They are potential thermal DM candidates, extending WIMPs towards low masses.

As already said, the new physics might be **light and very weakly coupled.** Feeble DM interactions are phenomenologically motivated and even predicted in models that explain the present DM abundance from dynamical processes in the early Universe. So, the reason of negative results is not the lack of energy, but the problem of detection, luminosity, background or detector performance.

It is assumed that **light dark matter (LDM)** [1020], not seen at LEP, must be neutral under SM gauge interactions and requires a light mediator between SM and Dark Sector, which can decay either to LDM or to SM through the portal couplings.

Exploring this case over a large range of couplings/masses requires a variety of facilities [1021].

The cosmic history of FIMP DM (Fig. 31-28) often leads to predict **long-lived** mediator particles in laboratory experiments. LHC plays a role in searching for such particles, in complementarity with **low-energy experiments**, beam dump and missing-energy experiments. See Fig. 31-29 [1022].

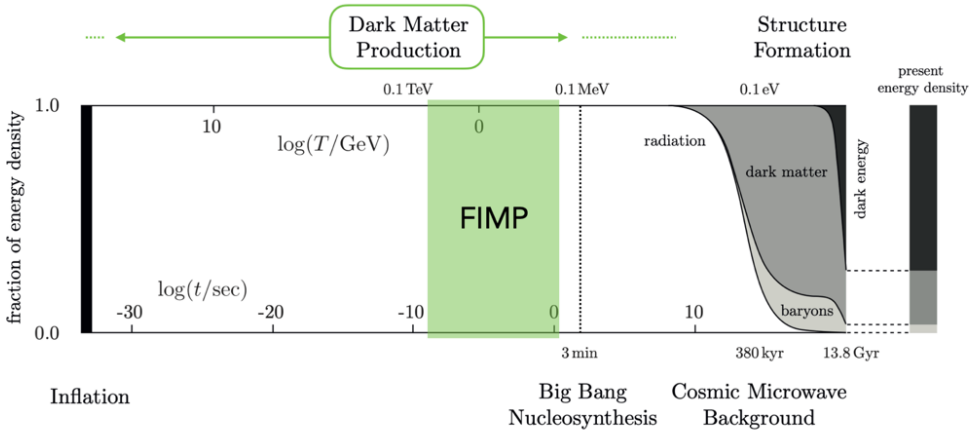


Fig. 31-28: FIMPs location in the timeline of Universe [1023].

Reference [1024] summarizes the various types of FIPS, classified according to the **portal** giving access to them, and explains how to detect them. Of the portals listed in Section 31.1, let us consider here the Vector Portal and dark photon mediators.

Figure 31-30 gives current limits and expected sensitivities of proposed experiments for **dark photons mediators** decaying to LDM. For the same decaying to SM particles see Fig. 31-13. It also lists the actors, present or future.

To end the tour, in Section 31.3 we will finally consider very weakly coupled sub-eV particles, as **Axions.**

[1020] Physics Briefing Book: Input for the European Strategy for Particle Physics Update 2020. CERN-ESU-004, https://arxiv.org/abs/1910.11775 , chapters 2, and 9
see also https://cerncourier.com/a/search-for-wisps-gains-momentum/
C. Antel *et al.,* Feebly-Interacting Particles: FIPs 2022 Workshop Report, https://arxiv.org/abs/2305.01715
[1021] Physics Briefing Book: Input for the European Strategy for Particle Physics Update 2020, https://arxiv.org/abs/1910.11775
[1022] ibid and B. Batell *et al.,* Exploring Dark Sector Portals with High Intensity Experiments. in Snowmass, 2022, https://arxiv.org/abs/2207.06905v3
[1023] S. Westhoff, FIMP Dark Matter at the LHC. https://arxiv.org/abs/2312.13373
[1024] Physics Briefing Book: Input for the European Strategy for Particle Physics Update 2020. CERN-ESU-004, https://arxiv.org/abs/1910.11775 , chapter 9

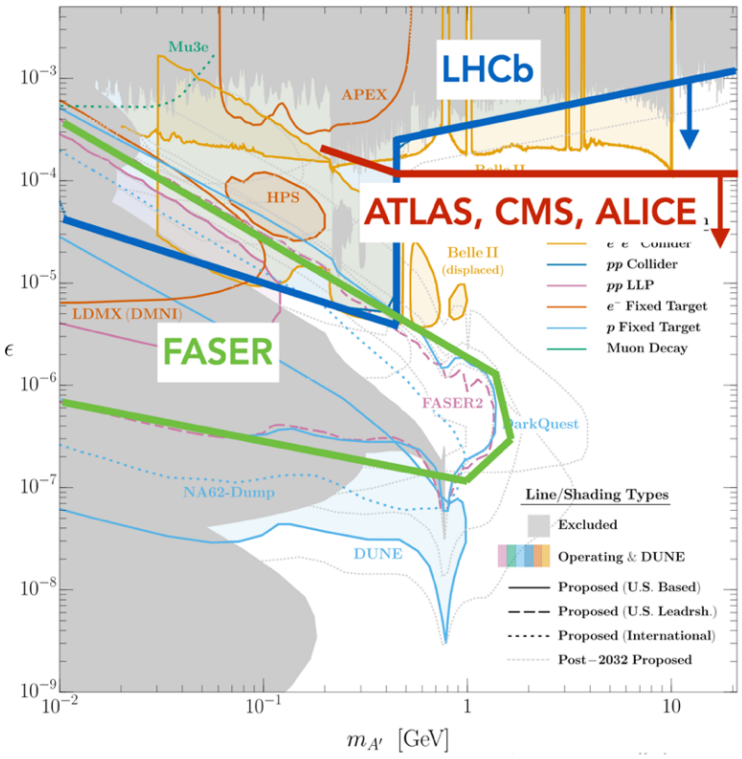


Fig. 31-29: Dark photon searches: mass versus kinetic mixing ϵ [1025].

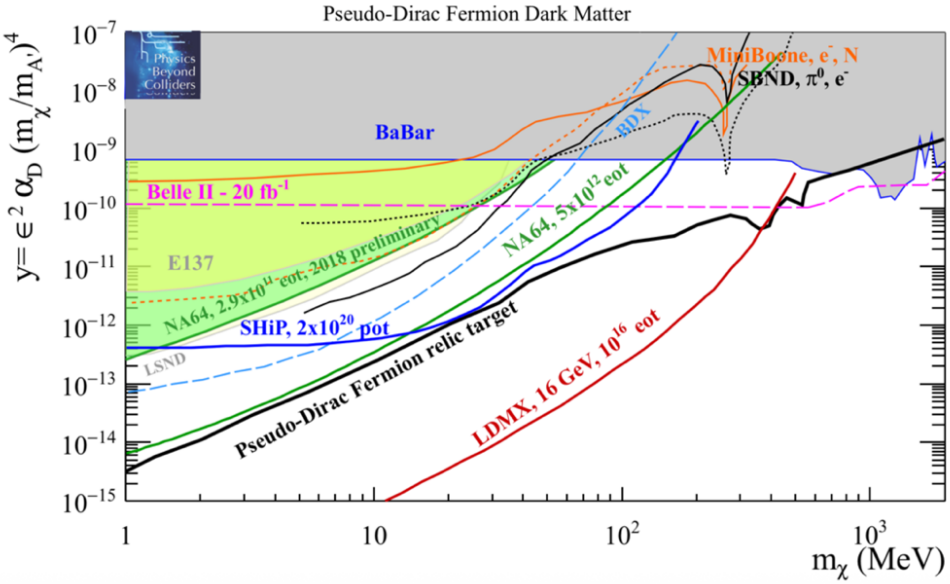


Fig. 31-30: Dark Photon decaying to Pseudo-Dirac fermion DM particle. Prospects are compared to the current bounds (solid areas) and future experimental landscape (other solid and dashed lines). ε is the mixing between the dark photon mediator and the SM photon that defines the SM-mediator coupling. In the limit computation one assumes a dark coupling constant value $\alpha_D = 0.1$ and a fixed ratio of the mediator-DM masses [1026].

[1025] ibid , see also J. Beacham *et al.,* Physics Beyond Colliders at CERN: Beyond the Standard Model Working Group Report. https://arxiv.org/abs/1901.09966

[1026] ibid

31.2.6 Direct DM detection strategies

Figure 31-31 shows a nice summary of the **direct Dark Matter detection strategies**, presenting the various types of detectors according to the signals they use.

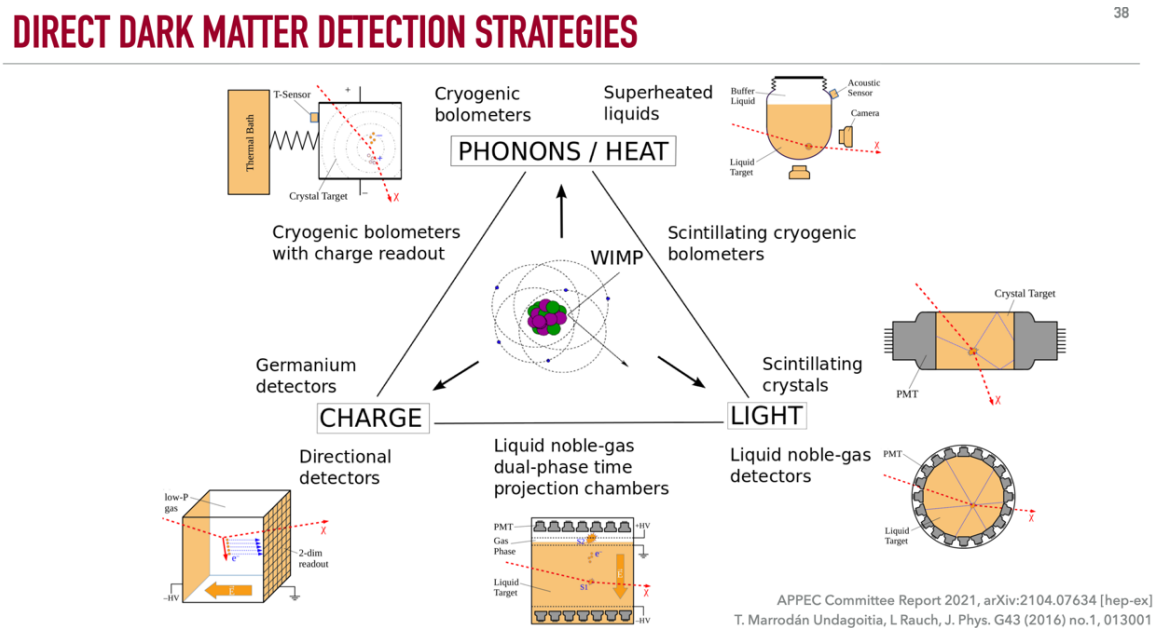


Fig. 31-31: Direct Dark Matter detection strategies [1027].

31.3 Axions and Axion-Like Particles

31.3.1 Presentation of the axion

See the delicious paper of Pierre Sikivie [1028] explaining the axion with a Pooltable analogy.

The SM quarks masses are described by the Yukawa matrices m_q. We saw in Chapter 14 that the **physical CP violation angle** is $\bar{\theta} = \vartheta - \arg(\det m_q)$, where ϑ is the coefficient of the Lagrangian term $\frac{g_s^2}{32\pi^2} G_{a\mu\nu}\tilde{G}^{a\mu\nu}$. As said in Chapter 14, experimental upper bounds on **electric dipole moments** (Section 32.2) require $\bar{\theta} < 10^{-10}$. We must understand why gluon topological effects, as alluded to in Section 7.4.5, do not generate large CP violation in QCD.

The popular solution is through the **Peccei–Quinn (PQ) mechanism** [1029], introducing a new global anomalous symmetry which is then **spontaneously broken at the PQ scale f_a**, giving rise to a **pseudo-Nambu–Goldstone boson (PNGB) called axion** [1030]. The axion ground state dynamically forces the

[1027] B. von Krosigk, Dark Matter Searches. 32nd Rencontres de Blois, France, 2021, https://indico.cern.ch/event/997281/contributions/4574201/attachments/2330505/3971353/von%20Krosigk.pdf
[1028] P. Sikivie, The Pooltable Analogy to Axion Physics. https://arxiv.org/abs/hep-ph/9506229
[1029] R. D. Peccei The Strong CP Problem and Axions. https://arxiv.org/abs/hep-ph/0607268
[1030] Recap: **Nambu–Goldstone bosons** (**NGBs**) appear necessarily in models exhibiting spontaneous breakdown of continuous symmetries. They are massless if the spontaneously broken symmetry is not also explicitly broken. If, instead, the symmetry is not exact, i.e. explicitly broken as well as spontaneously broken, then the bosons that emerge are not massless, though they typically remain relatively light, and are called pseudo-Nambu–Goldstone bosons.

theory to be CP-symmetric by setting $\bar{\theta} = 0$. The idea is thus to effectively **promote $\bar{\theta}$ to a field a(t,x)** for which the value a = 0 is energetically favourable.

Box 31-1 recaps some algebra relevant to the PQ mechanism [1031]. For a primer on axion see Ref. [1032].

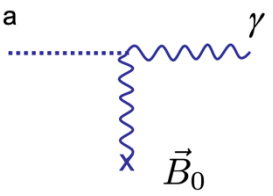
Gauge interactions are invariant under chiral transformations.
Let us consider the Yukawa term of the Lagrangian.

$L_Y = -G_d \bar{q}_L \phi d_R - G_u \bar{q}_L \phi_C u_R$ + herm.conj. with $\phi_C = i\tau_2 \phi^*$

The first term is invariant under

$q_L \to \exp(-\frac{i\alpha}{2}) q_L \quad d_R \to \exp(+\frac{i\alpha}{2}) d_R \quad u_R \to \exp\left(+\frac{i\alpha}{2}\right) u_R$, if $\phi \to \phi \exp(-i\alpha)$

But ϕ_C does not behave as ϕ. PQ introduced a second Higgs doublet ϕ_2 to replace ϕ_C and transforming as ϕ. The Yukawa term and the full Lagrangian have an extra $U(1)_{PQ}$ symmetry which allows to rotate θ to zero. The strong CP problem is solved, but the price to pay is to introduce the axion, a Goldstone boson not "eaten" in the symmetry breaking.



Name	Equations
Gauss's law	$\nabla \cdot \mathbf{E} = \rho - g_{a\gamma\gamma} \mathbf{B} \cdot \nabla a$
Gauss's law for magnetism	$\nabla \cdot \mathbf{B} = 0$
Faraday's law	$\nabla \times \mathbf{E} = -\dot{\mathbf{B}}$
Ampère–Maxwell law	$\nabla \times \mathbf{B} = \dot{\mathbf{E}} + \mathbf{J} + g_{a\gamma\gamma} (\dot{a}\mathbf{B} - \mathbf{E} \times \nabla a)$
Axion field's equation of motion	$\ddot{a} - \nabla^2 a + m_a^2 a = -g_{a\gamma\gamma} \mathbf{E} \cdot \mathbf{B}$

Box 31-1: Top left: the axion [1033]; top right: axion conversion to γ . Bottom: Maxwell equations with axion [1034] (Figure by P. Sikivie).

The axion gets its mass $m_a \approx m_\pi f_\pi / f_a$ by coupling to the QCD condensate, with an inverse **relation between mass and PQ scale**, but the value is unknown.

The axion's interactions are set by its **pseudo-scalar nature**. One expects the axion's couplings to be inversely proportional to the scale of symmetry breaking, thus proportional to its mass. Mixing with π^0 generates **coupling of axions to γ**. Axions can thus be detected [1035] by **converting them to γ in a strong magnetic field**, motivating most experiments. $L_{a\gamma\gamma} = \frac{1}{4} g_{a\gamma\gamma}\, a\, F_{\mu\nu} \tilde{F}^{\mu\nu}$ (remember $F_{\mu\nu} \tilde{F}^{\mu\nu} \sim \vec{E} \cdot \vec{B}$) defines the coupling [1036]. Via its coupling to nuclear and electron spins, axion DM would cause them to precess, as in a magnetic field.

[1031] For an alternative to the axion to solve the strong CP problem see F. Feruglio *et al.,* Solving the strong CP problem without axions. https://arxiv.org/abs/2406.01689
[1032] F. Yu, Primer on Axion Physics, https://arxiv.org/abs/2308.08612
F. Chadha-Day, J. Ellis and D. J. E. Marsh, Axion Dark Matter: What is it and Why Now? https://arxiv.org/abs/2105.01406
[1033] See Chapter 5 of the excellent book of P. D. B. Collins, A. D. Martin, E. J. Squires, Particle Physics and Cosmology, Copyright © 1989 by John Wiley & Sons, Inc.
[1034] https://en.wikipedia.org/wiki/Axion
[1035] P. Sikivie, Invisible Axion Search Methods. https://arxiv.org/abs/2003.02206.pdf
[1036] Please refer to https://arxiv.org/abs/2003.02206.pdf to see in more details the role of anomalies and the field structure of the Lagrangian, hence the specific scenarios quoted later.

31.3.2 Scenarios

One considers now **"invisible axion"** mechanisms [1037], too weakly coupled to have been already found.

By removing the relation quoted for the QCD axion, one creates the world of **ALPs** (**axion-like particles**), hypothetical light PNGBs, appearing in the spontaneous breaking of a symmetry. Masses and couplings span many orders of magnitude. In certain parameter regions they are, as axions, **good candidates for DM,** as prototype of non-thermal or freeze-in production mechanisms.

We enter here the domain of **ultra-light (sub-eV) DM**. Given their **high occupation number**, these objects ($\lesssim$ about 0.7 keV) must be **bosonic** and the effect of halo DM on experiments are more **wavelike**. Axion DM consists of the energy stored in spatial and temporal gradients, as well as potential energy, of the axion field, a(t,x). QCD effects produce an effective periodic potential in which the axion field moves. The oscillations of the axion field about the minimum of the potential, the so-called **misalignment mechanism**, generate a cosmological population of cold axions whose abundance depends on the axion mass. Quoting [1038]:*"It occurs when a particle's field has an initial value that is not at or near a potential minimum. This causes the field to oscillate around the nearest minimum, eventually dissipating energy by decaying into other particles until the minimum is attained. For axions created in the early Universe, the initial values are random because axions are massless in the hot plasma. Near QCD critical temperature, axions possess a T-dependent mass that enters a damped oscillation until the potential minimum is reached."*

As **specific axion scenarios**, let us mention the Kim–Shifman–Vainshtein–Zakharov (KSVZ) and the Dine–Fischler–Srednicki–Zhitnitskii (DFSZ) axion, which predict a specific coupling between axions and γ, guiding searches. The latter has already been excluded from 2.7 to 4.2 μeV, or 0.65 to 1 GHz.

Figures 31-32 to 31-34 give experimental and theoretical restrictions of the axion mass [1039], **showing in particular** stellar and astrophysical bounds, which give the best indications on the allowed values.

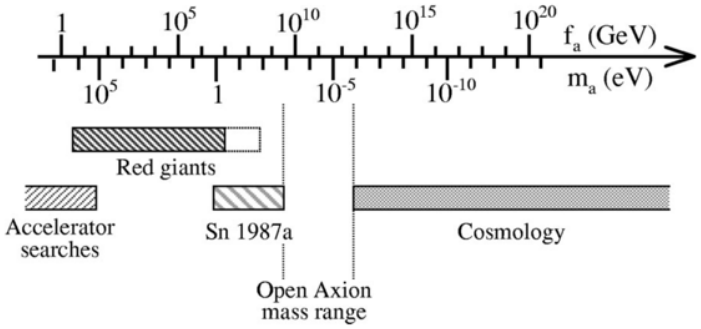


Fig. 31-32: Experimental and theoretical restrictions to axion mass [1040].

[1037] L. Darmé *et al.,* Invisible decays of axion-like particles: constraints and prospects. https://arxiv.org/abs/2012.07894
L. Di Luzio *et al.,* The landscape of QCD axion models. https://arxiv.org/abs/2003.01100
[1038] https://en.wikipedia.org/wiki/Misalignment_mechanism
[1039] L. D. Duffy and K. van Bibber, Axions as Dark Matter Particles. https://arxiv.org/abs/0904.3346
K. Saikawa, Axion as a non-WIMP dark matter candidate. https://arxiv.org/abs/1709.07091
[1040] S. J. Asztalos *et al.,* Searches for Astrophysical and Cosmological Axions. *Ann.Rev.Nucl.Part.Sci.* 56 (2006) 293-326. https://www.annualreviews.org/content/journals/10.1146/annurev.nucl.56.080805.140513,
R. Bradley *et al.,* Microwave cavity searches for dark-matter axions.
https://www.researchgate.net/publication/254744184_Microwave_cavity_searches_for_dark-matter_axions#pf6

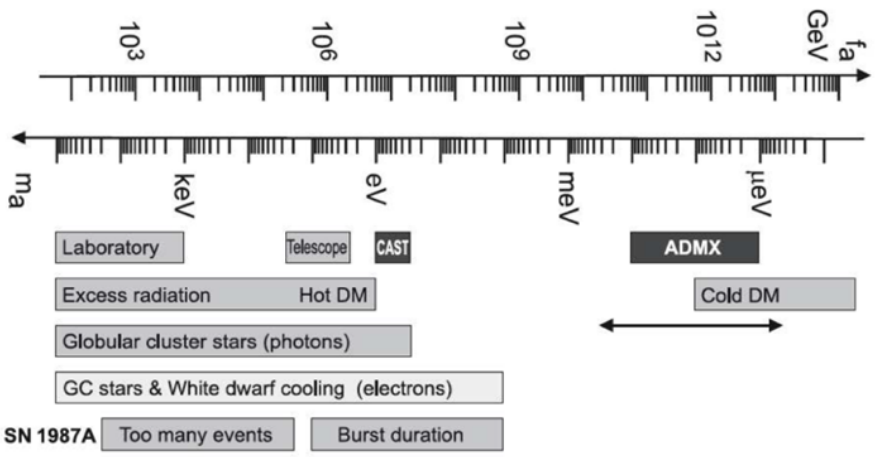


Fig. 31-33: Constraints on the PQ-scale f_a and corresponding m_a from astrophysics, cosmology and laboratory experiments [1041].

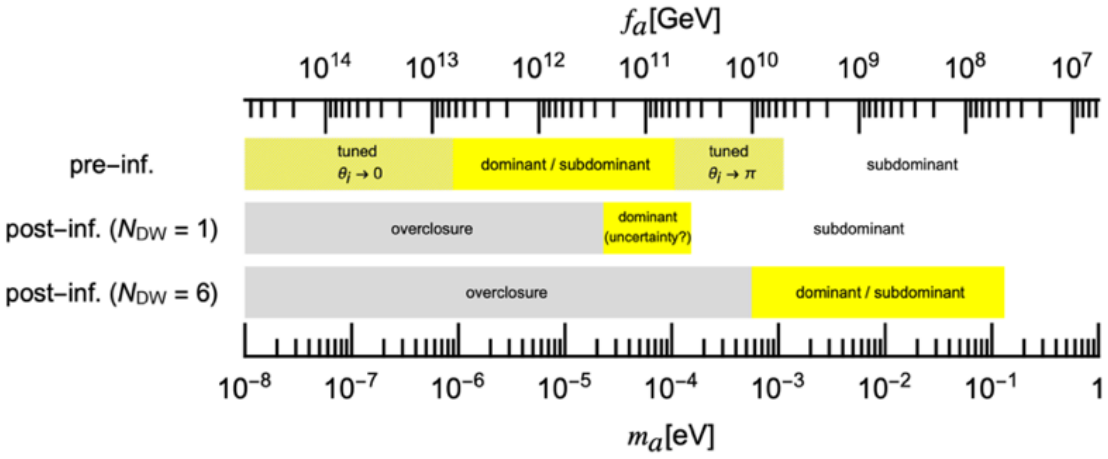


Fig. 31-34: Mass ranges predicted in various cosmological scenarios [1042].

31.3.3 Searches for axions

We will first recall the variety of the searches for axions, either **assumed as existing in the cosmos**, as DM halo, or **emitted from the sun**, or by **creating them in the lab** at colliders or from lasers. Then we will go through plots showing the results or expectations of these searches in the plane of **mass versus axion-photon coupling $g_{a\gamma\gamma}$.**

Figure 31-35 illustrates the different methods used to search for axions, as **cosmological objects,** in particular from the sun, or objects **created on Earth.**

[1041] L. D. Duffy, K. van Bibber, Axions as Dark Matter Particles. https://arxiv.org/abs/0904.3346
L. Baudis and S. Profumo, Dark Matter. https://pdg.lbl.gov/2024/reviews/rpp2024-rev-dark-matter.pdf
US cosmic vision: https://arxv.org/abs/1707.04591
[1042] K. Saikawa, Axion as a non-WIMP dark matter candidate. https://arxiv.org/abs/1709.07091

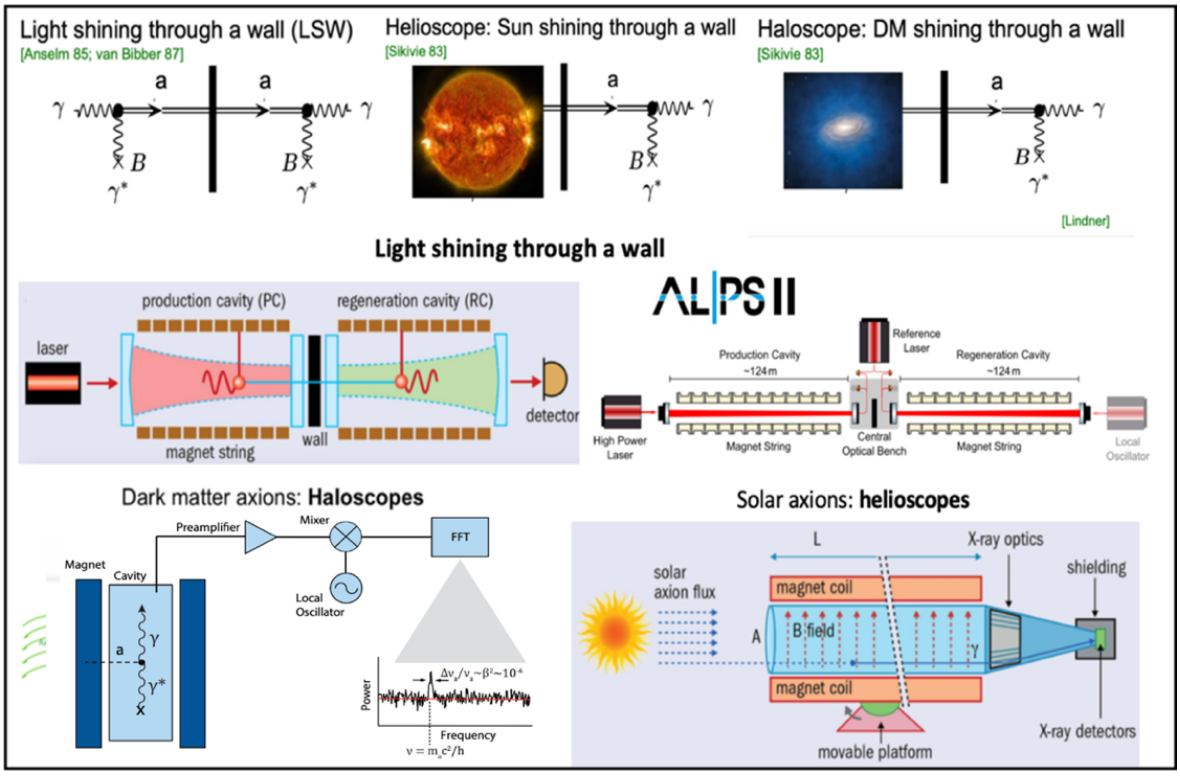


Fig. 31-35: From top: the three ways of searching for axion; light shining through a wall; halo-and helioscopes. Figure built from several references [1043].

The axion has motivated many collaborations of various sizes. The **Axion Dark Matter Experiment** (**ADMX**) uses **resonant cavities** in a powerful magnet, which amplify the signal of photons converted from DM halo axions via the Primakoff conversion occurring in the strong magnetic field, a method conceived by Pierre Sikivie. New resonant **haloscopes** attempt to extend and accelerate the frequency coverage and improve sensitivity. To probe higher axion masses above the reach of conventional cavities, new concepts are being pursued, as dielectric haloscopes and dish antenna experiments.

DESY plans three larger scale axion experiments exploiting the **light-shining-through-a-wall** technique, **solar axion** and **axion DM** searches: ALPS II, BabyIAXO and MADMAX (Magnetized Disc and Mirror Axion Experiment) [1044].
After CAST (**C**ERN **A**xion **S**olar **T**elescope), IAXO (**I**nternational **Ax**ion **O**bservatory) will be a new **axion helioscope**, searching for solar axions/ALPs with the axion-γ coupling down to a few 10^{-12} GeV^{-1}, for $m_a \leq 0.016$ eV.

Many other collaborations have flourished, as the **H**aloscope **A**t **Y**ale **S**ensitive **T**o **A**xion **C**DM (HAYSTAC) or ABRACADABRA. A list of acronyms is available at the end of the chapter.

[1043] A. Lindner *et al.*, Search for WISPs gains momentum. https://cerncourier.com/a/search-for-wisps-gains-momentum/
S. M. Lewis, Status of the ADMX-HF Experiment. https://inspirehep.net/files/a12f559c20164940fd70406ba67c0f86
[1044] D. Heuchel, A. Lindner and I. Oceano, The DESY axion search program. https://arxiv.org/abs/2302.11934
One can exploit the E-field oscillations from axions in a strong B field by using transitions between materials with different dielectric constants: at interfaces, the discontinuity of these oscillations is balanced by radiation from the surface. One can for instance use many magnetised dielectric discs in parallel placed in front of a mirror.

31.3.4 Axion exclusions

Figure 31-36 gives an overview of the relevant ALP parameter space and of the experiments exploring or to explore it [1045].

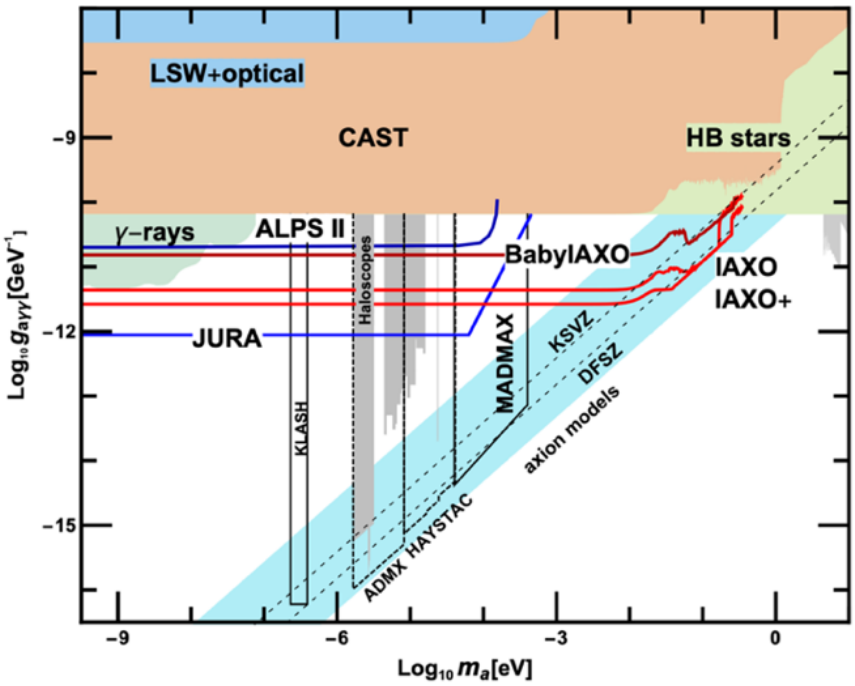


Fig. 31-36: Current exclusion of ALPs and axions coupling to photons in the sub-eV mass-scale with experimental prospects. γ-rays and Horizontal Branch stars give astrophysical limits. Pure laboratory experiments are in blue, helioscopes in red and haloscopes in grey. The turquoise shaded region indicates the typical coupling range expected for QCD axion models.

31.3.5 Collider searches

Colliders [1046] can produce ALPs resonantly or in exotic decays of the *Z* or Higgs bosons, such as $Z \rightarrow a\gamma$, $h \rightarrow aZ$, $h \rightarrow aa$. Other channels are vector boson fusion and associated production at e^+e^- colliders.

Figure 31-37 gives a summary plot of constraints on the parameter space spanned by the ALP mass and ALP-photon coupling. The right enlarged display shows the constraints from collider searches [1047].

ALPs search in heavy ion collisions (Fig. 31-38) [1048]

The production of an ALP in an ultra-peripheral ion collision proceeds via photon fusion (Fig. 31-38 left).

[1045] Physics Briefing Book: Input for the European Strategy for Particle Physics Update 2020. CERN-ESU-004, chapter 9, and references therein. https://arxiv.org/abs/1910.11775
See also I. G. Irastorza and J. Redondo, New experimental approaches in the search for axion-like particles. https://arxiv.org/abs/1801.08127
J. Jaeckel and A. Ringwald, The Low-Energy Frontier of Particle Physics. https://arxiv.org/abs/1002.0329
[1046] CERN-ESU-012 (see above), D. d'Enterria, Collider constraints on axion-like particles. https://arxiv.org/abs/2102.08971
[1047] M. Bauer *et al.,* Axion-Like Particles at Future Colliders. https://arxiv.org/abs/1808.10323
[1048] S. Knapen *et al.,* LHC limits on axion-like particles from heavy-ion collisions. https://arxiv.org/abs/1709.07110
D. d'Enterria *et al.,* Opportunities for new physics searches with heavy ions at colliders. https://arxiv.org/abs/2203.05939

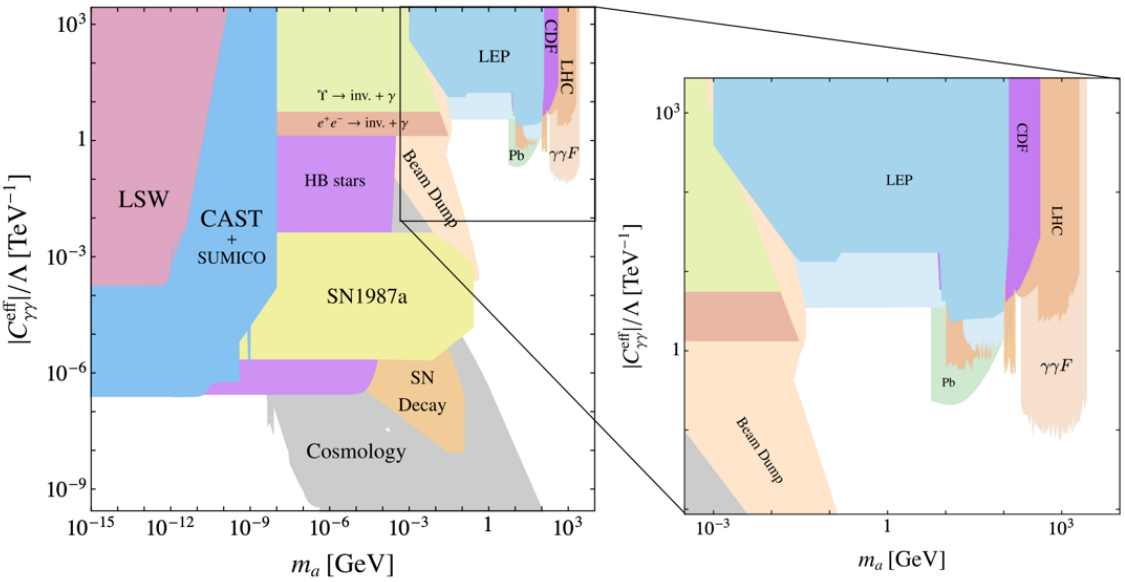


Fig. 31-37: The effective Wilson coefficients $C^{\rm eff}_{\gamma\gamma}$ determines the interactions of the ALPs with the SM particles, therefore their production and their decay. The usual decay constant of the axion f_a is related to the new physics scale Λ by $\Lambda / |C^{\rm eff}_{\gamma\gamma}| = 32\pi^2 f_a$.

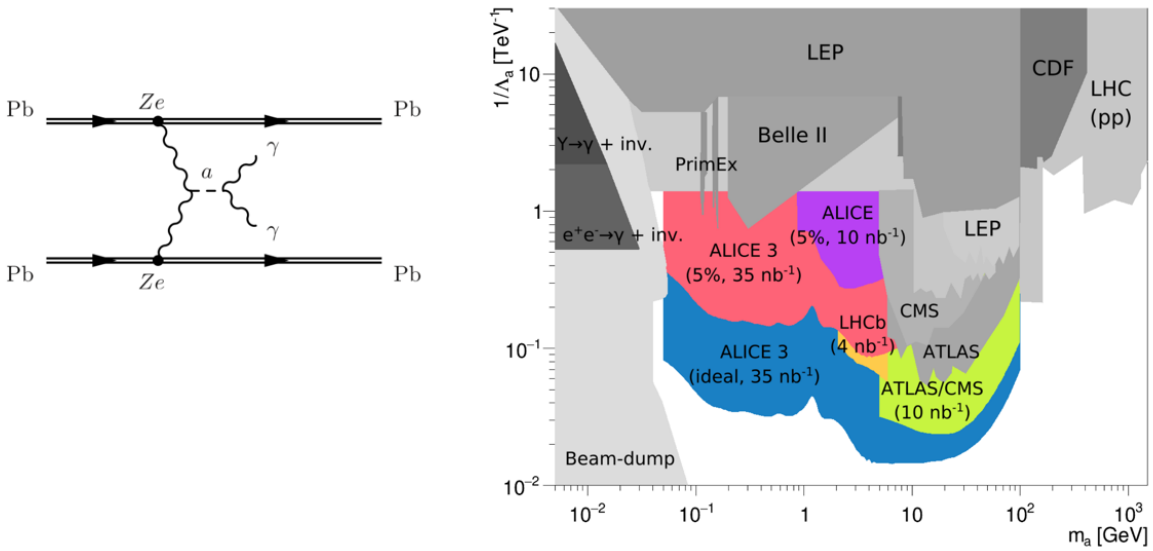


Fig. 31-38: Left: the relevant diagram for ALP production in heavy ion collisions. Right: Bounds in the (m_a, $1/\Lambda_a$) plane from existing (grey) and future (coloured, with heavy ions at the LHC) ALP searches. It is the same as Fig. 20-11.

31.3.6 Overview of searches

Figure 31-39 and the very complete Fig. 31-40 give an overview of the exclusion plot for ALP (axion)–γ coupling and offer a list of all experiments and processes involved.

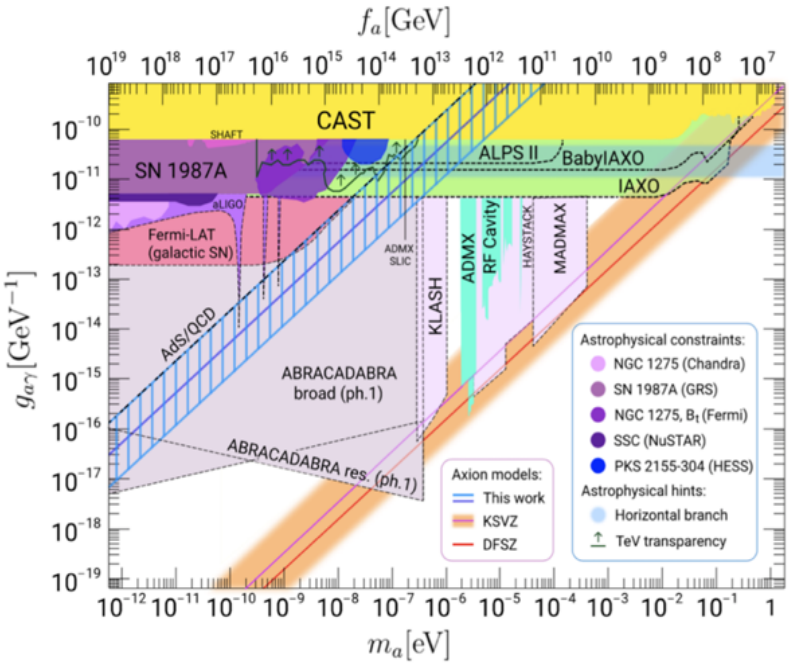


Fig. 31-39: Axion-photon coupling as a function of axion mass and decay constant for various axion models. The plot shows the existing and predicted constraints (dotted lines) from experiments together with those derived from astrophysical data and theoretical models [1049].

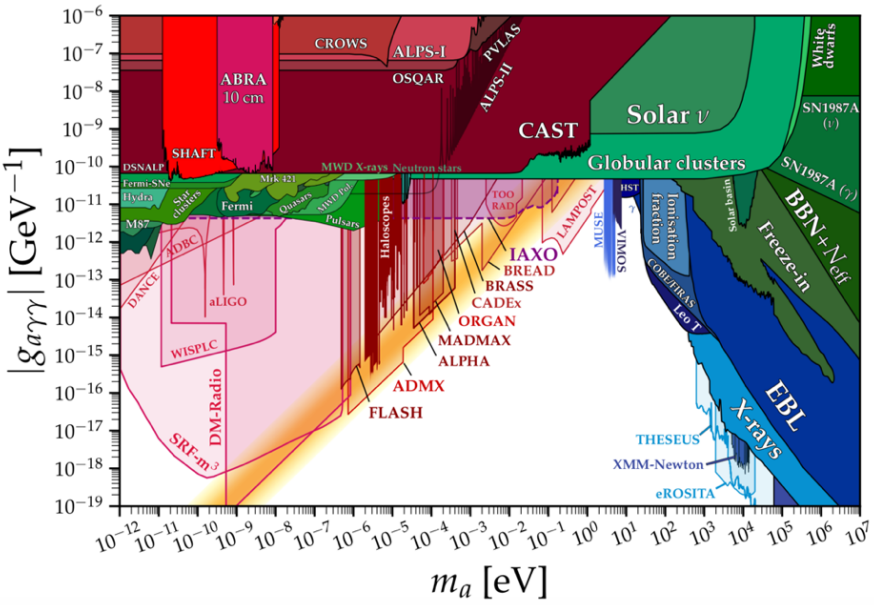


Fig. 31-40: Overview of results, prospects, and hints in the axion/ALP parameter space [1050]. Tables 31-3 and 31-4 will be useful, as well as Ref. [1051] explaining separately the various regions of this plot.

[1049] D. Heuchel *et al.,* The DESY axion search program. https://arxiv.org/abs/2302.11934 , A. Ringwald *et al.,* Axions and Other Similar Particles. https://pdg.lbl.gov/2021/reviews/rpp2021-rev-axions.pdf

[1050] Ibid (https://arxiv.org/abs/2302.11934)

[1051] A. Berlin, Direct Detection of Light Dark Matter. https://indico.fnal.gov/event/22303/contributions/247351/attachments/157883/206785/Berlin_Snowmass_TF_CF.pdf

31.3.7 Detection concepts, detector target materials and technologies

Before closing these chapters on DM searches, one should underline the prodigious variety and ingenuity of the detectors invented and built for these searches. This is illustrated in Figs. 31-41 to 31-43, as well as in Tables 31-3 and 31-4. Other informative references may be of interest [1052].

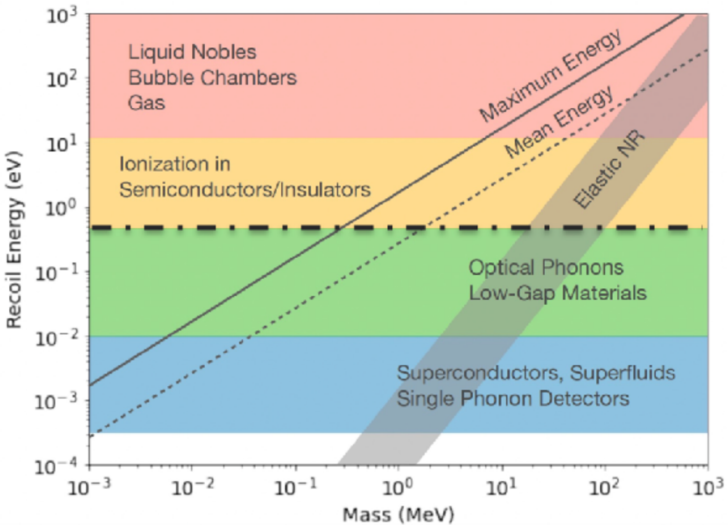


Fig. 31-41: Illustration of regions of DM mass kinematically accessible with different detection concepts, detector target materials, and technologies, depending on the energy deposited in detector by the particle. Elastic and inelastic nuclear recoils are indicated. The lines labelled "Maximum Energy" and "Mean Energy" corresponding to DM moving at the galactic escape velocity v_{esc} ~ 544 km/s or the mean velocity v_{mean} ~ 220 km/s, respectively [1053].

Figure 31-42 gives the ranges of sensitivity or applicability of different quantum sensors (QS) to searches for BSM physics. QS are mostly appropriate for searches for light and ultra-light DM, but they can also intervene as part of HEP detectors. And besides DM search, QS may play a role in other topics, as study of neutrino properties, tests of fundamental symmetries, searches for electric dipole moments (Section 32.2) and measurements of fundamental constants (Section 26.4).

Figure 31-43 shows the roadmap concerning R&D on a set of quantum and emerging detectors.

31.3.8 More information on axions

Tables 31-3 and 31-4 give an overview of direct DM Axion searches in Europe as well as a summary of methods, including definition of acronyms.

And finally, Fig. 31-44 illustrates the theoretically predicted axion DM mass ranges as well as excluded mass ranges by experiments. Table 31-5 shows the conclusion by Pierre Sikivie, presented at the 2024 Moriond meeting.

[1052] M. Battaglieri *et al.,* US Cosmic Visions: New Ideas in Dark Matter 2017: Community Report. https://arxiv.org/abs/1707.04591

[1053] R. Essig *et al.,* Snowmass 2021 Cosmic Frontier: The landscape of low-threshold dark matter direct detection in the next decade. https://arxiv.org/abs/2203.08297
D. Baxter, Experimental dark matter searches at masses below the GeV mass scale. IDM 2024, https://agenda.infn.it/event/39713/contributions/231099/attachments/123525/181178/lowmass_071024.pdf

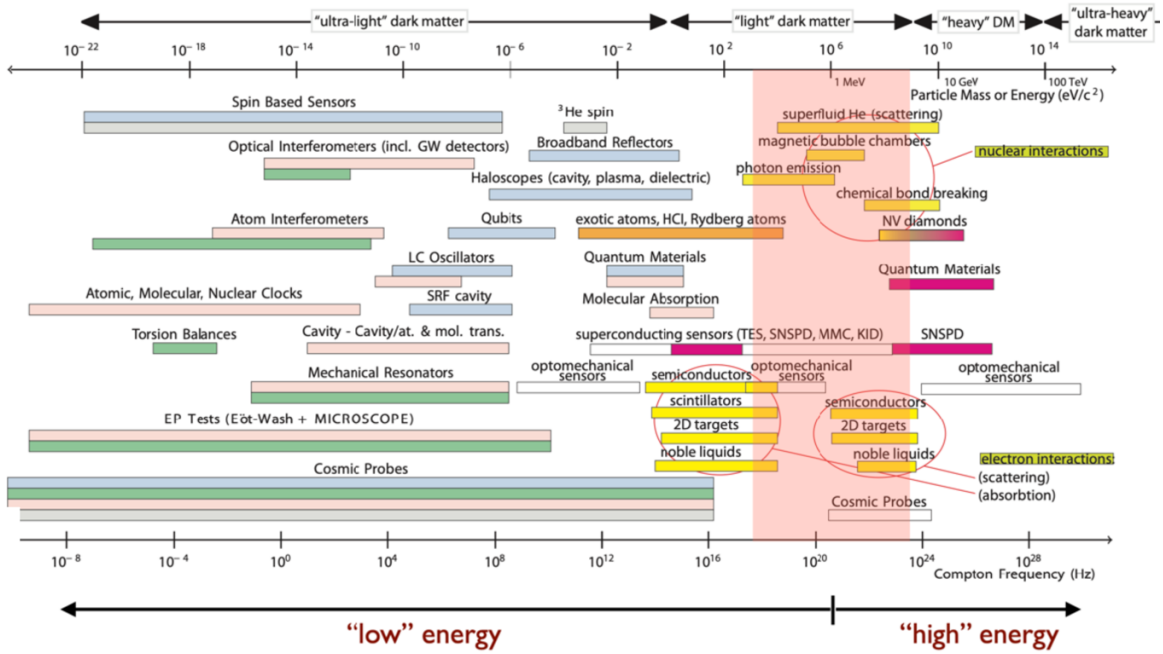


Fig. 31-42: Ranges of applicability of different quantum sensor techniques to search for BSM physics [1054].

On the left side of Fig. 31-42 appear in particular the atom interferometers. Given the wavelike character of ultralight DM, one can conceive their potential role for both DM searches and gravitational waves detection. Ref. [1055] presents a potential experiment and offers all references on the topic.

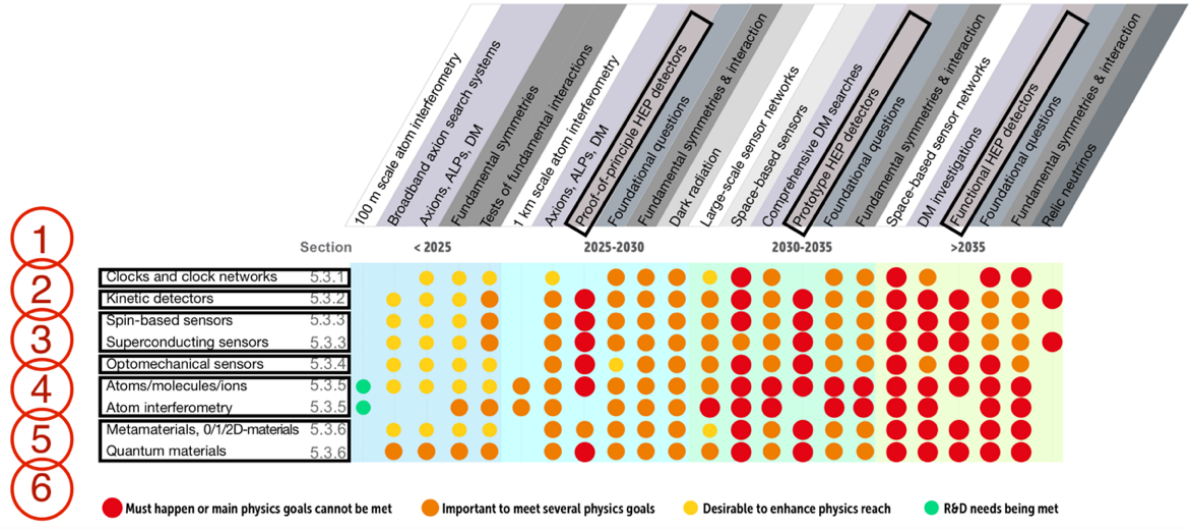


Fig. 31-43: RECFA Detector R&D roadmap 2021. Quantum and Emerging Technologies Detectors. The 6 families of detectors versus their applications in physics, in particular axions and ALPs searches [1056].

[1054] M. Doser, Quantum Particle Detectors. ICHEP Prague July 2024, https://indico.cern.ch/event/1291157/contributions/5958231/attachments/2901053/5087438/ICHEP_Quantum22.7.2024v3.pdf
S. D. Bass and M. Doser, Quantum sensing for particle physics. https://arxiv.org/abs/2305.11518
[1055] C. Baynham *et al.,* Letter of Intent: 100m Atom Interferometer Experiment at CERN. https://arxiv.org/abs/2509.11867
[1056] The 2021 ECFA detector research and development roadmap. https://cds.cern.ch/record/2784893

name	timing	mass target	location
MADMAX	data-taking 2025	$> 50\mu$eV	DESY
QUAX a-gamma	data-taking now	$\sim 37\mu$eV	Frascati
BRASS	data-taking 2020	$> 50\mu$eV	Hamburg
RADES	data-taking now	$\sim 33\mu$eV	CERN
KLASH	CDR in 2019	$< \mu$eV	Frascati

Experiment	**Location (country)**	**RF frequency (GHz)**	**Axion mass (μeV)**	**Coupling $g_{a\gamma\gamma}$ (GeV^{-1})**
ADMX	Univ. of Washington	0.645–2 (10)	2.66–8.2 (41)	2×10^{-16}
CULTASK	CAPP/IBM (Korea)	1.35–1.6, 2–2.5	5.4–6.4, 8–9	1×10^{-15}
CAST-CAPP	CERN (Switzerland)	5.25–6.25	21–25	1×10^{-14}
HAYSTAC	Yale Univ. (US)	5.6–5.8	22.4–23.2	1×10^{-14}
ORGAN	Univ. of Western Australia (Australia)	15–50	60–200	2×10^{-12}

Table 31-3: Top: overview of small and mid-scale experiments (in Europe) for direct DM Axion search. Bottom: haloscope projects [1057].

Methods	**advantage**	**disadvantage**
LSW	Model independent, broadband sensitivity in the mass m_a	signal suppressed by $g_{\gamma a}^4$ mass reach limited to $\lesssim$ meV
Helioscopes	Less model dependent, broadband mass coverage up to $m_a \sim$ 1eV	signal is suppressed by $g_{\gamma a}^4$ or $g_{\gamma e(N)}^2 g_{\gamma a}^2$
Haloscopes	Highly sensitive search. Can confirm DM nature of axion/ALP	Needs Axion/ALP to be DM, Cover narrow m_a window

ADMX: Axion Dark Matter eXperiment
CAPP: Center for Axion and Precision Physics research
CAST: CERN Axion Solar Telescope
CULTASK: CAPP Ultra Low Temperature Axion Search in Korea
EQuS: Engineered Quantum Systems
KAIST: Korea Advanced Institute of Science and Technology
HTSC: High-Temperature Super-Conductor
IBS: Institute for Basic Science
HAYSTAC: Haloscope At Yale Sensitive To Axion Cold dark matter
HEMT: High Electron Mobility Transistor
JPA: Josephson Parametric Amplifier
NHMFL: National High Magnetic Field Laboratory
ORGAN: Oscillating Resonant Group AxioN
SQUID: SUperconducting Quantum Interference Device

Table 31-4: Top: summary of methods. Bottom: definition of acronyms [1058].

[1057] M. S. Carena *et al.,* Strategic Search Plan for Axions and Axion-like-particles. CERN ESU-012, https://cds.cern.ch/record/2788559/files/CERN-ESU-012.pdf
[1058] ibid

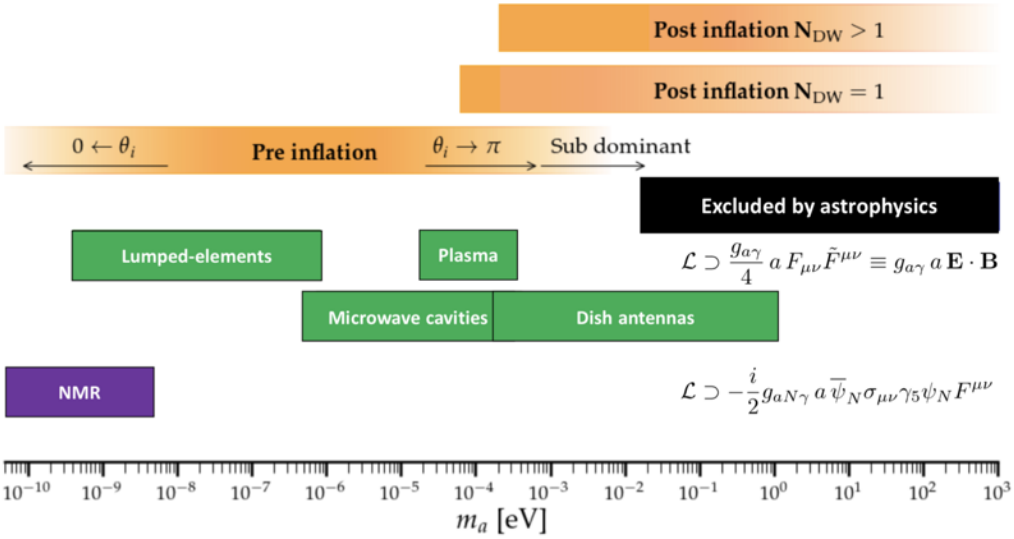


Fig. 31-44: Theoretically predicted axion DM mass ranges (orange bands). Axion mass range excluded by astrophysics (black band). Axion DM ranges probed by various haloscopes (green bands). Axion DM ranges probed by Nuclear Magnetic Resonance methods (NMR, violet band) [1059].

Conclusions	
• Axions solve the strong CP problem	• A population of cold axions is naturally produced in the early universe which may be the dark matter today
• Axion dark matter is detectable	• Axion dark matter has distinctive properties in large scale structure formation

Table 31-5: Conclusion by P. Sikivie at the 58th Rencontres de Moriond – Electroweak Interactions and Unified Theories 2024 [1060].

31.4 The dark stars

We explore now the possibility that DM is made of **dark cosmological compact objects**.

31.4.1 The contribution of microlensing

The contribution of **microlensing** to the search of DM is fascinating and important [1061]. *"A lensing effect occurs when a massive compact object (lens) passes close enough to a source's line of sight to produce gravitational images not intercepted by the lens"* (Fig. 31-45).

[1059] A. Ringwald, Axion dark matter (theory & experiment). https://arxiv.org/abs/2311.11660
[1060] P. Sikivie, Axion Dark Matter. Moriond EW 2024, https://indico.in2p3.fr/event/32664/contributions/137018/attachments/83759/124752/1_PSikivie-v1.pdf
[1061] B. Paczynski. Gravitational Microlensing by the Galactic Halo. *ApJ, 304:1, 1986.*
T. Blaineau *et al.,* New limits from microlensing on Galactic black holes in the mass range 10 $M_\odot$ < M < 1000 $M_\odot$. https://arxiv.org/abs/2202.13819

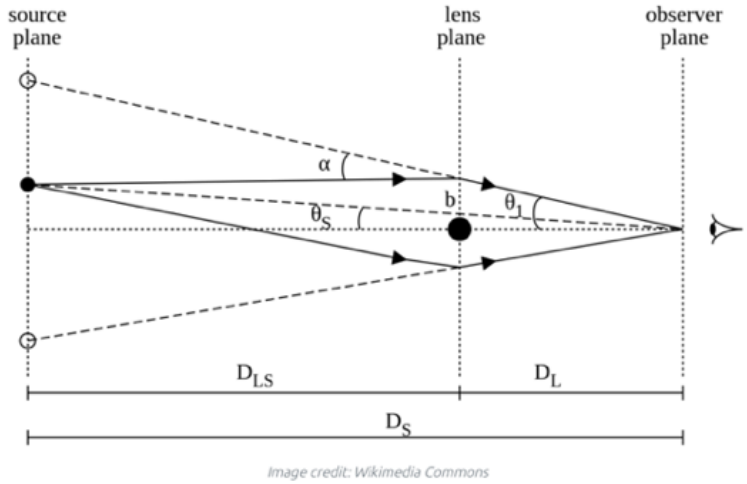


Fig. 31-45: Principle of lensing (wiki).

If the lens mass is small (planet or star) the displacement of light is not observed easily, but the **apparent brightening of the source** may still be detected. The lens passes by the source in some time span (~ the time taken for the lens to move across by an Einstein Radius, ER [1062]) and as the alignment changes, the source's apparent brightness changes, as Figs. 31-46 and 31-47 show. This transient astronomical event is called **microlensing**. In terms of angles we have the following hierarchy: real radius of the objects involved << radius of gravitational influence of the lens on the light of the object (ER) << radius of the luminous object due to diffraction.

The observation of lensing events allowed to put a limit on the contribution of dark astronomical objects "lenses" to the dark matter of the Universe as a function of mass (Fig. 31-48).

Since the most probable microlensing event is a star passing in front of another star [1063], with one single spot visible at the time of lensing, the region of one solar mass is the weak point of the method.

It is remarkable that, observed years later, a microlensing event region shows object and lens (two stars), merged during the event, now separated [1064] (Fig. 31-49).

[1062] Gravitational lensing: https://www.astro.umd.edu/~miller/teaching/astr422/lecture13.pdf
[1063] P. Mroz *et al.,* Microlensing optical depth and event rate toward the Large Magellanic Cloud based on 20 years of OGLE observations. Results are "*consistent with lensing by stars in the Milky Way disk and the LMC itself and demonstrate that massive and intermediate-mass black holes cannot comprise a significant fraction of dark matter.*" https://arxiv.org/abs/2403.02398
[1064] S. Kozlowski *et al.,* The first direct detection of a gravitational μ-lens toward the galactic bulge. https://arxiv.org/abs/astro-ph/0701488

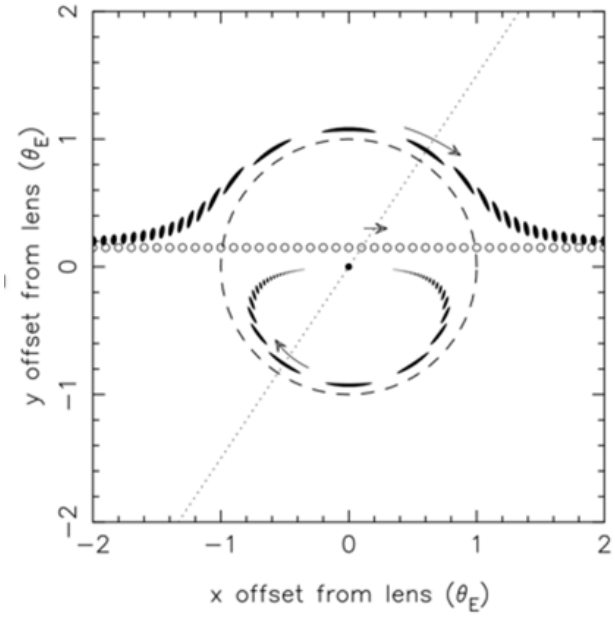


Fig. 31-46: Details of microlensing. A microlensing event seen at "perfect" resolution. The axes show angular offsets on the sky from the lens (central dot) in units of the Einstein angle; the dashed circle is the Einstein ring. The series of small open circles shows the "true" source position at successive timesteps. For each source position, there are two images (solid blobs) collinear with the lens and source, as indicated by the dotted line; the arrows illustrate their motion [1065].

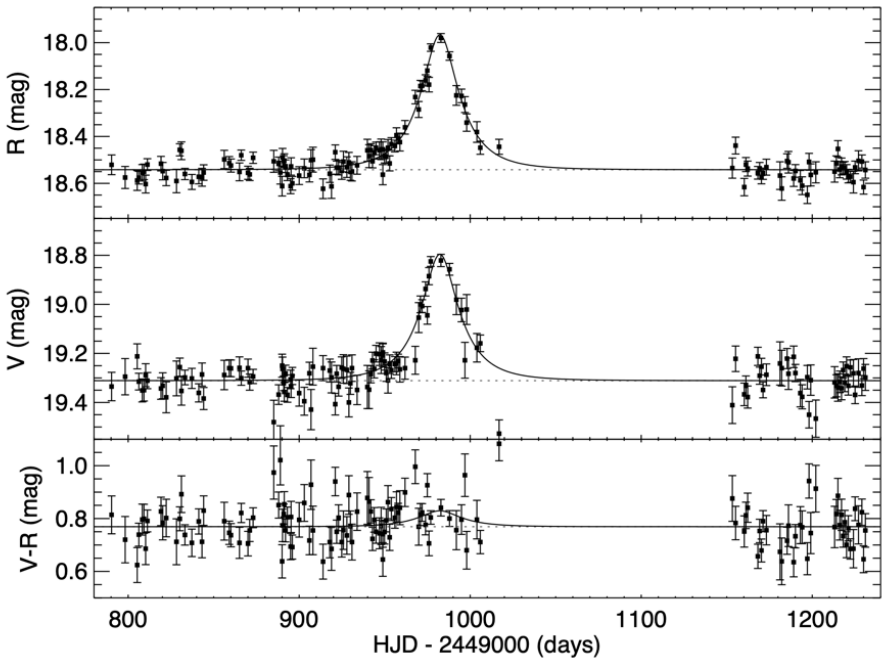


Fig. 31-47: A microlensing event. Light curve of the MACHO-95-BLG-37 event [1066].

[1065] W. Sutherland, Gravitational Microlensing - A Report on the MACHO Project. https://arxiv.org/abs/astro-ph/9811185
[1066] S. Kozlowski *et al.,* The first direct detection of a gravitational μ-lens toward the galactic bulge. https://arxiv.org/abs/astro-ph/0701488

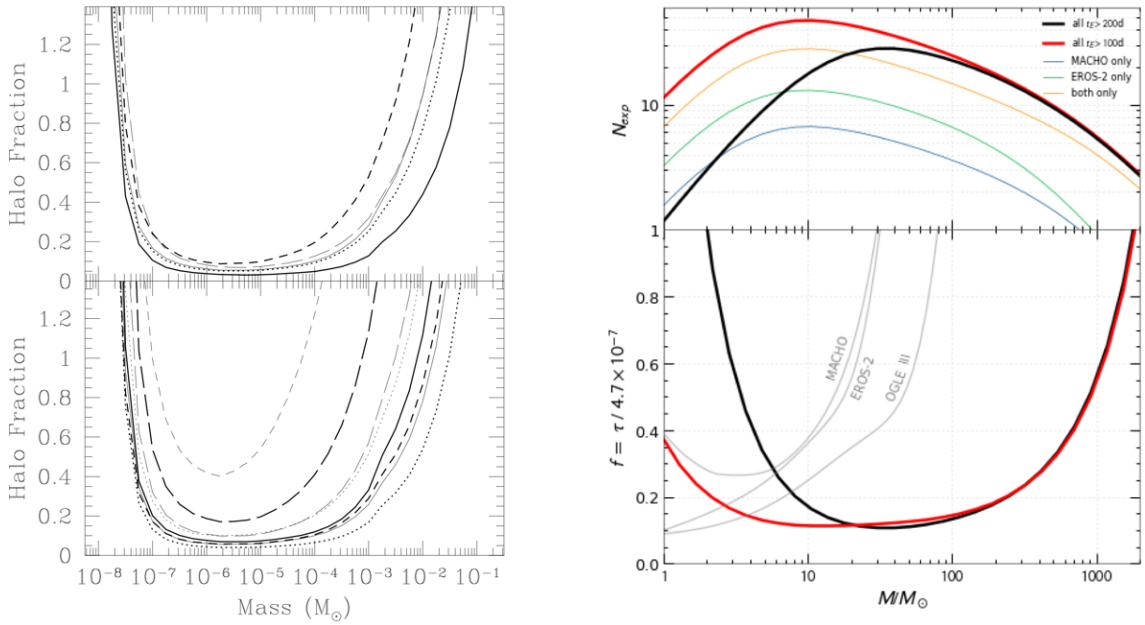


Fig. 31-48: Left: Halo fraction upper limit (95% CL) versus lens mass for the five EROS models (top) and the eight MACHO models (bottom) [1067]. Right: 95% CL upper limits on the fraction of the halo mass in the form of compact objects [1068].

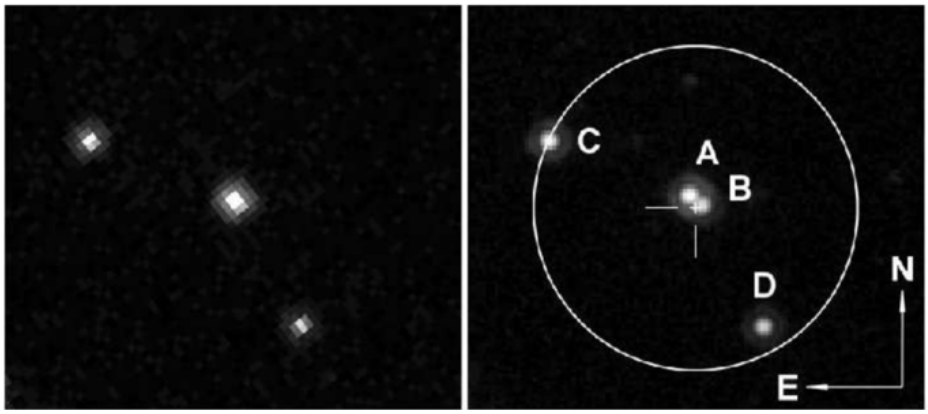


Fig. 31-49: HST images of the MACHO-95-BLG-37 event location. Left: 3.71 yr after microlensing; right: 8.95 yr after microlensing.

31.4.2 A brief account of Weak Gravitational Lensing

Weak Gravitational Lensing (WGL) distorts the shape and size of images of distant galaxies, due to the gravitational influence of matter along the line of sight. These distortions due to the large-scale structure in the Universe (Cosmic Shear) can be used to extract significant results for cosmology [1069].

[1067] EROS and MACHO collaborations, EROS and MACHO combined limits on planetary mass dark matter in the galactic halo. https://arxiv.org/abs/astro-ph/9803082

[1068] T. Blaineau *et al.,* New limits from microlensing on Galactic black holes in the mass range 10 $M_\odot$ < M < 1000 $M_\odot$. https://arxiv.org/abs/2202.13819

[1069] M. Kilbinger, Cosmology with cosmic shear observations: a review. https://arxiv.org/abs/1411.0115

Such images are **coherently deformed** by the tidal field of matter inhomogeneities along the line of sight. By measuring **galaxy shape correlations**, one can study the properties and evolution of structure on large scales, as well as the geometry of the Universe.

The usual approach to extract cosmological information from WGL surveys is to compute the **two-point correlation function or power spectrum** from data and compare to an expectation from theory.

Exploiting WGL is motivated by the fact that visible matter represents only about 13–14% of the matter of the Universe, the rest being dark. The mass distributions recovered by weak lensing can thus be referred to as **mass-maps of the dark matter** of the Universe.

The properties of the WGL effect depend on all the mass density integrated around the line of sight and on the cosmological angular distances between the observer, the lenses and the source.

WGL appears as the most promising tool to understand the nature of dark matter and to constrain the cosmological model describing the Universe.

The goal of WGL study is to solve the following **inverse problem**: how to derive a dark matter mass map from the measured shear field. Ref. [1070] suggests the complexity of such studies.

Figure 31-50 compares to Planck results those of 3 galaxy surveys obtained through WGL. The correlation functions (CF) are the angular CF of the lens galaxies, the CF of the tangential shear of sources with lens galaxy positions, the CFs of different components of the ellipticities of the source galaxies.

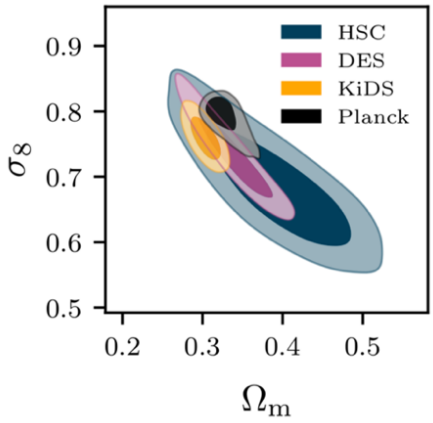


Fig. 31-50: This figure presents cosmological constraints from the 3×2pt combination for DES Y3 [1071], KiDS-1000 [1072] and HSC Y3 [1073] in comparison with early Universe measurements from the *Planck* satellite assuming the ΛCDM model. σ_8 is defined as a cosmological parameter that quantifies the amplitude of density fluctuations in the Universe on a scale of 8 h^{-1} Mpc.

Future weak lensing surveys such as LSST/Rubin, Euclid, and Roman are already planned in order to cover a large fraction of the sky with large accuracy and observe billions of galaxies over unprecedented areas, dramatically improving statistical precision.

[1070] J. Prat and D. Bacon. Weak Gravitational Lensing. https://arxiv.org/abs/2501.07938
[1071] DES Collaboration, Dark Energy Survey Year 3 Results. Cosmological Constraints from Galaxy Clustering and Weak Lensing. https://arxiv.org/abs/2105.13549
[1072] C. Heymans *et al.,* KiDS-1000 Cosmology: Multi-probe weak gravitational lensing and spectroscopic galaxy clustering constraints. https://arxiv.org/abs/2007.15632
[1073] R. Dalal *et al.,* Hyper Suprime-Cam Year 3 Results: Cosmology from Cosmic Shear Power Spectra. https://arxiv.org/abs/2304.00701

31.4.3 Primordial black holes: presentation

According to General Relativity, a region of mass M forms a **black hole (BH)** if it falls within its Schwarzschild radius $R_S \equiv 2\,GM/c^2$. BHs could exist over a wide range of mass scales, but astrophysical processes could only produce them above a solar mass.

BHs of several solar masses ($M_\odot$) are formed at the end of evolution of ordinary stars, "Intermediate Mass Black Holes" (IMBHs) of stars above 100 $M_\odot$. "Supermassive Black Holes" (SMBHs), with masses from $10^6\,M_\odot$ to $10^{10}\,M_\odot$, reside in active galactic nuclei (AGN). The Milky Way has one of mass $4 \times 10^6\,M_\odot$ and BHs with mass of around $10^8\,M_\odot$ power quasars. There is now overwhelming evidence for these astrophysical types of BHs, but they can only provide a small fraction of the dark matter density [1074] .

BHs could also have formed in the early Universe and these are called **"primordial" black holes (PBH)** [1075].

Figure 31-51 [1076], starting from the top and rotating anti-clockwise (small mass first), show the wide range of masses of BHs, from microphysics to macrophysics. PBHs may concern various areas of physics, from quantum gravity ($M_P \sim 10^{-8}$ kg) to the whole visible Universe, but one ignores whether PBHs formed in any of these mass ranges.

Historically, the founding papers on PBHs appeared in the 1970s, followed by two decades of mild interest, although the idea led to **Hawking radiation**. Attention rose after the MACHOs **microlensing results** in 1996, but the main rise occurred after the first LIGO-Virgo **gravitational wav**e events in 2016.

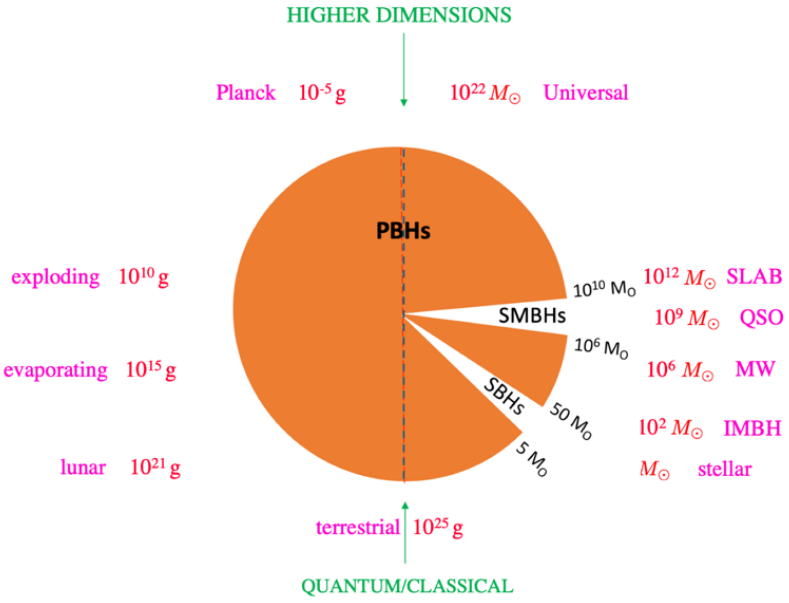


Fig. 31-51: This diagram indicates the mass of various types of black holes. Quantum emission is suppressed by accretion of the CMB to the right of the bottom point.

[1074] For a universe of critical density $R_{Hubble} = S_{chwarzschild}$

[1075] B. J. Carr and A. M. Green, The History of Primordial Black Holes. https://arxiv.org/abs/2406.05736
B. J. Carr *et al.*, Observational Evidence for Primordial Black Holes: A Positivist Perspective.
https://arxiv.org/abs/2306.03903

[1076] See B. J. Carr and A. M. Green above (2406.05736). Associating the Moon and MQ may surprise. It means that a BH of M_{Moon} , slightly hotter than CMB, slightly evaporates.

Formation and accretion

According to the Friedmann equation the cosmological density at time t after the Big Bang, when expansion is driven by radiation, is $\rho_r \sim (3/32\pi)/(Gt^2)$ and, from $R_S = 2\,GM/c^2$, the density required for making a BH is $\rho \sim (3/32\,\pi)\,c^6/(G^3M^2)$. Equality of these densities suggests that PBHs would initially have a mass $M = c^3t/G$. Numerically: 1 picosecond of age (~ EW transition) leads to 4×10^{23} kg (Earth mass = 6×10^{24} kg, Moon mass = 7×10^{22} kg). 10 microsecond (~ QCD transition) leads to 4×10^{30} kg (Sun mass = 2×10^{30} kg, R_S = 2.9 km). For curiosity 1s of age gives 4×10^3 kg, 10^{-23} s gives 4×10^{12} kg.

So, at the difference of astrophysical BHs, PBHs can be **lighter than a solar mass**. Realising that PBHs might be light led Hawking to study their quantum properties and discover that BH **radiate thermally** with a temperature $T = \hbar c^3/(8\pi\, G\, M\, k_B)$ and **evaporate** on timescale $\tau(M) = 5120\,\pi G^2 M^3/\hbar c^4$, those lighter than 10^{12} kg evaporating within the current age of the Universe. For light enough PBHs Hawking radiation is important and must enter their phenomenology. For $M = 10^{11}$ kg, $\tau \sim 10^{10}$ years. For 1 M_{Moon}, T = 4.5 K (CMB is at 2.7 K).

Here are the expressions of **evaporation time versus mass**:

$$t_{\text{ev}} = \frac{5120\pi G^2 M^3}{\hbar c^4} = \frac{480 c^2 V}{\hbar G} \approx 3.396 \times 10^{-16}\,\text{s} \left(\frac{M}{\text{kg}}\right)^3 \approx 2.140 \times 10^{67}\,\text{years} \left(\frac{M}{M_\odot}\right)^3$$

Formation of PBH can result from **inflationary density perturbations** if they are large enough to generate an interesting abundance of them. Since inflation exponentially reduces the number density of any PBHs formed earlier, the horizon mass at the end of inflation sets a lower limit on the mass of PBHs which are subsequently observable.

PBHs formation may also happen during matter-domination. Moreover, it may result from **phase transitions**, with a special concern of the **quark-hadron transition** at the QCD epoch.

Detailed studies of PBH formation concluded that the fraction of the Universe collapsing into PBHs, the **collapse fraction β**, must be tiny even if PBHs provide all of the dark matter. This requires fine-tuning β and fine tuning of the density fluctuations which generates the PBH. If PBHs provide dark matter, one can also ask why PBH and baryon densities are so close. On this last point, one can argue that PBHs forming at the QCD epoch would necessarily have $\beta \sim \eta$, where η is the **cosmological baryon-to-photon ratio** ($6.12 \pm 0.04 \times 10^{-10}$) if they provide the dark matter. Hence a baryogenesis scenario in which such a PBH formation naturally generates this relation and explains why the two densities are comparable [1077].

Evaporations and constraints

Products resulting from the **PBH evaporation** may lead to visible effects, whose non-observation can set strong constraints on PBH mass and abundance.

PBHs with initial mass $M_* \sim 10^{12}$ kg, which formed at 10^{-23} s and had the size of a proton, would be evaporating now and lighter ones would have evaporated earlier. On the other hand, evaporation would be suppressed for heavier PBHs, cooler than the CMB, namely any BH heavier than 4.54×10^{22} kg, which would accrete rather than evaporate. PBHs with mass $M \sim 2 \times 10^{11}$ kg, hotter than the QCD confinement scale, should emit quark-gluon jets which then fragment.

Figure 31-52 gives early limits on the collapse fraction (mind: scale is in gram).

[1077] P. Widerin and C. Schmid, Primordial black hole formation caused by the QCD transition? https://arxiv.org/abs/astro-ph/9801163
J. Garcıa-Bellido *et al.,* A common origin for baryons and dark matter. https://arxiv.org/abs/1904.11482

Further work gave a more precise value for the initial mass of a PBH evaporating today: $M_* \approx 5 \times 10^{11}$ kg. The constraints on β(M) for PBHs with initial mass $M \lesssim 10^{14}$ kg were extended and improved by studies of the effects of PBH evaporation on the early Universe, as on Big Bang Nucleosynthesis and diffuse γ population. These constraints are shown in Fig. 31-53 [1078].

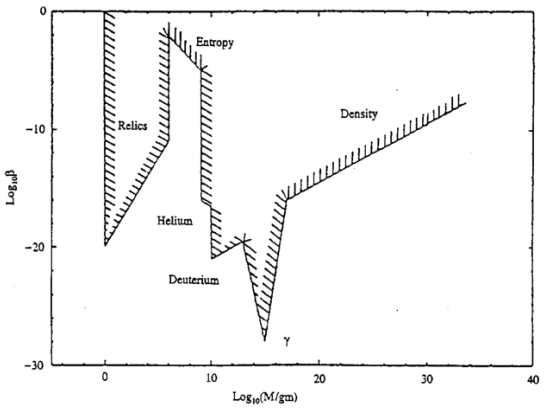


Fig. 31-52: The collapse fraction β(M) [1079].

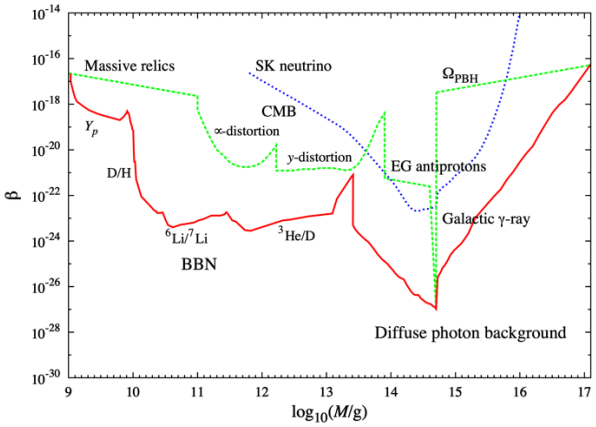


Fig. 31-53: Evaporation constraints on β(M), the fraction of Universe collapsing into PBHs of mass M (mind: scale in g).

31.4.4 Primordial black hole searches

Until the mid-1990s there was no evidence for PBHs and no strong reason to associate them to the DM problem.

Excitement started in 1996, when **gravitational microlensing (GML)** searches for massive compact halo objects (**MACHOs**), presented above, suggested that DM could be BH of mass 0.5 $M_\odot$. Alternative GML candidates could be excluded and it was understood that PBHs of this mass might naturally form at the quark-hadron phase transition. With further data, the MACHO collaboration found that solar-mass compact objects could comprise only 20% of the dark matter and others GML observations excluded compact objects in the mass range 10^{-7} $M_\odot$ to 10 $M_\odot$ from providing a substantial fraction of it (Fig. 31-48). A GML survey of the Andromeda galaxy (M31) extended the range of masses constrained by GML down to 10^{19} kg (10^{11} $M_\odot$). Lighter PBHs cannot be searched for by optical observations of main-sequence stars, because of the size of the source stars and wave-optics effects.

The Milky Way GML constraints have now been extended to larger masses, $M \sim 10^3$ $M_\odot$, by combining data from different surveys to obtain sensitivity to longer duration events.

From Ref. [1080] one reads: "*Microlensing observations of stars and quasars suggest that PBHs of around 1 $M_\odot$ could provide much of the dark matter in galactic halos. Provided the mass and dark matter fraction of the PBHs is large enough, the associated Poisson fluctuations could generate the first bound objects at a much earlier epoch than in the standard cosmological scenario.*"

Figure 31-56 gives a summary of positive evidences for this scenario.

[1078] B. J. Carr and A. M. Green, The History of Primordial Black Holes. https://arxiv.org/abs/2406.05736

[1079] ibid

[1080] B. J. Carr *et al*., Observational Evidence for Primordial Black Holes: A Positivist Perspective. https://arxiv.org/abs/2306.03903
M. M. Waldrop, Primordial black holes could hold the key to dark matter mysteries. https://doi.org/10.1073/pnas.2211215119

Significant improvements in calculations of the abundance and mass function of PBHs followed. The status of the constraints in 2021 is shown in Fig. 31-54.

After GML, LIGO/Virgo detection of **gravitational waves (GW)** from the mergers of BH with masses of 10–100 $M_{\odot}$ much interest started in PBHs, as explanation of some of these events and as dark matter. Although all the LIGO-VIRGO-KAGRA detections are thought to involve astrophysical BH, the masses are larger than initially expected and some appear in mass gaps disfavouring stellar remnants. One surprise of LIGO/VIRGO GW detection was indeed that both BH were around 30 times the sun mass – somewhat high for what one thought possible from a supernova, but consistent with the PBH assumption, since estimates predict a small peak in this mass range, as illustrated in Fig. 31-55 (Chapter 34).

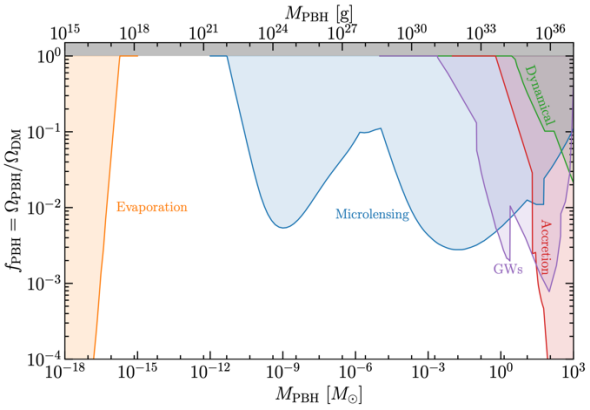


Fig. 31-54: Constraints on the fraction of DM in the form of PBHs, as a function of mass, assuming all PBHs have the same mass [1081].

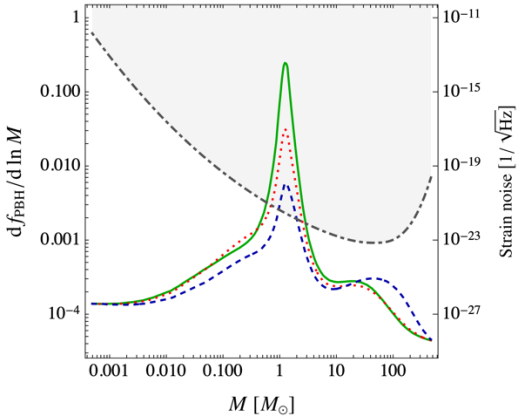


Fig. 31-55: Spectral density of the PBH dark matter fraction as a function of PBH mass. The green solid line indicates the standard scenario. Also shown is the LIGO sensitivity curve (grey dot-dashed line) for equal-mass mergers and using the maximal GW frequency $f_{max} \approx 4400\ M_{\odot}/M$ for the conversion from frequency to mass [1082].

This shift towards the search for **positive evidence for PBHs** is described in Ref. [1083].

Further evidence and constraints came from other domains: evaporation, dynamical, accretion and nucleosynthetic effects.

In 2019 calculation of **the evaporation spectra produced by any population of PBHs** was available [1084]. Various observations (e.g. of MeV gamma-rays) were used to tightly constrain the abundance of PBHs lighter than 10^{17} g and limits on evaporating PBHs were reviewed in 2023. Cosmic structure, dwarf galaxies and supermassive black holes contributed also to generate new ideas.

About the **generation of cosmic structure**, provided the mass and dark matter fraction of the PBHs are large enough, they could generate the **first bound objects at a much earlier epoch** than in the standard

[1081] B. J. Carr and A. M. Green, The History of Primordial Black Holes. https://arxiv.org/abs/2406.05736
[1082] ibid (Ref. https://arxiv.org/abs/2306.03903)
[1083] S. Clesse and J. Garcia-Bellido, Seven Hints for Primordial Black Hole Dark Matter. https://arxiv.org/abs/1711.10458
[1084] A. Arbey and J. Auffinger, Calculation of the Hawking evaporation spectra of any black hole distribution. https://arxiv.org/abs/1905.04268 , see also https://cds.cern.ch/record/2674326?ln=en
A. Arbey and J. Auffinger, Physics Beyond the Standard Model with BlackHawk. v2.0. https://arxiv.org/abs/2108.02737 , see also https://cds.cern.ch/record/2778056

scenario. An observational consequence could be the recent detection of **high-redshift objects**, as dwarf galaxies, in particular from recent JWHT observations, quoted in Section 30.5.

As for Super Massive BH (SMBH) in galactic nuclei, the usual view is that they form from dynamical processes **after galaxies**, but this is becoming increasingly challenged. It is unclear that SMBHs can form fast enough in the standard model, so a suggestion is that these objects – or at least their seeds – could form **before galaxies.** Then unusually massive galaxies at z > 10 could offer the evidence that structure formation is accelerated by 10^9 $M_\odot$ PBHs making up 10^{-6}–10^{-3} of the dark matter.

Fig.31-56 gives a summary of positive evidence for PBHs. These come from PBH-attributed signals from supernovæ (SNe), various micro-lensing surveys (Gaia, HSC, OGLE, MACHO), POINT-AGAPE pixel-lensing (P-A), gravitational waves (LVK), ultra-faint dwarf galaxies (UFDGs), supermassive black holes (SMBHs), core/cusp (C-C) profiles for inner galactic halos, and correlations of the source-subtracted cosmic infrared and X-ray backgrounds (CIB-XRB) [1085].

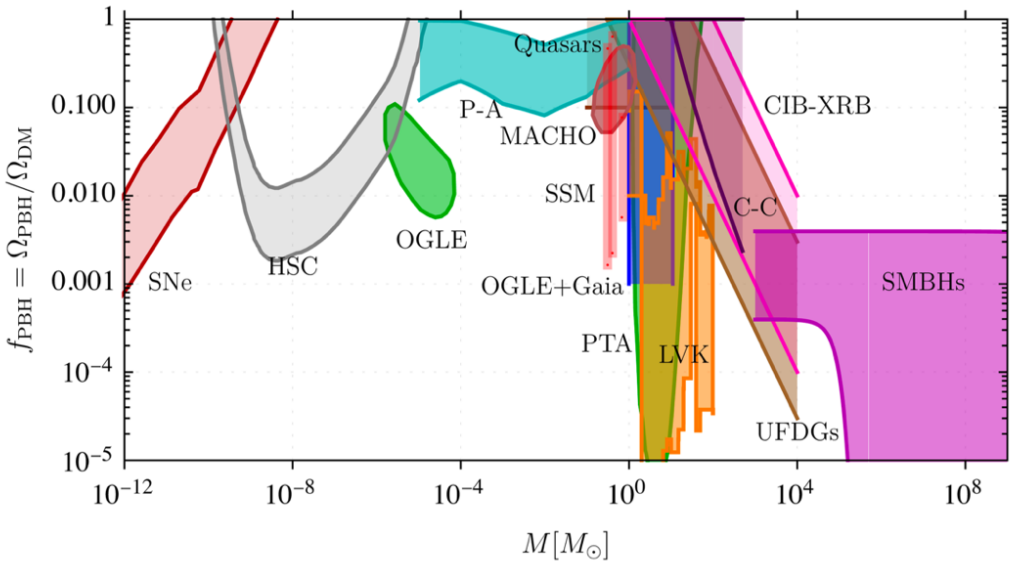


Fig. 31-56: Summary of positive evidence for PBHs in terms of f_{PBH} values required by or consistent with the claimed detections.

Quoting Ref. [1086]: "*Even if PBHs provide only a small fraction of the dark matter, they could explain various other observational conundra, and sufficiently large ones could seed the supermassive black holes in galactic nuclei or even early galaxies themselves. We argue that PBHs would naturally have formed around the electroweak, quantum chromodynamics and electron-positron annihilation epochs, when the sound-speed inevitably dips. This leads to an extended PBH mass function with a number of distinct bumps, the most prominent one being at around 1 $M_\odot$, and this would allow PBHs to explain much of the evidence in a unified way.*"

[1085] B. Carr *et al*., Observational Evidence for Primordial Black Holes: A Positivist Perspective. https://arxiv.org/abs/2306.03903
[1086] ibid

Figure 31-57 [1087] shows in more details constraints on f(M) for a monochromatic mass function, from evaporations (red), lensing (blue), gravitational waves (GW) (grey), dynamical effects (green), accretion (light blue), CMB distortions (orange) and large-scale structure (LSS, purple).

One can be bolder and build scenarios in which PBH form at various phase transitions and explain facts. For instance, one may assume a quasi-scale-invariant mass spectrum such as might be produced by a variant of slow-roll inflation, as shown in Fig. 31-58 [1088] with different spectral index n_S values. The bumps correspond to the **EW and QCD phase transitions and e^+e^- annihilation**. Several constraints are shown (M means microlensing), as well as GW events (vertical lines).

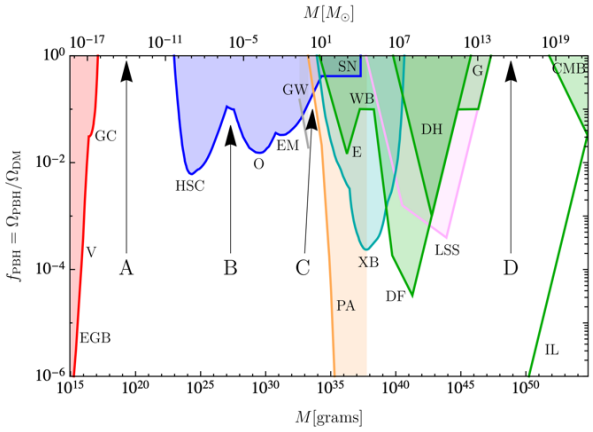


Fig. 31-57: Details on constraints on f(M). See text for explanations.

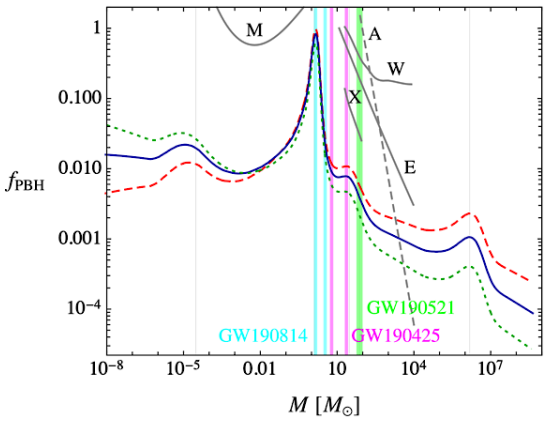


Fig. 31-58: Mass spectrum with bumps at various transitions. From light to heavy: EW, QCD phase transitions and e^+e^- annihilation.

Still quoting Ref. [1089]: *"The existence of PBH is likely to be confirmed or excluded within the next decade and the expectations. there has been much interest in PBHs in recent years and this has prompted more sophisticated studies of their expected characteristics and consequences. PBHs as a solution of the dark matter problem maybe in the asteroidal and solar mass ranges. The former view is not excluded by current observations. The latter view is driven by the claimed evidence but is more controversial due to the constraints in this mass region."*

Back to JWST: this telescope has identified the emergence of a population of (unusually) massive galaxy sources (> 10^{10} $M_\odot$) at z > 7–10, less than 700 Myr after the Big Bang. The early Universe, younger than one billion years, seems densely populated by well-developed galaxies and quasars (SMBHs) that should not have had time to form within the standard ΛCDM cosmology. Among possible explanations, as said above, massive PBHs, which were created first in the early Universe at a pre-stellar epoch, could seed galaxy and quasar formation in the very young Universe.

Let us close on these optimistic notes and quote a curiosity: the so-called "asteroid-mass window", $10^{17} \lesssim m \lesssim 10^{22}$ g, is also quite fashionable [1090].

[1087] B. Carr and F. Kuhnel, Primordial black holes as dark matter candidates. https://arxiv.org/abs/2110.02821
[1088] ibid
[1089] B. Carr *et al.*, Observational Evidence for Primordial Black Holes: A Positivist Perspective. https://arxiv.org/abs/2306.03903
[1090] M. Gorton and A. M. Green, How open is the asteroid-mass primordial black hole window? https://arxiv.org/abs/2403.03839

32. Some very hot topics

32.1 Neutrinos: a key question remains

As said in Chapter 19, one of today's great secrets remains [1091]: the nature, Dirac or Majorana, of massive neutrinos. A Majorana neutrino would be its own antiparticle (Fig. 32-1).

32.1.1 Neutrinoless double beta decay

Currently, **neutrinoless double beta decay (0νββ)** [1092] is the only known feasible way to prove the Majorana property of neutrinos (Fig. 32-2) [1093]. But it is a most difficult enterprise. Its discovery would transform our fundamental understanding of neutrinos and matter in the Universe. A lot of experimental and theoretical efforts have been put towards its discovery.

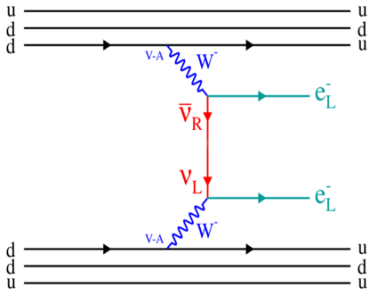


Fig. 32-1: The neutrinoless process.

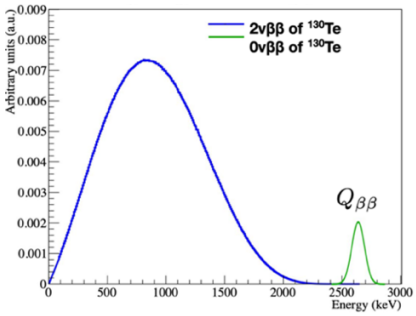


Fig. 32-2: The electron energy spectrum, example of ^{130}Te.

The goal, mββ, the **effective Majorana mass**, is related to basic ν properties (Chapter 19) as shown in Figs. 32-3 and 32-4. Table 32-1 gives information on techniques and isotopes used.

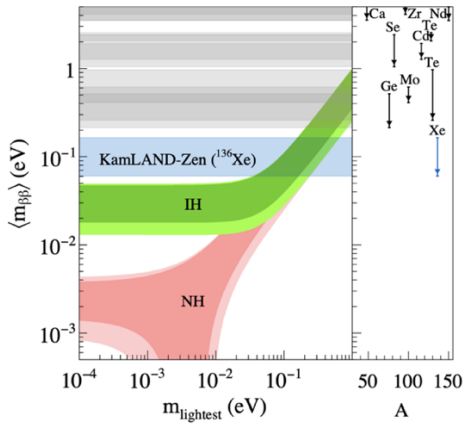


Fig. 32-3: The effective mass <mββ> versus the presently unknown lightest neutrino mass [1094].

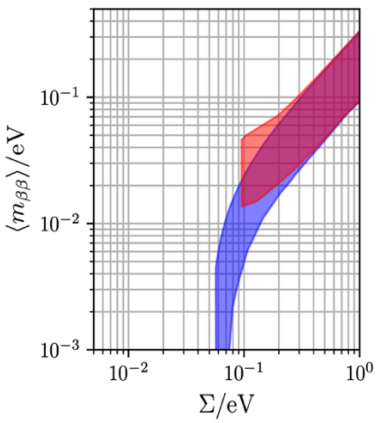


Fig. 32-4: The effective mass <mββ> versus the cosmological observable Σ [1095].

[1091] C. Adams *et al.,* Neutrinoless Double Beta Decay. https://arxiv.org/abs/2212.11099
[1092] B. J. P. Jones, The Physics of Neutrinoless Double Beta Decay: A Primer. https://arxiv.org/abs/2108.09364
[1093] I. Nutini, Neutrinoless Double Beta Decay and Inference on Neutrino Mass and Nature. https://agenda.infn.it/event/42052/?print=1
[1094] B. J. P. Jones, The Physics of Neutrinoless Double Beta Decay: A Primer. https://arxiv.org/abs/2108.09364
[1095] M. J. Dolinski *et al.,* Neutrinoless Double-Beta Decay: Status and Prospects. https://arxiv.org/abs/1902.04097

Isotope	Technique	$T^{0\nu}_{1/2}$	$m_{\beta\beta}$ (eV)	Year Published
^{48}Ca	CaF_2 scint. crystals	$> 5.8 \times 10^{22}$ y	<3.5-22	2008 [65]
^{76}Ge	^{76}Ge detectors	$> 1.8 \times 10^{26}$ y	<0.079-0.180	2020 [12]
^{82}Se	Zn^{82}Se bolometers	$> 4.6 \times 10^{24}$ y	<0.263-0.545	2022 [19]
^{96}Zr	Thin metal foil within TPC	$> 9.2 \times 10^{21}$ y	<3.9 - 19.5	2009 [66]
^{100}Mo	$Li_2{}^{100}MoO_4$ bolometers	$> 1.8 \times 10^{24}$ y	<0.28-0.49	2022 [18]
^{116}Cd	$^{116}CdWO_4$ scint. crystals	$> 2.2 \times 10^{23}$ y	<1.0-1.7	2018 [67]
^{128}Te	TeO_2 bolometers	$> 3.6 \times 10^{24}$ y	<1.5-4.0	2022 [68]
^{130}Te	TeO_2 bolometers	$> 2.2 \times 10^{25}$ y	<0.090-0.305	2022 [69]
^{136}Xe	Liquid Xe scintillators	$> 2.3 \times 10^{26}$ y	<0.036-0.156	2022 [13]
^{150}Nd	Thin metal foil within TPC	$> 2 \times 10^{22}$ y	1.6-5.3	2016 [70]

Natural abundance
Energy of peak
Phase space factor

Isotope	$G^{0\nu}$ (10^{-14} y^{-1})	$Q_{\beta\beta}$ (keV)	Nat. ab. (%)
^{48}Ca	6.35	4273.7	0.187
^{76}Ge	0.623	2039.1	7.8
^{82}Se	2.70	2995.5	9.2
^{96}Zr	5.63	3347.7	2.8
^{100}Mo	4.36	3035.0	9.6
^{110}Pd	1.40	2004.0	11.8
^{116}Cd	4.62	2809.1	7.6
^{124}Sn	2.55	2287.7	5.6
^{130}Te	4.09	2530.3	34.5
^{136}Xe	4.31	2461.9	8.9
^{150}Nd	19.2	3367.3	5.6

Table 32-1: Top: Technique and present limits per isotope [1096]; bottom: information on isotopes [1097].

We recall the basic formulae relating effective mass and ν masses through the elements U_{ei} of the leptonic mixing matrix and giving the half life, where $G^{0\nu}$ is a phase space factor and $M_{0\nu}$ is a nuclear matrix element

$$\langle m_{\beta\beta} \rangle = \left| \sum U_{ei}^2 m_i \right| \qquad \left(T_{1/2}^{0\nu}\right)^{-1} = G^{0\nu} |M_{0\nu}|^2 \left(\frac{\langle m_{\beta\beta} \rangle}{m_e}\right)^2$$

But the relation between the 0νββ decay rate and the neutrino mass is subject to large theoretical uncertainties, as it requires the knowledge of **nuclear matrix elements (NME).**

So far, experiments agree with the null-signal hypothesis, placing lower limits on the isotopes half-life $T_{1/2,}$ translating into upper bounds on $m_{\beta\beta}$ for a given NME.

Figure 32-5 and the following ones allow to compare their bounds and various aspects of their potential.

[1096] M. Agostini *et al.,* Toward the discovery of matter creation with neutrinoless ββ decay. https://arxiv.org/abs/2202.01787
C. Adams *et al.,* Neutrinoless Double Beta Decay. https://arxiv.org/abs/2212.11099
[1097] B. J. P. Jones, The Physics of Neutrinoless Double Beta Decay : A Primer. https://arxiv.org/abs/2108.09364

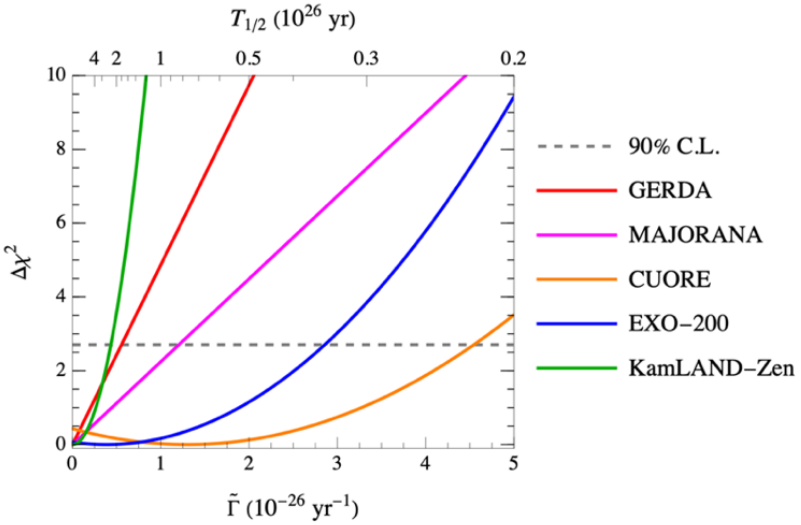


Fig. 32-5: $\Delta\chi^2$ profiles for experiments versus the 0νββ inverse half time (bottom abscissa) and half-life (top abscissa) of related isotope [1098] .

32.1.2 Backgrounds

A major problem concerns the **background level**. Figures 32-6 and 32-7 give estimates for various programs.

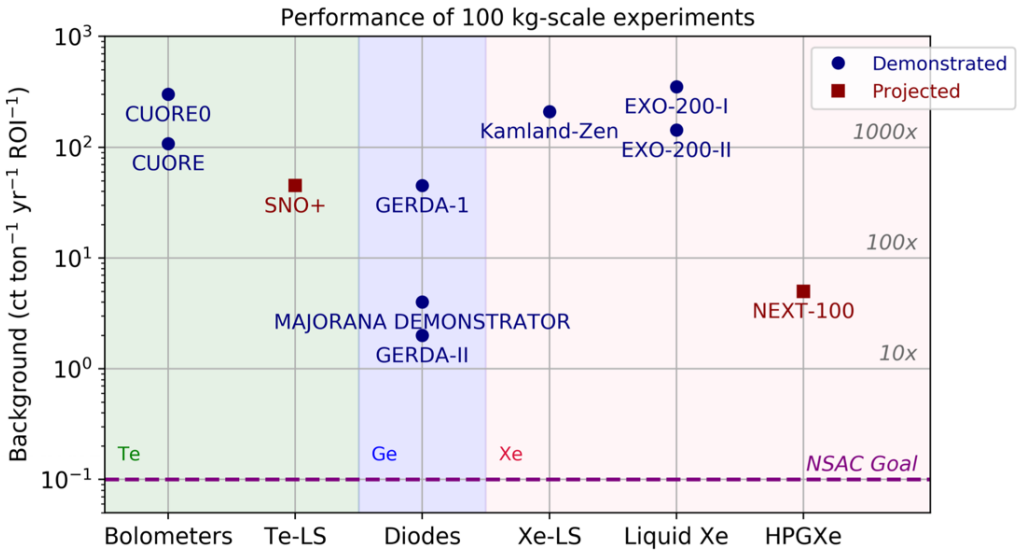


Fig. 32-6: Approximate background indices in present (100kg scale) programs [1099].

[1098] F. Pompa *et al.,* Impact of nuclear matrix element calculations for current and future neutrinoless double beta decay searches. https://arxiv.org/abs/2303.10562 . The a, b, c coefficients introduced in this reference and derived from the info given by each experiment allow to build the $\Delta\chi^2$. Actually, CUORE now reaches a half-life of $T_{1/2} > 3.5$ 1025 yr (90% CL). See https://www.science.org/doi/10.1126/science.adp6474
See also I. Nutini, New results from the CUORE experiment. Moriond EW 2024.
https://indico.in2p3.fr/event/32664/contributions/137004/attachments/83746/124733/1_INutini-v1.pdf

[1099] B. J. P. Jones, The Physics of Neutrinoless Double Beta Decay : A Primer. https://arxiv.org/abs/2108.09364

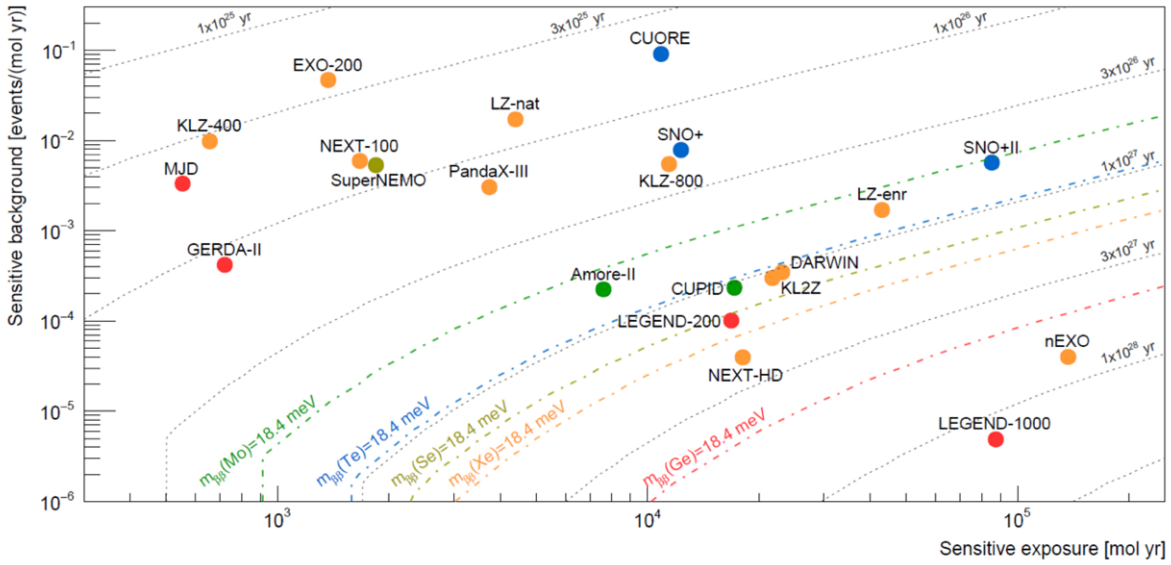


Fig. 32-7: Experiments and their sensitive background versus exposure [1100].

32.1.3. Interpretation and identification

The interpretation of 0νββ decay and, if discovered, the identification of the mechanism requires an ambitious theoretical program, in particular the calculation of the **hadronic and nuclear matrix elements**. One must compute 0νββ decay rates with minimal model dependence and quantified theoretical uncertainty, which requires progress in particle and nuclear effective field theories (EFTs), lattice QCD and ab-initio nuclear-many-body methods. Figures 32-8 and 32-9 give an idea of the dispersion of these estimates.

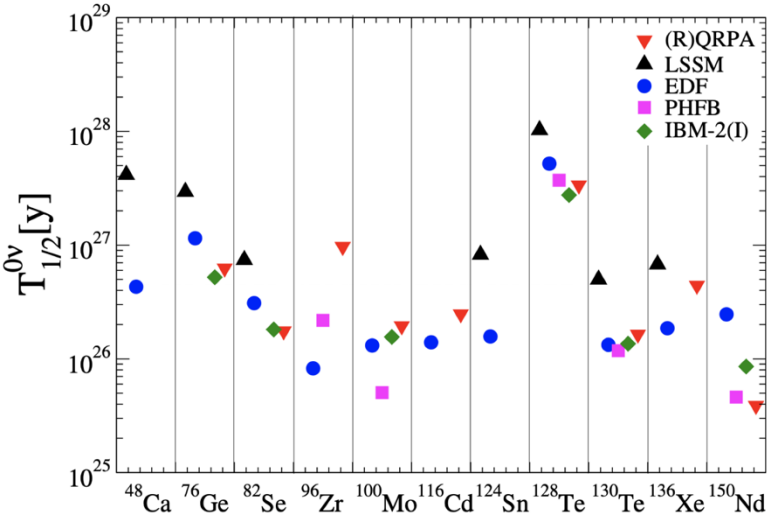


Fig. 32-8: Predictions for the half-life of 0νββ in a given reference model with different calculated nuclear matrix elements [1101].

[1100] R. Cesarano, LEGEND: Large Enriched Germanium Experiment for Neutrinoless ββ Decay. https://agenda.infn.it/event/38205/contributions/222314/attachments/117044/168935/2024-03-04-Cesarano-LaThuile2024.pdf
[1101] B. J. P. Jones, The Physics of Neutrinoless Double Beta Decay: A Primer. https://arxiv.org/abs/2108.09364

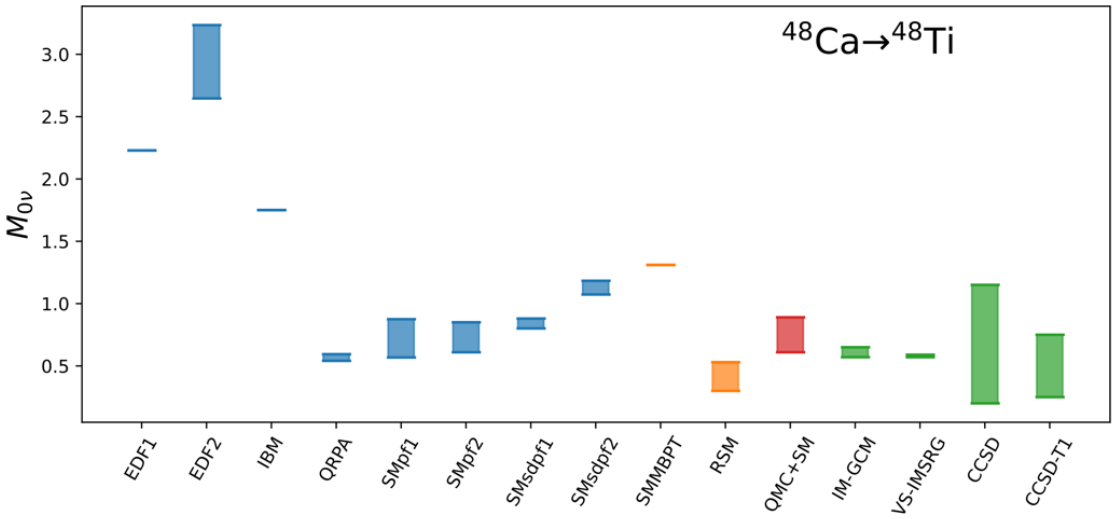


Fig. 32-9: NME (M0ν) for 0νββ 48Ca → 48 Ti [1102].

32.1.4 Current and future experiments

Table 32-2 and Fig. 32-10 give details about current and future experiments.

Experiment	Isotope	ε [mol·yr]	b [events/(mol·y)]	PSF [yr^{-1} eV^{-2}]
LEGEND-1000	^{76}Ge	8736	$4.9 \cdot 10^{-6}$	$2.36 \cdot 10^{-26}$
SuperNEMO	^{82}Se	185	$5.4 \cdot 10^{-3}$	$10.19 \cdot 10^{-26}$
CUPID	^{100}Mo	1717	$2.3 \cdot 10^{-4}$	$15.91 \cdot 10^{-26}$
SNO+II	^{130}Te	8521	$5.7 \cdot 10^{-3}$	$14.2 \cdot 10^{-26}$
nEXO	^{136}Xe	13700	$4.0 \cdot 10^{-5}$	$14.56 \cdot 10^{-26}$

Table 32-2: Future experiments performances and phase space factor [1103].

SuperNEMO continues to exploit a unique and powerful technique initiated by NEMO-3 (Fig. 32-11) with reconstruction of the topology, energy and timing of decays. Commissioning of its Demonstrator in Modane is proceeding [1104].

The next generation of experiments, Legend-1000, KAMLAND-ZEN-1T and nEXO, will cover the inverted ordering (IO) scenario (Fig. 32-12) [1105]. About ν masses, one will follow the evolution of the three methods illustrated by Figs. 19-8 to 19-10.

[1102] C. Adams *et al.,* Neutrinoless Double Beta Decay. https://arxiv.org/abs/2212.11099

[1103] F. Pompa *et al.,* Impact of nuclear matrix element calculations for current and future neutrinoless double beta decay searches. https://arxiv.org/abs/2303.10562
The a, b, c coefficients, introduced in this reference and derived from the info given by each experiment allow to build the $\Delta\chi^2$. Actually, CUORE now reaches a half-life of $T_{1/2} > 3.5\ 10^{25}$ yr (90% CL).
See https://www.science.org/doi/10.1126/science.adp6474

[1104] X. Aguerre *et al.,* Calorimeter Commissioning of the SuperNEMO demonstrator. https://arxiv.org/abs/2412.18021

[1105] S. Mertens, 0νββ and direct neutrino mass measurements. ICHEP 2024,
https://indico.cern.ch/event/1291157/contributions/5958324/attachments/2901872/5089559/Mertens_ICHEP_final.pdf

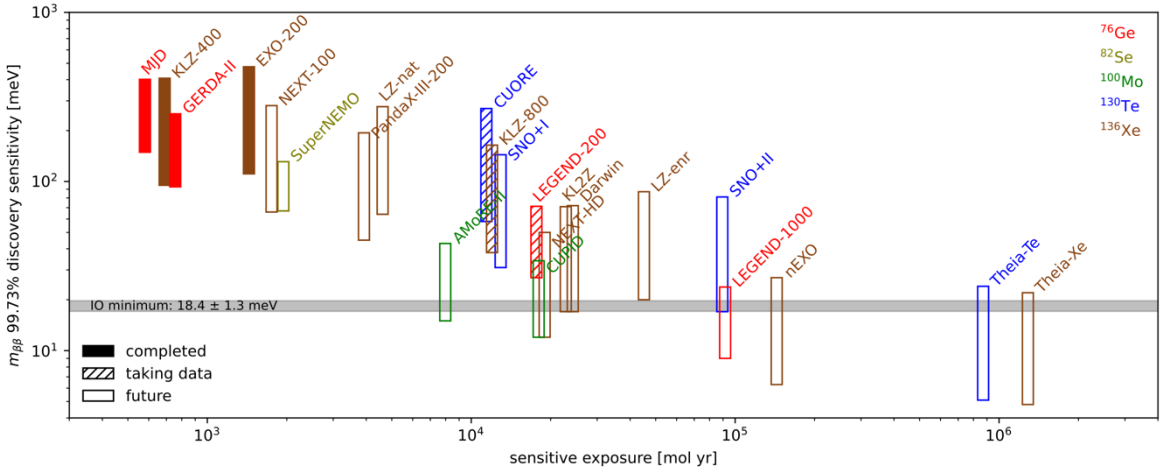


Fig. 32-10: Discovery sensitivity of current and upcoming 0νββ experiments for different mechanisms of lepton number violation [1106].

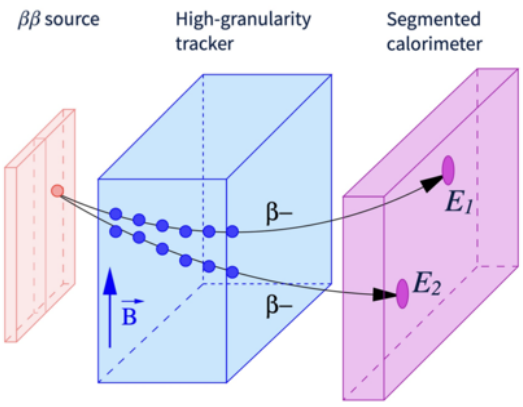


Fig. 32-11: The NEMO method.

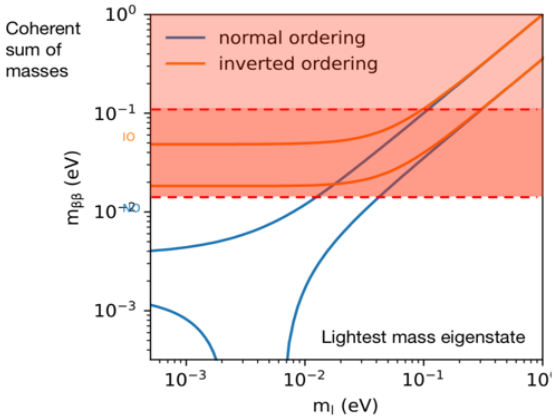


Fig. 32-12: Towards covering the IO.

To recall the complexity of such analyses Fig. 32-13 shows the CUORE spectrum. Table 32-3 list experiments in progress, in preparation or planned and Table 32-4 shows experiments in progress, in preparation or planned, with different information.

[1106] C. Adams *et al.,* Neutrinoless Double Beta Decay, https://arxiv.org/abs/2212.11099

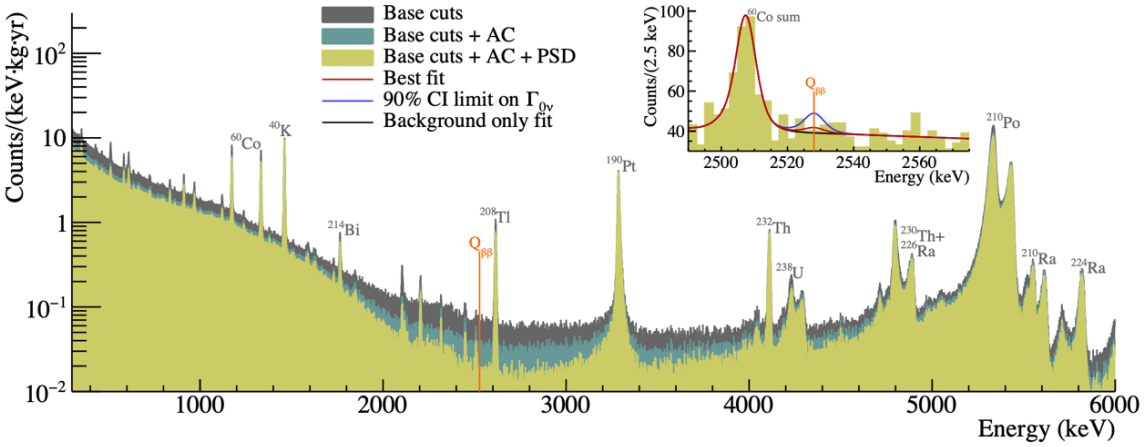


Fig. 32-13: The CUORE physics spectrum [1107], with zoom on the region of interest.

Experiment	Isotope	Mass	Technique	Present Status	Location
CANDLES-III [124]	^{48}Ca	305 kg	$^{nat}CaF_2$ scint. crystals	Operating	Kamioka
CDEX-1 [125]	^{76}Ge	1 kg	^{enr}Ge semicond. det.	Prototype	CJPL
CDEX-300ν [125]	^{76}Ge	225 kg	^{enr}Ge semicond. det.	Construction	CJPL
LEGEND-200 [16]	^{76}Ge	200 kg	^{enr}Ge semicond. det.	Commissioning	LNGS
LEGEND-1000 [16]	^{76}Ge	1 ton	^{enr}Ge semicond. det.	Proposal	
CUPID-0 [19]	^{82}Se	10 kg	Zn^{enr}Se scint. bolometers	Prototype	LNGS
SuperNEMO-Dem [126]	^{82}Se	7 kg	^{enr}Se foils/tracking	Operation	Modane
SuperNEMO [126]	^{82}Se	100 kg	^{enr}Se foils/tracking	Proposal	Modane
Selena [127]	^{82}Se		^{enr}Se, CMOS	Development	
IFC [128]	^{82}Se		ion drift SeF_6 TPC	Development	
CUPID-Mo [17]	^{100}Mo	4 kg	Li$^{enr}MoO_4$,scint. bolom.	Prototype	LNGS
AMoRE-I [129]	^{100}Mo	6 kg	^{40}Ca$^{100}MoO_4$ bolometers	Operation	YangYang
AMoRE-II [129]	^{100}Mo	200 kg	^{40}Ca$^{100}MoO_4$ bolometers	Construction	Yemilab
CROSS [130]	^{100}Mo	5 kg	$Li_2{}^{100}MoO_4$, surf. coat bolom.	Prototype	Canfranc
BINGO [131]	^{100}Mo		Li$^{enr}MoO_4$	Development	LNGS
CUPID [28]	^{100}Mo	450 kg	Li$^{enr}MoO_4$,scint. bolom.	Proposal	LNGS
China-Europe [132]	^{116}Cd		$^{enr}CdWO_4$ scint. crystals	Development	CJPL
COBRA-XDEM [133]	^{116}Cd	0.32 kg	^{nat}Cd CZT semicond. det.	Operation	LNGS
Nano-Tracking [134]	^{116}Cd		^{nat}CdTe. det.	Development	
TIN.TIN [135]	^{124}Sn		Tin bolometers	Development	INO
CUORE [10]	^{130}Te	1 ton	TeO_2 bolometers	Operating	LNGS
SNO+ [136]	^{130}Te	3.9 t	0.5-3% ^{nat}Te loaded liq. scint.	Commissioning	SNOLab
nEXO [29]	^{136}Xe	5 t	Liq. ^{enr}Xe TPC/scint.	Proposal	
NEXT-100 [137]	^{136}Xe	100 kg	gas TPC	Construction	Canfranc
NEXT-HD [137]	^{136}Xe	1 ton	gas TPC	Proposal	Canfranc
AXEL [138]	^{136}Xe		gas TPC	Prototype	
KamLAND-Zen-800 [13]	^{136}Xe	745 kg	^{enr}Xe disolved in liq. scint.	Operating	Kamioka
KamLAND2-Zen [41]	^{136}Xe		^{enr}Xe disolved in liq. scint.	Development	Kamioka
LZ [139]	^{136}Xe	600 kg	Dual phase Xe TPC, nat./enr. Xe	Operation	SURF
PandaX-4T [119]	^{136}Xe	3.7 ton	Dual phase nat. Xe TPC	Operation	CJPL
XENONnT [140]	^{136}Xe	5.9 ton	Dual phase Xe TPC	Operating	LNGS
DARWIN [141]	^{136}Xe	50 ton	Dual phase Xe TPC	Proposal	LNGS
R2D2 [142]	^{136}Xe		Spherical Xe TPC	Development	
LAr TPC [143]	^{136}Xe	kton	Xe-doped LR TPC	Development	
NuDot [144]	Various		Cherenkov and scint. in liq. scint.	Development	
THEIA [145]	Xe or Te		Cherenkov and scint. in liq. scint.	Development	
JUNO [146]	Xe or Te		Doped liq. scint.	Development	
Slow-Fluor [147]	Xe or Te		Slow Fluor Scint.	Development	

Table 32-3: List of experiments in progress, in preparation or planned [1108].

[1107] D. Q. Adams *et al.,* Latest results from the CUORE experiment. https://inspirehep.net/files/5e629ae5beefba669f6f47baaf9ab543

[1108] C. Adams *et al.,* Neutrinoless Double Beta Decay. https://arxiv.org/abs/2212.11099

Isotope	Exposure [kg · yr]	$T_{1/2}$ [yr] at 90%	$m_{\beta\beta}$ [meV]	Experiment
^{76}Ge	~ 6632	$\sim 10^{28}$	XXX	LEGEND (planned) [179]
^{76}Ge	~ 1325	$\sim 10^{27}$	XXX	LEGEND (planned) [179]
^{76}Ge	110.7	$> 1.8 \cdot 10^{26}$	$< 79 - 180$	GERDA [18]
^{76}Ge	64.5	$> 8.3 \cdot 10^{25}$	$< 113 - 269$	Majorana [25]
^{82}Se	~ 1300	$\sim 10^{26}$	XXX	SuperNEMO (demo) [14]
^{82}Se	5.29	$> 4.6 \cdot 10^{24}$	$< 263 - 545$	CUPID-0 [21]
^{100}Mo	~ 1715	$\sim 10^{27}$	XXX	CUPID [15]
^{100}Mo	1.47	$> 1.8 \cdot 10^{24}$	$< 280 - 490$	CUPID-Mo [22]
^{128}Te	78.56	$> 3.6 \cdot 10^{24}$	XXX	CUORE [23]
^{130}Te	1300	$> 2 \cdot 10^{26}$	XXX	SNO+ [20]
^{130}Te	200	$> 3.5 \cdot 10^{26}$	XXX	CUORE [24]
^{130}Te	288.8	$> 2.2 \cdot 10^{25}$	$< 90 - 305$	CUORE [24]
^{136}Xe	~ 5000	$\sim 10^{27} - 10^{28}$	XXX	nEXO (planned) [19]
^{136}Xe	970	$> 2.3 \cdot 10^{26}$	$< 36 - 156$	KamLAND-Zen [26]
^{136}Xe	100	$> 5.9 \cdot 10^{25}$	XXX	NEXT (demo) [16]
^{136}Xe	234.1	$> 3.5 \cdot 10^{25}$	$< 93 - 286$	EXO-200 [17]

Table 32-4: List of experiments in progress, in preparation or planned, with different information [1109].

32.2 Electric Dipole Moments

Observing an Electric Dipole Moment (EDM) in any physical system (electron, neutron, proton, atom, molecule) would be **a sign of new physics**. In case of maximum CP symmetry breaking, an EDM, with the sensitivity of current measurements, would give access to BSM mass scales far superior to those offered by a collider (see also Fig. 32-26).

32.2.1 EDM limits

Figure 32-14 recalls the limits reached over the years for electrons and neutrons.

The best for the **neutron EDM** comes from the nEDM @PSI experiment: $|d_n| < 1.8 \times 10^{-26}\ e$ cm. Figure 32-15 shows the expected future evolution.

Figure 32-16 gives the limits of **electron EDM** with access to new physics for one- and two-loop effects. All current experiments use **AMO** (Atomic, Molecular and Optical) techniques. The solid line indicates the most sensitive, the shade the potential progress. The best limit comes from Ref. [1110] and as second the **ACME** experiment [1111]. These experiments are briefly described below. Figure 32-17 gives the limits for the neutron and the proton (indirect) and the sensitivities expected for the proton and the deuteron in the **storage ring method**.

Observing a signal in a single system will undoubtedly mark the discovery of new physics but will be insufficient to discriminate between BSM models. It will have to be observed, or be set limits, in other systems. This will require a **coordinated experiment-theory program** between disciplines, PP, nuclear and AMO, also offering opportunities for search of dark matter, dark energy, axions. Theoretical progress in various areas will be needed to improve the interpretation of experimental results.

[1109] G. van Goffrier, Nuclear and Particle Physics Aspects of Neutrinoless Double-Beta Decay (Thesis). https://inspirehep.net/files/3a781c838d4a7a7757021ef953329c42

[1110] T.S. Roussy *et al.,* A new bound on the electron's electric dipole moment. https://arxiv.org/abs/2212.11841

[1111] V. Andereev *et al.,* Improved limit on the electric dipole moment of the electron. *Nature 562 (2018) 7727, 355-360*

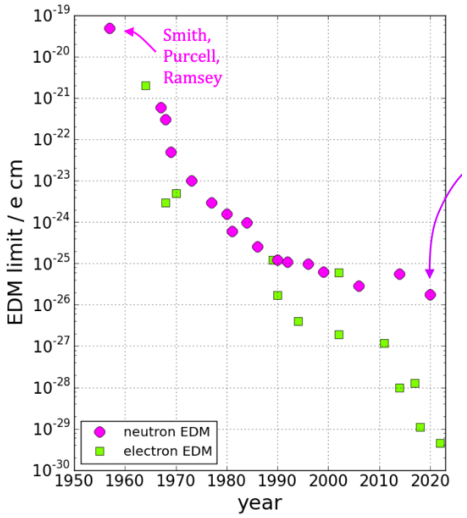


Fig. 32-14: Evolution of EDM limits since the 1950's. Purple arrow at the right side indicates the best limit from the nEDM experiment @PSI [1112].

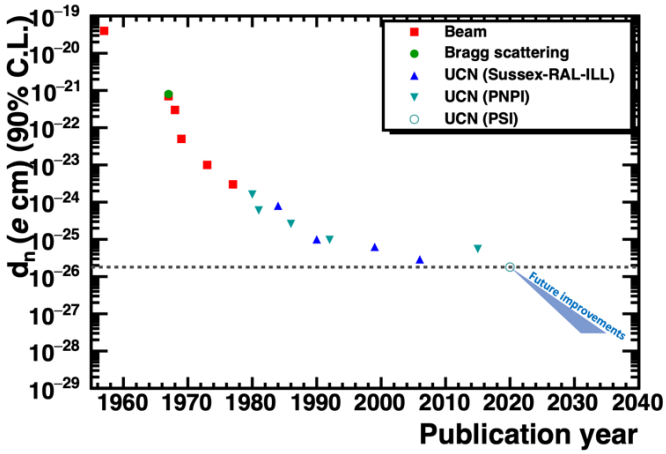


Fig. 32-15: Evolution of the nEDM results and projected future improvements [1113].

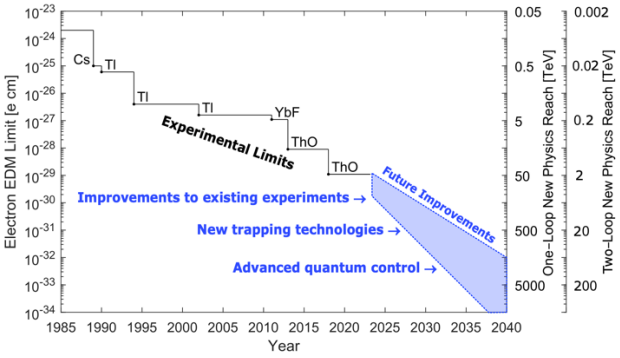


Fig. 32-16: Limits of electron EDM versus time [1114].

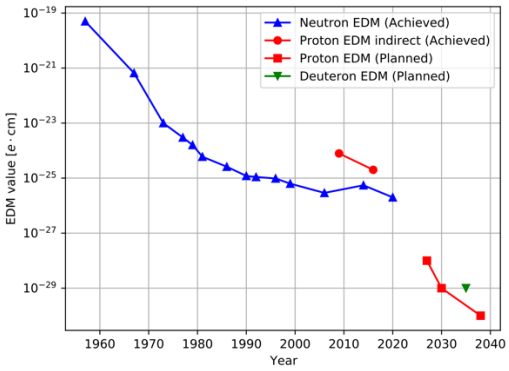


Fig. 32-17: Limits of n, p and deuteron EDM versus time [1115].

Another legitimate question is to ask what such results on EDMs **have actually set as limits or even excluded in some physics sectors**, or which features must be added to ensure their survival (see the right side of Fig. 32-16). A question [1116] is for instance: "Does the Electron EDM Preclude EW Baryogenesis?" (this is alluded to in Section 24.1.5). Some more in the next section.

[1112] G. Pignol, The n2EDM experiment. Presentation in Moriond EW (2023), https://indico.in2p3.fr/event/29681/contributions/122511/attachments/76508/111037/08-GPignol-v1.pdf
C. Abel *et al.,* Measurement of the Permanent Electric Dipole Moment of the Neutron. *Phys.Rev.Lett. 124, 081803 (2020),* https://journals.aps.org/prl/pdf/10.1103/PhysRevLett.124.081803

[1113] R. Alarcon *et al,* Electric dipole moments and the search for new physics. https://arxiv.org/abs/2203.08103

[1114] R. Alarcon *et al.,* Electric dipole moments and the search for new physics. https://arxiv.org/abs/2203.08103

[1115] ibid

[1116] Y-Z. Li *et al.,* Does the Electron EDM Preclude Electroweak Baryogenesis? https://arxiv.org/abs/2404.19197

32.2.2 More on two of the last eEDM experiments

An eEDM $\vec{d}_e = d_e \hat{s}$ with $\hat{s}$ a unit vector along the electron spin, subject to an electric field $\vec{\mathcal{E}}$ has an energy of $-\vec{d}_e \cdot \vec{\mathcal{E}}$. The idea of an eEDM search is to measure the energy shift when $\hat{s}$ is **aligned with $\vec{\mathcal{E}}$ compared with when it is anti-aligned.** Since the shift scales with the size of $\vec{\mathcal{E}}$, many eEDM experiments use **electrons embedded inside polar molecules**, where intramolecular electric fields can be ~ **five orders of magnitude larger** than what can be directly applied in the lab. Modest external electric fields are sufficient to align these internal electric fields in the lab frame by orienting the molecules.

Reference [1117] uses **HfF^+ molecular ions**. In an **applied electric field of ~58 V cm^{-1}**, the EDM sensitive state of the molecule is split into a series of doublets. In two of them (Fig. 32-18 left), the molecule is oriented: in the upper doublet the intramolecular axis is parallel to the applied field, in the lower doublet it is antiparallel. This intramolecular axis defines the direction of an **effective electric field,** E_{eff} = 23 GV cm^{-1} active on the spin of one of the valence e^-. In the presence of a small B field, the two states in a doublet correspond to the spin of this valence electron being **aligned or anti-aligned with E_{eff}.**

On a coherent superposition of the two spin states the experiment measures the energy difference using **Ramsey spectroscopy,** with coherent evolution up to 3 seconds. The eEDM will give a contribution to this energy, $\pm 2 d_e E_{eff}$, with opposite sign in the two doublets. The measurement is performed simultaneously on spatially overlapping clouds of ions prepared in each of the doublets. The difference between the measured energies is the *science signal*.

The sequence starts by producing and radiofrequency trapping about 20 000 ions **in a trap**, shown in Fig. 32-18 right, with the fields applied, the rotating electric bias field $\vec{\mathcal{E}}_{rot}$ and the quadrupole magnetic field $\vec{B}^0$. An imaging microchannel plate and phosphor screen assembly allows, when needed, to count the population of molecular ions by detecting Hf^+ ions after photodissociation.

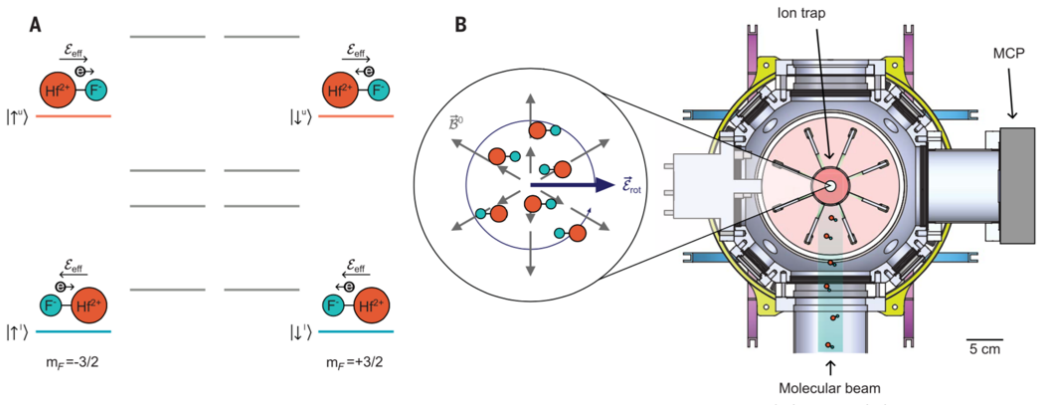


Fig. 32-18: The up and down doublets with opposite relative orientation (left); the trap and its fields (right).

Then follows a very elaborate sequence of preparation of states, Ramsey procedure, cleaning out of unwanted spin states and counting the relevant ion populations, repeated with opposite initial spin state and with different coherent evolution times.

[1117] T. S. Roussy *et al.,* An improved bound on the electron's electric dipole moment. https://jila.colorado.edu/sites/default/files/2023-08/eEDM_Science_2023.pdf

The subsequent analysis leads to $d_e = (-1.3 \pm 2.0\,\text{stat} \pm 0.6\,\text{syst}) \times 10^{-30}$ e cm, consistent with zero and giving an upper bound of $|d_e| < 4.1 \times 10^{-30}$ e cm at 90% confidence.

The ACME experiment [1118] uses a **cryogenic molecular beam of the heavy polar molecule ThO.** The molecules are prepared in a metastable electronic state, which has two valence electrons with parallel spins. In this state, the EDM of one of these valence electrons experiences a huge effective **intramolecular electric field**, $E_{eff} \sim 75$ GV/cm. The second valence electron serves to cancel the magnetic moment of the first, so the molecule is less sensitive to magnetic field-induced torques.

To measure d_e, a **spin precession measurement** is performed on pulses of $^{232}Th^{16}O$ molecules coming from a cryogenic buffer gas beam source. The molecules enter a magnetically shielded vacuum chamber that contains **uniform parallel electric and magnetic fields**. They are optically pumped into the "H" electronic EDM sensitive state, which present two sets of states, one with the **molecular axis aligned with the electric field, and the other anti-aligned**, corresponding to opposite directions of the effective intramolecular E-field, and undesired polarizations are optically pumped out of the H state. The molecules precess in the fields, and one reads out the accumulated phase with polarized lasers. By **reversing the E field**, one can reverse the amount of precession accumulated from the eEDM; taking the difference between these two phases yields the eEDM. The result is $|d_e| < 8.7 \times 10^{-29}$ e cm.

The impact of these results on the eEDM is considered as major on a number of theories. One is **EW baryogenesis** that was considered in Chapter 24 [1119]. We will come back to this point in Section 32.4.

The estimate of the eEDM [1120] generated in a BSM theory has, at one loop, the following magnitude $d_e \sim \frac{e a_0 \alpha}{2} \frac{g^2}{2\pi} \sin\Phi_{CP} \frac{m_e^2}{M^2}$, where M is the typical mass of new particles, with effective coupling g to the electron, and Φ_{CP} is the phase that describes how strongly the interaction violates CP. Assuming for instance $\sin\Phi_{CP} = 1$ and $g^2 = \alpha$, the formula and the limit on d_e gives M = 40 TeV! Hence the spectacular peak of d_e in Fig. 32-26.

32.2.3 Some more on neutron EDM

The measurement of the neutron electric dipole moment (nEDM) [1121] belongs to the very important fundamental physics experiments at low energy. It is a very promising route for finding new physics beyond the SM.

In parallel electric and magnetic fields, the neutron spin precesses around the fields at an angular frequency given by $\omega = 2(\mu B + d E)/\hbar$. The EDM term can be separated from the magnetic term by taking the difference of the frequency measured in parallel and anti-parallel field configurations. But the electric term is extremely small. For $d = 10^{-26}$ e cm and E = 15 kV/cm, the spin would only complete about **two full turns per year**, due to the electric term. From the formula on the expected uncertainty $\sigma(d_n) = \hbar/(2\,E\,T\,\alpha\sqrt{N})$ one sees that the key requirements are a long interaction time T with a large electric field E, a high flux of neutrons N and a precise control of the magnetic field.

[1118] P.W. Hess, Improving the Limit on the Electron EDM: Data Acquisition and Systematics Studies in the ACME Experiment. Doctoral dissertation, Harvard University, 2014. http://nrs.harvard.edu/urn-3:HUL.InstRepos:12274320
https://inspirehep.net/files/0414eff02dfbec0bb2841ab42712a22b
https://jdoyle.hsites.harvard.edu/tho-electron-edm

[1119] D. Bödeker and W. Buchmüller, Baryogenesis from the weak scale to the grand unification scale. https://arxiv.org/abs/2009.07294

[1120] T. S. Roussy *et al.,* An improved bound on the electron's electric dipole moment. https://www.science.org/doi/10.1126/science.adg4084 and
https://jila.colorado.edu/sites/default/files/2023-08/eEDM_Science_2023.pdf

[1121] E. Chanel *et al.,* The Pulsed Neutron Beam EDM Experiment. https://arxiv.org/abs/1812.03987
B. W. Filippone, Worldwide Search for the Neutron EDM. https://arxiv.org/abs/1810.03718

We recall that the latest measured value of the nEDM upper limit is 1.8×10^{-26} e·cm (90% CL).

It used **ultracold neutrons (UCNs).** UCN have kinetic energies below about 300 neV, corresponding to velocities below 8 m/s, and temperatures below 4 mK. This energy is the same as the neutron **optical potential** of some materials. Thus, **material bottles** can be used to store UCNs (Section 32.5). This energy corresponds also to the potential difference of a neutron raised by 3 m in the Earth's gravitational field, or to the potential difference of a 5 Tesla magnetic field gradient acting on the neutron magnetic moment. UCN are totally reflected on material surfaces. Stored, they can be manipulated and studied for a time as long as their lifetime of ~ 15 minutes.

UCN are produced either from a reactor or from a lead spallation target, as the PSI UCN source [1122].

Figure 32-19 [1123] recalls upper limits of the nEDM compared to others EDMs. Table 32-5 summarizes the ongoing searches for a nEDM using UCN [1124]. The last column gives the EDM sensitivity after several years of running.

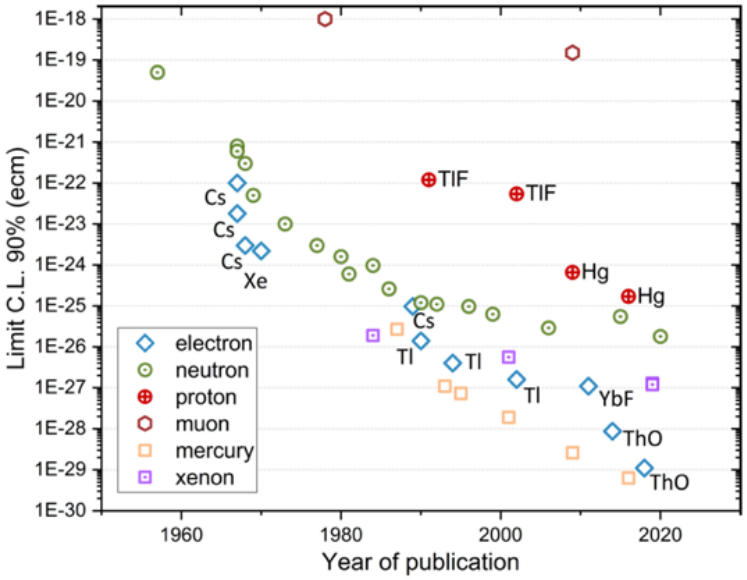


Fig. 32-19: History of upper EDM limits (CL 90%) as function of the year of publication.

32.2.4 A nice by-product

As we saw in Section 31.3, abundant DM particles as axions could be just described as a **classical coherently oscillating field**. ALPs could induce EDMs of neutrons [1125] via their coupling to gluons (as with the QCD-term) and those EDMs would be oscillating at the Compton frequency of the axion field. Ignoring this frequency, one must perform a broad search at all accessible ones. For the nEDM experiment, this is the range of **inverse time scales of the measurements**, from single cycle duration of a few minutes to several years of data taking, covering 6 orders of magnitude.

Figure 32-20 shows the laboratory exclusion of DM axion-like particle obtained using UCN at PSI [1126].

[1122] B. Lauss and B. Blau, UCN, the ultracold neutron source - neutrons for particle physics. https://arxiv.org/abs/2104.02457
[1123] K. Kirch and Ph. Schmidt-Wellenburg, Search for electric dipole moments. https://arxiv.org/abs/2003.00717
[1124] B. W. Filippone, Worldwide Search for the Neutron EDM. https://arxiv.org/abs/1810.03718
[1125] K. Kirch and B. Lauss, Ultracold Neutrons. https://arxiv.org/abs/2006.04568
[1126] ibid

Experiment	UCN Source	Cell	Technique	Sensitivity x10^{-28} e-cm
ILL-PNPI	ILL turbine PNPI-SD_2	Vac.	Ramsey technique for ω E=0 cell for magentometry	Phase 1 < 100 Phase 2 < 10
PSI nEDM	SD_2	Vac.	Ramsey, Cs + Hg co-mag. ^{3}He, Hg, Cs magnetom.	Phase 1 < 100 Phase 2 < 20
Munich/ILL	SD_2@FRMII LHe@ILL	Vac.	Ramsey + Hg co-mag. + external ^{3}He/Cs mag.	Phase 1 < 50 Phase 2 < 5
TRIUMF (TUCAN)	LHe-II	Vac.	Ramsey technique with Hg + Xe co-mag.	< 50
SNS nEDM	LHe-II	LHe	Cryo-HV, n-^{3}He capture for ω, SQUIDS+Critical dressing	< 5
JPARC	SD_2	Vac.	Under Devlopment	< 5(?)
LANL EDM	SD_2	Vac.	Ramsey with Hg	< 50

Table 32-5: Summary of the ongoing searches for a neutron EDM using Ultra Cold Neutrons.

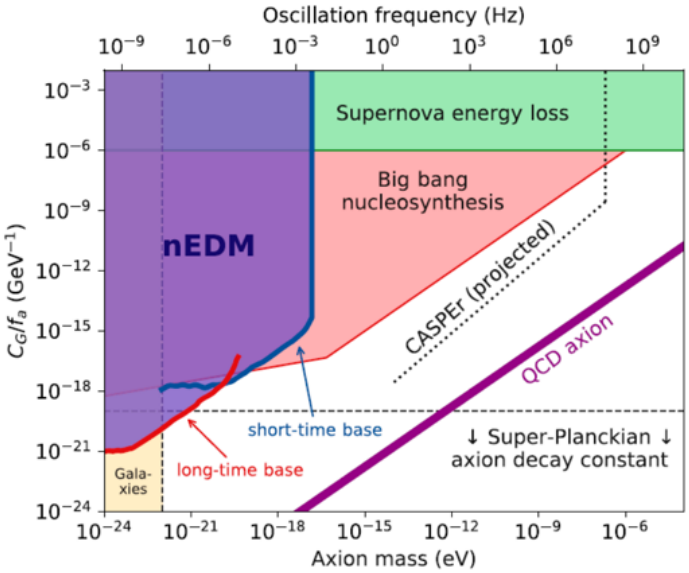


Fig. 32-20: It shows the laboratory exclusion of DM axion-like particle that would generate oscillating neutron EDM signal. Ordinate is the normalized coupling strength of ALPs to gluons in the neutron.

32.3 Still more on FCNCs

We touched on the subject of FCNCs in Chapter 8. Neutrino non-zero masses show the violation of lepton flavour (LFV). But no LFV in the interactions between **charged leptons** (CLFV) has yet been observed, while many models predict some. Searches of potential decays of this type involve many programs.

Figure 32-21 [1127] gives the numerous limits of the LFV decays of the tau lepton and Table 32-6 [1128] lists the upper limits of the relevant BRs concerning mesons and bosons (90% CL).

[1127] See the impressive paper by M. Ardu and G. Pezzullo, Introduction to Charged Lepton Flavor Violation. https://arxiv.org/abs/2204.08220

[1128] ibid , Table drawn from their table, which gives CLs and references.

For the top, limits ~ 10^{-5} are put on the BR of processes as t → uγ, uZ, cZ (Fig. 8-9). BR (t → e μ q) limits are shown in Table 32-7 [1129]. Even the Higgs boson is the object of such studies.

Among the CLFV experiments, **muons have so far taken centre stage** [1130], see the MEG [1131] and SINDRUM [1132] experiments.

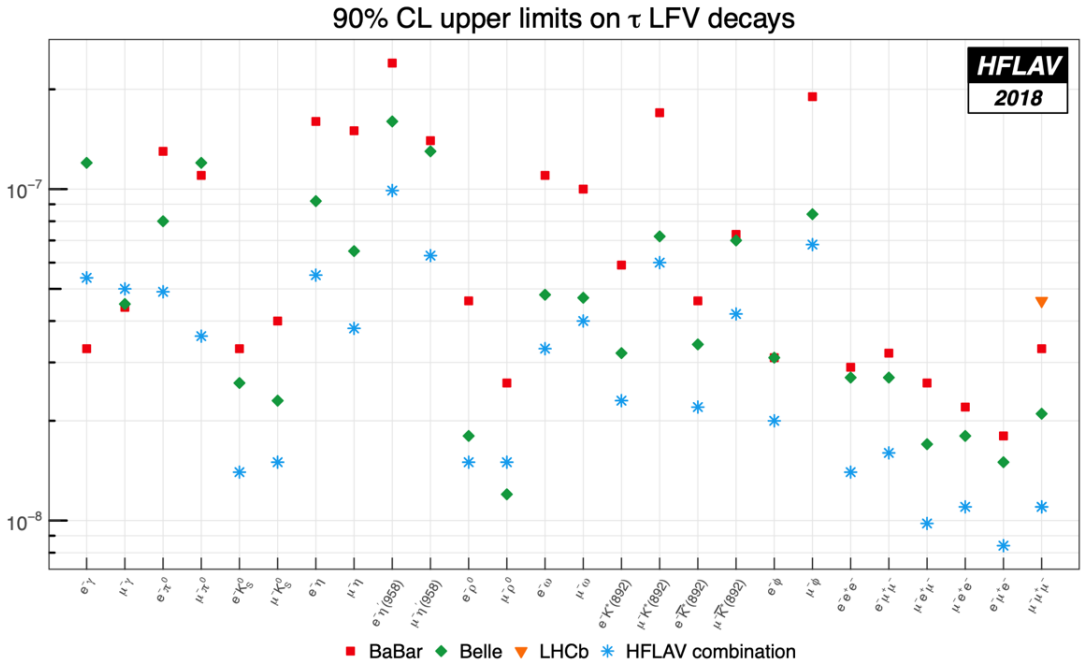


Fig. 32-21: Limits of the LFV decays of the tau lepton.

In the SM with ν masses the μ → e γ process (Fig. 32-22) is described by the penguin diagram and is proportional to the off-diagonal elements of the PMNS matrix. Due to chirality conservation it is also proportional to the ν masses. With the present ν oscillation data, one can estimate the branching ration BR_{SM} (μ → e γ) ~ 10^{-55}. However, μ → e γ decay might turn to a direct manifestation of physics BSM, in particular SUSY.

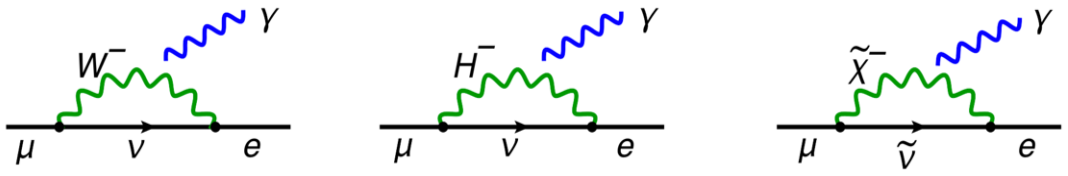


Fig. 32-22: μ → e γ processes [1133].

[1129] L. Skinnari, Top Measurements at ATLAS & CMS. la Thuile 2024, https://agenda.infn.it/event/38205/contributions/219717/attachments/117202/169224/skinnari_TopMeasurements_LaThuile2024.pdf
[1130] A. Knecht *et al.,* Science Case for the new High-Intensity Muon Beams HIMB at PSI. https://arxiv.org/abs/2111.05788
[1131] L. Galli, The MEG experiment result and the MEG II status. *Nuovo Cim.C 41 (2018) 1-2, 42*
J. Adam *et al.,* The MEG detector for $\mu^+ \rightarrow e^+\gamma$ decay search. https://arxiv.org/abs/1303.2348
[1132] SINDRUM Collaboration, Search for the decay $\mu^+ \rightarrow e^+e^+e^-$. *Nucl. Phys.B 299 (1988) 1-6*
[1133] M. Davidkov and D. I. Kazakov, $\mu \rightarrow e\gamma$ Decay Rate in the MSSM with Minimal Flavour Violation. https://arxiv.org/abs/1102.1582

Process	Experiment	Limit
$\mu^+ \to e^+\gamma$	MEG	4.2×10^{-13}
$\mu^+ \to e^+e^-e^+$	SINDRUM	1.0×10^{-12}
$\mu^-\mathrm{N} \to e^-\mathrm{N}$	SINDRUM-II	$6.1(7.1) \times 10^{-13}$ Ti
$\mu^-\mathrm{N} \to e^+\mathrm{N}'$	SINDRUM-II	5.7×10^{-13}
$\tau\pm \to e^\pm\gamma$	BaBar	3.3×10^{-8}
$\tau^\pm \to \mu^\pm\gamma$	BaBar	4.4×10^{-8}
$\tau \to eee$	Belle	2.7×10^{-8}
$\tau \to \mu\mu\mu$	Belle	2.1×10^{-8}
$\tau \to \mu ee$	Belle	1.8×10^{-8}
$\tau \to e\mu\mu$	Belle	2.7×10^{-8}
$\tau \to \pi^0 e$	Belle	8.0×10^{-8}
$\tau \to \pi^0 \mu$	BaBar	1.1×10^{-7}
$\tau \to \eta e$	Belle	9.2×10^{-8}
$\tau \to \eta \mu$	Belle	6.5×10^{-8}
$\tau \to \rho^0 e$	Belle	1.8×10^{-8}
$\tau \to \rho^0 \mu$	Belle	1.2×10^{-8}
$\pi^0 \to \mu e$	KTeV	3.6×10^{-10}
$K_L^0 \to \pi^0\mu^+e^-$	kTeV	7.6×10^{-11}
$K_L^0 \to \mu e$	BNL E871	4.7×10^{-12}
$K^+ \to \pi^+\mu^+e^-$	BNL E865	1.3×10^{-11}
$J/\psi \to \mu e$	BESIII	1.5×10^{-7}
$J/\psi \to \tau e$	BESIII	7.5×10^{-8}
$J/\psi \to \tau\mu$	BESII	2.6×10^{-6}
$B^0 \to \mu e$	LHCb	2.8×10^{-9}
$B^0 \to \tau e$	BaBar	2.8×10^{-5}
$B^0 \to \tau\mu$	LHCb	1.4×10^{-5}
$B \to K\mu e$	BaBar	3.8×10^{-8}
$B \to K^*\mu e$	BaBar	5.1×10^{-7}
$B^+ \to K^+\tau e$	BaBar	4.8×10^{-5}
$B^+ \to K^+\tau\mu$	BaBar	3.0×10^{-5}
$B_s^0 \to \mu e$	LHCb	1.1×10^{-8}
$B_s^0 \to \tau\mu$	LHCb	4.2×10^{-5}
$Z^0 \to \mu e$	ATLAS	7.5×10^{-7}
$Z^0 \to \tau e$	OPAL	9.8×10^{-6}
$Z^0 \to \tau\mu$	DELPHI	1.2×10^{-5}
$h \to \mu e$	ATLAS	6.1×10^{-5}
$h \to \tau e$	CMS	2.2×10^{-3}
$h \to \tau\mu$	CMS	1.5×10^{-3}

Table 32-6: Limits of the relevant BRs concerning mesons and bosons.

Int. type	BR (t → eμu)×10^{-7}	BR (t → eμc)×10^{-7}
Tensor	0.32	4.98
Vector	0.22	3.69
Scalar	0.12	2.16

Table 32-7: BR (t → eμq) limits.

Further research is provided by MEG II [1134], COMET [1135], Mu2e [1136] (Fermilab, US) and Mu3e [1137] at PSI [1138].

[1134] M. Meucci on behalf of the MEG II Collaboration, MEG II experiment status and prospect. https://arxiv.org/abs/2201.08200

[1135] M. J. Lee, COMET Muon Conversion Experiment in J-PARC. https://www.frontiersin.org/journals/physics/articles/10.3389/fphy.2018.00133/full

[1136] M. T. Hedges, The Mu2e experiment — Searching for charged lepton flavor violation. https://arxiv.org/abs/2210.14317

[1137] G. Hesketh *et al.,* The Mu3e Experiment. https://arxiv.org/abs/2204.00001

[1138] About PSI and its achievements: https://en.wikipedia.org/wiki/Paul_Scherrer_Institute#Energy_and_the_Environment C. Hoffman, K. Kirch and A. Signer (editors), Review of Particle Physics at PSI (PSI2020). SciPost Phys. Proc. 5, (2021), https://scipost.org/SciPostPhysProc.5

About KEK and J-PARK https://en.wikipedia.org/wiki/KEK

The goal of the MEG II experiment [1139] is the search for the LFV decay $\mu \to e\gamma$, with a sensitivity below 10^{-33}, 10 times better than phase-1 MEG experiment. Presently MEG-MEG II reach BR < 3.1×10^{-13}, see Ref.[1140].

MEG II is also good at measuring low energy e^+e^- pairs and can, exploiting a different reaction, (p +^{7}Li), check the possible existence of the 17 MeV particle candidate suggested elsewhere [1141].

Figure 32-23 shows the layout of MEG and MEG II. Figure 32-24 displays SINDRUM II and Fig. 32-25 the COMET experiment at J-PARK (Japan). Figure 32-26 summarizes the reach in new physics scale of present and future facilities, from generic dimension six operators.

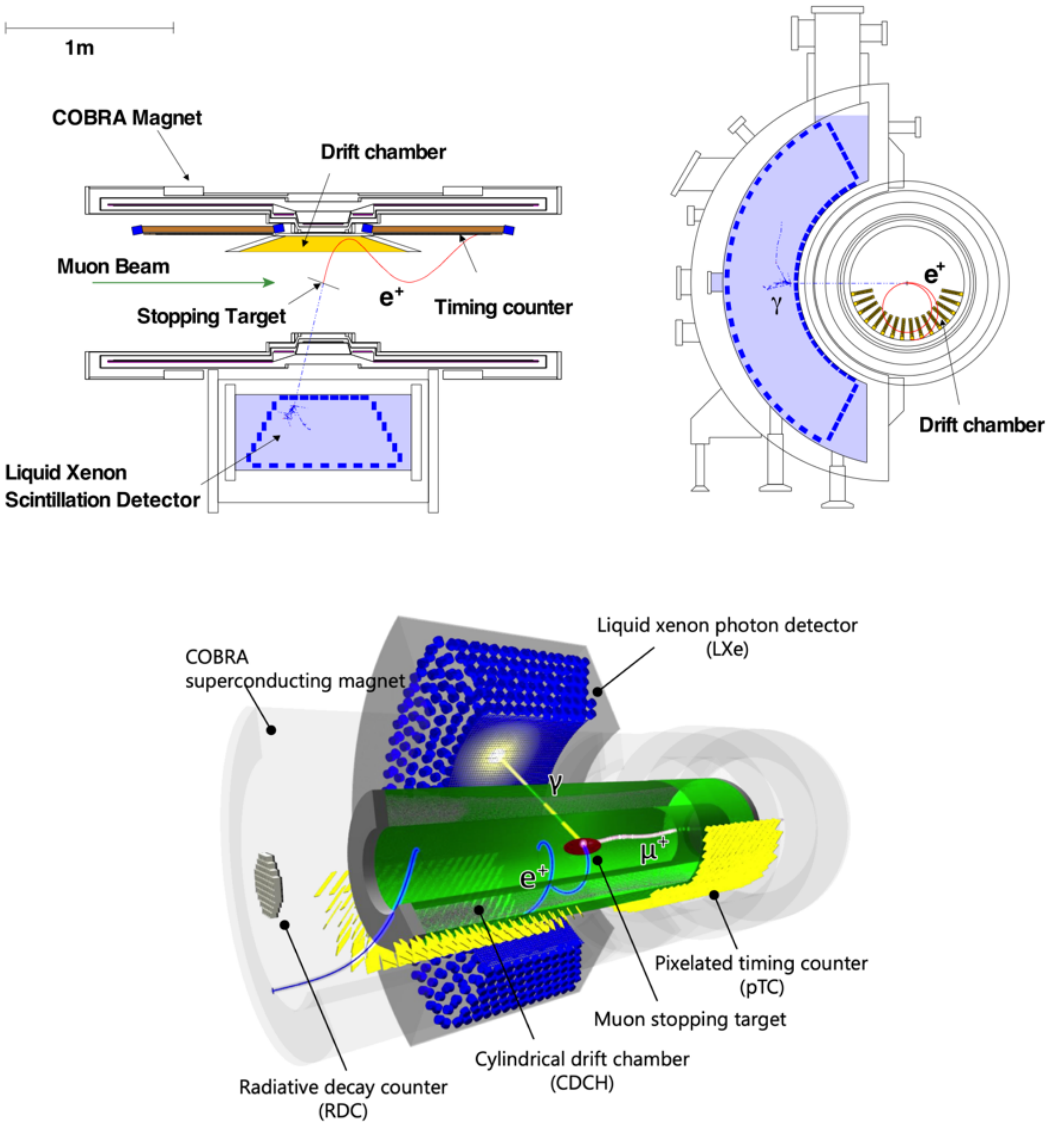


Fig. 32-23: The MEG (top) and MEGII (bottom) experiments.

[1139] F. Renga, Lepton Flavour Violation with the MEG-II Experiment. https://inspirehep.net/files/9253f71e917d0b4bf80febbf4427a836

[1140] F. Renga, Chasing muon decays: recent results from MEG II. la Thuile 2024, https://agenda.infn.it/event/38205/contributions/221666/attachments/117155/169144/renga_LaThuile2024.pdf

[1141] Mixed signals from X17. https://cerncourier.com/mixed-signals-from-x17/

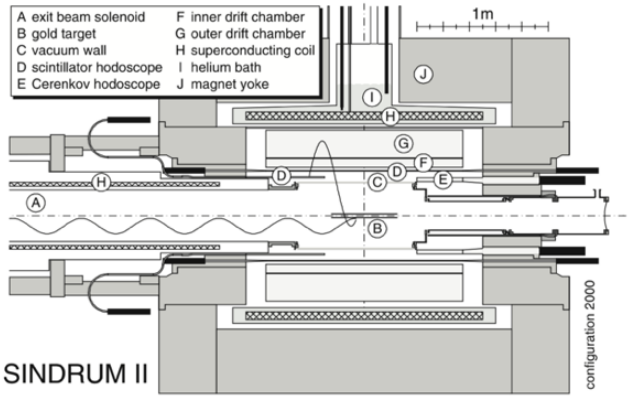


Fig. 32-24: SINDRUM II.

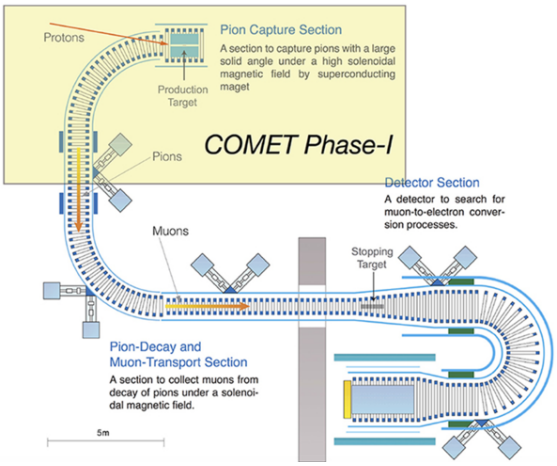


Fig. 32-25: COMET at J-PARK, Japan.

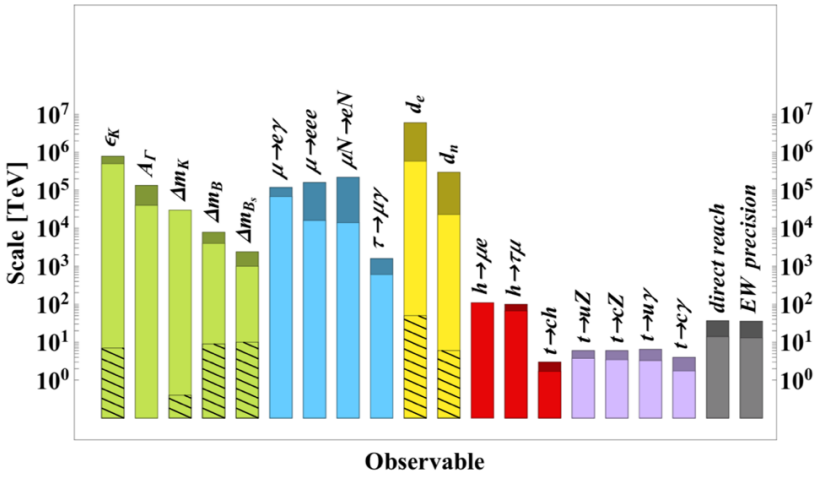


Fig. 32-26: Reach in new physics scale of present and future facilities, from generic dimension six operators. Colour coding of observables is: green for mesons, blue for leptons, yellow for EDMs, red for Higgs flavoured couplings and purple for the top quark. The blue region shows the impact of MEG II, Mu3e, Mu2e, COMET [1142].

[1142] Physics Briefing Book: Input for the European Strategy for Particle Physics Update 2020. CERN-ESU-004, and references and caveats therein. https://arxiv.org/abs/1910.11775 , p. 67

32.4 GUTs, Proton decay searches and the Neutron lifetime problem

The free proton is a stable particle, whose spontaneous decay into other particles has never been observed. Neutrons can be transformed into protons by β decay. A free neutron decays this way within about 15 minutes.

32.4.1 Proton decay searches, history and prospects

Proton decay is possible in Grand Unification scenarios through processes like the ones shown in Fig. 32-27.

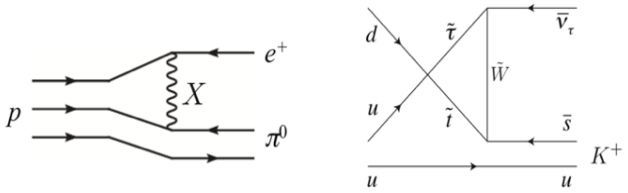


Fig. 32-27: Proton decay processes.

Let us start with some history [1143].

We saw in Chapter 9 (Fig. 9-14) the strange way how the quest for p decay started. The following tables [1144] list in detail the first attempts to observe p decay by Cherenkov technique (Table 32-8) or calorimetry (Table 32-9).

Status of nucleon lifetime experiments—Čerenkov technique (August 1981)

Collaborative institutions	University of Cal/Irvine University of Michigan Brookhaven National Lab	Harvard University Purdue University University of Wisconsin	University of Pennsylvania Brookhaven National Lab
Location	Morton Salt Mine, Painesville, Ohio	Silver King Mine, Park City, Utah	Homestake Gold Mine, Lead, South Dakota
Depth (km water equivalent)	1.7 kmwe	1.7 kmwe	4.4 kmwe
Detector mass (kilotons)	10 KT total ~5 KT fiducial	0.8 KT water, surrounded by mirrors and lead/gas tube shower counter	0.3 KT total 0.15 KT fiducial

Table 32-8: Proton decay searches by Cherenkov technique.

Status of nucleon lifetime experiments—Sampling calorimeter technique (August 1981)

Collaborative Institutions	Tata Institute, Bombay Osaka City University University of Tokyo	CERN INFN Frascati University of Milan University of Turin	University of Minnesota Argonne National Lab Oxford University	Orsay École Polytechnique Saclay
Location	Kolar Gold Fields, South India	Mont Blanc Auto Tunnel (Garage 17) Franco-Italian Border	Soudan Iron Mine, Vermillion, Minnesota	Fréjus Auto Tunnel Franco-Italian Border
Depth (km water equivalent)	7.6 kmwe	5.0 kmwe	1.8 kmwe	4.5 kmwe
Detector Mass (kilotons)	0.14 KT total ~0.10 KT fiducial	0.15 KT total	30 ton total (prototype)	1.5 KT total 1.0 KT fiducial

Table 32-9: Proton decay searches by calorimetry.

[1143] D. Perkins, Proton Decay Experiments.
https://www.annualreviews.org/content/journals/10.1146/annurev.ns.34.120184.000245
D. Treille, Nucleon Lifetime Experiments. https://lib-extopc.kek.jp/preprints/PDF/1981/8112/8112048.pdf
[1144] Tables extracted from M. Goldhaber and L. R. Sulak, An Overview of Current Experiments in Search of Proton Decay.
https://inspirehep.net/files/49a4f982f63e5c447ba1e8e61d25ff5d

To these early experiments, let us add KamiokaNDE (Kamioka Nucleon Decay Experiment, Gifu, Japan; 1983–1985, 1985–1990, 1990–1995) and especially Super-Kamiokande (**SK**, water-Cherenkov detector, Gifu, Japan; 1996–now) met in Chapter 19 as the discoverer of the non-zero mass of neutrinos. The progress in the most promising avenue, Cherenkov detectors, is illustrated by these numbers:

- IMB: 3.3 kton (fid. vol.), 2000 PMTs (coverage 4%),
- KamiokaNDE: 0.88 kton (fid. vol.), 948 PMTs (coverage 20%),
- Super-Kamiokande (SK): 22.5 kton (fid. vol.), 11186 PMTs (coverage 40%).

The common point is that **none has observed proton decay**.

Figure 32-28 describes the SK detector. One of its 20 inches photomultipliers was shown in Chapter 6.

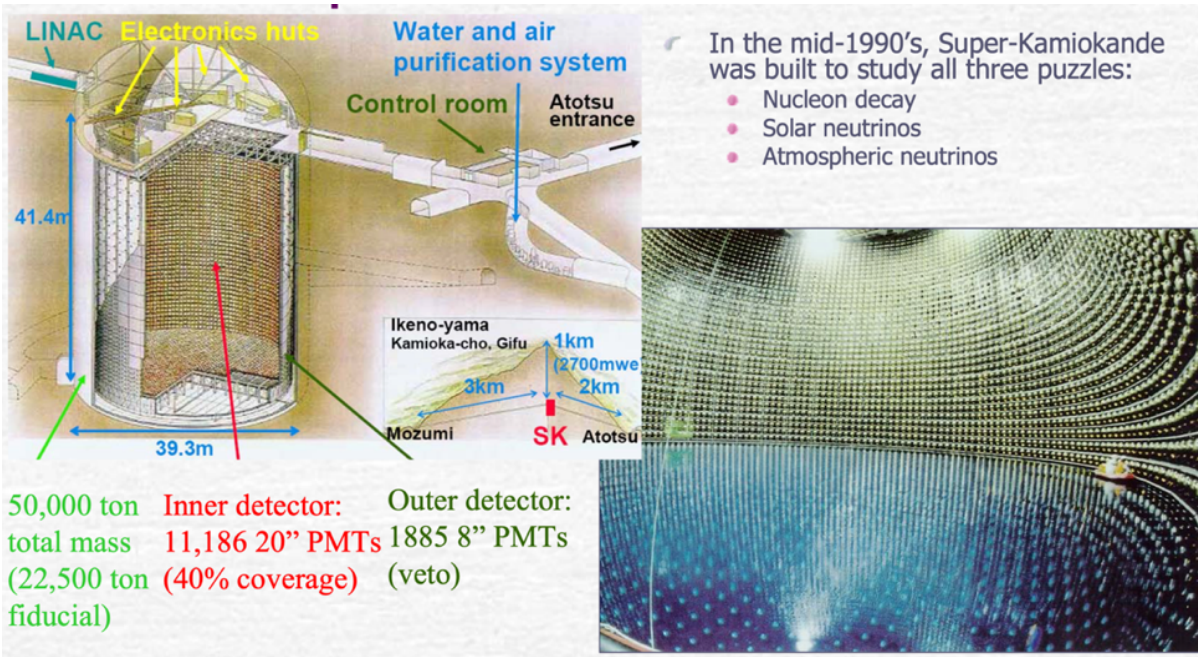


Fig. 32-28: The Super-Kamiokande detector [1145].

Figure 32-29 shows on the left side the signal expected from $p \rightarrow e^{+}\pi^{0}$ decay and, the right plot illustrates that no signal was observed [1146].

As described in Chapter 19, Super-Kamiokande made an outstanding career in all sectors of ν physics. New physics results with new neutron-tagging techniques by Gadolinium loading [1147] are expected. Figure 32-30 [1148] shows for example the sun seen with neutrinos (even by night ...) by this giant underground detector.

[1145] D. Casper, The Super-Kamiokande Experiment. https://www.slac.stanford.edu/econf/C040802/lec_notes/Casper/Casper.pdf
[1146] ibid , F. Dufour, Super-Kamiokande: latest results on neutrinos. https://llr.in2p3.fr/services/llr_seminaires/upload/2010_0510_Dufour_SuperK.pdf
[1147] K. Abe *et al.,* Second gadolinium loading to Super-Kamiokande. https://arxiv.org/abs/2403.07796
[1148] Super-Kamiokande official Website, Solar neutrinos. https://www-sk.icrr.u-tokyo.ac.jp/en/sk/about/research/

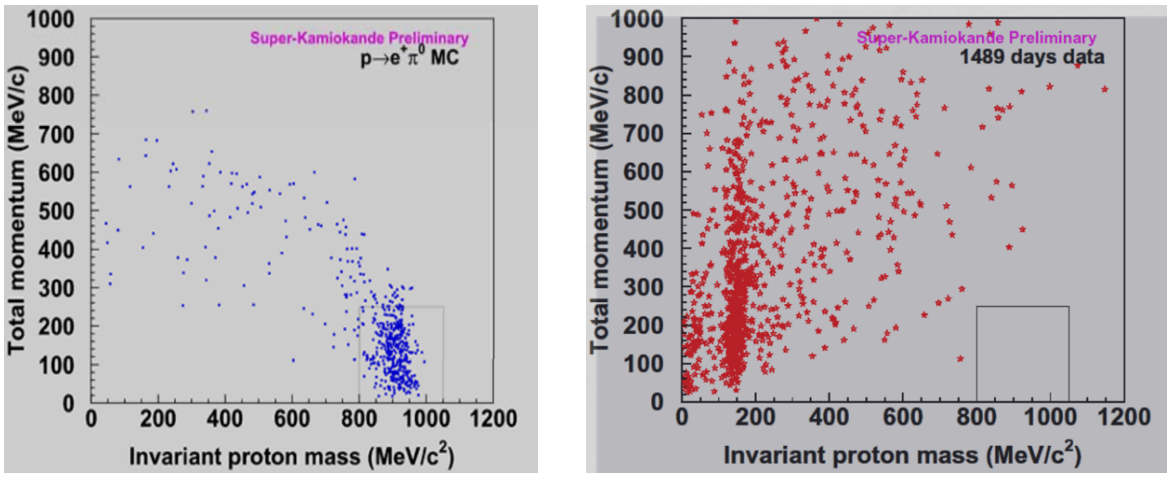


Fig. 32-29: The present limit on $p \rightarrow e^+ \pi^0$ is 2.4×10^{34} years. Left is the signal MC and right are the data. The black box shows the signal region.

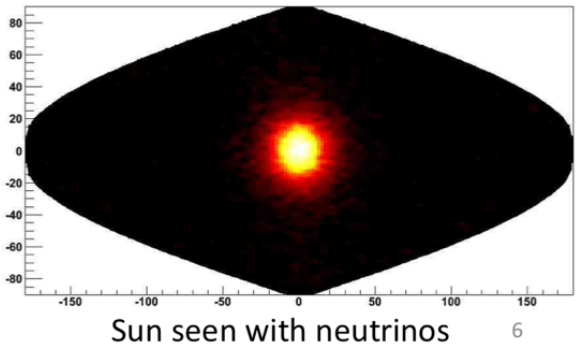


Fig. 32-30: The sun seen with neutrinos using observation data of Super-Kamiokande from 1996 to 2018.

After describing the past and present detectors, let us now resume the problematics of proton decay. Advances in the field of proton lifetime are expected from the DUNE (US) and HyperKamioka (Japan) neutrino programs.

Figure 32-31 gives the status of the set and expected lower bounds on the proton lifetime versus the expected ranges for various Grand Unification scenarios [1149]. Figure 32-32 illustrates the sensitivities expected from the main players in the game.

For example, in a minimal SU(5) SUSY model, in light of the LHC results, with scalar masses up to 30 TeV but with the mass parameter of the gauginos < 2 TeV, the proton lifetime in $\nu + K^+$ is probably about 10^{35} years [1150].

[1149] K. Abe *et al.,* Hyper-Kamiokande Design Report. https://arxiv.org/abs/1805.04163
The HK cavern excavation has been completed on July 31, 2025.
[1150] K. S. Babu *et al.,* Proton lifetime in minimal SUSY SU(5) in light of LHC results. https://arxiv.org/abs/2012.14411

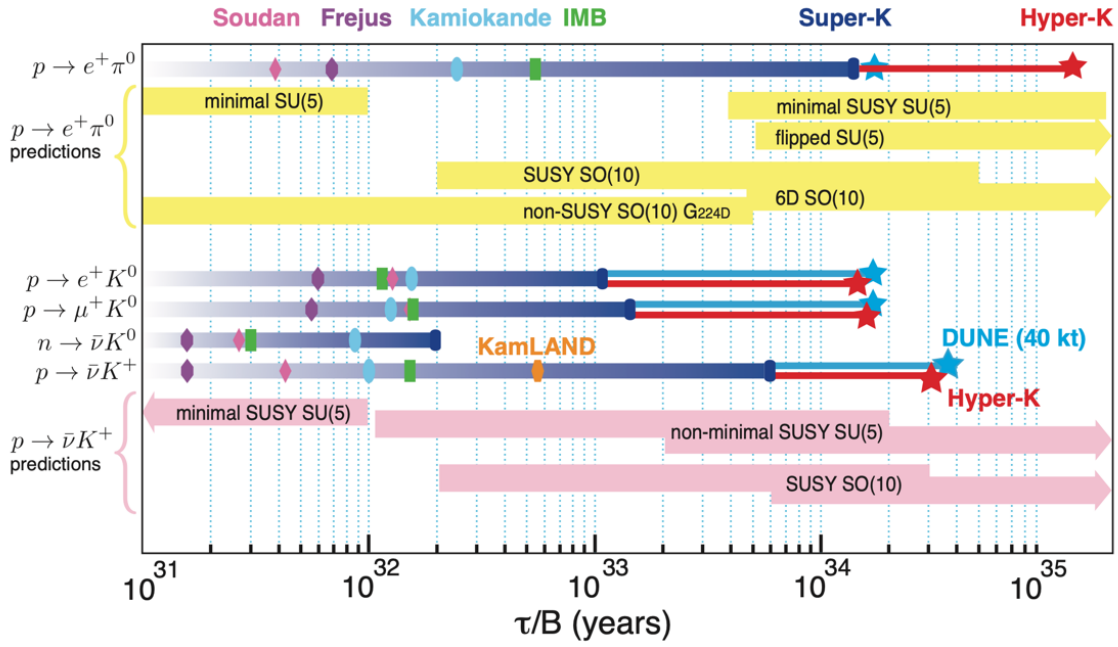


Fig. 32-31: A comparison of historical experimental limits on the rate of nucleon decay and projected limits for Hyper-Kamiokande and DUNE based on 10 years of exposure.

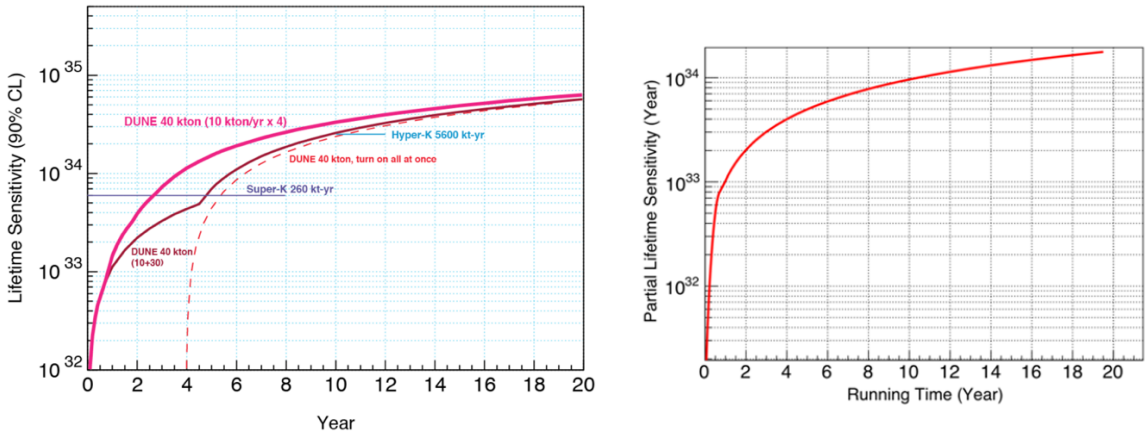


Fig. 32-32: Sensitivities of DUNE and HyperK [1151] (left) and sensitivity of JUNO [1152] (right).

After the violation of $L_e - L_\mu$ and $L_\mu - L_\tau$ observed via neutrino oscillations, the eventual violation of the baryon number B would suggest that there are **no true global symmetries** in nature and that the genuine symmetries are gauge symmetries [1153].

[1151] The DUNE Collaboration, The physics program for DUNE. https://arxiv.org/abs/1512.06148
[1152] A. Abusleme *et al.,* JUNO Sensitivity on Proton Decay Searches. https://arxiv.org/abs/2212.08502
[1153] E. Witten, Symmetry and Emergence. https://arxiv.org/abs/1710.01791

Table 32-10 gives the lifetime expectations and present status of various theory classes [1154].

Theory class	Proton lifetime (years)[15]	Ruled out experimentally?
Minimal SU(5) (Georgi–Glashow)	10^{30}–10^{31}	Yes
Minimal SUSY SU(5)	10^{28}–10^{32}	Yes
SUGRA SU(5)	10^{32}–10^{34}	Yes
SUSY SO(10)	10^{32}–10^{35}	Partially
SUSY SU(5) (MSSM)	~10^{34}	Partially
SUSY SU(5) – 5 dimensions	10^{34}–10^{35}	Partially
SUSY SO(10) MSSM G(224)	2×10^{34}	No
Minimal (Basic) SO(10) – Non-SUSY	< ~10^{35} (maximum range)	No
Flipped SU(5) (MSSM)	10^{35}–10^{36}	No

Table 32-10: Proton lifetime expectations and present status of various theory classes [1155].

32.4.2 More towards baryogenesis

This chapter and GUTs offer an occasion to come back to the obviously key problem of **baryogenesis** [1156].

Let us recall the **Sakharov conditions** [1157] for creating baryon asymmetry, a.k.a. baryogenesis.

1. Existence of a process that **violates the baryon number**.
2. C and CP Violation.
3. Departure from thermal equilibrium.

The hope was that GUTs would provide all conditions to generate this asymmetry. They necessarily break baryon number B. Heavy particles from GUTs (leptoquarks?), after T falls below their production threshold, lead to departure from thermal equilibrium. Their decay, if CP violating, may produce more baryons than anti-baryons.

However, the effect of **EW anomaly** changed the picture [1158]. Note that $\Delta(B - L) = 0$: the EW anomaly preserves B − L. Because of this process, the pre-existing B and L are converted to each other to find

[1154] Let us recap some relevant properties of the main GU groups considered. With a proper choice of representations, SU(5) is anomaly-free. SO(10) is naturally anomaly-free. In minimal SU(5), as in the SM, neutrinos have to be massless. Although the B and L global symmetries are broken in minimal SU(5), there still remains a B – L global U(1) symmetry and B—L is conserved. B and L evolving to values proportional to B – L, baryogenesis fails if initially B — L is 0. Since 2B = B + L + B – L, sphalerons, which keep B – L but change B + L, change B and erase it. The addition of ν_R to solve the ν mass problem and the violation of B — L would be rather ad hoc modifications of SU(5). But these features occur automatically in the rank-5 GUT SO(10). SU(5) being excluded by the limit on the p lifetime, the hope to rescue GUT baryogenesis seems to rest on SO(10) and the group E_6. But one should not forget that any GUT suffers from a severe hierarchy problem.

[1155] https://en.wikipedia.org/wiki/Proton_decay

[1156] H. Murayama, GUT, Neutrinos, and Baryogenesis. https://arxiv.org/abs/hep-ph/0208005
D. Bödeker and W. Buchmüller, Baryogenesis from the weak scale to the grand unification scale. https://arxiv.org/abs/2009.07294
A. Riotto, Theories of Baryogenesis. https://arxiv.org/abs/hep-ph/9807454
M. Trodden, Baryogenesis and Leptogenesis. https://www.slac.stanford.edu/econf/C040802/papers/L018.PDF
W. Buchmüller, Baryo- and leptogenesis. https://inis.iaea.org/records/rae7r-6as20

[1157] In 1967, 2 years after CP discovery, one year after the CMB discovery!

[1158] For a precise explanation of the effect see H. Murayama, GUT, Neutrinos, and Baryogenesis. https://arxiv.org/abs/hep-ph/0208005

the chemical equilibrium at B ∼ 0.35(B − L), L ∼ −0.65(B − L) [1159]**.** Even if there were both B and L, both of them **get washed out** if B − L was zero.

But unsuppressed **(B + L)-violating sphaleron** processes at high T excluded these models. The trivial equation B = (B + L)/2 + (B – L)/2 is significant: sphalerons only erase B + L but leave B – L untouched. Thus, a GUT baryogenesis scenario only works if it produces at high scale an asymmetry in B – L, what **SU(5) does not do.**

So, one was left with two scenarios: **electroweak baryogenesis and thermal leptogenesis.**

Electroweak baryogenesis tries to generate B = L at the time of the EW phase transition, so that they do not get washed out further by the EW anomaly (Chapters 7 and 24).

As we saw in Chapter 24, EW baryogenesis would allow to connect the cosmological matter-antimatter asymmetry with physics at the LHC and, moreover, with gravitational waves. The EW phase-transition and sphaleron processes are by now well understood. EW baryogenesis is a process far from thermal equilibrium. Since in the SM the phase transition is a smooth crossover, **extensions of the Higgs sector**, such as two-Higgs-doublet models, etc., are needed for EW baryogenesis. However, besides LHC constraints, stringent upper bounds on the electron EDM (Section 32.2) exclude most of the known models [1160].

One is led to construct models, where CP violation in baryogenesis and low-energy CP violation are decoupled, and the EW phase transition occurs at temperatures well above a TeV. Or one can turn to **strongly coupled composite Higgs models** in which EW baryogenesis is still possible, compatible with LHC constraints and low-energy precision experiments, which both need to be strengthened.

That B − L is left unchanged by sphaleron transitions opens the possibility of generating the B asymmetry from a L asymmetry. This is **leptogenesis** [1161], trying to generate L≠0, but no B, from **neutrino physics**, well before the EW phase transition, and L partially converted to B due to the EW anomaly. If an asymmetry in L is produced, sphaleron transition will reprocess it and convert it into B, because B + L = 0, the final baryon asymmetry is B ≃ −L. This brings us back to neutrino physics and adding **RH Majorana neutrinos** to the SM [1162] (see Sections 19.6,19.7 and 19.9).

Thermal leptogenesis, closely related to ν masses, a process close to thermal equilibrium, is well understood. See Ref. [1163], the reference from which the following remarks arise.

Originally leptogenesis was based on a GUT-scale (SO (10)) seesaw mechanism with hierarchical heavy Majorana neutrinos. Estimates, based on GUT models, yield the right order of magnitude for the observed matter-antimatter asymmetry. In the one-flavour approximation, successful leptogenesis leads to a preferred mass window for the light neutrinos that is consistent with the cosmological upper bound on **the sum of neutrino masses**, and to a lower bound on the heavy Majorana neutrino masses.

However, the standard temperature scale of thermal leptogenesis (T ∼ 10^{10} GeV) can be significantly lowered by **flavour effects**, which keep the qualitative picture, but relax the neutrino mass bounds.

[1159] ibid., these non-trivial relations need an explanation suggested in the previous reference.

[1160] D. Bödeker and W. Buchmüller, Baryogenesis from the weak scale to the grand unification scale. https://arxiv.org/abs/2009.07294

[1161] M. Fukugita and T. Yanagida, Baryogenesis without grand unification. *Phys. Lett. 174, 45 (1986).*

[1162] Majorana neutrinos have no defined L number, but processes involving them, as 0νββ decay, induce $\Delta L = \pm 2$. Majorana removes the neutrino/antineutrino distinction but not the left/right difference. Lepton number conservation still holds, but it is thanks to the handedness of the neutrinos involved. The overlap between L and R-handed particles (down to the subtle difference between handedness and chirality) is very small and vanishes in the limit $v \to c$ of which neutrinos are very close. Hence, concerning the usual low-mass active neutrinos, the doubt about their nature subsists.

[1163] D. Bödeker and W. Buchmüller, Baryogenesis from the weak scale to the grand unification scale. https://arxiv.org/abs/2009.07294

For **quasi-degenerate heavy neutrinos,** this temperature can be lowered to the weak scale. CP-violating oscillations of sterile neutrinos can lead to successful leptogenesis even for GeV neutrino masses. When mass differences between the heavy ν are comparable to the heavy ν decay widths (called resonant leptogenesis) thermal leptogenesis with out-of-equilibrium decays of heavy Majorana (sterile) neutrinos can work down to masses around the electroweak scale, once the CP asymmetries in their decays are resonantly enhanced.

Leptogenesis with even lighter sterile neutrinos that have masses O(GeV) is possible via CP-violating oscillations among sterile neutrinos. As seen in Chapter 19, **the νMSM** is an extension of the SM by three sterile neutrinos, of which the two heavier ones ($N_{2,3}$), highly mass degenerate, can generate the baryon asymmetry and the lightest (N_1) is available as a DM candidate. This minimal extension might account for neutrino oscillations, baryogenesis, and dark matter.

0νββ is sensitive to the **effective mass m_{ee}** (see Fig. 19-9), for which experiments (Section 32.1) set limits $m_{ee} \leq 100$ meV. Cosmological observations measure **the sum of neutrino masses.** The situation is summarized in Fig. 32-33 which links the three ways of access to neutrino masses.

An important ingredient of leptogenesis is the **CP-violating phases** in the neutrino mass matrices (Chapter 19). The observation of 0νββ decay would constrain the Majorana phases.

A measurement of a total neutrino mass $m_{tot} \sim 100$ meV with an uncertainty of ~10 meV is challenging, but it would have a strong impact on our understanding of leptogenesis.

A new development is the possibility of probing high-scale leptogenesis with **gravitational waves**. This includes the seesaw mechanism and a high scale of B−L breaking.

We recall that in the ΛCDM one assumes that neutrinos are free streaming after 1 MeV, follow the relativistic Fermi-Dirac spectrum, have a temperature $T_\nu = (4/11)^{1/3}\ T_\gamma$ and a negligible lepton asymmetry. Their properties are then [1164] :

$$\sum m_\nu < 0.072\,\mathrm{eV} \quad \textit{(Planck 2018 + DESI 2024)}$$
$$\Delta N_{\mathrm{eff}} = -0.10 \pm 0.21\,(68\%\,\mathrm{CL}) \quad \textit{(BBN)}$$
$$N_{\mathrm{eff}} = 2.92^{+0.36}_{-0.37}\,(95\%\,\mathrm{CL}) \quad \textit{(Planck 2018)}$$

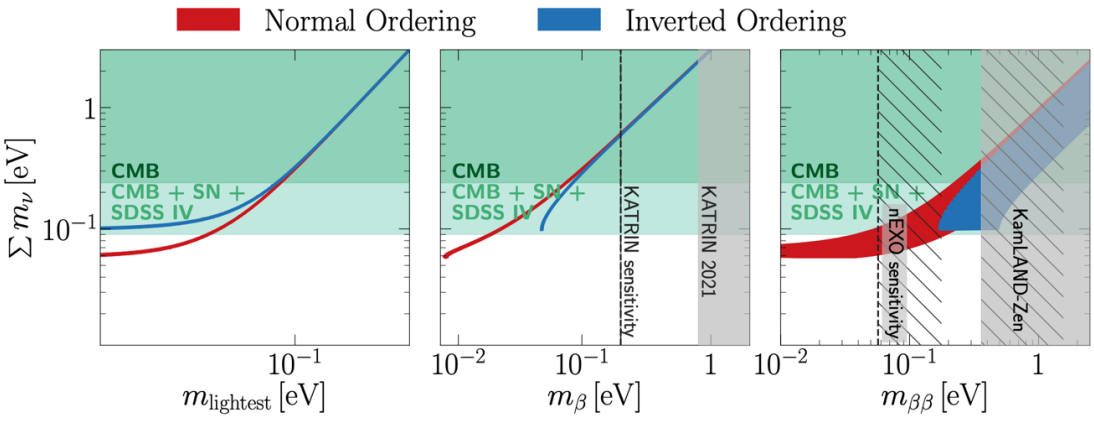


Fig. 32-33: Theoretical predictions and current bounds for the sum of neutrino masses Σm_ν as a function of three quantities characterizing the neutrino masses [1165].

[1164] I. M. Oldengott, Cosmological Constraints on Neutrinos. https://indico.cern.ch/event/1335188/contributions/6137377/attachments/2951231/5187828/NeutrinosCosmology.pdf

[1165] E. Di Valentino *et al.,* Neutrinos in Cosmology. https://arxiv.org/abs/2404.19322

32.4.3 The Neutron problem

If we move to the **neutron**, a problem arises [1166]. Two methods are generally used to measure their lifetime: the **beam method** and the so-called **"bottle" method**. For example, the UCNτ experiment [1167] uses the second. A trap – the "bottle" – is filled with a known number of ultra-cold neutrons, held in suspension by magnetic fields. Depending on whether one or other of these measurement methods is used, the lifetime of the neutron differs by 9 seconds! τ_{bottle} = 878.4 ± 0.5 s versus τ_{beam} = 888.45 ± 1.65 s. New physics or forgotten systematics?

Theoretically we expect $\tau_n = \frac{4908.7(1.9)s}{|V_{ud}|^2\ (1+3g_A^2\ )}$. Figure 32-34 shows the results.

This disagreement has consequences on the abundances of light elements resulting from primordial nucleosynthesis (Section 30.3).

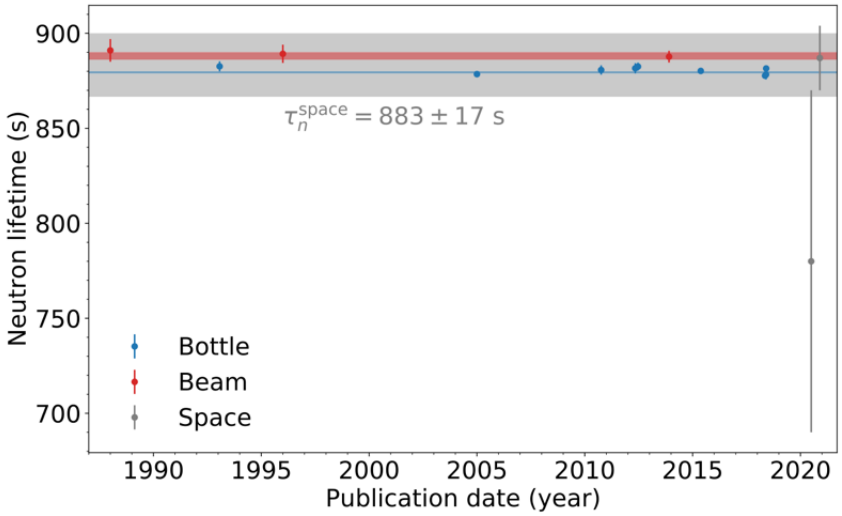


Fig. 32-34: The neutron lifetime measurements [1168].

Figure 32-35 shows the mass fraction of Helium-4 (Y_p) and relative abundance of deuterium (D/H) versus neutron lifetime, τ_n. NACRE II and PRIMAT are two different abundance predictions. The vertical lines are averages of the lifetimes obtained by the different methods, beams, bottles and space. The horizontal orange shaded regions are the primordial PDG abundances. Subaru and CEO do not agree [1169].

Some physicists [1170] count on instruments on a lunar mission, measuring the escape of neutrons produced by cosmic ray interactions, to get a 3rd independent method, arbitrating between the first two.

[1166] S. Paul, The Puzzle of Neutron Lifetime. https://arxiv.org/abs/0902.0169
[1167] F. M. Gonzalez *et al.,* Improved neutron lifetime measurement with UCNτ. https://arxiv.org/abs/2106.10375
[1168] J. T. Wilson, Measurement of the free neutron lifetime using the neutron spectrometer on NASA's Lunar Prospector mission. *Phys.Rev.C104 045501,* https://journals.aps.org/prc/pdf/10.1103/PhysRevC.104.045501
[1169] T. Chowdhury and S. Ipek, Neutron Lifetime Anomaly and Big Bang Nucleosynthesis. https://arxiv.org/abs/2210.12031
[1170] CERN Courier, Jan/Feb 2022 p 11. Space-based data probe neutron lifetime, https://cds.cern.ch/record/2799462/files/CERNCourier2022JanFeb-digitaledition.pdf

A quite different hypothesis appears in Ref. [1171]: the possible existence of a neutron excited state.

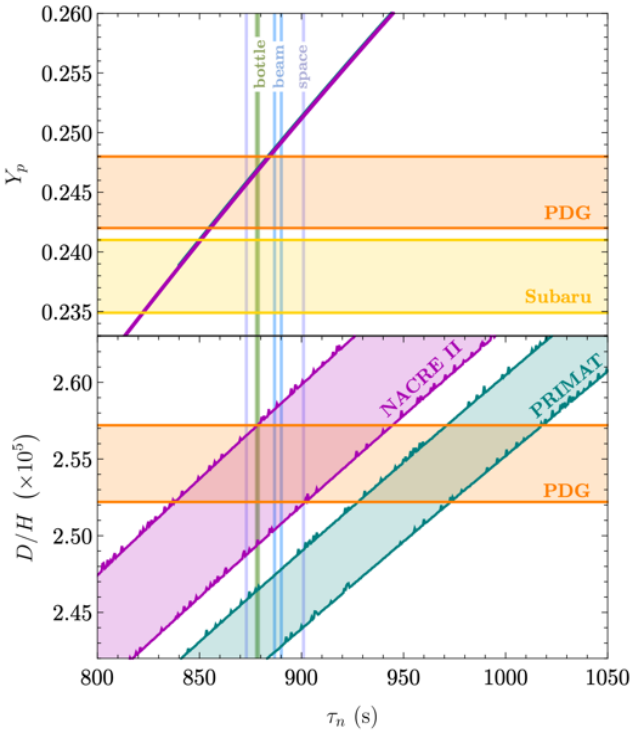


Fig. 32-35: Mass fraction of Helium-4 (Y_p) and relative abundance of deuterium (D/H) as a function of the neutron lifetime τ_n.

[1171] B. Koch and F. Hummel, An exciting hint towards the solution of the neutron lifetime puzzle? https://arxiv.org/abs/2403.00914

33. A singular point: The Paul-Scherrer-Institute

Section 32.3 illustrated the role of PSI experiments in muon rare decays and FCNC searches. Section 32.4 dealt with neutron lifetime which is part of PSI's programme with the SPECT experiment. The role of PSI appeared also in Chapter 7 concerning the proton structure and in Section 32.2 on EDMs searches. It is thus worth, putting together these topics, to illustrate the physics output of this relatively small but most active laboratory.

The proton accelerator facility of the Paul Scherrer Institute (PSI) [1172] with its ring cyclotron, among the world's most powerful ones (average beam power of up to 1.4 MW, beam current of over 2 mA), generates high-intensity beams of pions, muons and ultracold neutrons.

Many of the particle physics experiments performed at PSI concern low-energy interactions of electrons, muons, protons, neutrons, and pions and use the high beam fluxes to precisely measure the parameters of the SM or to search for possible physics beyond the SM with improved sensitivity.

As we pointed out, the PSI abundant and remarkable physics results are scattered between the various topics in our document:

- proton physics (Chapter 5), as a very precise determination of its radius exploiting muonic atoms. The MUSE experiment (Section 5.4), proposing to measure $l\,p \to l\,p$ with l being both $e^{\pm}$ and $\mu^{\pm}$, offers the opportunity to compare e p and μ p scattering within the same experimental setup;
- EDM searches with cold neutrons provided by the Swiss Spallation Neutron Source (SINQ) and the PSI Ultra Cold Neutron (UCN) source and with muonium (Section 32.2);
- Searches for flavour changing neutral currents in muon decay (Section 32.3).

One can add that the most precise measurements of pionic hydrogen and deuterium have been performed at PSI. The most accurate determination of the mass of the negatively charged pion, m_{π^-}, was obtained from measurements of X-ray transition energies in pionic atoms. The weak muonic decay mode of charged pions, dominating over the electronic mode, allowed to measure the mass of π^+ as $m_{\pi^+} = 139.570\,21(14)$ MeV. This yields a new quantitative measure of CPT invariance in the pion sector: $(m_{\pi^+} - m_{\pi^-})/m_{\pi}(\text{av}) = (-2.9 \pm 2.0) \times 10^{-6}$, an improvement by two orders of magnitude.

In a Review of Particle Physics at PSI [1173], PSI has summarized its physics output and Table 33-1 [1174] illustrates well its variety and importance.

[1172] https://www.psi.ch/en , https://en.wikipedia.org/wiki/Paul_Scherrer_Institute ,
C. Hoffman, K. Kirch and A. Signer (editors), Review of Particle Physics at PSI (PSI2020). SciPost Phys. Proc. 5, (2021), https://scipost.org/SciPostPhysProc.5

[1173] C. Hoffman, K. Kirch and A. Signer (editors), Review of Particle Physics at PSI (PSI2020). SciPost Phys. Proc. 5, (2021), https://scipost.org/SciPostPhysProc.5

[1174] G. Colangelo *et al.,* A theory vade mecum for PSI experiments. https://scipost.org/SciPostPhysProc.5.005/pdf

	experiment	section	process / particles / (bound states)
[1]	muon decay	6	$\mu^+ \to e^+ \nu_e \bar{\nu}_\mu$
[2]	MuLan	16	$\mu^+ \to e^+ \nu_e \bar{\nu}_\mu$
[3]	SINDRUM	7	$\mu^+ \to e^+ ee$, $\mu^+ \to e^+ \nu_e \bar{\nu}_\mu ee$, $\pi^+ \to e^+ \nu_e ee$, $\pi^0 \to ee$
[4]	SINDRUM II	8	$\mu^- {}^{A}_{Z}N \to e^- {}^{A}_{Z}N$ for Au, Pb, Ti
[5]	MEG	19	$\mu^+ \to e^+\gamma$, $\mu^+ \to e^+ \nu_e \bar{\nu}_\mu \gamma$, $\mu^+ \to e^+ X \to e^+ \gamma\gamma$
[6]	Mu3e	20	$\mu^+ \to e^+ ee$, $\mu^+ \to e^+ \nu_e \bar{\nu}_\mu ee$
[7]	Mspec, Mu-Mass	29	$M = (\mu^+ e^-)$, μ^+
[8]	MACS	9	$M = (\mu^+ e^-) \leftrightarrow \bar{M} = (\mu^- e^+)$
[9]	CREMA	21	$(\mu^- p)$, $(\mu^- d)$, $(\mu^-$He$)$, p, d, He
[10]	muX	22	$(\mu^- {}^{A}_{Z}N)$, ${}^{248}_{96}$Cm, ${}^{226}_{88}$Ra
[11]	MUSE	23	$e^\pm p \to e^\pm p$, $\mu^\pm p \to \mu^\pm p$
[12]	MuCap	17	$\mu^- p \to \nu_\mu n$
[13]	MuSun	18	$\mu^- d \to \nu_\mu nn$
[14]	pionic hydrogen	14	$(\pi^- p)$, $(\pi^- d)$
[15]	pionic helium	26	$(\pi^- e^-$ ^{4}He$^{++})$, π^-
[16]	nTRV	15	$n \to p e^- \bar{\nu}_e$
[17]	nEDM	27	n, n
[18]	indirect nEDM	28	n / dark matter / exotic
[19]	negative pions	10	$(\pi^- p)$, π^-
[20]	positive pions	11	$\pi^+ \to \mu^+ \nu_\mu$, π^+, ν_μ
[21]	neutral pions	12	$\pi^- p \to \pi^0 n$, π^0
[22]	PiBeta	24	$\pi^+ \to \pi^0 e^+ \nu_e$, $\pi^+ \to e^+ \nu_e (+\gamma)$, $\mu^+ \to e^+ \nu_e \bar{\nu}_\mu \gamma$
[23]	PEN	25	$\pi^+ \to e^+ \nu_e (+\gamma)$, $\mu^+ \to e^+ \nu_e \bar{\nu}_\mu \gamma$

Table 33-1. Processes and particles (bound states) that are investigated at PSI, where the driving interaction to be studied is indicated by the colour as follows: BSM, weak, weak and try to learn about strong, EM, EM and try to learn about strong, strong. In addition, the mass or charge radius of particles are measured. The section number refers to the Review of Particle Physics at PSI.
To this Table one can even add Refs. [1175] and [1176].

[1175] G. R. Araujo *et al.,* Determination of the Muon Lifetime in ^{76}Se with the MONUMENT experiment. https://arxiv.org/abs/2510.23401

[1176] K. A. Beyer *et al.,* Modern approach to muonic x-ray spectroscopy demonstrated through the measurement of stable Cl radii. https://arxiv.org/abs/2506.08804

34. Brief status of the physics of gravitational waves

The follow-up of the evolution of the famous binary pulsar [1177] (the cumulative shift of the periastron time versus year, Fig. 34-1) has dissipated questions concerning the reality of the emission of gravitational waves **(GW)** and the understanding of the amount of energy radiated.

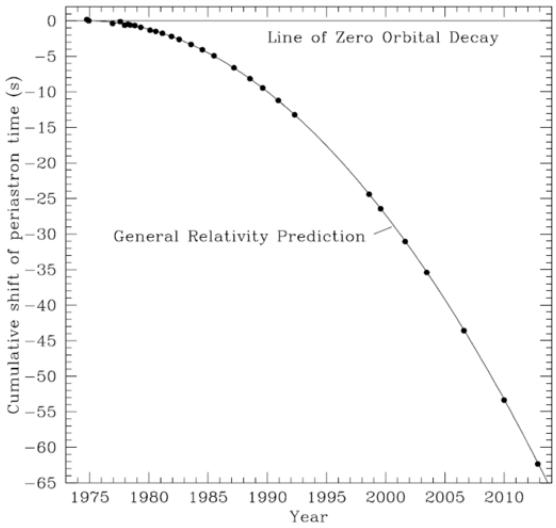


Fig. 34-1: Evolution of the binary pulsar.

The next step was the direct detection of GWs. Figure 34-2 [1178] gives the spectrum of GW to be expected. We will focus on some results of terrestrial interferometers **(TI),** assumed to be familiar to the reader [1179].

Figure 34-3 [1180] gives the expected signal of a merger of two BH in terms of strain evolution. The first GW event [1181] (Fig. 34-4) appeared just as shown in Fig. 34-3. In Fig. 34-4 “shifted” means corrected by the propagation of the wave front at c.

Figure 34-5 shows that the interferometers managed to master their noise strain at the needed level [1182] to be sensitive to astronomical events.

[1177] https://fr.wikipedia.org/wiki/PSR_B1913%2B16
PSR B1913+16 was discovered in 1974 by radioastronomers R.A. Hulse and J.H. Taylor (Nobel Prize 1993).
N. Christensen, Gravitational Waves: Now and in the Future.
https://indico.cern.ch/event/1335188/contributions/6137374/attachments/2951358/5188019/Christensen_blois_2024.pdf
Work by T. Damour and N. Deruelle showed that in GR the gravitational force acting on the pulsar propagated from its companion at light speed, in the form of waves, and that this propagation caused a slow decrease in its orbital period.
https://www.ihes.fr/~damour/Conferences/DamourDeruelleAIHP86.pdf

[1178] C. Jia, Gravitational Waves Through Time: Scientific Significance, Detection Techniques, and Recent Breakthroughs. https://arxiv.org/html/2312.16198v2

[1179] D. V. Martynov *et al.,* The Sensitivity of the Advanced LIGO Detectors at the Beginning of Gravitational Wave Astronomy. https://arxiv.org/abs/1604.00439

[1180] LIGO Collaboration, How we searched for merging black holes and found GW150914. http://ligo.org/science-summaries/GW150914CBC/

[1181] B. P. Abbott *et al.,* Observation of Gravitational Waves from a Binary Black Hole Merger. *Phys. Rev. Lett.116, 061102*
https://journals.aps.org/prl/abstract/10.1103/PhysRevLett.116.061102
https://www.ligo.caltech.edu/image/ligo20160211a

[1182] N. Christensen, Gravitational Waves: Now and in the Future.

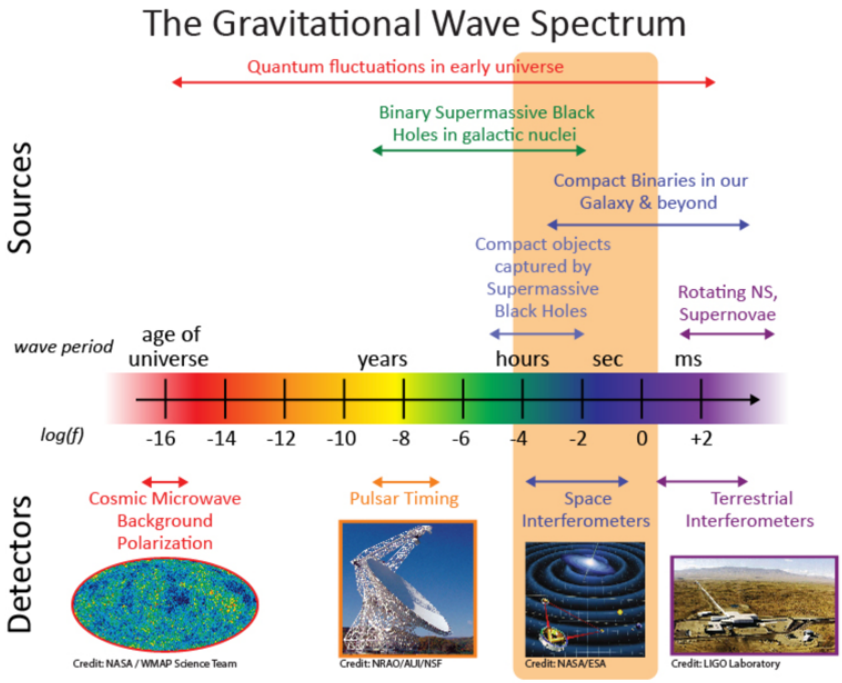


Fig. 34-2: The spectrum of GW to be expected and the various detection techniques used to probe the gravitational wave spectrum. Image from NASA.

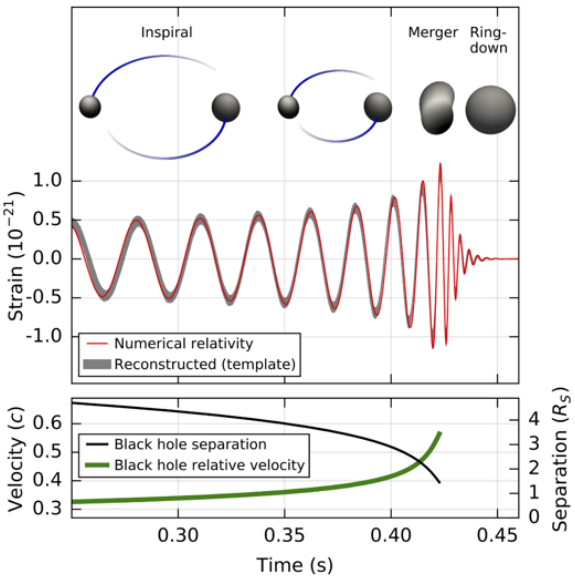


Fig. 34-3: Expected signal of a BH merger.

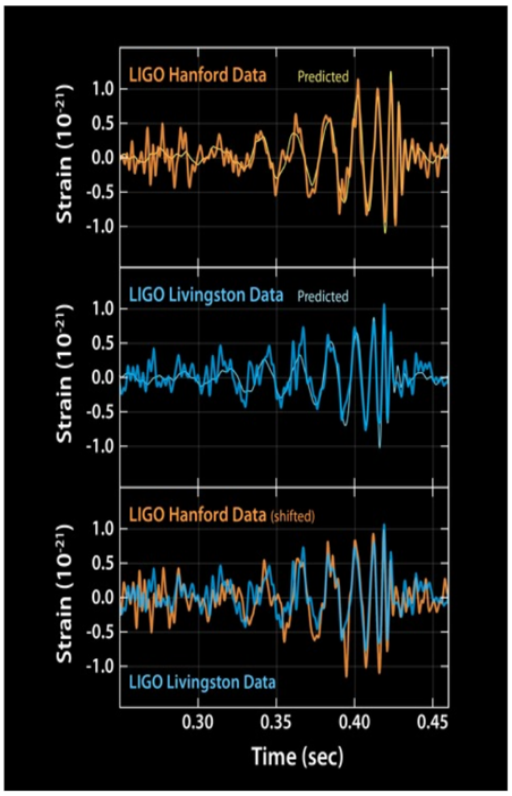


Fig. 34-4: The first merging. September 14, 2015 at 09:50:45 UTC.

https://indico.cern.ch/event/1335188/contributions/6137374/attachments/2951358/5188019/Christensen_blois_2024.pdf

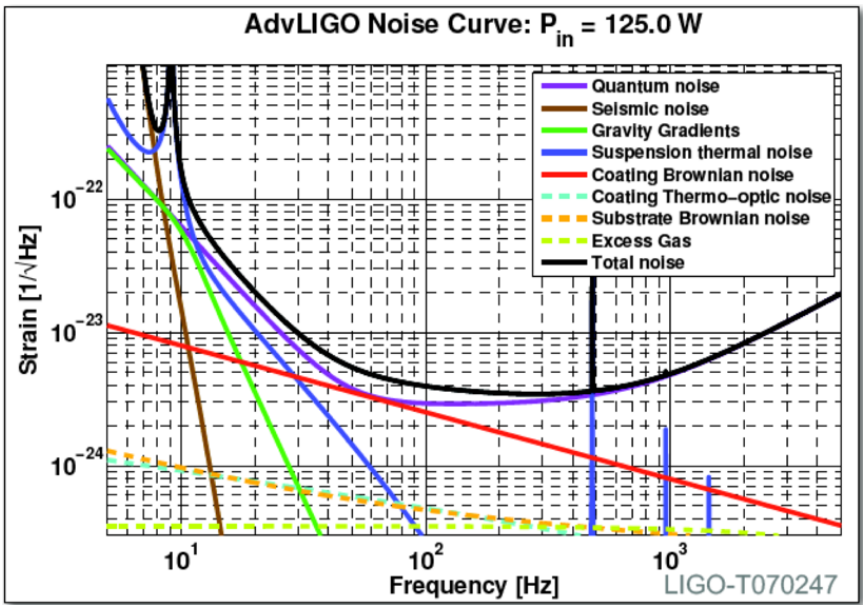


Fig. 34-5: Strain of AdvLIGO versus frequency.

Figure 34-6 shows the evolution of the number of candidates with years and Fig. 34-7 gives a sample of them in the plot of the two masses of the mergers [1183].

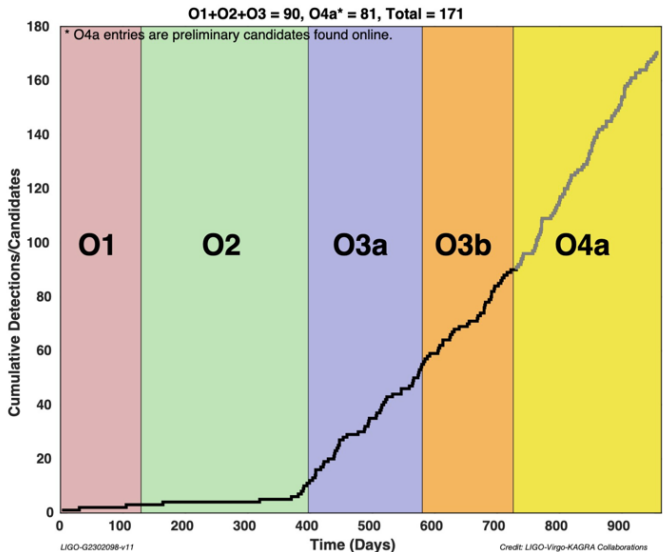


Fig. 34-6: Evolution of the number of candidates. Credit LIGO–Virgo–KAGRA.

[1183] N. Christensen, Gravitational Waves: Now and in the Future. https://indico.cern.ch/event/1335188/contributions/6137374/attachments/2951358/5188019/Christensen_blois_2024.pdf On February 11, 2016, the LIGO Scientific Collaboration and Virgo Collaboration announced the first confirmed observation of gravitational waves from colliding black holes. http://ligo.org/detections/gw150914/

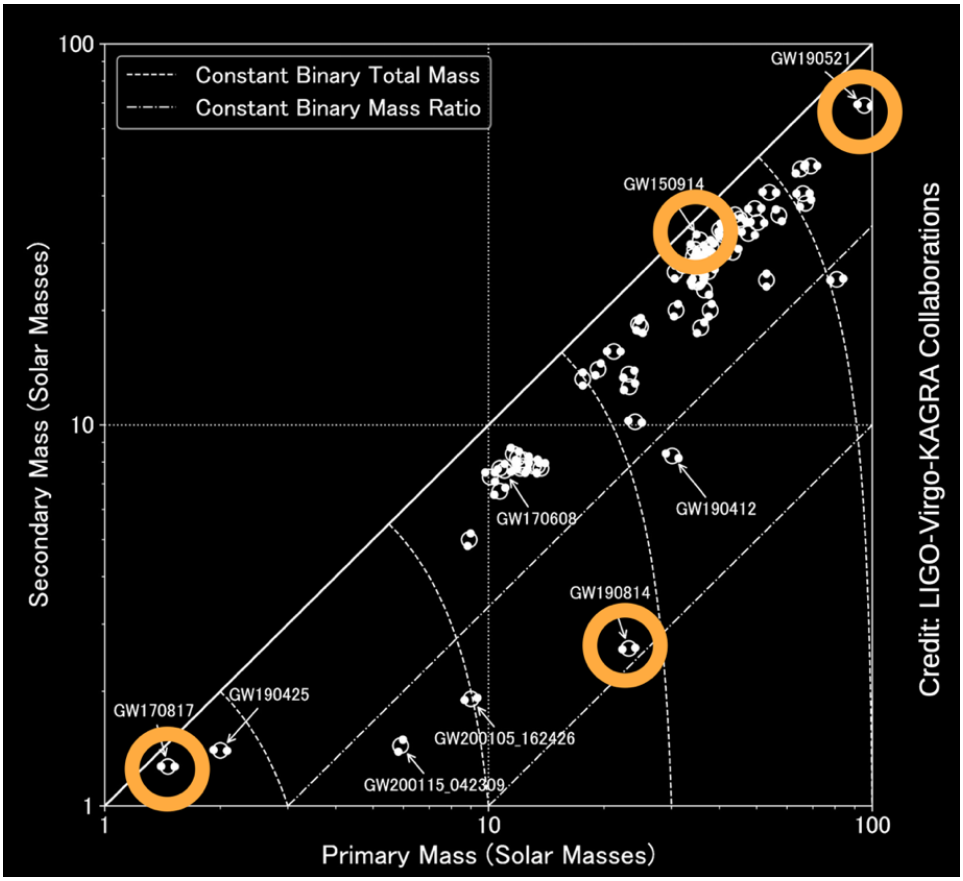


Fig. 34-7: Sample of events in the plot of the two masses of the mergers.

Figure 34-8 [1184] gives the mass distribution of the primary merger, showing a peak at small masses, a few solar masses, as expected (e.g. N-stars, below $M_S \sim 2\ M_\odot$, or already mergers of them) and a slight one in the surprising 30 to 40 $M_\odot$ region (Section 31.4). Figure 34-9 [1185] shows that the mergers rate change with z.

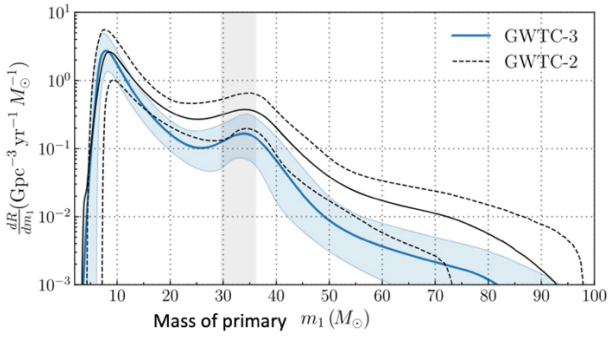


Fig. 34-8: Mass distribution of the primary merger.

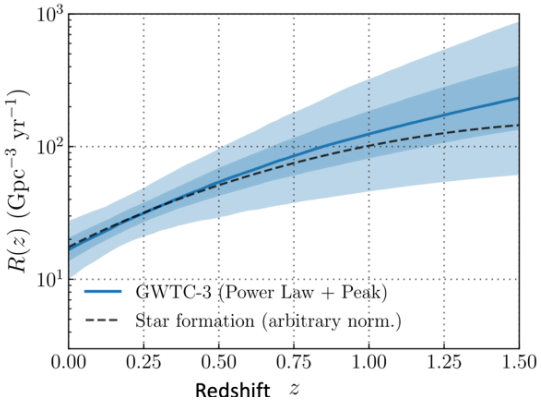


Fig. 34-9: Change of the mergers rate with z.

[1184] S. Nissanke, New perspectives onto the Universe in the era of Gravitational Wave (GW) Physics, 42nd International Conference on High Energy Physics, Praha, 2024.
https://indico.cern.ch/event/1291157/contributions/5958354/attachments/2901957/5091832/ICHEPPraha_2024_wide_nissanke_final.pdf
[1185] ibid

This document does not intend to discuss the evolution of the field. However, Table 34-1 [1186] suggests that the next generation of interferometers (ET (Einstein Telescope), CE (Cosmic explorer)) will dwarf the present results and extend to nearly the whole space the probed volume (Fig. 34-10 [1187]).

Network	N	N_1	N_{10}	N_{100}	M
HLV	48	0	16	48	19
HLVKI	48	0	48	48	7
1ET+2CE	990k	14k	410K	970k	12

Table 34-1: The Next generation of interferometers. Expected number of binary NS detections per year N; localized with a resolution of < 1, < 10 and < 100 square degrees, N_1, N_{10} and N_{100}, respectively, and median localization error M (in sq. deg.), in a network consisting of LIGO-Hanford, LIGO-Livingston and VIRGO (HLV), HLV, KAGRA and LIGO-India (HLVKI) and 1 Einstein Telescope and 2 Cosmic Explorer detectors (1ET+2CE).

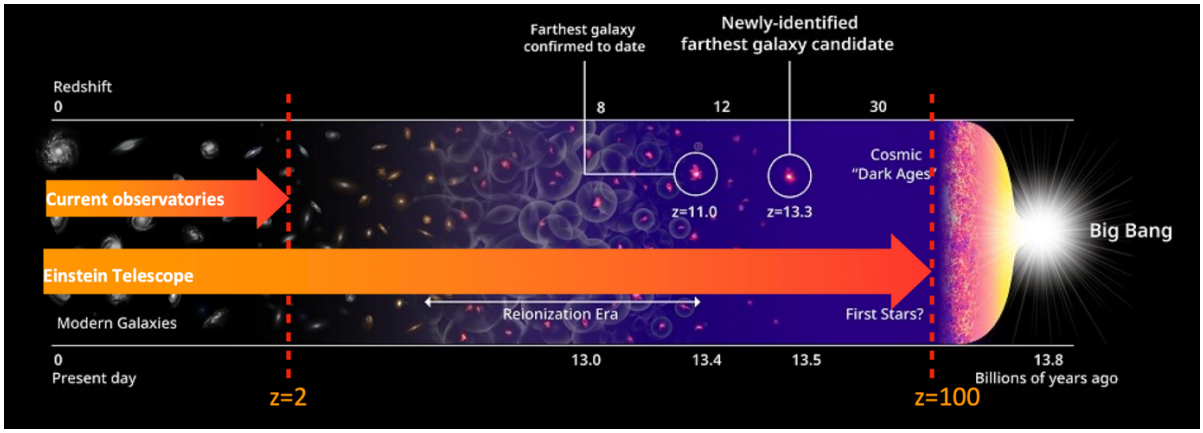


Fig. 34-10: Evolution of the probed volume.

Another line of study of GW of very low frequencies is the exploitation of the quasi-perfect clocks offered by pulsars [1188], as suggested in Fig. 34-11. Several datasets exist, with many pulsars recorded on long time spans. Nano-Hz band is explored. The Pulsar Timing Array (PTA) dataset content is given by Table 34-2.

The observed evolution of the separation angle between pulsars as a function of the separation angle magnitude shows a slight effect (Fig. 34-12). It is however too early to draw any conclusion**.**

[1186] ibid , B. S. Sathyaprakash *et al.,* Multimessenger Universe with Gravitational Waves from Binary Systems. https://arxiv.org/pdf/1903.09277

[1187] S. Nissanke, New perspectives onto the Universe in the era of Gravitational Wave (GW) Physics, 42nd International Conference on High Energy Physics, Praha, 2024. https://indico.cern.ch/event/1291157/contributions/5958354/attachments/2901957/5091832/ICHEPPraha_2024_wide_nissanke_final.pdf

[1188] S. Babak, Pulsar Timing Array. https://indico.cern.ch/event/1335188/contributions/6139295/attachments/2952148/5189736/04_babak.pdf

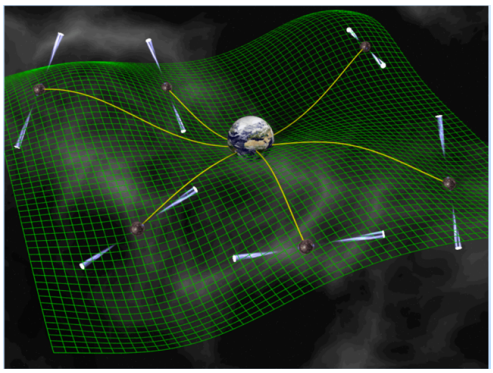


Fig. 34-11: Distant pulsars send regular radio pulses as highly accurate clocks. To allow measurements the axes must point at us. A passing GW would change the arrival time of the pulse [1189].

Credits: Kuo Liu

IPTA DR3 dimensions

- In total **121** pulsars in full DR3;
  - The biggest / most sensitive PTA dataset ever made !!

Dataset	Number of pulsars	Time span	Frequency range
EPTA DR2	25	24.5 yr	283 – 5107 MHz
NANOGrav 15-yr	68	15.9 yr	302 – 3988 MHz
PPTA DR3	24	18.1 yr	704 – 4032 MHz
InPTA DR1	15	3.5 yr	300 – 1460 MHz
MeerKAT DR2	83	4.5 yr	856 – 1712 MHz
CHIME DR1	11	2.5 yr	400 – 800 MHz
LOFAR+NenoFar	17	9.6 yr	35 – 190 MHz
IPTA DR3	121	~25 yr	~30 – 5000 MHz

Table 34-2: The International Pulsar Timing Array (IPTA) datasets.

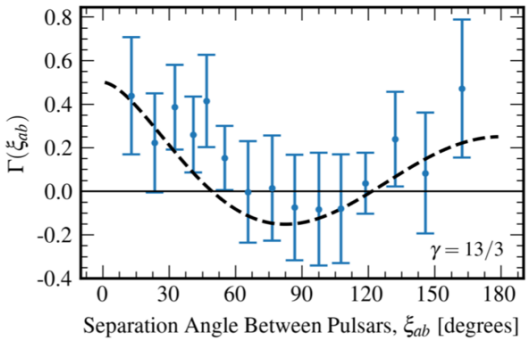


Fig. 34-12: Possible evidence for an excess low-frequency signal with phase-coherent inter-pulsar correlations in the NANOGrav 15-year data set [1190].

[1189] N. Christensen, Gravitational Waves: Now and in the Future. https://indico.cern.ch/event/1335188/contributions/6137374/attachments/2951358/5188019/Christensen_blois_2024.pdf

[1190] G. Agazie *et al.,* The NANOGrav 15-year Data Set: Evidence for a Gravitational-Wave Background. https://arxiv.org/abs/2306.16213

35. Astroparticle Physics

Here is a very short and sketchy account of what happened in the field of astroparticle physics. Several excellent papers present the domain [1191].

35.1 Overview

The origin of the field is generally attributed to the 'discovery' of cosmic rays by Victor Hess in the early 1910's (Nobel Prize 1936).

Strongly motivated by the discovery of **neutrino oscillations** (Chapter 19), the field has developed a lot both theoretically and experimentally since the early 2000s [1192]. Its filiation with the active cosmic ray physics of the fifties is obvious but aims and scales have changed.

Besides studying messengers from the heaven, the field of astroparticles covers many other topics: search for and study of **rare natural phenomen**a (double beta decay, possibly neutrinoless, etc.), search for peculiar or a priori forbidden properties of matter (as **electric dipole moments, proton decay**, etc.), as well as **gravitational waves detection**. We have treated apart some of these subjects.

To put some order, one usually lists the following sections:

- ***High-energy cosmic-ray physics and astrophysics;***
- ***particle cosmology;***
- ***particle astrophysics;***
- ***related astrophysics: supernova, active galactic nuclei, cosmic abundances, dark matter, etc.;***
- ***high-energy, VHE and UHE gamma-ray astronomy;***
- ***high- and low-energy neutrino astronomy;***
- ***instrumentation and detector developments related to the above-mentioned fields.***

In this document, the contributions of astroparticle physics to SM and BSM studies (neutrino masses, DM search, etc., were given priority over their other facets, namely the discovery and study of **cosmic messengers** [1193] and of **their sources**, topics of great interest but requiring the competence and collaboration of astrophysicists having a good understanding of objects and mechanisms of the field. This last chapter brings some correction to this assumed bias.

[1191] J. Ellis, Astroparticles and Cosmology: Learning from Cosmic and Gamma Rays. https://inspirehep.net/files/3a8d6467add3a7f817b712111ea38cdd
G. Gelmini, Cosmology and Astroparticles, https://arxiv.org/abs/hep-ph/9606409
R. Alves Batista *et al.,* EuCAPT White Paper: Opportunities and Challenges for Theoretical Astroparticle Physics in the Next Decade. https://arxiv.org/abs/2110.10074
P. Tinyakov *et al.,* Astroparticle physics with compact objects**.** https://arxiv.org/abs/2110.12298
M. Ackermann and K. Helbing, Searches for beyond-standard-model physics with astroparticle physics instruments. https://arxiv.org/abs/2402.18894

[1192] C. Spiering, Cherenkov detectors in astroparticle physics. https://arxiv.org/abs/2304.02340

[1193] A. de Angelis, Fundamental Physics With Cosmic High-Energy Gamma Rays. https://arxiv.org/abs/1610.08245
F. Halzen, The Observation of High-Energy Neutrinos from the Cosmos: Lessons Learned for Multimessenger Astronomy. https://arxiv.org/abs/2110.01687

The fast development of the field led to design new types of infrastructure and new detection methods, underground laboratories, special telescopes, antennas and satellite experiments, observing neutrinos, gamma rays and cosmic rays at the highest energies [1194].

Figure 35-1 [1195] illustrates the different detection techniques of cosmic-ray air showers.

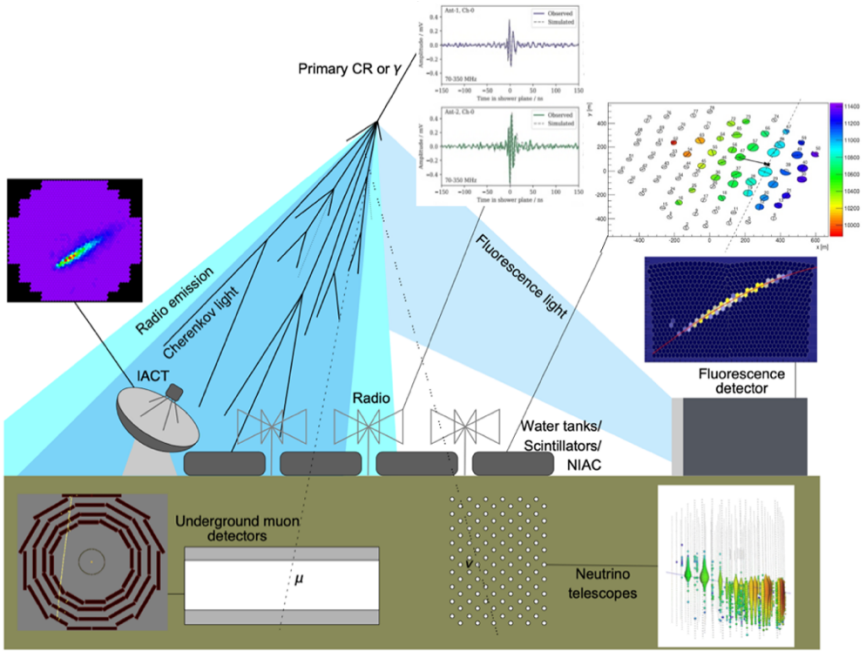


Fig. 35-1: The various methods of detection cosmic ray air shows are shown for illustration.

For **neutrinos and gamma rays**,[1196] **Cherenkov techniques** are widely used in astroparticle experiments, using various detection principles. For early ground observations of gamma astronomy see Ref. [1197]. Table 35-1 gives examples of the location, radiation medium and techniques of present detectors.

Location	Cherenkov Medium	Technique	Example
Underground	Ultrapure water	Ring imaging	Super-Kamiokande
Underwater/ice	Natural water/ice	Timing optical radio	 IceCube RNO-G (Greenland)
Ground	Atmosphere	Imaging	H.E.S.S.
	Atmosphere water in tanks	Timing Timing	TAIGA HAWC
Space, balloons	e.g. NaF	Ring imaging	AMS

Table 35-1: Location, detection principles and examples of experiments [1198].

[1194] F. G. Schroeder *et al.,* Snowmass UHECR Whitepaper*:* Requirements on Future Instrumentation, https://inspirehep.net/files/ce42ad172113e7bc1ffd0153784d2ac6
W. Hofmann and J. Hinton, Detectors for high-energy messengers from the Universe. https://arxiv.org/abs/1912.07473
[1195] ibid
[1196] D. Semikoz, Multi-messenger observations with cosmic rays, gamma-rays and neutrinos, present status and future perspectives. https://inspirehep.net/files/802fb71604ed94bd10eaa241d7434b6e
[1197] P. Fleury, Gamma Astronomy - Results from Ground Observations.
https://inspirehep.net/files/705ba70be9902da75e5cf6c3fdc9bbfb
[1198] C. Spiering, Cherenkov Detectors in Astroparticle Physics. https://arxiv.org/abs/2304.02340

35.2 Imaging Atmospheric Cherenkov Telescopes

Gamma-ray astronomy has now been extended to the TeV energy range. The number of identified TeV gamma-ray sources has been multiplied by 100: first PeV ones have been detected. The improved angular resolution of Imaging Atmospheric Cherenkov Telescopes (IACTs) reveals more about the morphology of these sources.

Table 35-2 provides the basic parameters of three major IACTs for high-energy gamma ray physics.

	H.E.S.S.	MAGIC	VERITAS
Altitude	1800 m	2200 m	1270 m
Dish diameter	4× 12 m 1× 28 m	2× 17 m	4×12 m
Nb. of pixels	4× 960 1× 2048	2× 576	4× 499
Field of view	5°	3.5°	3.5°
Start of operation	2003/2012	2004/2009	2007

Table 35-2: Basic parameters for H.E.S.S., MAGIC and VERITAS [1199].

Geiger-mode Avalanche Photodiodes (G-APDs), also called SiPMs, have the potential to significantly improve the sensitivity of IACT, which was successfully demonstrated with the FACT telescope [1200].

The Cherenkov Telescope Array Observatory (CTAO) is the next-generation ground-based gamma-ray observatory currently under construction. It will consist of two arrays of telescopes, one in the Northern Hemisphere and one in the Southern Hemisphere, designed to provide full-sky coverage for very high-energy gamma-ray astronomy. The project uses three types of telescopes to detect gamma rays: Large-Sized Telescopes (LSTs), Medium-Sized Telescopes (MSTs), and Small-Sized Telescopes (SSTs). These telescopes are designed to cover a wide range of gamma-ray energies, from 20 GeV to about 300 TeV (four orders of magnitude), and one expects to achieve a 10 times better sensitivity than H.E.S.S., MAGIC, and VERITAS. Table 35-3 gives the main parameters of the three telescope types used for CTA [1201].

	LST	MST	SST
energy range of optimization	20-150 GeV	0.15-5 TeV	5-300 TeV
optical design	parabolic	Davies-Cotton	Schwarzchild-Couder
primary dish diameter	23 m	12 m	4.3 m
focal length	28 m	16 m	2.15 m
total weight	100 tonne	82 tonne	17.5 tonne
type of camera sensors	PMTs	PMTs	SiPMs
number of pixels	1855	1855 (NectarCam) 1764 (FlashCam)	2048
camera FoV	4.3°	~7°	8.8°

Table 35-3: Main Parameters for the three telescopes types for CTA [1202].

[1199] ibid

[1200] H. Anderhub *et al.,* FACT—The first Cherenkov telescope using a G-APD camera for TeV gamma-ray astronomy. https://www.sciencedirect.com/science/article/abs/pii/S0168900210023466?via%3Dihub
T. Bretz *et al.,* FACT - The First G-APD Cherenkov Telescope: Status and Results https://arxiv.org/abs/1308.1512

[1201] M. Martinez on behalf of the CTA Consortium, Introduction to the CTA Project. https://inspirehep.net/files/f27ec275ed2edf3b5687d1a82028f842
CTAO homepage: https://www.ctao.org
R. Zanin on behalf of the CTA Observatory, CTA Consortium and LST Collaboration, Cherenkov Telescope Array: the World's largest VHE gamma-ray observatory. https://be.research-collection.ethz.ch/server/api/core/bitstreams/36cd6b3c-31fd-4296-a1a0-4afe2fc7f1de/content

[1202] ibid

Figure 35-2 [1203] illustrates the foreseen LST-part of the CTA project in La Palma (Spain) compared to the proposed telescopes of different sizes in Paranal (Chile). Figure 35-3 [1204] shows a picture from a CTA LST (diameter 23 m) operational in La Palma since 2020.

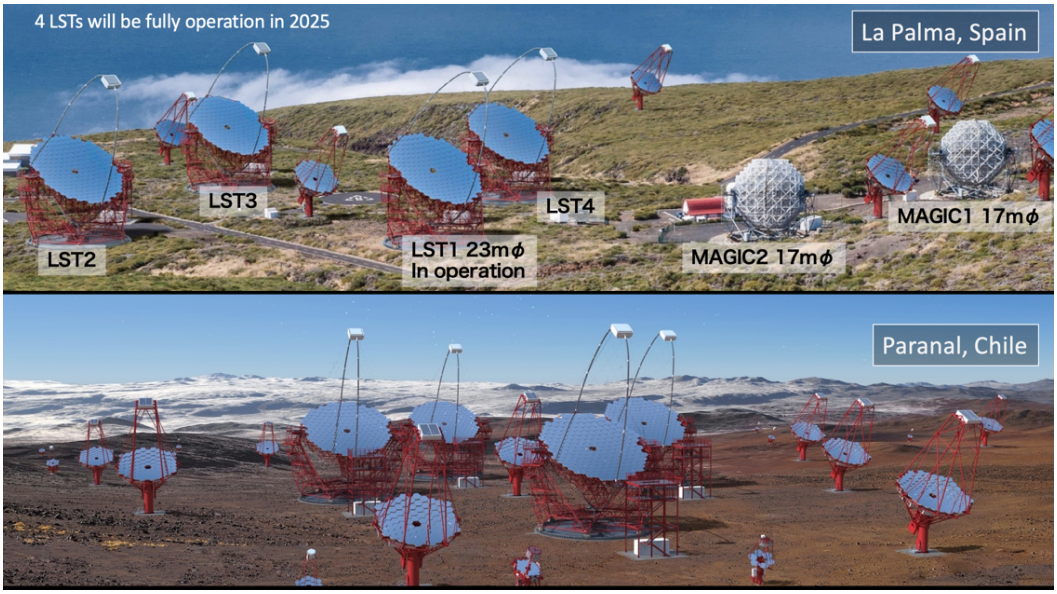


Fig. 35-2: Top: Status of the LST project in La Palma (Spain). Bottom: all telescope sizes in Paranal (Chile) [1205].



Fig. 35-3: Picture from a CTA LST operational in La Palma since 2020. LST (diameter = 23 m): mirror area of 400 m^2 (left) and size comparison of the CTA telescopes (right).

35.3 Neutrino telescopes and other instruments like e.g. air shower detectors using water tanks

The sensitivity of **neutrino telescopes** has been improved by almost a factor 1000, and the detection of a diffuse flux and of point sources of energetic ν gave access to the "**high-energy neutrino sky**".

[1203] M. Teshima, CTA -LST Project.
https://indico.cern.ch/event/877521/contributions/5084733/attachments/2523872/4340360/2022_1007_CTA_LST.pdf
[1204] ibid
[1205] On 2 July 2025, ESO signed, on behalf of the CTAO, a major contract with a consortium of Chilean companies to build the telescope foundations for the MSTs and SSTs on the CTAO-South site, located near ESO's Paranal Observatory in Chile.

This remarkable progress is due to a variety of factors: much larger detectors, more elaborate technology, more refined analysis methods, better sites, complementary detection methods combined and a "**multi-messenger approach**".

Considering **neutrinos** (Chapter 19), Table 35-4 [1206] lists the large neutrino telescopes. Dates are given for first data, completion and termination, respectively.

Experiment	Milestones	Location	Size (km^3)
NT200	1993/1998/2015	Lake Baikal	10^{-4}
AMANDA	1996/2000/2009	South Pole	0.015
ANTARES	2006/2008/2021	Mediterr. Sea	0.010
IceCube	2004/2010/ -	South Pole	1.0
GVD	2015/2026/ -	Lake Baikal	(0.5) 1.0
KM3NeT/ARCA	2015/2027/ -	Mediterr. Sea	1.2
KM3NeT/ORCA	2017/2026/ -	Mediterr. Sea	(0.001) 0.007
IceCube Gen2	2028/2035/ -	South Pole	8
KM3NeT Phase 3	2028/ - / -	Mediterr. Sea	≈3

Table 35-4: Past, present and future neutrino telescope projects. The number in brackets correspond to the 2022 status.

At altitudes of more than about 3 km above sea level, cosmic-ray showers down to a few hundred GeV can reach the ground. E.g. arrays of water tanks can observe these charged particles via the emitted Cherenkov light. Table 35-5 [1207] lists the present air shower detectors recording the Cherenkov light generated by charged particles in water tanks (plus eventually scintillators and air Cherenkov detectors).

	Pierre Auger	IceTop	HAWC	LHAASO
Location	Chile	South Pole	Mexico	Tibet
Altitude	1.4 km	2.9 km	4.1 km	4.4 km
Area	3000 km^2	1 km^2	0.02/ 0.05 km^2	1 km^2
Primary	CR (γ, ν)	CR	CR, γ	CR, γ
Energy threshold	$10^{17.5}$ eV	10^{14}eV	10^{11} eV	10^{11} eV

Table 35-5: Examples of present air shower detectors recording the Cherenkov light generated by charged particles in water tanks. CR stands for charges cosmic rays.

Considering the highest energy cosmic rays, the two main existing arrays are described in Table 35-6. Figures 35-4 and 35-5 [1208] give the **energy and identity patterns of the most energetic CR.** Figure 35-5 shows the effective < X_{max} >, i.e. the depth of the position of the shower maximum, as function of the Energy (E/eV,) as measured by Auger and TA. However, one should add the following remark: The TA Collaboration measures an effective distribution of the shower maximum and compares it to simulations which undergo same selection as the data. According to the authors, the measured average and variance of X_{max} will not match those of the true distribution. On the other hand, the Pierre Auger Collaboration attempts an unbiased measurement, introducing fiducial cuts which reduce the statistics. The different approaches of the two collaborations means that they are not measuring the

[1206] C. Spiering, Cherenkov Detectors in Astroparticle Physics. https://arxiv.org/abs/2304.02340
[1207] ibid
[1208] E. Zas, Beyond the Galaxy: UHECR results from the Pierre Auger Observatory and the Telescope Array. https://iopscience.iop.org/article/10.1088/1742-6596/632/1/012104/pdf

same quantity, so that the values obtained cannot be directly compared to one another. Nevertheless, the two sets of measurements have been superposed and shown in the right panel of Fig. 35-4. As pointed out by the authors, this figure must therefore be interpreted with great care.

			Auger	TA
SD	Average latitude		35.3° N	39.4° S
	Average altitude		1,400 m	1,400 m
	Surface area		3,000 km^2	700 km^2
	Lattice		1.5 km hexagon	1.2 km square
	Detector	Type	water-Cherenkov	Plastic scintillator
		Size	10 m^2 × 1.2 m	(2×) 3 m^2 × 1.2 cm
		Sampling	25 ns	20 ns
FD	Sites		4	3
	Telescopes	Number	24	36
		Size	13 m^2	6.8 m^2/3 m^2
		Field of view	28.5° × 30°	16° × 14°/18° × 15°
		Pixels	440	256

Table 35-6: Comparison of characteristics of the Pierre Auger Observatory and the Telescope Array [1209]. The low energy extensions for each observatory, HEAT and TALE, are not included.

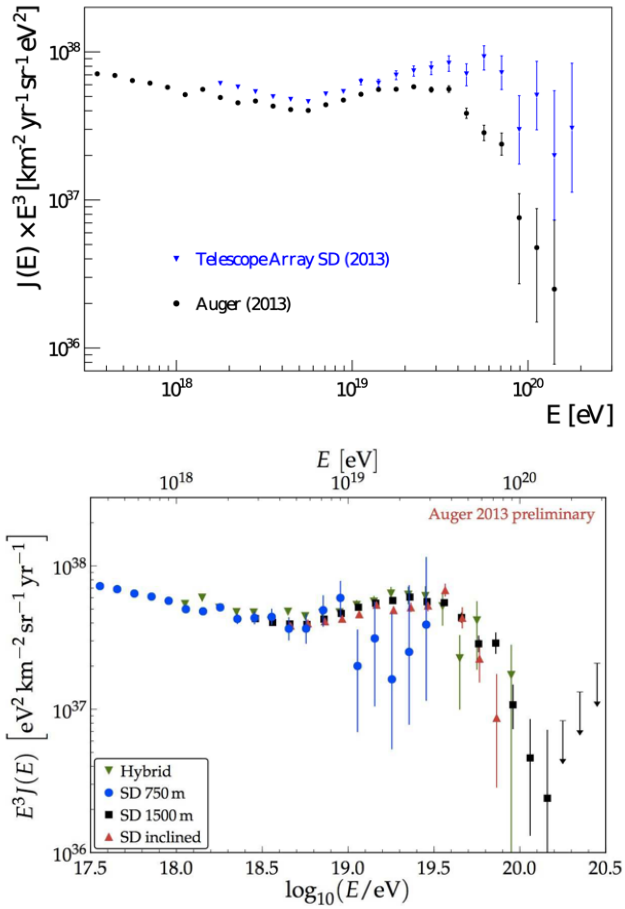


Fig. 35-4: Top: energy spectra obtained with the Pierre Auger Observatory (black dots) and the Telescope Array (blue triangles). Only statistical uncertainties are plotted. Bottom: Comparison of the four energy spectra obtained with the Auger Observatory.

[1209] ibid

Quoting [1210]: *"The energy spectrum measurements agree below 50 EeV and display the ankle at about 5 EeV. For energies greater than 50 EeV, both spectra clearly indicate **a suppression** but there are some important discrepancies. TA results are consistent with models in which protons are accelerated and they interact with the CMB producing **the GZK cut-off**. The Auger spectrum can only be made consistent with such scenario if the **fluxes at the sources are suppressed** at similar energies. But such a scenario is in fact in tension with some sets of data from the Auger Observatory."*

Composition studies also show discrepancies between both experiments. Auger data indicate a **transition from light to heavier elements** starting at E ~ 4 EeV. As an example of input of PP to the field of astrophysics see Ref. [1211] .

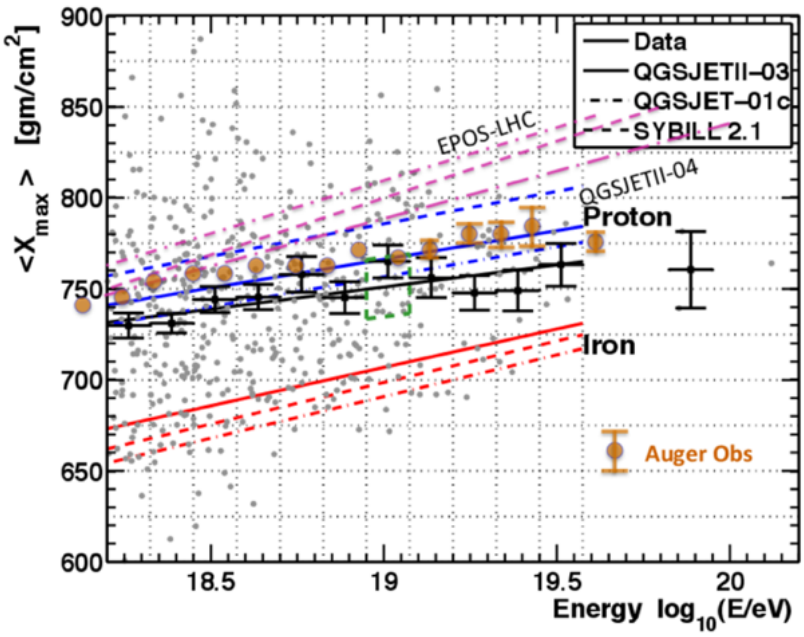


Fig. 35-5: Effective < X_{max} > (depth of the position of the shower maximum) measured at the Telescope Array (small black squares) and < X_{max} > obtained from the Auger Observatory data with fiducial cuts (large brown circles) compared to expectations for the effective X_{max} measured by the TA for proton (blue) and iron (red). For more information see text.

Leaving the ground and the large arrays, let us close by illustrating **two satellite telescopes** which by their conception, their careful design and their achieved longevity have changed our knowledge and understanding of cosmic messengers.

35.4 The Alpha Magnetic Spectrometer

AMS-01 [1212] was a pioneering experiment, designed to be the first large magnetic spectrometer to be operated in space. At the heart of AMS-01 was a permanent cylindrical magnet, layers of silicon tracking detectors, time-of-flight and Cherenkov counters. AMS-01 was installed on the Space Shuttle Discovery during a 10-days mission in 1998 and demonstrated the feasibility to operate a large magnetic spectrometer in space. From the about 80 million events collected several new physics

[1210] ibid
[1211] G. Graziani, LHCb inputs to astroparticle physics. https://cds.cern.ch/record/2682147/files/graziani_EPS_astroLHCb.pdf
[1212] https://en.wikipedia.org/wiki/Alpha_Magnetic_Spectrometer , https://ams02.space/what-is-ams/ams-01

results were obtained (e.g. the Helium – Antihelium ratio, lepton and proton spectra in near earth orbit), advancing our understanding of cosmic rays and their properties [1213]. The data also allowed to investigate whether antimatter exists in our Universe today in a measurable quantity [1214].

After the successful flight of the prototype, the AMS Collaboration started to design the AMS-02 (or AMS for short) detector [1215], to be installed at the International Space Station (ISS). The instrument which eventually resulted from a long evolutionary process has been called *"the most sophisticated particle detector ever sent into space"* and was installed at the ISS in May 2011.

AMS (Fig. 35-6) is the first and only instrument measuring simultaneously particles, anti-particles and the chemical composition of cosmic ray (CR) nuclei in a broad energy range and over a solar cycle. AMS has collected more than 250 billion CR events, measuring with unprecedented precision different components of the charged CR up to few TeV. It provided inputs to a better understanding of their production and propagation. This includes fluxes of positrons, electrons, antiprotons, protons, and nuclei from helium to silicon and beyond. Results on time variation of CR fluxes associated with solar activity on different time scales have been obtained.

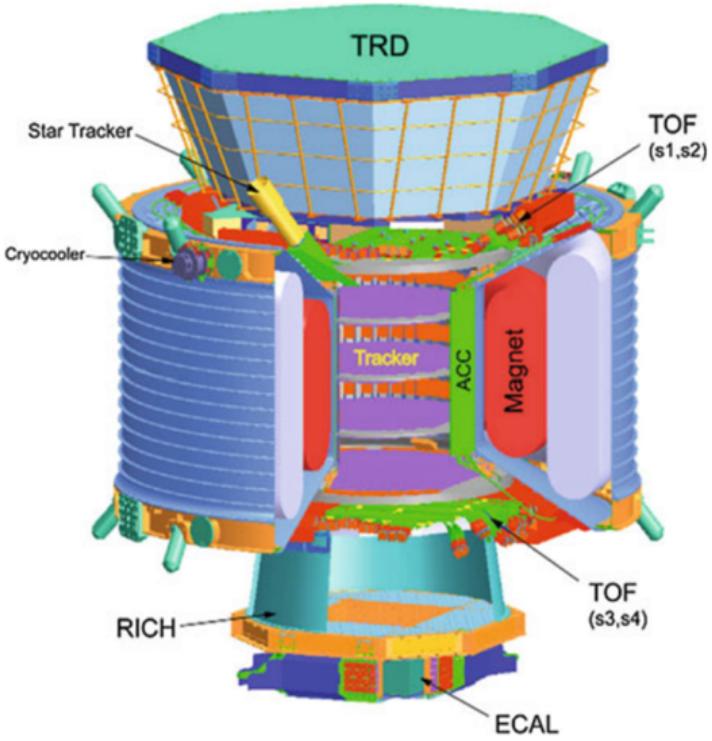


Fig. 35-6: AMS detector on the ISS showing the main sub-detector elements and their functions.

As an external payload on the ISS until at least 2030, AMS [1216] will continue to collect and analyse an increasing set of data at highest energies which will provide new insights in this field and will allow to continue exploring new physics and astrophysics phenomena.

[1213] M. Aguilar, *et al.,* Relative Composition and Energy Spectra of Light Nuclei in Cosmic Rays: Results from AMS-01. 2010 ApJ 724 329, https://iopscience.iop.org/article/10.1088/0004-637X/724/1/329
U. Becker, AMS-01: First flight, first results; future AMS-02.https://doi.org/10.1063/1.1291488
[1214] H. Anderhub, A. Biland and F. Pauss, Search for antimatter in space with the Alpha Magnetic Spectrometer. Nuclear Physics News, Vol. 12, No. 1, 2002, https://doi.org/10.1080/10506890208235633
[1215] AMS homepage, https://ams02.space
[1216] J. Bedugo, AMS Highlights. https://cds.cern.ch/record/2813963/files/document.pdf

Figures 35-7 and 35-8 illustrate some of the many results obtained by AMS. Figure 35-7 shows the electron and positron spectra with 1.9 million positrons and 28.1 million electrons. The spectra clearly show a different behaviour, commonly referred to as positron excess. It is consistent with the existence of a new source of high-energy positrons with a characteristic cut-off energy, as predicted by the existence of dark matter or other astrophysical processes.

AMS can determine the charge of cosmic ray particles with multiple subdetectors independently and can thus resolve ions up to iron (Z = 26) and nickel (Z = 28). With large event numbers and precise charge and rigidity determination, AMS measures the cosmic-ray ion fluxes with high accuracy. Figure 35-8 shows the combined results.

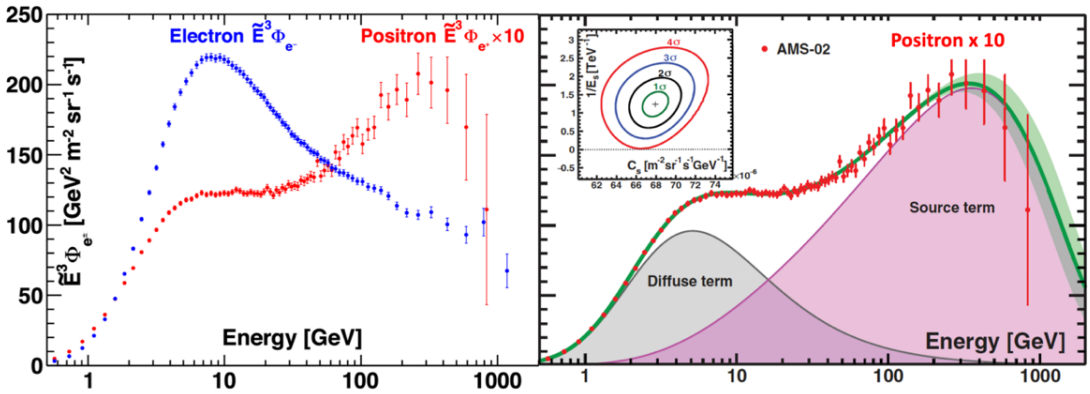


Fig. 35-7: AMS e^- (blue) and e^+ (red points, multiplied by 10) spectra. Plotted is the mean energy value $\tilde{E}^3$ of each measurement bin multiplied by the electron or positron flux Φ of as a function of energy (left). The positron spectrum is fitted with a diffused (power law) term plus a source (power law with exponential cut-off) term (right) [1217].

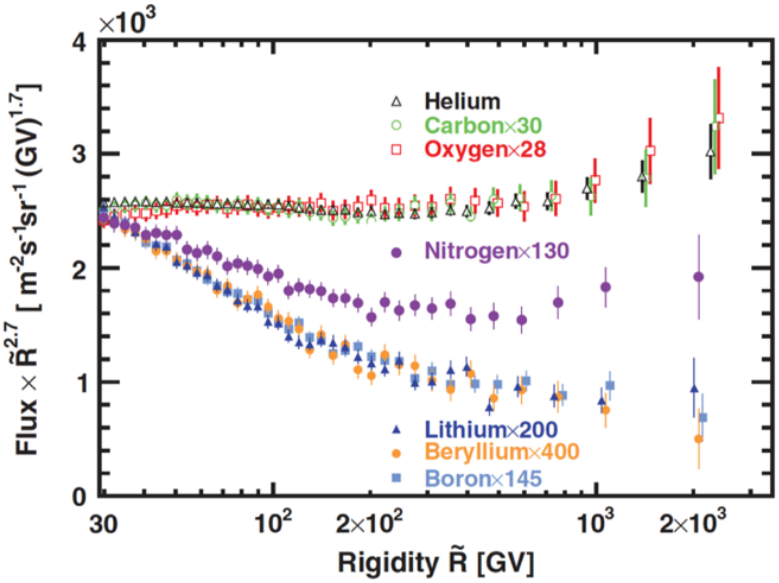


Fig. 35-8: AMS measurements of cosmic ray ion fluxes. Plotted is the cosmic ray ion fluxes multiplied by $\tilde{R}^{2.7}$, where $\tilde{R}$ is the weighted average rigidity of each data bin. For display purposes only, the fluxes were rescaled as indicated in the plot [1218].

[1217] Y.- H. Chang, Latest Results from the AMS Experiment. https://inspirehep.net/files/8b50e2312f541d6b927455e09d2f9729

[1218] ibid

35.5 The Large Area Telescope

The **Large Area Telescope (LAT)**, [1219] the primary instrument for the **Fermi Gamma-ray Space Telescope (Fermi)** [1220], formerly called the **Gamma-ray Large Area Space Telescope** (**GLAST**) mission, is an imaging, wide field-of-view, high-energy gamma-ray (GR) telescope, covering the energy range from 30 MeV to more than 300 GeV. It remains in excellent operating condition after more than ten years in space and there are no consumables that will limit its lifetime.

Figure 35-9 [1221] shows a schematic diagram of the LAT and a picture in space. The telescope's dimensions are 1.8 m × 1.8 m × 0.72 m and it has a mass of 2789 kg. Figure 35-10 shows a picture from 2009, at that time the deepest and best-resolved portrait of the gamma-ray sky.

The LAT has achieved a wide range of scientific goals, as exploring the HE GR sky and Investigating the origin of isotropic diffuse emissions. It has probed particle acceleration mechanisms in various astrophysical sources, including active galactic nuclei (AGNs), pulsars, and supernova remnants. It studied the HE emissions of GR bursts (GRB)and other transient sources. A GRB that was detected by the GR Burst Monitor (GBM) and followed up by the LAT was **coincident with the first neutron star-neutron star merger observed with LIGO and Virgo**. The LAT detected also a flaring of gamma-ray emission from an active galaxy in association with the detection of a high-energy ν from the same direction by the IceCube ν detector, **first association between ν and γ emission from an active galaxy**. By using HE γ Fermi-LAT helped to study the early Universe and the origin of DM. The mission still produces excellent science in the new frontiers of multi-messenger (MM) astrophysics, that it contributed to open. In addition to MM science, the LAT and Fermi are expected to centrally participate in coming advances in multi-wavelength studies, and detection of transient sources with the new telescopes and sky surveys completed or in active development.

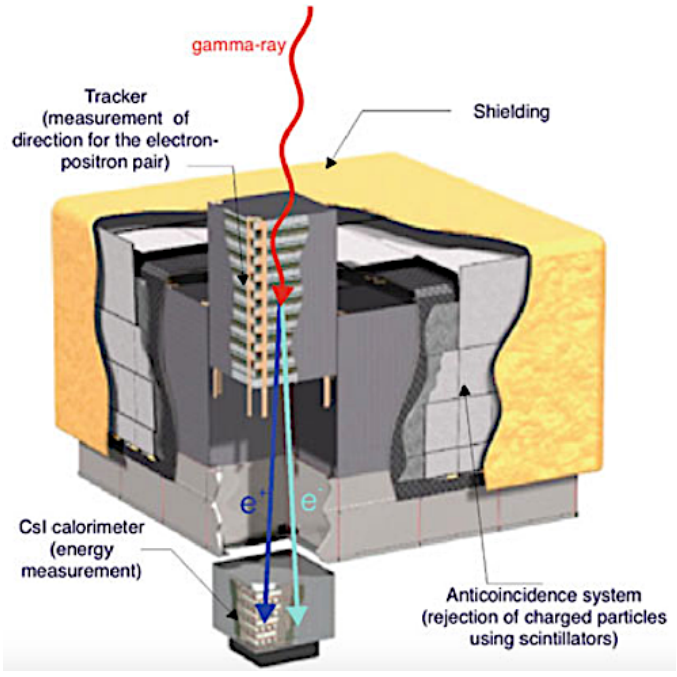


Fig. 35-9: Schematic diagram of the LAT.

[1219] R. Pillera, Science highlights of the Fermi-LAT. https://inspirehep.net/files/13c6c2f2f033c0e765e95dfc6185d09f
[1220] https://web.archive.org/web/20221207174345/https://fgst.slac.stanford.edu/
[1221] W. B. Atwood *et al.,* The Large Area Telescope on the *Fermi Gamma-Ray Space Telescope* Mission. https://iopscience.iop.org/article/10.1088/0004-637X/697/2/1071/pdf

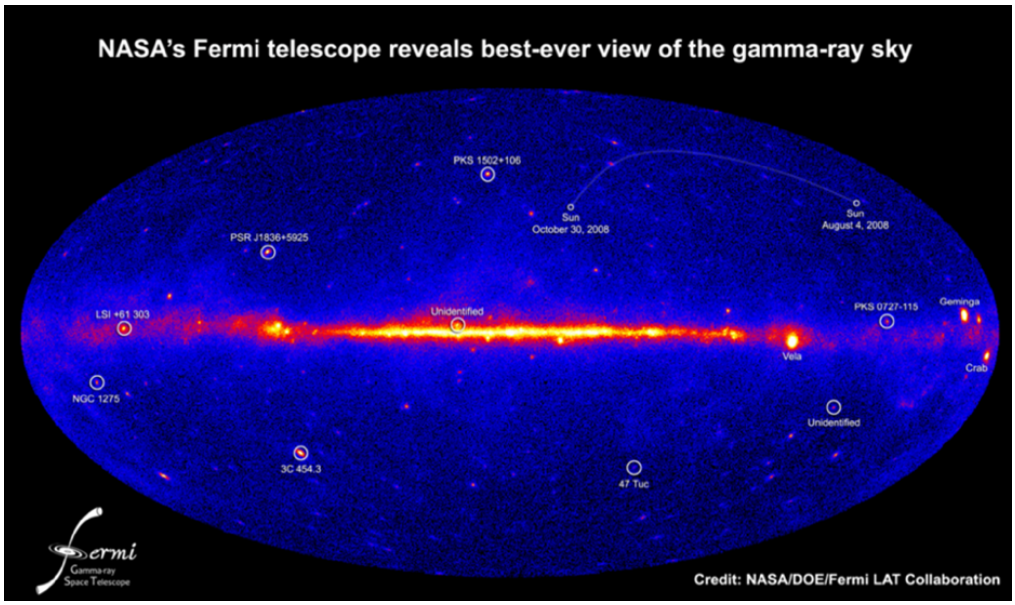


Fig. 35-10: The image shows how the sky appears at energies more than 150 million times greater than that of visible light [1222].

***Apologies**: It would lead us too far to review the status and progress of the great astronomical instruments in all wavelengths, up to radio astronomy. But it is clear that any new information on cosmic objects may potentially, through indirect steps, tell more on questions relevant to particle physics. Description of the physics cases of these big projects, as SKA, are sketched in Ref. [1223]. Another relationship between the fields concerns the similitude of the means needed in terms of size, number of items to be built, computing means required, data volume expected, analysis methods to be implemented to search for new effects. These similarities already led to agreements between SKA and CERN, a priori quite different fields [1224].*

*In Chapter 34, on the fascinating topic of **gravitational waves (GW)**, we just referred to a summary of results [1225], to the next to come major interferometer [1226] and to a promising future technique of GW detection [1227].*

[1222] Fermi comes to CERN (2009): https://cds.cern.ch/record/1187556

[1223] L. Harvey-Smith, After the SKA - Radio Astronomy in 2049. https://arxiv.org/abs/1212.1858
R. Fender, High energy astrophysics with the next generation of radio astronomy facilities. https://arxiv.org/abs/0810.0951
G. Heald and P. Serra, Panoramic Radio Astronomy: Wide-field 1-2 GHz research on galaxy evolution. https://arxiv.org/abs/0911.4018
D. Semikoz, Multi-messenger observations with cosmic rays, gamma-rays and neutrinos, present status and future perspectives. 2019 *J. Phys.: Conf. Ser. 1263 012009,* https://iopscience.iop.org/article/10.1088/1742-6596/1263/1/012009/pdf

[1224] https://cerncourier.com/a/ska-and-cern-co-operate-on-extreme-computing/

[1225] R. Abbott *et al.,* GWTC-3: Compact Binary Coalescences Observed by LIGO and Virgo during the Second Part of the Third Observing Run. https://arxiv.org/abs/2111.03606

[1226] A. Chiummo, for the ET Collaboration, The Einstein Telescope: status of the project. https://inspirehep.net/files/e5cdb436e68e352f3813b214020ca406
M. Armano *et al.,* In-depth analysis of LISA Pathfinder performance results: Time evolution, noise projection, physical models, and implications for LISA. https://arxiv.org/abs/2405.05207

[1227] R. S Lynch, Pulsar timing array. 2015 *J. Phys.: Conf. Ser. 610 012017* https://iopscience.iop.org/article/10.1088/1742-6596/610/1/012017

36. Some conclusions

With multiple apologies for all insufficiently treated topics, let us look again at the overall scenery.

Without any doubt, the last eight decades, since the end of the Second World War, from the conception of QED to the Higgs boson discovery, represent an amazing period, which saw the birth and blooming of a new branch of science: **Particle Physics.**

Intellectually and technically, in parallel and in interaction with the mutations of **electronics and computing,** with the revolutions of **cosmology**, with the progress of other physics domains, as **condensed matter physics**, it was a long series of breakthroughs. This is illustrated in Fig. 36-1.

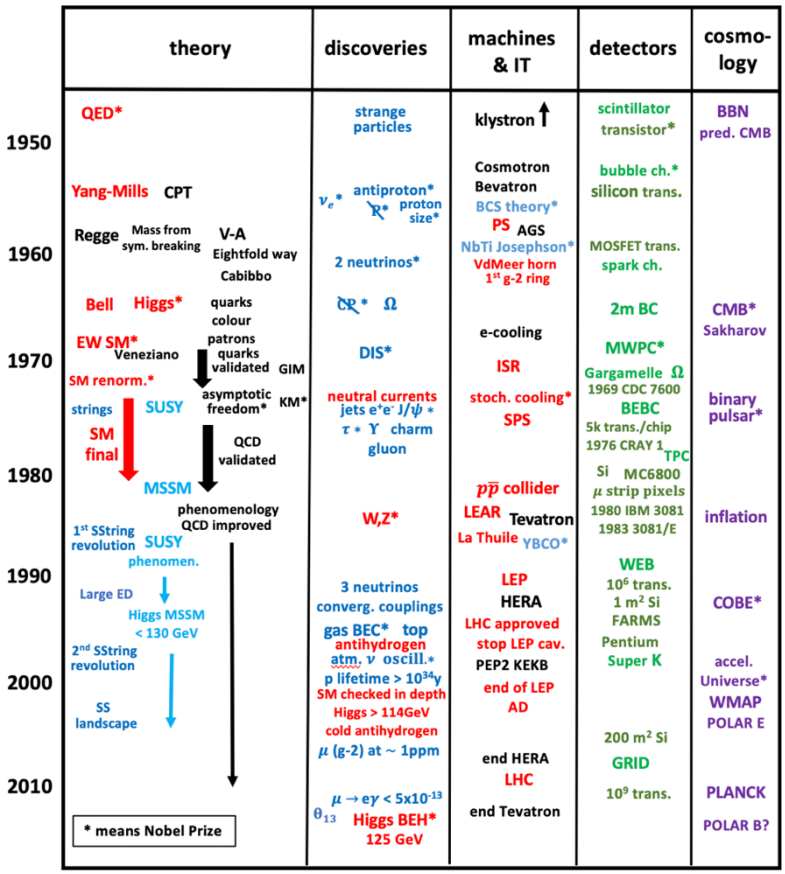


Fig. 36-1: Schematic presentation of the impressive progress made over the past 70 years in theory, machines, IT and detectors as well as major discoveries in particle physics and cosmology (same as Fig. 2-4).

The advent of the Higgs boson, a **totally new physical object**, marks a beginning of speculations, not an end. Facing the questions it raises, as hierarchy, vacuum metastability, let us risk guesswork, allow for conjectures, be bold. Is the Higgs field linked to inflation, are hierarchy and metastability connected, etc.?

The SM is a prodigious construction, but it is **manifestly incomplete**. Big questions are asked: the nature of the neutrino? CP in strong interaction and axion? Origin of baryogenesis? Proton decay? Are true symmetries all gauge symmetries? – and many more.

A burst of intellectual and instrumental innovations is motivated by the presumed existence of a **Dark Sector**. Some instruments are of modest size. Particle Physics is not exclusively bound to gigantism.

Smaller but sophisticated machines provide major results. A diversified physics program is maintained. But don't forget that Dark Matter as part of Particle Physics is an assumption, even if a compelling one.

Nevertheless, the quest of higher energy is still considered as a must. The de Broglie inverse relation between resolution and energy is unavoidable!

It is understandable that large new projects considered are subject to criticism, and their possible questionable aspects must be minimised. But they should also be put in the **correct perspective** and at a global scale, for example for energy consumption [1228]. Thus, if the CERN electricity consumption seems large on the Geneva's scale, it is 10^{-5} of the world energy. Is that acceptable for a world-leading laboratory covering a **unique field of most fundamental research**, which implies worldwide about 17 500 scientists from more than 80 countries?

One should also realise that in matter of funding the "principle of communicating vessels" is illusory. As history tells, funds refused to some sector of research are not guaranteed to be granted to another one or to a more virtuous domain.

Let us recall that Particle Physics belongs to the domain of **exact science**! The muon g–2 agreement between theory and experiment is demonstrated at the 10^{-6} level and the possibility of a tiny mismatch invited to go on improving both. One must fight for ultimate precision in all sectors and try to better illustrate the virtues of this quest of precision. Fighting for accuracy, again and again, has many implications.

A key of the game implies first a continued and still improved intensive and close **collaboration between theory and experiment.**

A priori considerations are dangerous. All topologies should be explored. We should look for more discoveries with great vigilance! We should not miss anything at the LHC or elsewhere! While awaiting new discoveries, one should continue to develop an **Effective Field Theory approach** to LHC physics.

An essential corollary of these objectives is that physics measurements and analyses are **increasingly difficult**! **Cross-checking** of programs and experiences is absolutely necessary! Coordination and comparisons between experiments are mandatory: secretiveness is no longer relevant.

In the making of physics, a number of errors will occur and must be corrected, and this will be easier if **openness** is the attitude. An overall program of analyses, as exhaustive as possible, should be defined, which is the role of the research management. Open discussions, as in the Moriond spirit, should be the rule.

It is important to try to avoid fake news as much as possible. On the late "750 GeV", one reads on wiki*: "The event highlighted the desire in the community for the LHC to discover a fundamentally new particle, and the difficulties in searching for a signal which is unknown a priori".*

Last but not least, **vigorous R&D programs**, which were the key to success, must be maintained in all relevant domains, accelerators, detectors, electronics and advanced information technology.

Let us also remember that even if Particle Physics first evokes *"high-energy atom smashers",* many technologies have been developed along its course that find **wide applications in society**.

The approved HL-LHC will bring 10 times more data. This is a very ambitious goal. While discussing about the long-term future, let us achieve and exploit this major upgrade, and ensure that the field continues to attract the best young minds.

[1228] CERN uses annually 1.3 TWh of electricity. The world electricity consumption in 2022 was 24 398 TWh, which is about 20% of the world final energy consumption.